REPUBLIC OF LEBANON
COUNCIL FOR DEVELOPMENT
AND RECONSTRUCTION

الجمهورية اللبنانية
مجلس الإنماء والإعمار

MISE A JOUR DES ETUDES ET ASSISTANCE TECHNIQUE POUR LA CONSTRUCTION DU BARRAGE DE BISRI

BARRAGE BISRI

AVANT PROJET DETAILLE

PIECE 4 : NUMERICAL STABILITY ANALYSIS

February 2015

DAR AL HANDASAH NAZIH TALEB & PARTNERS
دار الهندسة نزيه طالب وشركاه
Founded 1956

NOVEC
CDG DEVELOPPEMENT

ITASCA
Consultants, s.a.s.

Rapport
15R-004

25/03/2015

To the attention of
Mr. A. F. CHRAIBI
NOVEC

Numerical stability analysis and subsidence evaluation of the Bisri dam in Lebanon under seismic loading

Author : CATALANO Emanuele
Review : BILLAUX Daniel
Approval : BILLAUX Daniel

ITASCA CONSULTANTS, S.A.S.

64, Chemin des Mouilles,
F-69134 ECULLY Cedex
Tel: 33 (0)4 72 18 04 20
Fax : 33 (0)4 72 18 04 21
Email : itasca@itasca.fr
Web site : www.itasca.fr

MODIFICATIONS

Version	Modifications	Date
A1	**First version**	**05/02/2015**
A*2*	**Corrections following comments during review meeting on February 23, 2015**	**25/03/2015**

INDEX

LIST OF FIGURES

1. REFERENCES

[1] NOVEC, Barrage de Bisri – Etudes et Assistance pour la construction du barrage. Mission I : Actualisation de l'étude géologique d'avant-projet détaillé. Février 2013

[2] Darendeli, M. B. (2001), Development of a new family of normalized modulus reduction and material damping curves. *Austin, Texas: The University of Texas.*

[3] Erdik M., Sesetyan K., Demircioglu M.B., Harmandar E. (2014), Assessment of site-specific earthquake hazard for Bisri Dam, Lebanon, *Bogaziçi University, Kandilli Observatory and Earthquake Research Institute, Departement of earthquake engineering.*

[4] Gazetas G., Dakoulas P. (1991) Aspects of seismic analysis and design of rockfill dams. *Second International Conference on Recent Advances in Geotechnical Earthquake Engineering and Soil Dynamics* (1991: Matrch 11 - 15; St. Louis, Missouri): 1851-1888.

[5] Itasca Consulting Group, Inc. (2011), FLAC (Fast Lagrangian Analysis of Continua) user's manuals, *Minneapolis, MN*.

[6] Itasca Consulting Group, Inc. , UBCHYST - A total stress hysteretic model, *Minneapolis, MN*.

[7] Kunar, R. R., P. J. Beresford and P. A. Cundall (1977) A Tested Soil-Structure Model for Surface Structures, *Proceedings of the Symposium on Soil-Structure Interaction*, Roorkee University, India, Vol. 1, pp. 137-144. Meerut, India.

[8] Lysmer, J., and R. L. Kuhlemeyer (1969) Finite Dynamic Model for Infinite Media, *J. Eng. Mech.*, 95(EM4), 859-877.

[9] Roblee, C., and Chiou, B. (2004) A proposed geoindex model for design selection of non-linear properties for site response analysis. *Proc., NSF/PEER Int. Workshop on Uncertainties in Nonlinear Soil Properties and their Impact on Modeling Dynamic Soil Response* Univ. of California at Berkeley, Berkeley.

[10] Seed, H. B. W., R. T.; Idriss, I.M. & Tokimatsu, K. 1986. Moduli and Damping Factors for Dynamic Analyses of Cohesionless Soils, *Journal of Geotechnical Engineering*, ASCE 112 (11): 1016-1032.

[11] Sun J.I., Golesorkhi R. and Seed H. B. (1988) Dynamic Moduli and Damping Ratios for Cohesive Soils. *Earthquake Engineering Research Centre Report no. 88-15*, University of California, Berkeley.

[12] J.A. Schneider, L. Hoyos, P.W. Mayne, E.J. Macari, G.J. Rix. Field and laboratory measurements of dynamic shear modulus of piedmont residual soils, *Behavioral Characteristics of Residual Soils*, GSP 92, ASCE, Reston, 1999, pp. 12–25.

[13] A.H. Hammama, M. Eliwab, Comparison between results of dynamic & static moduli of soil determined by different methods , *HBRC Journal* (2013) 9, 144-149

2. INTRODUCTION

The Bisri dam is a clay-core earthfill dam to be built over a heterogeneous quaternary lacustrine deposit, 120 meters thick, not fully consolidated. Lithological sections surveys and reconnaissance wells show that this deposit is composed of coarse alluvium (more present in the upper part of the alluvium deposit), clays and silts with intercalated sand lenses of varying thickness. This dam on the Bisri River in Lebanon will be about 70 m high and will have a span of about 700 m at the crest.

Concerning the seismic risks evaluation, the site is characterized by the close proximity of the Roum fault in the valley and the presence of the Yammouneh fault about ten kilometers to the east. An assessment of site-specific earthquake hazard for the Bisri site was conducted by experts from the department of earthquake engineering of the Kandilli Observatory and Earthquake Research Institute, Bogaziçi University [3], providing seismic records which can be considered as characteristic of the site.

ITASCA Consultants S.A.S. (ITASCA) has been asked by NOVEC to perform a numerical simulation, using the software FLAC *(Fast Lagrangian Analysis of Continua)*, to evaluate the stability of the Bisri dam, in the framework of the design studies to be performed by NOVEC and its partners. Fully dynamic 2D simulations are performed to evaluate the subsidence induced by the seismic motion.

In this report, the 2D numerical model of the dam is described in detail. The physical properties of both the foundation and the dam materials are presented. Also, details about the numerical model, with a special emphasis to the boundary conditions which were adopted, are given.

Details about the constitutive behavior of materials are given, related to both the dam construction phase and the subsequent dynamic loading.

Two different geometries are tested, which will be named in the report as “Reference Cross Section” and “Real Cross Section”. For both geometries, the numerical results will be presented in two main sections:

- a first section relative to the dam construction phase: the evolution of foundation settlements is presented, during the construction of the embankment and the upstream filling of the dam;
- a second section relative to the dynamic analysis: the subsidence caused by the earthquake will be evaluated, graphically presented and discussed.

The materials that compose the foundation are identified in Figure 2-1. In the numerical model, labeled groups are created to identify the materials that compose both the dam and the foundation. They are summarized below.

The dam materials are grouped as follows:

- The dam clay core (label “1_Core”);
- The rockfill (“2_Rockfill”);
- The compacted gravel (“3_Comp_Gravel”).

The foundation layers are:

- A layer of alluvial sand (“A1_Alluv_Sand”);
- A layer of alluvial clayey silt (“A2_ClayeySilt”);
- A layer of alluvial gravel (“A3_Alluv_Gravel”).

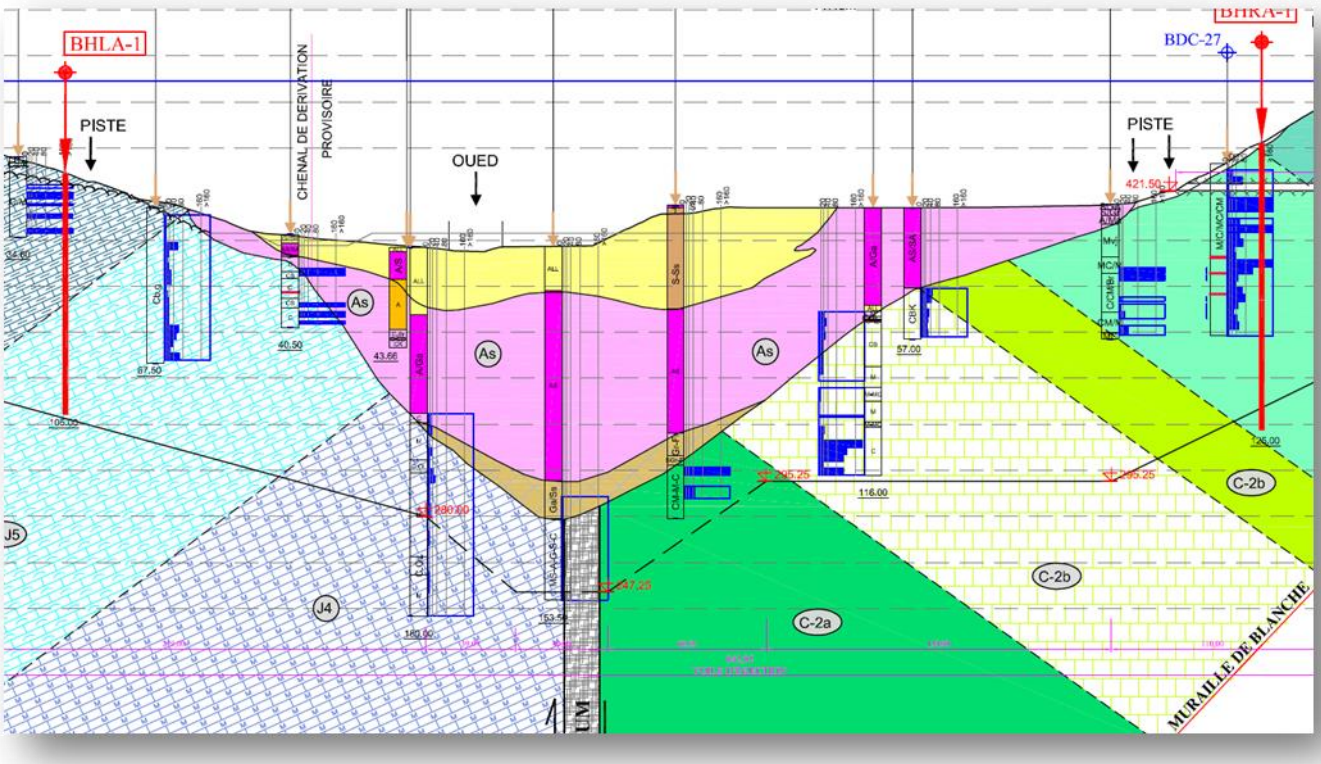

All-ss	Alluvions (sable et sable silteux)
As	Argile silteuse - Argile à galets
	Graviers et fragments de roches

ÂGE			DESCRIPTION
QUATER-NAIRE			TERRAIN DE COUVERTURE
			DEPOT LACUSTRE
CRETACE	CRETACE SUPERIEUR	C4	CENOMNIEN DOLOMIE MASSIVE / CALCAIRE LITE A SILEX/ MARNES / CALCAIRE INFERIEUR
		C3	ALBIEN (BARRE A CARDIUM) : CALCAIRE ORANGE-JAUNÂTRE, DUR, CRISTALLIN, KARSTIFIE MARNES ET MARNO-CALCAIRE VERT-JAUNÂTRE A ABONDANTES COQUILLES
	CRETACE INFERIEUR	C2b	APTIEN SUPERIEUR (FALAISE DE BLANCHE): CALCAIRE LITHOGRAPHIQUE BEIGE A POINTS ROUGES A ORBITOLINES, CRISTALLIN, DUR, KARSTIFIE, TRES FRACTURE
		C2a	APTIEN INFERIEUR (MARNE A PISOLITHES): ALTERNANCE DE SABLE, D'ARGILE, DE MARNE DE CALCAIRE GRESEUX DETRITIQUE, DE SABLE FERRUGINEUX GENERALEMENT PEU CIMENTE
		C1	CRETACE INFERIEUR : GRES DE BASE ; ALTERNANACE DE SABLE , D'ARGILE, DE MARNE,DE SABLE FERRUGINEUX CIMENTE, PARFOIS TRES DUR, DE TUF PARFOIS CIMENTE ET DE CINERITES
JURASSIQUE		J 7	KIMMERIDGIEN CALCAIRE GRIS, OOLITHIQUE, CRISTALLIN, DUR, KARSTIFIE. A NIVEAUX MARNEUX
		J 6	PORTLANDIEN CALCAIRE FIN,MASSIF, RAREMENT OOLITHIQUE, OCRE TANTOT A POINTS ROUGES. A SILEX. CRISTALLIN. DURE PEU KARSTIFIE.
		J 5	ARGILE, MARNE ET CALCAIRE MARNEUX
		J 4	CALCAIER OOLITHIQUE FOSSILIFERE MARNE ET CALCAIRE MARNEUX

Figure 2-1: Cross section of the alluvium foundation and bedrock (provided by NOVEC)

3. THE BISRI DAM MODEL

3.1. Physical and mechanical properties of materials

3.1.1. Static properties

The physical and mechanical parameters of the foundation materials, which were extrapolated on the base of geological and geotechnical information relative to the site [1] are reported in Table 3-1. Also, the physical and mechanical properties of the materials which are intended to compose the embankment are summarized as they were furnished by NOVEC.

Material	Dry density	Porosity	Cohesion	Friction	Dilatancy	Young's modulus	Poisson's ratio
	$[kg/m^3]$	[-]	$[kPa]$	[°]	[°]	$[MPa]$	[-]
DAM - Clay Core	1740	0.26	10	25	0.0	20	0.25
DAM - Rockfill	1780	0.42	0.0	50	0.0	80	0.25
DAM - Compacted Gravel	1780	0.42	0.0	40	0.0	300	0.25
A1 – Alluvional Sand	1520	0.46	0.0	30	0.0	80	0.33
A2 – Alluvional Clayey Silt	1340	0.51	0.0	22	11	40	0.33
A3 – Alluvional Gravel	1700	0.3	0.0	35	17.5	80	0.33

Table 3-1 : physical and mechanical properties of materials

Soil dilatancy is considered only for highly confined zones. This is due to the limitation of the employed model which doesn't allow to take into account of the dependency of dilatancy on the current value of shear deformation. For low confinement and large strains, dilatancy in the plastic regime causes very high volumetric deformations, causing the simulation to crash due to incompatible deformations of the mesh. Finally, no dilatancy was set for low confinement zones.

3.1.2. Dynamic properties

The information concerning the dynamic properties of soil foundation layers come from downhole surveys/SPTs: an average shear wave velocity of about 200-220 m/s at a depth of about 70m from the ground surface was estimated (data furnished by NOVEC). The computation of the maximum shear modulus of the foundation materials takes this information into account. The following procedure was adopted:

- Computation of static shear moduli for the soil foundation layers, before the construction of the dam;
- Calibration of a multiplication factor between the static values of shear moduli and the dynamic ones, to ensure that the latter agree with the shear wave velocity information.

The profile of shear wave velocity that was computed for the soil foundation layers is presented below. The following expression was used:

$$V_s = \sqrt{\frac{G_{max,dyn}}{\rho}} \qquad (1)$$

where ρ_{soil} is the soil mass density, and the maximum dynamic shear modulus $G_{max,dyn}$ $G_{dynamic}$ is computed as:

$$G_{max,dyn} = 3 \cdot G_{static} \qquad (2)$$

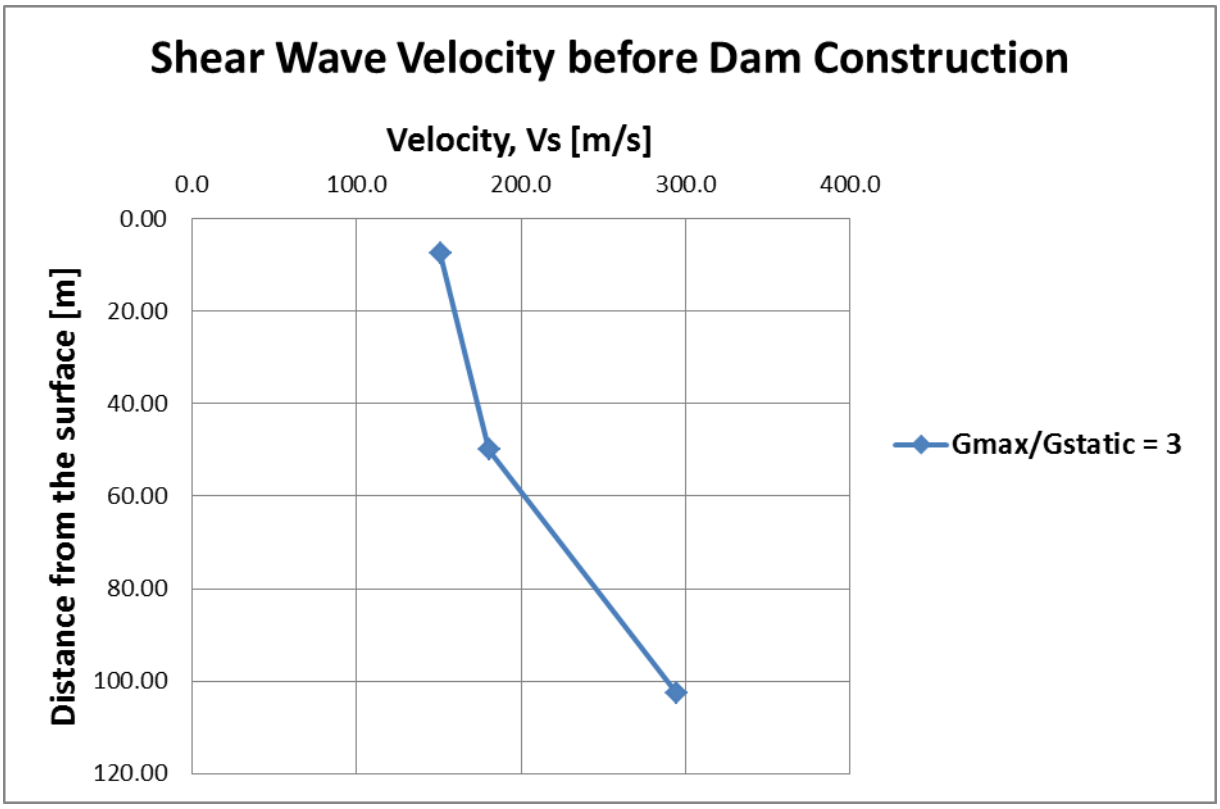

Figure 3-1: Profile of shear wave velocity along the foundation

It is recalled, that the difference between static and dynamic loading is that the second induces very small elastic shear strain, typically in the order of 0.001%, while shear strains for static loading of foundations are generally in the 0.1–0.01% range [12] [13]. The value of the *static* shear modulus, G_{static}, is then relative to elastic conditions during static loading, whereas the value of *maximum dynamic* shear modulus, $G_{max,dyn}$, is relative to elastic conditions during dynamic loading. During

the dynamic simulation, the value of shear modulus varies according to the level of shear deformation. G_{dyn} refers to the value taken by the shear modulus during the simulation.

A factor of 3 was finally adopted to compute the values of maximum dynamic shear modulus for the foundation materials.

3.2. Constitutive behavior of materials

As already mentioned in the introduction, for the two geometries that were tested, a *quasi-static* simulation of the dam construction is performed and analyzed, before a second simulation relative to the dynamic analysis.

To simulate the dam construction phase, the constitutive model has a non-linear elastic part (compressibility and shear modulus depend on confining stress) and a Mohr-Coulomb failure envelope. This is used to reproduce the mechanical behavior of both the foundation and the dam materials. The only exception is the bedrock layer, which is assumed elastic in all simulations. The definition of the bulk and shear moduli of materials for this phase is presented in section 3.2.1.

Regarding the dynamic analysis, the UBCHyst constitutive model is adopted. UBCHyst (Byrne and Naesgaard 2010) has been developed at University of British Columbia for dynamic analyses of soil subjected to earthquake loading. It is intended to be used in permeable granular soils where excess pore water would dissipate as it is generated. The model has been implemented in the two dimensional finite difference program FLAC (Itasca, 2011). Details about this method are given in section 3.2.2.

3.2.1. Static simulation - Non-linear elasticity and Mohr-Coulomb failure criterion

A nonlinear-elastic-Mohr-Coulomb model is used to model the whole soil structure. Only the bedrock layer is assumed to be elastic.

For the dam and the foundation materials, the variation of the Young's modulus with confining stress obeys the following expression:

$$E = E_0 \sqrt{\frac{\sigma_c}{p_{atm}}} \qquad (3)$$

where σ_c is the confining stress and p_{atm} is the atmospheric pressure. Then, Young moduli take the values listed in Table 3-1 when $\sigma_c = p_{atm}$.

The bulk and shear moduli are then computed using the well-known expressions, coming from elasticity theory for homogeneous isotropic materials:

$$K = \frac{E}{3(1-2\nu)} \qquad (4)$$

$$G = \frac{E}{2(1+\nu)} \qquad (5)$$

The Mohr-Coulomb model is the conventional plastic model used to represent shear failure in soils and rocks. The failure envelope implemented by FLAC corresponds to a Mohr-Coulomb criterion (shear yield function) with tension cutoff (tensile yield function).

Details about the implementation of the Mohr-Coulomb constitutive model in the software *FLAC* are given in Appendix 1, section 7.1.

3.2.2. Dynamic simulation – The UBCHyst Model

The UBCHyst model [6] has been developed at University of British Columbia for dynamic analyses of soil subjected to earthquake loading. In order to speed up the computations the FISH source code was converted to C++ and compiled as a DLL.

The UBCHyst model is intended to be used with "undrained" strength parameters in low permeability clayey and silty soils, or in highly permeable granular soils where excess pore water pressure would dissipate as it is generated. The model has been implemented in the two dimensional finite difference program FLAC (Itasca, 2011).

No pore pressure generation, induced by the cyclic shear loading during the earthquake, is assumed to take place. Then, liquefaction is not admitted to occur in sandy layers. No flow computation is done during the numerical analysis. An effective stress analysis is performed, considering a constant hydrostatic profile of water pressure.

The essence of this hysteretic model is that the tangent shear modulus G_t is a function of the peak shear modulus G_{max} times a reduction factor that is a function of the developed stress ratio and the change in stress ratio to reach failure. This function is as shown in equation (6) and illustrated in Figure 3-2.

$$G_t = G_{max}\left(1 - \left(\frac{\eta_1}{\eta_{1f}}\right)^{n_1} \cdot R_f\right)^n \qquad (6)$$

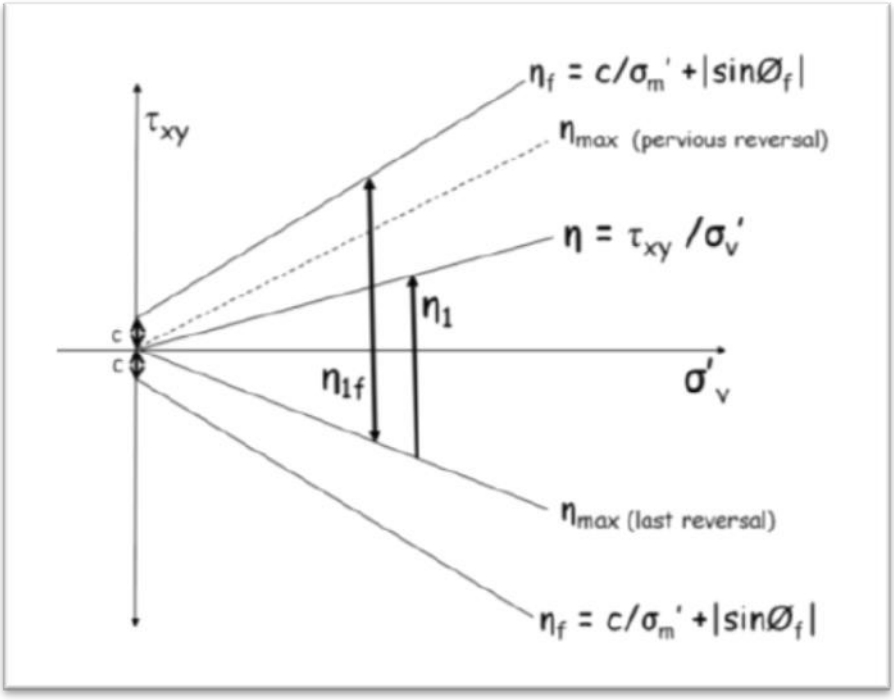

Figure 3-2 : UBCHyst model key variables (from Byrne and Naesgaard 2010)

Where:

- η is the stress ratio τ_{xy}/σ_v' ;
- η_1 is the stress ratio τ_{xy}/σ_v' since last reversal $(\eta - \eta_{max})$;
- η_{max} is the maximum stress ratio at the last reversal ;
- η_{1f} is the change in stress ratio to reach failure envelope in direction of loading $(\eta_f - \eta_{max})$;
- $\eta_f = \sin(\phi_f) + c \cdot \cos(\phi_f)/\sigma_v'$;
- τ_{xy} is the developed shear stress in horizontal plane;
- σ_v' is the vertical effective stress;
- ϕ_f is the friction angle.

and n_1, R_f and n are calibration parameters.

Stress reversals occur if the absolute value of the mobilized stress ratio (η) is less than the previous value and a cross-over occurs if τ_{xy} changes sign. A stress reversal causes η_1 to be reset to 0 and η_{1f} to be recalculated. However, the program retains the previous reversals ($\eta_{1,old}$ and $\eta_{1f,old}$) so that small hysteretic loops that are subsets of larger loops do not change the behavior of the large loop. With the above equation the tangent shear modulus varies throughout the loading cycle to give hysteretic stress-strain loops.

The input variables for the UBCHyst model are:

- The total strain increment tensor, which is determined by the solver for each computational step by means of the equation of motion and by means of the stress state, evaluated using the constitutive law in the previous step;
- The stresses tensor evaluated in the previous step;
- The stress ration parameters such as η_1, η, η_{max}, η_{1f}, η_f which have been evaluated in the previous step.

The output variables are:

- The new stress tensor σ_{ij};
- The new stress ratio parameters η_1, η, η_{max}, η_{1f}, η_f;
- The new shear modulus using eq. (6).

3.2.2.1. Calibration of UBCHyst free parameters

The calibration of the free parameters of the UBCHyst model is an essential operation to ensure the soil in the numerical model to behave in a relevant way. A set of calibrated parameters define a strength modulus reduction curve (G_t/G_{max} vs γ_{xy}) which is characteristic of the material (see Appendix 2, section 8.1). The behavior of a soil sample under cyclic loading depends essentially on two aspects:

- the mechanical properties of the material;
- the confining stress.

The calibration of the free parameters for the UBCHyst model consists in running cyclic shear tests on soil samples, at a prescribed confining stress representative of the *in situ* conditions. In the present work, the following procedure has been adopted:

- the quasi-static simulation of the dam construction is performed (phase 1);
- for each dam and foundation material, a range of confining stresses is extrapolated, as it can be measured at the end of the quasi-static phase and prior to the dynamic loading;
- within these ranges, a set of parameters is calibrated, for each material and for every 200kPa confining stress interval, thus performing ad-hoc cyclic shear tests on soil samples.

The reference behavior for each calibration is given by appropriate strength modulus reduction and damping curves, available in literature, and representative of the material under question. The reference curves that were chosen are presented hereafter.

3.2.1. Mechanical damping and material response

Natural dynamic systems exhibit some degree of damping of the vibration energy within the system; otherwise, the system would oscillate indefinitely when subjected to driving forces. Damping is due, in part, to energy loss as a result of internal friction in the intact material and slippage along interfaces, if these are present.

For a dynamic analysis, the damping in the numerical simulation should reproduce in magnitude and form the energy losses in the natural system when subjected to a dynamic loading. In soil and rock, natural damping is mainly hysteretic (i.e., independent of frequency). The UBCHyst constitutive model integrates hysteretic damping, as a function of the level of cyclic shear deformation. The model calibration consists in comparing its uniform cyclic response to that inferred from published modulus reduction and damping curves (Darendeli, 2001 [2]). The simple shear test is preferred over triaxial loading because the loading path, with rotation of principal axes, more closely resembles the stress path during earthquake loading [6].

The model overestimates the damping response at medium to large (>0.1%) shear strains [6]. The reason for this overestimation of damping factor appears to be the width of the hysteresis loop in the UBCHyst model.

3.2.1.1. Reference modulus reduction curves

A literature review was performed to find reference modulus reduction and damping curves. The main references (cited below) are:

- Gazetas G., Dakoulas P. (1991) [4], whose work was concentrated in seismic analysis of rockfill dams;
- Roblee, C., and Chiou, B. (2004) [9], that provides guidelines for the design selection of non-linear properties for site response analysis;
- Seed, H. B. W., R. T.; Idriss, I.M. & Tokimatsu, K. 1986., [10] that provides moduli and damping factors for dynamic analyses of cohesionless soils;

- Sun J.I., Golesorkhi R. and Seed H. B. (1988) [11], that provides dynamic moduli and damping ratios for cohesive soils.

The reference curves that were chosen for the clay core (material group '1_Core') and clayey foundation material (group A2_ClayeySilt) are represented on Figure 3-3 and Figure 3-4.

The strength modulus reduction curve and damping curves in Figure 3-3 and Figure 3-4, according to Sun et al. [11], are representative of fine-grained soils and clays with a PI (Plastic Index) between 20 and 40 (low to medium plasticity), consistent with the fine-grained borrowed material, for which a plastic index between 10% and 39% was measured [1].

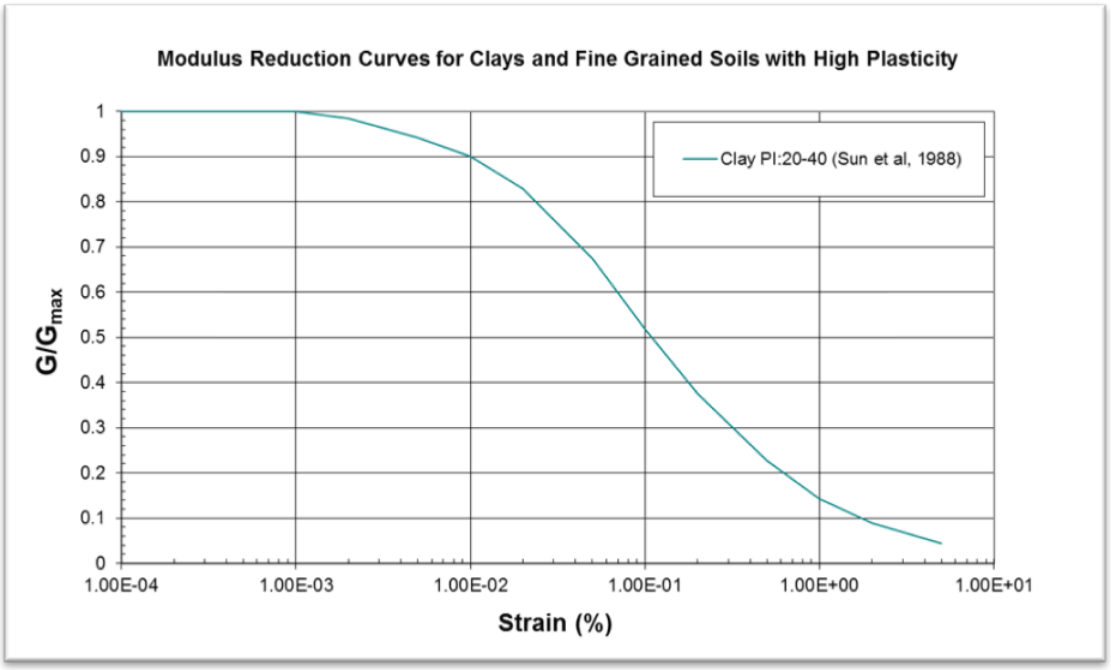

Figure 3-3 : Reference strength modulus reduction curve for the fine-grained materials (dam core and clayey foundation layer)

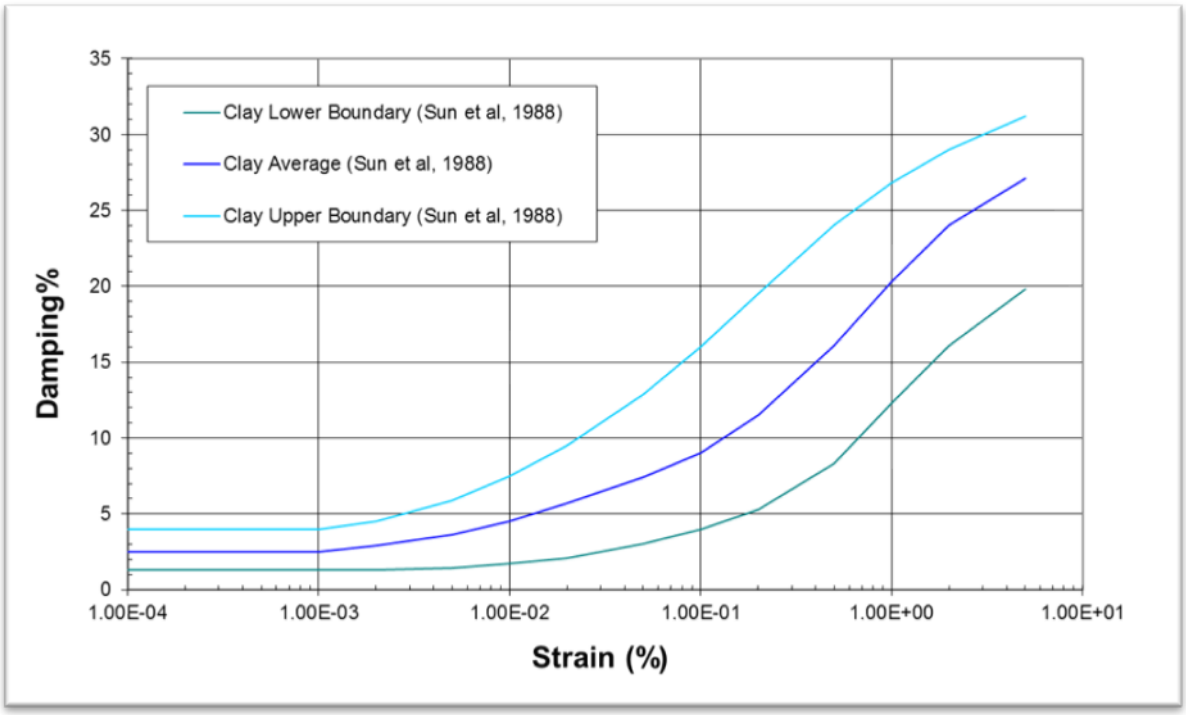

Figure 3-4 : Reference damping curve for the fine-grained materials (dam core and clayey foundation layer)

Concerning the rockfill (material group '2_Rockfill'), the strength modulus reduction and damping curves from Gazetas (1991, [4]) were chosen as reference (Figure 3-5 and Figure 3-6).

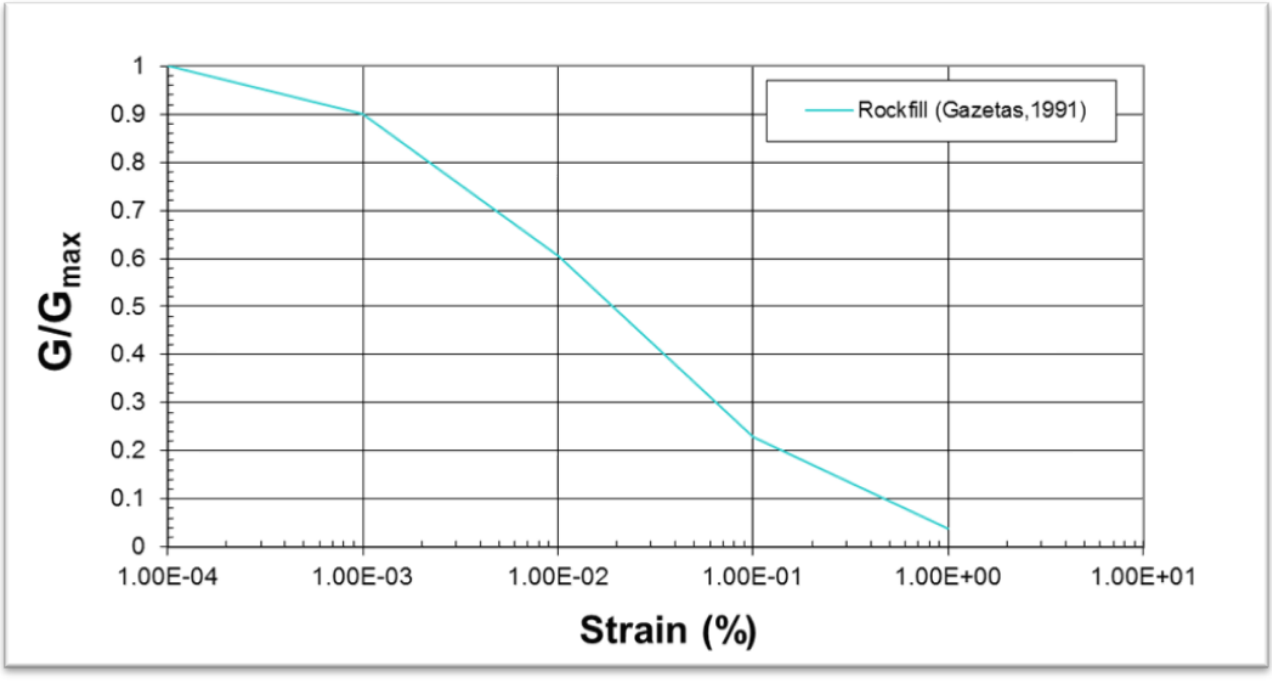

Figure 3-5 : Reference strength modulus reduction curve for the rockfill

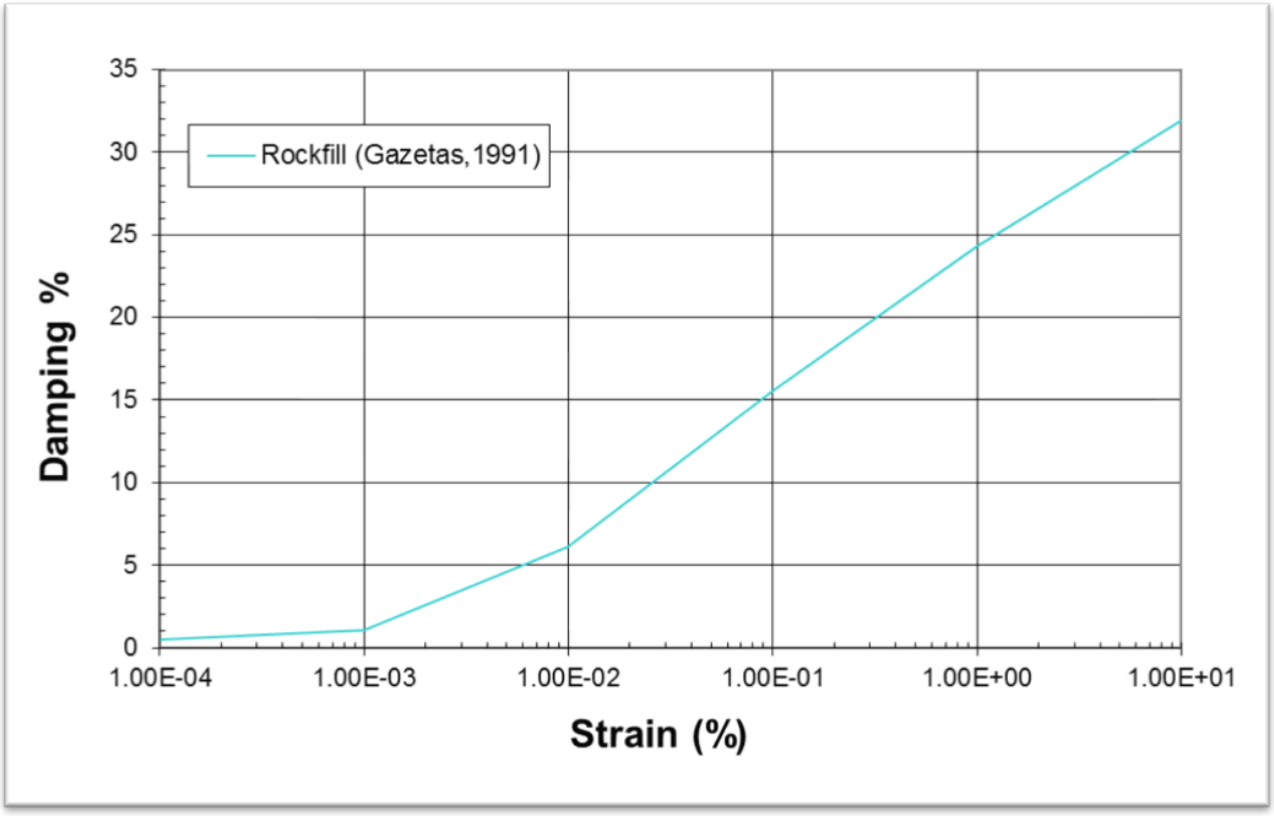

Figure 3-6 : Reference damping curve for the rockfill

Seed et al. [10] reference curves (Figure 3-7 and Figure 3-8) were chosen for gravelly materials (groups '3_CompactedGravel' and 'A3_Alluvial_Gravel'), whereas curves recommended by Roblee and Chiou, 2004 (Figure 3-9 and Figure 3-10, [9]) were considered as appropriate for the alluvial sandy foundation layer (group 'A1_Alluvial_Sand').

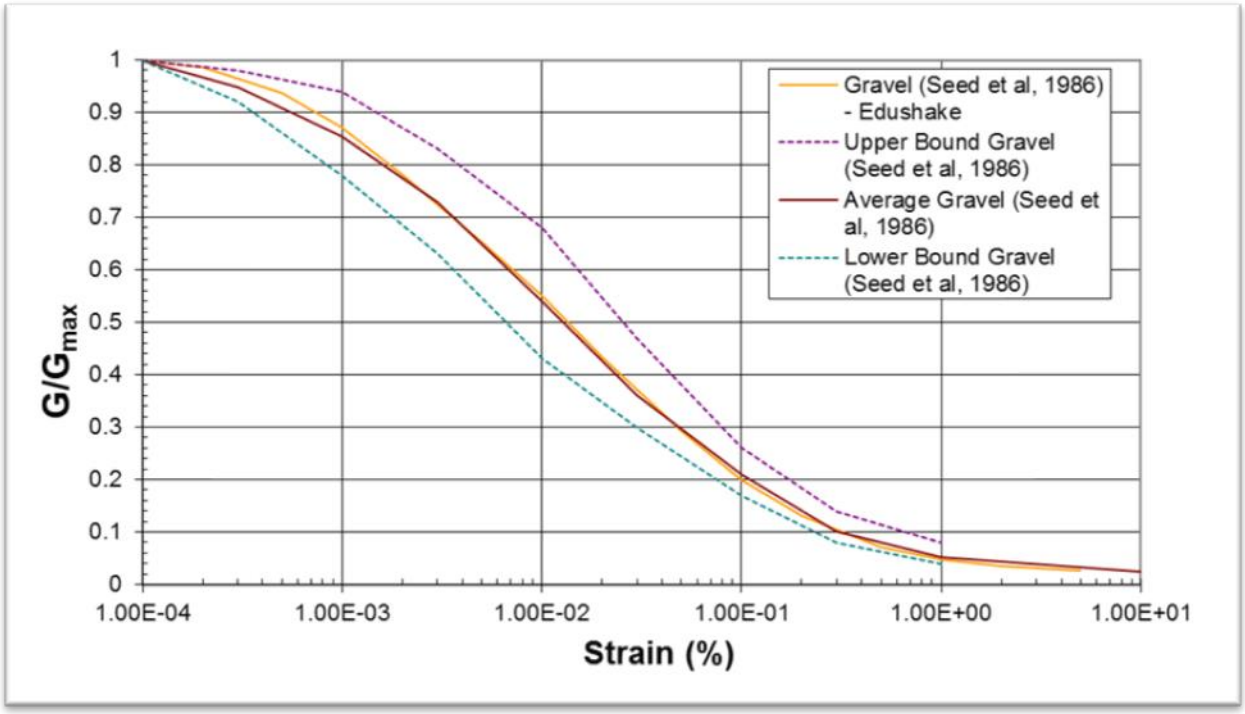

Figure 3-7 : Reference strength modulus reduction curve for the gravel (compacted gravel and gravelly foundation layer)

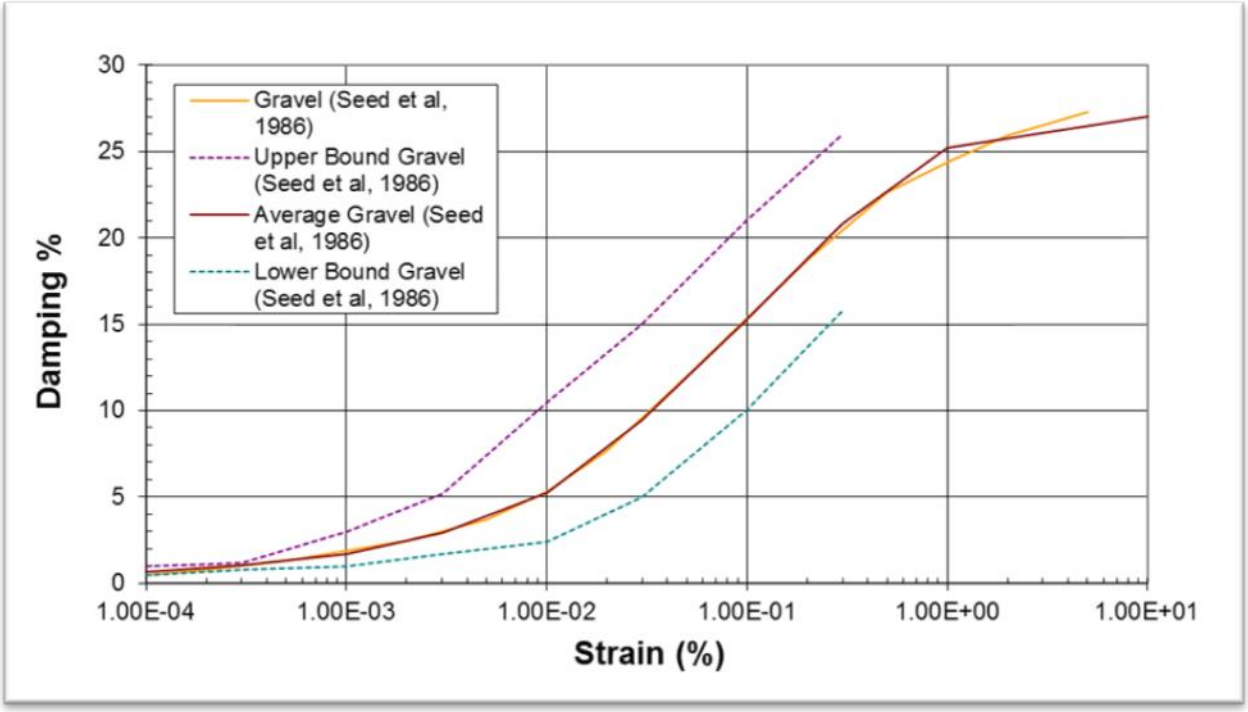

Figure 3-8 : Reference damping curve for the gravel (compacted gravel and gravelly foundation layer)

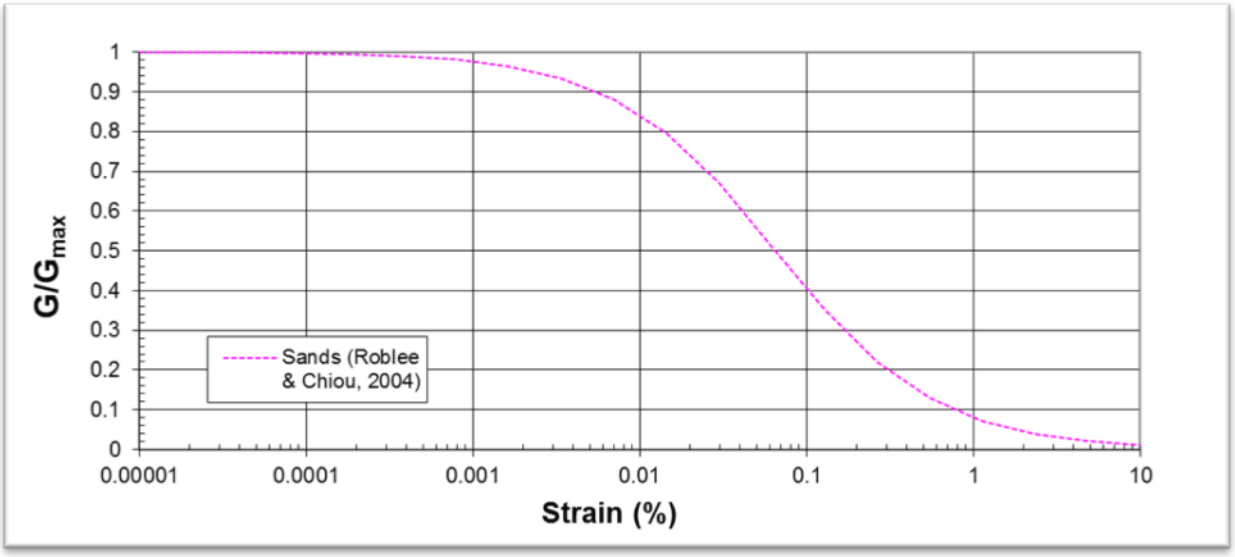

Figure 3-9 : Reference strength modulus reduction curve for the sandy materials (alluvial sandy foundation layer)

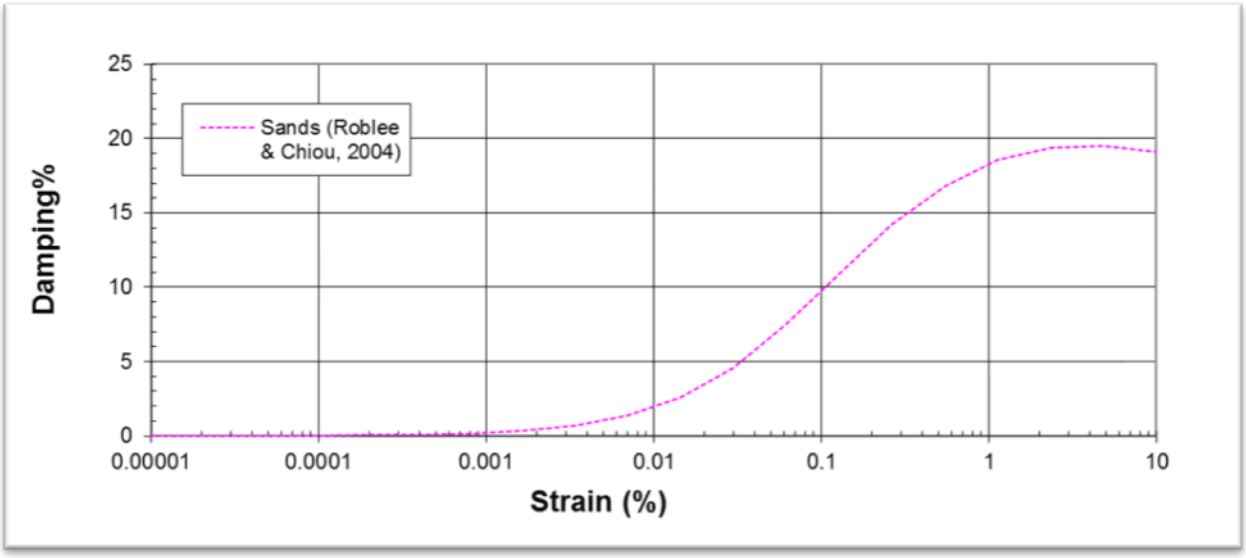

Figure 3-10 : Reference damping curve for the sandy materials (alluvial sandy foundation layer)

3.2.1.2. Rayleigh damping

In time-domain programs, Rayleigh damping is commonly used to provide damping that is approximately frequency-independent over a restricted range of frequencies. Although Rayleigh damping embodies two viscous elements (in each of which the absorbed energy is dependent on frequency), the frequency-dependent effects are arranged to cancel out at the frequencies of interest.

When hysteretic damping is in operation, a very low Rayleigh damping may be used (e.g., 0.2%) to remove high frequency noise that is not well managed by hysteretic damping.

In the present work, the frequency range of the Rayleigh damping to be used for nonlinear dynamic simulations is chosen from the results of elastic linear simulations, which are presented in section 4.6.1. During nonlinear dynamic simulations, Rayleigh damping will be imposed in the predominant range of frequencies measured during the elastic simulations.

3.3. Signal processing

Information related to the seismicity of the Bisri site is taken from the report "Assessment of site-specific earthquake hazard for Bisri Dam – Lebanon", prepared at the Bogaziçi University for the Council for Development and Reconstruction of the Republic of Lebanon.

The following design basis ground motion spectra were used to generate the earthquake signals:

- The Operating Basis Earthquake (OBE) is determined as the probabilistically assessed earthquake ground motion for an average return period of 144 years (Figure 3-11). Horizontal and vertical design basis spectra for the OBE were provided. The response spectrum is provided for 5% damping and for the free-field engineering bedrock outcrop.
- The Safety Evaluation Earthquake (SEE) is the maximum level of ground motion for which the dam should be designed or analyzed. For the earthquake resistant design of the Bisri Dam the SEE level ground motion was determined (Figure 3-12) to correspond to the 84-percentile deterministic MCE (i.e. median plus one standard deviation). The horizontal and vertical design basis spectra for the SEE were provided. The response spectrum is provided for 5% damping and for the free-field engineering bedrock outcrop.

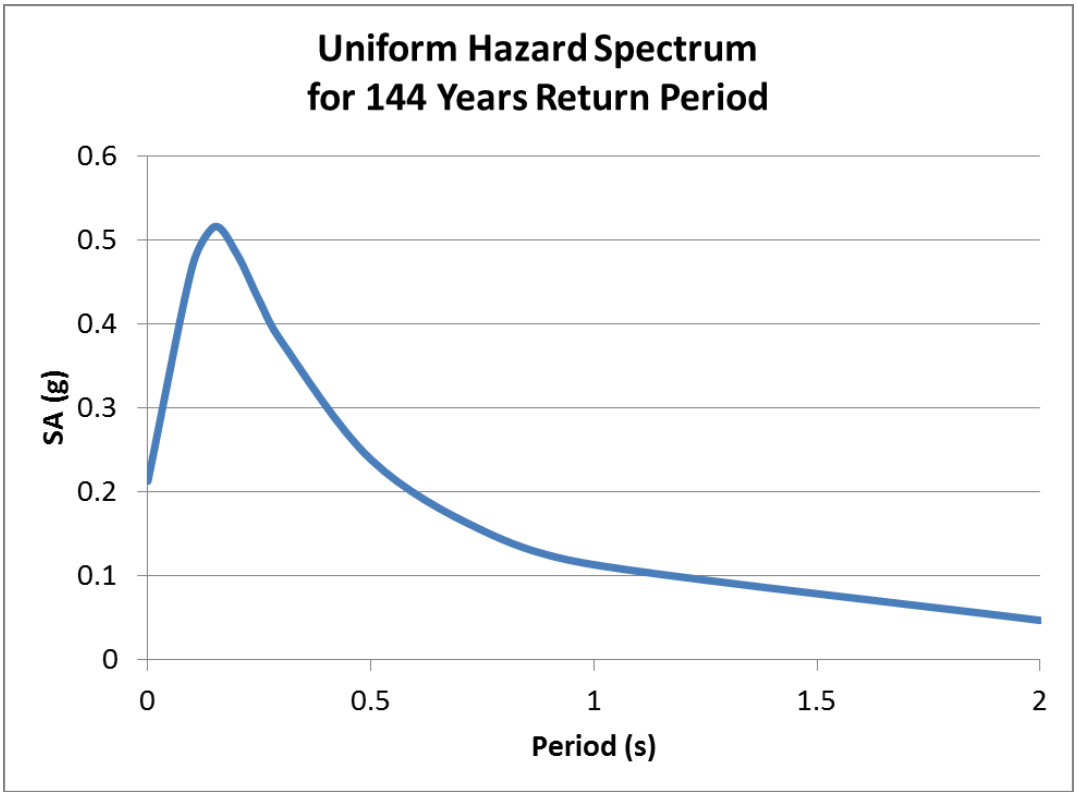

Figure 3-11 : Uniform Hazard Spectrum corresponding to 144 years return period for the Bisri Dam site [3]

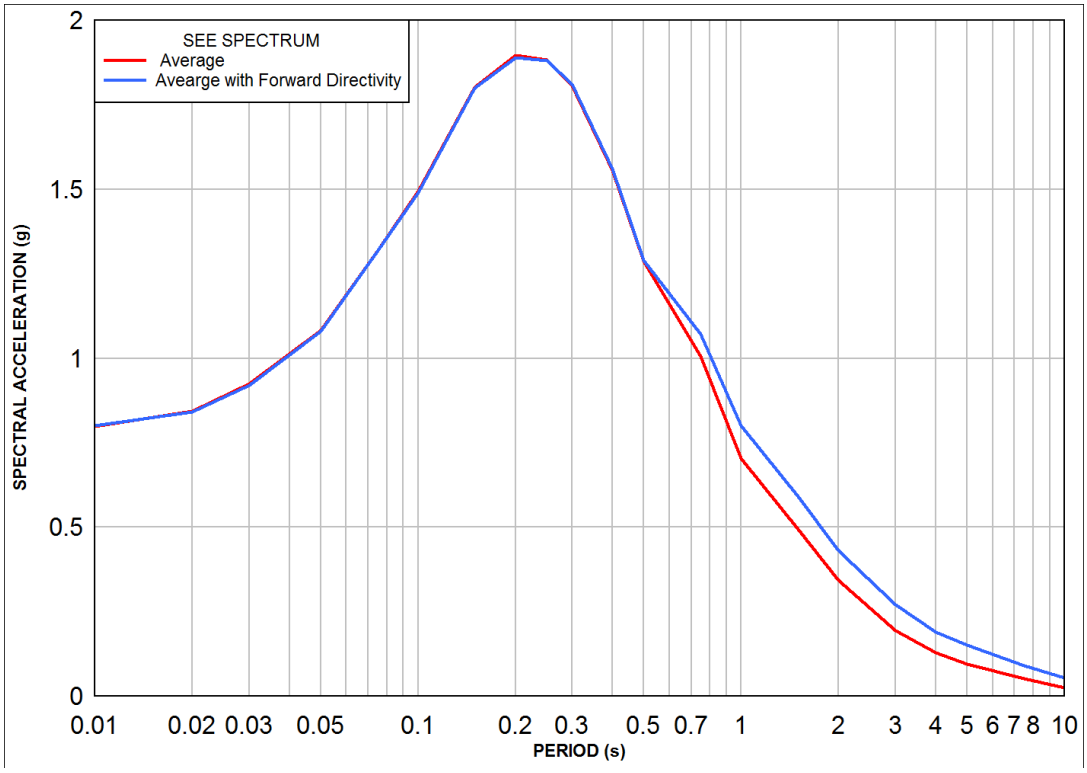

Figure 3-12 : The average and the directivity modified design basis response spectra. [3]

3.3.1. SEE and OBE design earthquakes

Figure 3-13, Figure 3-14 and Figure 3-15 show the acceleration histories of the SEE design earthquakes.

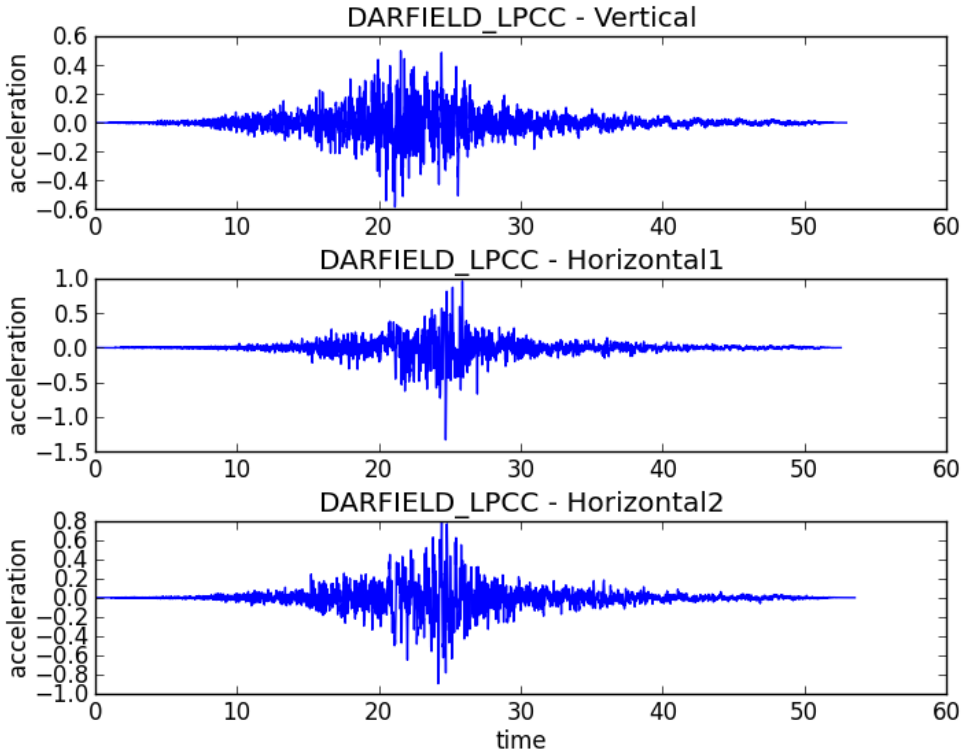

Figure 3-13 : SEE Darfield LPCC – Acceleration time history

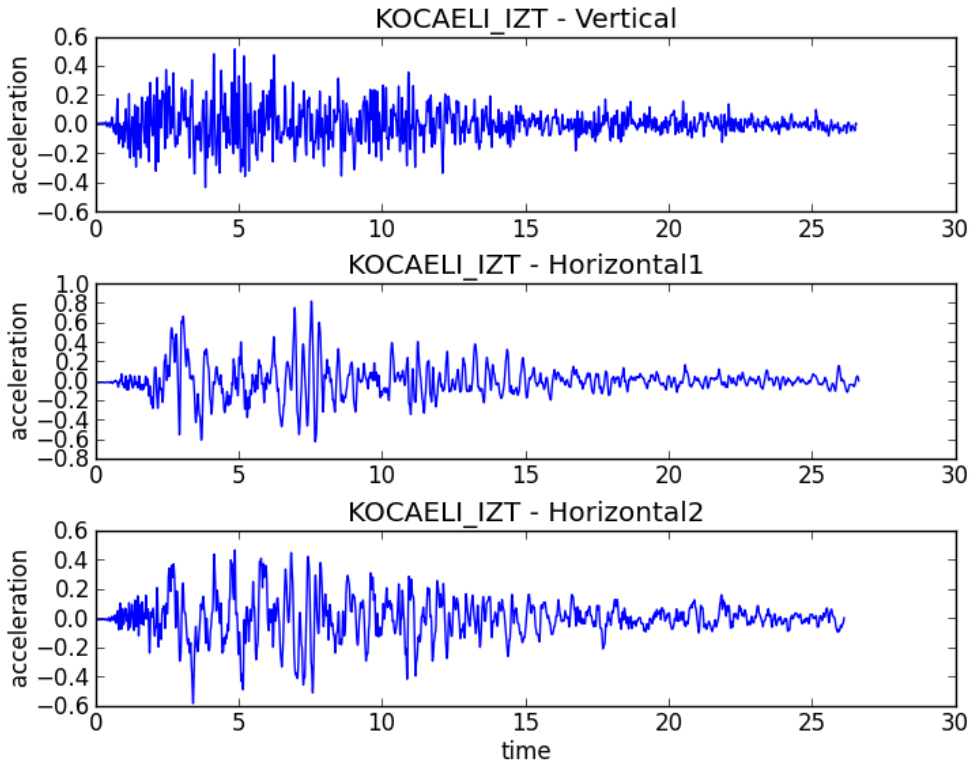

Figure 3-14 : SEE Kocaeli IZT – Acceleration time history

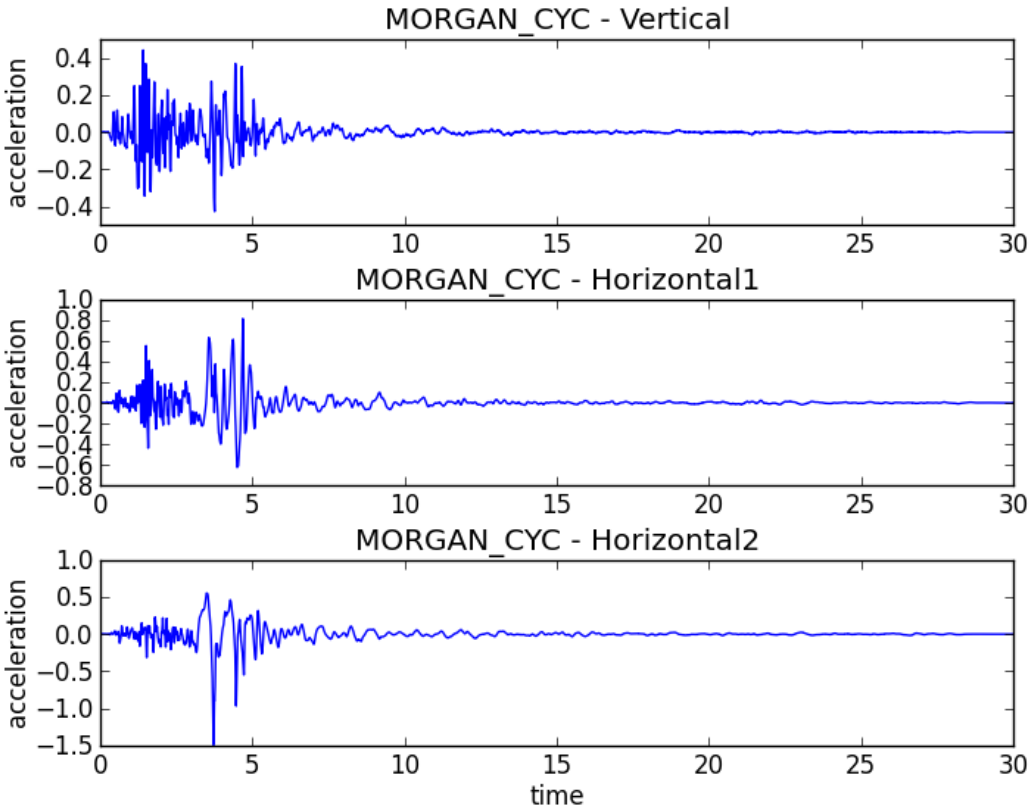

Figure 3-15 : SEE Morgan CYC – Acceleration time history

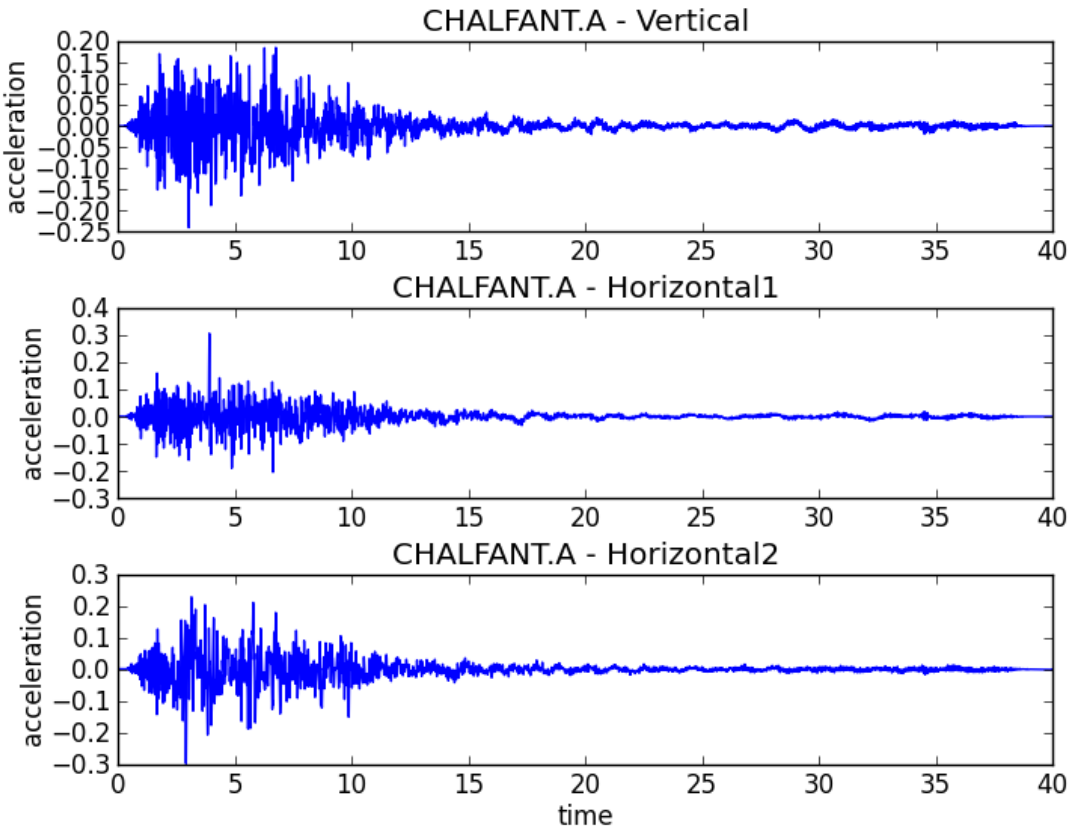

Figure 3-16 : OBE Chalfant A – Acceleration time history

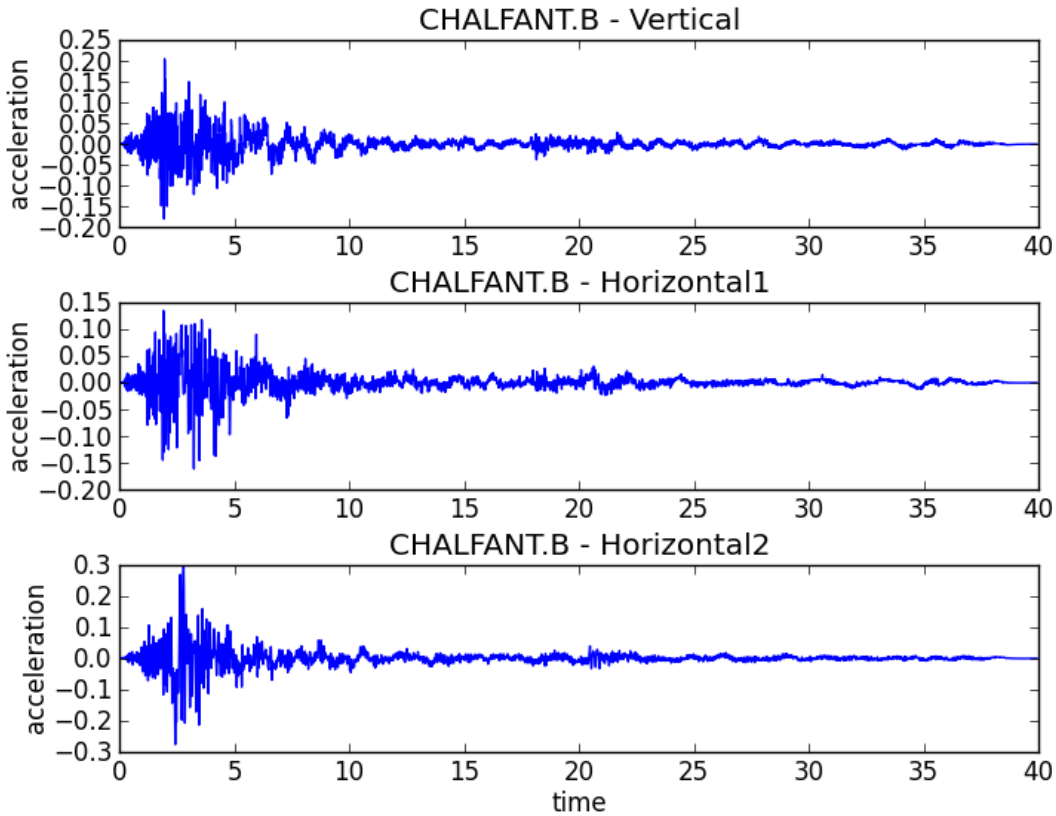

Figure 3-17 : OBE Chalfant B – Acceleration time history

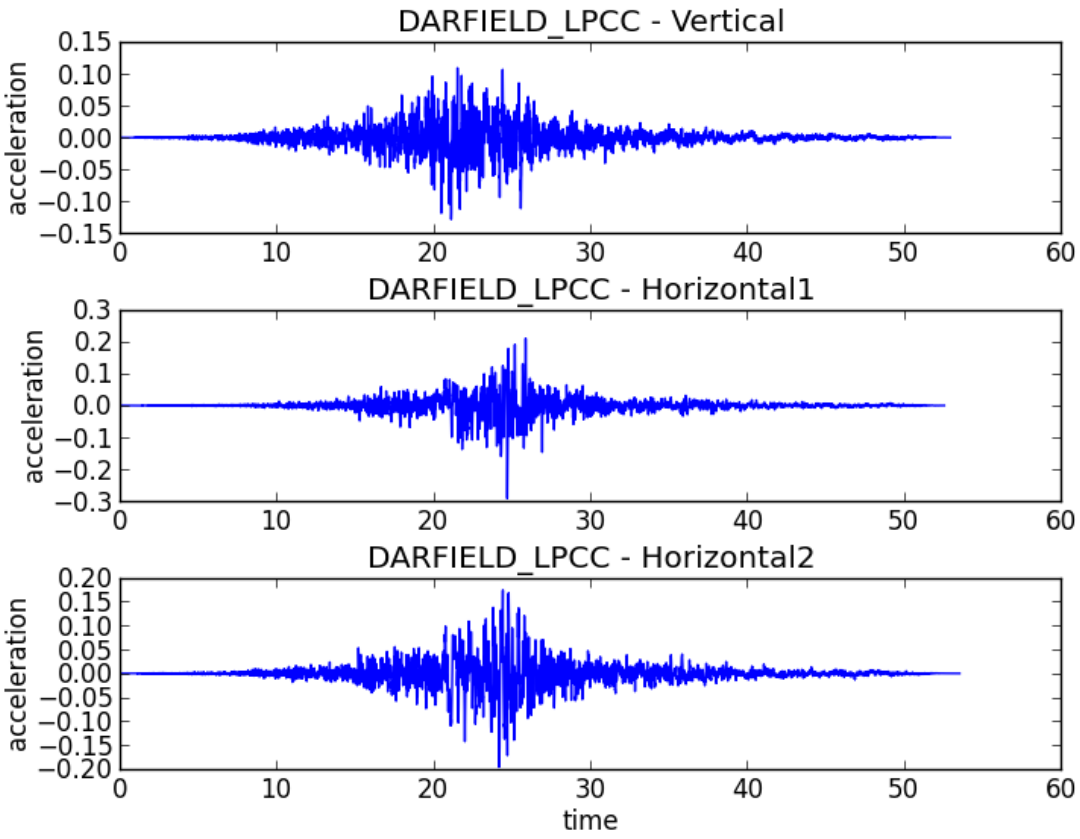

Figure 3-18 : OBE Darfield LPCC – Acceleration time history

The following table summarizes the peak ground accelerations (PGA) of the design SEE and OBE seismic records that were adopted for the dynamic simulations.

SEE EARTHQUAKE				
		PGA [g]		
Name		Vertical	Horizontal 1	Horizontal 2
Darfield LPCC		+ 0.5 / - 0.58	+ 0.96 / - 1.33	+ 0.79 / - 0.89
Kocaeli IZT		+ 0.51 / - 0.43	+ 0.82 / - 0.63	+ 0.47 / - 0.59
Morgan CYC		+ 0.44 / - 0.43	+ 0.81 / - 0.62	+ 0.55 / - 1.49

OBE EARTHQUAKE				
		PGA [g]		
Name		Vertical	Horizontal 1	Horizontal 2
Chalfant A		+ 0.19 / - 0.24	+ 0.31 / - 0.20	+ 0.23 / - 0.30
Chalfant B		+ 0.20 / - 0.18	+ 0.13 / - 0.16	+ 0.30 / - 0.28
Darfield LPCC		+ 0.11 / - 0.13	+ 0.21 / - 0.29	+ 0.17 / - 0.20

Table 3-2 : PGA of design SEE and OBE earthquakes

3.3.2. Significant duration of earthquakes

Computational times are directly proportional to the duration of the applied signal. This can be a problem for large (and thus fairly long earthquake). It is therefore standard procedure to keep only the significant part of the signal for computations. Arias intensity is used to define the cut, with the following rationale.

A good measure of damage to freestanding structures (applicable as well to anchored structures) is the combination of the horizontal PGA and the horizontal PGV/PGA. The higher the PGA and PGV/PGA, the more damaging is a particular waveform. Many structures can easily withstand very high PGA values provided that the period of this pulse is very short (low PGV/PGA) - in this case there is no time to coherently accelerate the structure in one direction so it doesn't really feel the high acceleration.

These damaging pulses are basically always located within the 5-95% duration of the earthquake, defined on the base of the Arias intensity. The Arias intensity is a measurement of the force of an earthquake, obtained by integration of the acceleration with respect to the time. It is a parameter that characterizes the intensity of an earthquake, like "IM" parameters ("Intensity Measures", e.g. PGA) and this intensity is indicative of the probability that a structure undergoes instability, or of the potential of liquefaction of soils.

The correction of the earthquake duration on the base of Arias intensity consists in cutting the initial part of the signal, up to 5% of Arias Intensity, and the final part as well, corresponding to the 95-100% interval and therefore keeping 90% of the Arias intensity.

However, in the case of Bisri Dam simulations, it was chosen to reduce the duration of the design earthquakes on the base of a 1%-99% Arias Intensity correction only. This was considered to be a good compromise between the reduction of the earthquake duration (reduction of computational time), and the conservation of the main characteristics of the original signal, especially in terms of damaging pulses. The consequences of the described correction on the original signal will be discussed in section 3.3.5.

3.3.3. High-frequencies filtering

The design of a *FLAC* model grid depends on two main conditions:

- For those parts of the model where the largest stress gradients (and thus largest strains) are expected (i.e. at the dam top and adjacent layers), the zoning is fine enough for a correct representation of the mechanical behavior;
- Numerical distortion of the propagating wave can occur in a dynamic analysis as a function of the modeling conditions. Both the frequency content of the input wave and the wave-speed characteristics of the system will affect the numerical accuracy of wave transmission. *Kuhlemeyer and Lysmer (1973)* show that for accurate representation of wave transmission through a model, the maximal spatial element size, Δl, must be smaller than approximately one-tenth to one-eighth of the wavelength associated with the highest frequency component of the input wave:

$$\Delta l < \frac{\lambda}{10} \qquad (7)$$

For dynamic input with a high peak velocity and short rise-time, the Kuhlemeyer and Lysmer requirement may necessitate a very fine spatial mesh and a corresponding small timestep. The

consequence is that reasonable analyses may be prohibitively time- and memory-consuming. In such cases, it may be possible to adjust the input by recognizing that most of the power for the input history is contained in lower-frequency components. By filtering the history and removing high-frequency components, a coarser mesh may be used without significantly affecting the results.

Fourier transforms of seismic signals are built to define a maximum frequency for the FLAC grid design. An example is given in section 3.3.5, where the signal processing of the SEE Kocaeli IZT is presented in detail.

3.3.4. Baseline correction

If a "raw" acceleration or velocity record from a site is used as a time history, the *FLAC* model may exhibit continuing velocity or residual displacements after the motion has finished. This is particularly true when a reduced duration of the earthquake is considered, as described in section 3.3.2: the truncated signals at the beginning and at the end of the seismic record correspond indeed to velocities which are subtracted from the signal, reflected in residual displacements that would not present if we were using the original signal.

The baseline correction consists in determining a low frequency wave which, when added to the original history, produces a final displacement which is zero. It is worth noticing that as long as the velocity time history is not affected significantly, the physics of the *FLAC* simulation will not be affected by this operation.

In the case of dynamic simulations for the Bisri Dam, all the original signals correspond to **no final displacements** at the end of the earthquake. This is no more the case after the reduction of the earthquake duration based on Arias Intensity considerations. The baseline correction is then performed on all the seismic signals that were adopted.

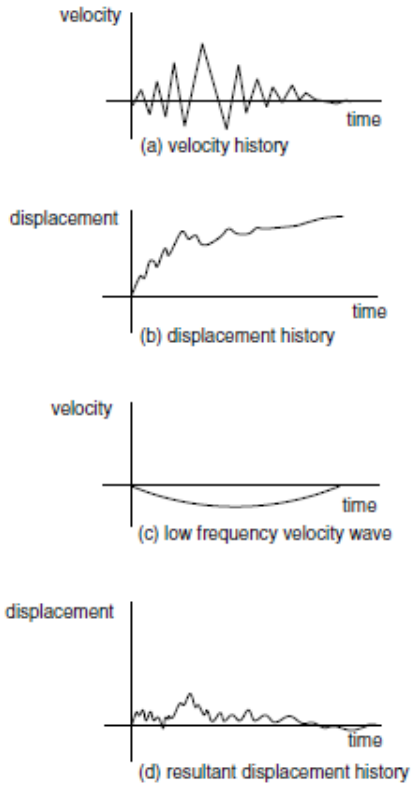

Figure 3-19 : The baseline correction process [5]

3.3.5. Signal processing of Kocaeli IZT SEE design earthquake

In this section an example of signal processing will be detailed, whereas only the original and final seismic signal will be given for all the others design earthquakes. The exact same procedure is used for all earthquakes. The earthquake which is considered in this section is the SEE earthquake labeled “Kocaeli IZT”.

Figure 3-20, Figure 3-21 and Figure 3-22 show the two horizontal and the vertical components of the original acceleration time history, respectively. Figure 3-23, Figure 3-24 and Figure 3-25 show the three components of acceleration, after reduction of the total duration of the earthquake on the base of the Arias Intensity.

Fourier Transforms of seismic signals were built, to define a maximum frequency for the FLAC grid design (figures from Figure 3-26 to Figure 3-28**Erreur ! Source du renvoi introuvable.** give an example). The FLAC grid for the Bisri dam model was finally designed for a maximum frequency of 15Hz. It is worth to compare the time histories before and after this operation to make sure that the peaks of accelerations and/or velocities are conserved.

Figure 3-29 and Figure 3-30 show the velocity time history before and after the filtering process and the baseline correction, for the horizontal 1 (H1) component of Kocaeli IZT earthquake. Figure 3-31, Figure 3-32, Figure 3-33 and Figure 3-34 show the same for the H2 and V components. It is worth noticing that there is no significant variation of velocity time histories, which is the condition for the signal processing operations to be relevant. Figure 3-35, Figure 3-36 and Figure 3-37 show the low frequency velocity issued of the baseline correction operation for the H1, H2 and V components, respectively. As can be seen, the velocities added to the signal range from 0 to 2cm/s.

Figure 3-38 to Figure 3-46 show the final acceleration, velocity and displacement histories that were used for the dynamic simulation. Only the displacement history differs noticeably from the original: the FLAC model being sensitive to input velocities rather than input displacements, this doesn’t affect the physics of FLAC simulation and its results.

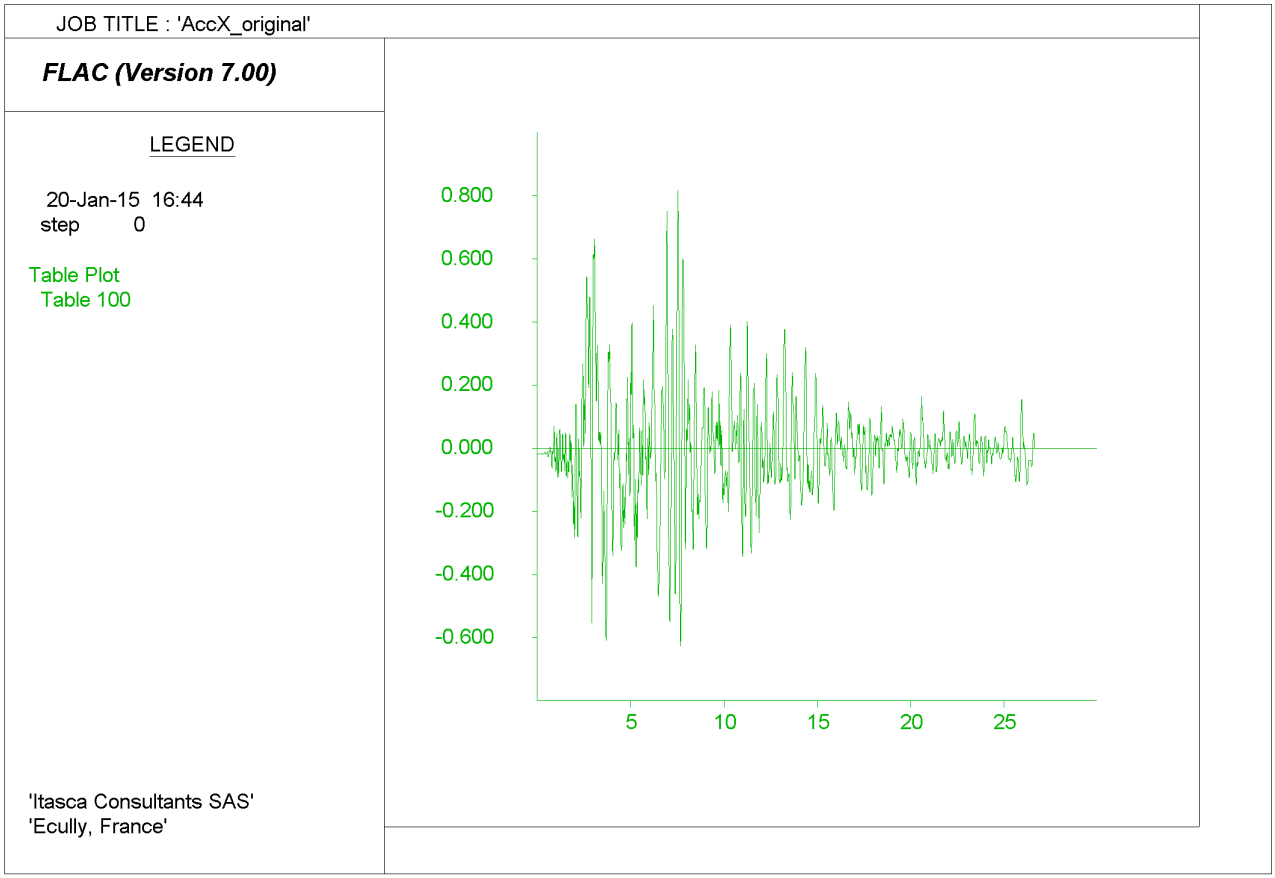

Figure 3-20: KOCAELI IZT – Horizontal 1 (H1) acceleration – Original acceleration time history

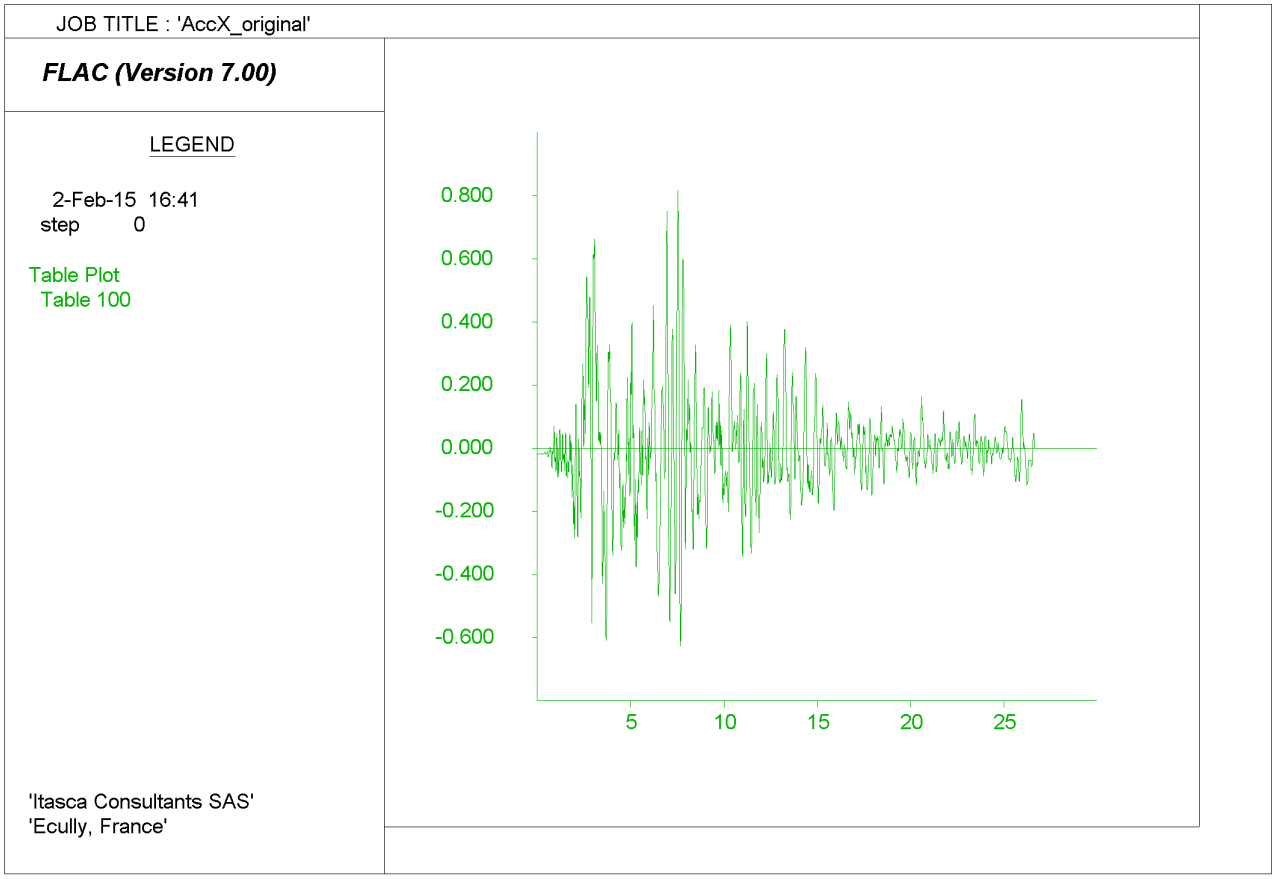

Figure 3-21: KOCAELI IZT – Horizontal 2 (H2) acceleration – Original acceleration time history

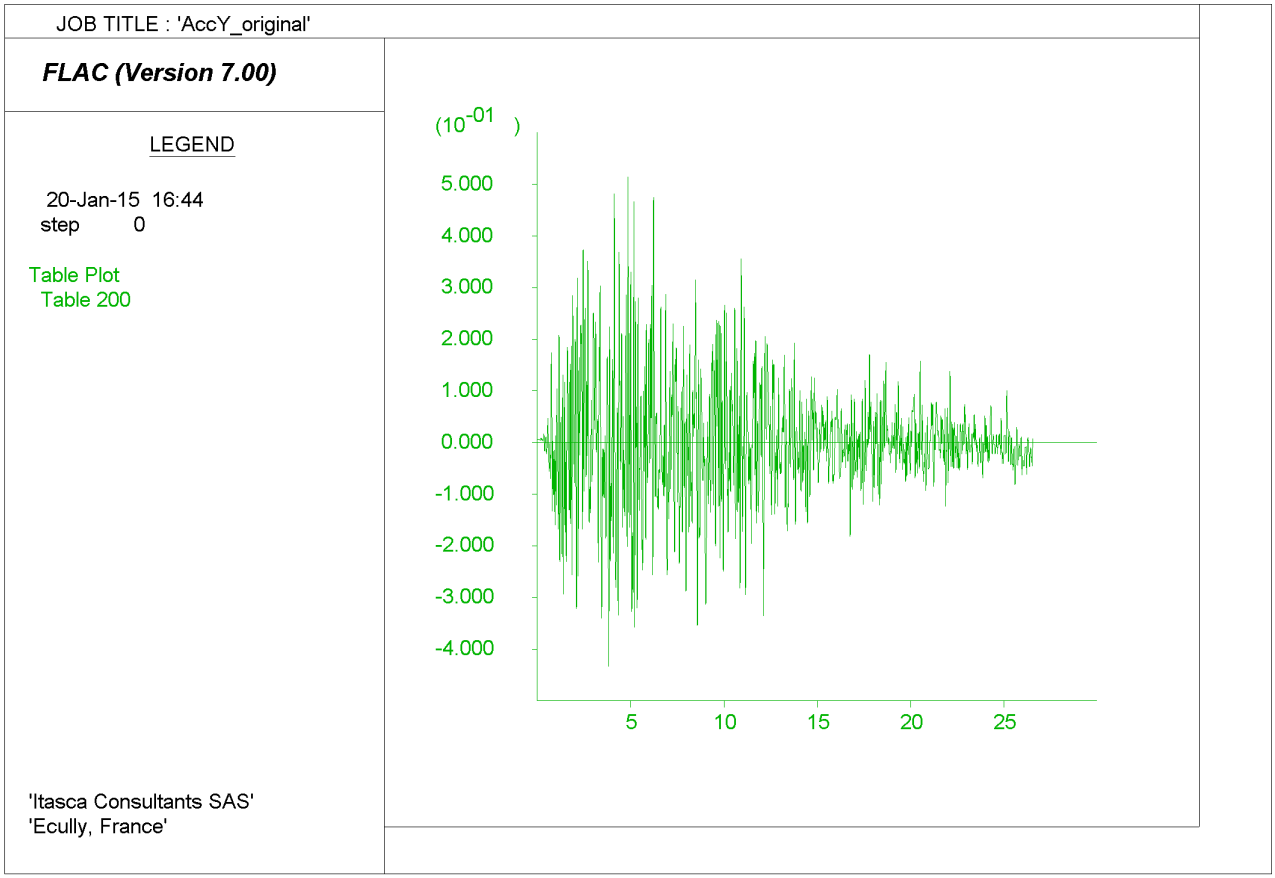

Figure 3-22: KOCAELI IZT – Vertical (V) acceleration – Original acceleration time history

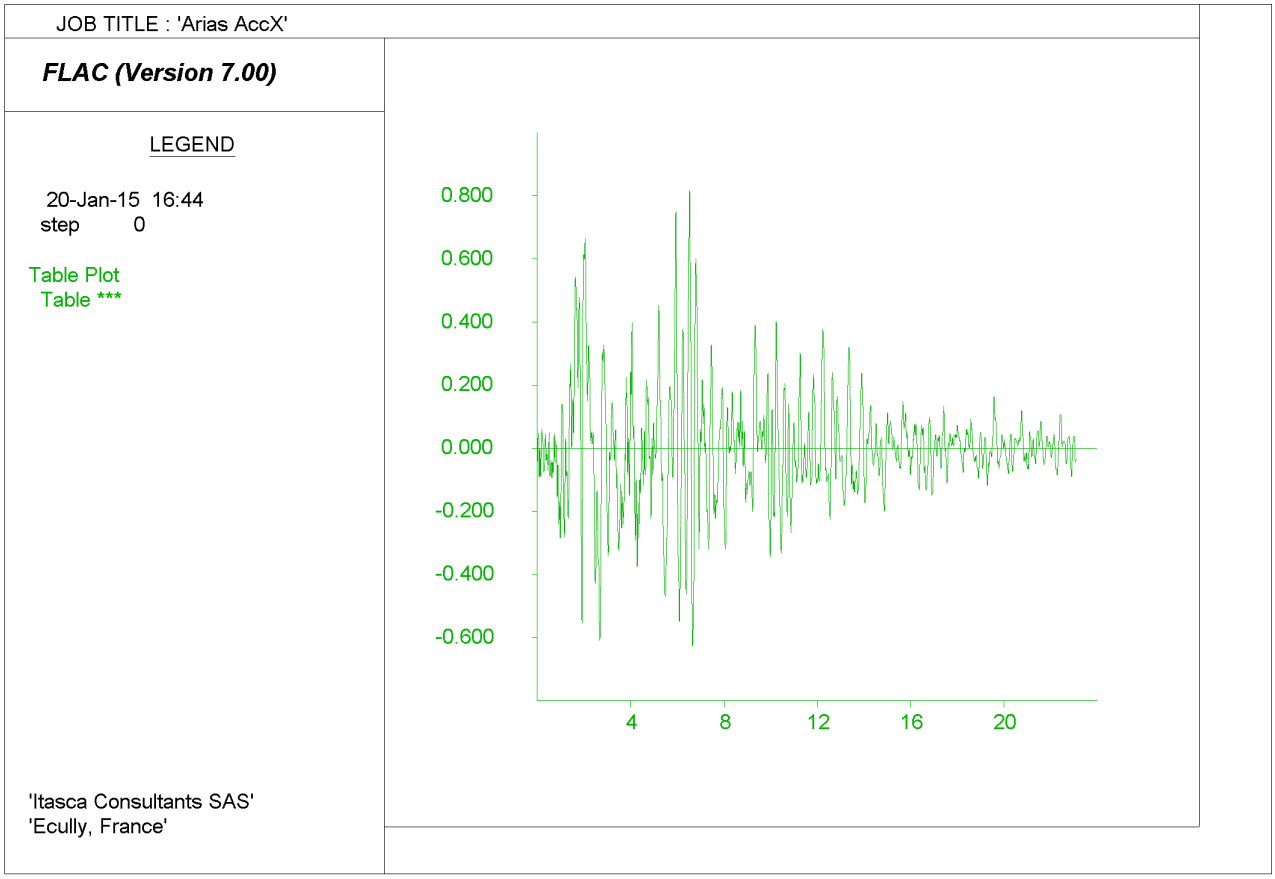

Figure 3-23: KOCAELI IZT – H1 acceleration – 1-99 significant duration based on Arias Intensity

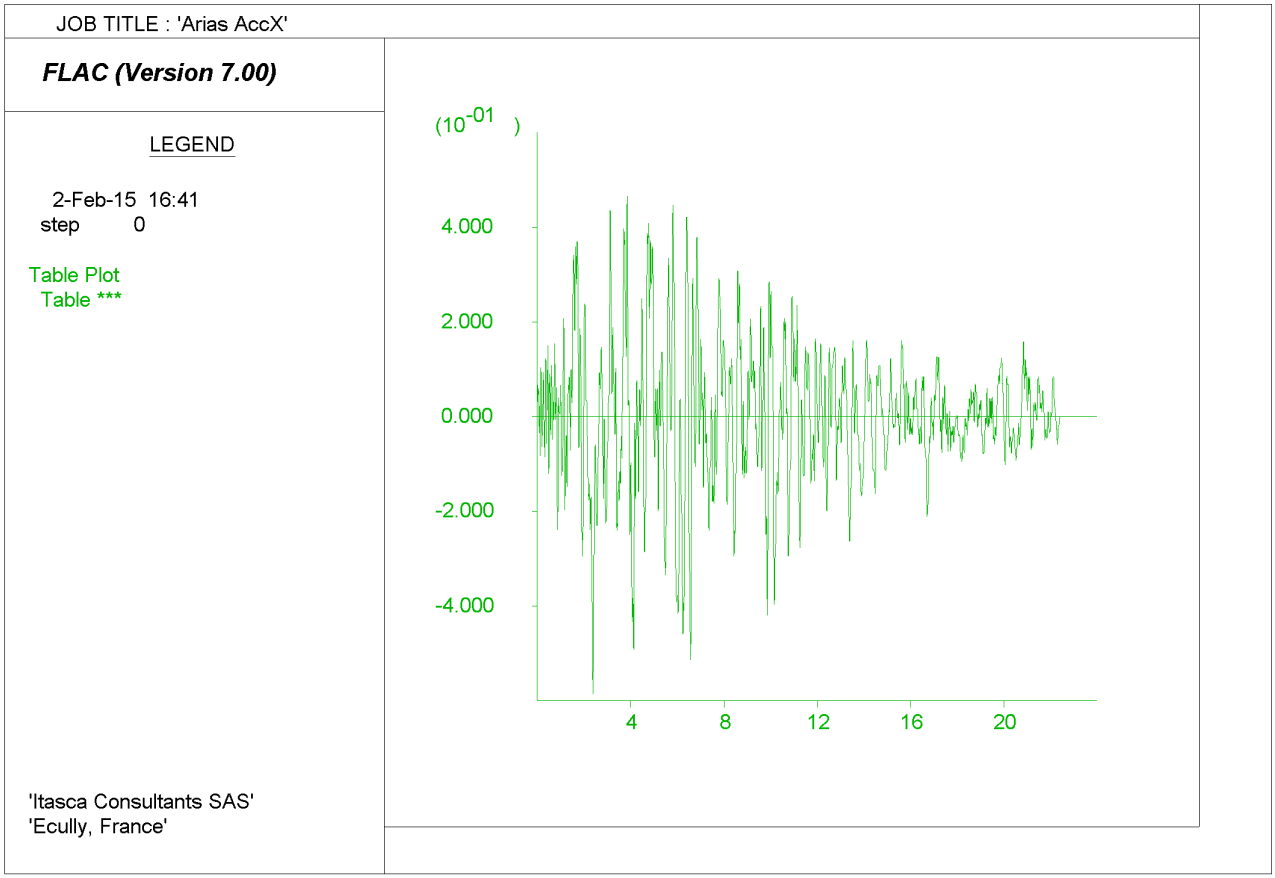

Figure 3-24 : KOCAELI IZT – H2 acceleration – 1-99 significant duration based on Arias Intensity

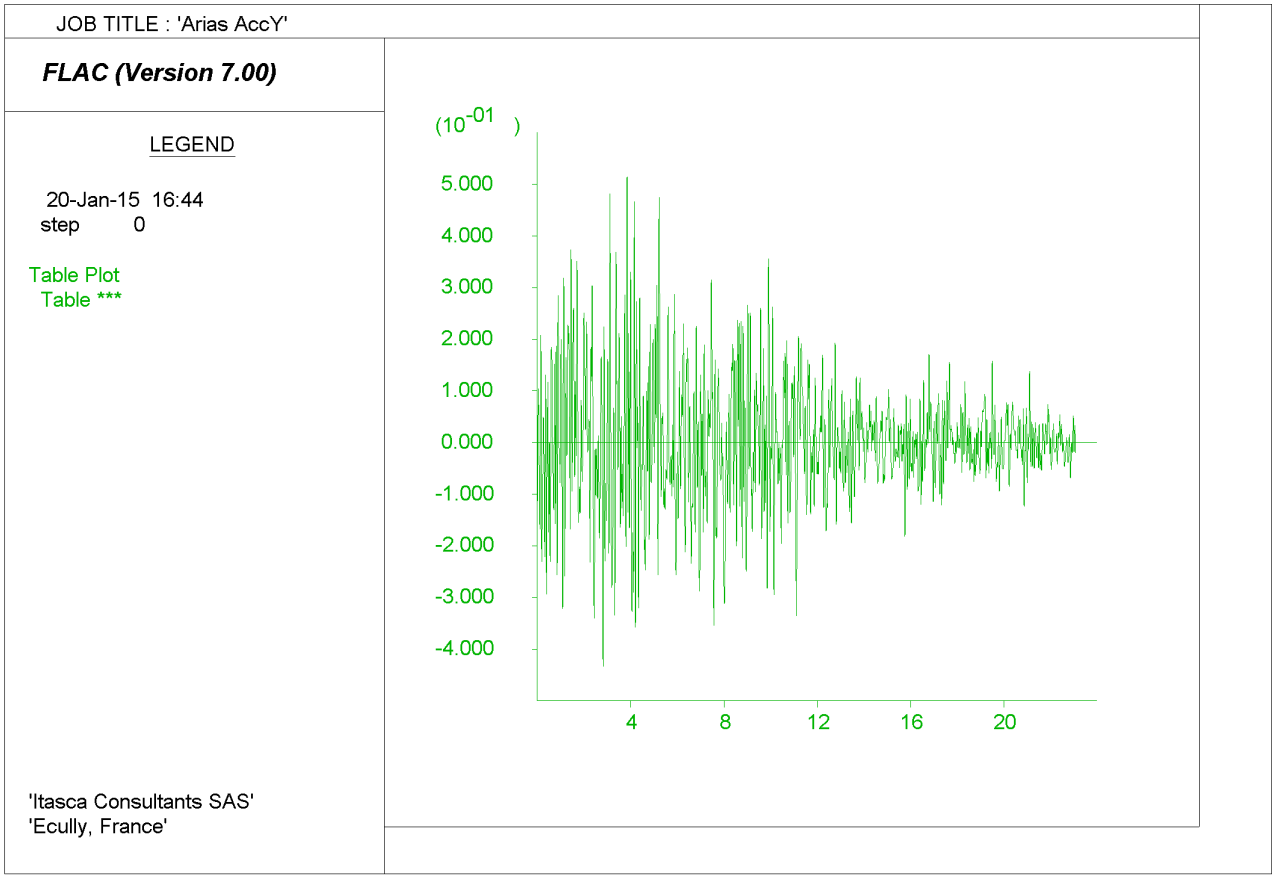

Figure 3-25: KOCAELI IZT – V acceleration – 1-99 significant duration based on Arias Intensity

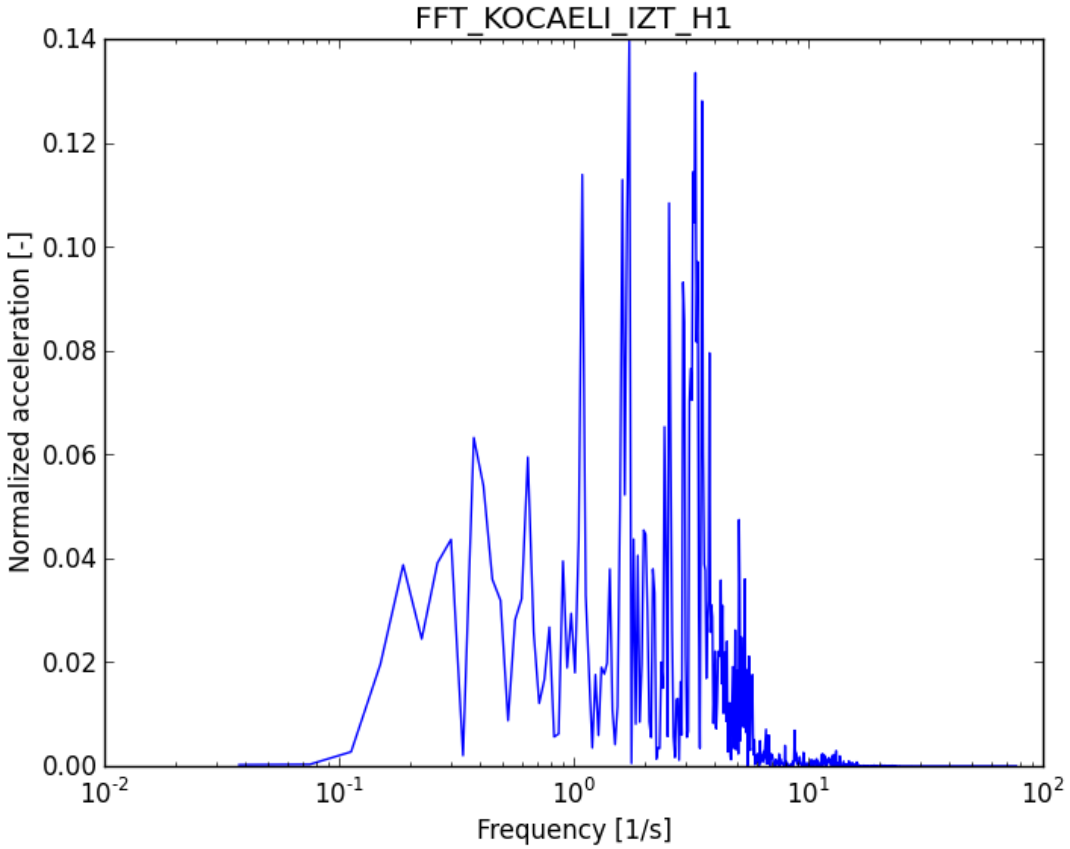

Figure 3-26 : Fourier Transform of horizontal (H1) acceleration of SEE Kocaeli IZT

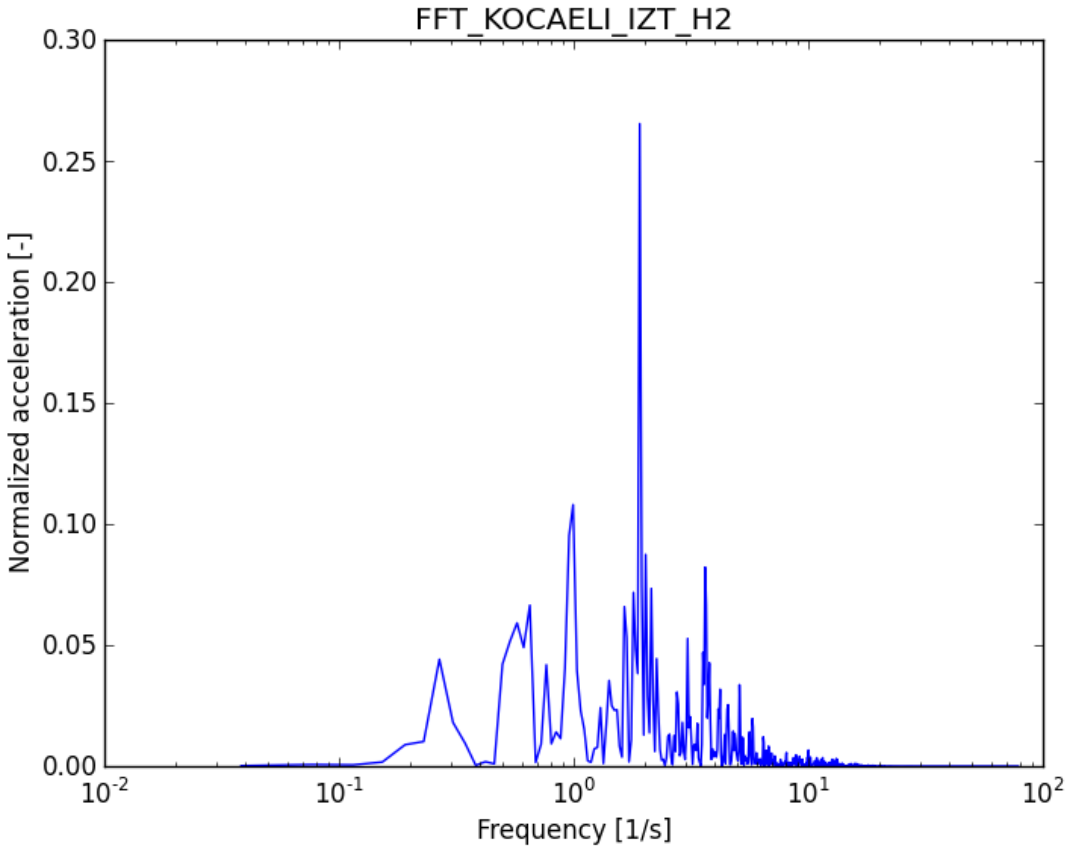

Figure 3-27: Fourier Transform of horizontal (H2) acceleration of SEE Kocaeli IZT

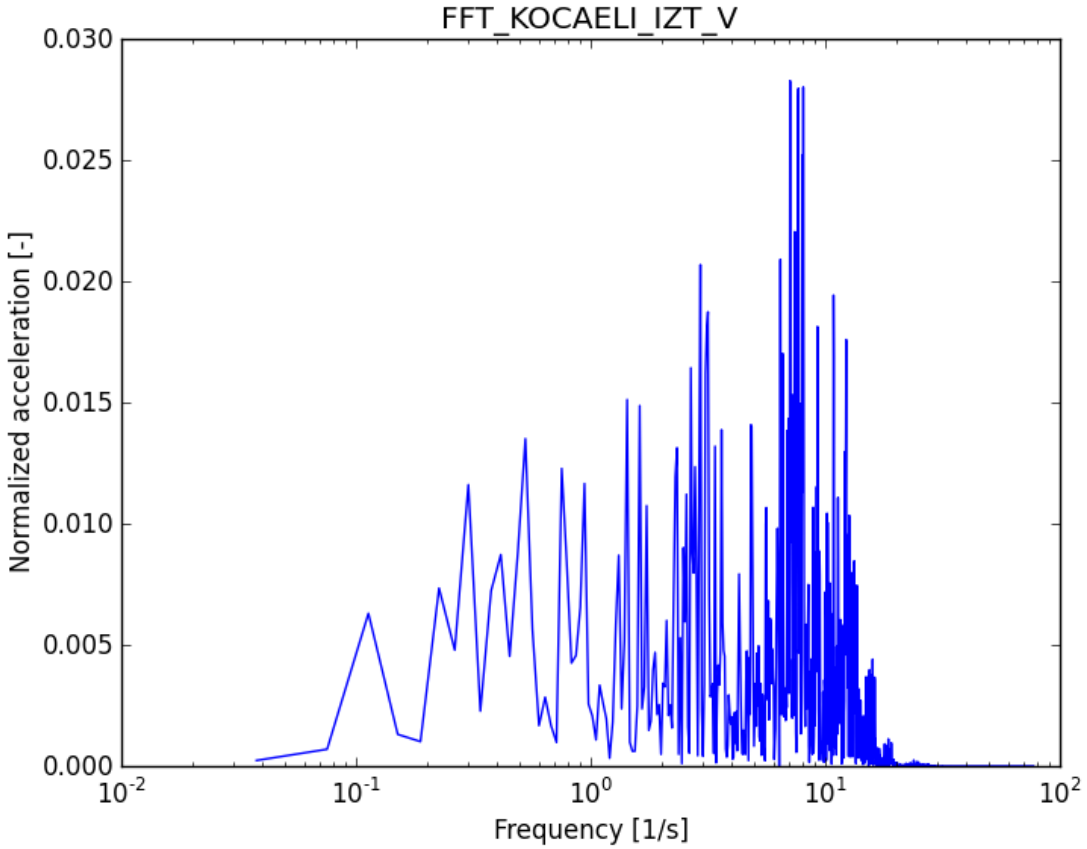

Figure 3-28: Fourier Transform of vertical (V) acceleration of SEE Kocaeli IZT

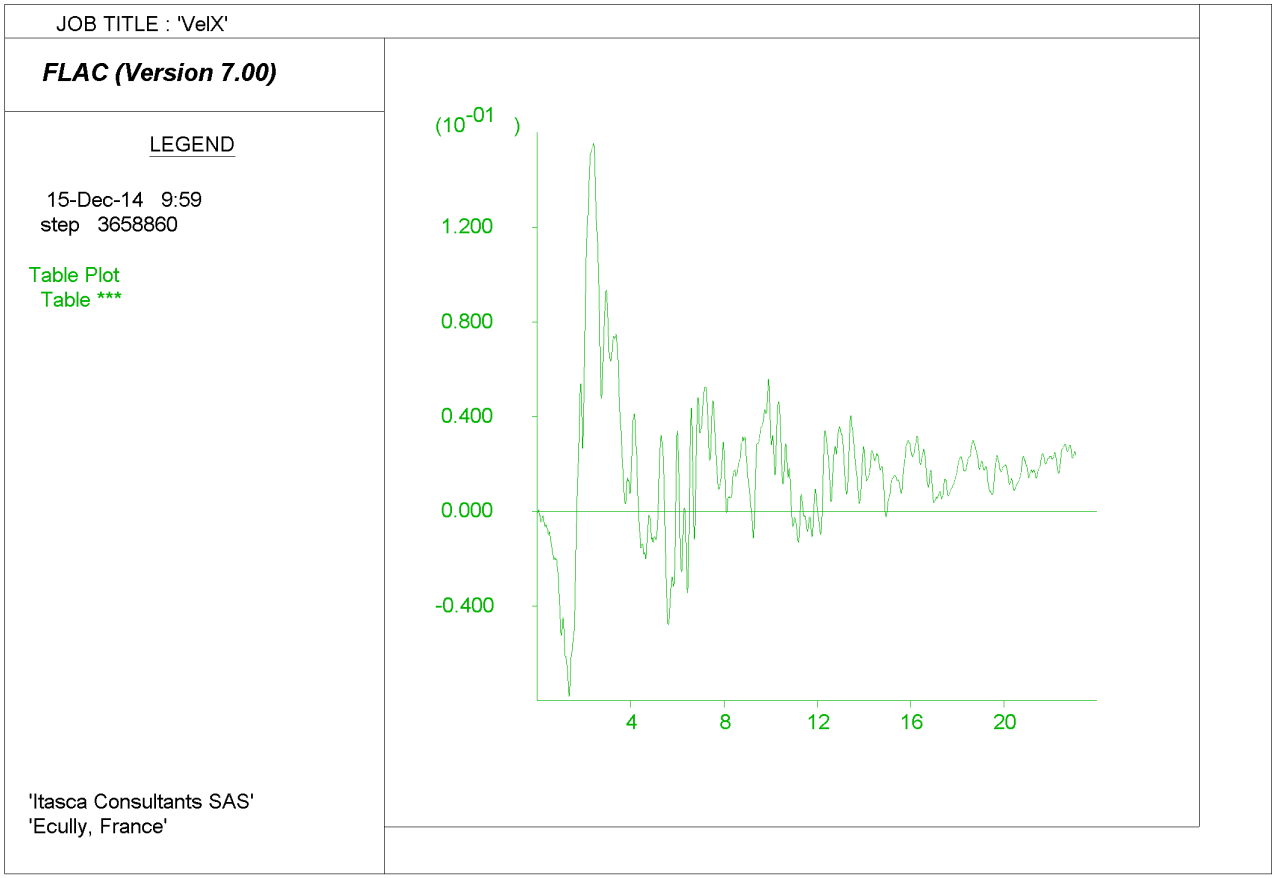

Figure 3-29 KOCAELI IZT – H1 velocity before filtering process and baseline correction

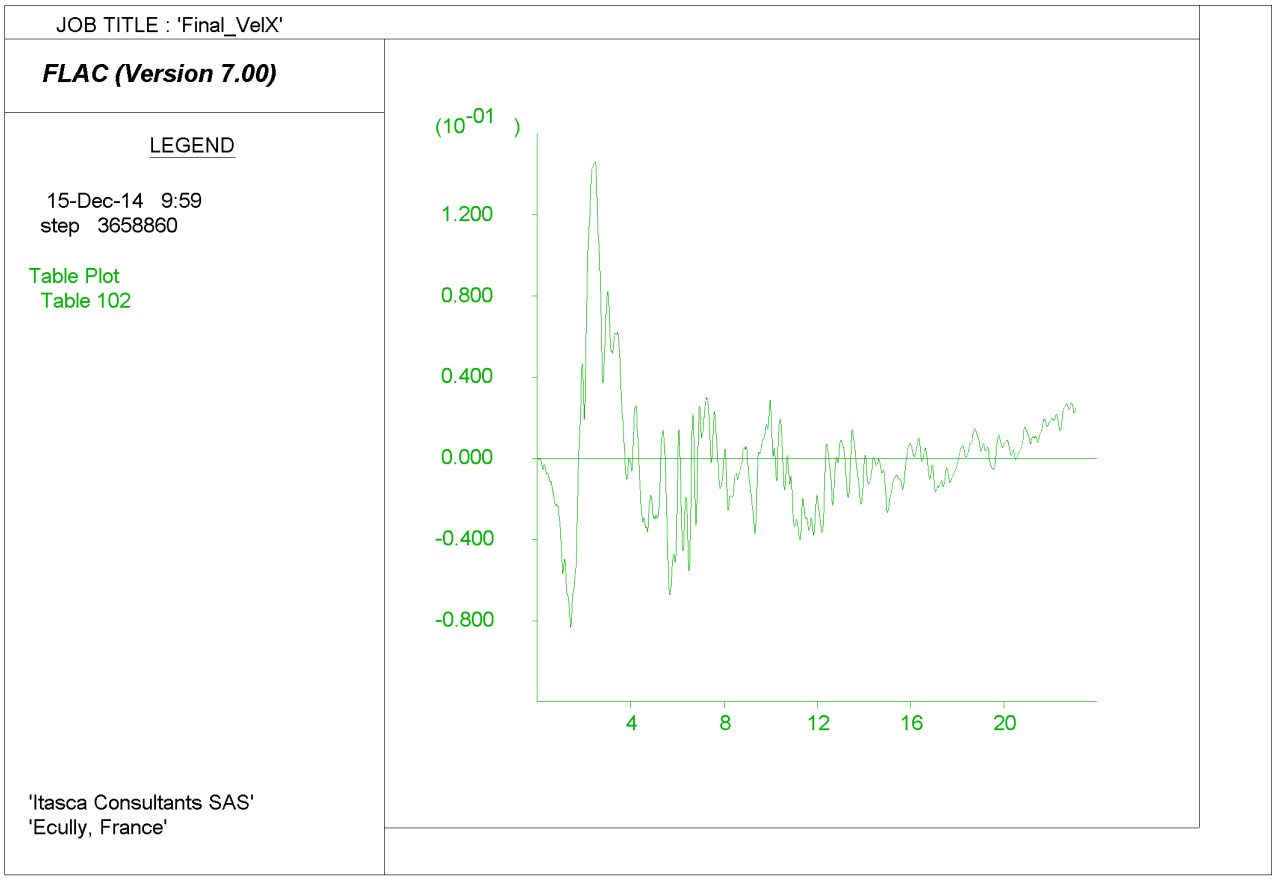

Figure 3-30: KOCAELI IZT – H1 velocity after filtering process and baseline correction

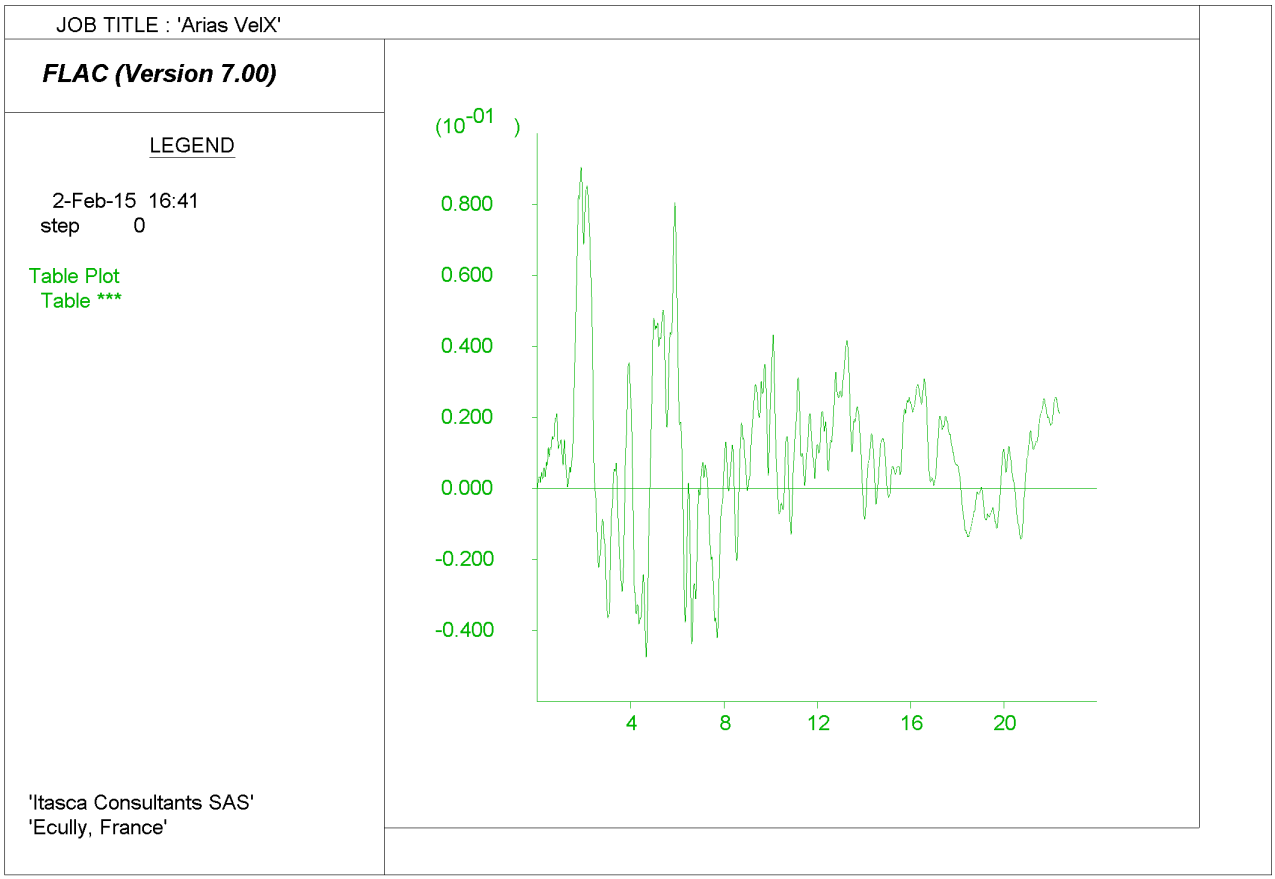

Figure 3-31 KOCAELI IZT – H2 velocity before filtering process and baseline correction

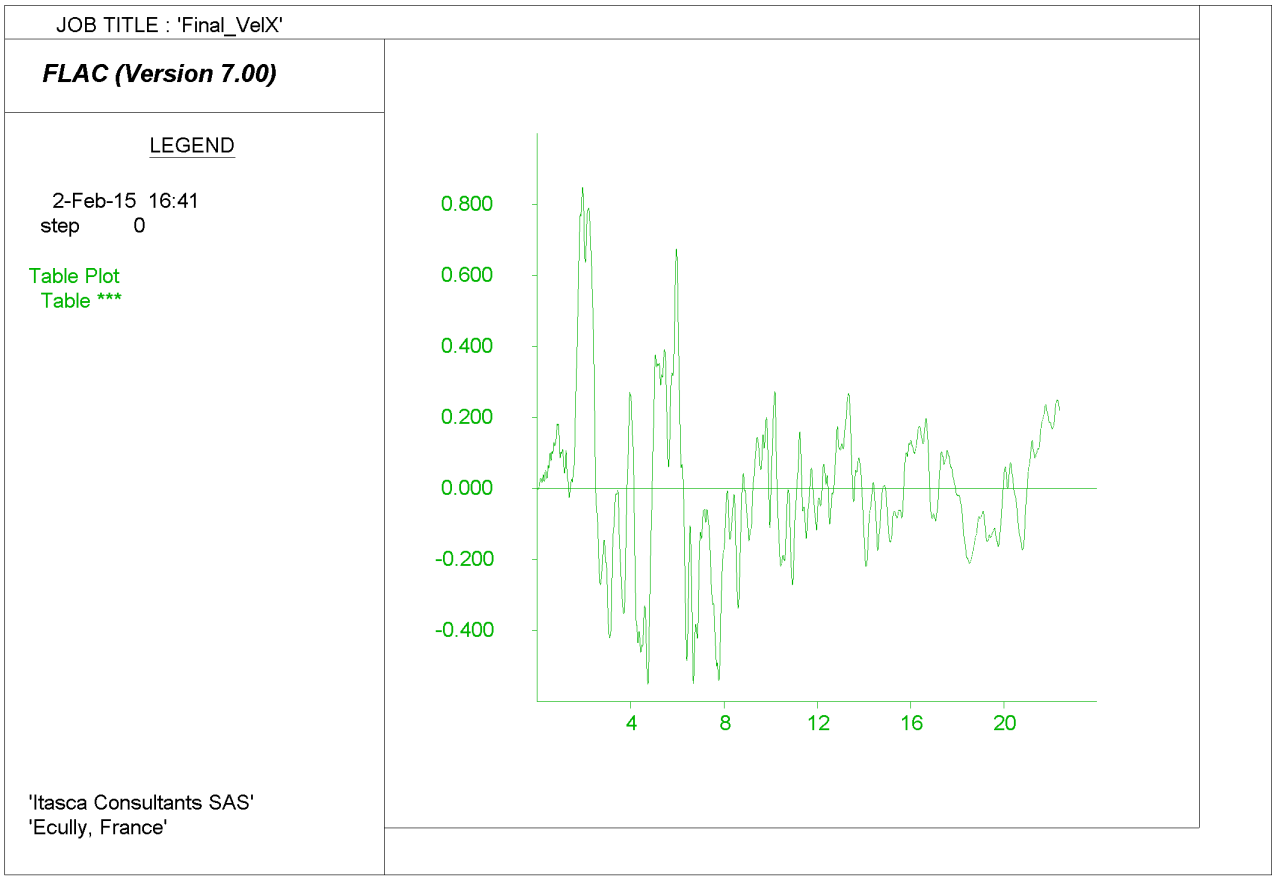

Figure 3-32 KOCAELI IZT – H2 velocity after filtering process and baseline correction

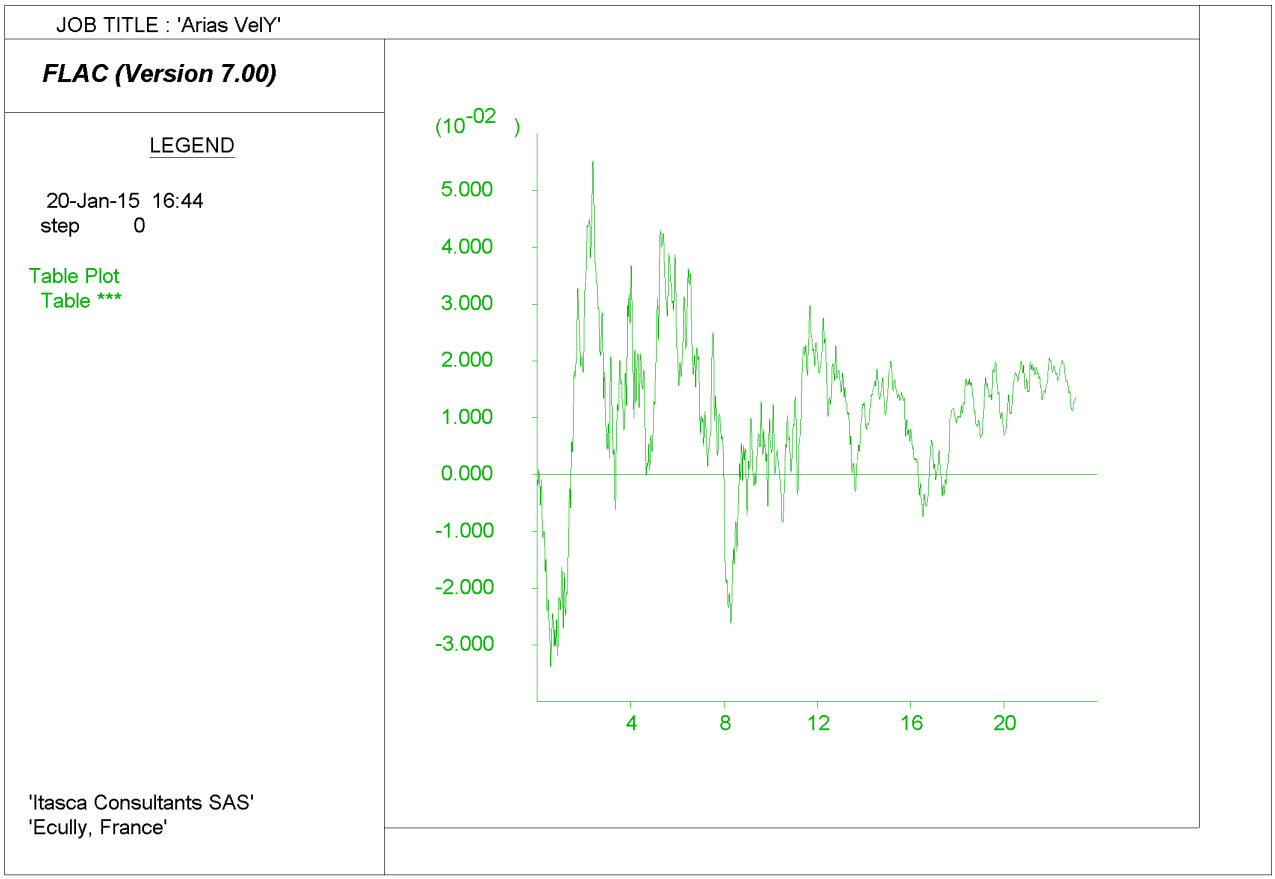

Figure 3-33 KOCAELI IZT – V velocity before filtering process and baseline correction

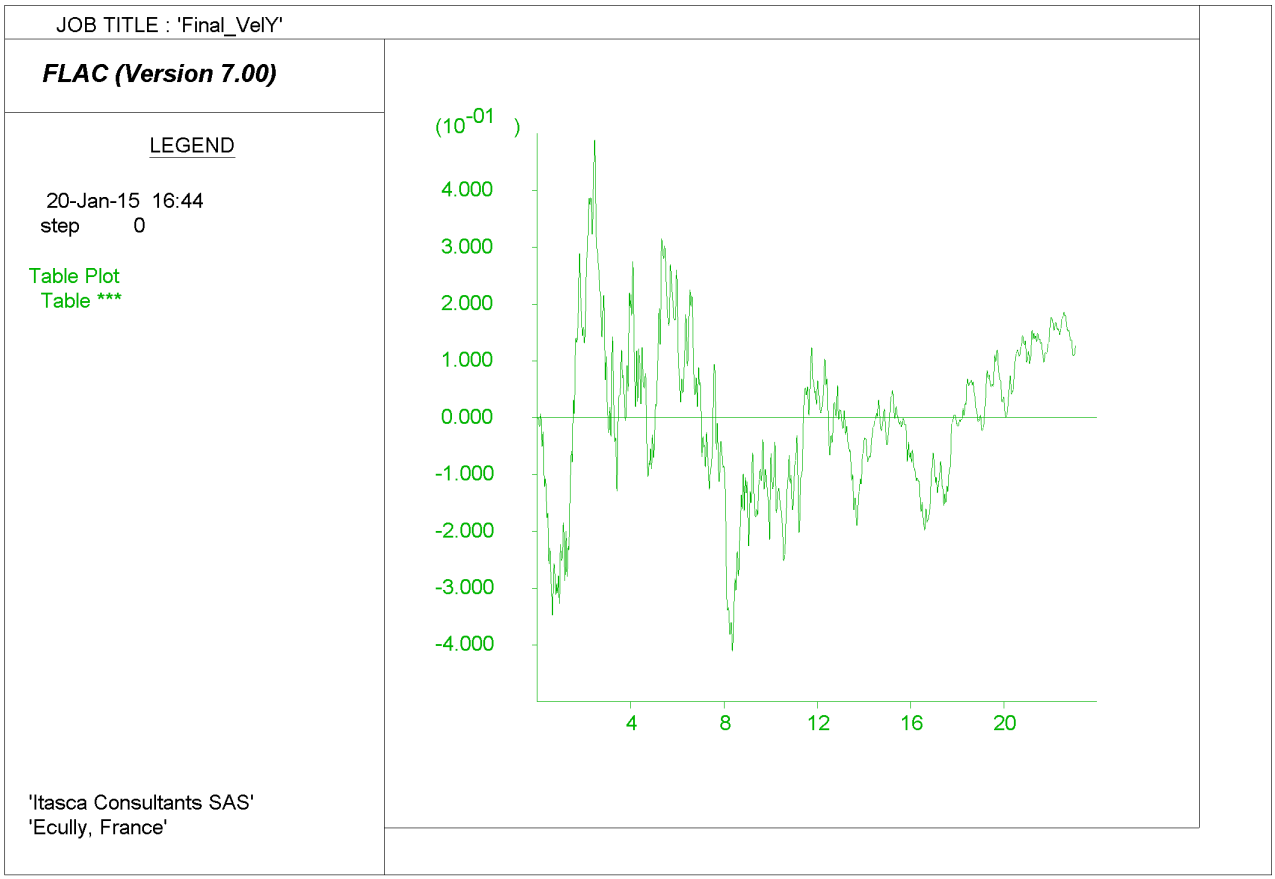

Figure 3-34 KOCAELI IZT – V velocity after filtering process and baseline correction

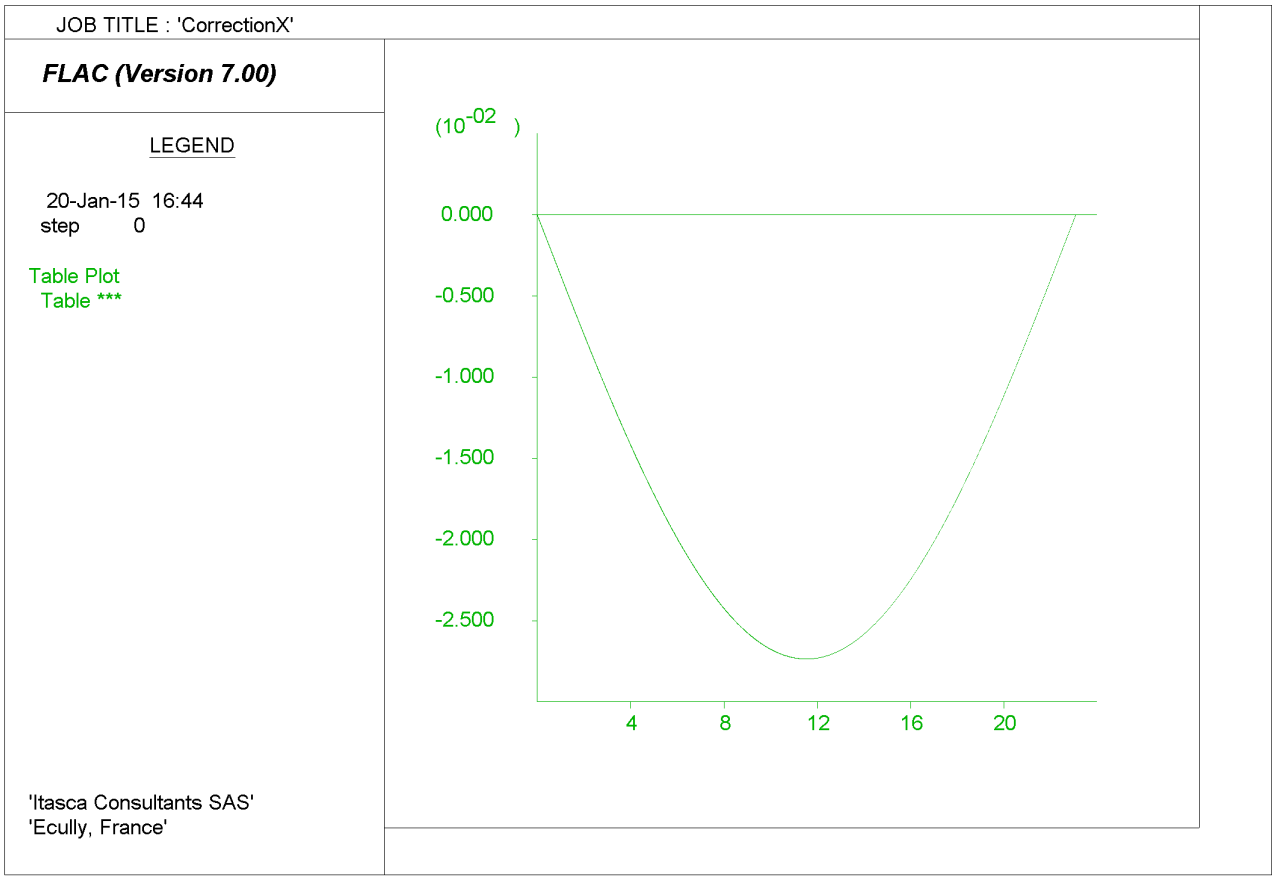

Figure 3-35 : KOCAELI IZT – Baseline Correction - H1 low frequency velocity

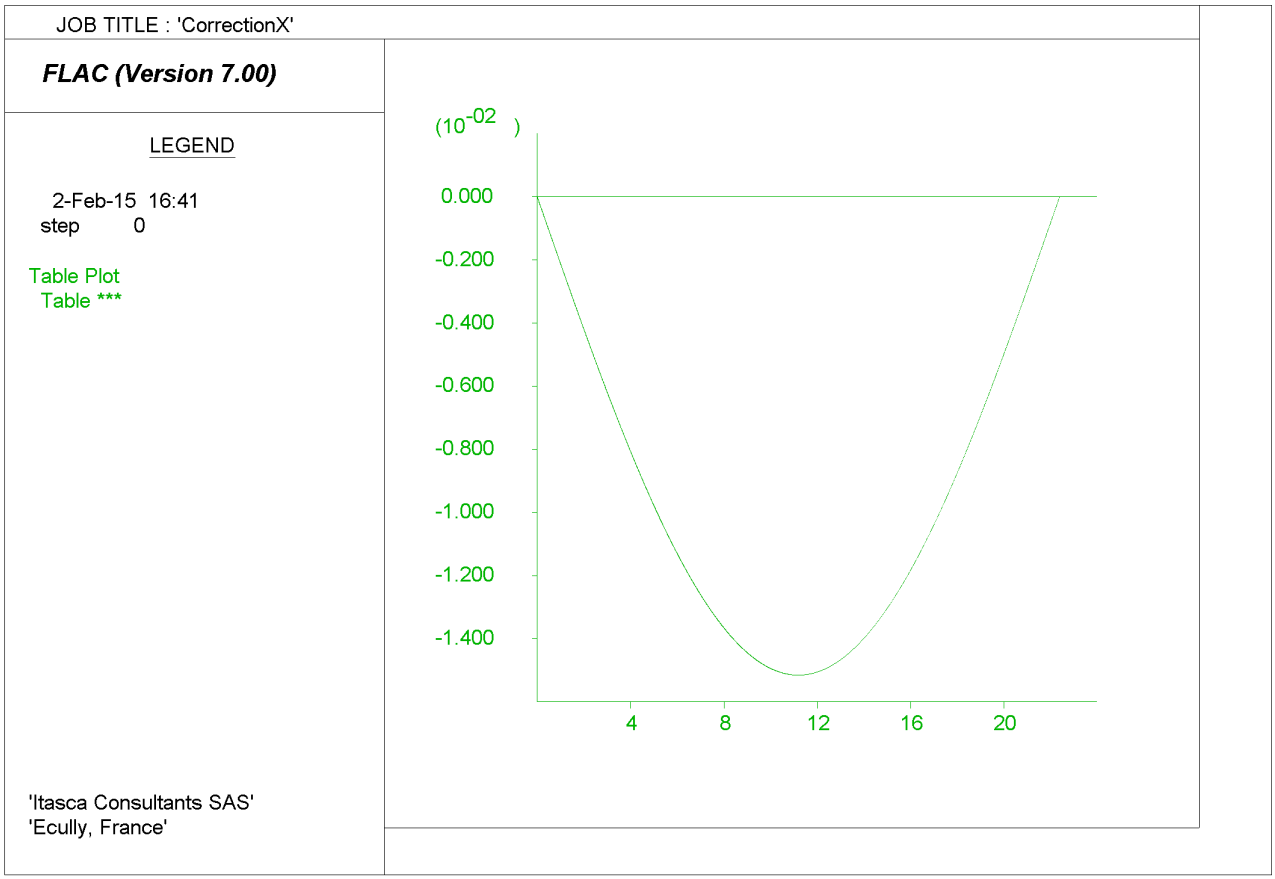

Figure 3-36: KOCAELI IZT – Baseline Correction – H2 low frequency velocity

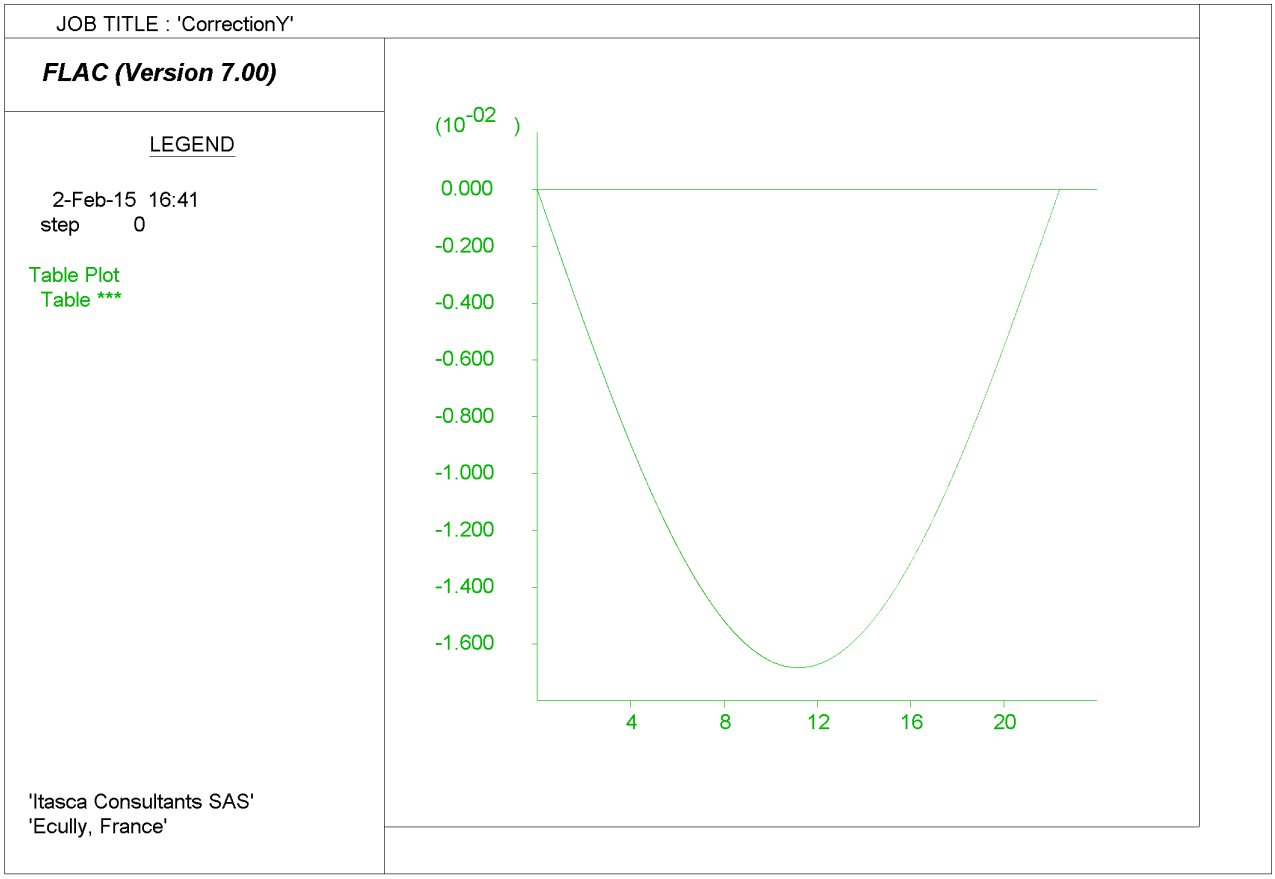

Figure 3-37: KOCAELI IZT – Baseline Correction - V low frequency velocity

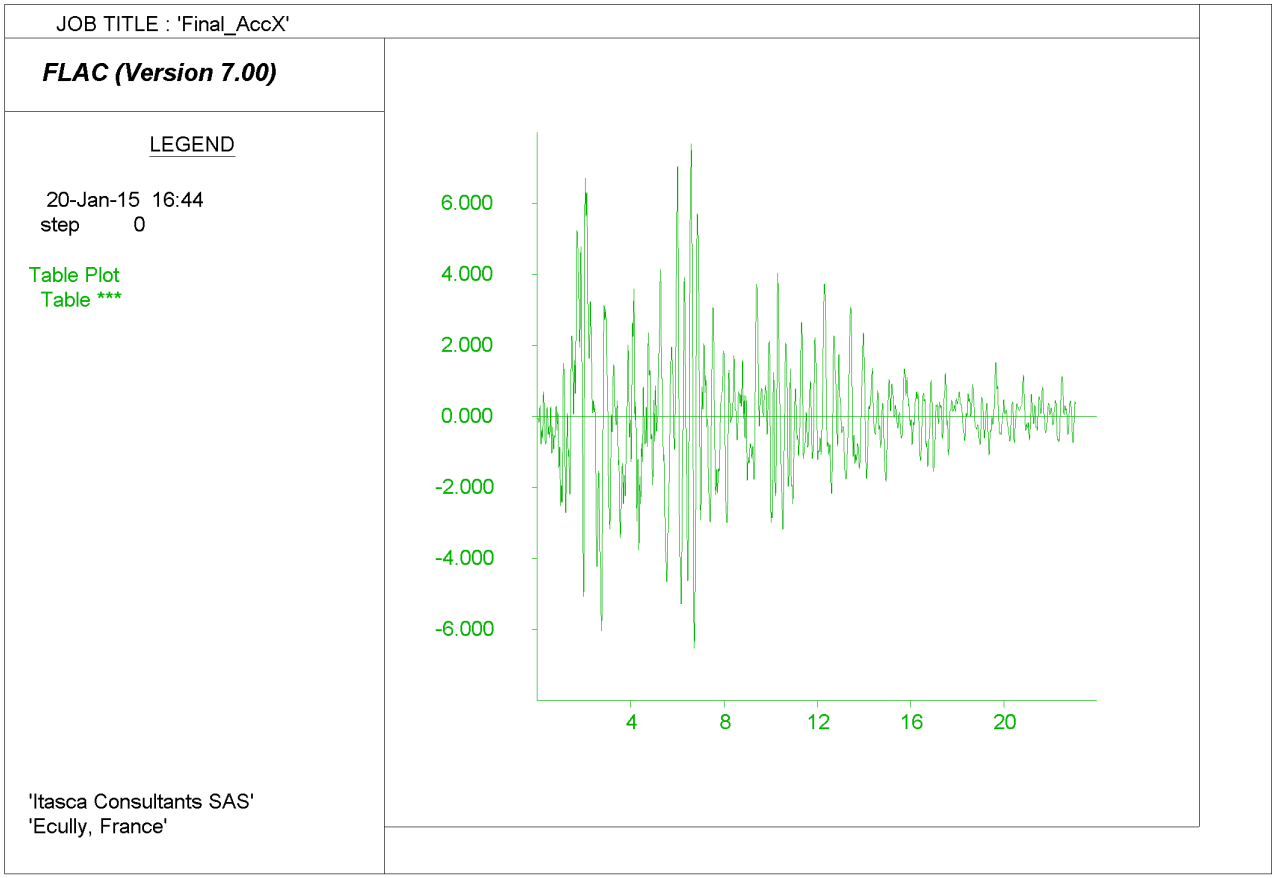

Figure 3-38 KOCAELI IZT – Final H1 acceleration time history

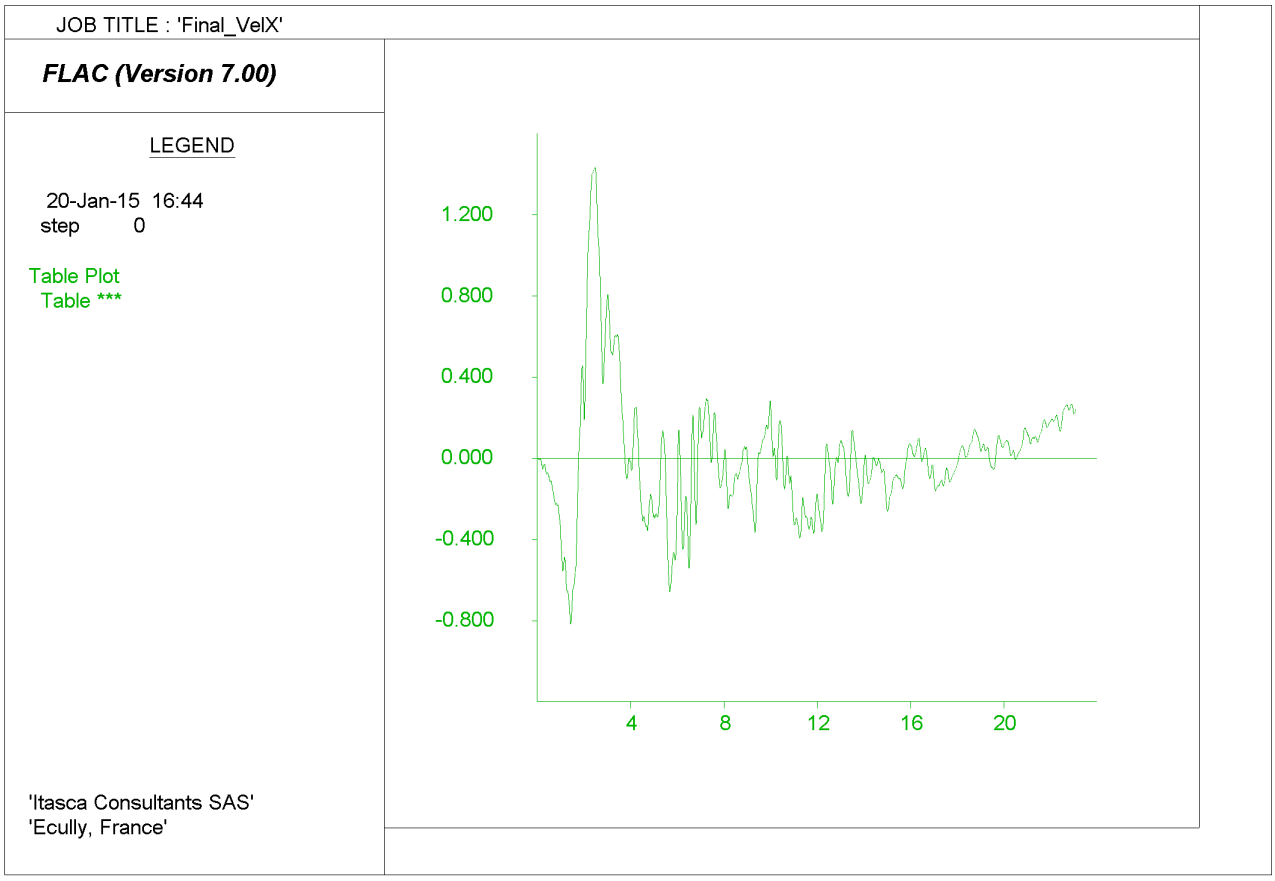

Figure 3-39 KOCAELI IZT – Final H1 velocity time history

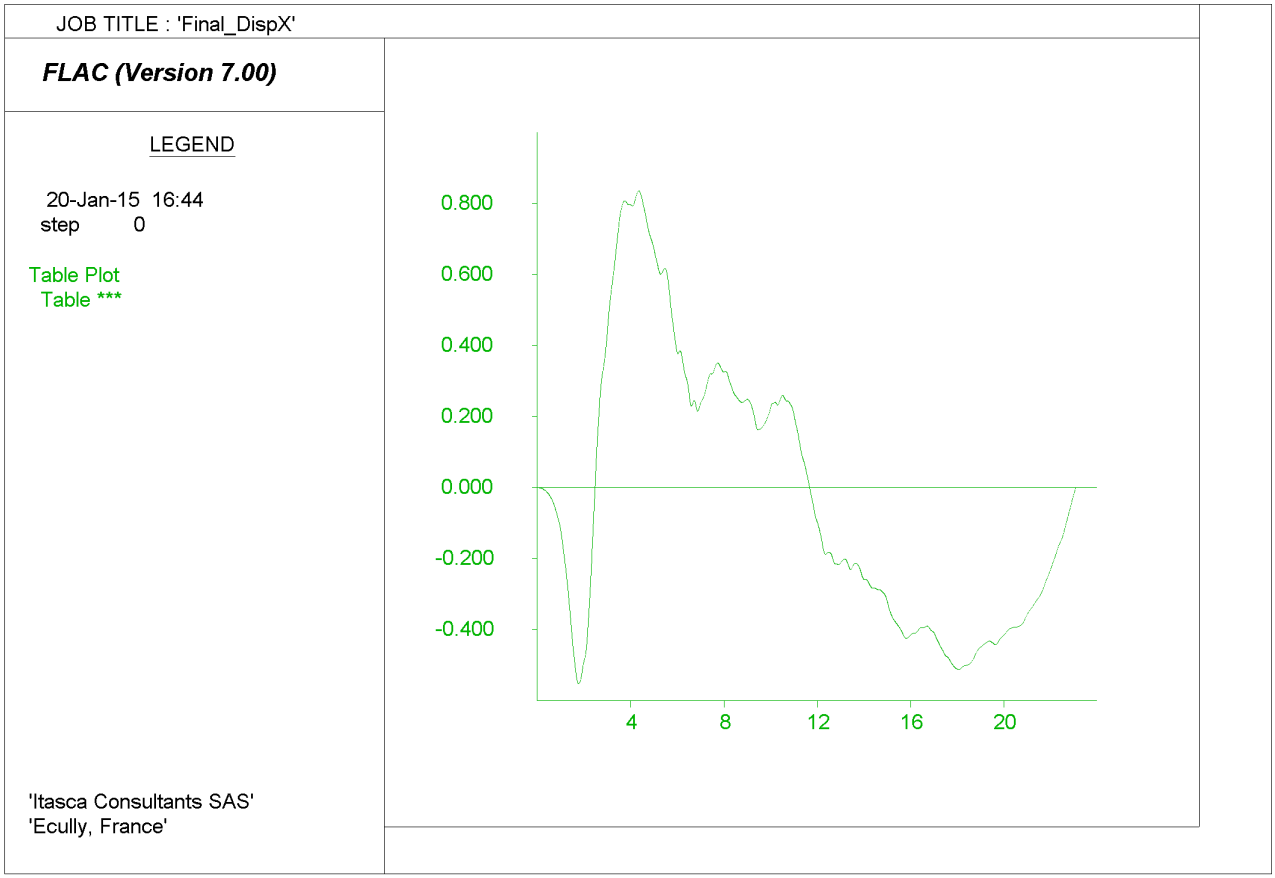

Figure 3-40 KOCAELI IZT – Final H1 displacement time history

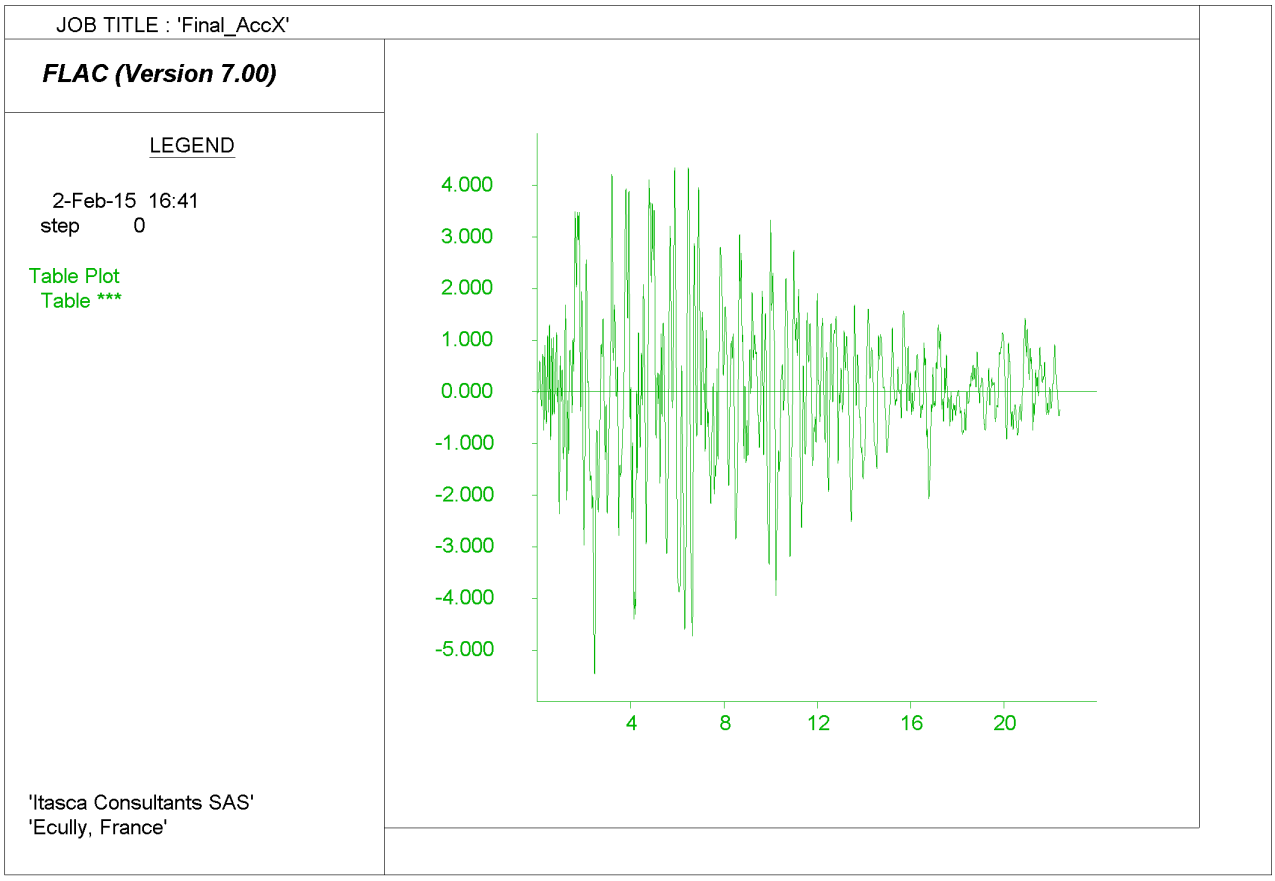

Figure 3-41 KOCAELI IZT – Final H2 acceleration time history

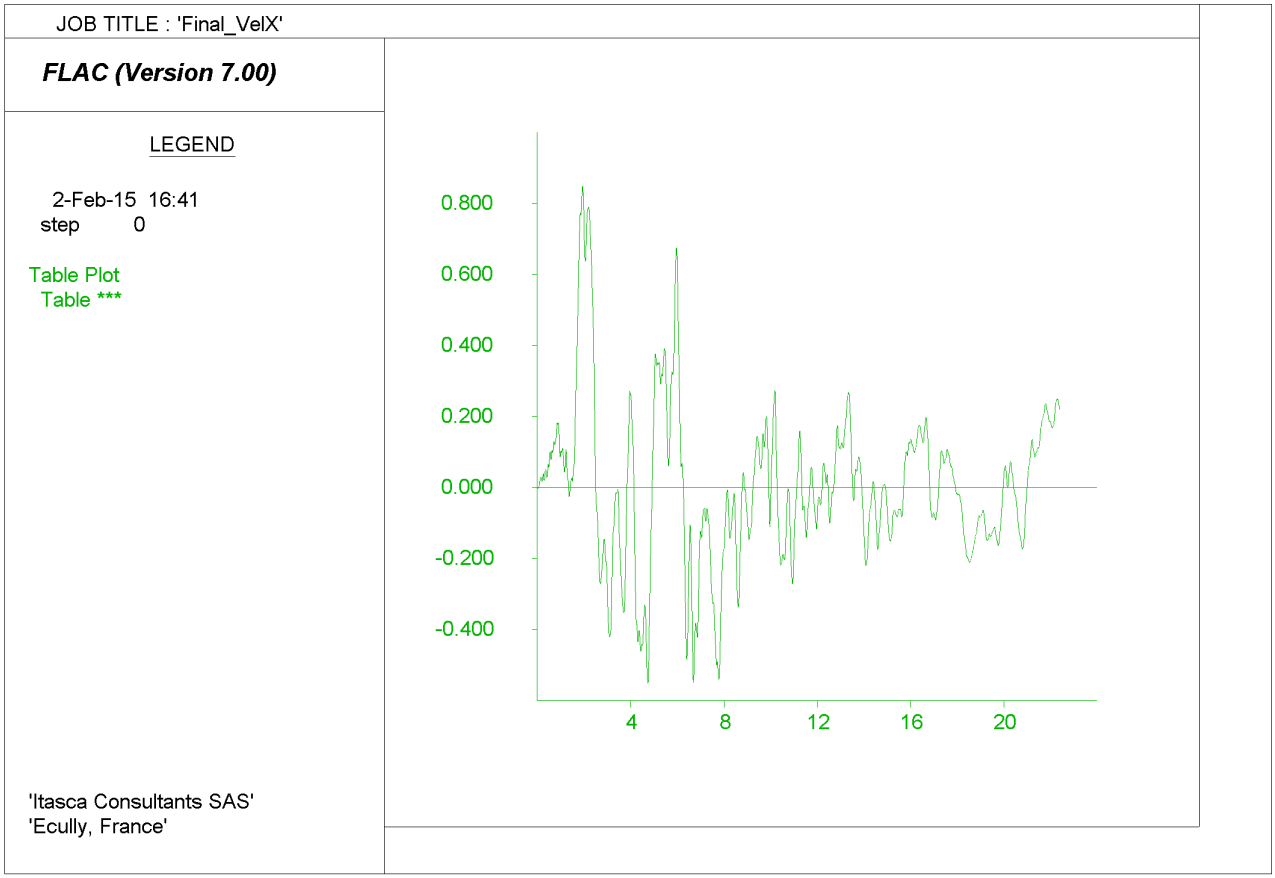

Figure 3-42 KOCAELI IZT – Final H2 velocity time history

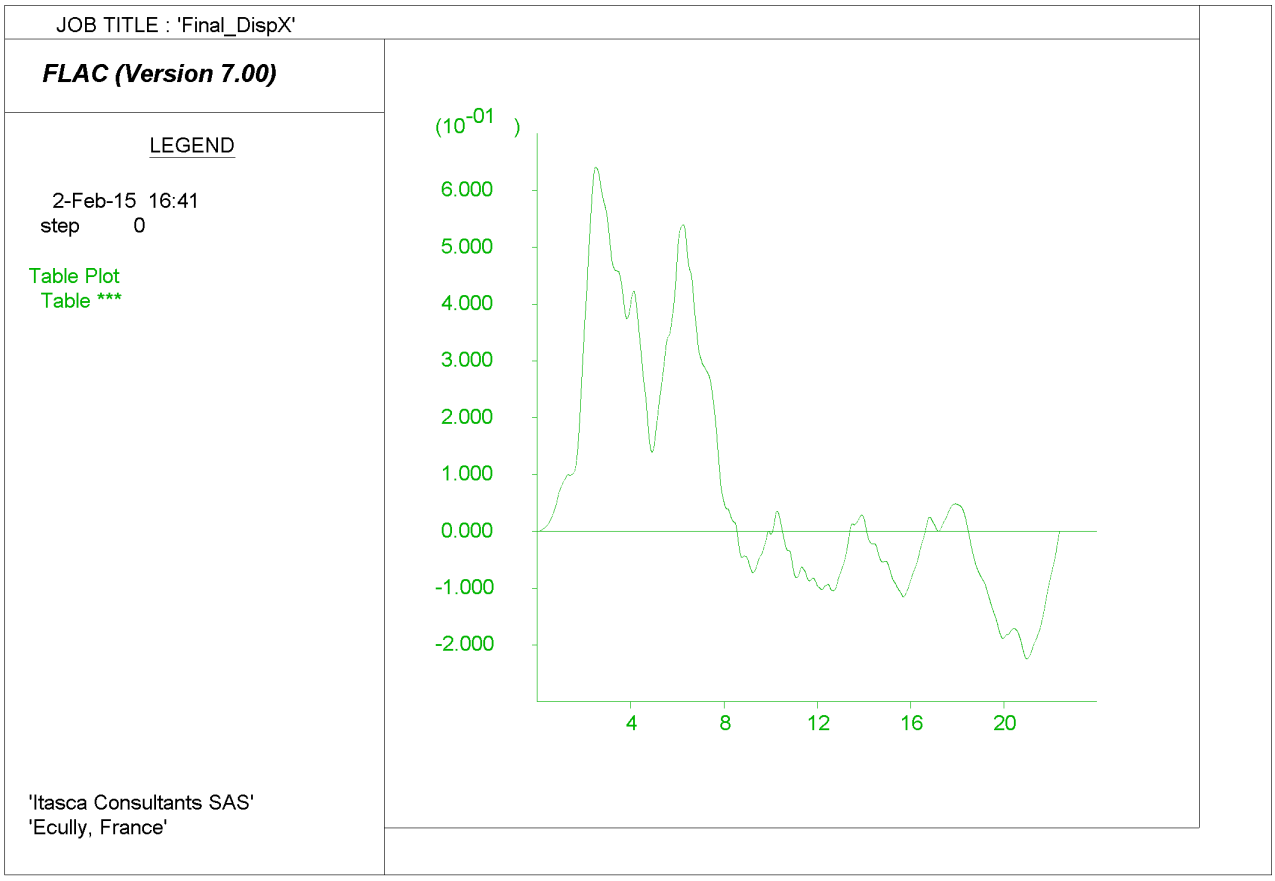

Figure 3-43 KOCAELI IZT – Final H2 displacement time history

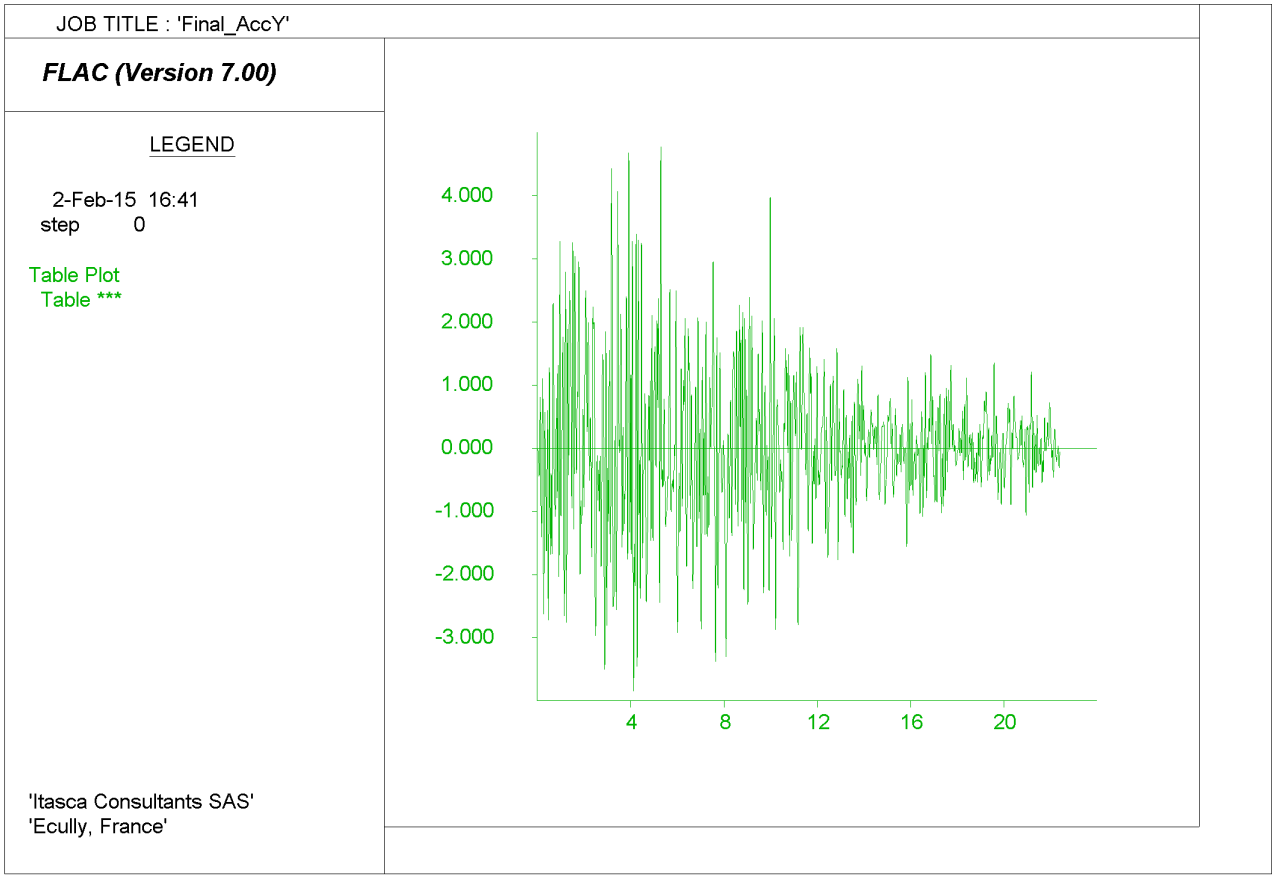

Figure 3-44 KOCAELI IZT – Final V acceleration time history

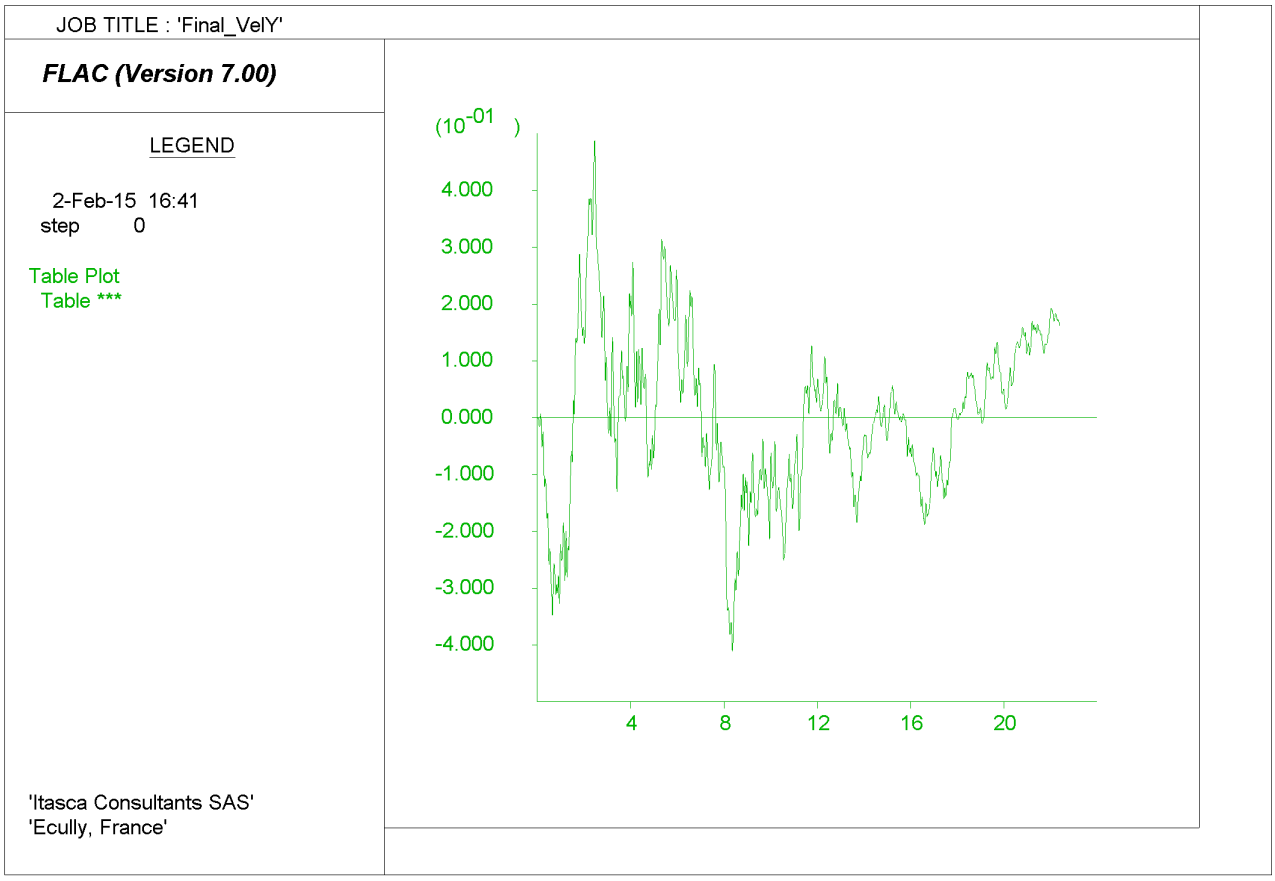

Figure 3-45 KOCAELI IZT – Final V velocity time history

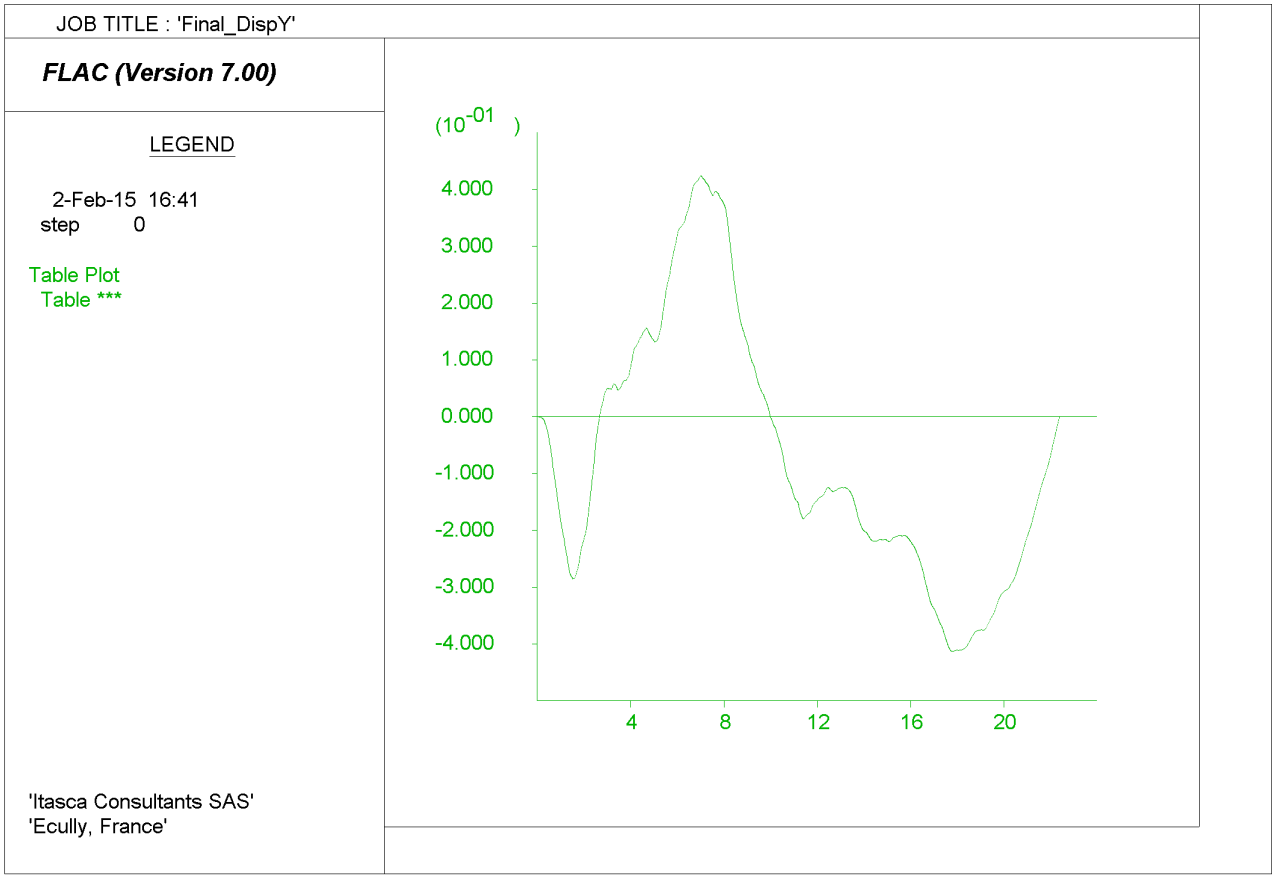

Figure 3-46 KOCAELI IZT – Final V displacement time history

3.4. Boundary conditions

3.4.1. Quiet boundaries

The modeling of geomechanics problems involves media which, at the scale of the analysis, are better represented as unbounded. Numerical methods relying on the discretization of a finite region of space require that appropriate conditions be enforced at the artificial numerical boundaries. In static analyses, fixed or elastic boundaries (e.g., represented by boundary-element techniques) can be realistically placed at some distance from the region of interest.

In dynamic problems, however, such boundary conditions cause the reflection of outward propagating waves back into the model and do not allow the necessary energy radiation. The use of a larger model can minimize the problem, since material damping will absorb most of the energy in the waves reflected from distant boundaries. However, this solution leads to a large computational burden. The alternative is to use quiet (or absorbing) boundaries. Several formulations have been proposed. The viscous boundary developed by Lysmer and Kuhlemeyer (1969, [8]) is used in FLAC. It is based on the use of independent dashpots in the normal and shear directions at the model boundaries. The method is almost completely effective at absorbing body waves approaching the boundary at angles of incidence greater than 30◦. For lower angles of incidence, or for surface waves, there is still energy absorption, but it is not perfect. However, the scheme has the advantage that it operates in the time domain. Its effectiveness has been demonstrated in both finite-element and finite-difference models (Kunar et al. 1977, [7]).

The quiet-boundary scheme proposed by Lysmer and Kuhlemeyer (1969) involves dashpots attached independently to the boundary in the normal and shear directions. The dashpots provide viscous normal and shear tractions given by:

$$t_n = -\rho C_p v_n \qquad (8)$$

$$t_s = -\rho C_s v_s \qquad (9)$$

where v_n and v_s are the normal and shear components of the velocity at the boundary, ρ is the mass density and C_p and C_s are the *p*- and *s*- wave velocities.

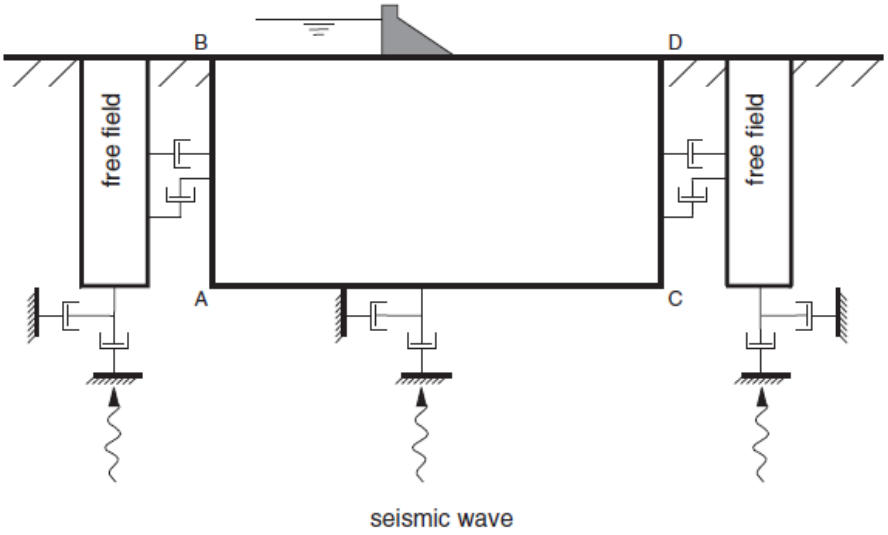

Figure 3-47 Model for seismic analysis of surface structures and free-field mesh

3.4.2. Free-field boundaries

Numerical analysis of the seismic response of surface structures requires the discretization of a region of the material adjacent to the foundation. The seismic input is normally represented by plane waves propagating upward through the underlying material. The boundary conditions at the sides of the model must account for the free-field motion which would exist in the absence of the structure.

Here, we use a procedure which "enforces" the free-field motion in such a way that boundaries retain their non-reflecting properties (i.e., outward waves originating from the structure are properly absorbed). This approach was used in the continuum finite-difference code NESSI (*Cundall et al.*). A technique of this type was developed for *FLAC*, involving the execution of a one-dimensional free-field calculation in parallel with the main-grid analysis.

The lateral boundaries of the main grid are coupled to the free-field grid by viscous dashpots to simulate a quiet boundary (see Figure 3-47), and the unbalanced forces from the free-field grid are applied to the main-grid boundary. In this way, plane waves propagating upward suffer no distortion at the boundary because the free-field grid supplies conditions that are identical to those in an infinite model.

When the main grid is uniform, and there is no surface structure, the lateral dashpots are not exercised because the free-field grid executes the same motion as the main grid. However, when the main-grid motion differs from that of the free field (due, say, to a surface structure that radiates

secondary waves, which is the case here), then the dashpots act to absorb energy in a manner similar to the action of quiet boundaries.

The free field performs a small-strain calculation, even if the main grid is executing in large-strain mode. In this case, the results will be approximately correct, provided the deformations near the free-field boundaries are relatively small (e.g., compared to grid dimensions).

3.5. Seismic signal input

Dynamic input can be applied either in the x- or y-direction corresponding to the xy-axes for the model, or in the normal and shear directions to the model boundary. Certain boundary conditions cannot be mixed at the same boundary segment. One restriction when applying velocity or acceleration input to model boundaries is that these boundary conditions cannot be applied along the same boundary as a quiet (viscous) boundary condition, because the effect of the quiet boundary would be nullified. To input seismic motion at a quiet boundary, a stress boundary condition is used (i.e., a velocity record is transformed into a stress record and applied to a quiet boundary). A velocity wave may be converted to a stress wave using the formulae:

$$\sigma_n = 2(\rho C_p)\, v_n \qquad (10)$$

$$\sigma_s = 2(\rho C_s)\, v_s \qquad (11)$$

The formulae assume plane-wave conditions. The factor of two accounts for the fact that the applied stress must be double that observed in an infinite medium, since half the input energy is absorbed by the viscous boundary.

3.5.1. Validation of the seismic input in the Bisri Dam model

In this section the input of the seismic signal into the FLAC model of Bisri site is presented. As described into the seismic analysis report [3], the SEE and OBE design earthquakes are provided for the free-field engineering bedrock outcrop. The outcrop motion is simply twice the upward propagating wave train motion. Thus, the upward propagating wave that will be imposed at the base of the model will be half the outcrop motion.

A short simulation was performed, by considering a unique layer representing a 300 meters thick bedrock (see Figure 3-48). The signal at the surface is measured and compared to the outcrop original signal. The results shown are relative to the Kocaeli IZT SEE earthquake.

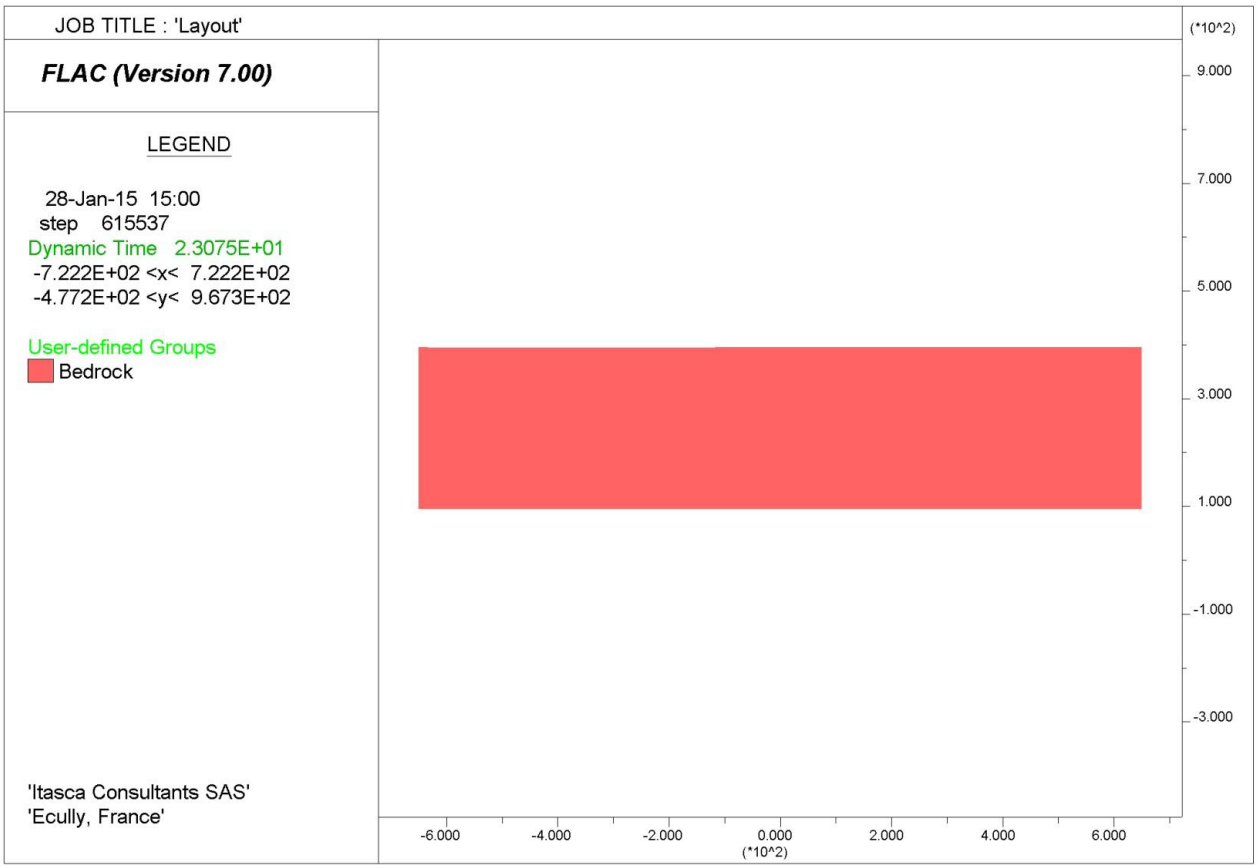

Figure 3-48 : Input of seismic signal – Signal transmission through a 300m thick bedrock layer

Figure 3-49 and Figure 3-50 show a direct comparison between the signals measured at the top of the model and the original outcrop signal. A difference can be noticed: peak accelerations associated to high frequencies are not reproduced in the model, due to filtering process described in section 3.3.3.

A second simulation was performed, this time considering the foundation layers that characterize the Bisri site. At the base of the embankment foundation (120 meters thick), a bedrock layer (180 meters thick) is added. This layer, which behaves elastically throughout the simulation, is added to the model to realistically transmit the signal to the foundation layers. The new layout is represented in Figure 3-51.

Figure 3-52 and Figure 3-53 show again the signal that was measured at the top of the model and the comparison with the bedrock outcrop motion, to observe the influence of the foundation layers. It can be seen how accelerations can be both amplified and reduced. Fourier transforms of those signals help with interpretation: low frequency waves are amplified, whereas high frequency waves are reduced (see from Figure 3-54 to Figure 3-57).

The amplification of the vertical component of acceleration through the soil foundation layers is in fact quite important. This may be due to the fact that *drained* mechanical properties are adopted for the foundation layers. A simulation was performed, adopting an undrained bulk modulus for the clayey silt layer of the soil foundation. The results that were obtained are presented in Appendix 5 (section 11). They show only small differences.

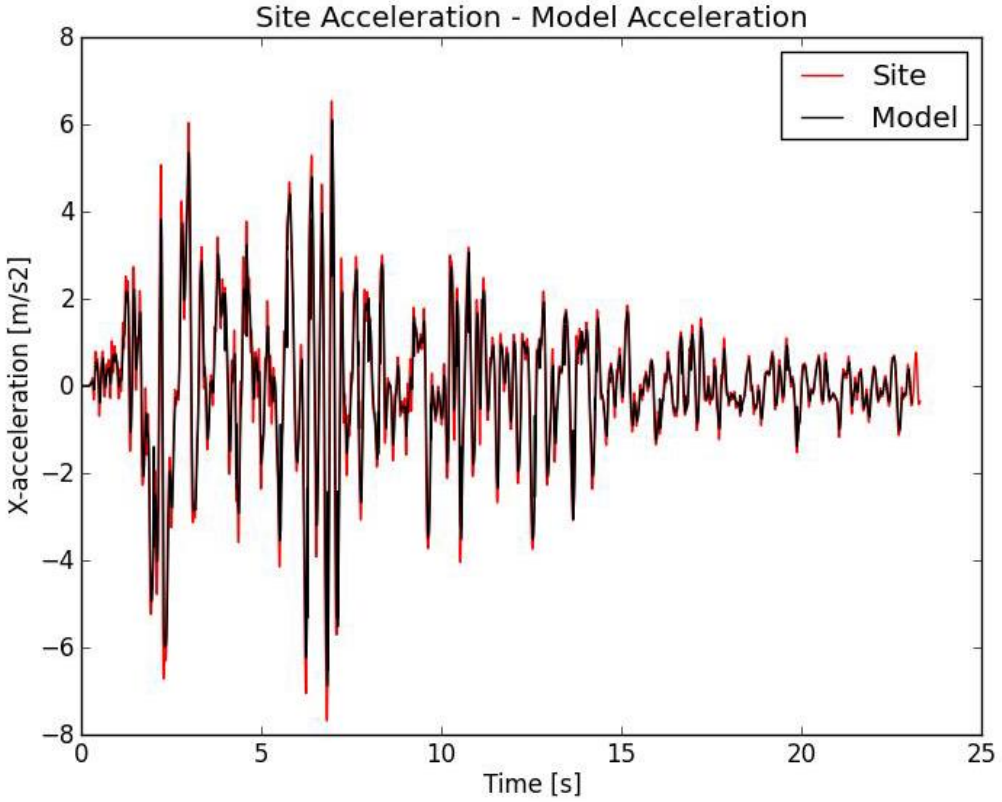

Figure 3-49 : Input of seismic signal – Horizontal acceleration through the bedrock layer

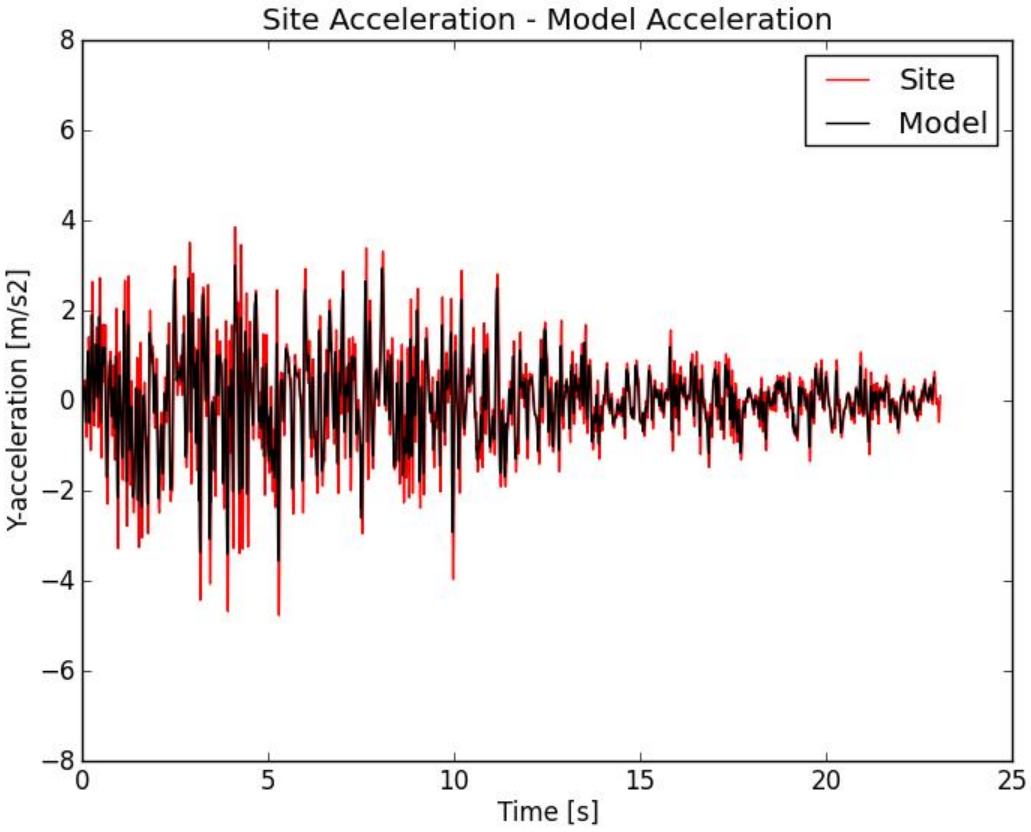

Figure 3-50 : Input of seismic signal – Vertical acceleration through the bedrock layer

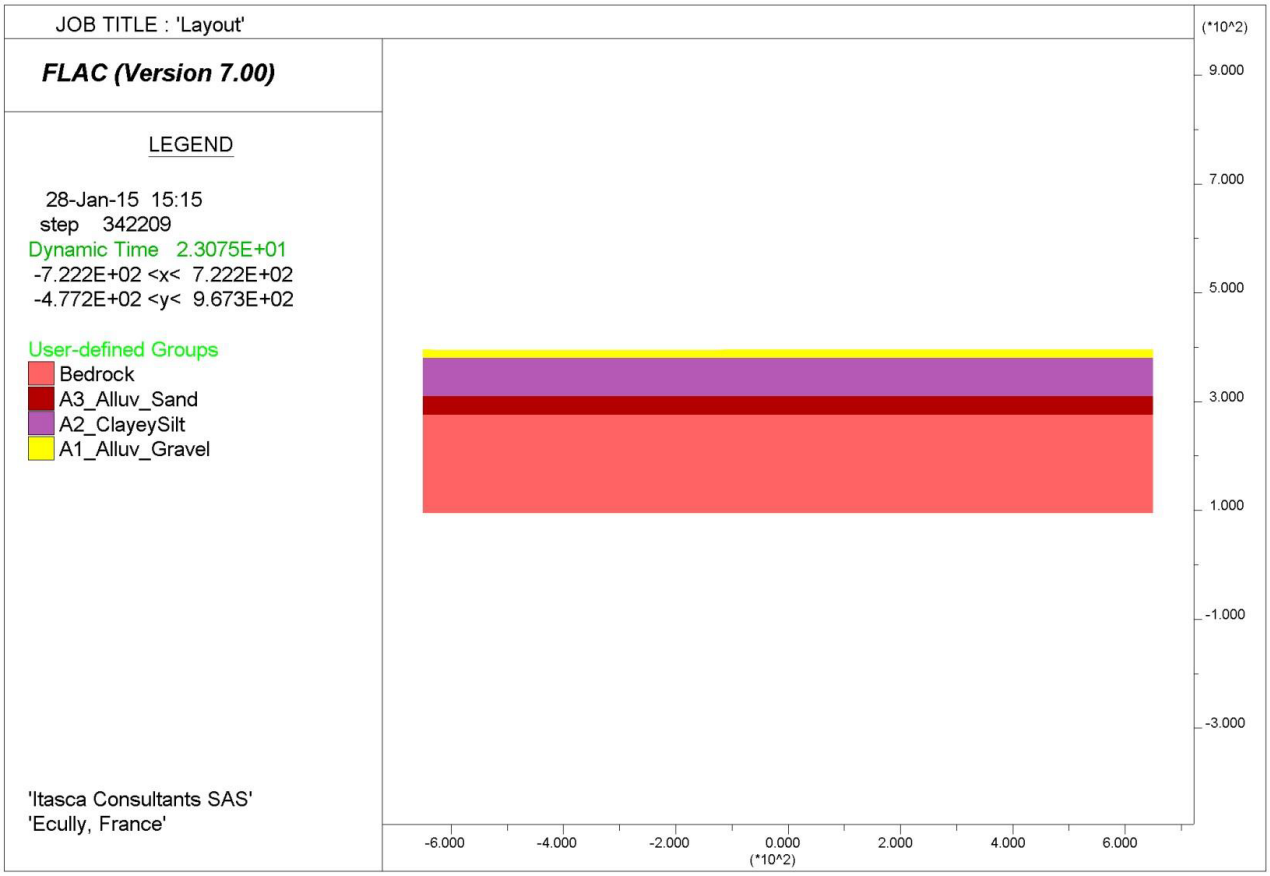

Figure 3-51 : Input of seismic signal – Signal transmission through bedrock-foundation layers

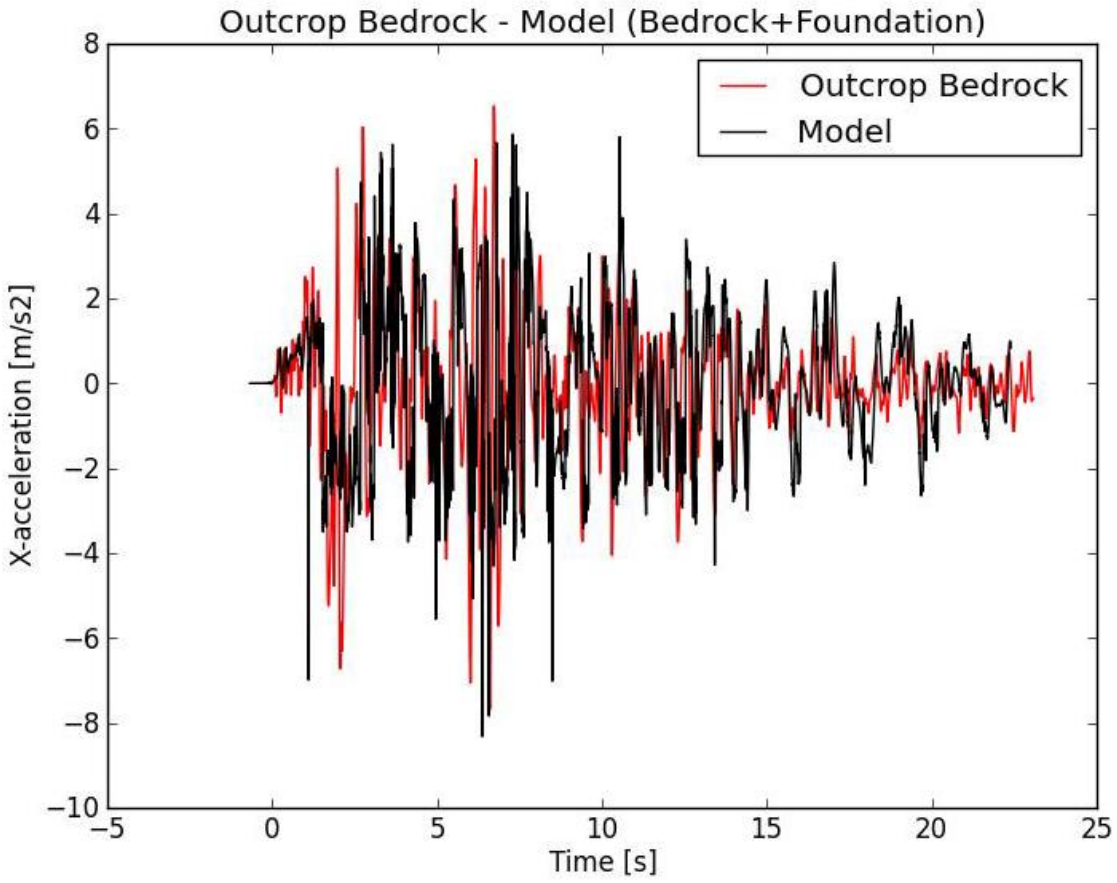

Figure 3-52 : Input of seismic signal – Horizontal acceleration through the bedrock-foundation layers

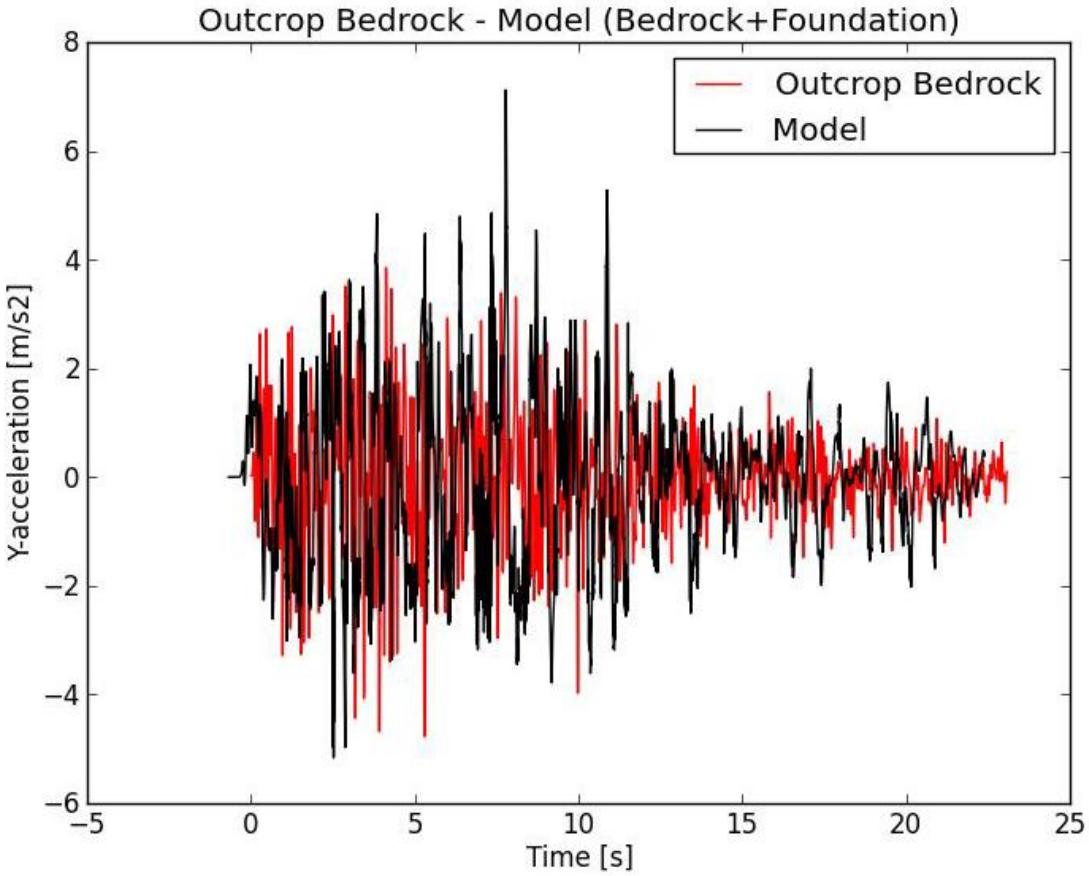

Figure 3-53 : Input of seismic signal – Vertical acceleration through the bedrock-foundation layers

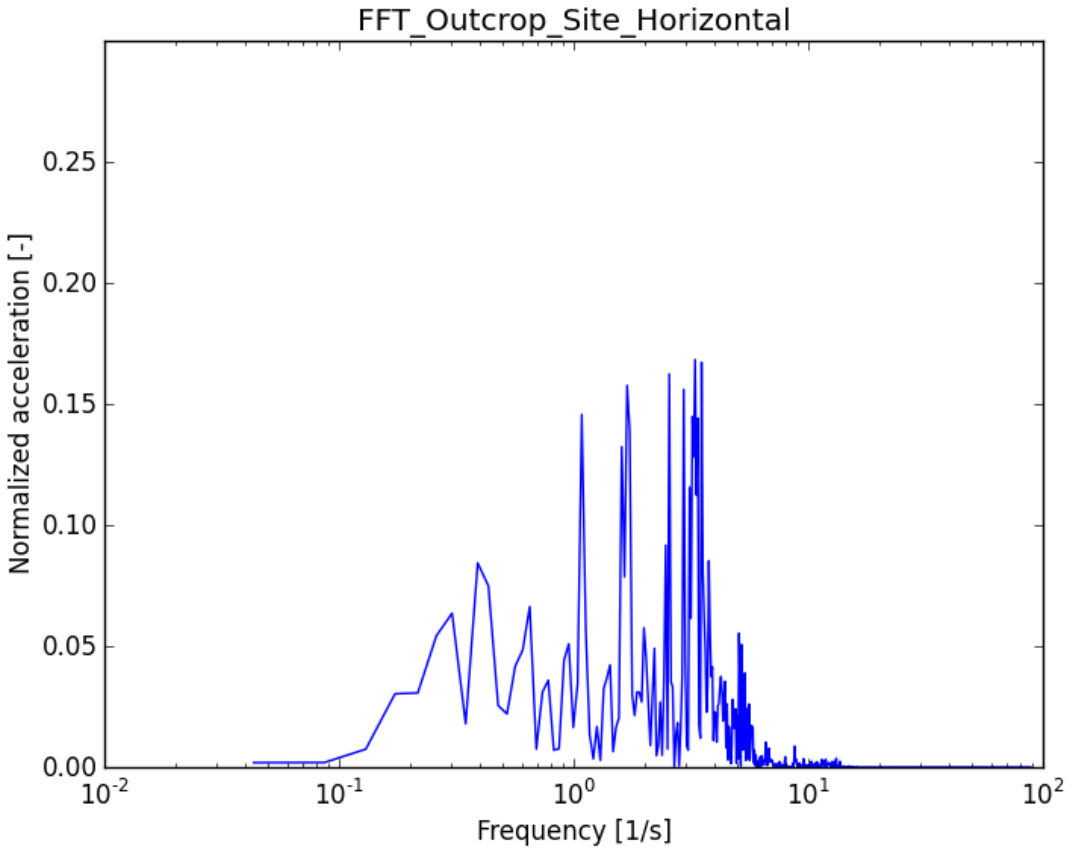

Figure 3-54 : Input of seismic signal – Fourier transform of outcrop horizontal acceleration

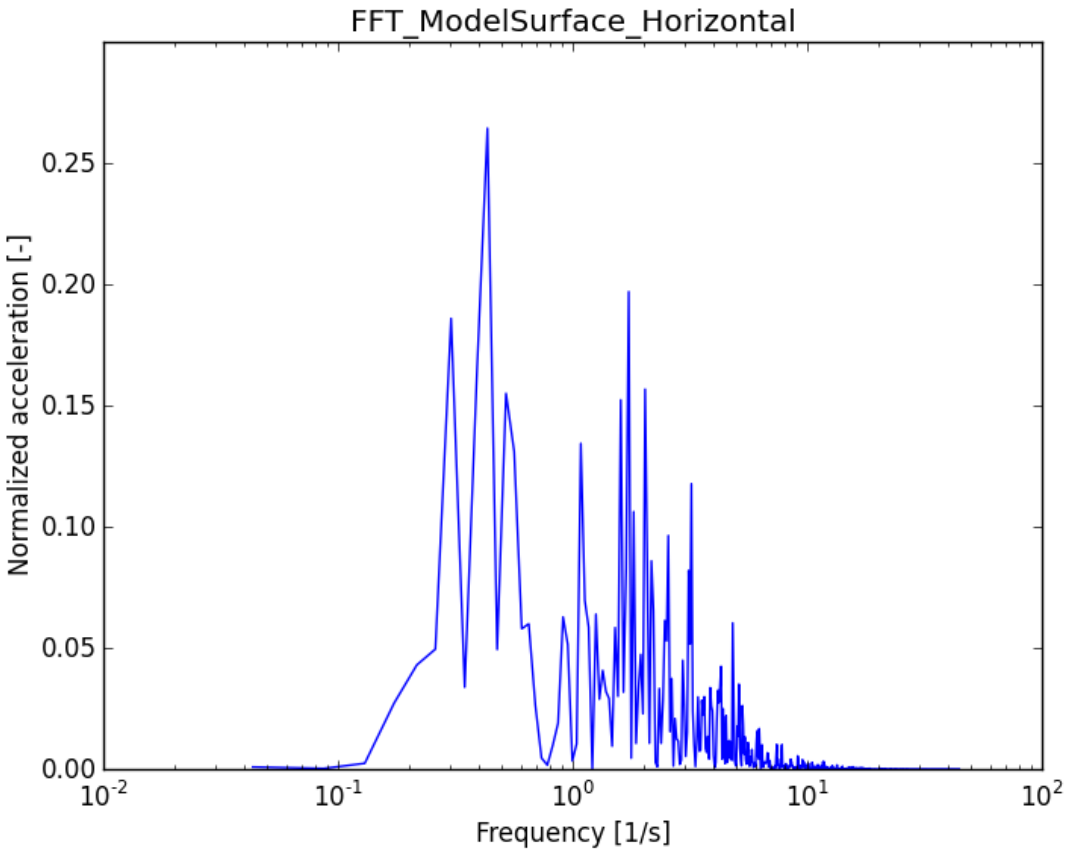

Figure 3-55 : Input of seismic signal – Fourier transform of horizontal acceleration measured at model surface

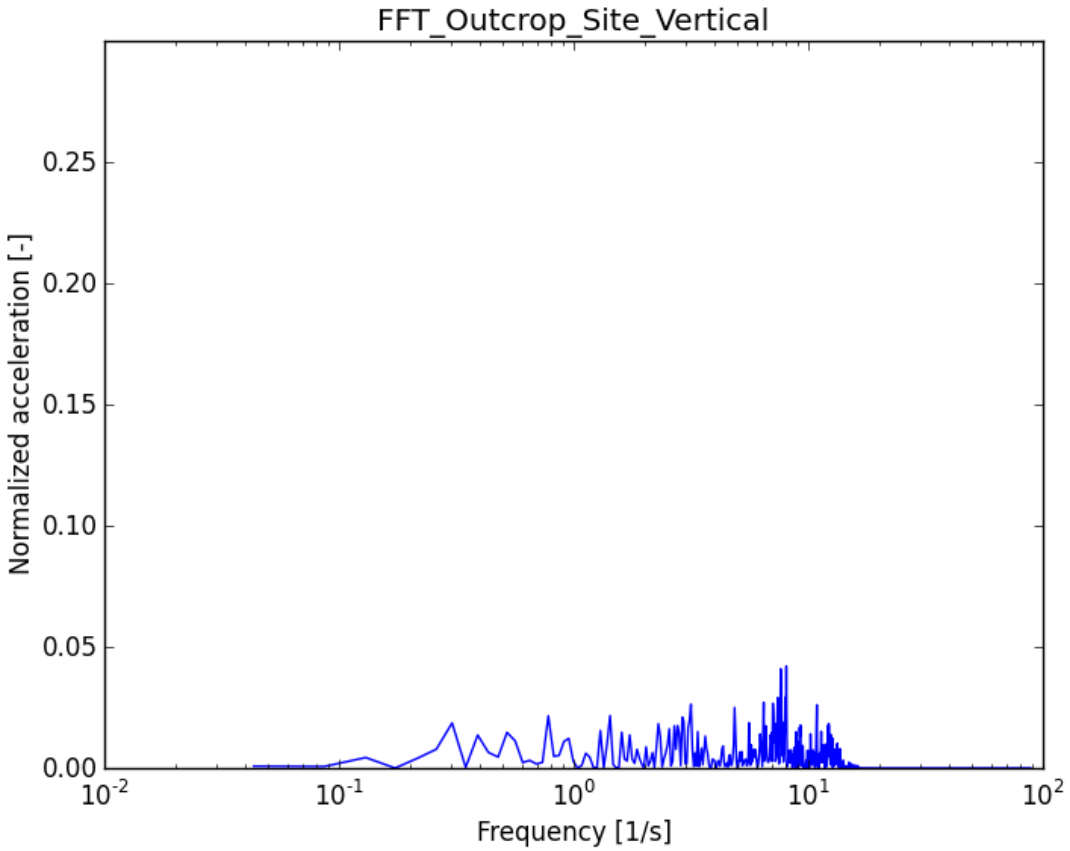

Figure 3-56 : Input of seismic signal – Fourier transform of outcrop vertical acceleration

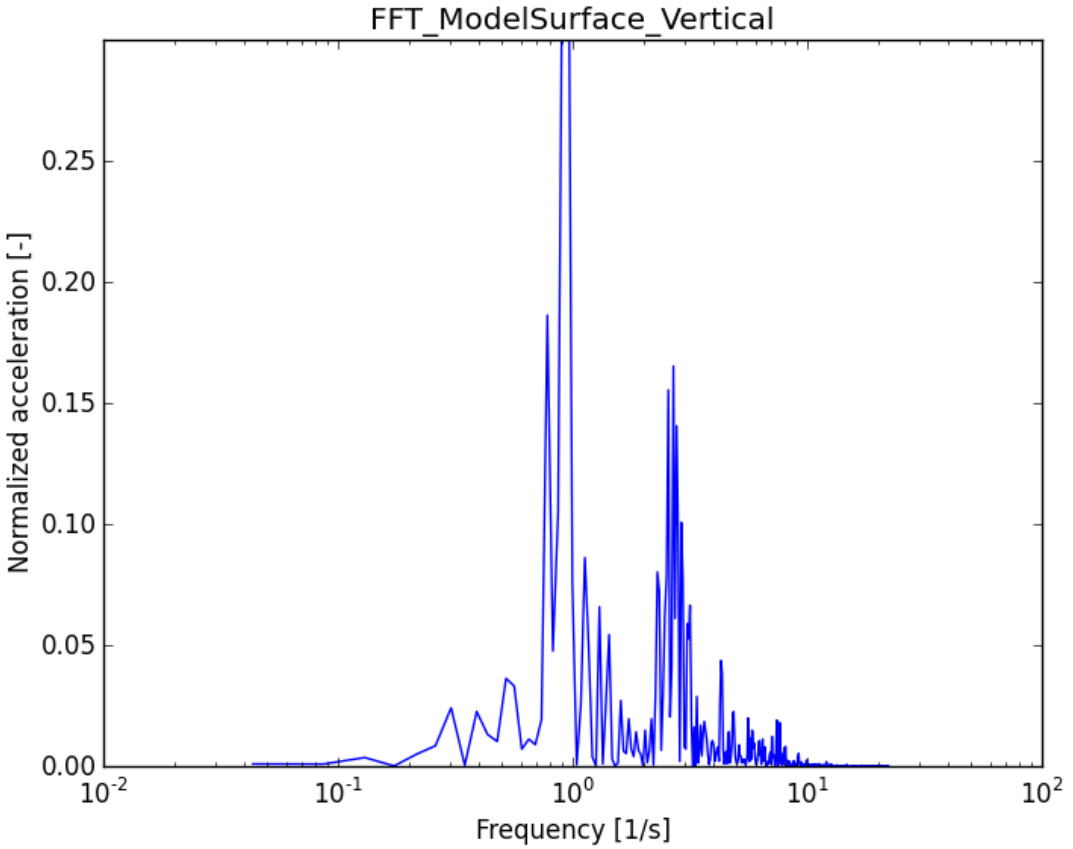

Figure 3-57 : Input of seismic signal – Fourier transform of vertical acceleration measured at model surface

3.6. Program of simulations

As mentioned in the introduction, two different dam-foundation profiles were studied.

The first profile, labeled “Reference Cross Section”, is an idealized profile of the foundation layers (perfectly horizontal layering). The dam profile, whose geometry will be detailed in the next section, aims at limiting differential horizontal displacements of the dam core. One important design constraint is related to the need of a deep cast in place wall, below the dam core, for controlling leakage through the foundation. This wall goes down to the bedrock. Such a wall can withstand only limited differential horizontal displacements after its construction. This is not a matter of earthquake behavior, but of displacements between the wall construction and the end of construction of the dam itself.
The quasi-static simulation of the reference cross section serves to validate the construction sequence, by checking such horizontal displacements. Note that the cast in place wall is not explicitly modeled.

The second profile that is tested, labeled “Real Cross Section”, is characterized by a more realistic foundation profile, according to the geological conditions of the Bisri site. The dam profile slightly differs from the *reference* case, to ensure a more stable behavior during dynamic loading.

A detailed comparison of the final results between the *reference* and the *real* cases will be presented.

4. REFERENCE CROSS SECTION

4.1. The geometry

The layout of the dam-foundation system is presented in Figure 4-1. As introduced in section 3.5, a 180 meters-thick, elastic, bedrock layer is placed at the base of the soil foundation. The latter has a total depth of 120 meters, and is made of (as introduced in section 2):

- A layer of alluvial sand ("A1_Alluv_Sand"), thickness = 15 meters;
- A layer of alluvial clayey silt ("A2_ClayeySilt"), thickness = 70 meters;
- A layer of alluvial gravel ("A3_Alluv_Gravel"), thickness = 35 meters.

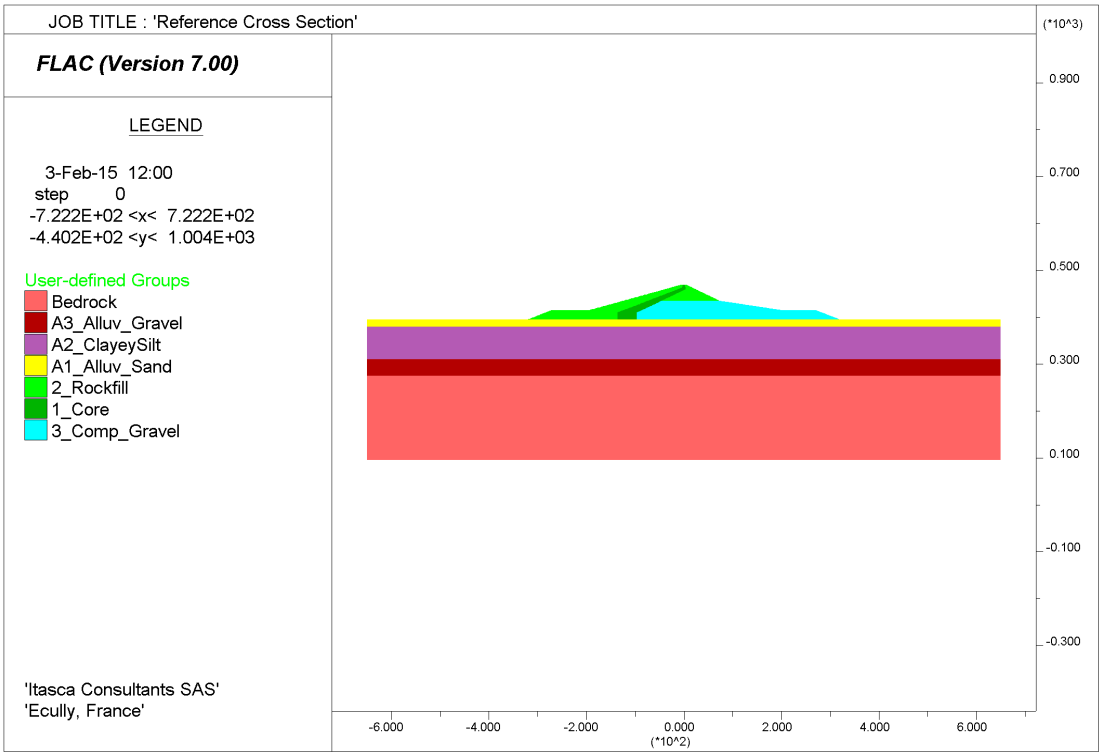

Figure 4-1 : Reference cross section – Layout

The embankment is 70 meters-high, and more than 600 meters-wide. It is made of:

- The dam clay core (label "1_Core");
- The rockfill, which is placed upstream and near the crest of dam on the downstream ("2_Rockfill");
- The compacted gravel, which is positioned along on the downstream ("3_Comp_Gravel").

A zoomed view on the embankment is given on Figure 4-2. Also, the position of the concrete wall is represented in blue in the same figure. Notably, the concrete wall goes from the base of the dam core, down to the top of the bedrock layer. The concrete wall is not introduced in the model. However, a special attention is given to horizontal displacements in this zone, to prevent any distress of the concrete wall due to dam construction. This approach is clearly conservative.

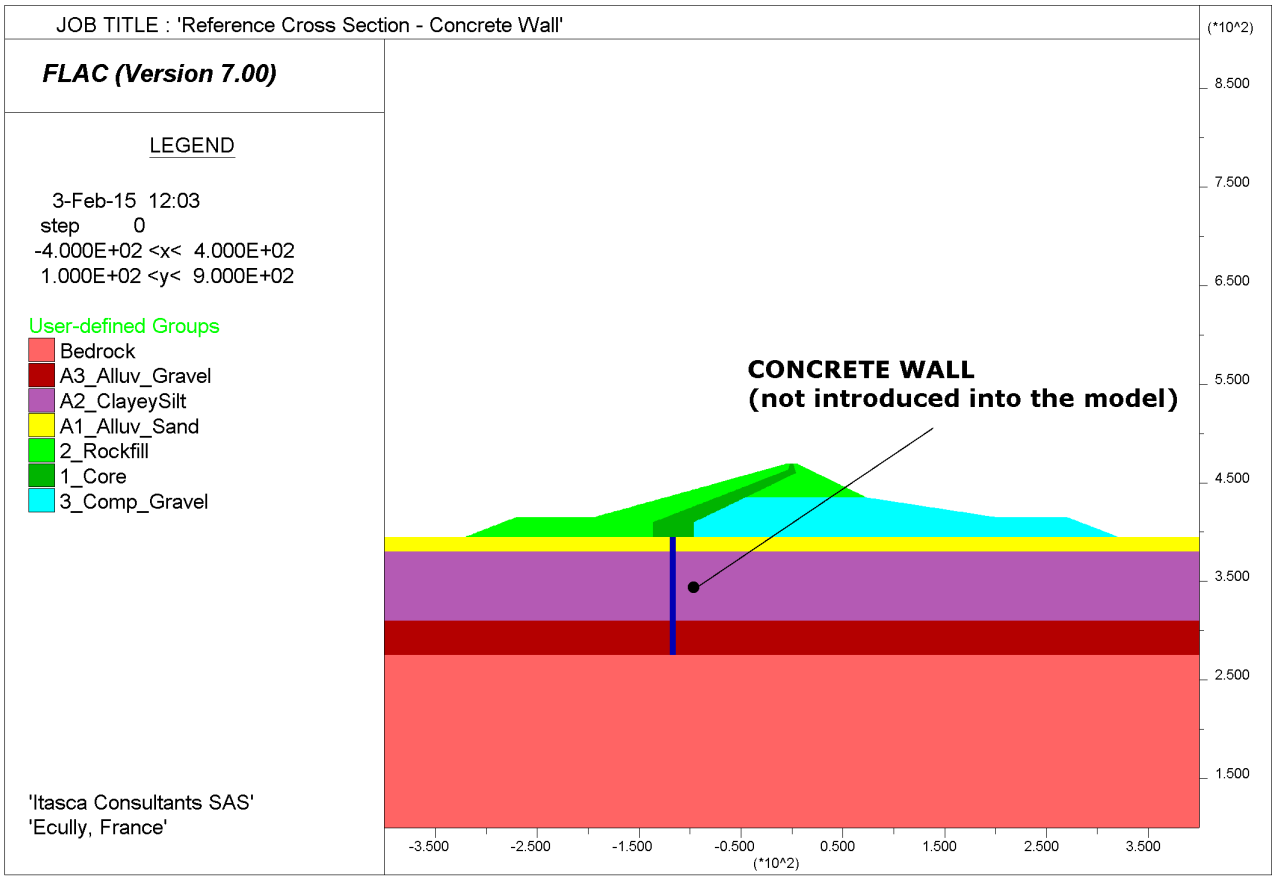

Figure 4-2 : Reference cross section – Concrete wall

4.2. Mechanical properties

As described in section 3.2.1, a nonlinear-elastic Mohr-Coulomb model is used to model the whole soil structure. The bedrock layer is assumed to be elastic. For the dam and the foundation materials, a variation of the Young's modulus with the confining stress is assumed.

Figure 4-3 and Figure 4-4 show the values of friction angle and dilatancy (see section 3.1.1).

Figure 4-5 and Figure 4-6 show the profiles of bulk modulus and shear modulus, respectively, for the soil foundation layers. These profiles refer to the foundation prior to the construction of the embankment. However, the soil layers are assumed to be consolidated.

The evolution of the confining stress, and its consequences on the value of bulk and shear moduli, is taken into account during the construction of the embankment and the reservoir filling on the upstream.

It is worth noticing, as already mentioned in section 3.1.2, that the multiplication factor (= 3) for the computation of the values of the dynamic maximum shear modulus ($G_{max,dyn}$) and dynamic bulk modulus, was estimated on the base of the values of Figure 4-5 and Figure 4-6, since the information on shear wave velocity of soil foundation layers refers to the condition prior the construction of the embankment.

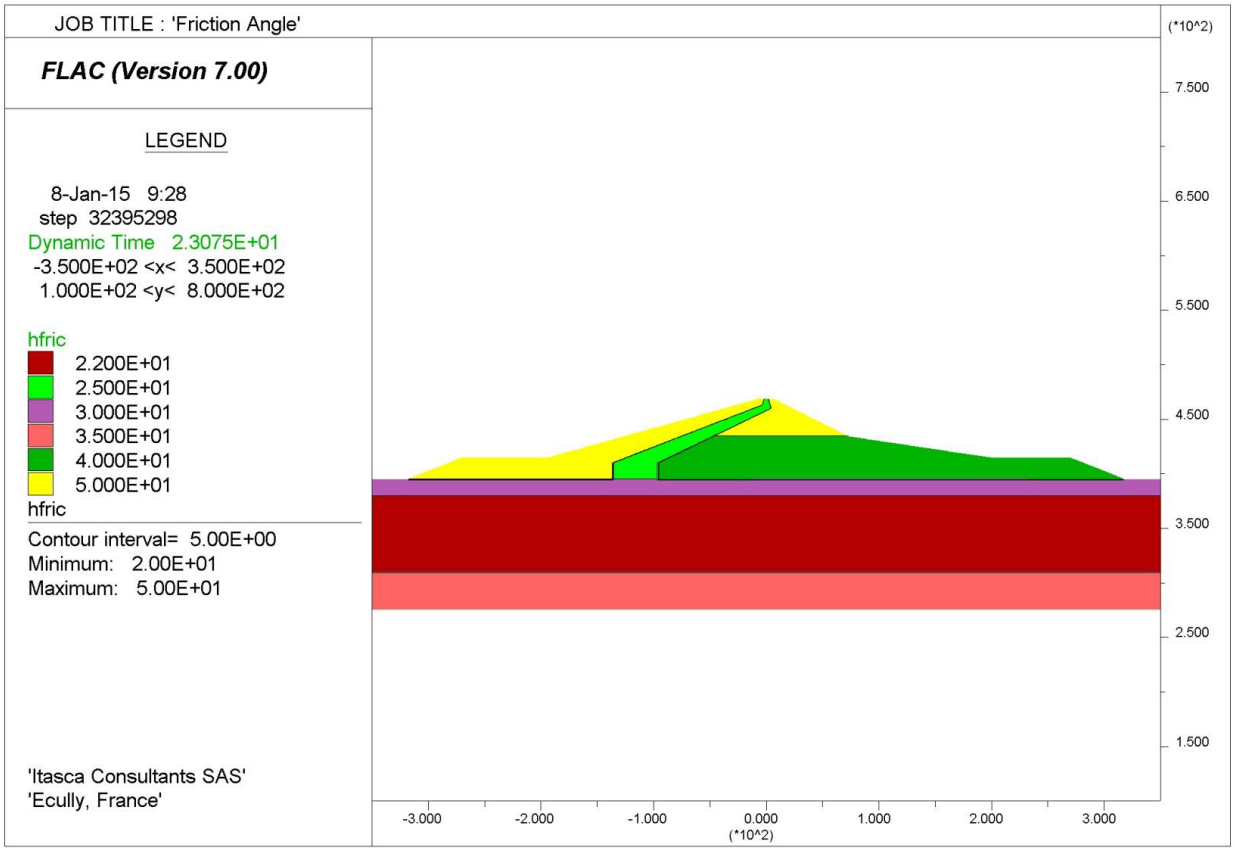

Figure 4-3 : friction angle of the soil foundation and the embankment

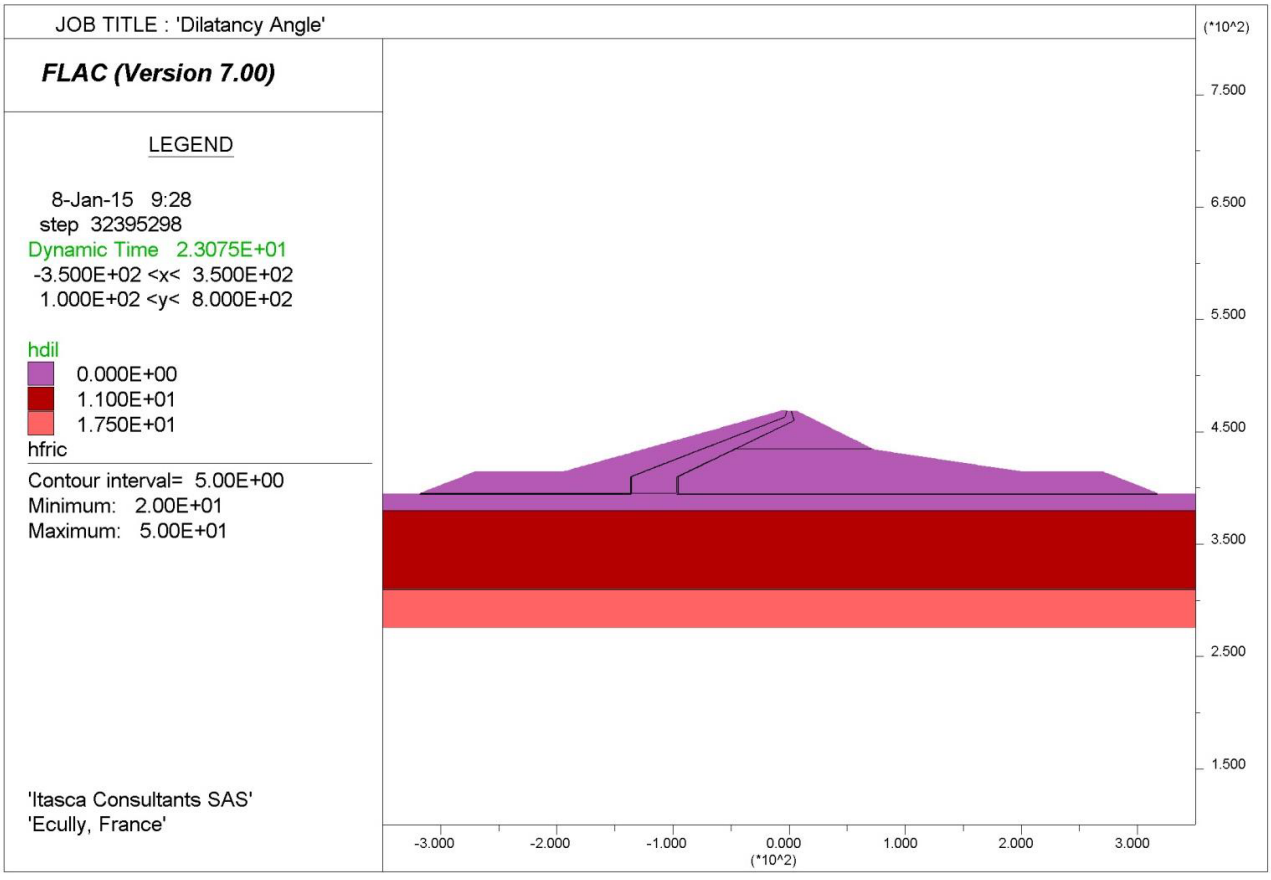

Figure 4-4 : dilatancy of the soil foundation and the embankment

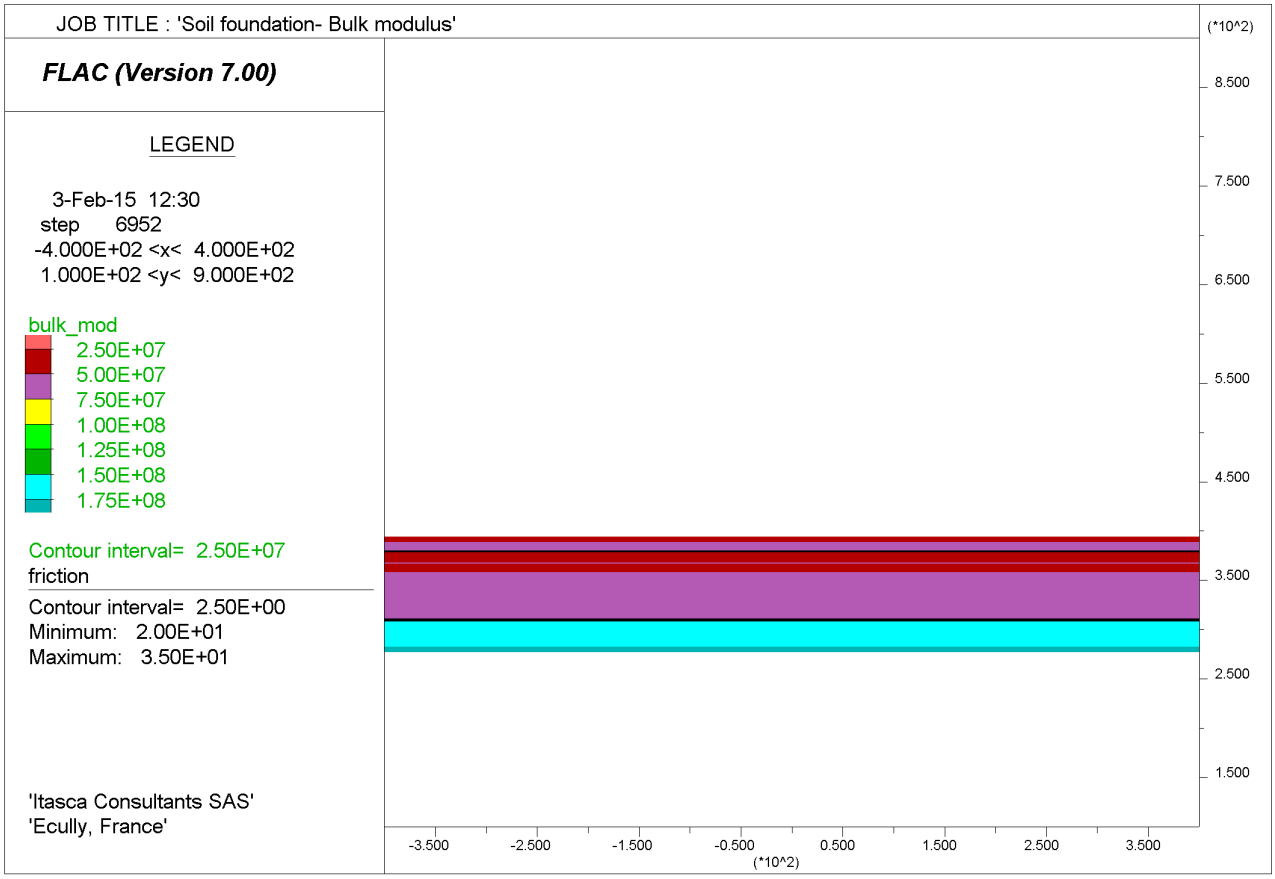

Figure 4-5 : bulk modulus of soil foundation layers (consolidated)

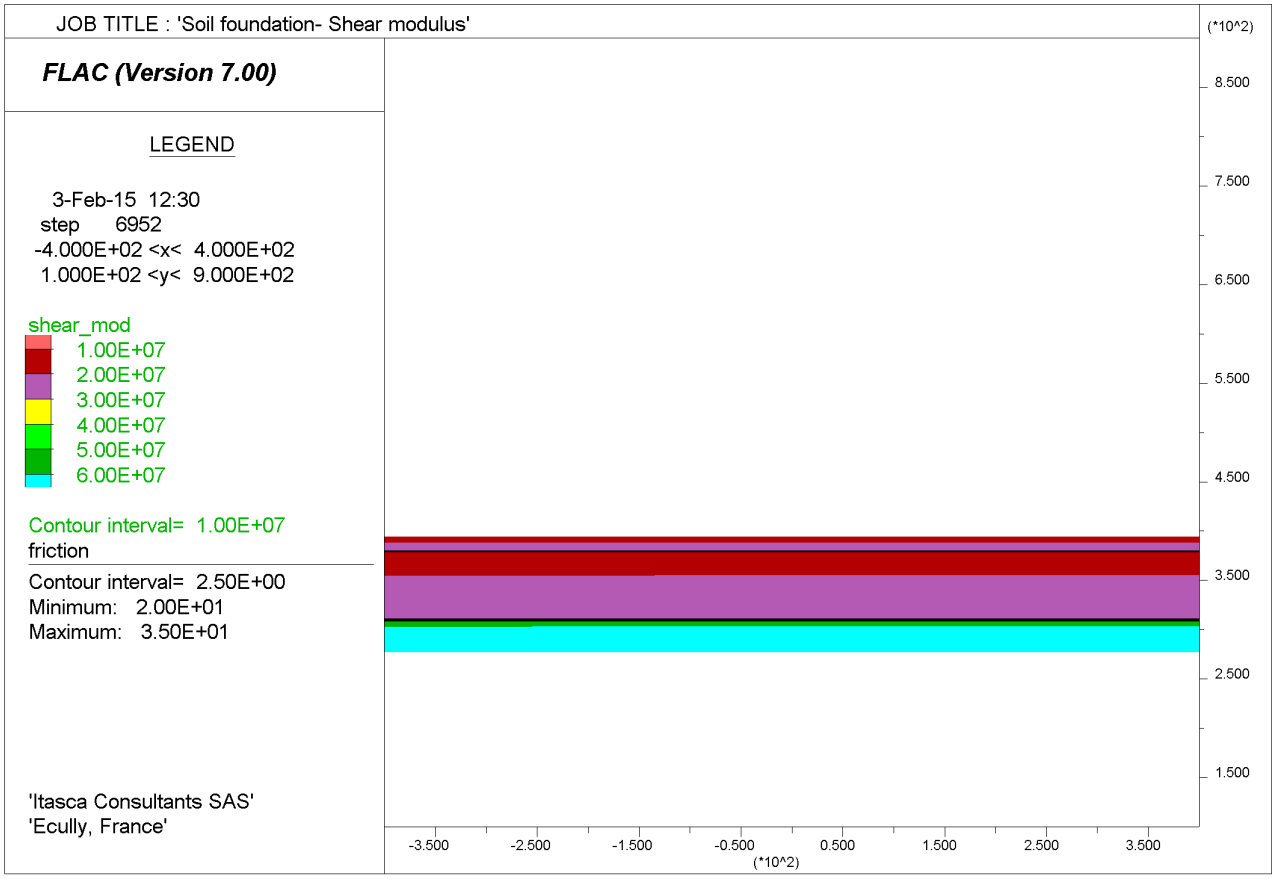

Figure 4-6: shear modulus of soil foundation layers (consolidated)

4.3. Hydraulic properties

The phreatic surface is assumed to coincide with the soil surface, i.e. at elevation 395 meters, at this stage and all along the construction of the embankment. Figure 4-7 shows the pore pressures profile.

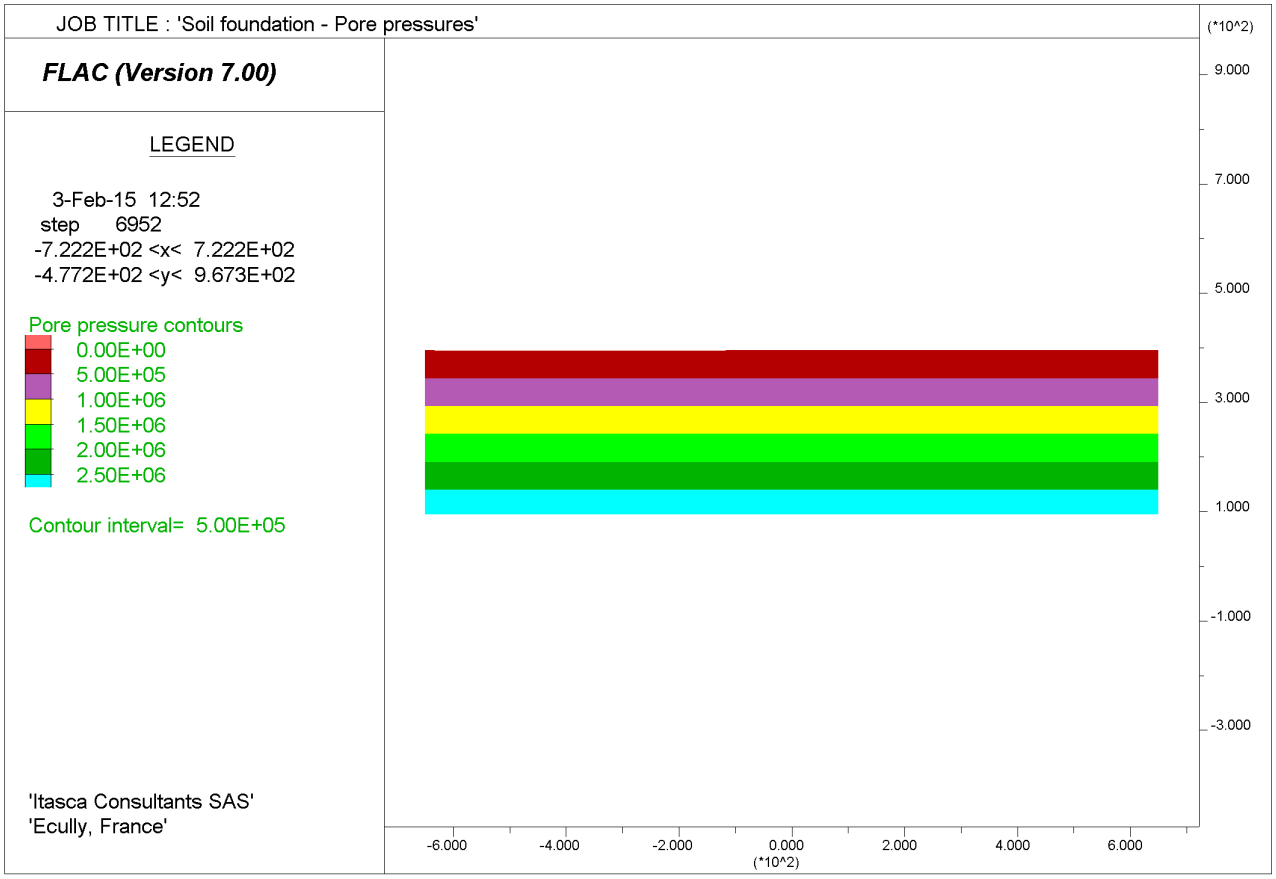

Figure 4-7 : embankment foundation – pore pressures profile (water level at the surface)

4.4. Stress initialization

Effective stresses are initialized using the following expressions:

$$\sigma'_{yy}(y) = (\gamma_{sat} - \gamma_w) \cdot y = \gamma' \cdot y \qquad (12)$$

$$\sigma'_{xx}(y) = k_0 \cdot \sigma'_{yy}(y) \qquad (13)$$

$$\sigma'_{zz}(y) = k_0 \cdot \sigma'_{yy}(y) \qquad (14)$$

The lateral earth pressure coefficient at rest, represented as K0, is assumed to be equal to 0.667 for the first 30 meters of foundation, since in this zone the compaction effects due to the construction of the embankment is assumed to be significant.

K0 = 0.5 below elevation 365 meters.

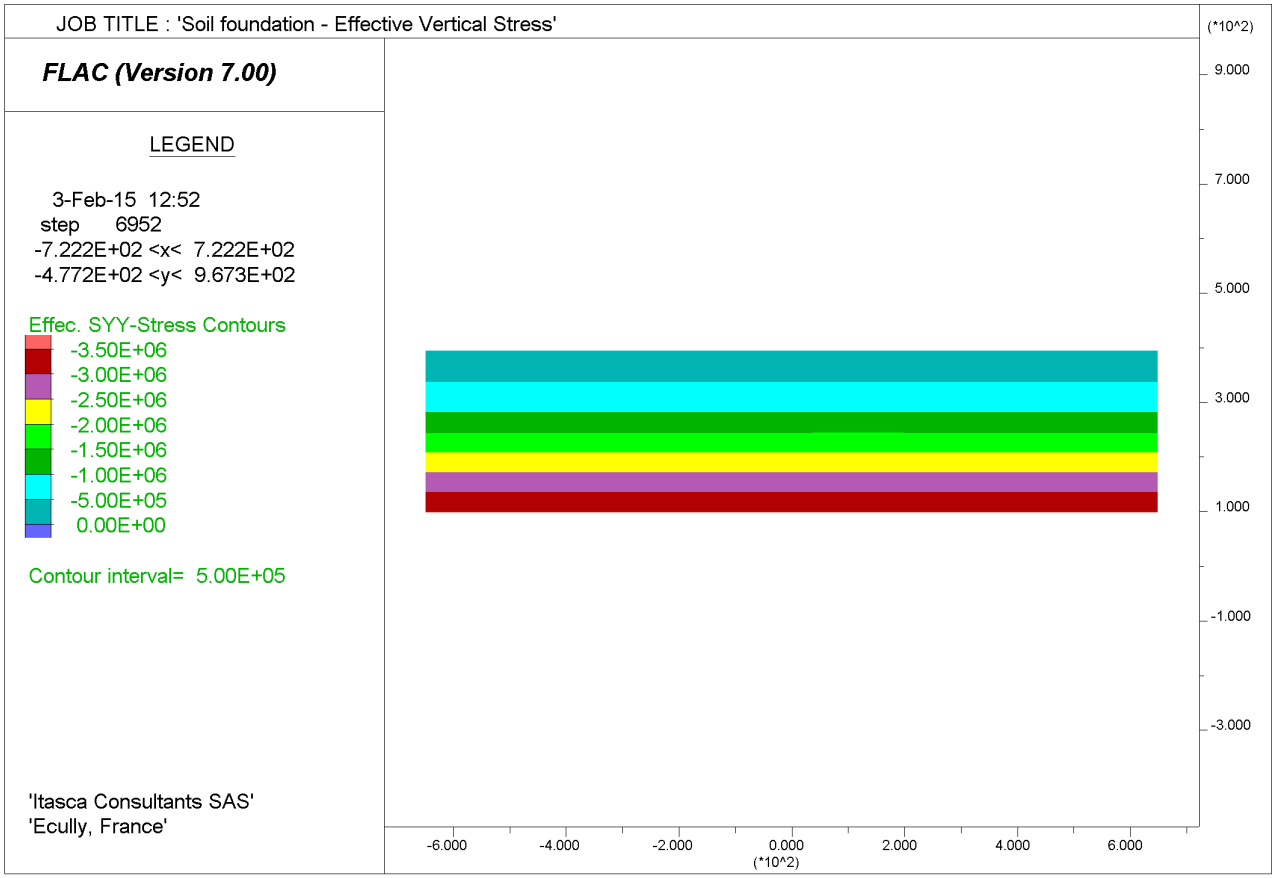

Figure 4-8 : effective vertical stress profile prior to the construction of the embankment

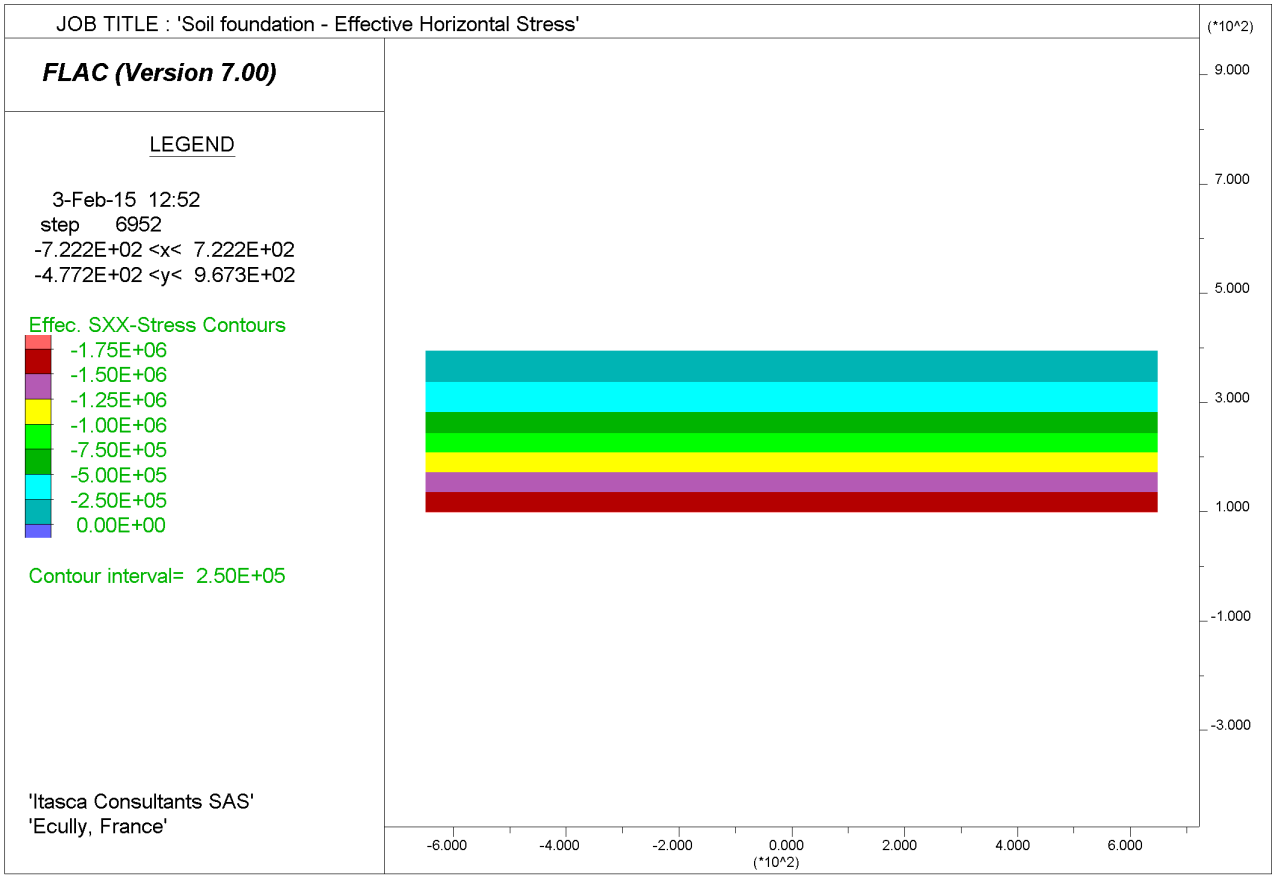

Figure 4-9: effective horizontal stress profile prior to the construction of the embankment

4.5. Simulation of embankment construction

In this section the simulation of the construction of the embankment is presented. The phases of construction, as they were communicated by NOVEC, are presented in this section. The evolution of horizontal and vertical displacement associated to each phase of construction, with special attention to horizontal displacements at the position of the concrete wall, will be detailed.

Three phases of construction of the embankment are forecasted:

- Phase 1 (Figure 4-10): layering (12 steps) of downstream compacted gravel (group "3_Comp_Gravel") and rockfill (group "2_Rockfill") up to elevation 462 meters;
- Phase 2 (Figure 4-11): layering (12 steps) of dam core (group "1_Core") and upstream rockfill, up to elevation 462 meters;
- Phase 3 (Figure 4-12): layering (2 steps) of the dam crest, up to elevation 469 meters.

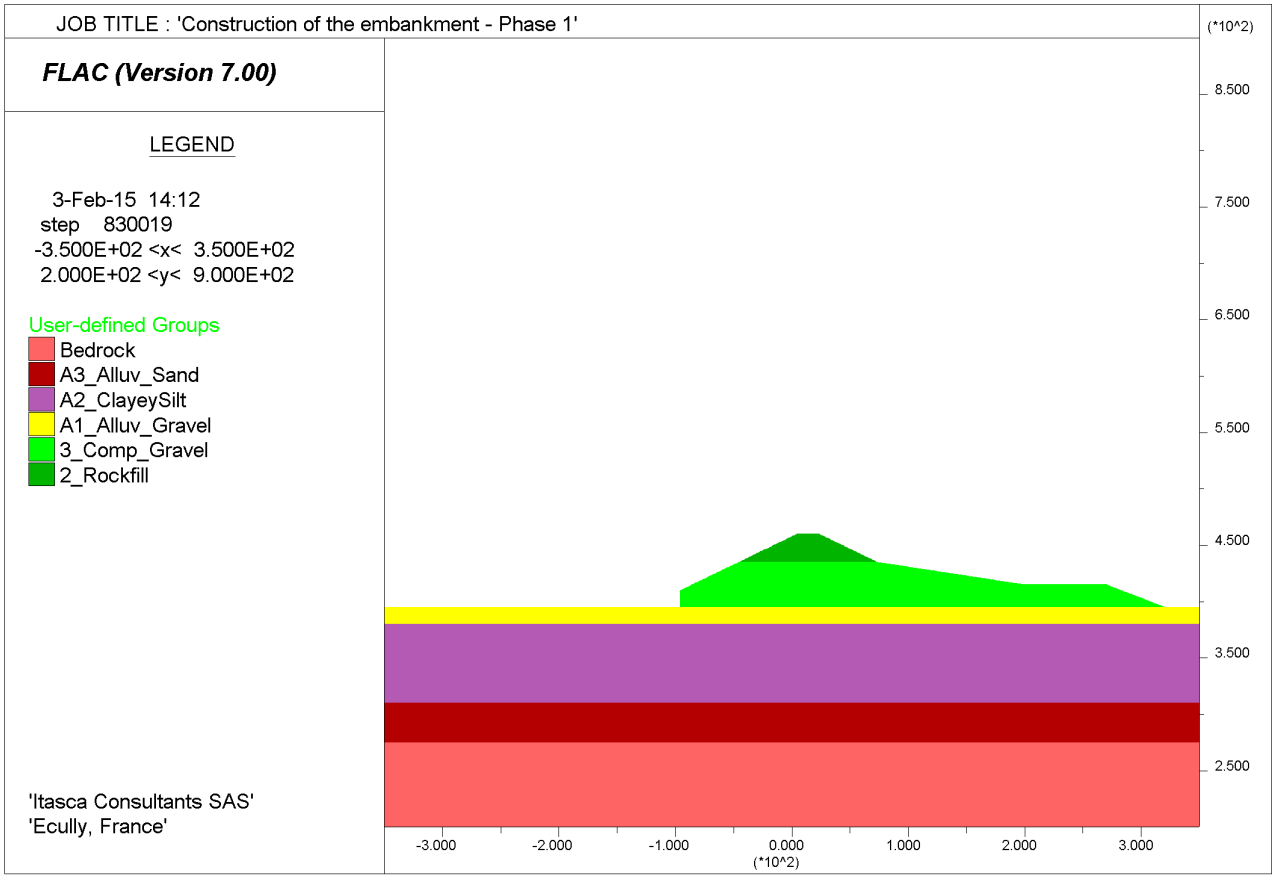

Figure 4-10 : Embankment construction – Phase 1

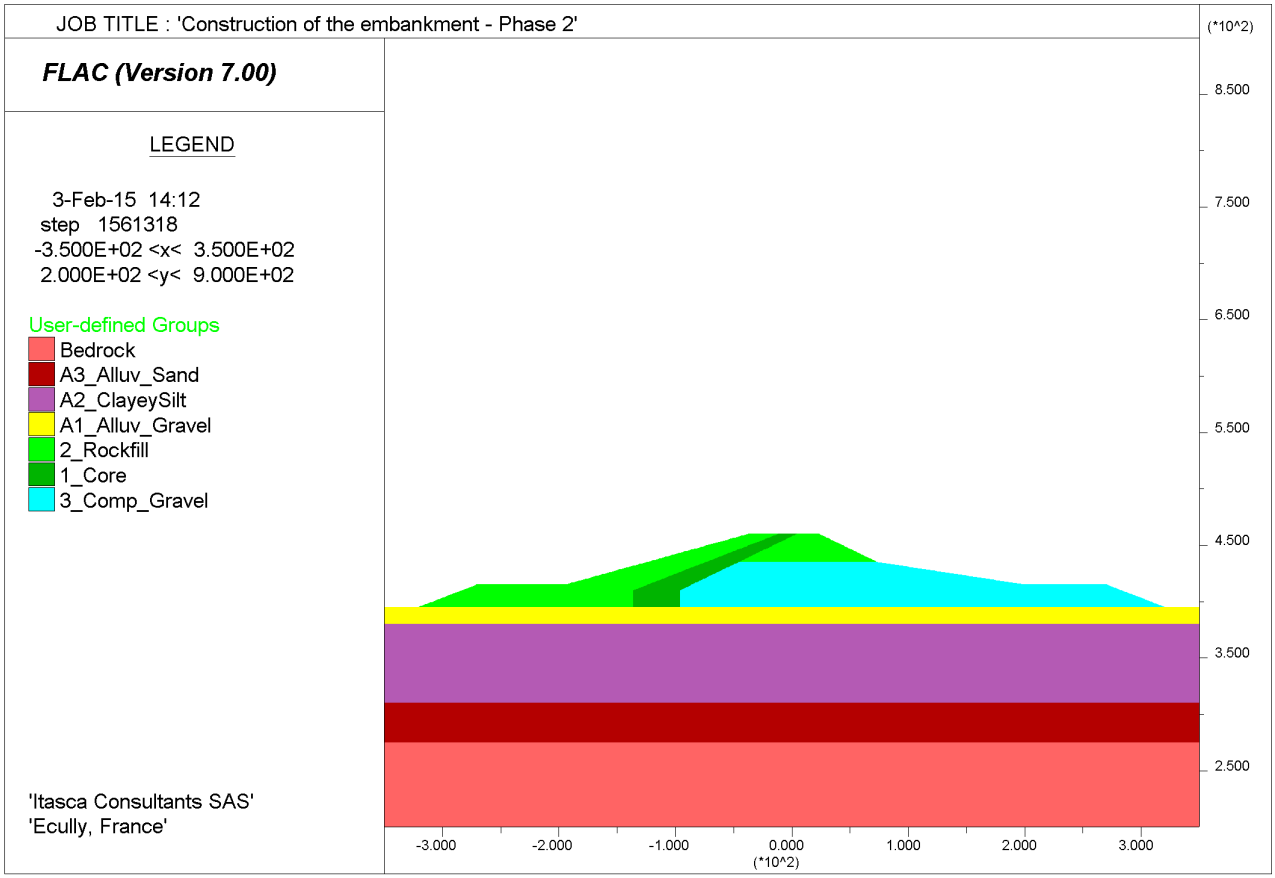

Figure 4-11: Embankment construction – Phase 2

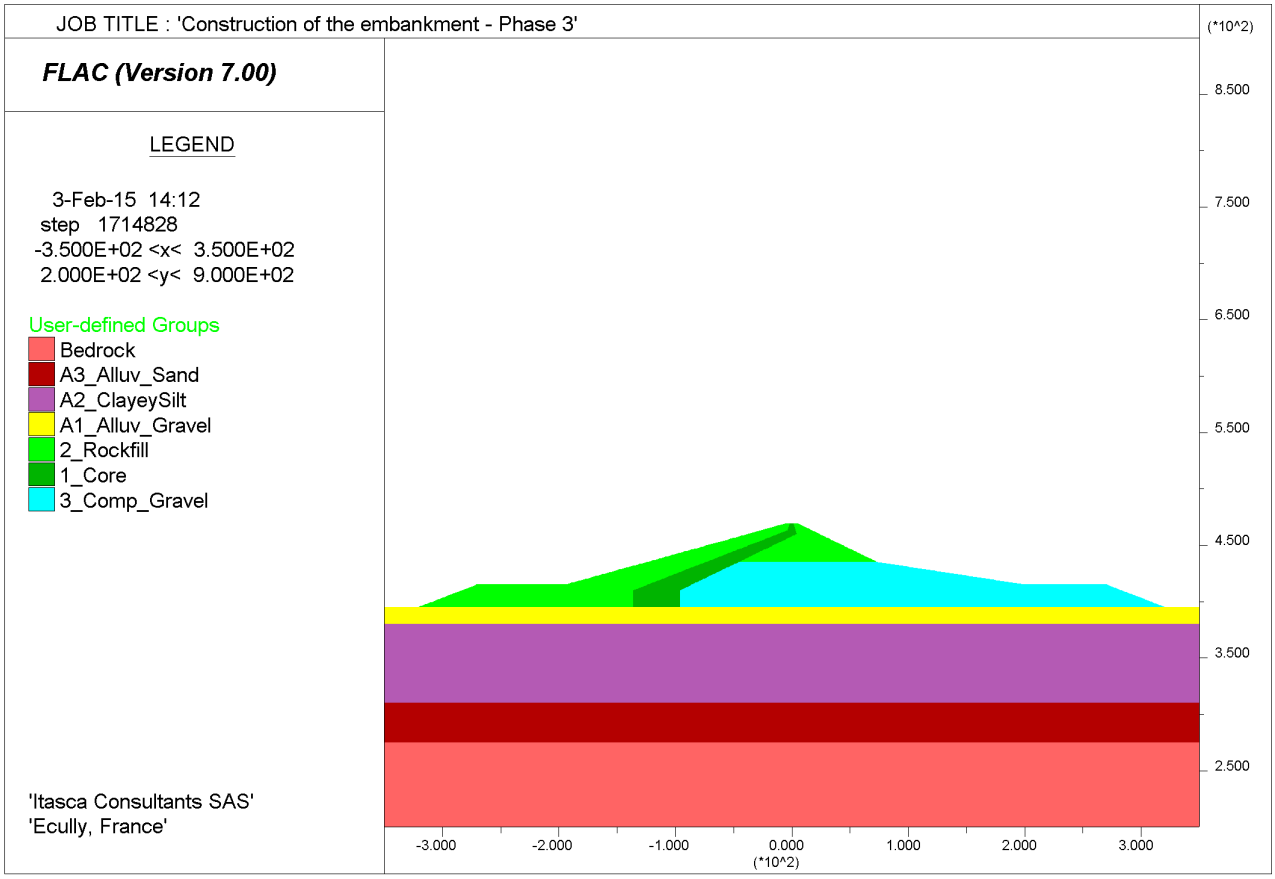

Figure 4-12: Embankment construction – Phase 3

4.5.1. Phase 1

The first phase (Phase 1) of embankment construction consists in the layering of downstream compacted gravel (group "3_Comp_Gravel") and rockfill (group "2_Rockfill") up to elevation 462 meters.

Figure 4-13 and Figure 4-14 show the horizontal and vertical displacements, respectively, at the end of this phase. It is worth noticing that the concrete wall is not placed yet at this stage. The intent, indeed, is that a large part of the horizontal displacements due to the construction of the embankment take place before the installation of the concrete wall.

The layering of layers of embankment was subdivided in 12 successive steps. The model is brought to equilibrium after the installation of each layer. This ensures that the simulation follows a realistic stress path.

The progressive installation of embankment layers is visible on Figure 4-15, where the horizontal displacements that are represented are measured at points 1 – 8 of Figure 4-16. It is recalled, to avoid all misunderstanding, that the concrete wall is not installed yet at this stage.

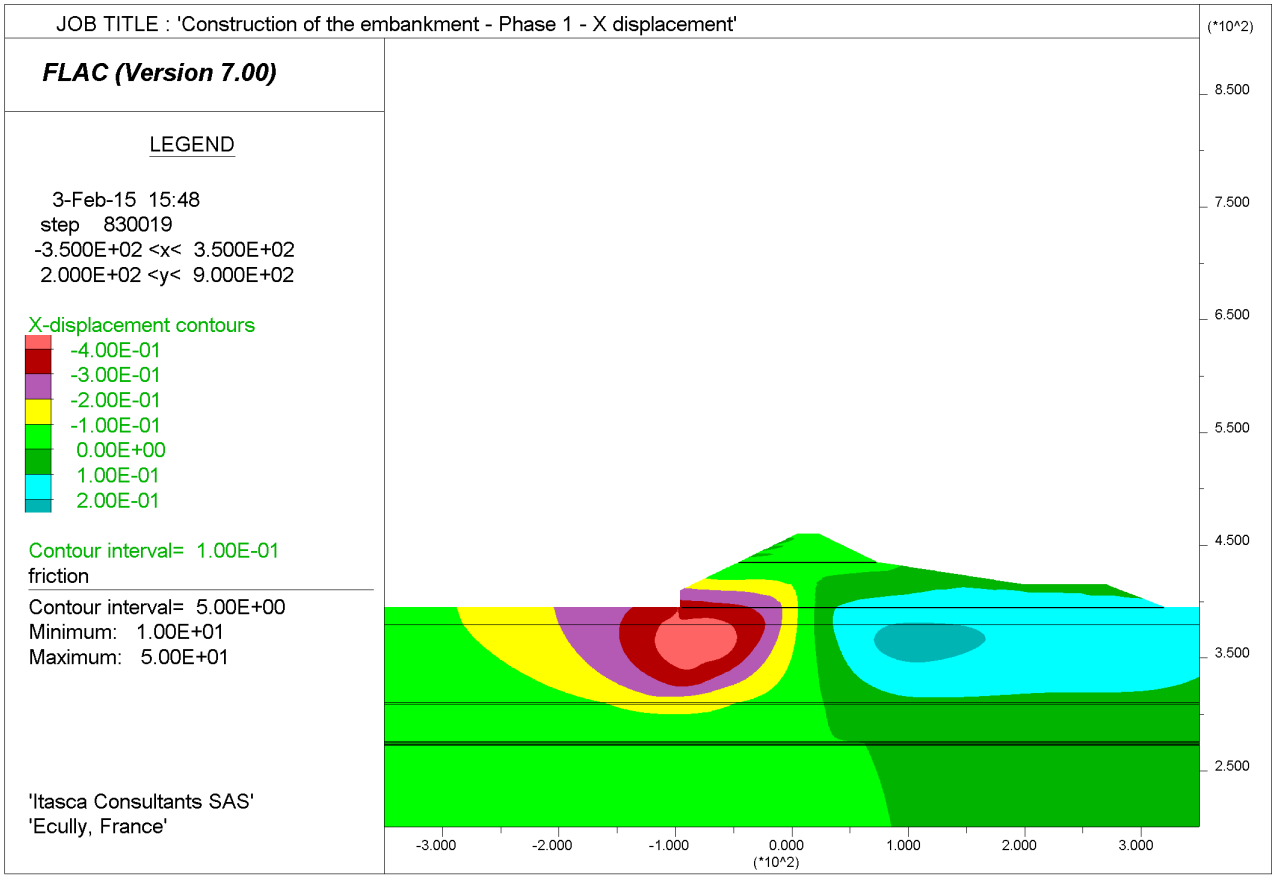

Figure 4-13 : Embankment construction – Phase 1 – Horizontal displacements

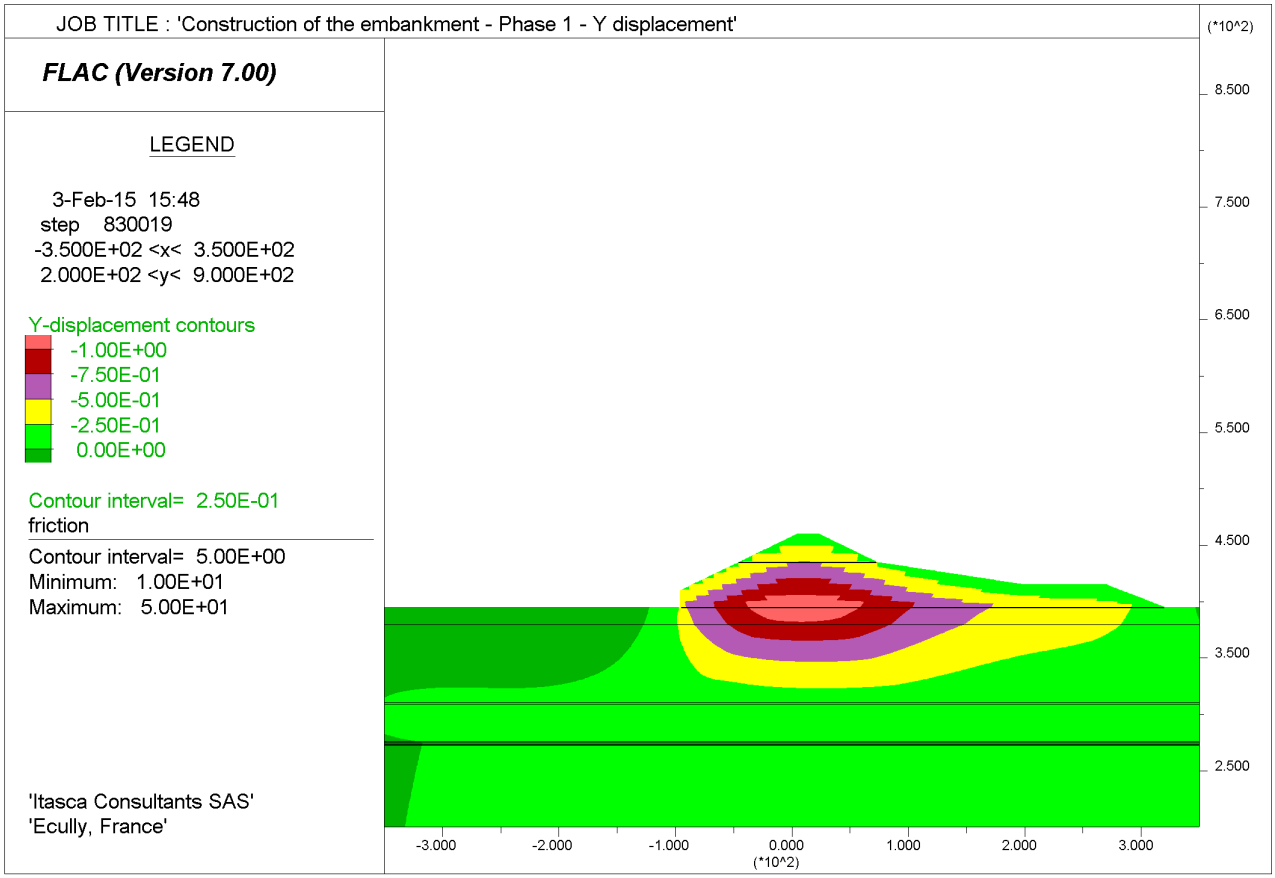

Figure 4-14: Embankment construction – Phase 1 – Vertical displacements

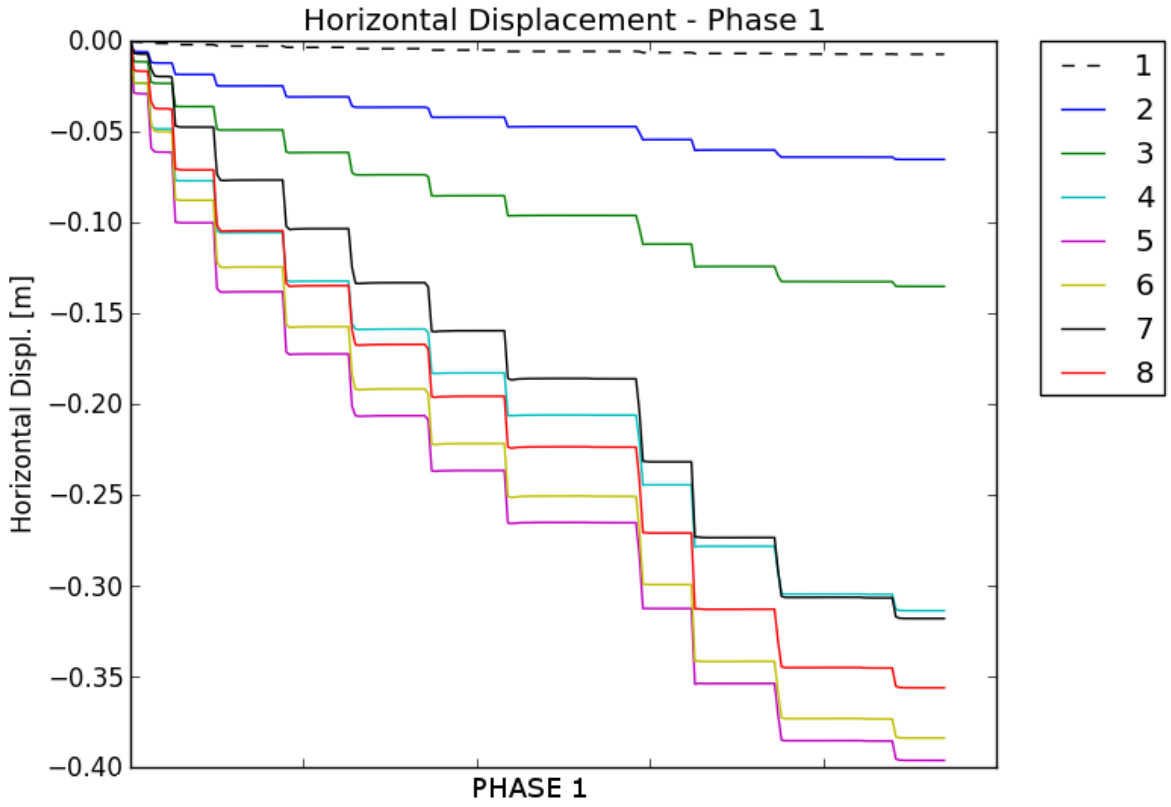

Figure 4-15 : Phase 1 - horizontal displacements measured at points 1-8 of Figure 4-16

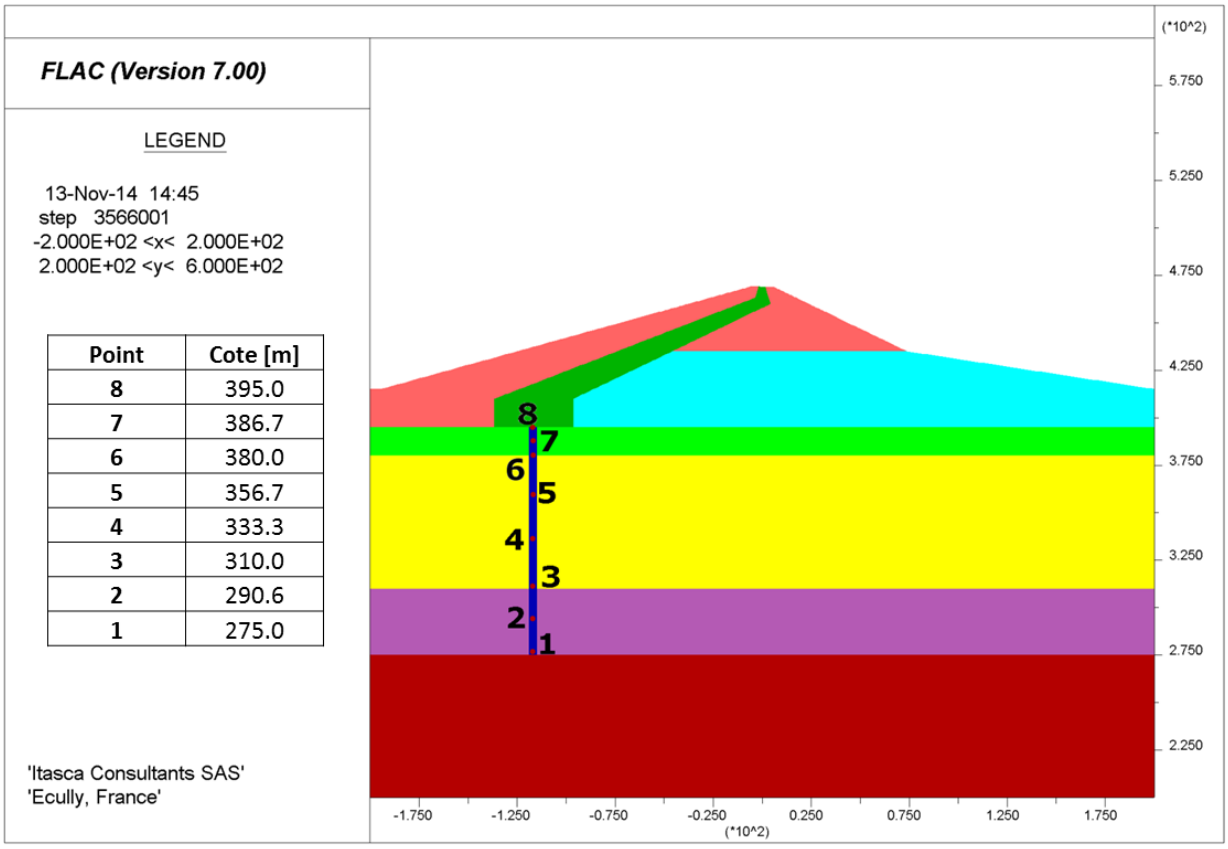

Figure 4-16 : virtual points of measurement of displacement (concrete wall is not modeled)

4.5.2. Phase 2

The second phase (Phase 2) of embankment construction consists in the layering (12 steps) of dam core (group "1_Core") and upstream rockfill, up to elevation 462 meters. The layering was subdivided in 12 successive steps. The model is brought to equilibrium after the installation of each layer.

Figure 4-17 and Figure 4-18 show the horizontal and vertical displacements, respectively, at the end of this phase.

The concrete wall is assumed to be installed before this phase. The induced extra horizontal displacements are therefore of interest to analyze the eventual occurrence of incompatible differential displacements which could damage it. Figure 4-19 shows the horizontal displacements, measured at the virtual points of Figure 4-16, with a differential displacement of 10cm at maximum between points 4 and 8, i.e. over a length of 61.7m.

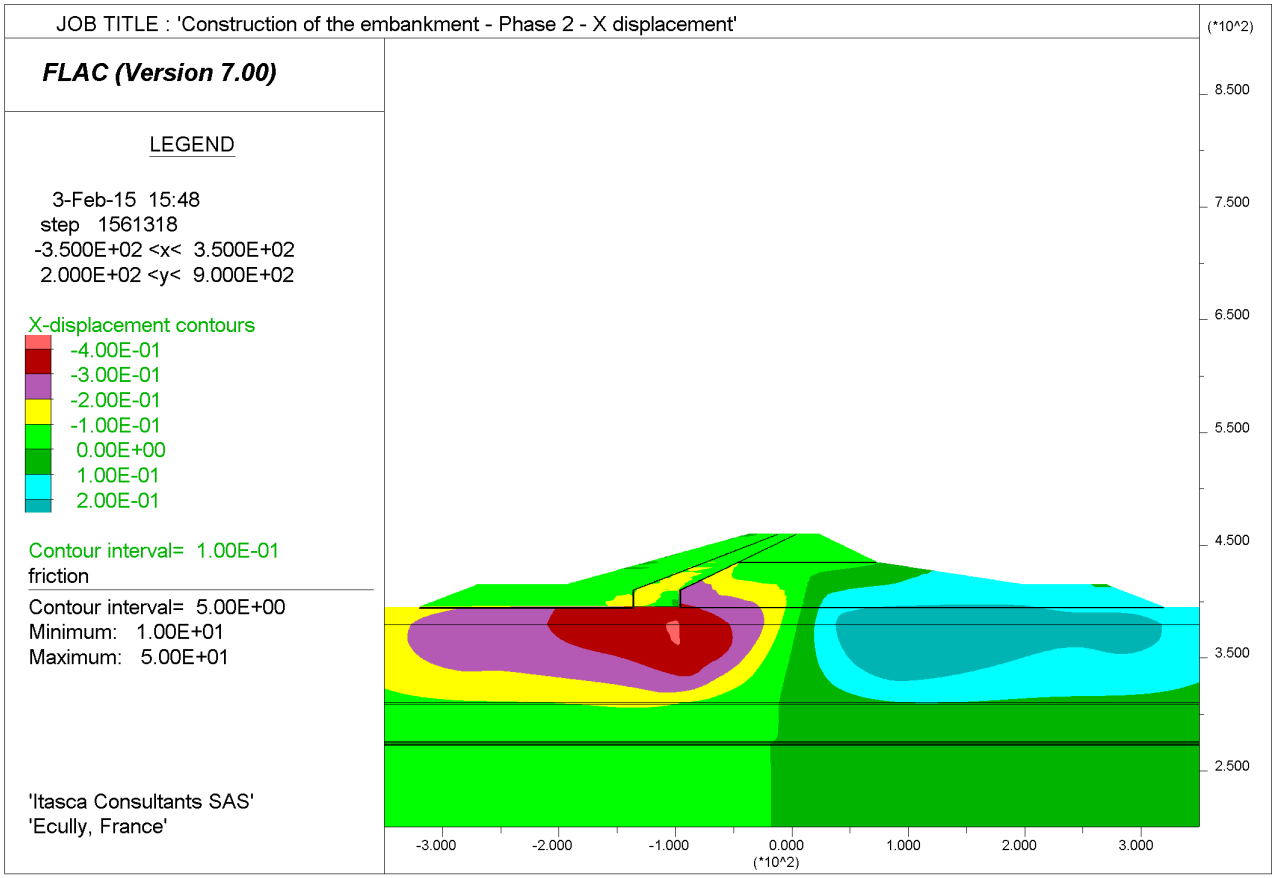

Figure 4-17 : Embankment construction – Phase 2 – Horizontal displacements

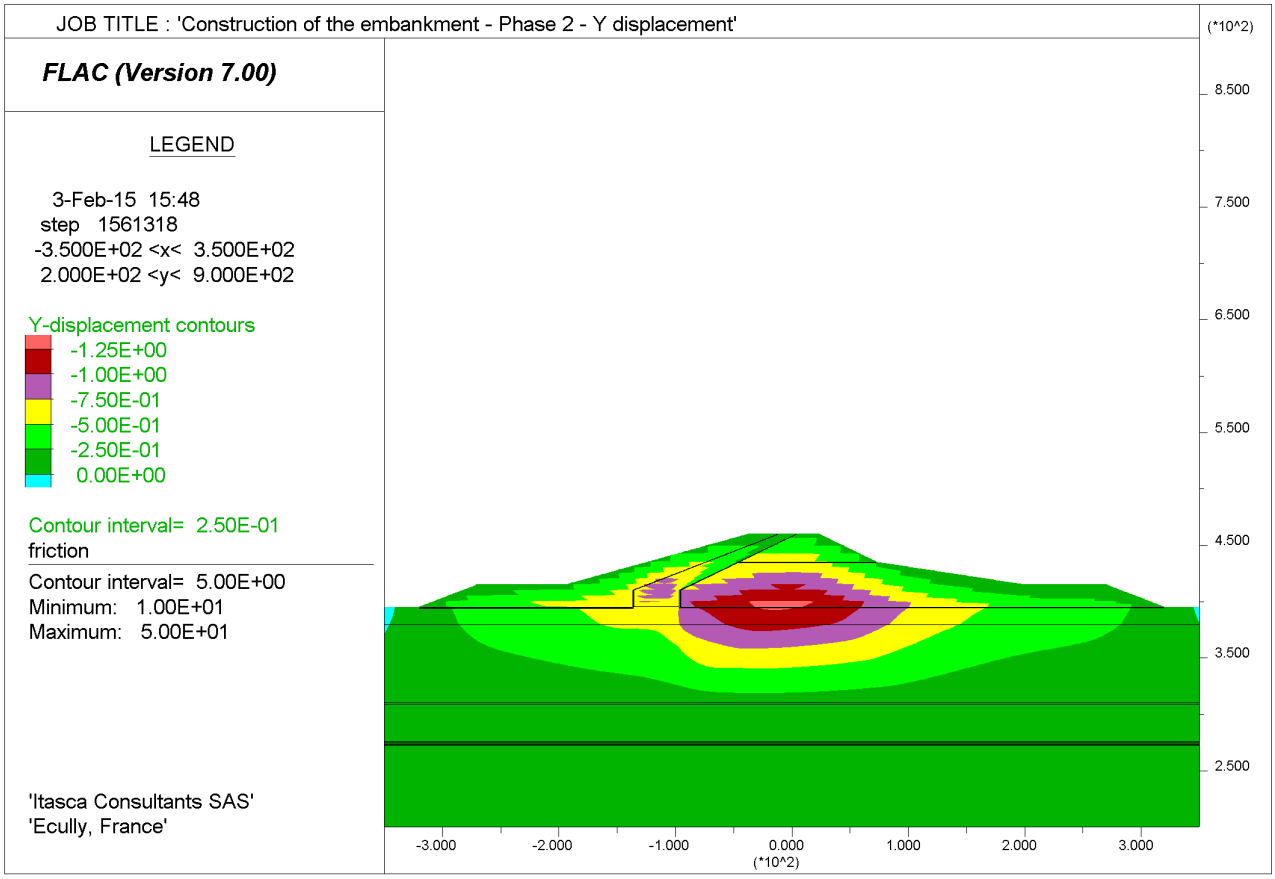

Figure 4-18: Embankment construction – Phase 2 – Vertical displacements

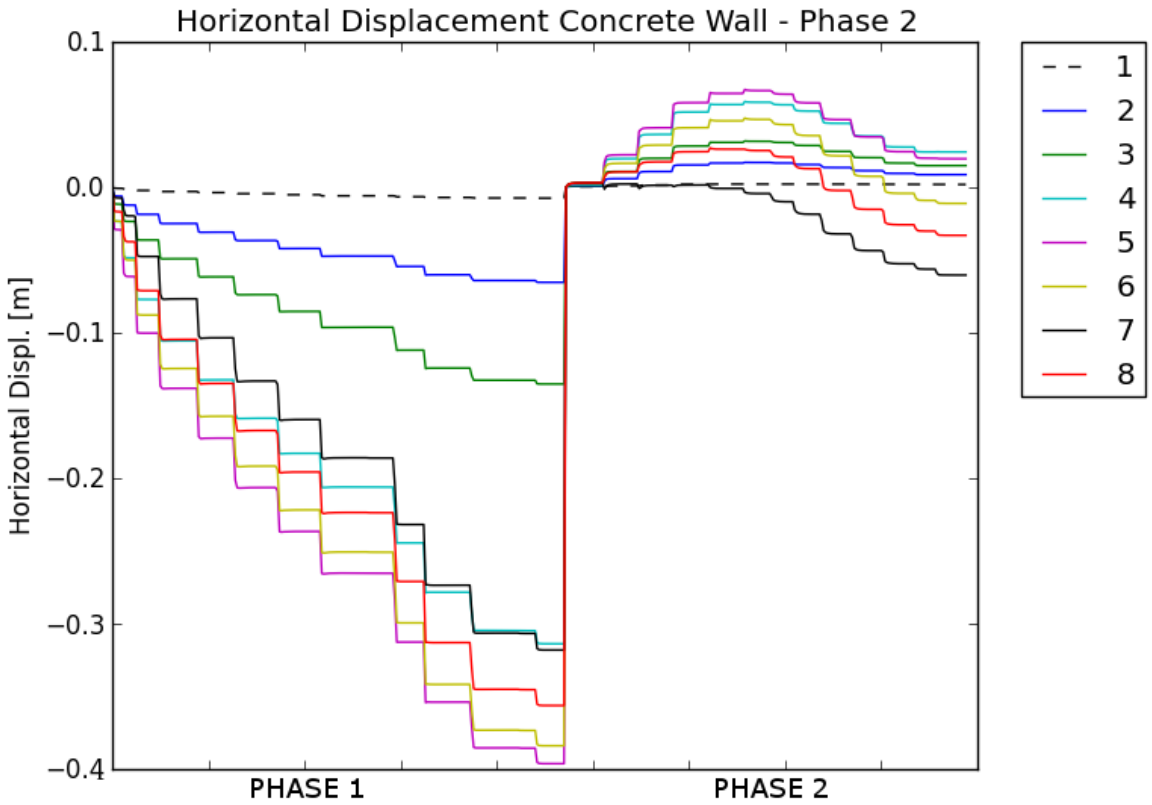

Figure 4-19 : Phase 2 - horizontal displacements measured at points 1-8 of Figure 4-16

4.5.3. Phase 3 – End of embankment construction

The third phase (Phase 3) of embankment construction consists in the layering (2 steps) of dam crest, up to elevation 469 meters.

Figure 4-20 and Figure 4-21 show the horizontal and vertical displacements, respectively, at the end of this phase. The maximum final vertical displacement, at the base of the dam and in the central axis, is about 1.25 meters.

The induced horizontal displacements of the concrete wall, after the installation of the dam crest, do not evolve significantly, as shown on Figure 4-22.

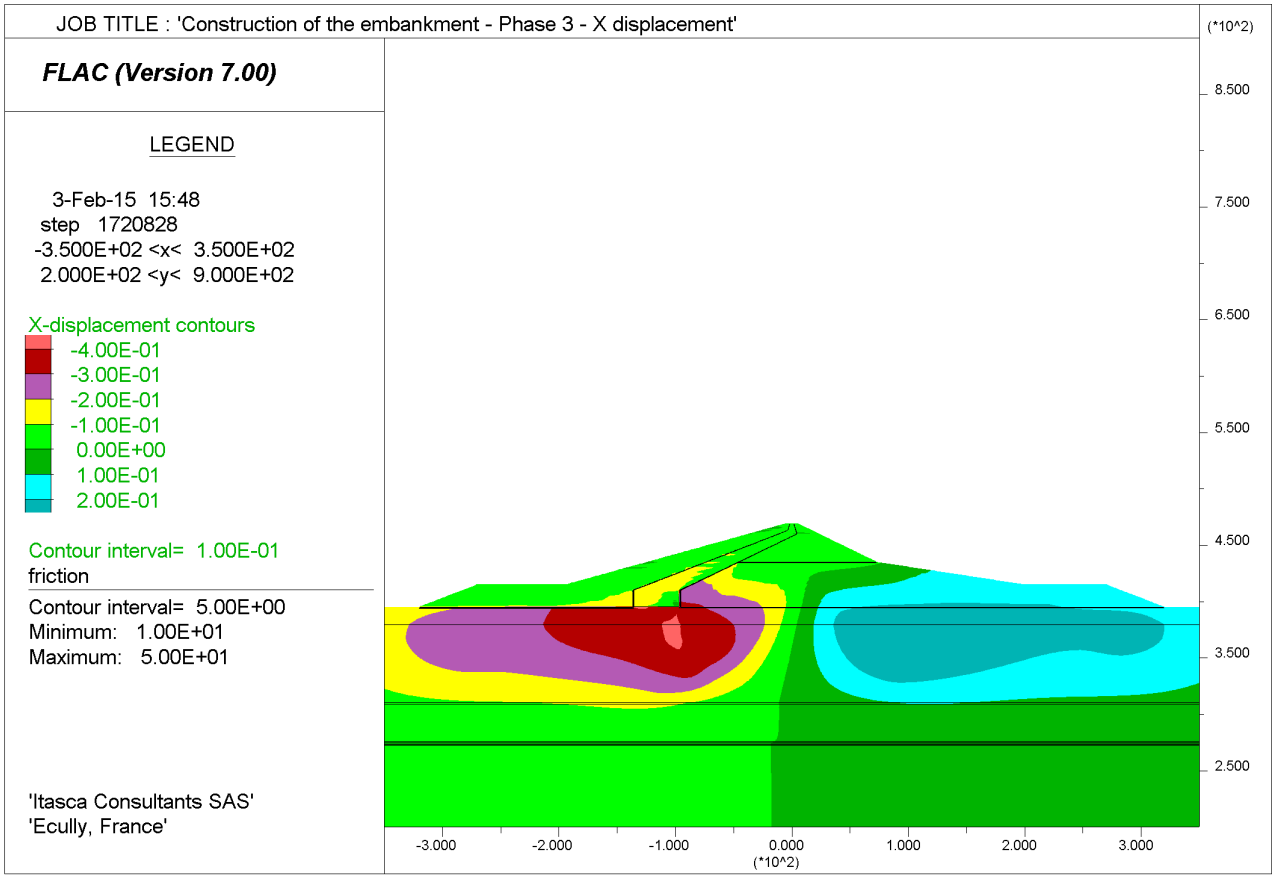

Figure 4-20 : Embankment construction – Phase 3 – Horizontal displacements

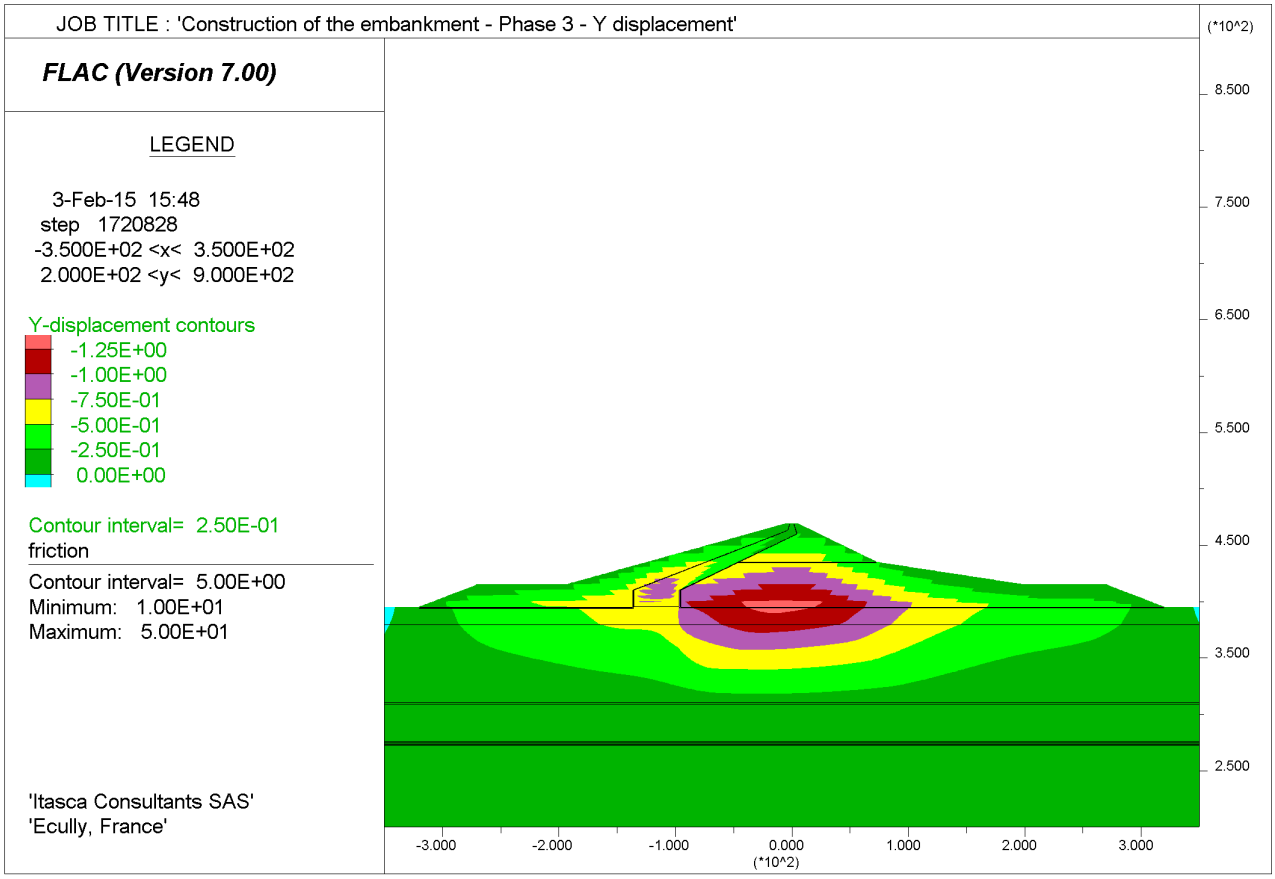

Figure 4-21 : Embankment construction – Phase 3 – Vertical displacements

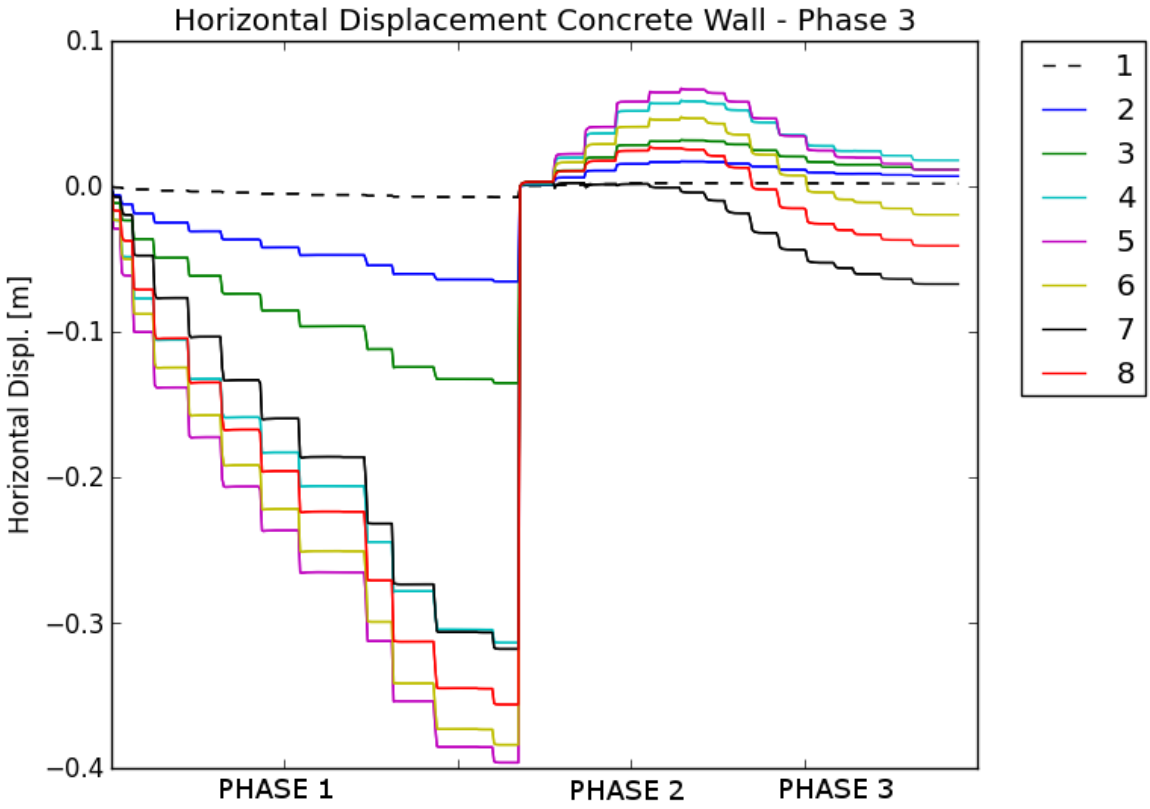

Figure 4-22 : Phase 3 - horizontal displacements measured at points 1-8 of Figure 4-16

4.5.4. Reservoir filling

After the construction of the embankment, the water level is raised on the upstream side, up to elevation 462 meters, which is supposed to be the maximum reservoir level. The rising is gradual and performed in 8 steps.

Figure 4-23 shows the final pore pressure profile at the end of this phase. The pore pressure profile will be maintained in this state all along the dynamic simulation (as mentioned in section 3.2.2, no pore pressure generation is allowed during the dynamic simulation).

Figure 4-24 shows a detail of the pore pressure profile in the embankment: the water is assumed to be perfectly drained by the rockfill and the compacted gravel. Therefore, the phreatic surface follows the interface between the dam core and the rockfill/compacted gravel, and continues along the base of the dam at the downstream.

Figure 4-25 and Figure 4-26 show the final profiles for horizontal and vertical displacements. Figure 4-27 and Figure 4-28 show the final profiles of the effective vertical and horizontal stresses, respectively.

Figure 4-29 shows the evolution of horizontal displacements at points 1 – 8 of Figure 4-16. The 8 steps of advancement of the rising water level can easily be recognized. The final relative horizontal displacement is around 0.35 meters between points 1 and 6, i.e. over a length of 105 meters.

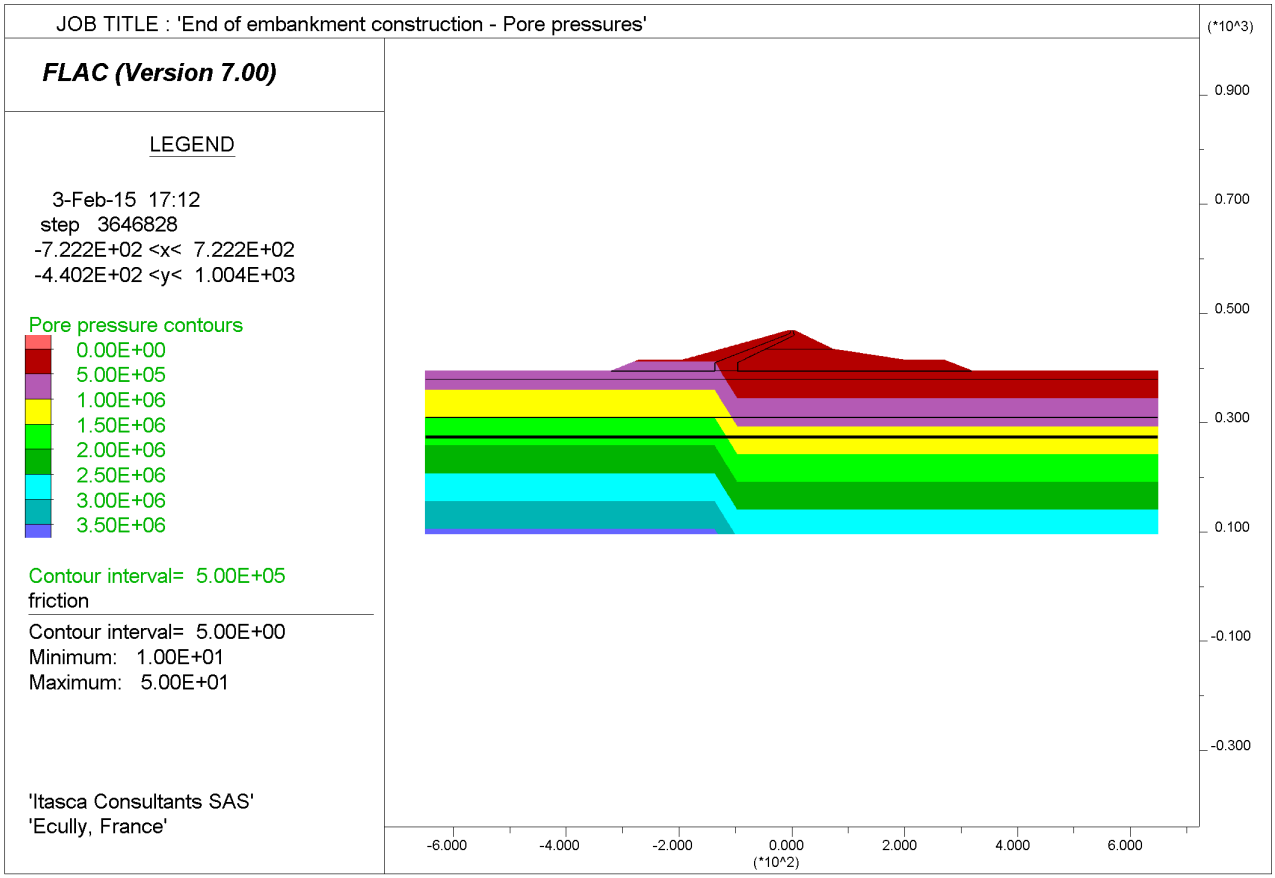

Figure 4-23 : upstream water filling – final pore pressure profile

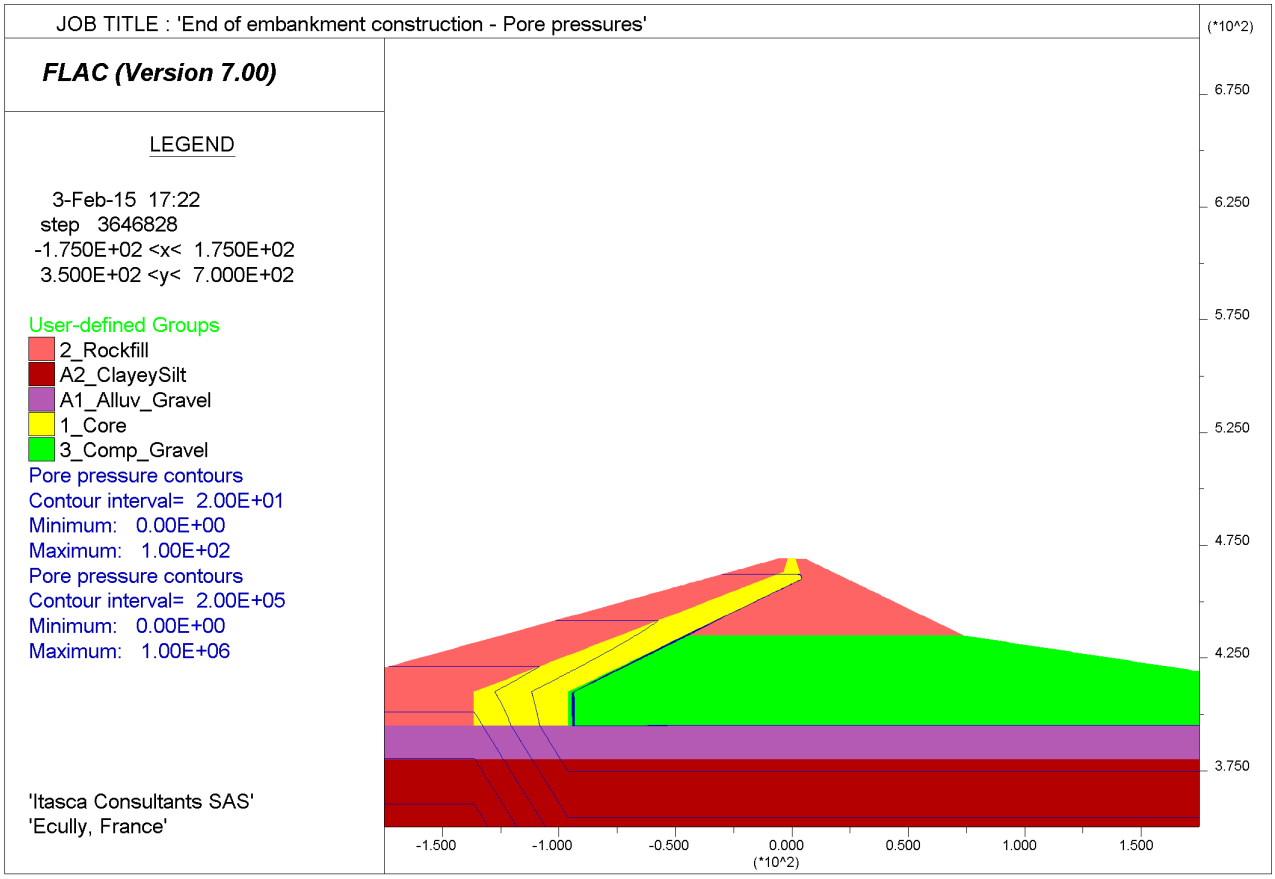

Figure 4-24 : upstream water filling – detail of pore pressure profile on dam core

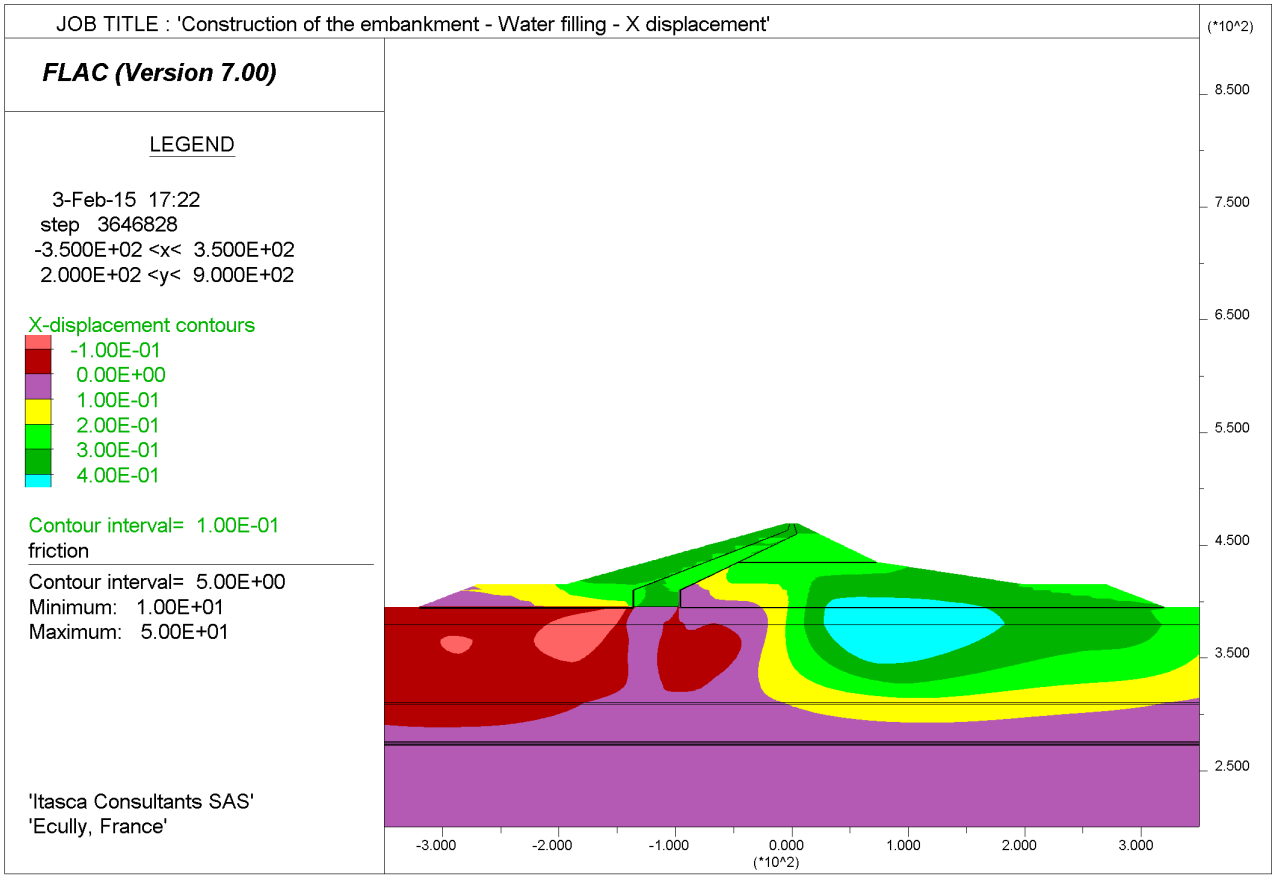

Figure 4-25 : embankment construction and upstream water filling – final horizontal displacements

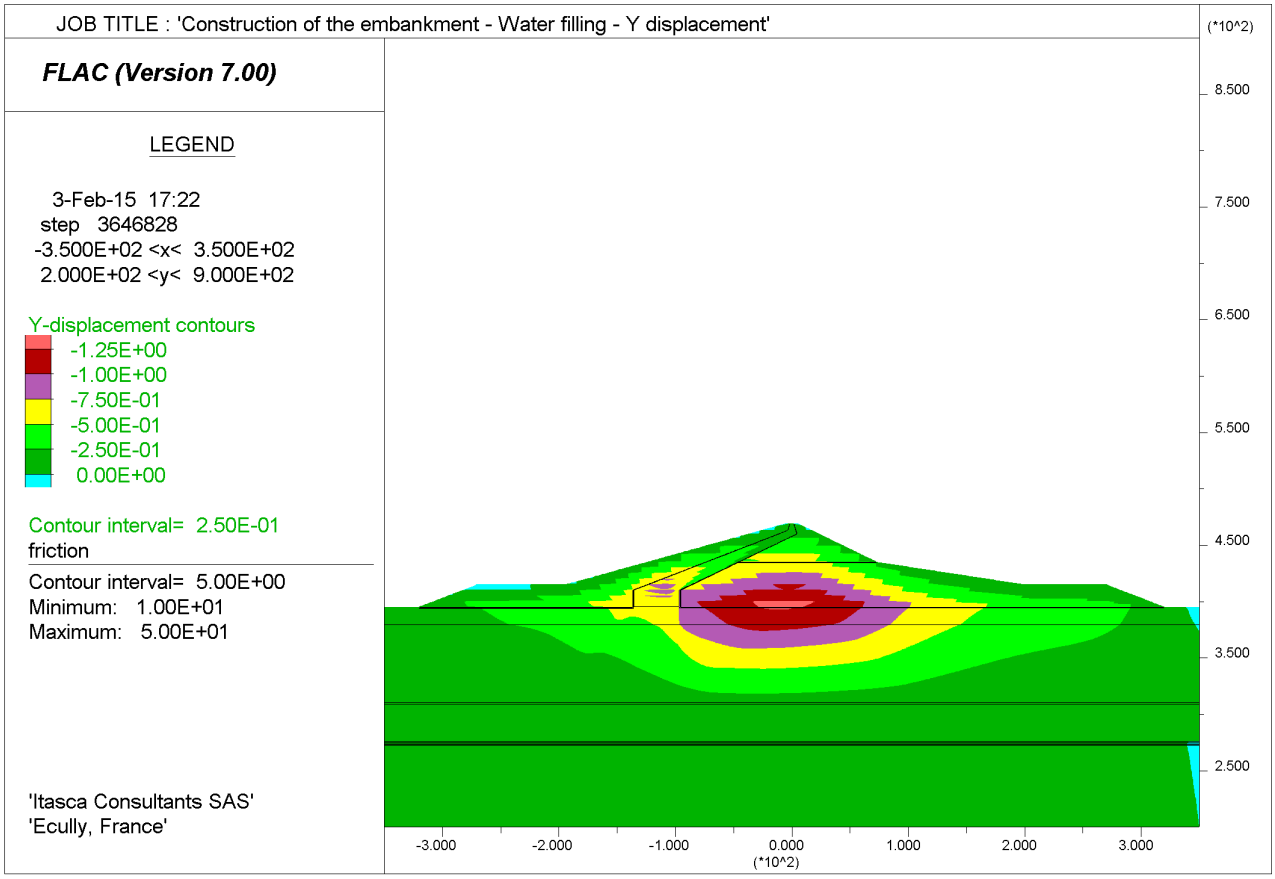

Figure 4-26: embankment construction and upstream water filling – final vertical displacements

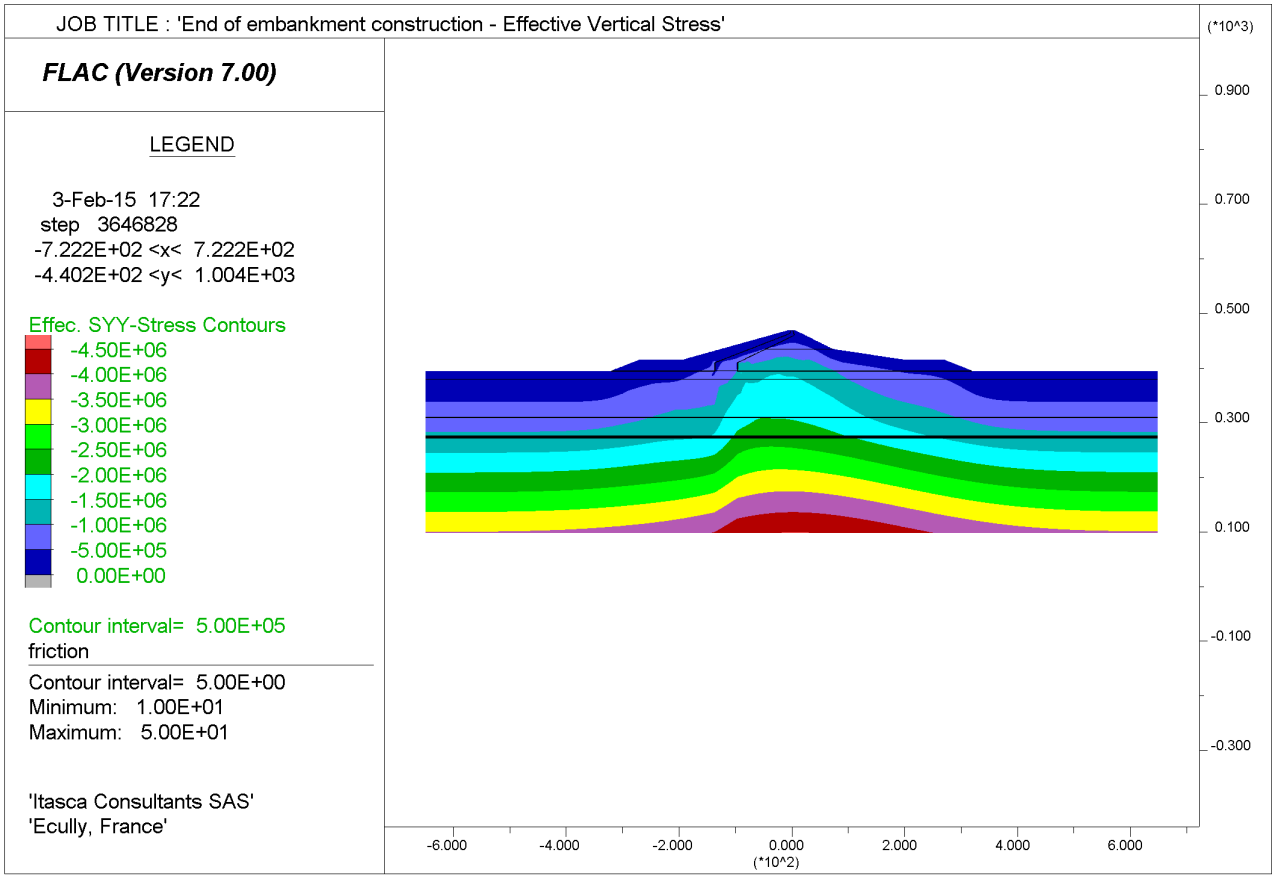

Figure 4-27: embankment construction and upstream water filling – final effective vertical stress

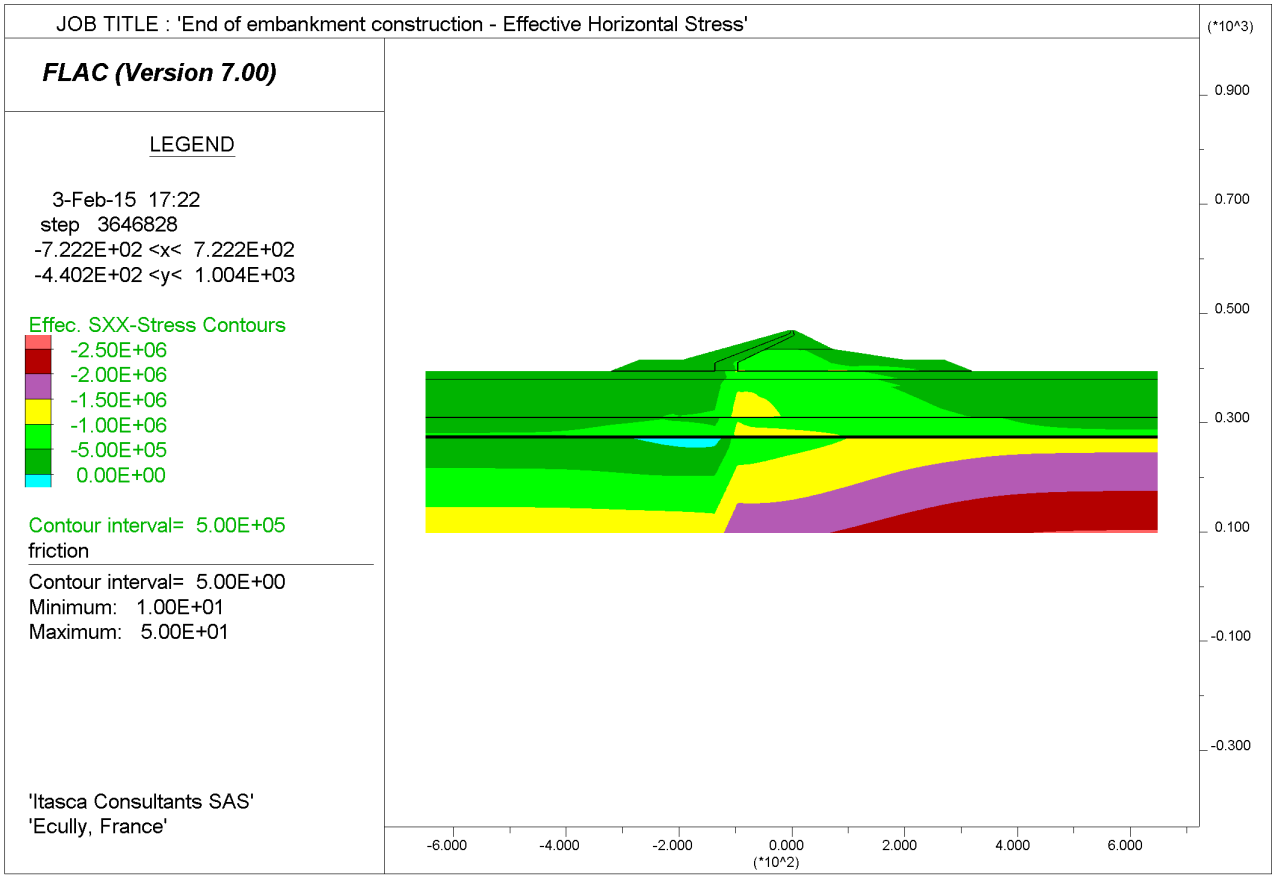

Figure 4-28: embankment construction and upstream water filling – final effective vertical stress

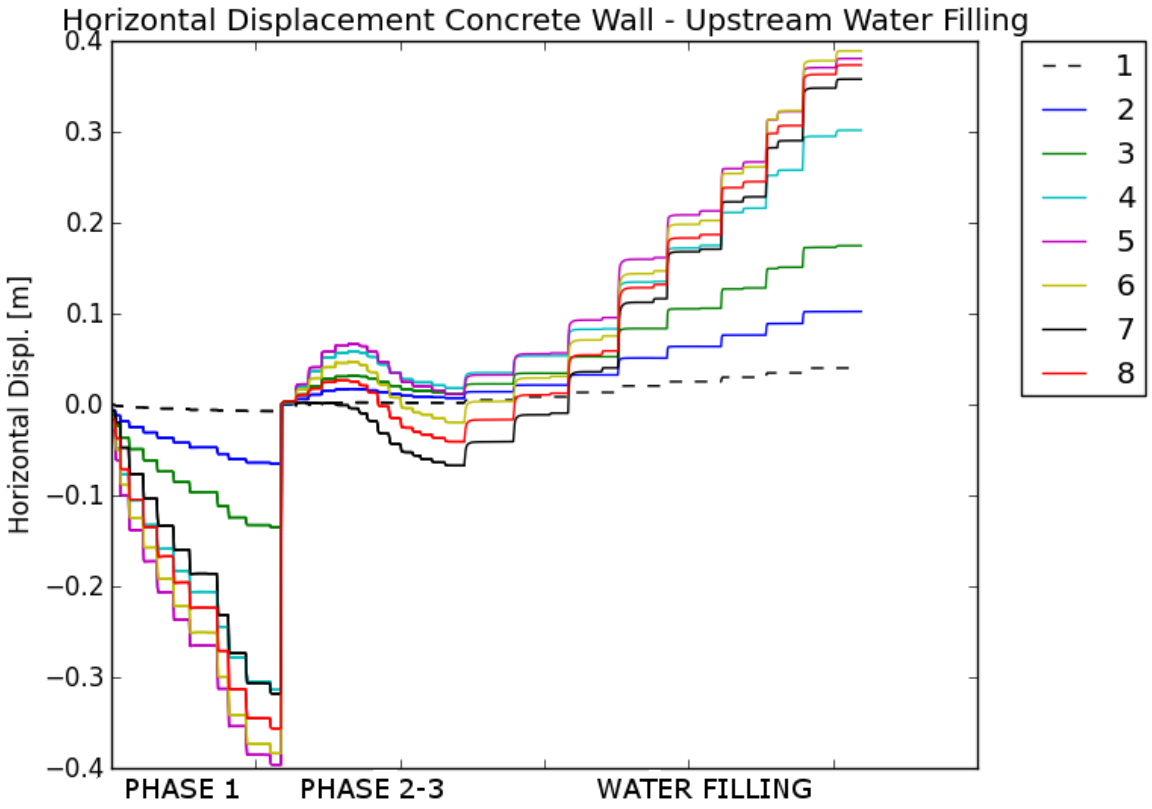

Figure 4-29: embankment construction and upstream water filling – final horizontal displacements measured at points 1 – 8 of Figure 4-16

4.5.5. Conclusions

The construction of the embankment was simulated by reproducing the three forecasted construction phases. The layering of the downstream compacted gravel and rockfill in a first stage (up to elevation 462.0 meters) is of great interest, since it allows the occurrence of a large part of horizontal displacements, prior to the installation of the concrete wall. The successive layering of the dam core, the upstream rockfill and the dam crest, do not constitute a problem for the concrete wall stability.

The final maximum vertical displacement is of about 1.25 meters, at the center of the embankment base.

After the completion of the embankment construction, the upstream water level is raised in 8 steps, up to elevation 462 meters. The relative displacement measured at the points (Figure 4-16) where the concrete wall will be installed, reaches a maximum of 35 centimeters over a length of more than 100 meters (points 1 – 6). The stability of the concrete wall is ensured at these conditions.

4.6. Dynamic simulation

The program of dynamic simulations consists of:

- A linear analysis of the dam-foundation system, considering the Operating Basis Earthquakes, presented in section 4.6.1. The linear analysis allows the identification of the zones which are susceptible to fail during the nonlinear dynamic simulation;
- Nonlinear dynamic analysis, considering the Operating Basis Earthquakes (section 4.6.2);
- Pseudo-static Newmark's Sliding Block Analysis, considering the Safety Evaluation Earthquakes, presented in section 4.6.3;
- Nonlinear dynamic analysis, considering the Safety Evaluation Earthquakes, section 4.6.4;
- Nonlinear dynamic analysis, considering a new configuration with the dam directly founded on the bedrock, and the Safety Evaluation Earthquakes, section 4.6.5.

As described in section 3.1.2, the values of the maximum dynamic shear modulus and dynamic bulk modulus are computed by applying a factor to the static values obtained at the end of the quasi-static phase of construction of the embankment and reservoir filling. This factor was estimated to be equal to 3, as described in section 3.1.2.

Values of the dynamic maximum shear modulus and dynamic bulk modulus are presented in Appendix 3, section 9.1.

4.6.1. OBE earthquake – Linear analysis

A linear analysis of the dam-foundation response is performed, considering the OBE earthquakes that were presented in section 3.3.1. The linear analysis allows verifying that the numerical simulation gives relevant results in elastic conditions, before performing the nonlinear elasto-plastic analysis.

Results from the linear analysis of the dam-foundation response to the OBE earthquake are also employed to perform a spectral analysis of the velocity records at virtual point C of Figure 4-31, thus at the "central point" of the embankment. The aim of this procedure is to identify the "flat" region which usually spans over a 3:1 frequency range that will be targeted by the Rayleigh damping. Rayleigh damping is considered to be frequency independent over a span of roughly 3:1 (or one-third) of the frequency range for the velocity record.

Figure 4-32 and Figure 4-33 show the horizontal and vertical velocity records at point C of Figure 4-31. Figure 4-34 and Figure 4-35 show the corresponding Fourier transform, on which it can be observed how the frequency range of velocity records goes up to 1.5Hz, with a central frequency of about 0.5Hz.
A 1% Rayleigh damping is finally introduced for a central frequency of 0.5Hz.

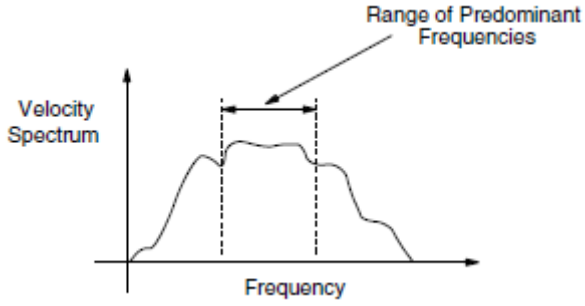

Figure 4-30 : plot of velocity spectrum versus frequency

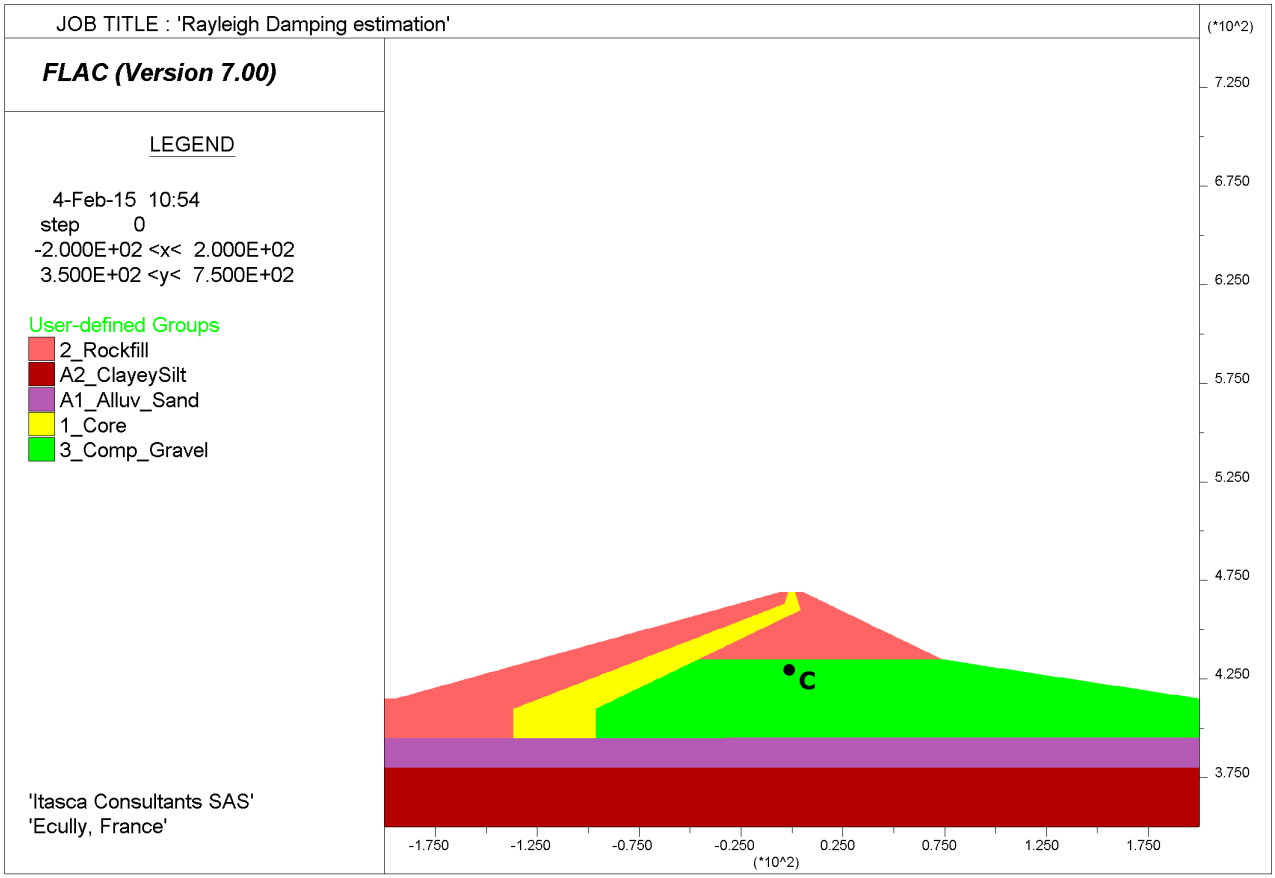

Figure 4-31 : virtual point of velocity measurement for Rayleigh damping estimation

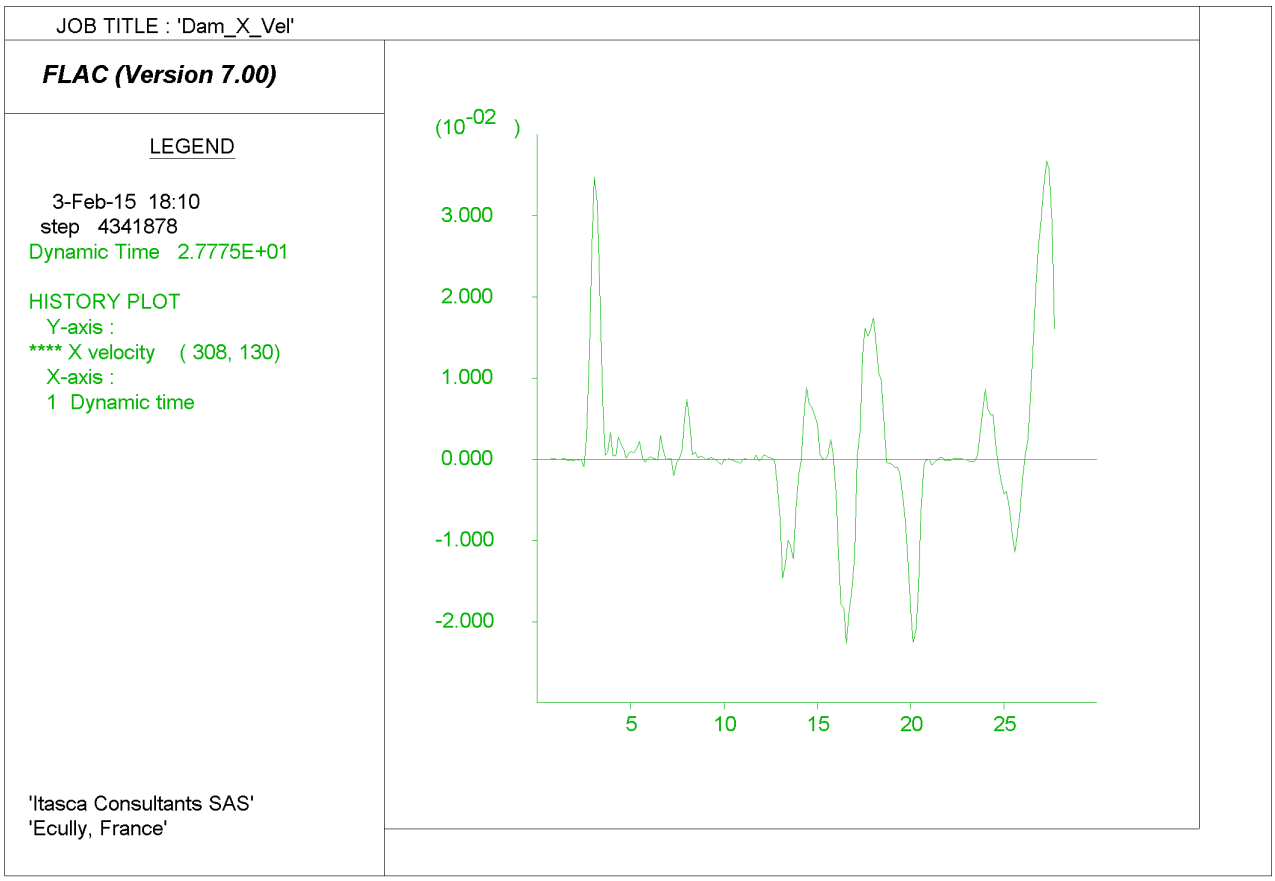

Figure 4-32 : history of horizontal velocity at point C of Figure 4-32

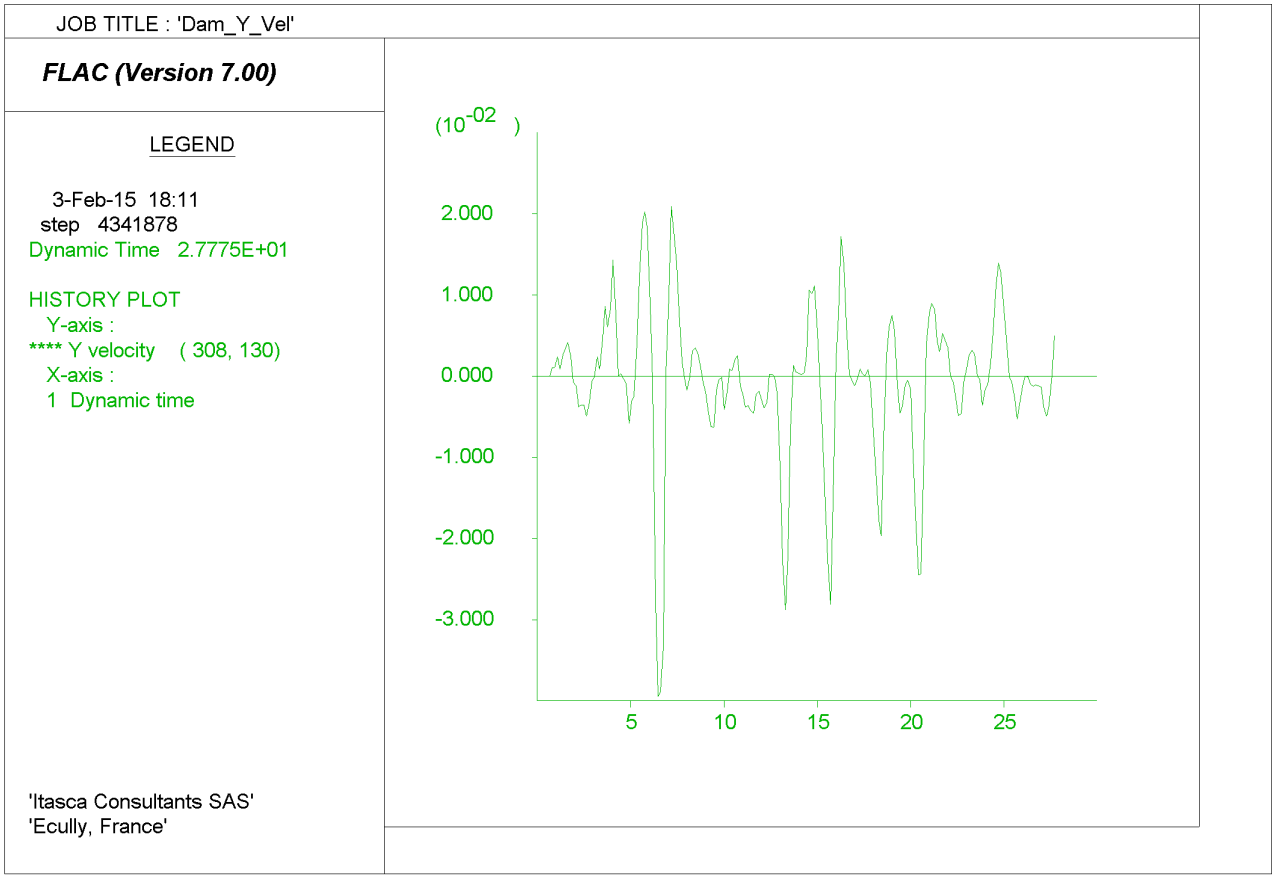

Figure 4-33 : history of vertical velocity at the point C of Figure 4-32

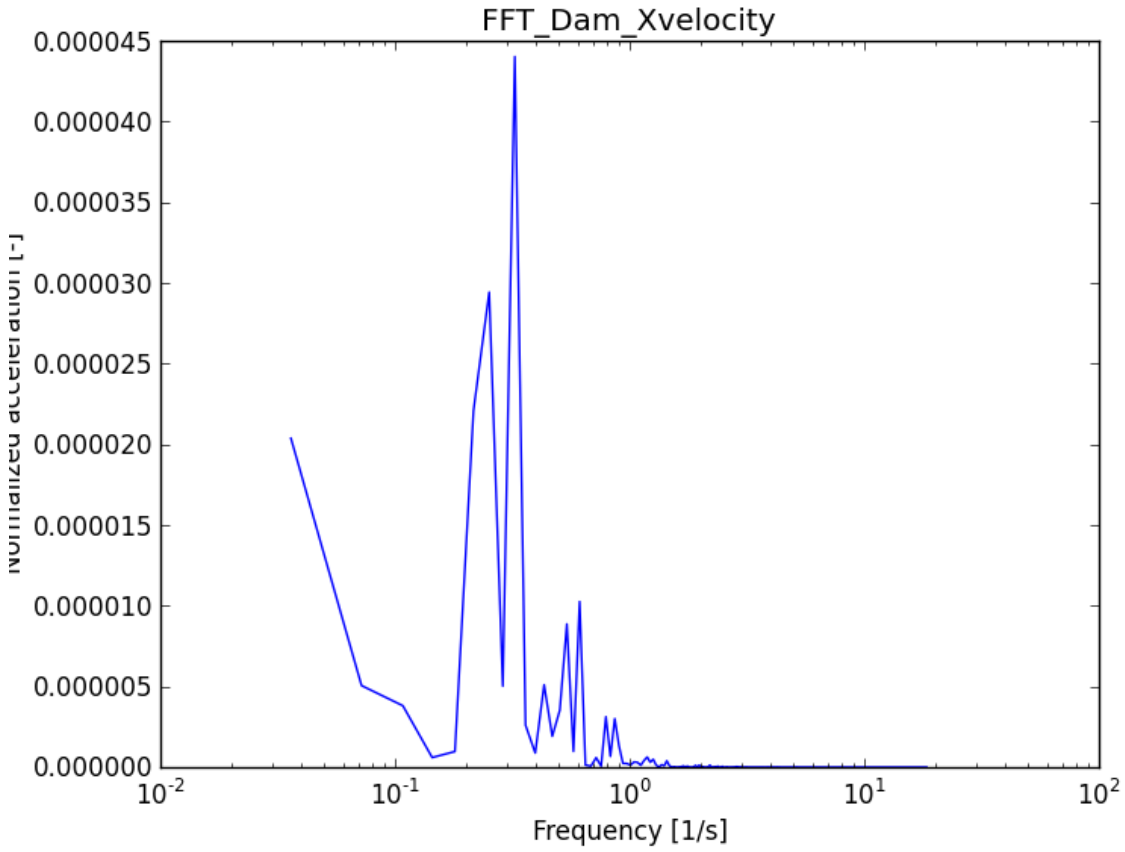

Figure 4-34 : Fourier transform of horizontal velocity of Figure 4-32

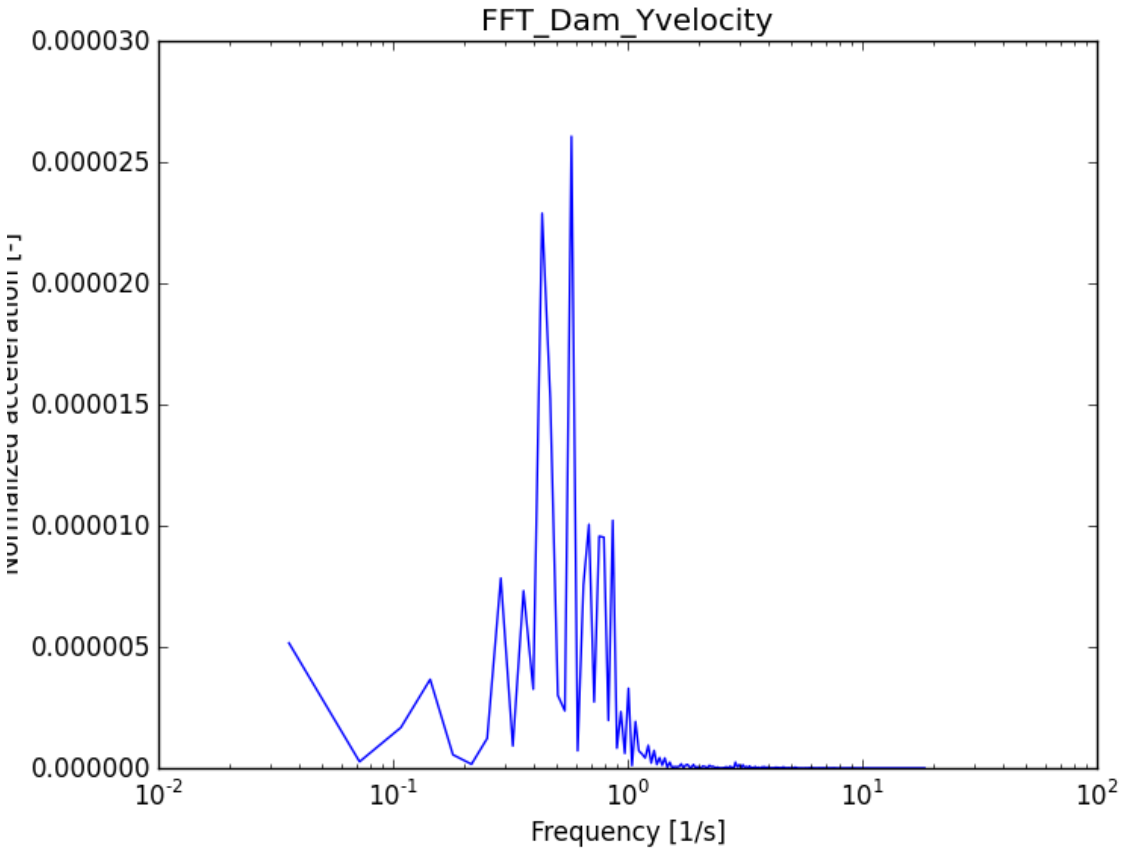

Figure 4-35: Fourier transform of vertical velocity of Figure 4-33

4.6.2. OBE earthquake – Nonlinear analysis

4.6.2.1. Histories of acceleration, velocity and displacement

In this section the histories of acceleration, velocity and displacement are presented, as they were measured at the following points:

- Base of the model;
- Top of the bedrock layer (base of the soil foundation);
- Top of the soil foundation (base of the embankment).

Histories are presented by comparing the records from two consecutive points, to allow understanding of the role played by each zone of the model, that is:

- From the base of the bedrock to the base of the soil foundation (section 4.6.2.1.1);
- From the base of the soil foundation to the base of the embankment (section 4.6.2.1.2).

This information is relative to the nonlinear dynamic simulation of the OBE earthquake Chalfant A (see section 3.3.1).

4.6.2.1.1. Base Bedrock – Top bedrock

Figure 4-36 and Figure 4-37 show the horizontal and vertical displacement, respectively, Figure 4-38 and Figure 4-39 the horizontal and vertical velocity, Figure 4-40 and Figure 4-41 the horizontal and vertical acceleration. As expected, the influence of the bedrock layer, elastic and very stiff (shear modulus 6.9 GPa), is very low.

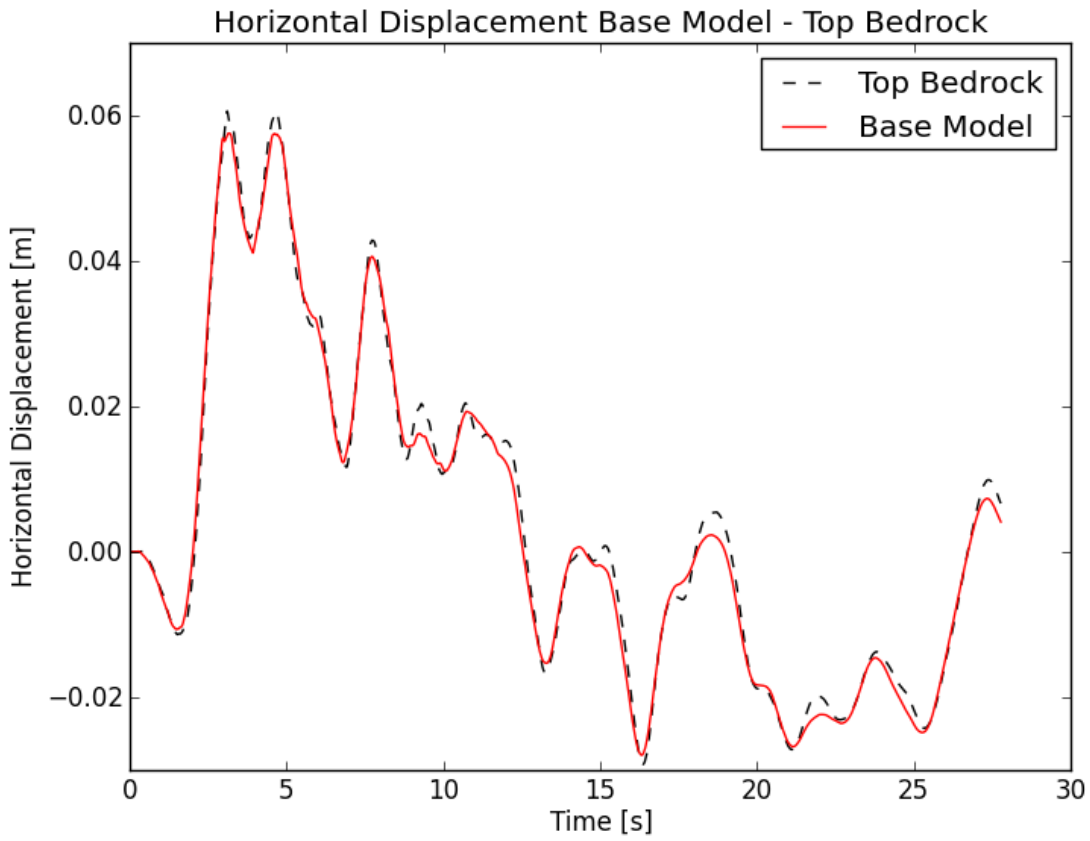

Figure 4-36: horizontal displacement base model – top bedrock

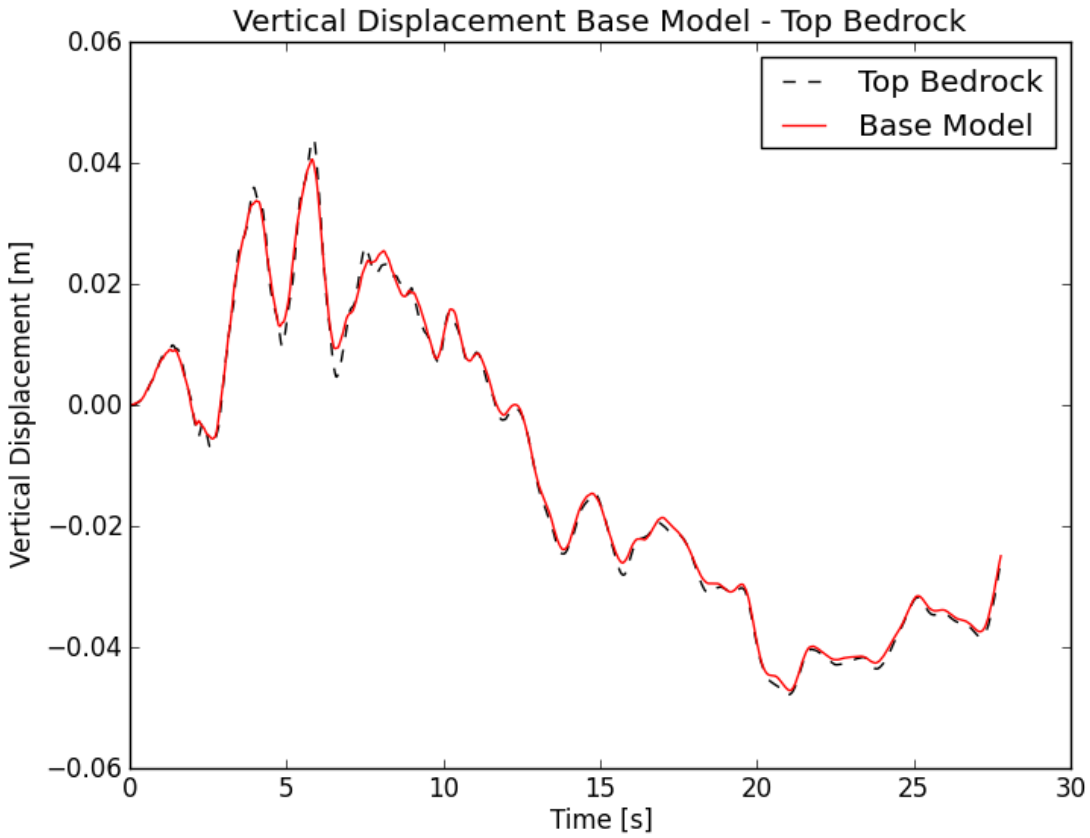

Figure 4-37: vertical displacement base model – top bedrock

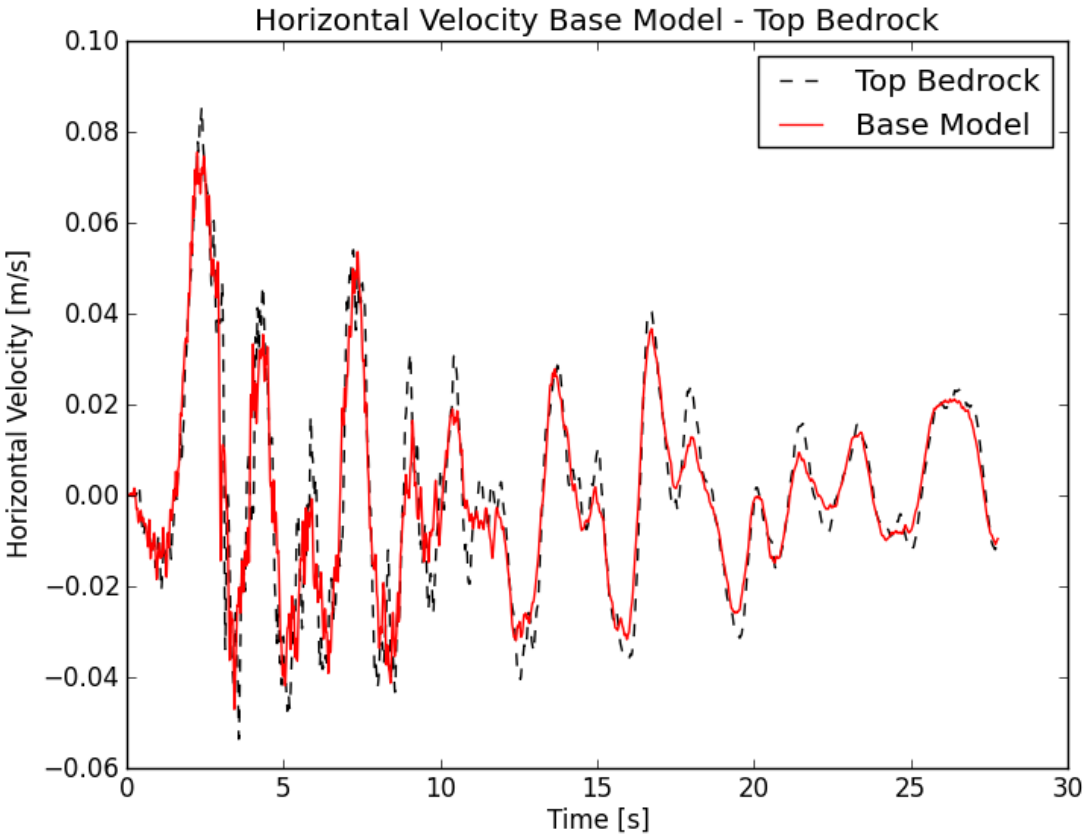

Figure 4-38: horizontal velocity base model – top bedrock

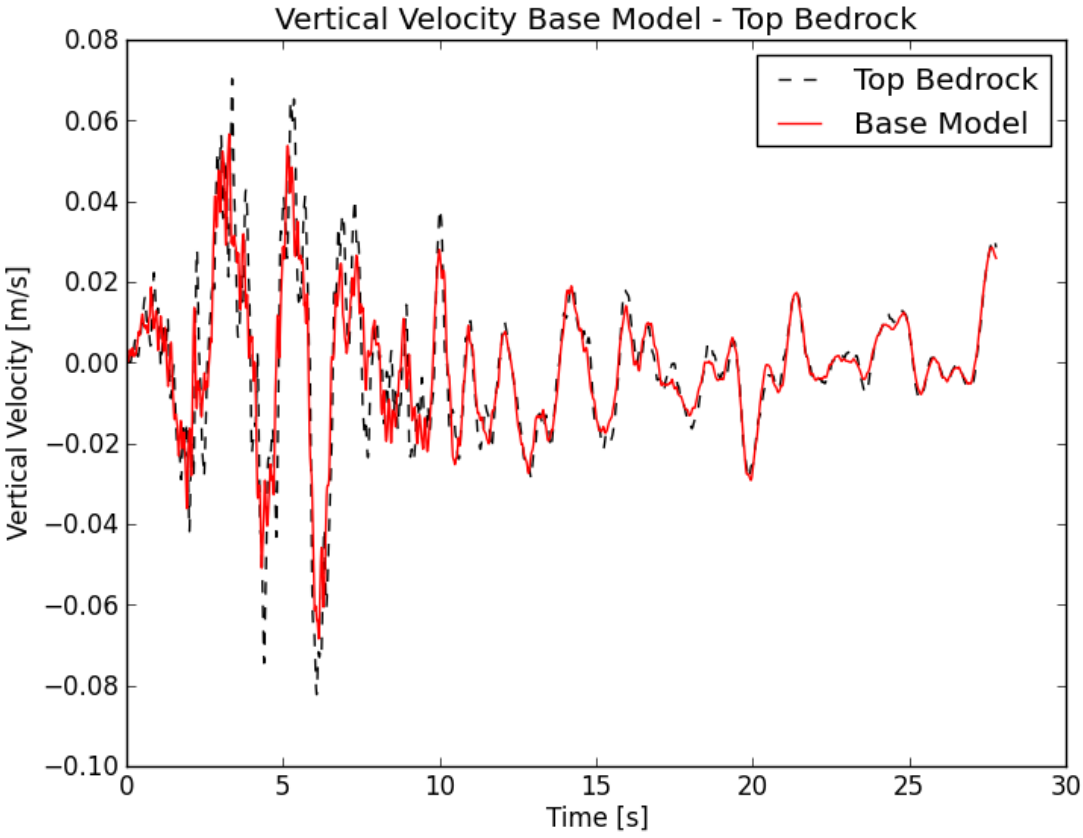

Figure 4-39: vertical velocity base model – top bedrock

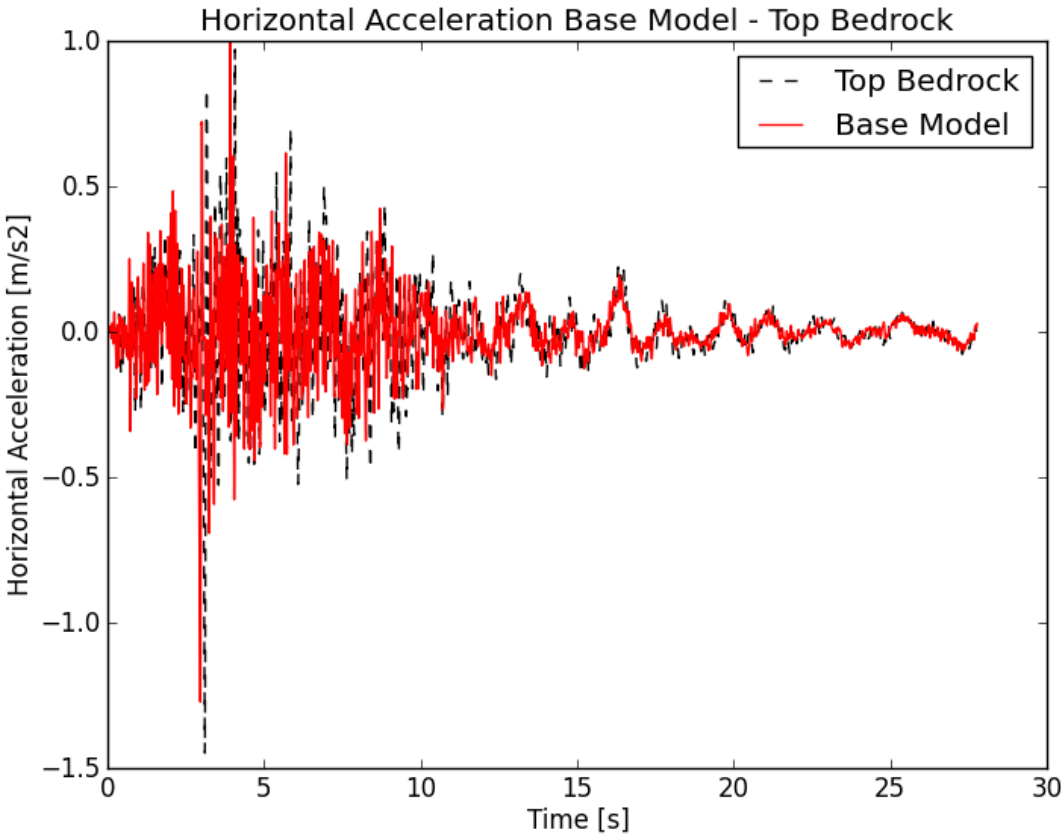

Figure 4-40: horizontal acceleration base model – top bedrock

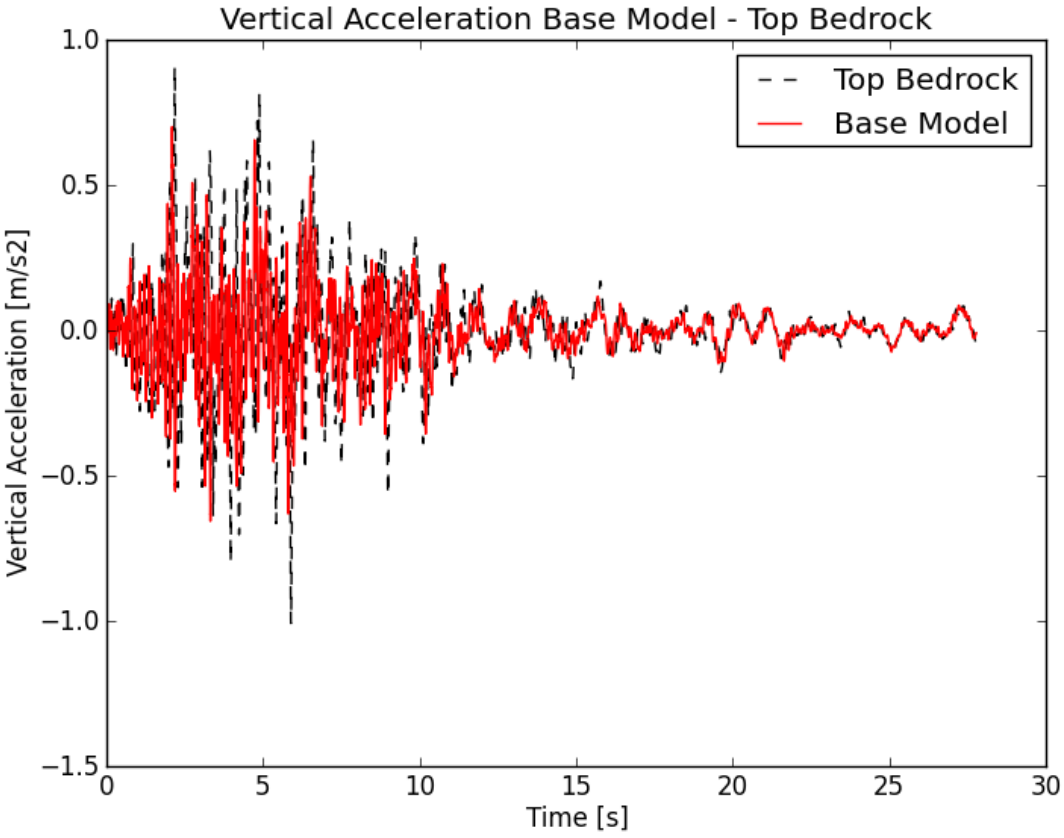

Figure 4-41: vertical acceleration base model – top bedrock

4.6.2.1.2. Base foundation – Top foundation

Figure 4-42 and Figure 4-43 show the horizontal and vertical displacement, respectively, as they were recorded at the base and at the top of the soil foundation (base of the embankment), during the nonlinear dynamic simulation. A strong amplification of the horizontal displacement is denoted. The soil foundation response is characterized by a period of oscillation of about 4s (frequency 0.25 Hz). As should be expected, the influence of the foundation layer is less pronounced concerning the vertical displacement.

Figure 4-44 and Figure 4-45 show the horizontal and vertical velocity, respectively, whereas Figure 4-46 and Figure 4-47 show the horizontal and vertical accelerations. Regarding the acceleration, it is interesting to notice how some peaks of horizontal acceleration, mainly associated to the highest frequencies, which are recorded at the base of the foundation, are reduced/dissipated through the foundation layer. Accelerations associated to lower frequencies are, on the other hand, amplified. This effect is less pronounced when looking at the vertical acceleration.

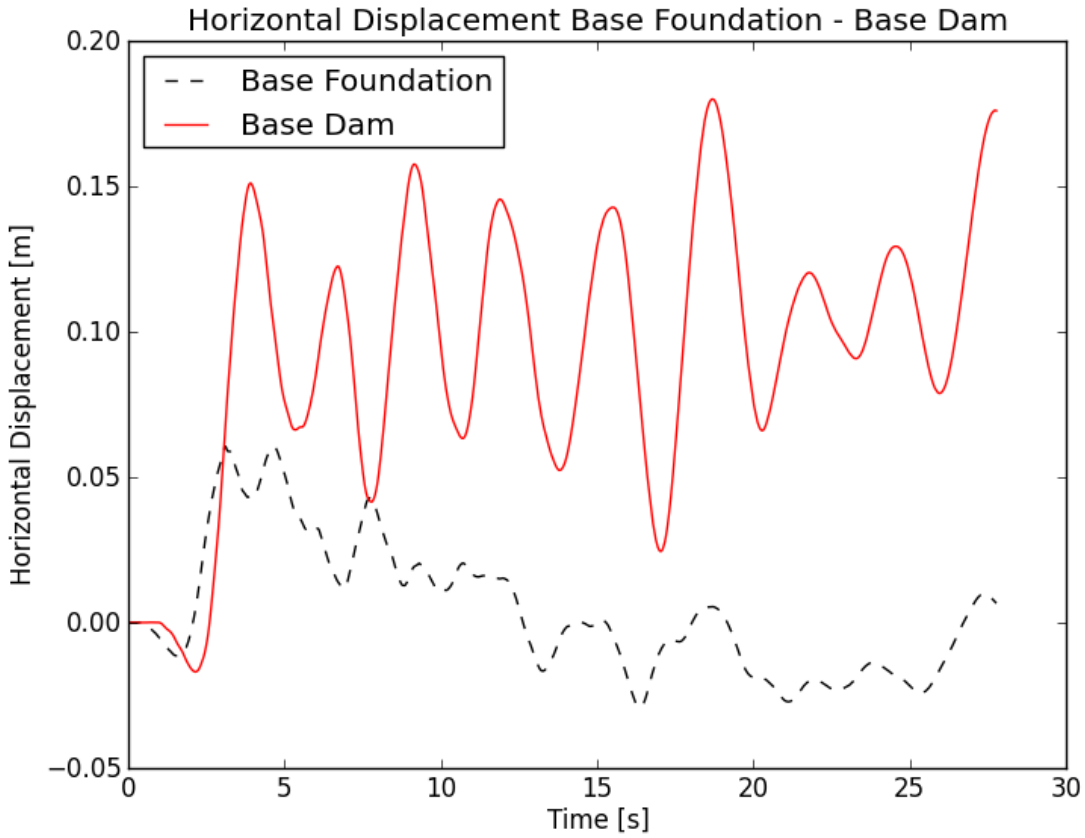

Figure 4-42: horizontal displacement base foundation – top foundation

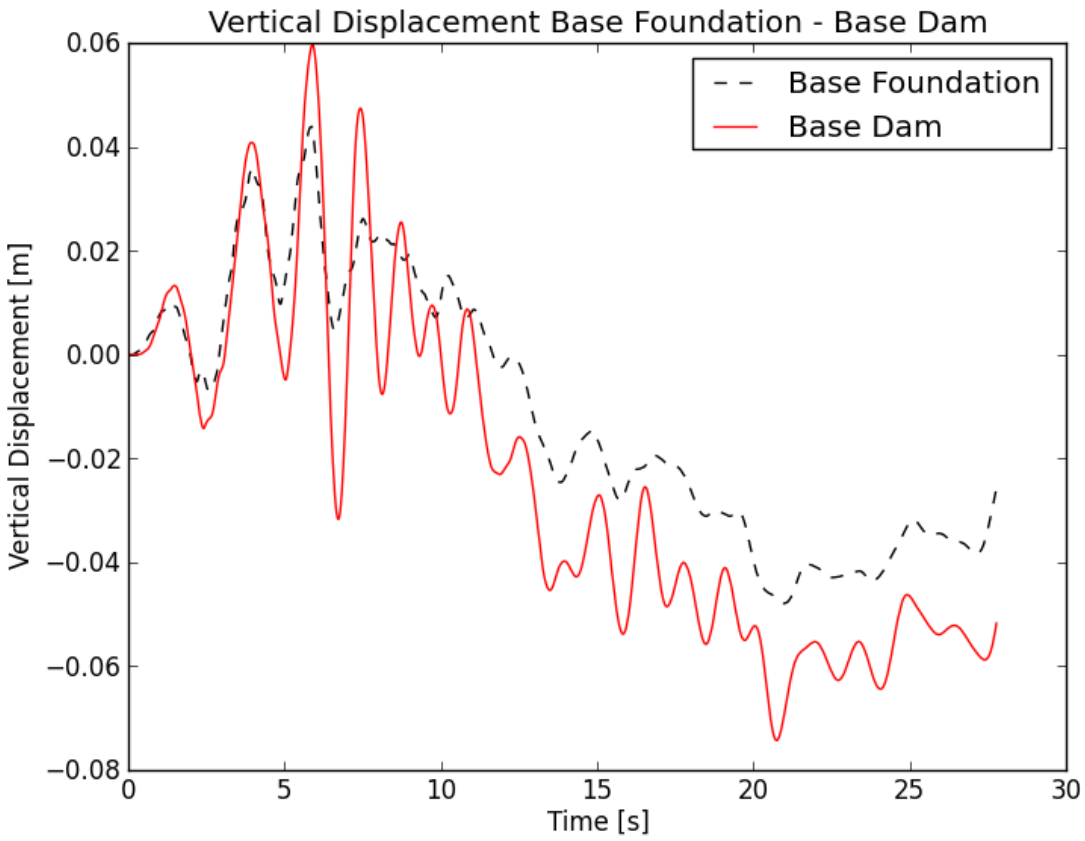

Figure 4-43: vertical displacement base foundation – top foundation

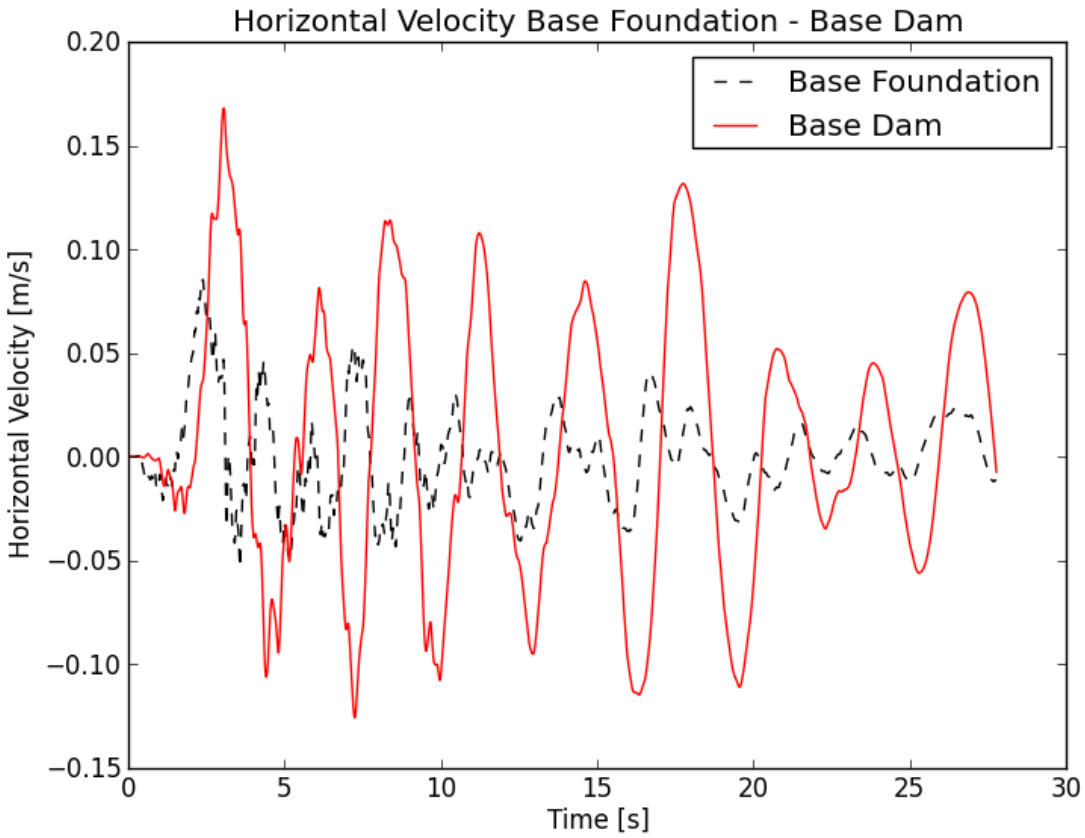

Figure 4-44: horizontal velocity base foundation – top foundation

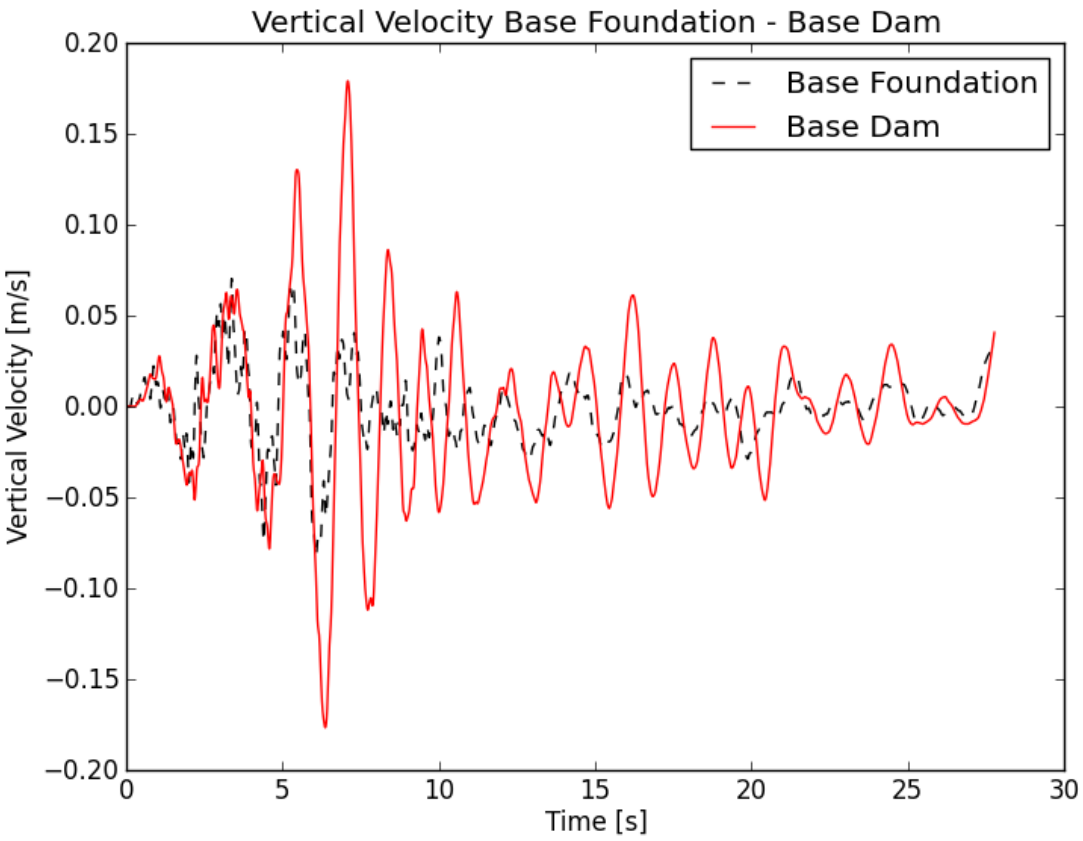

Figure 4-45: vertical velocity base foundation – top foundation

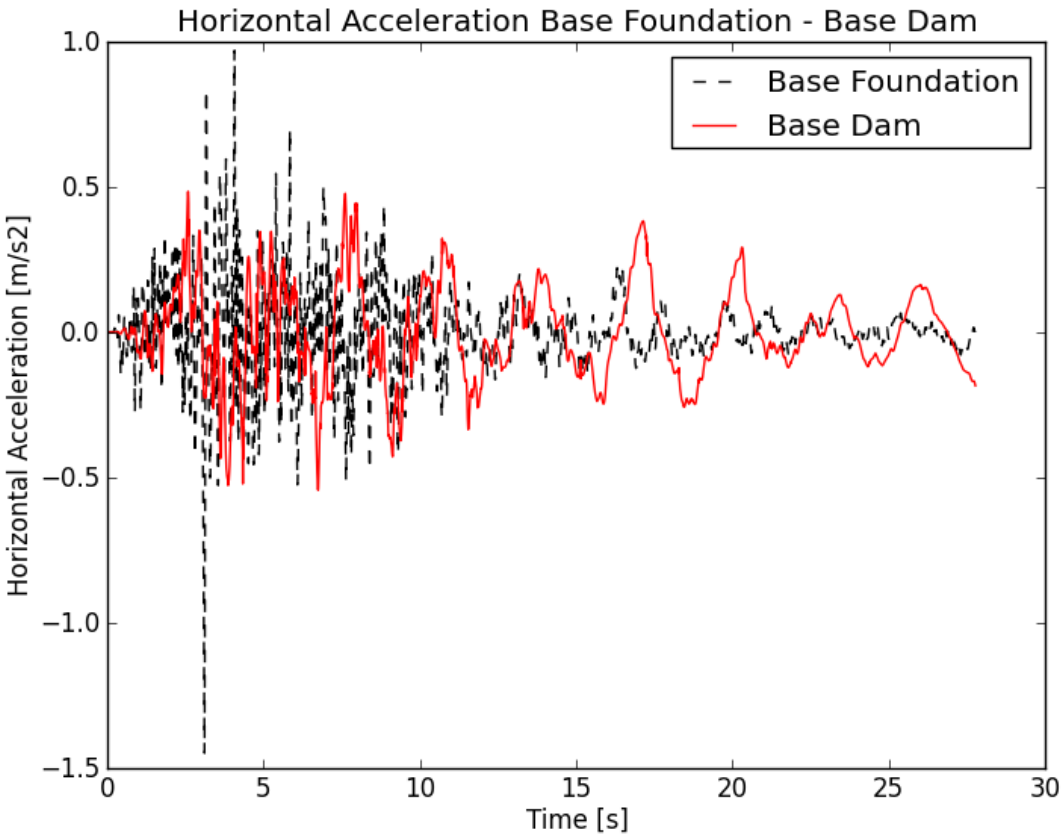

Figure 4-46: horizontal acceleration base foundation – top foundation

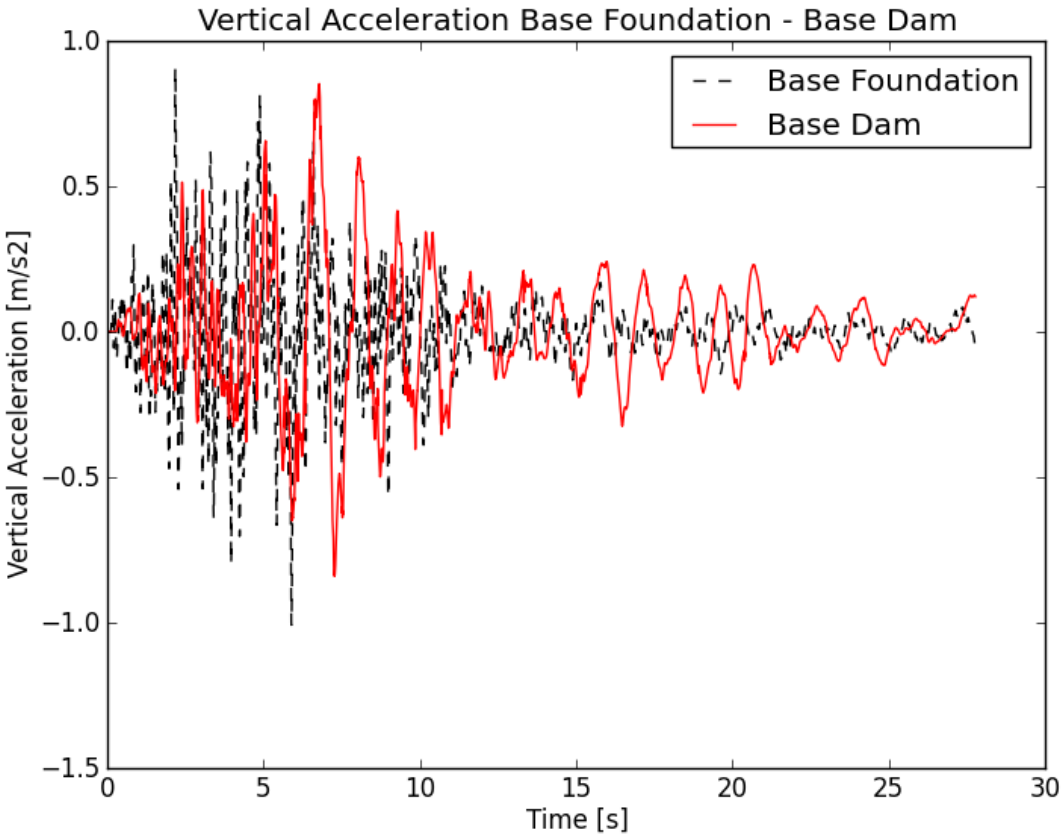

Figure 4-47: vertical acceleration base foundation – top foundation

4.6.2.2. Numerical results

The results of the nonlinear dynamic simulation of the dam-foundation response to the OBE earthquakes are presented in this section. In all cases the vertical displacement at the crest of the dam is only a fraction of the maximum admissible settlement of 4 meters.

Figure 4-48 and Figure 4-49 show the final horizontal and vertical displacements, respectively, corresponding to the OBE earthquake Chalfant A (PGA V +0.19 / -0.24 H1 +0.31 / -0.20). The maximum negative horizontal displacement (5cm) is located at the upstream foot, whereas the maximum positive displacements are more concentrated at the crest. Maximum vertical negative displacements occur upstream, close to the horizontal bench. Non-negligible displacements occur at the foot of the downstream embankment, which seems to be a zone susceptible to fail in case of more important solicitations.

The same considerations can be made for the OBE earthquake Chalfant A (PGA V +0.19 / -0.24 H2 +0.23 / -0.30). Figure 4-50 and Figure 4-51 show the final horizontal and vertical displacements, respectively.

The response of the dam-foundation system to the Chalfant B earthquake (PGA V +0.20 / -0.18 H1 +0.13 / -0.16) is again very similar to the previous cases; the displacement are lower in this case. Figure 4-52 and Figure 4-53 show the final horizontal and vertical displacements, respectively.

A more significant motion is detected upstream (foot/bench), in the case of the OBE earthquake Chalfant B (PGA V +0.20 / -0.18 H2 +0.30 / -0.28). Again, the downstream foot also undergoes a non-negligible motion.

The same trends are observed for the last three earthquakes tested. Figure 4-54 and Figure 4-55 show the final horizontal and vertical displacements, respectively, corresponding to the OBE earthquake Chalfant B (PGA V +0.20 / -0.18 H2 +0.30 / -0.28). Figure 4-56 and Figure 4-57 show the final horizontal and vertical displacements, respectively, corresponding to the OBE earthquake Darfield LPCC (PGA V +0.11 / -0.13 H2 +0.21 / -0.29). Figure 4-58 and Figure 4-59 show the final horizontal and vertical displacements, respectively, corresponding to the OBE earthquake Darfield LPCC (PGA V +0.11 / -0.13 H2 +0.17 / -0.20).

As a general comment to these results, the zones which appear to be more susceptible to undergo non-negligible motions are the upstream and downstream slopes. Upstream, the vertical displacements are more important than elsewhere in the model. The displacements at the crest are in all cases lower than 10cm.

The table below summarizes the maximum displacements that were observed at the dam crest.

OBE EARTHQUAKE					
		PGA [g]		Max Crest Displacements [m]	
Name		Vertical	Horizontal	Vertical	Horizontal
Chalfant A V-H1		+ 0.19 / - 0.24	+ 0.31 / - 0.20	-0.05	+0.23
Chalfant A V-H2			+ 0.23 / - 0.30	-0.06	+0.28
Chalfant B V-H1		+ 0.20 / - 0.18	+ 0.13 / - 0.16	-0.06	+0.25
Chalfant B V-H2			+ 0.30 / - 0.28	-0.07	+0.16
Darfield LLPC V-H1		+ 0.11 / - 0.13	+ 0.21 / - 0.29	-0.04	+0.13
Darfield LLPC V-H1			+ 0.17 / - 0.20	-0.05	-0.20

Table 4-1 : OBE earthquakes – Nonlinear analysis – Maximum crest displacements

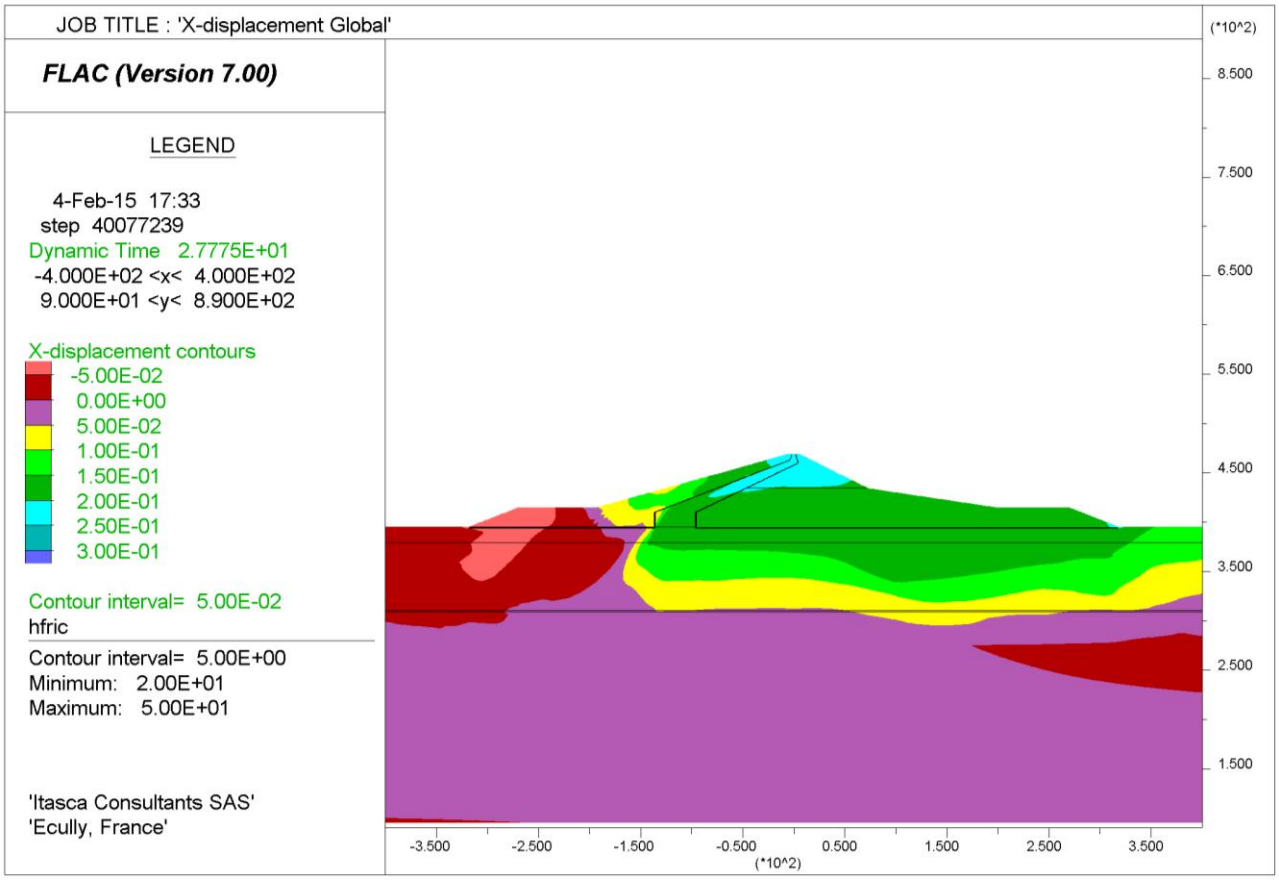

Figure 4-48 : Nonlinear analysis – OBE earthquake Chalfant A (V-H1)
Final horizontal displacements

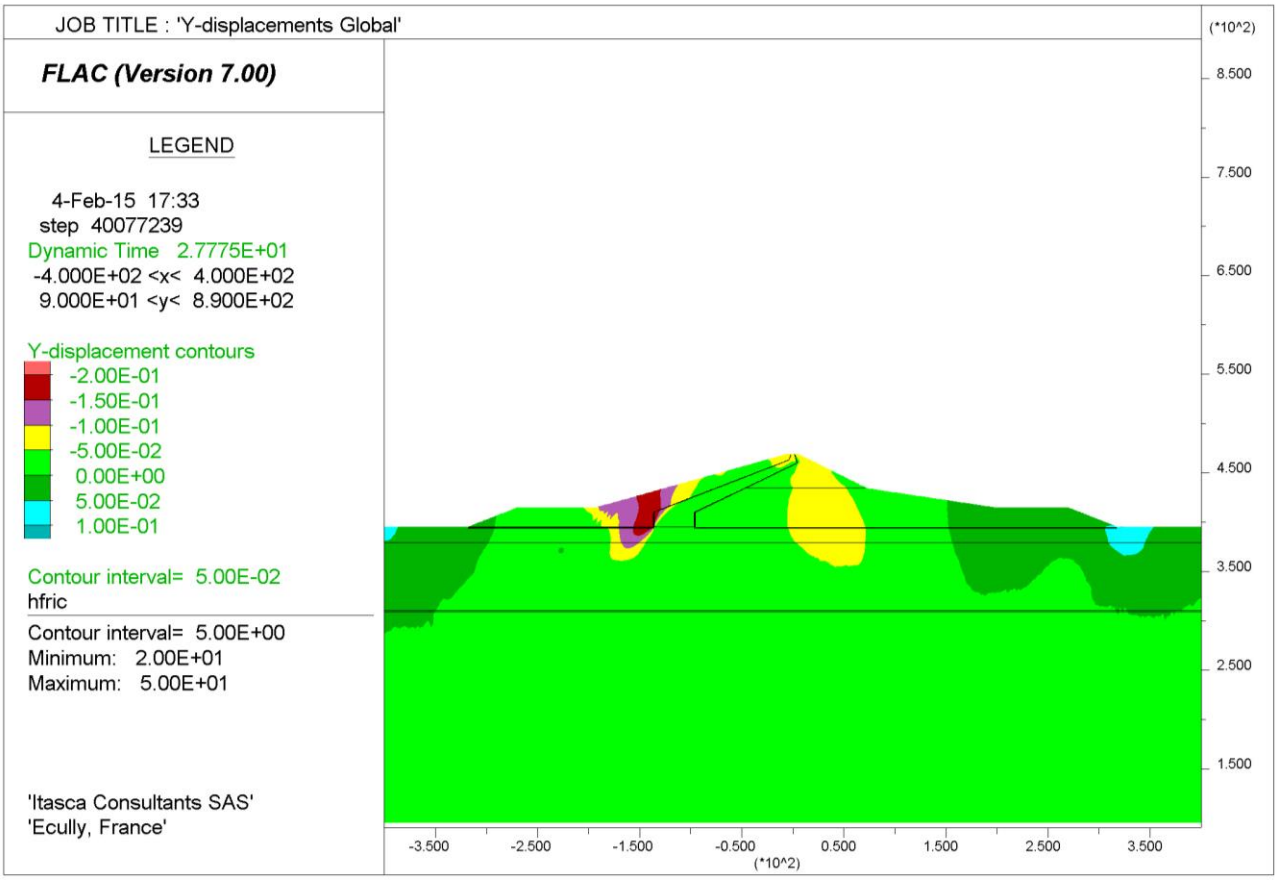

Figure 4-49 Nonlinear analysis – OBE earthquake Chalfant A (V-H1)
Final vertical displacements

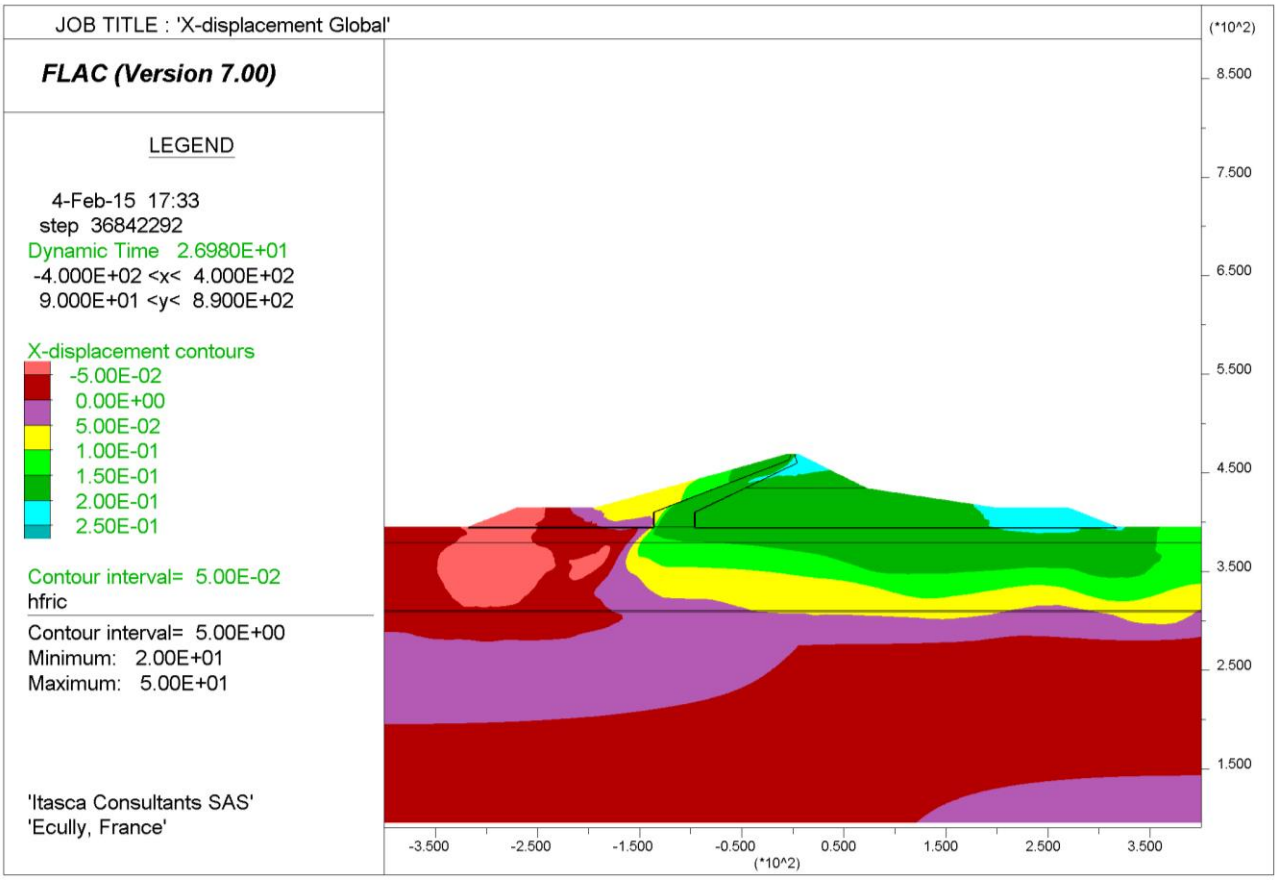

Figure 4-50 Nonlinear analysis – OBE earthquake Chalfant A (V-H2)
Final horizontal displacements

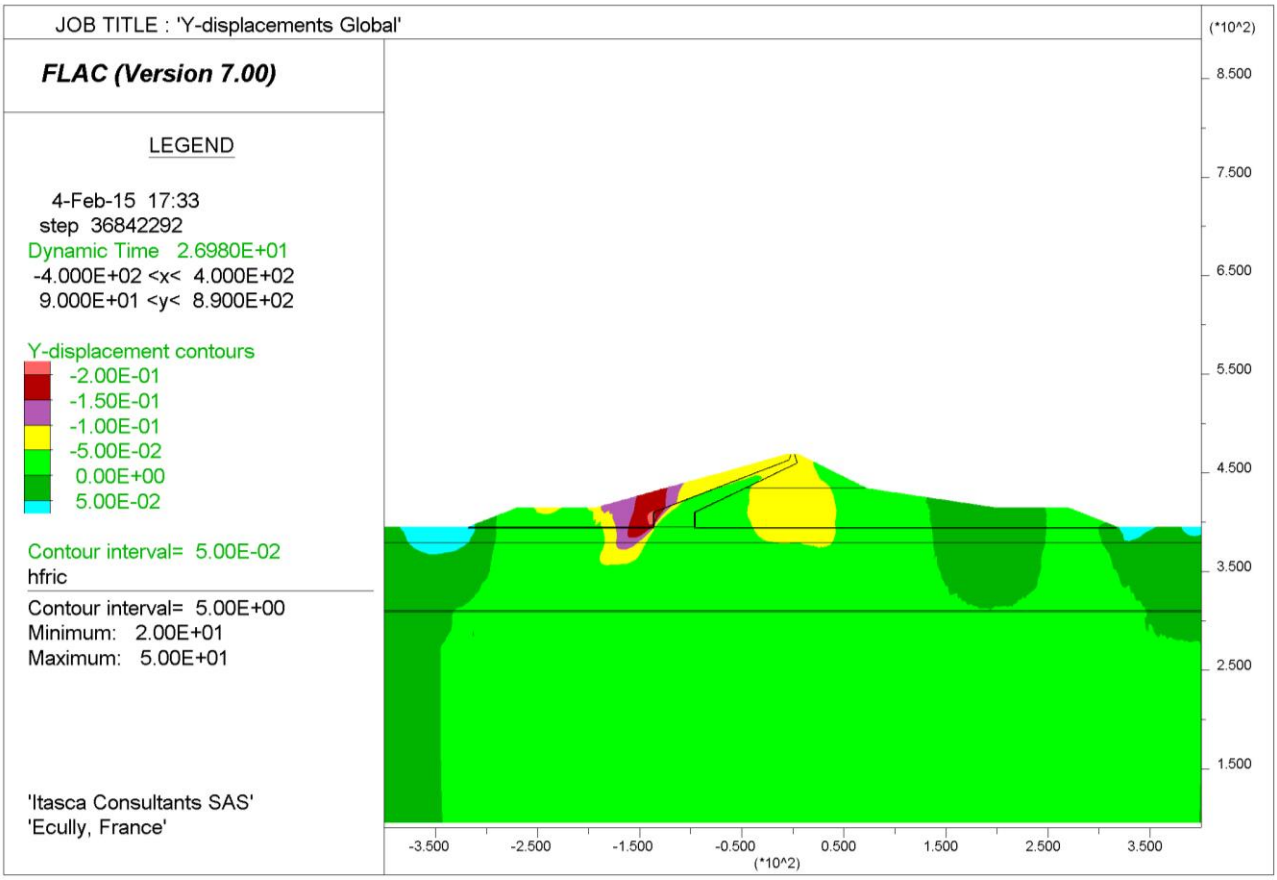

Figure 4-51 Nonlinear analysis – OBE earthquake Chalfant A (V-H2)
Final vertical displacements

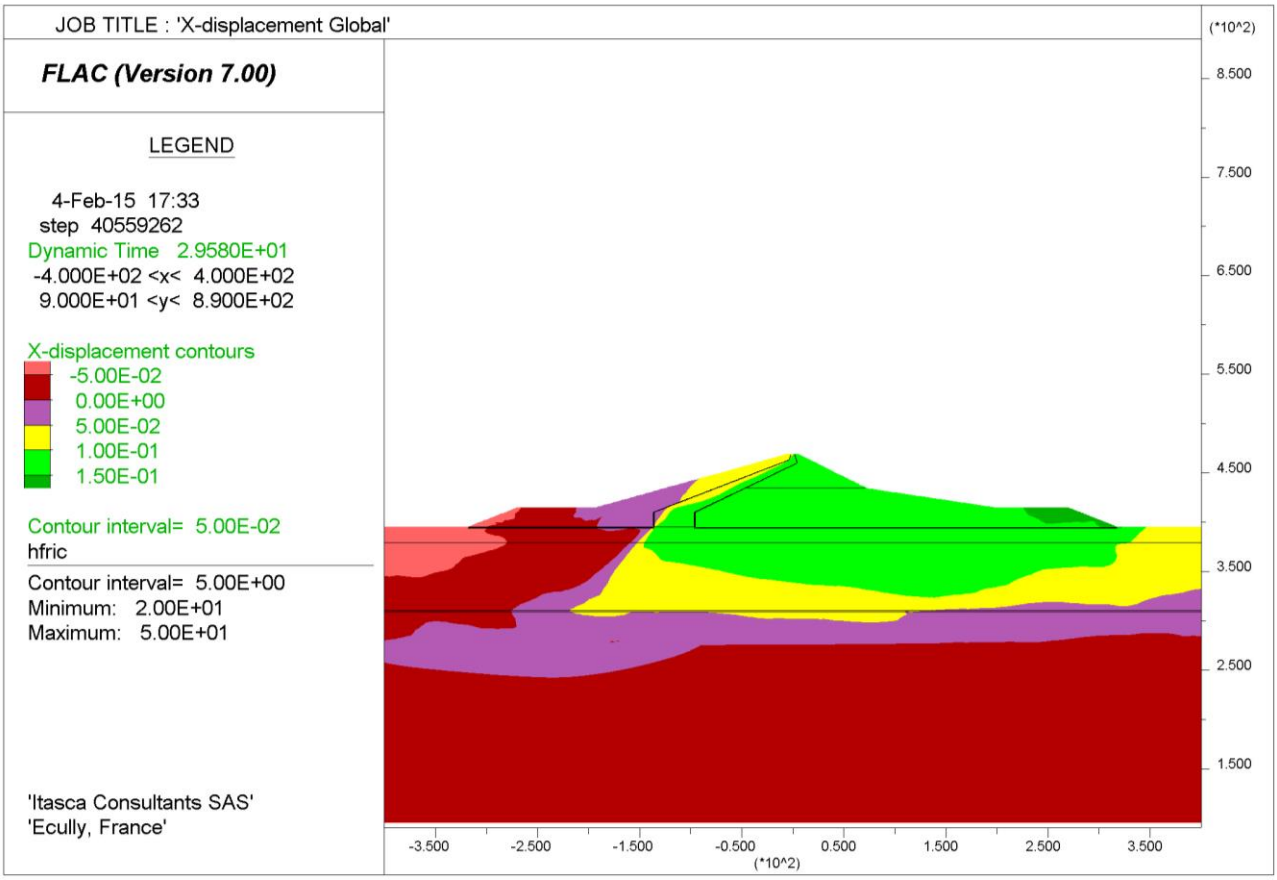

Figure 4-52 Nonlinear analysis – OBE earthquake Chalfant B (V-H1)
Final horizontal displacements

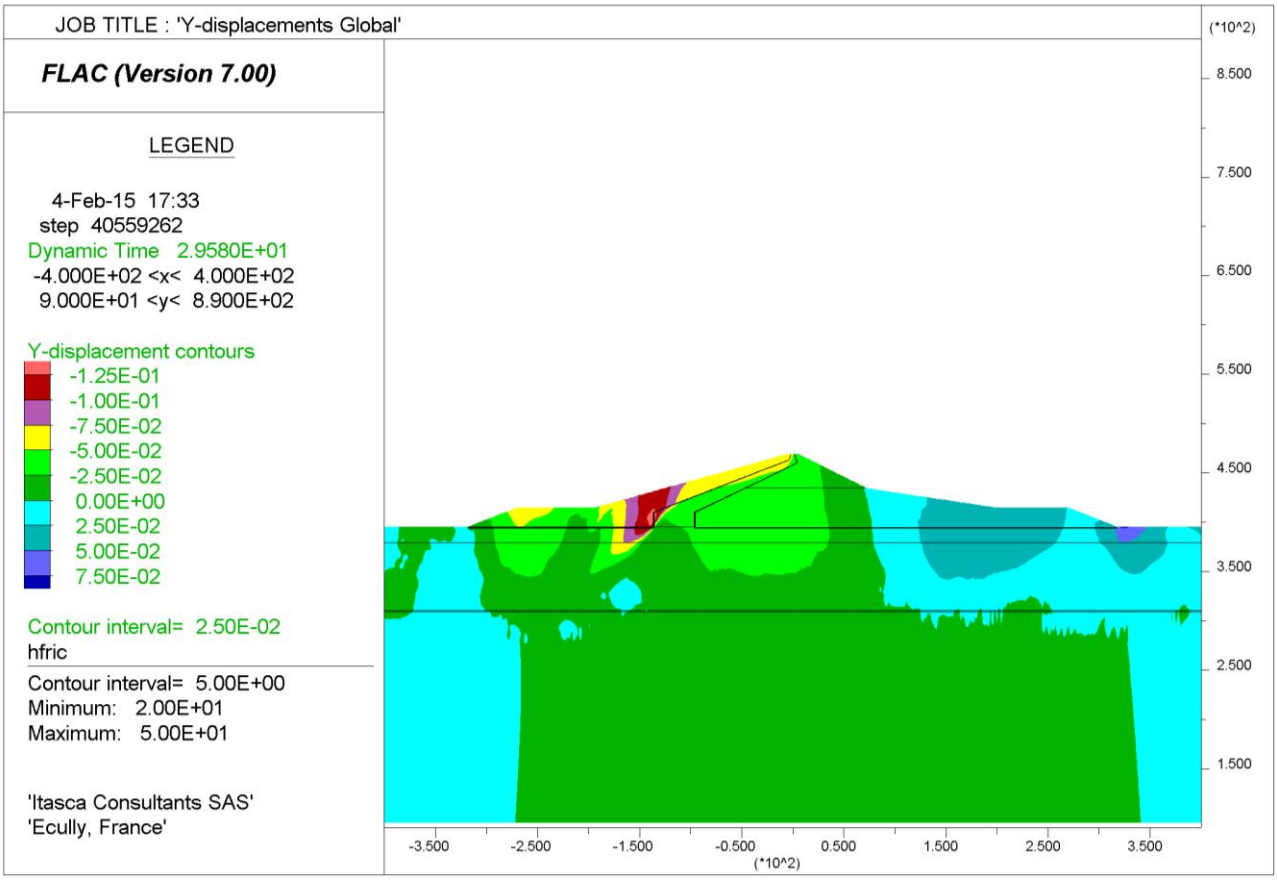

Figure 4-53 Nonlinear analysis – OBE earthquake Chalfant B (V-H1)
Final vertical displacements

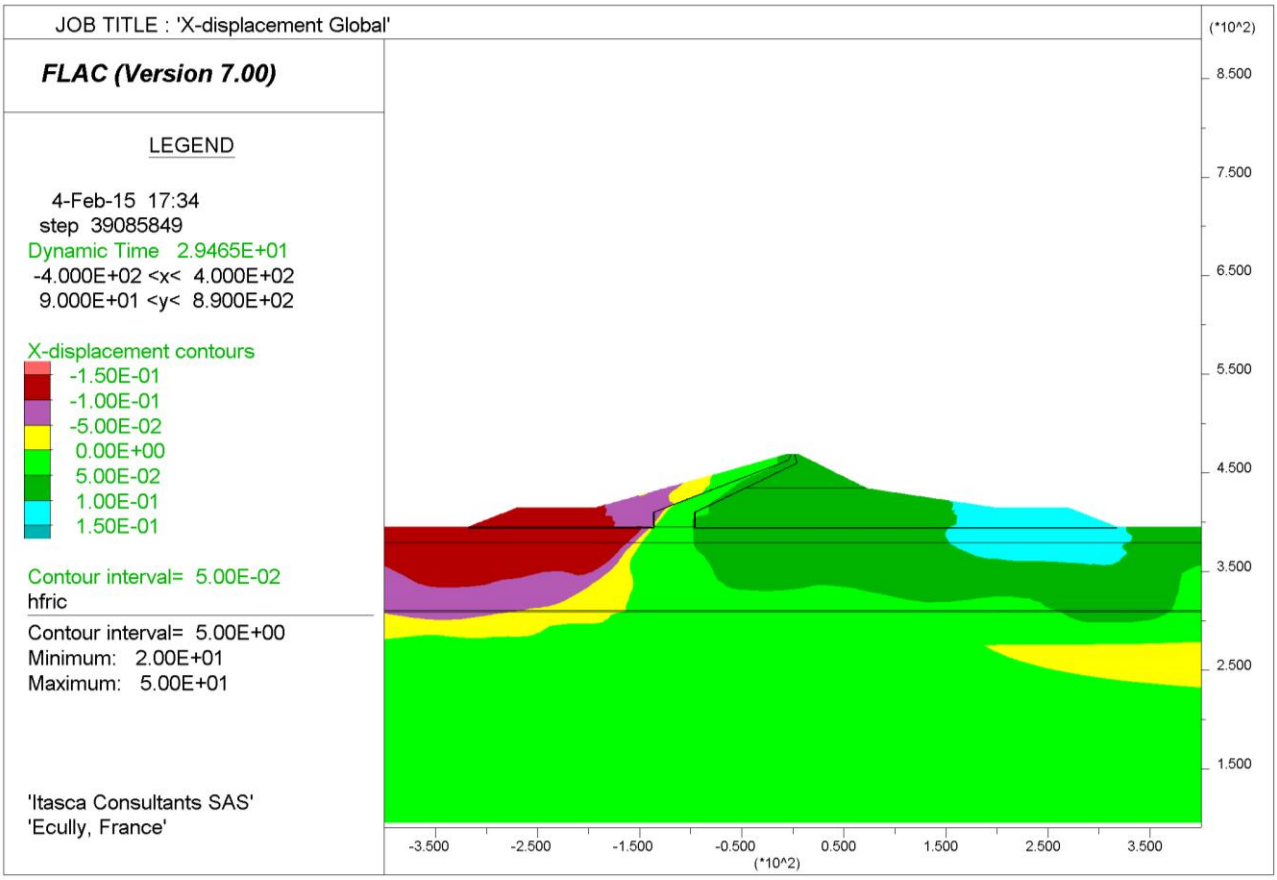

Figure 4-54 Nonlinear analysis – OBE earthquake Chalfant B (V-H2)
Final horizontal displacements

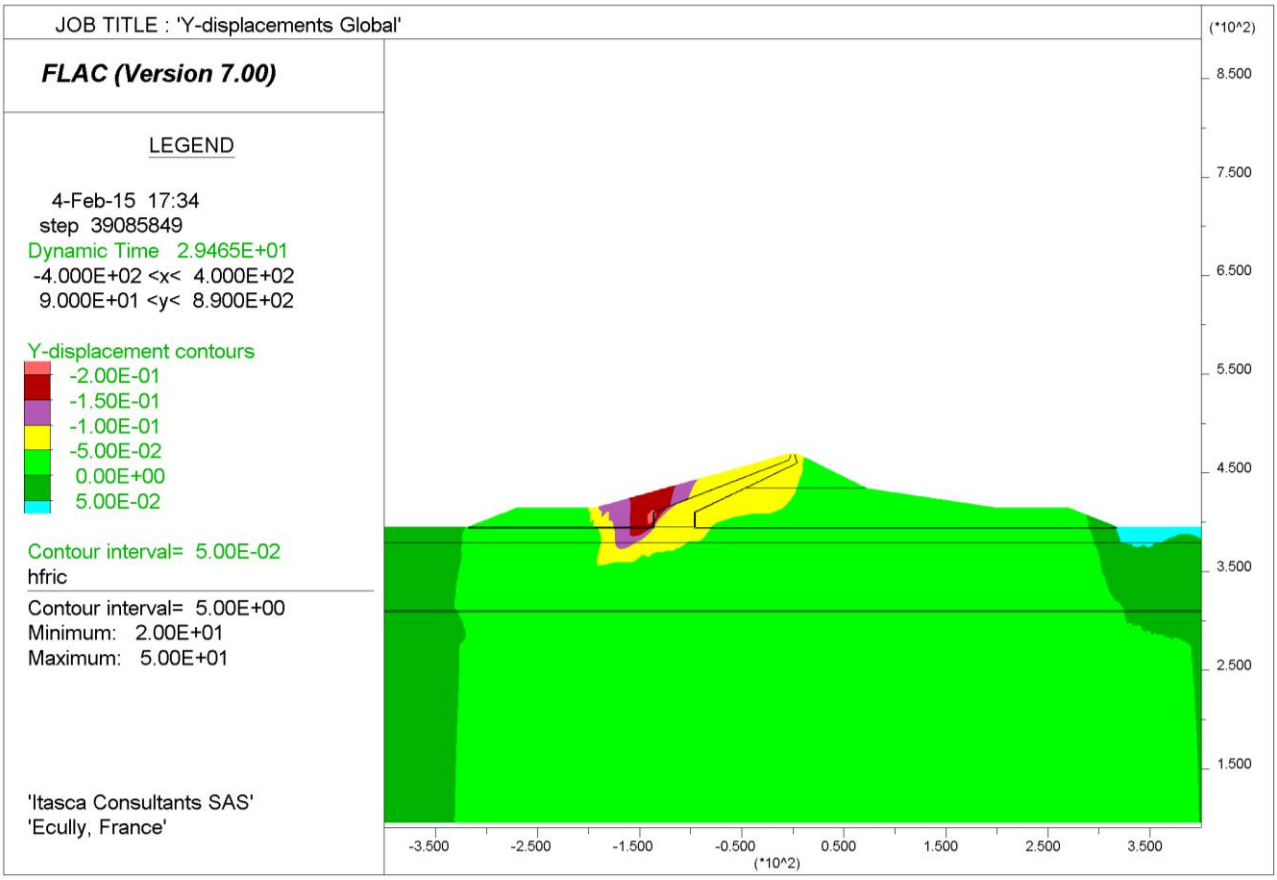

Figure 4-55 Nonlinear analysis – OBE earthquake Chalfant B (V-H2)
Final vertical displacements

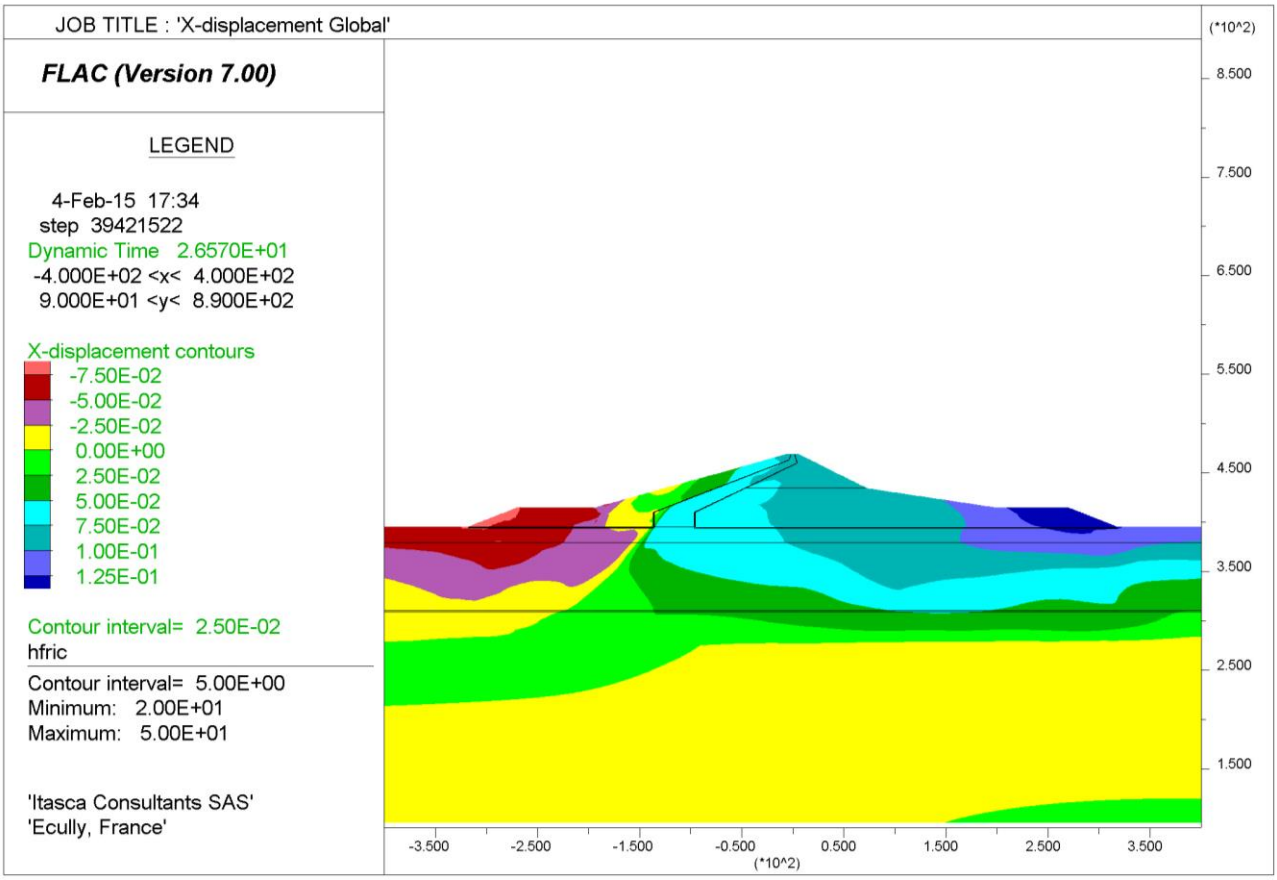

Figure 4-56 Nonlinear analysis – OBE earthquake Darfield LPCC (V-H1)
Final horizontal displacements

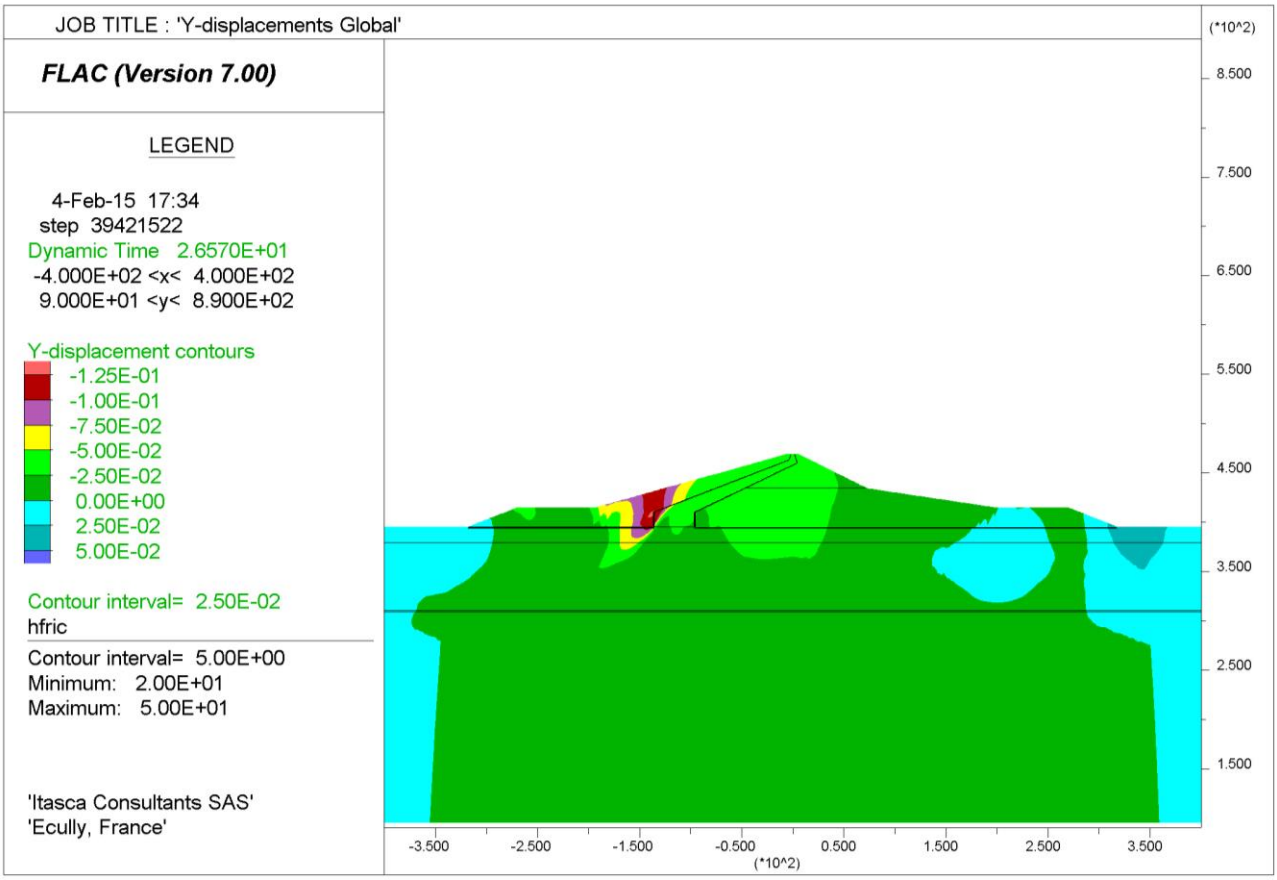

Figure 4-57 Nonlinear analysis – OBE earthquake Darfield LPCC (V-H1)
Final vertical displacements

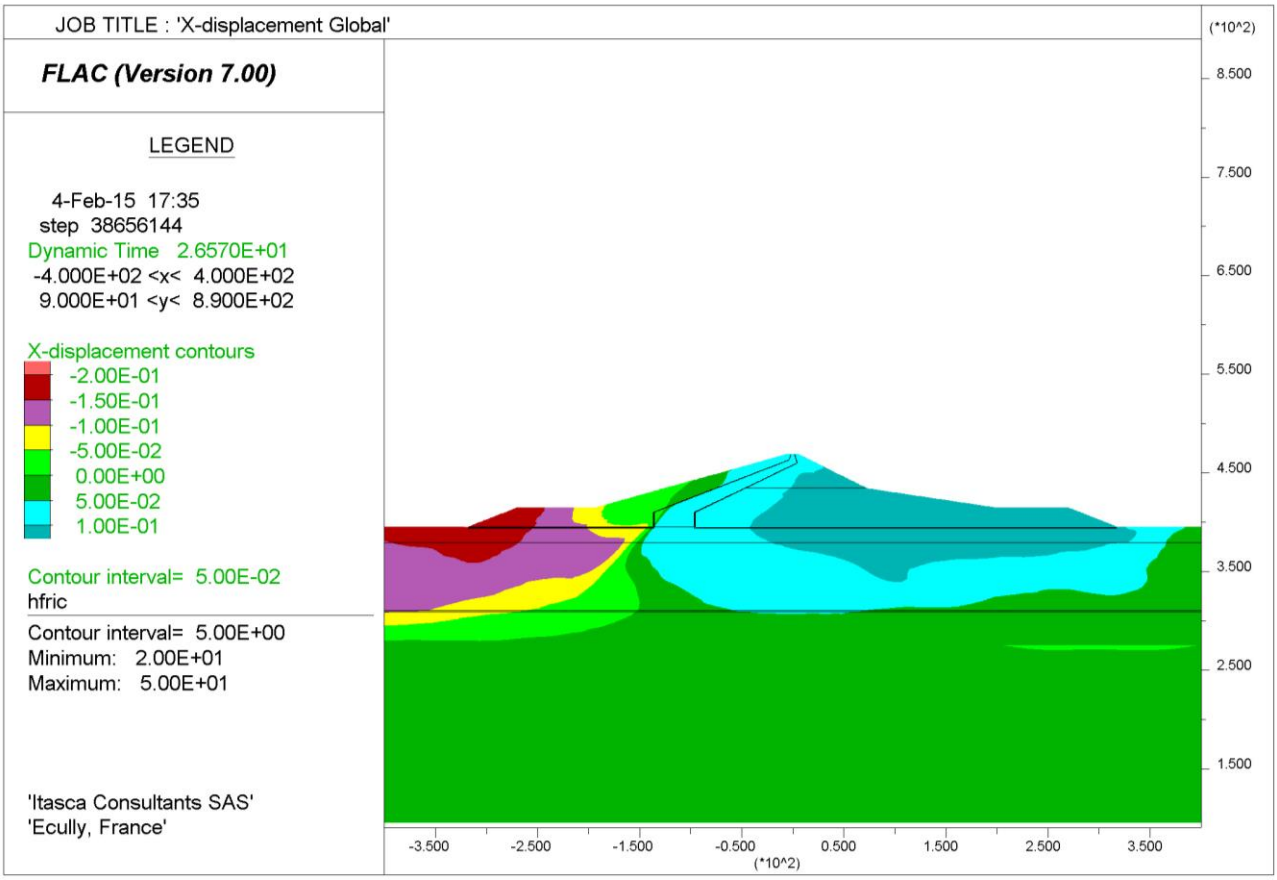

Figure 4-58 Nonlinear analysis – OBE earthquake Darfield LPCC (V-H2)
Final horizontal displacements

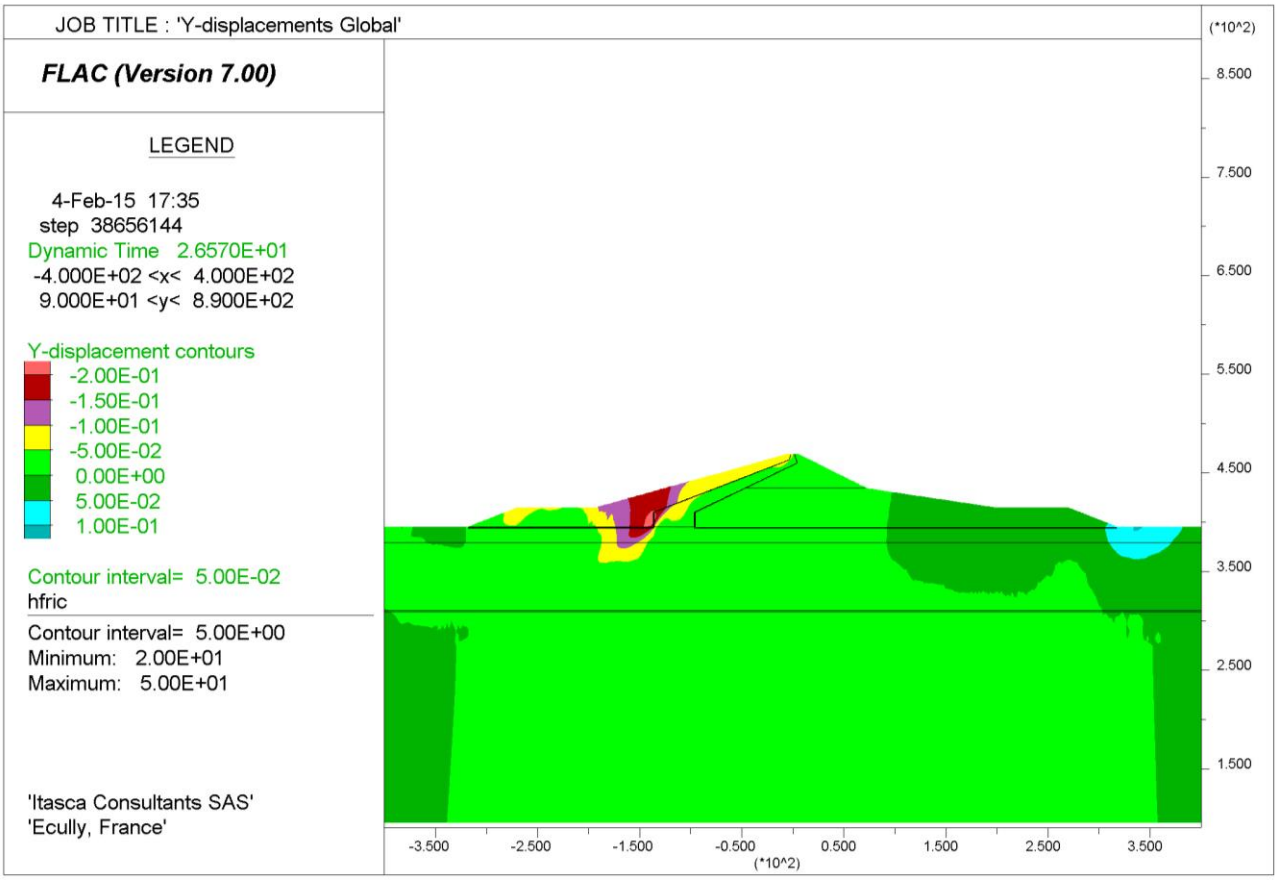

Figure 4-59 Nonlinear analysis – OBE earthquake Darfield LPCC (V-H2)
Final vertical displacements

4.6.3. SEE earthquake – Pseudo-static Newmark's Sliding Block Analysis

In this section the pseudo-static Newmark's Sliding Block analysis of the Bisri dam will be presented, considering the SEE earthquake Kocaeli IZT (V-H1, PGA V + 0.51 / - 0.43 H1 + 0.82 / - 0.63).

Newmark's analysis, when compared to a dynamic FLAC simulation, could be too pessimistic, since all accelerations beyond the limit acceleration (equal to Kh*g) are considered as source of permanent plastic deformations. Also, it could be too optimistic, since it doesn't take into account of the reduction of strength properties that occurs during cyclic loading. The values of maximum displacements give an idea of the order of magnitude of the displacements that are to be expected in the dynamic analysis, this latter allowing a more realistic reproduction of materials behavior under seismic loading.

The procedure that is adopted to perform such analysis is the following (see Figure 4-60):

a) An iterative procedure is adopted to determine the minimum seismic coefficient [*g* units] that causes failure of the dam-foundation structure;
b) Simple integration of acceleration time history using the yield acceleration determined in (a) as cut-off.

The vertical component of the seismic acceleration, that would lighten the soil, is neglected at this stage. This is not a conservative choice. A complete analysis, including both components of acceleration, will be performed in case a more conservative analysis will be needed.

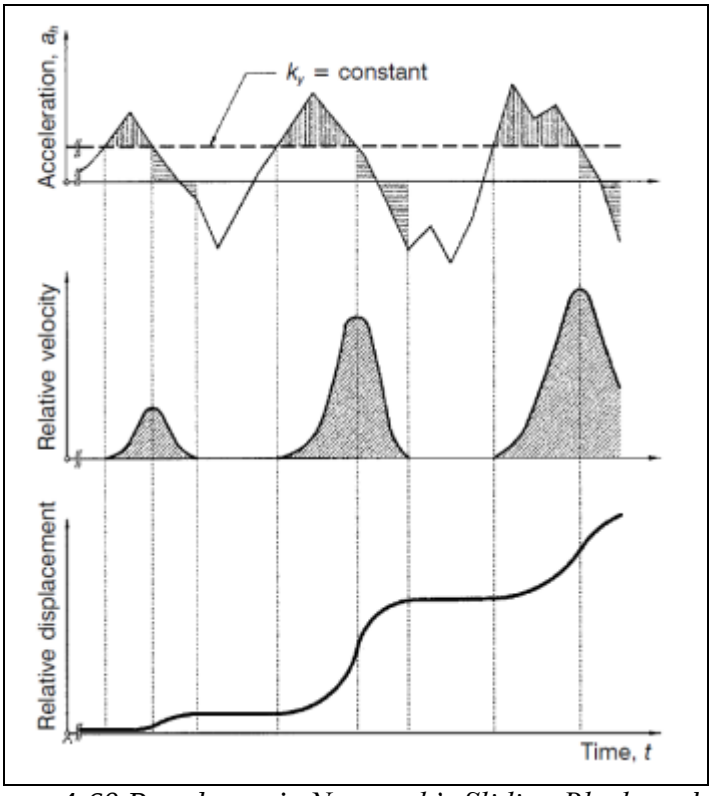

Figure 4-60 Pseudo-static Newmark's Sliding Block analysis

4.6.3.1. Downstream analysis

Coefficient Kh [*g* units] is varied (increased gradually) to determine the minimum seismic coefficient that causes failure of the dam-foundation structure (see Figure 4-61). A coefficient Kh=0.17 was found. Figure 4-62 and Figure 4-63 show the maximum shear increment and the plastic zones, as they were obtained for Kh=0.17.

It can be seen that the failure concerns both the dam and the foundation layers. Considering a yield acceleration equal to Kh*g, a relative acceleration can be computed (Figure 4-65).

The relative velocity (Figure 4-66) is then calculated by integrating the relative acceleration at the base of the sliding block with respect to time, not taking into account negative values.

The relative displacement is finally obtained by integration of the relative velocity (Figure 4-67). A relative displacement of more than 9 meters is computed.

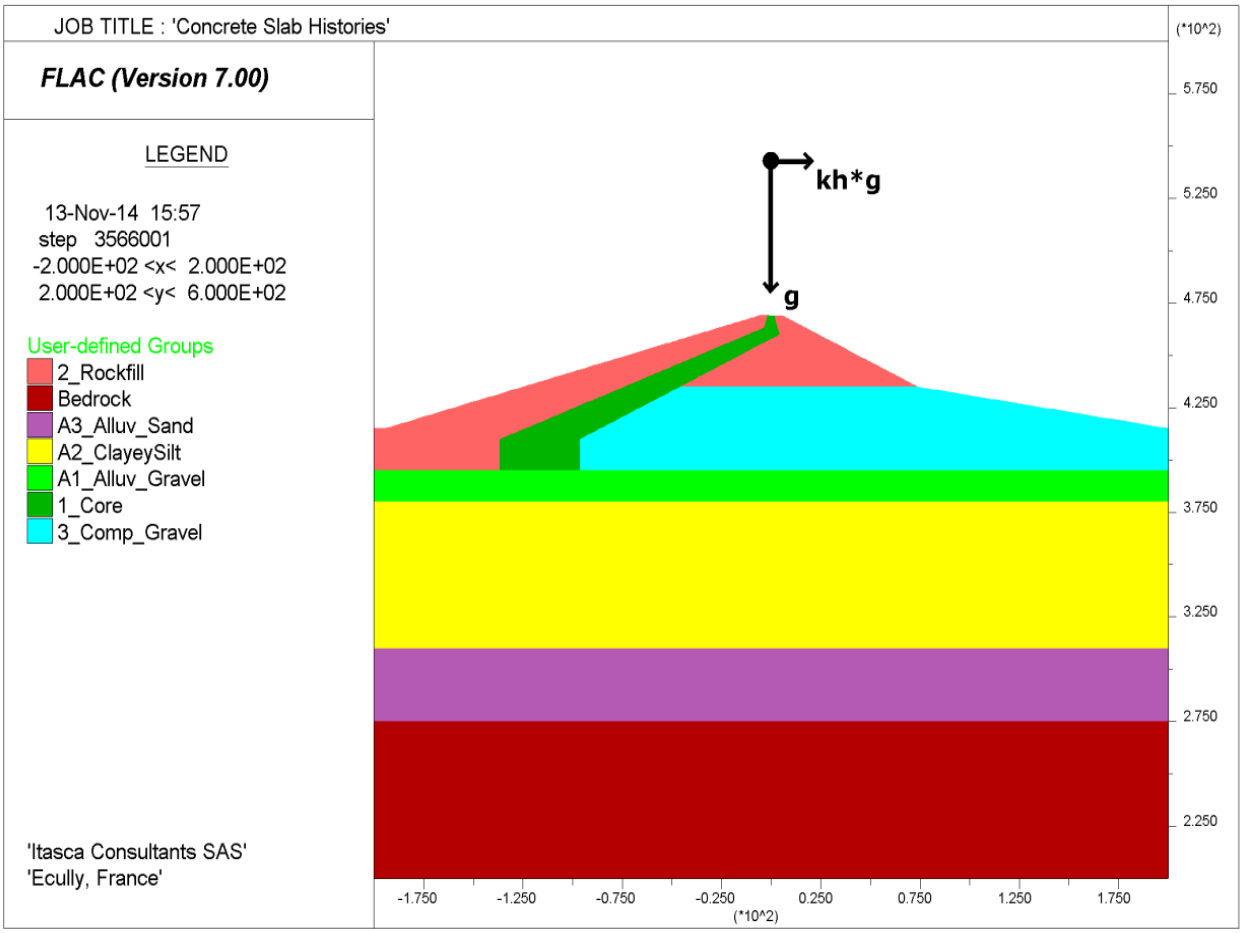

Figure 4-61 : Pseudo-static analysis - Downstream

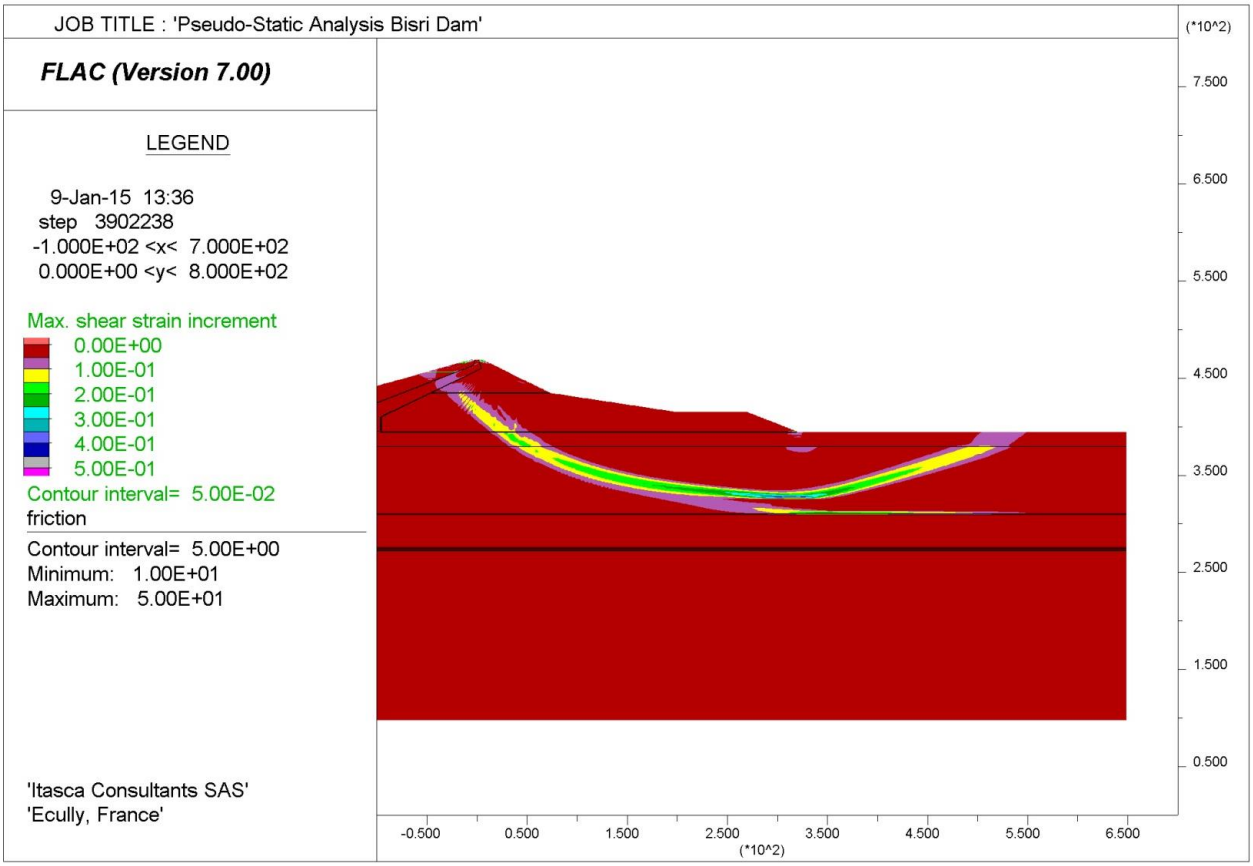

Figure 4-62 : Maximum shear strain increment – Downstream analysis (Kh = 0.17)

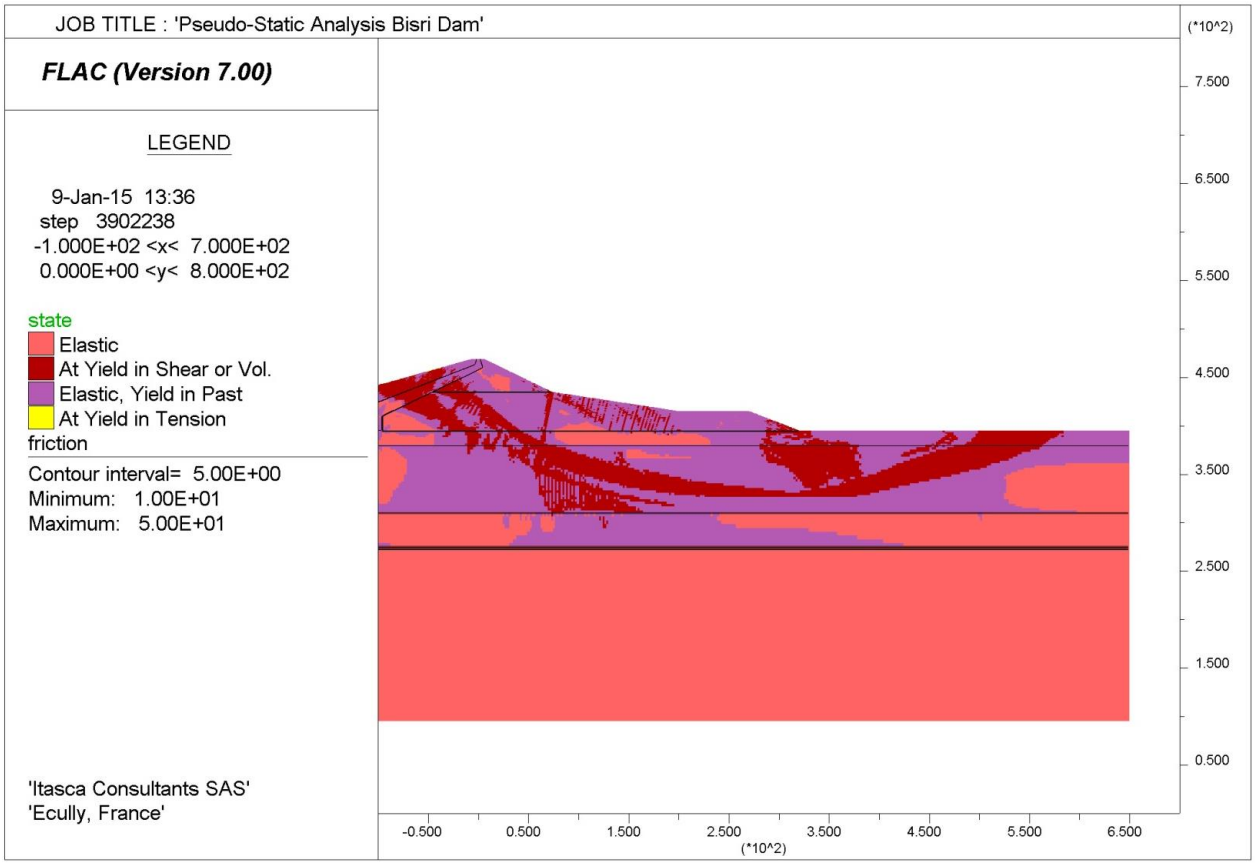

Figure 4-63 : Plastified zones – Downstream analysis (Kh = 0.17)

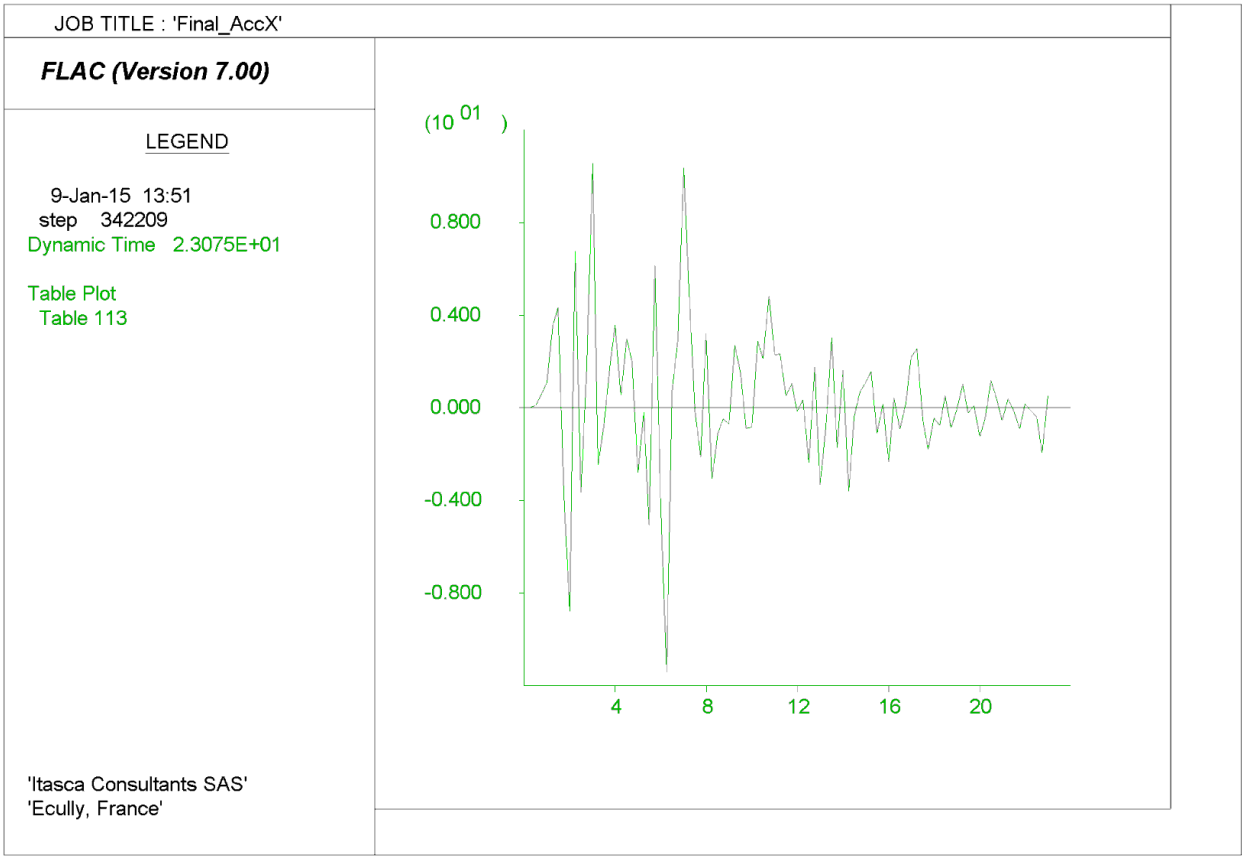

Figure 4-64 : Downstream analysis - Input horizontal acceleration a(t) (KOCAELI IZT V-H1)

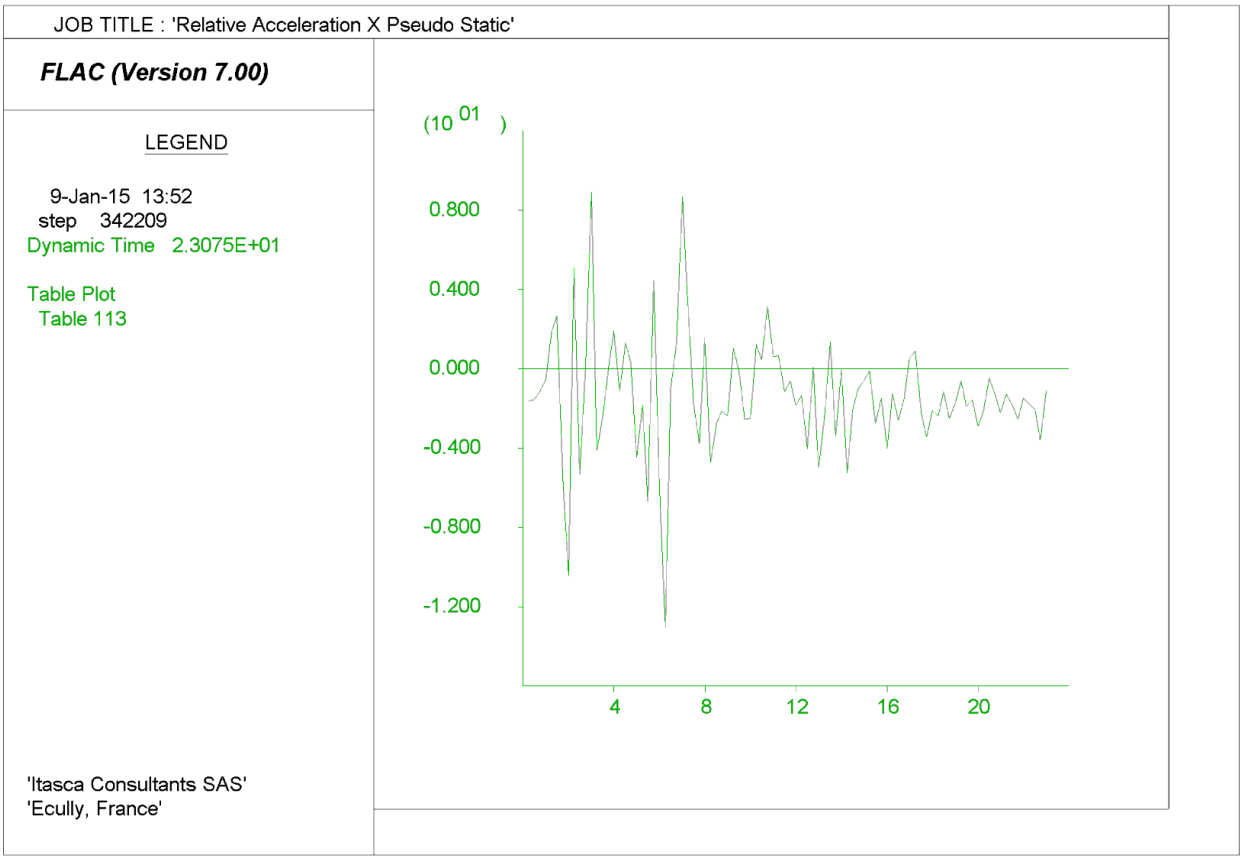

*Figure 4-65 : Downstream analysis - Relative horizontal acceleration ar(t) = a(t) – Kh*g*

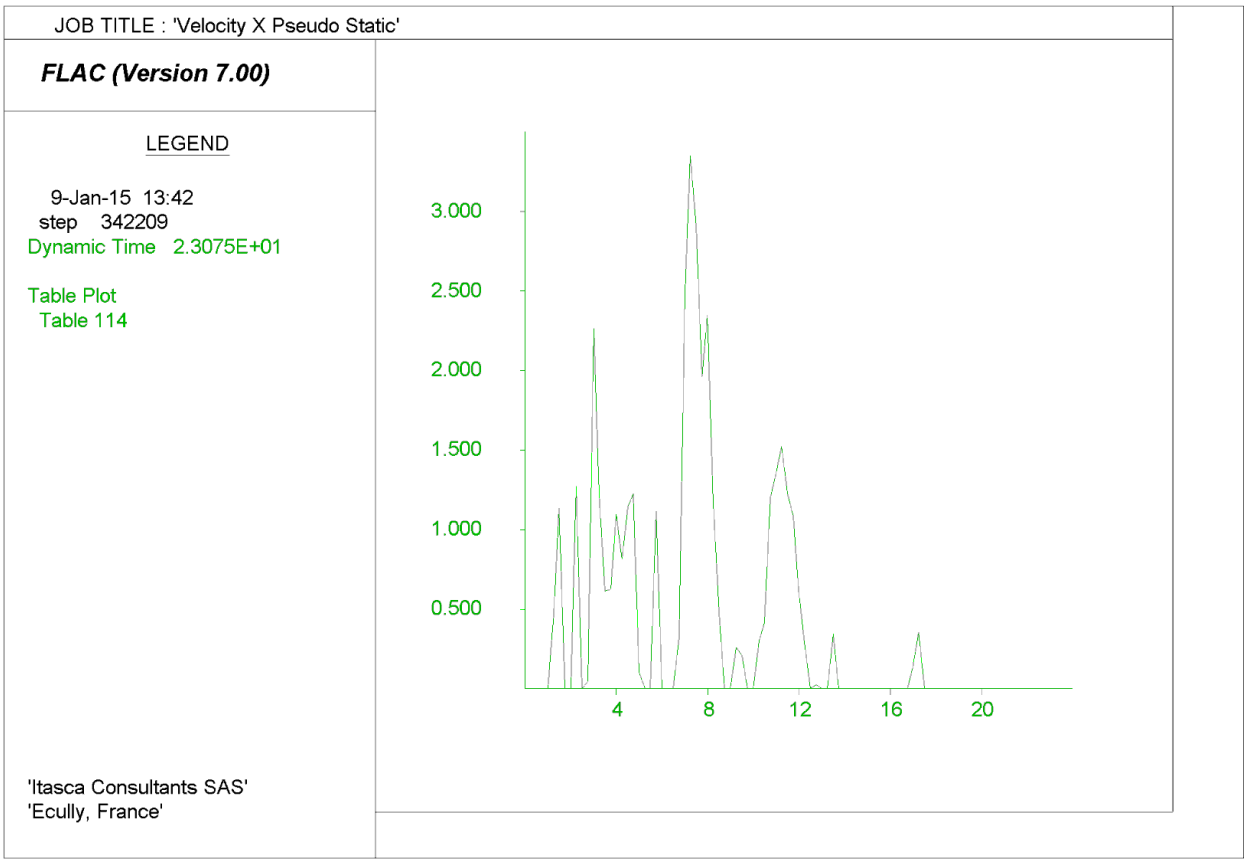

Figure 4-66 : Downstream analysis - Relative velocity (integration of relative acceleration)

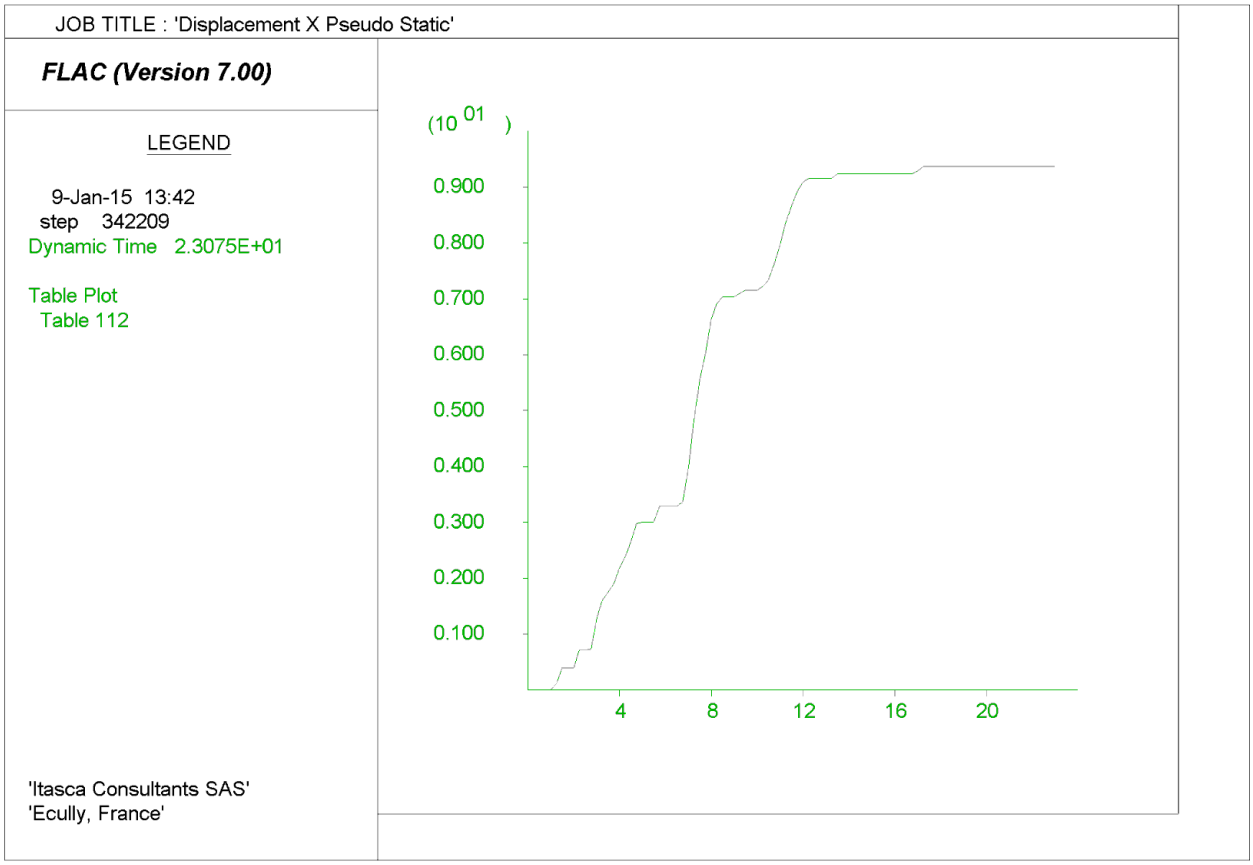

Figure 4-67 : Downstream analysis - Relative displacement (integration of relative velocity)

4.6.3.2. Upstream analysis

Similarly to what it was done for the downstream analysis, an upstream analysis is performed (see Figure 4-68). A coefficient Kh=-0.16 was found. Figure 4-69 and Figure 4-70 show the maximum shear increment and the plastified zones, as they were obtained for Kh = - 0.16.

Considering a yield acceleration equal to Kh*g, a relative acceleration is computed (Figure 4-72).

The relative velocity (Figure 4-73) is then calculated by integrating the relative acceleration with respect to time, not taking into account negative values.

The relative displacement is finally obtained by integration of the relative velocity (Figure 4-74). A negative relative displacement of more than 4 meters is computed.

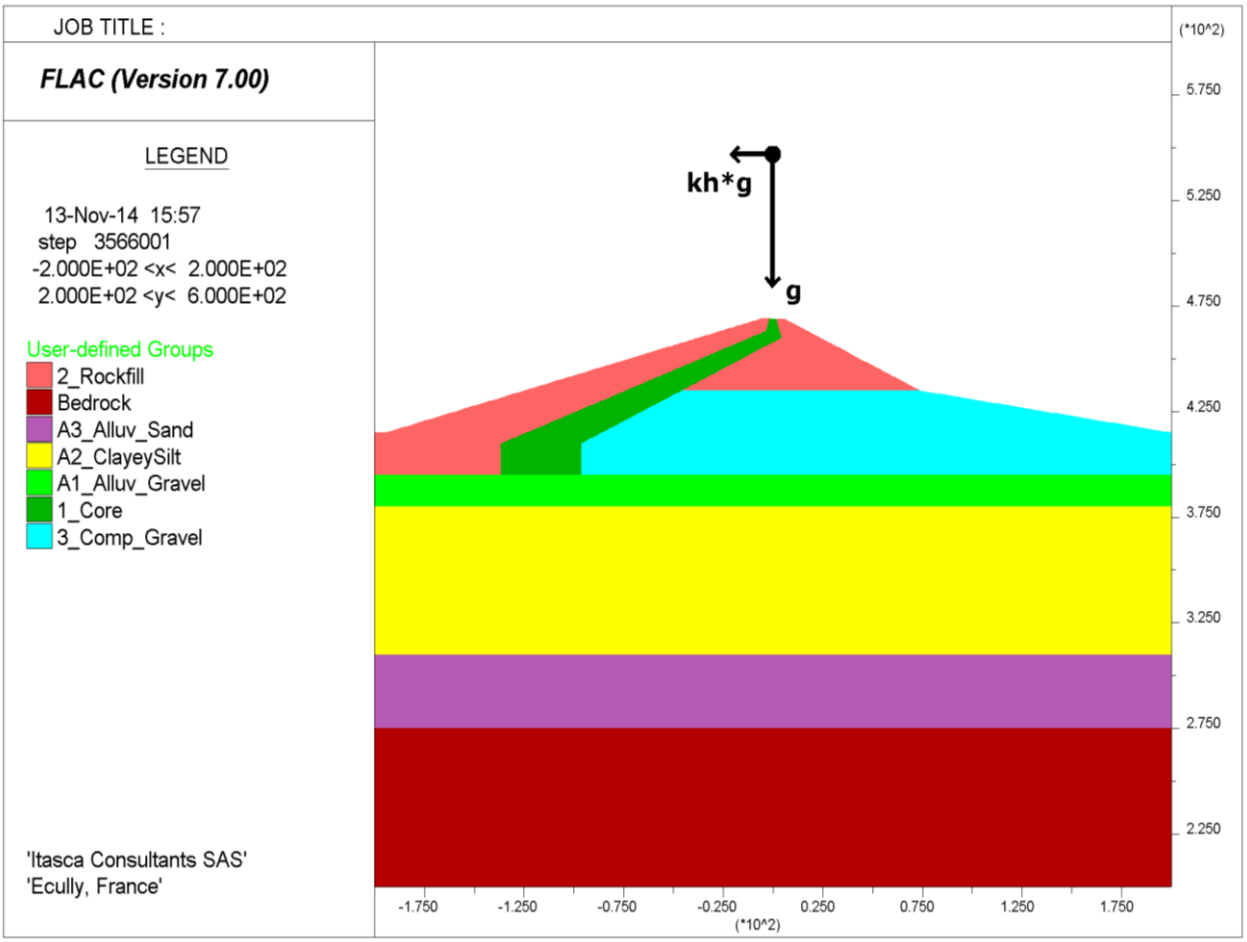

Figure 4-68 : Pseudo-static analysis - Upstream

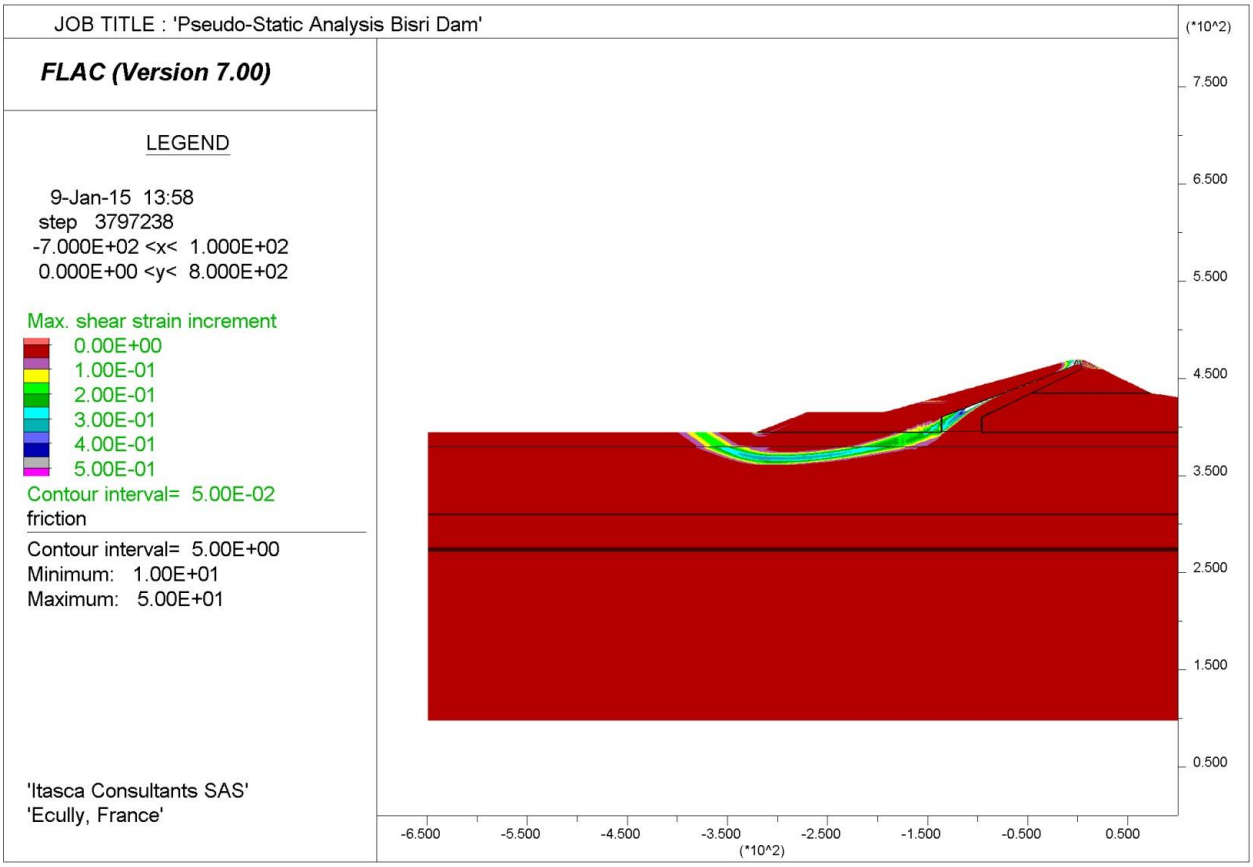

Figure 4-69 : Maximum shear strain increment – Upstream analysis (Kh = 0.17)

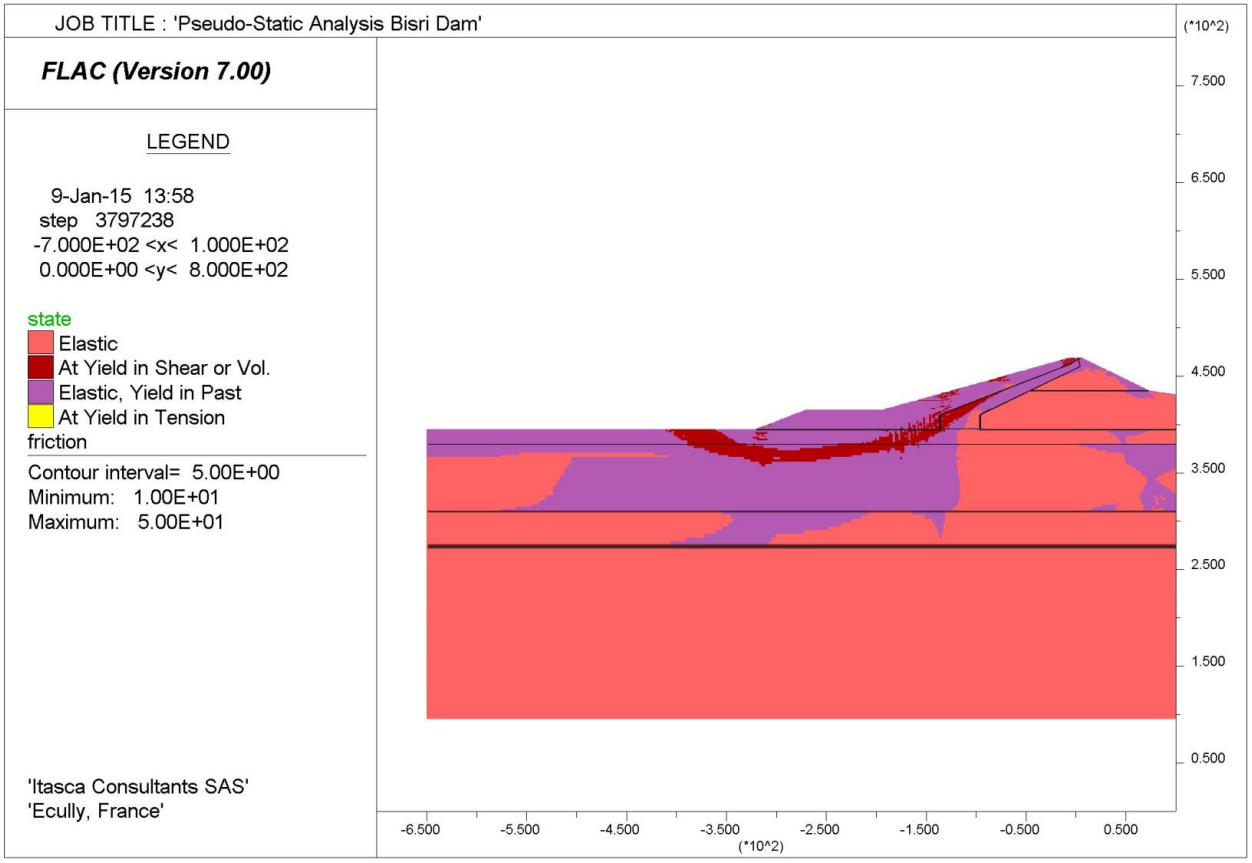

Figure 4-70 : Plasticized zones – Upstream analysis (Kh = 0.17)

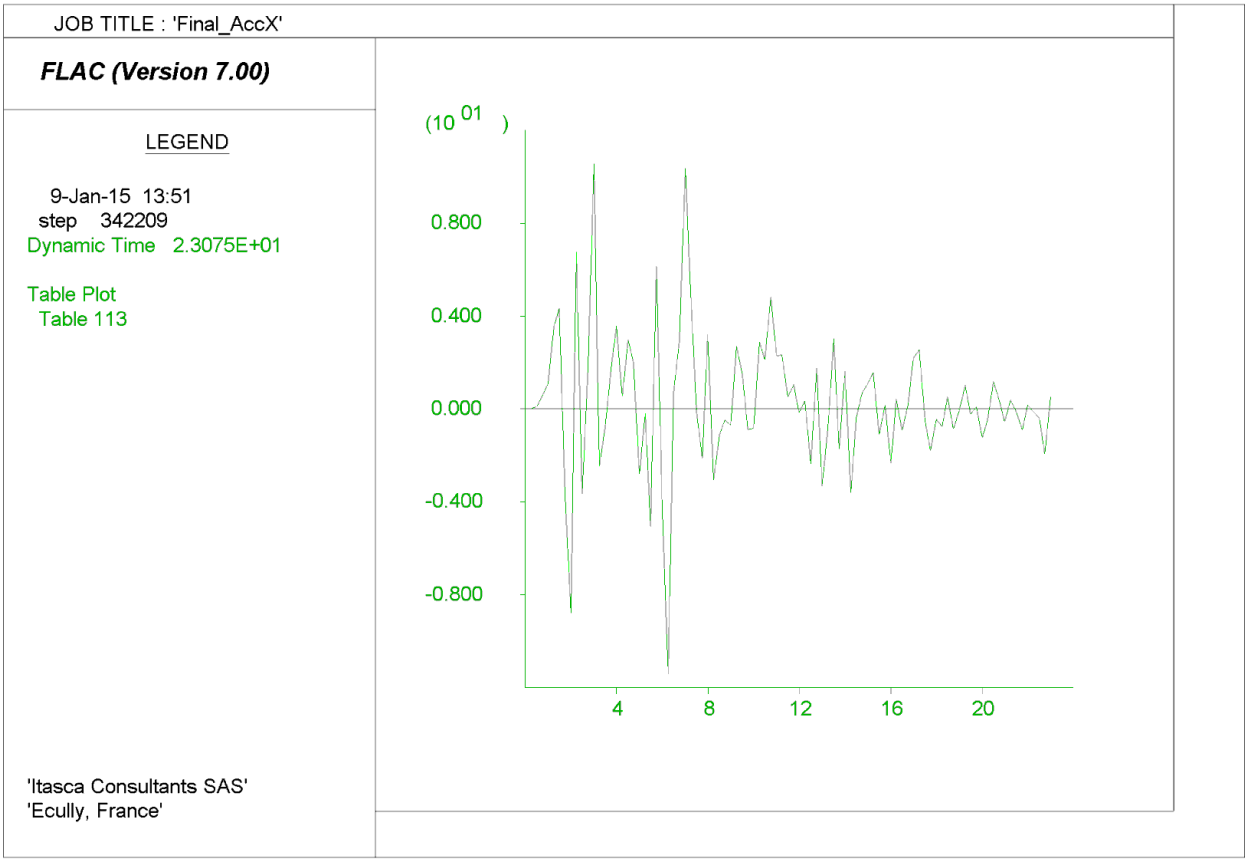

Figure 4-71 : Upstream analysis - Input horizontal acceleration a(t) (KOCAELI IZT V-H1)

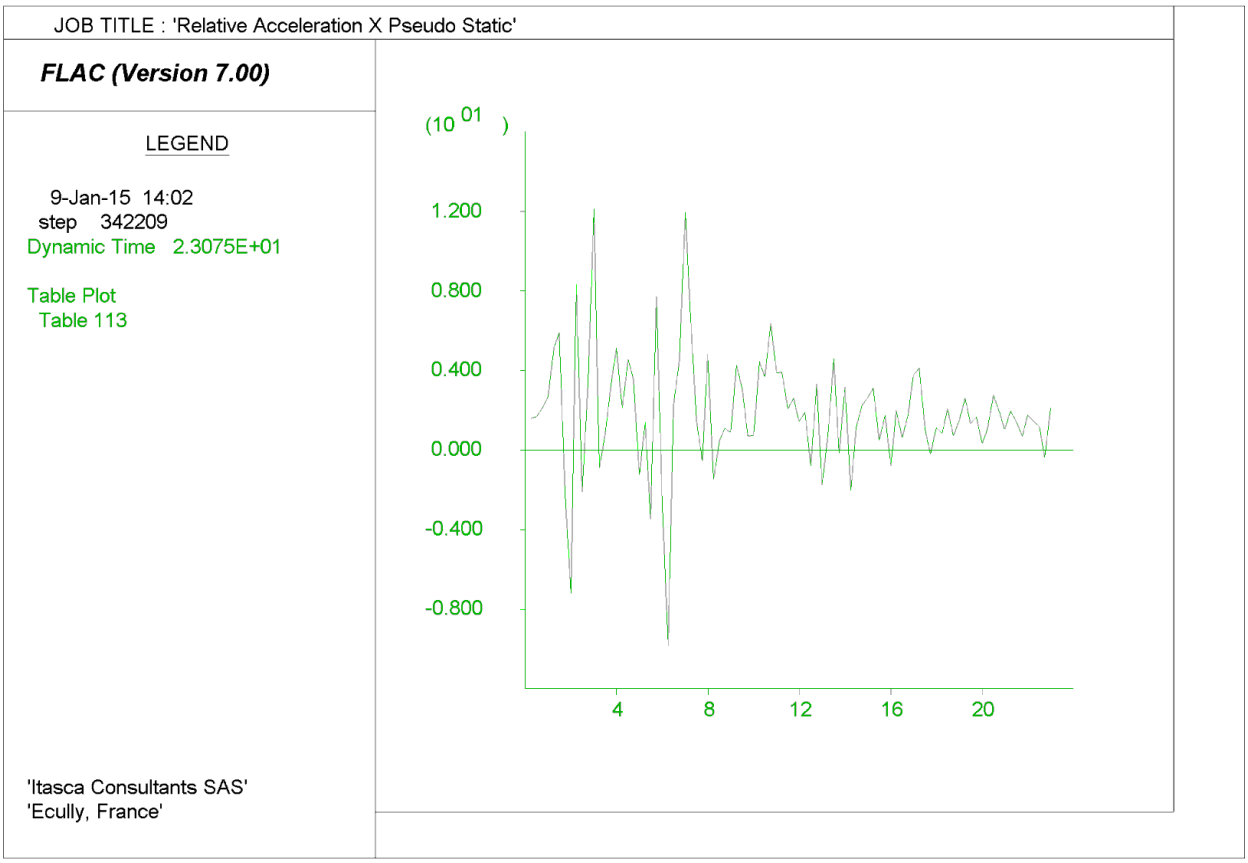

*Figure 4-72 : Upstream analysis - Relative horizontal acceleration ar(t) = a(t) – Kh*g*

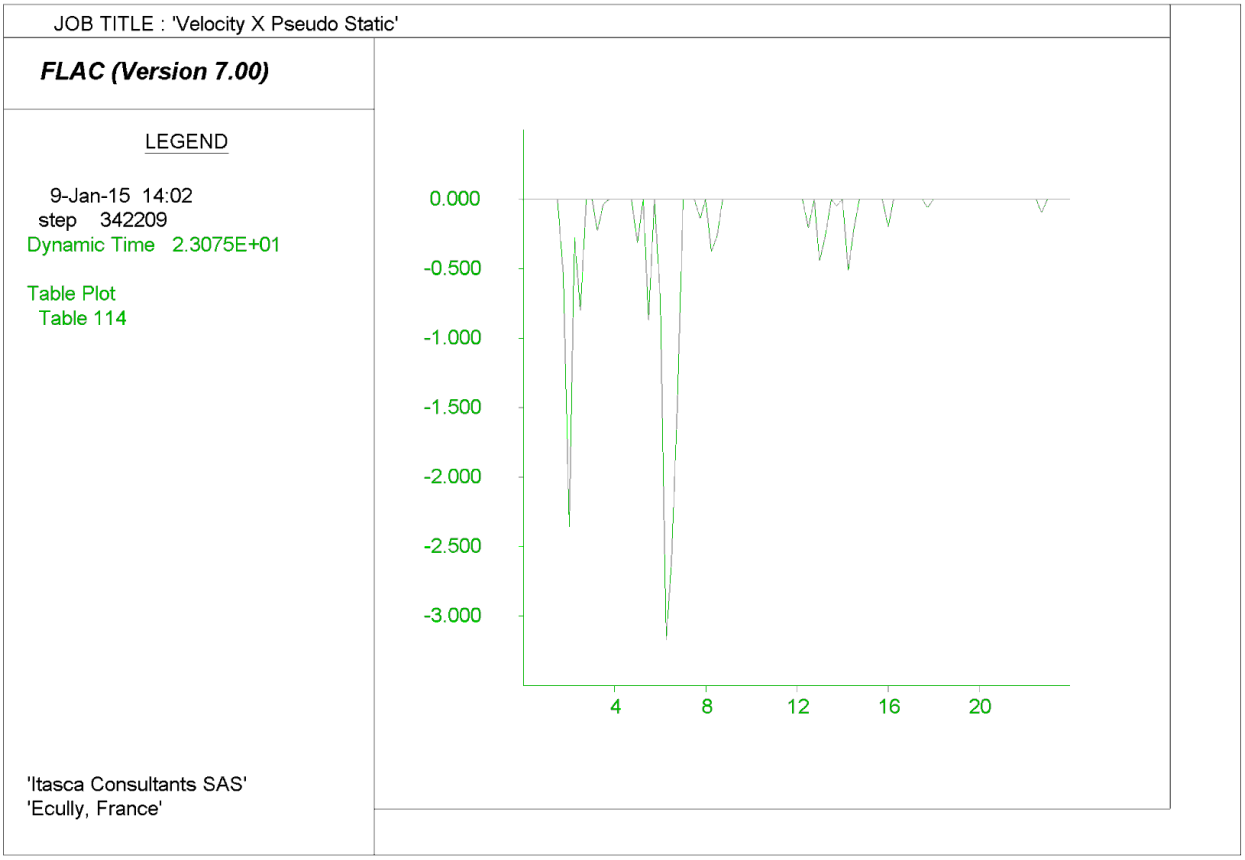

Figure 4-73 : Upstream analysis - Relative velocity (integration of relative acceleration)

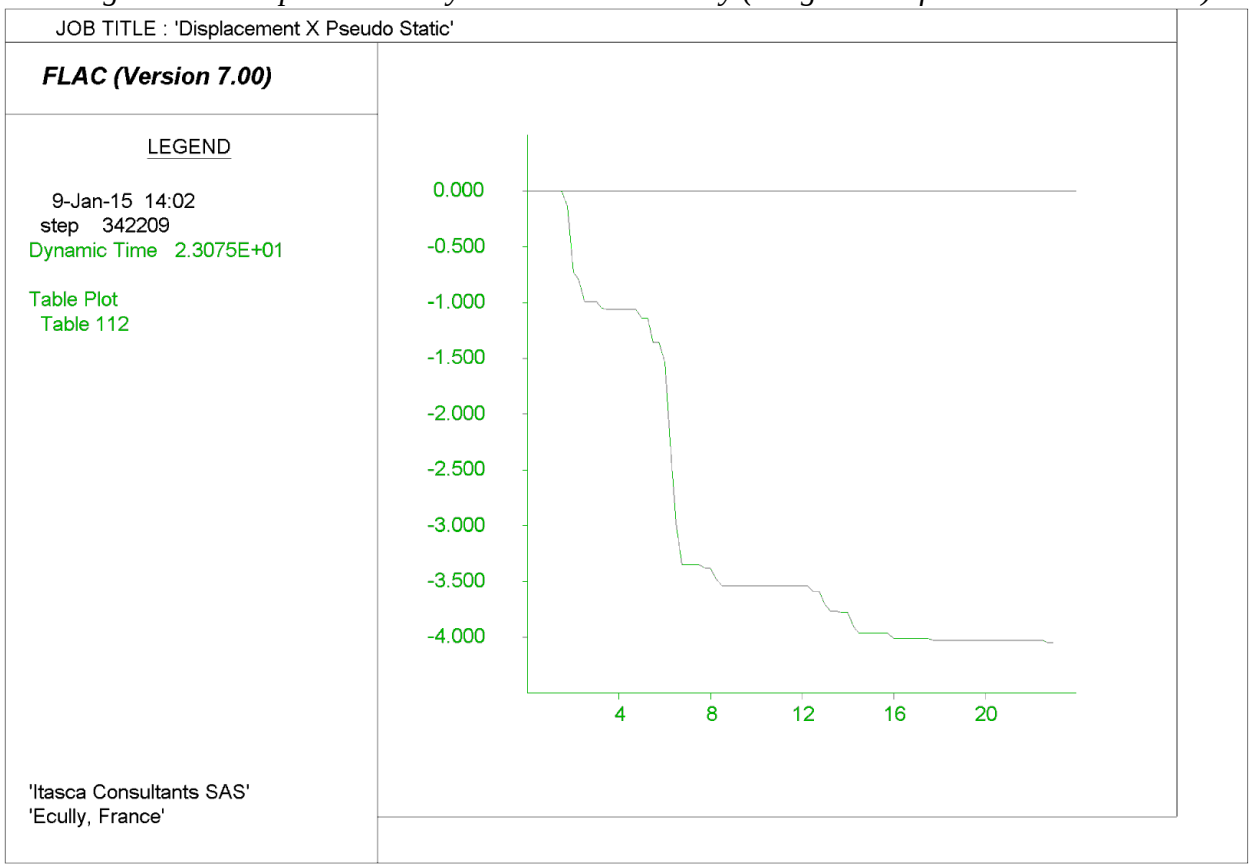

Figure 4-74 : Upstream analysis - Relative displacement (integration of relative velocity)

4.6.3.1. Summary of results and comments

The table below summarizes the results that were obtained. The measured displacements are very high. It is worth noticing that they have to be intended as rigid displacements of the sliding mass along the failure surfaces of Figure 4-62 and Figure 4-69.

SEE EARTHQUAKE - KOCAELI IZT V-H1			
		Pseudo-static Analysis	
Analysis		Kh [g]	Max Displacement
Downstream		0.17	> 9 m
Upstream		-0.16	> 4 m

Table 4-2 : Pseudo-static analysis – Summary of results

The correspondent displacement at the dam crest, noting as *D* the computed displacement along the failure surface (see Figure 4-75) and as α the angle between the vertical and the failure surface, can be computed. For the downstream analysis, an angle α equal to 43° can be measured, therefore a dam crest displacement of about 6.5m can be estimated. Concerning the upstream analysis, a dam crest vertical displacement of about 3m can be estimated, considering an angle α equal to 42° (see Figure 4-76).

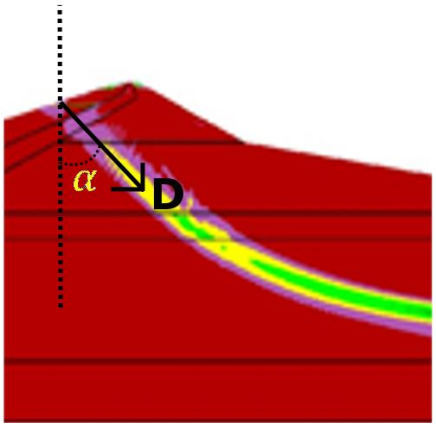

Figure 4-75 : Pseudo-static Newmark's downstream analysis – Displacement at the dam crest

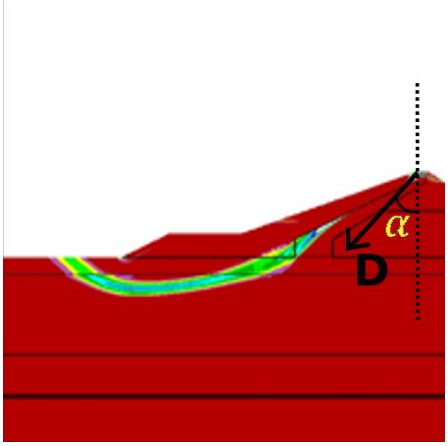

Figure 4-76 : Pseudo-static Newmark's upstream analysis – Displacement at the dam crest

4.6.4. SEE earthquake – Nonlinear analysis

The results issued from the nonlinear dynamic simulation of the dam-foundation response to the SEE earthquakes are presented in this section.

Table 4-3 summarizes the maximum displacements that were observed at the dam crest. Displacement fields for all the tested cases are plotted from Figure 4-79 to Figure 4-90. Horizontal displacements that could affect the stability of the slurry concrete wall are analyzed in section 4.6.4.1.

In all cases the vertical displacement at the crest of the dam is lower than 2 meters (maximum admissible displacement = 4 meters). The main instability processes concern the foot of the downstream embankment and the upstream slope. The foot of the downstream embankment plastifies for all the simulated cases. It is there that the maximum positive horizontal and vertical displacements are encountered. In one case - the Kocaeli IZT V-H1 earthquake - the maximum horizontal displacement is higher than 3 meters (Figure 4-83).

The upstream slope seems to be the most problematic zone. The instability concerns mainly the foot/bench zone in one case (Darfield V-H1, Figure 4-79 and Figure 4-80), whereas it is extended to all the upstream slope in two cases (Darfield V-H2, Figure 4-81 and Figure 4-82 and Kocaeli V-H2, Figure 4-85 and Figure 4-86). Sliding of the rockfill along the interface between the dam core and the rockfill occurs: this is confirmed by the plot of the maximum shear increment (Figure 4-77), and by the magnified grid deformation of Figure 4-78, where the relative sliding between the rockfill and the dam core is particularly evident close to the crest of the dam.

Figure 4-79 and Figure 4-80 show the final horizontal and vertical displacements, respectively, corresponding to the SEE earthquake Darfield LPCC (PGA V + 0.5 / - 0.58 H1 + 0.96 / - 1.33).
Figure 4-81 and Figure 4-82 show the final horizontal and vertical displacements, respectively, corresponding to the SEE earthquake Darfield LPCC (PGA V + 0.5 / - 0.58 H2 + 0.79 / - 0.89).
Figure 4-83 and Figure 4-84 show the final horizontal and vertical displacements, respectively, corresponding to the SEE earthquake Kocaeli IZT (PGA V + 0.51 / - 0.43 H1 + 0.82 / - 0.63).
Figure 4-85 and Figure 4-86 show the final horizontal and vertical displacements, respectively, corresponding to the SEE earthquake Kocaeli IZT (PGA V + 0.51 / - 0.43 H2 + 0.47 / - 0.59).
Figure 4-87 and Figure 4-88 show the final horizontal and vertical displacements, respectively, corresponding to the SEE earthquake Morgan (PGA V + 0.44 / - 0.43 H1 + 0.81 / - 0.62).
Figure 4-89 and Figure 4-90 show the final horizontal and vertical displacements, respectively, corresponding to the SEE earthquake Morgan (PGA V + 0.44 / - 0.43 H2 + 0.55 / - 1.49).

SEE EARTHQUAKE - REFERENCE CROSS SECTION					
		PGA [g]		Max Crest Displacements [m]	
Name		Vertical	Horizontal	Vertical	Horizontal
Darfield V-H1		+ 0.5 / - 0.58	+ 0.96 / - 1.33	-0.25	+0.60
Darfield V-H2			+ 0.79 / - 0.89	-1.00	-1.50
Kocaeli Izt V-H1		+ 0.51 / - 0.43	+ 0.82 / - 0.63	-0.90	+2.50
Kocaeli Izt V-H2			+ 0.47 / - 0.59	-1.00	-0.80
Morgan V-H1		+ 0.44 / - 0.43	+ 0.81 / - 0.62	-0.20	+0.40
Morgan V-H2			+ 0.55 / - 1.49	-0.20	+0.60

Table 4-3 : SEE earthquakes – Nonlinear analysis – Maximum crest displacements

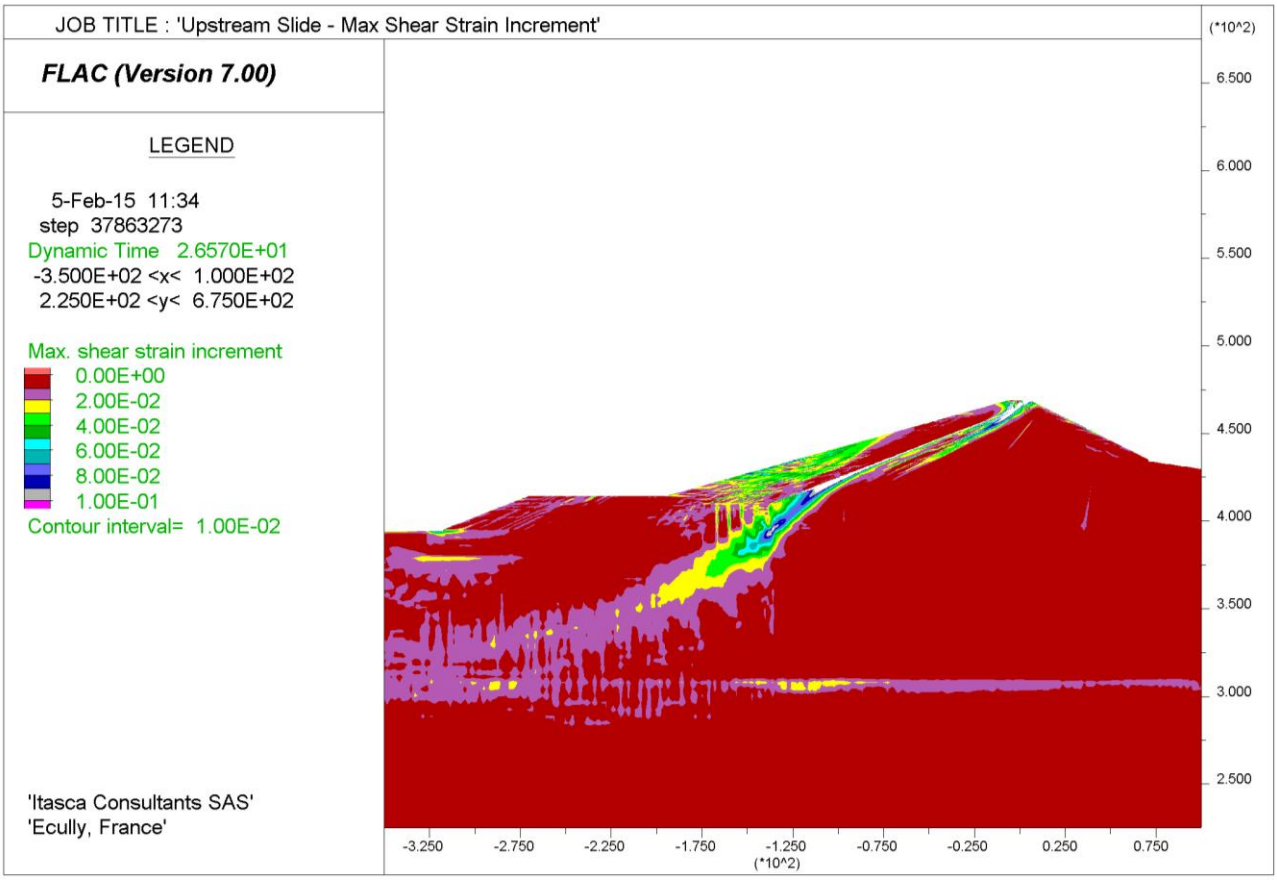

Figure 4-77 : Upstream rockfill sliding – Maximum shear strain increment (SEE Darfield V-H2)

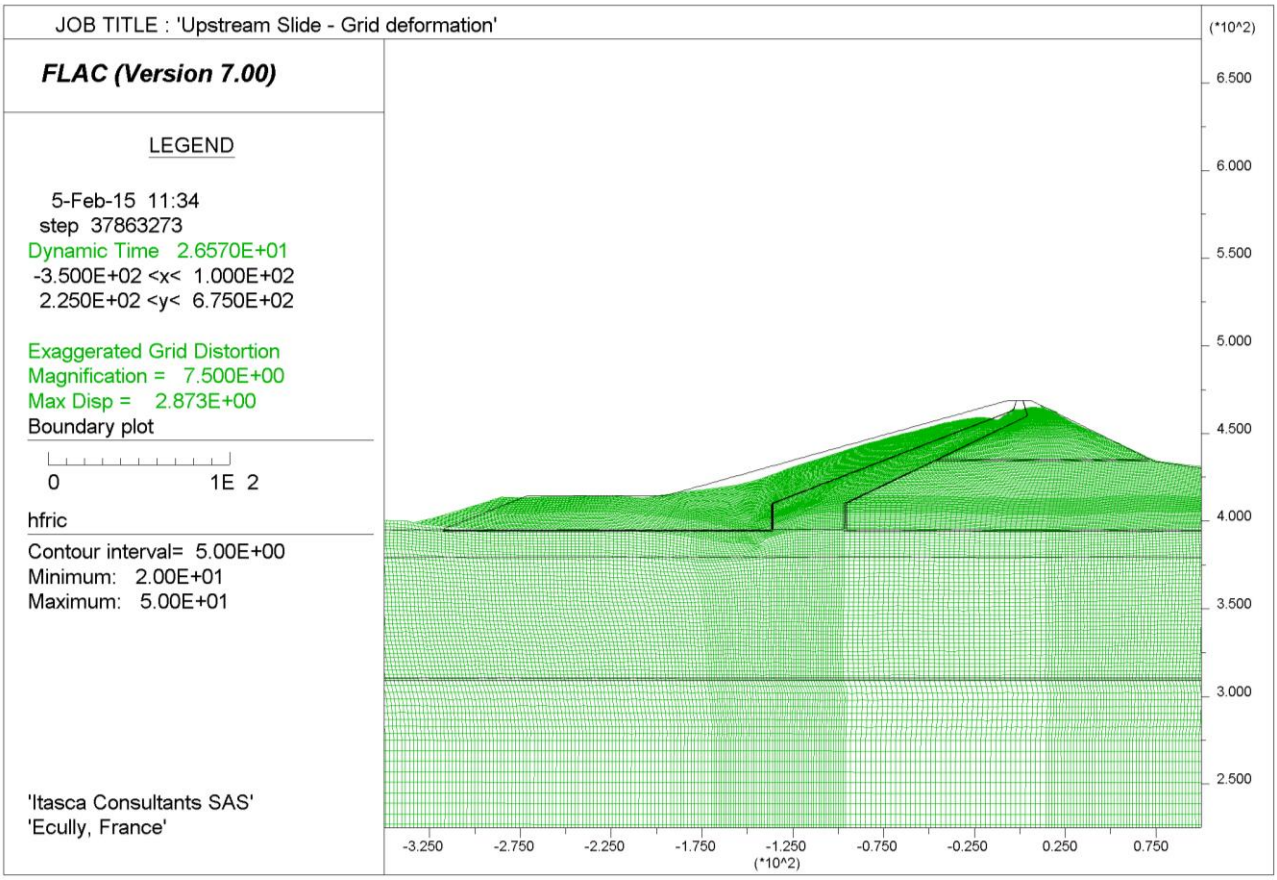

Figure 4-78: Upstream rockfill sliding – Grid magnified deformation (SEE Darfield V-H2)

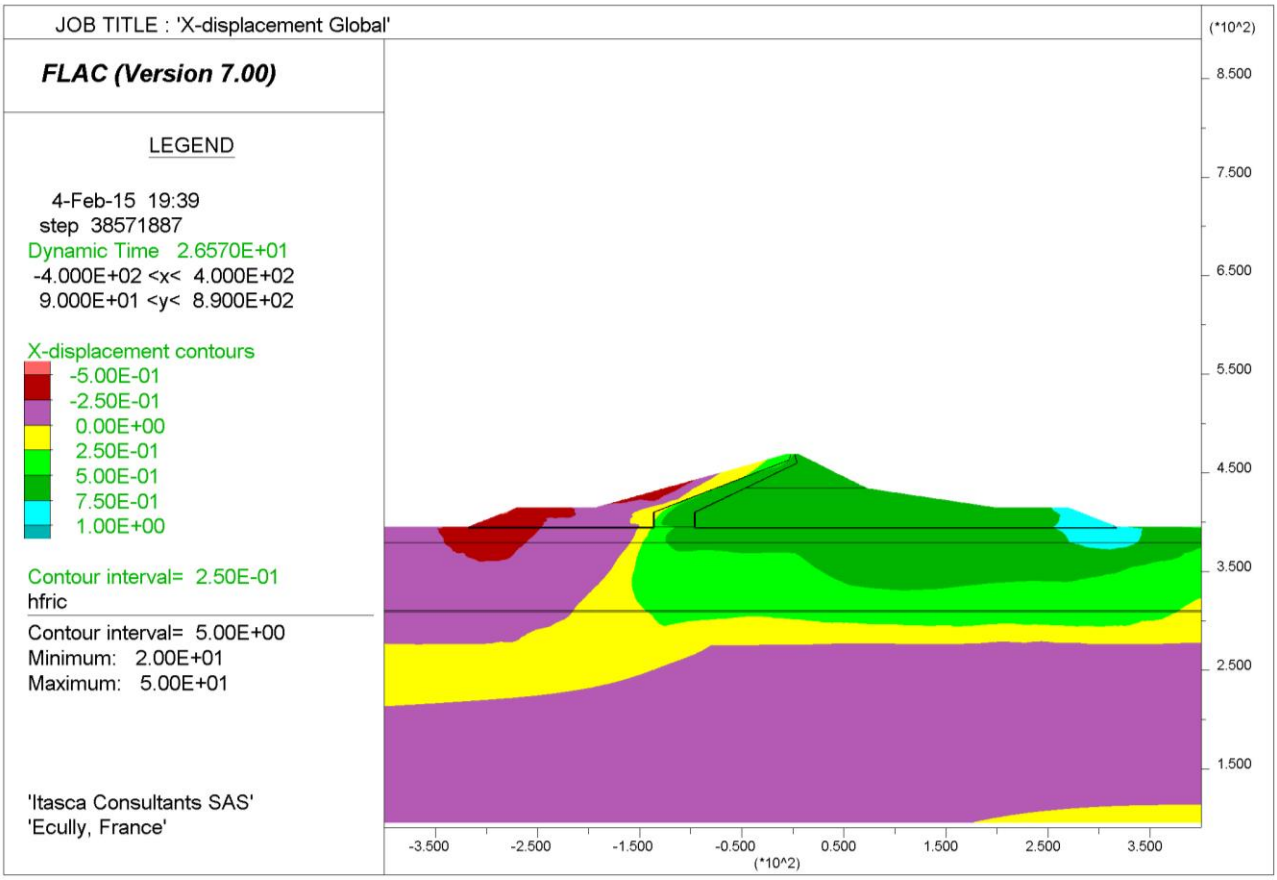

Figure 4-79 Nonlinear analysis – SEE earthquake Darfield LPCC (V-H1)
Final horizontal displacements

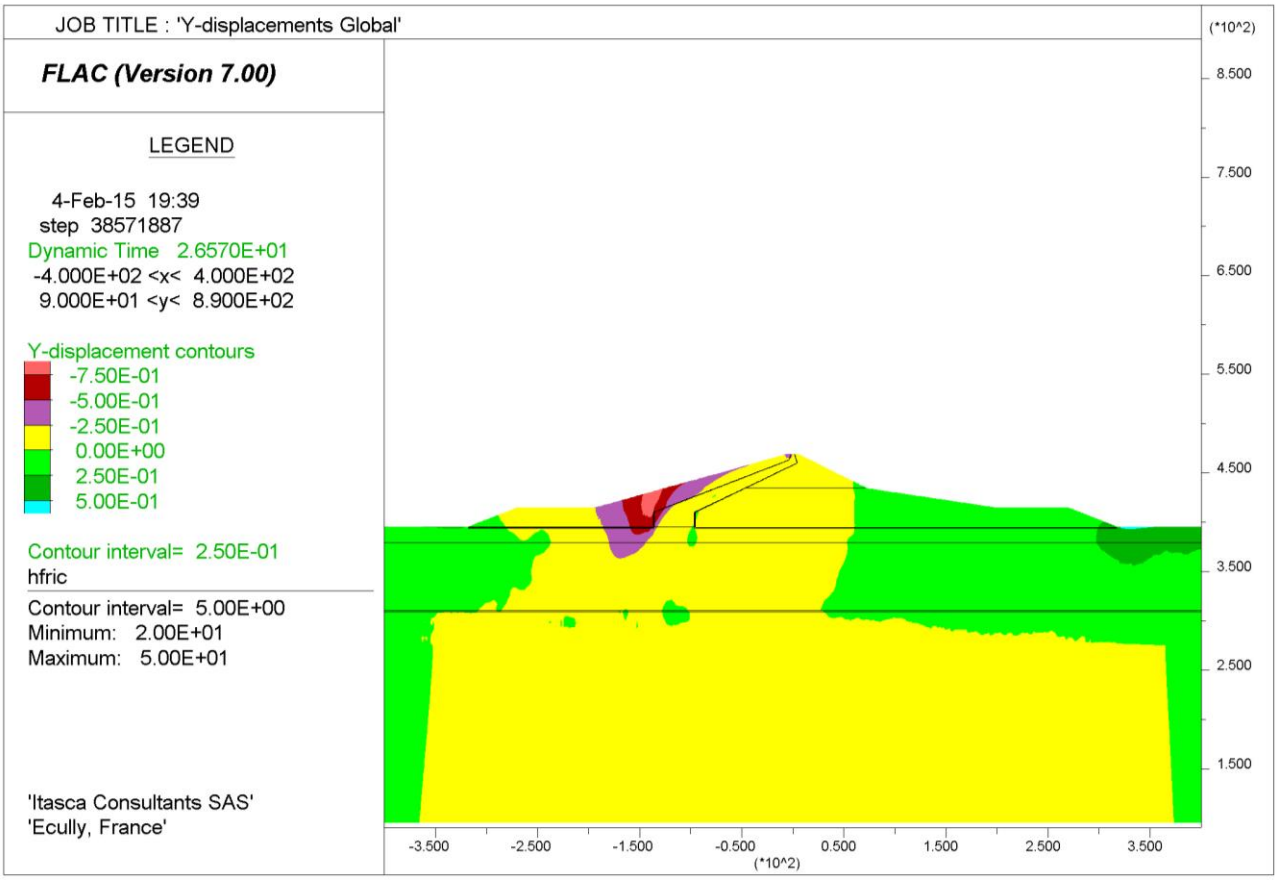

Figure 4-80 Nonlinear analysis – SEE earthquake Darfield LPCC (V-H1)
Final vertical displacements

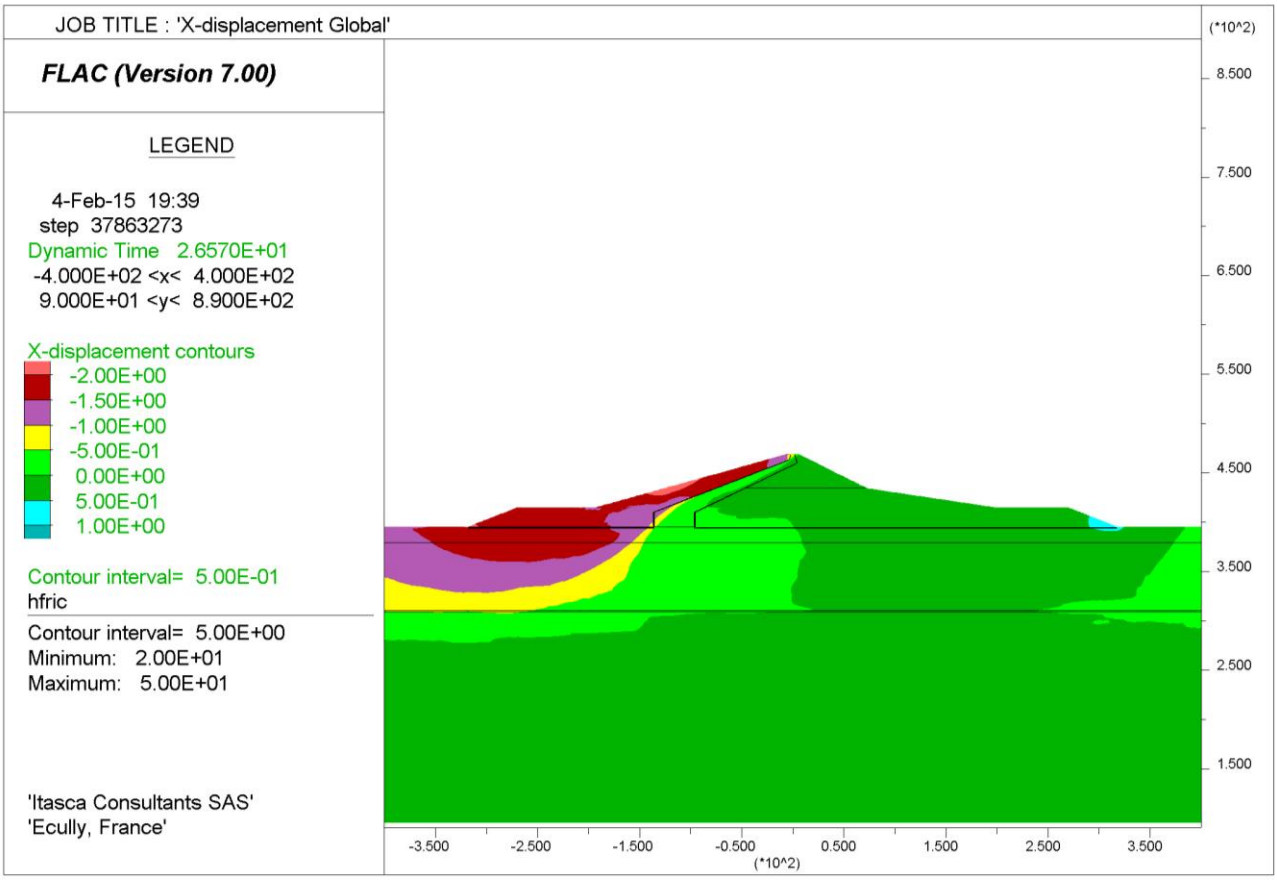

Figure 4-81 Nonlinear analysis – SEE earthquake Darfield LPCC (V-H2)
Final horizontal displacements

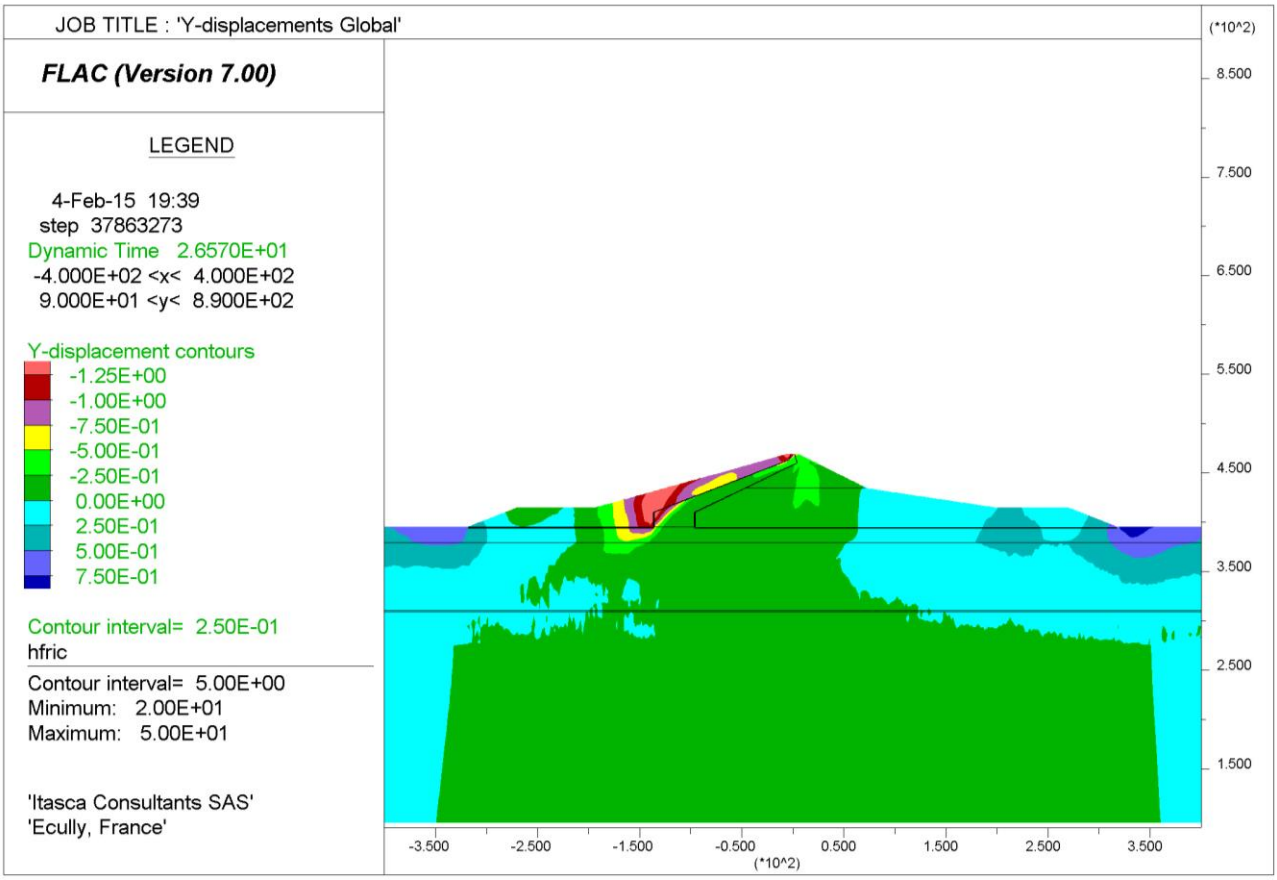

Figure 4-82 Nonlinear analysis – SEE earthquake Darfield LPCC (V-H2)
Final vertical displacements

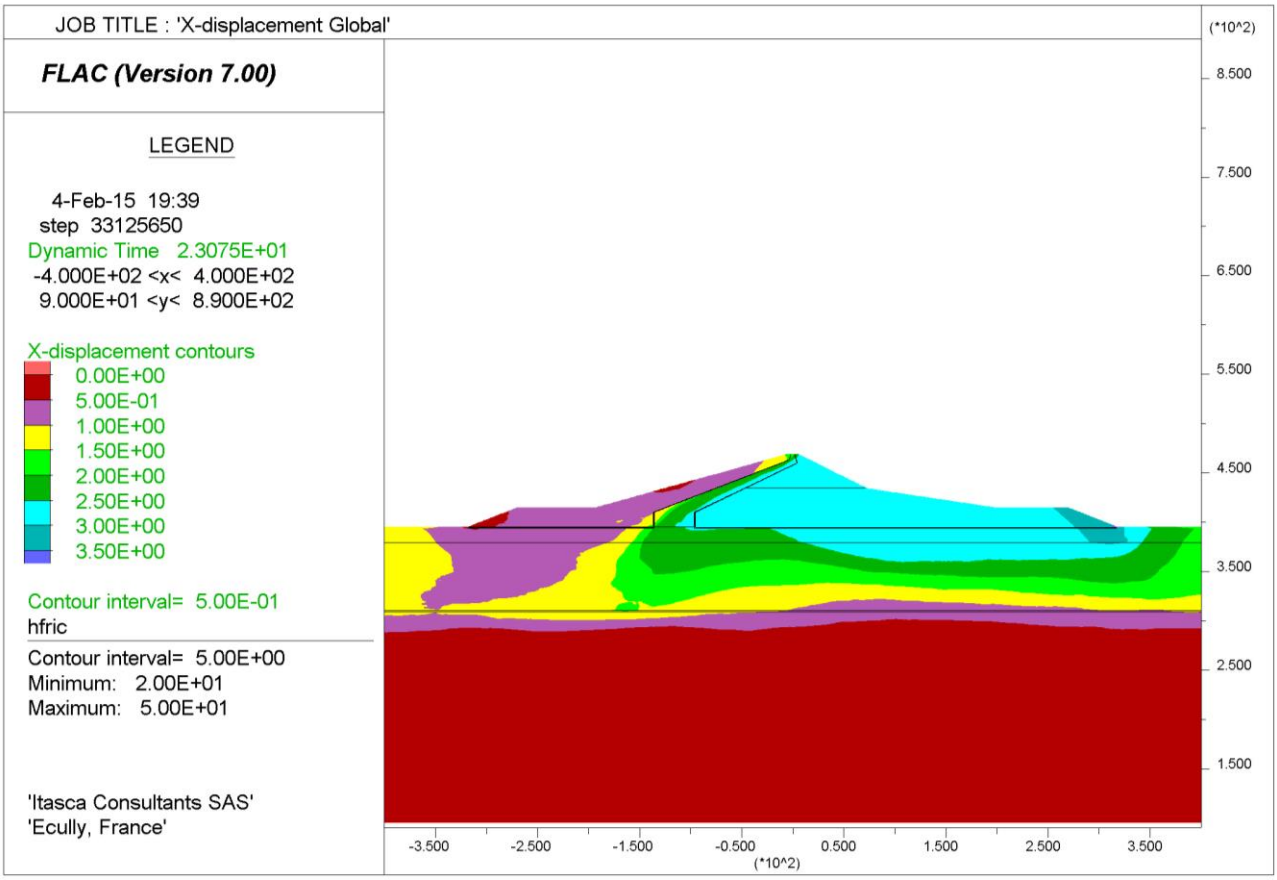

Figure 4-83 Nonlinear analysis – SEE earthquake Kocaeli IZT (V-H1)
Final horizontal displacements

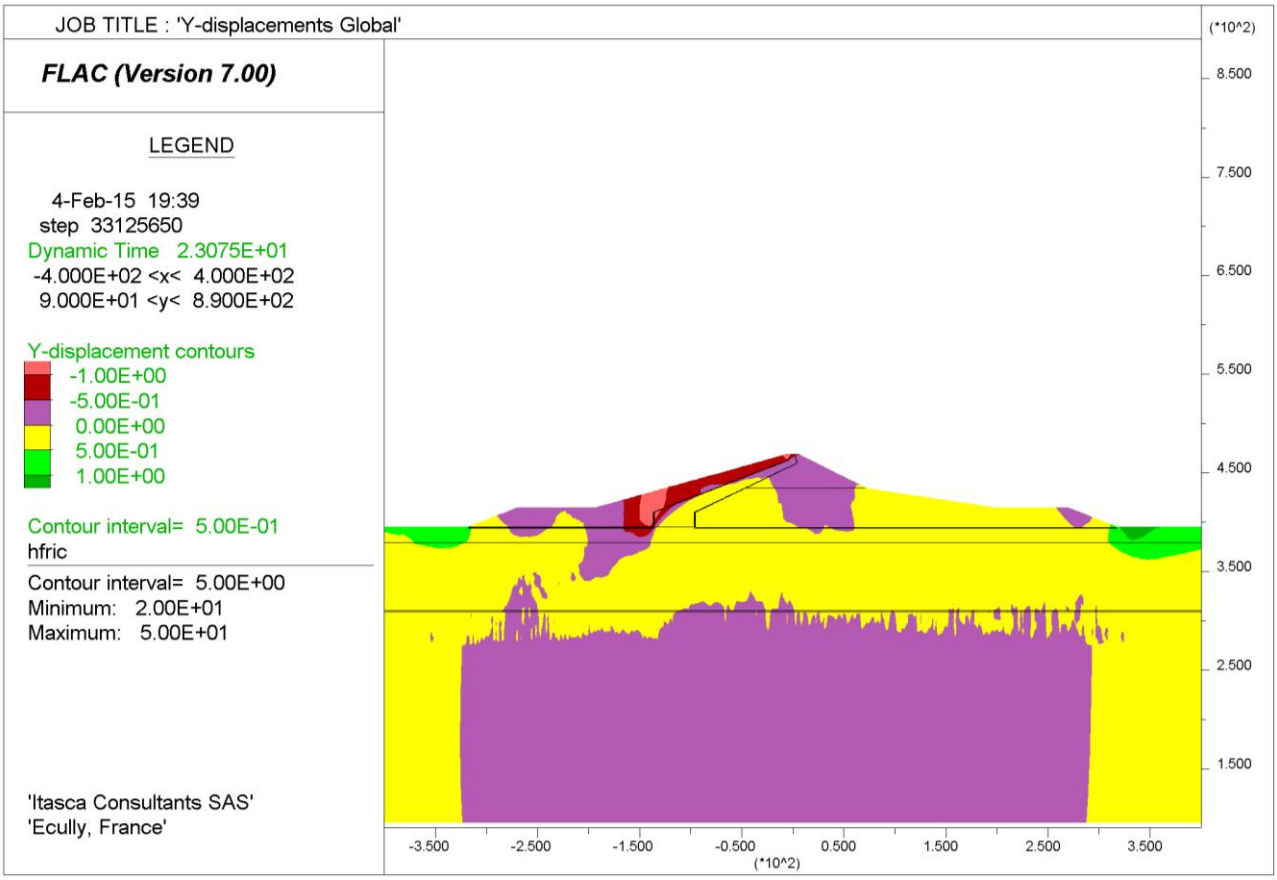

Figure 4-84 Nonlinear analysis – SEE earthquake Kocaeli IZT (V-H1)
Final vertical displacements

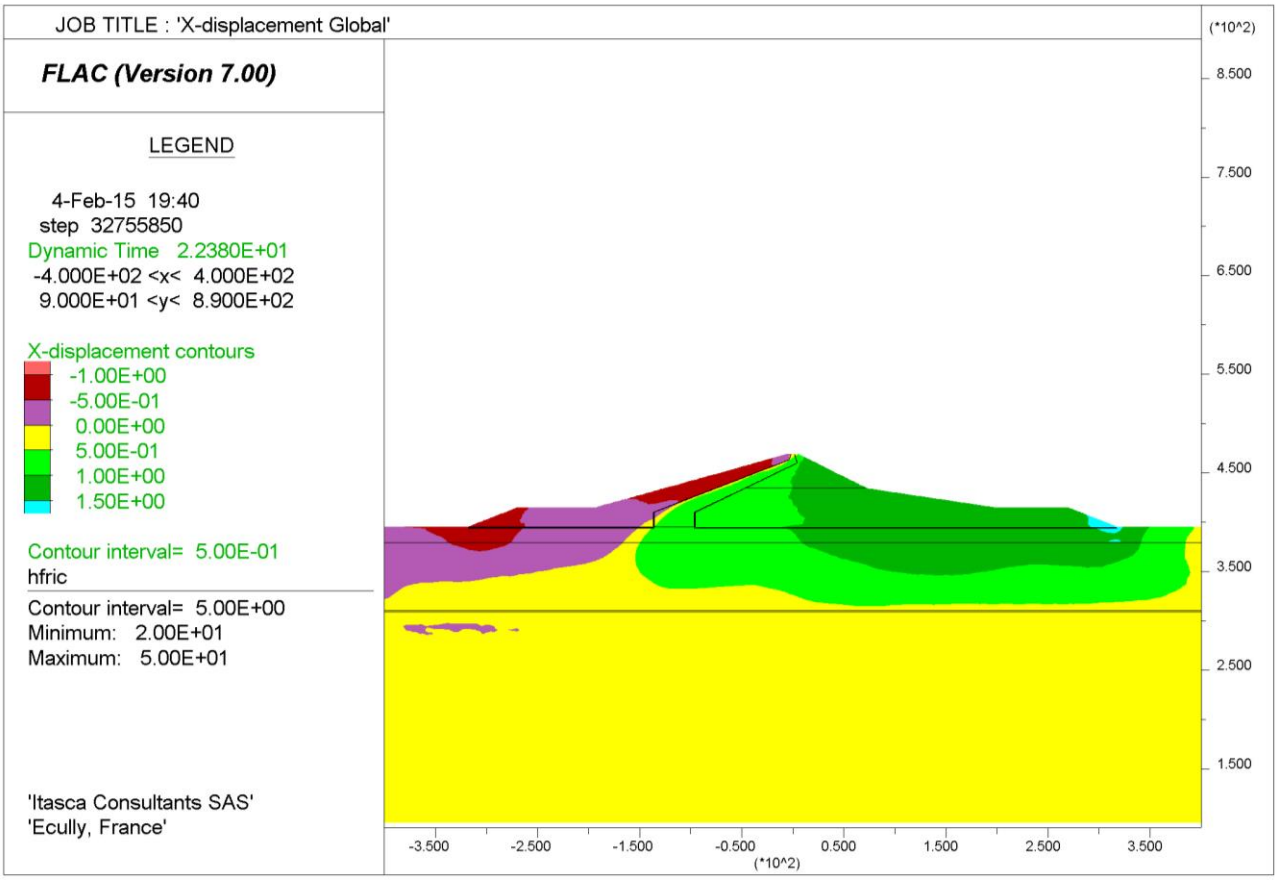

Figure 4-85 Nonlinear analysis – SEE earthquake Kocaeli IZT (V-H2)
Final horizontal displacements

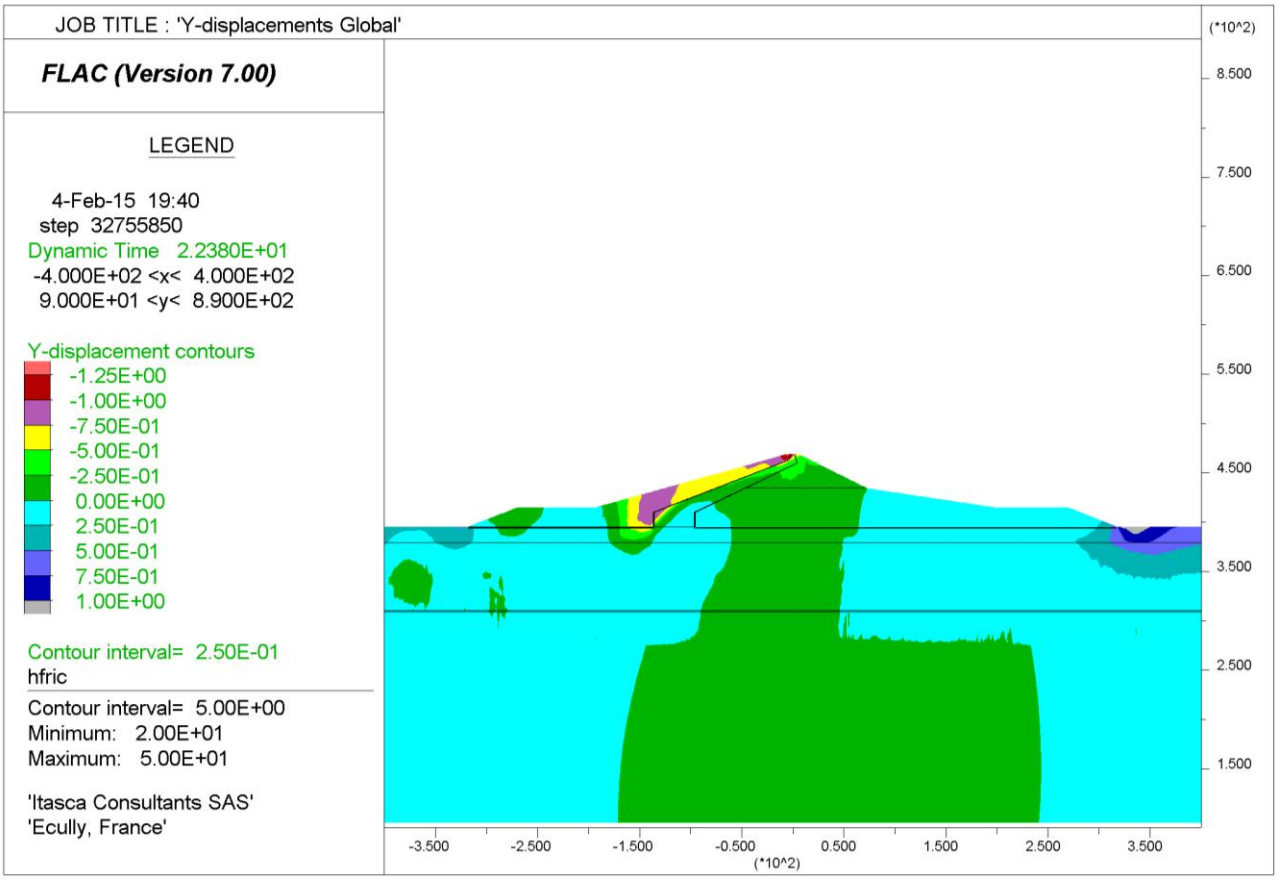

Figure 4-86 Nonlinear analysis – SEE earthquake Kocaeli IZT (V-H2)
Final vertical displacements

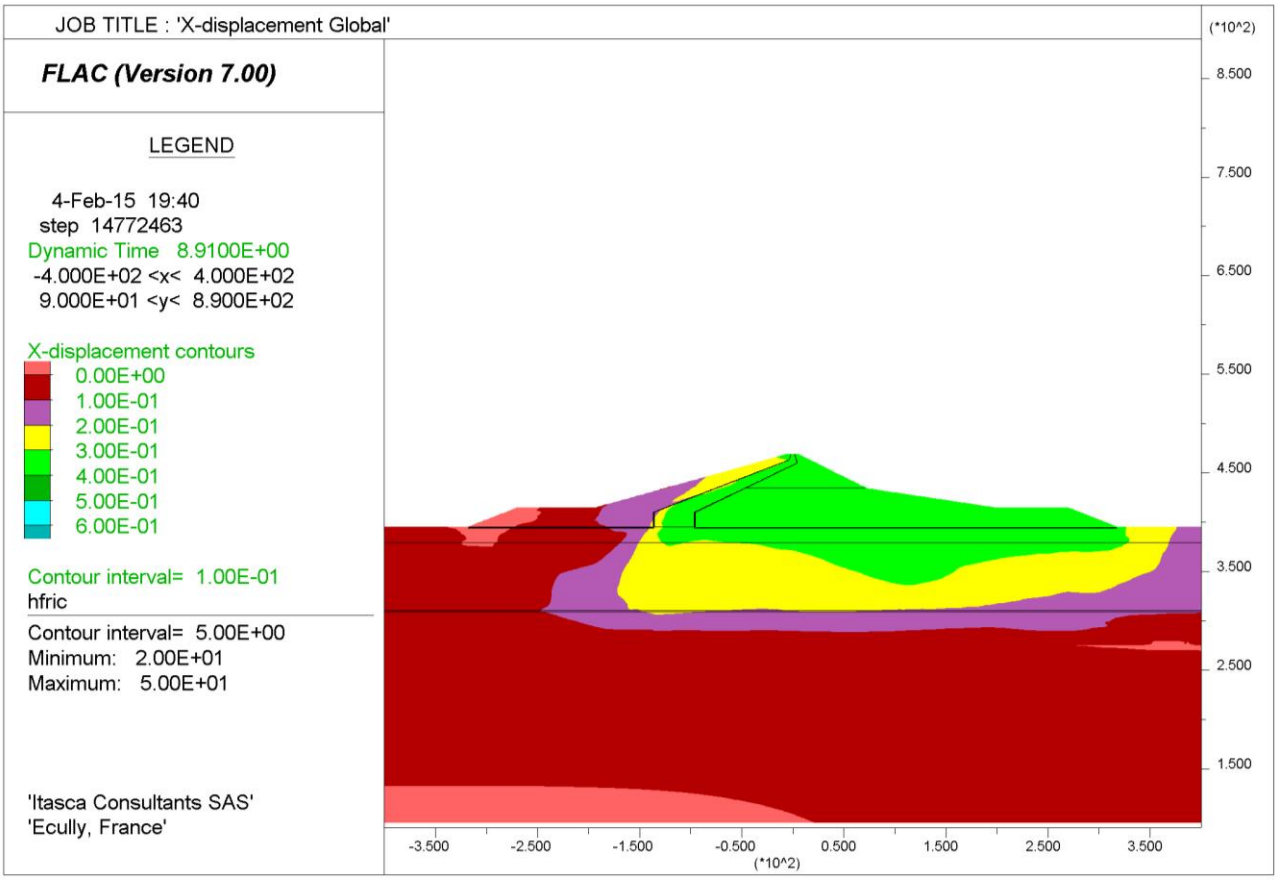

Figure 4-87 Nonlinear analysis – SEE earthquake Morgan (V-H1)
Final horizontal displacements

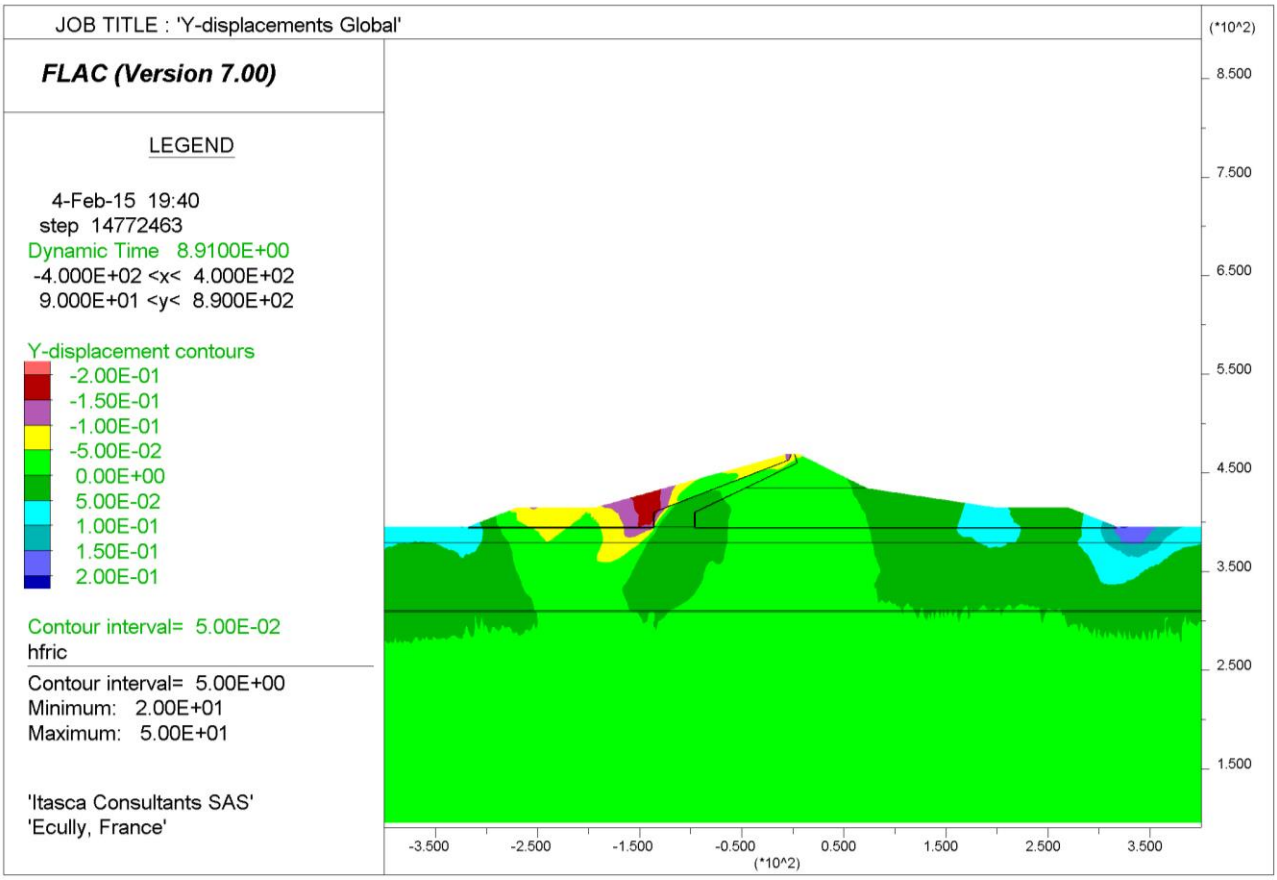

Figure 4-88 Nonlinear analysis – SEE earthquake Morgan (V-H1)
Final vertical displacements

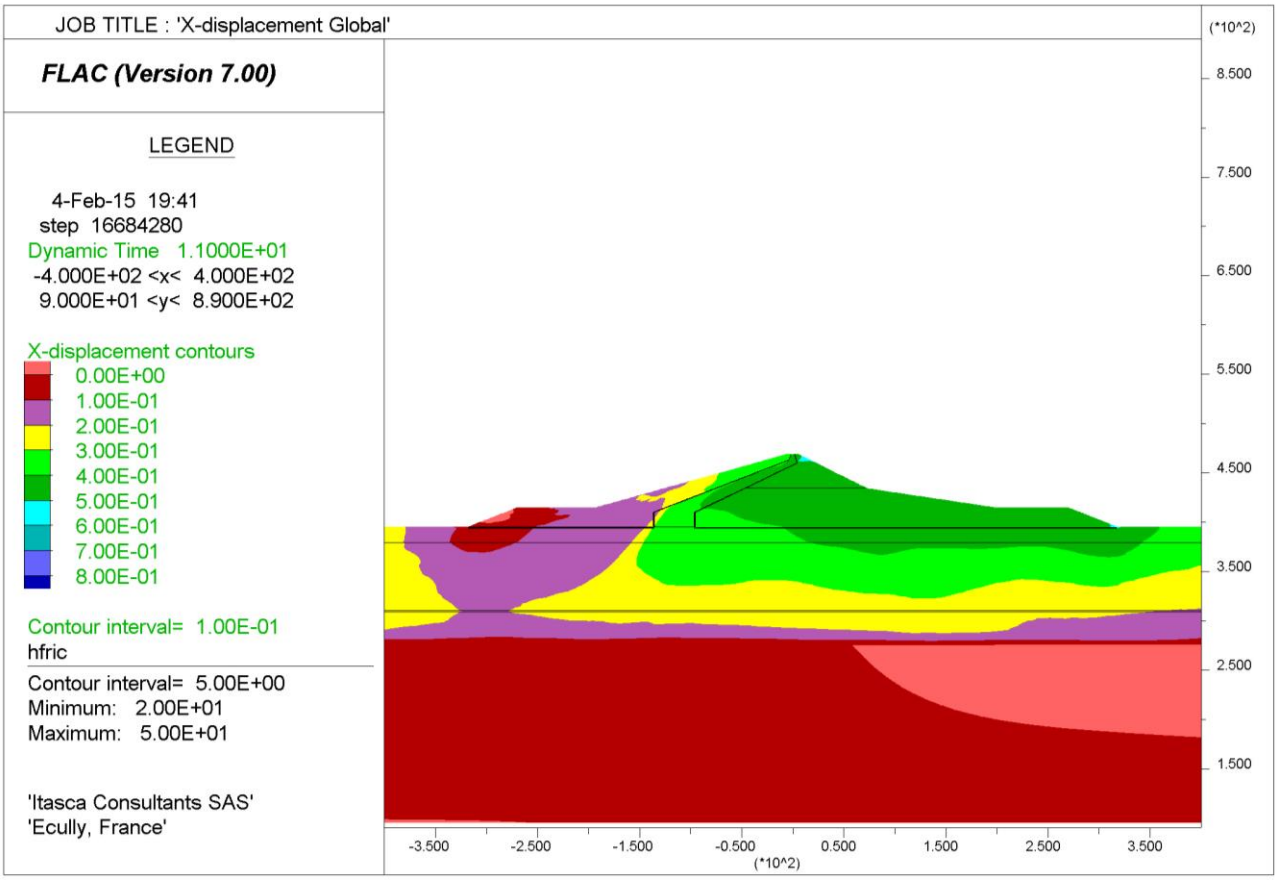

Figure 4-89 Nonlinear analysis – SEE earthquake Morgan (V-H2)
Final horizontal displacements

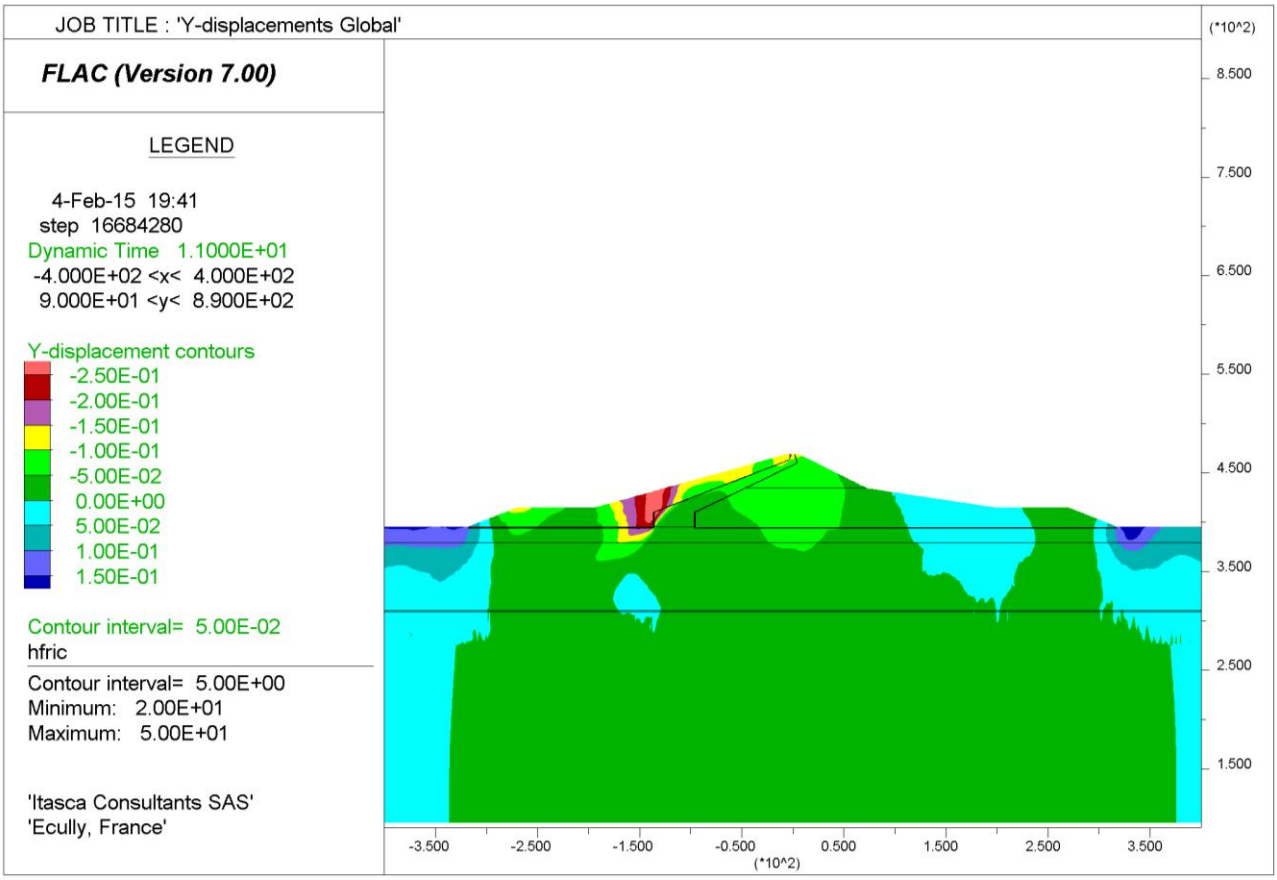

Figure 4-90 Nonlinear analysis – SEE earthquake Morgan (V-H2)
Final vertical displacements

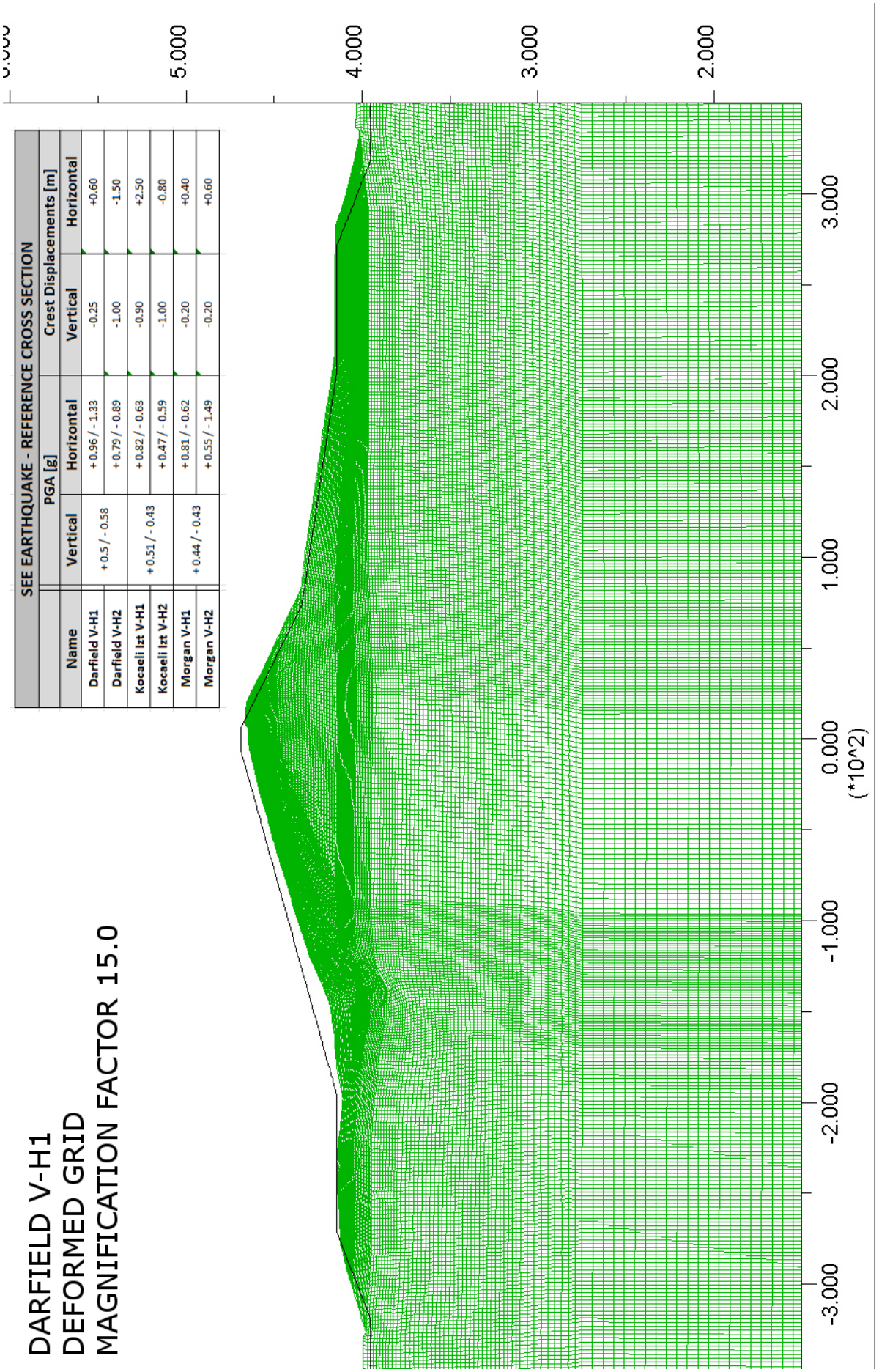

Figure 4-91 SEE earthquake Darfield (V-H1) – Deformed grid (magnification factor 15.0)

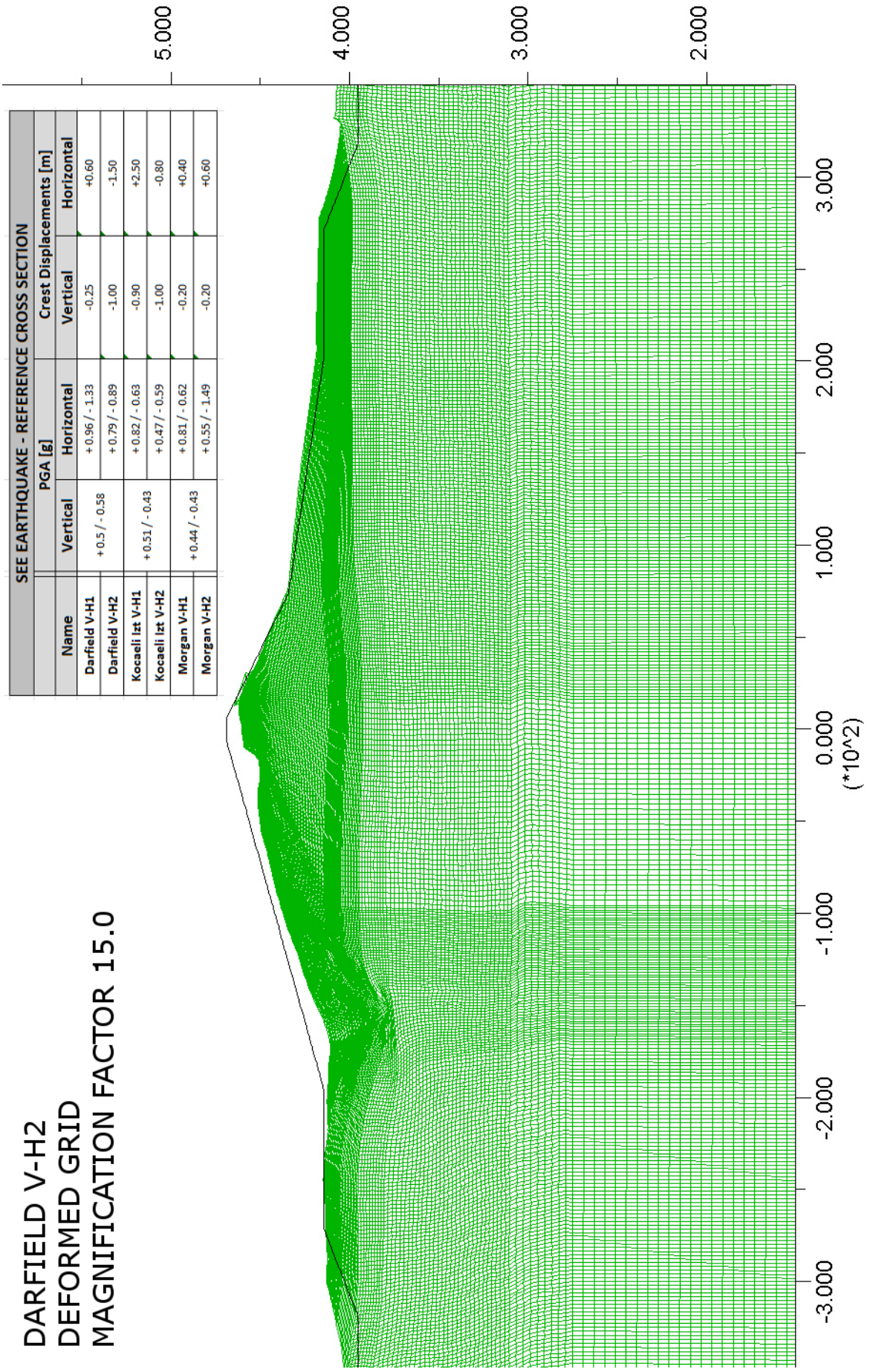

Figure 4-92 SEE earthquake Darfield (V-H2) – Deformed grid (magnification factor 15.0)

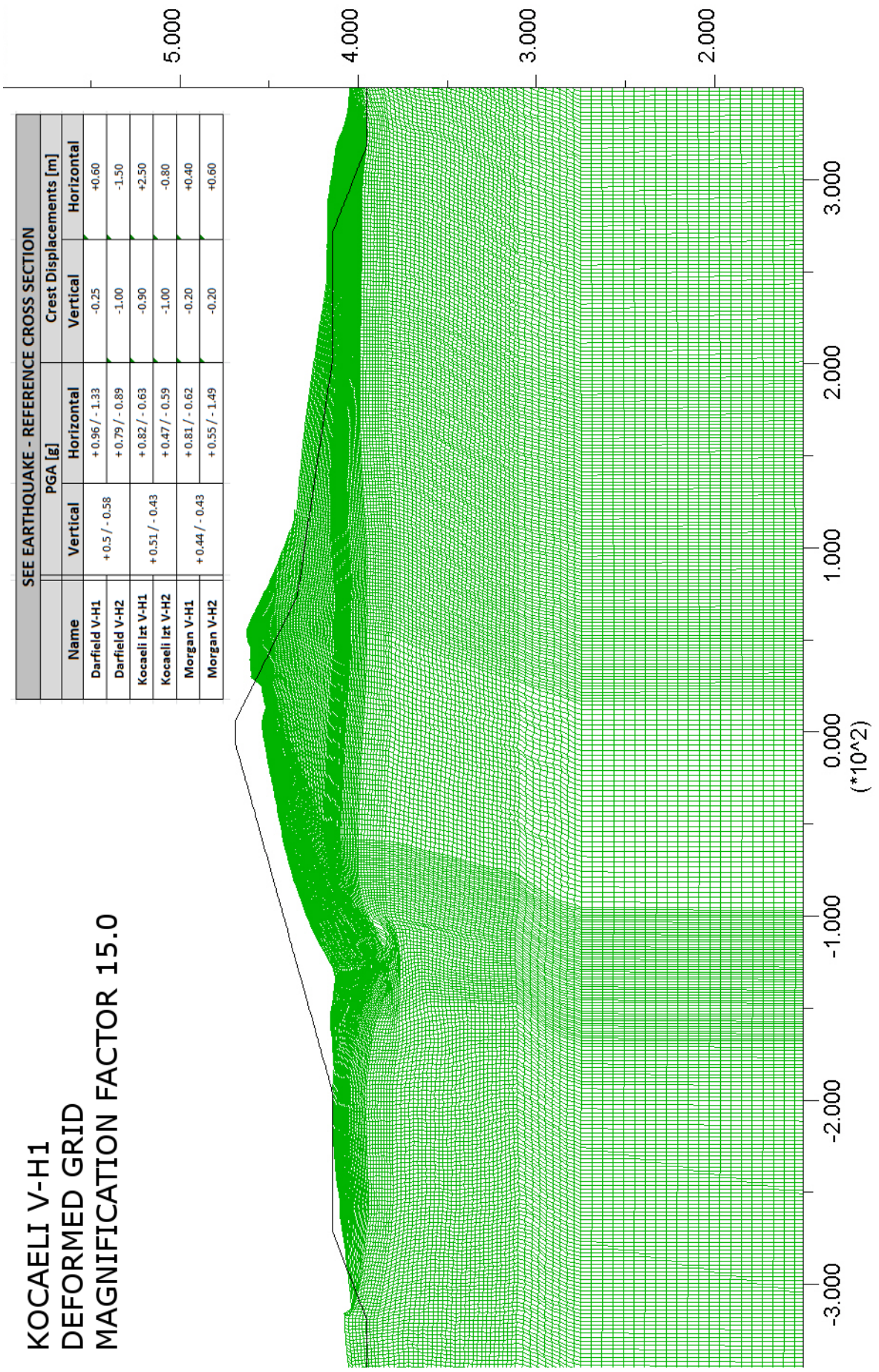

SEE EARTHQUAKE - REFERENCE CROSS SECTION					
	PGA [g]		Crest Displacements [m]	
Name	Vertical	Horizontal	Vertical	Horizontal
Darfield V-H1	+0.5 / - 0.58	+ 0.96 / - 1.33	-0.25	+0.60
Darfield V-H2		+ 0.79 / - 0.89	-1.00	-1.50
Kocaeli Izt V-H1	+0.51 / - 0.43	+ 0.82 / - 0.63	-0.90	+2.50
Kocaeli Izt V-H2		+ 0.47 / - 0.59	-1.00	-0.80
Morgan V-H1	+0.44 / - 0.43	+ 0.81 / - 0.62	-0.20	+0.40
Morgan V-H2		+ 0.55 / - 1.49	-0.20	+0.60

Figure 4-93 SEE earthquake Kocaeli (V-H1) – Deformed grid (magnification factor 15.0)

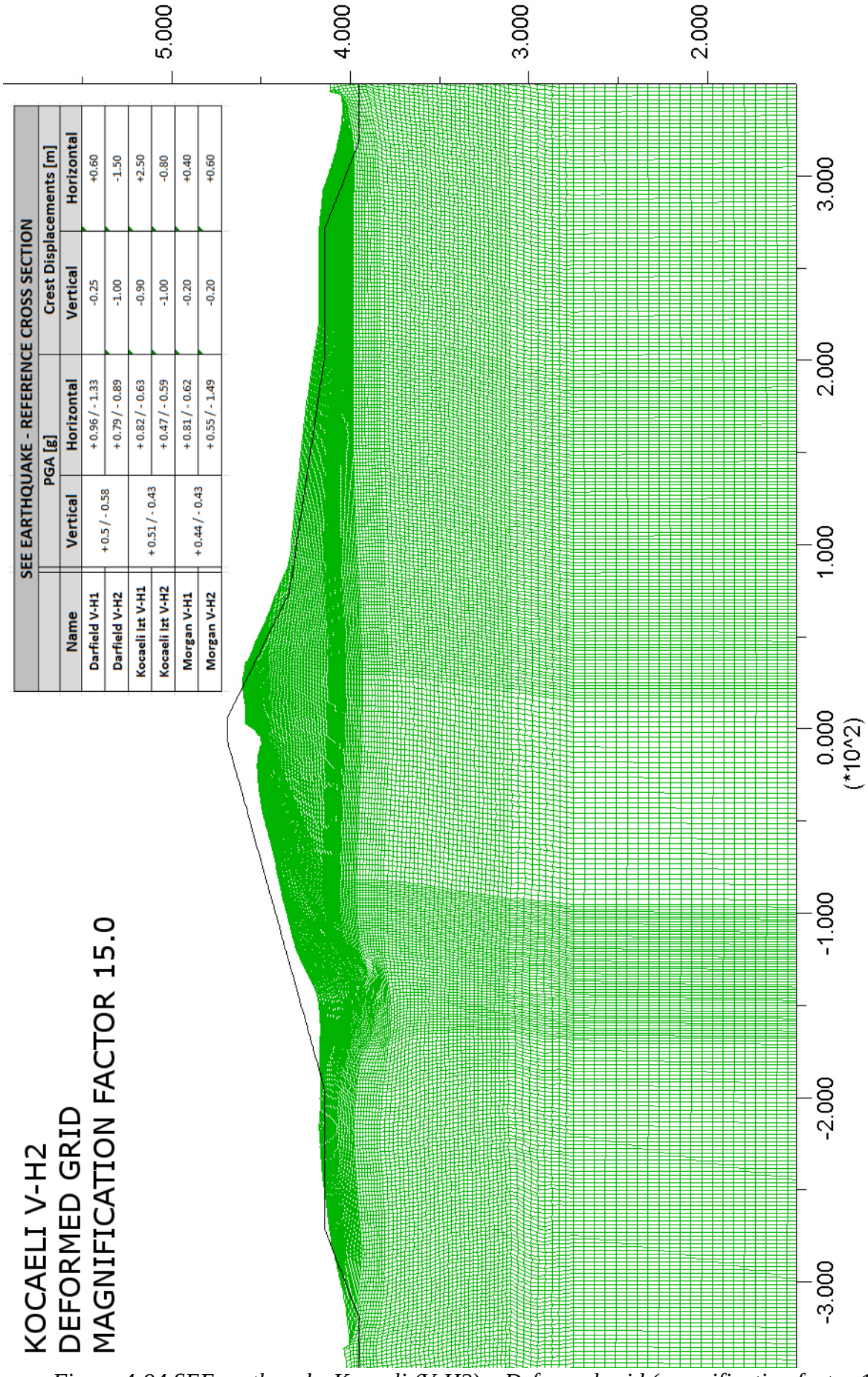

Figure 4-94 SEE earthquake Kocaeli (V-H2) – Deformed grid (magnification factor 15.0)

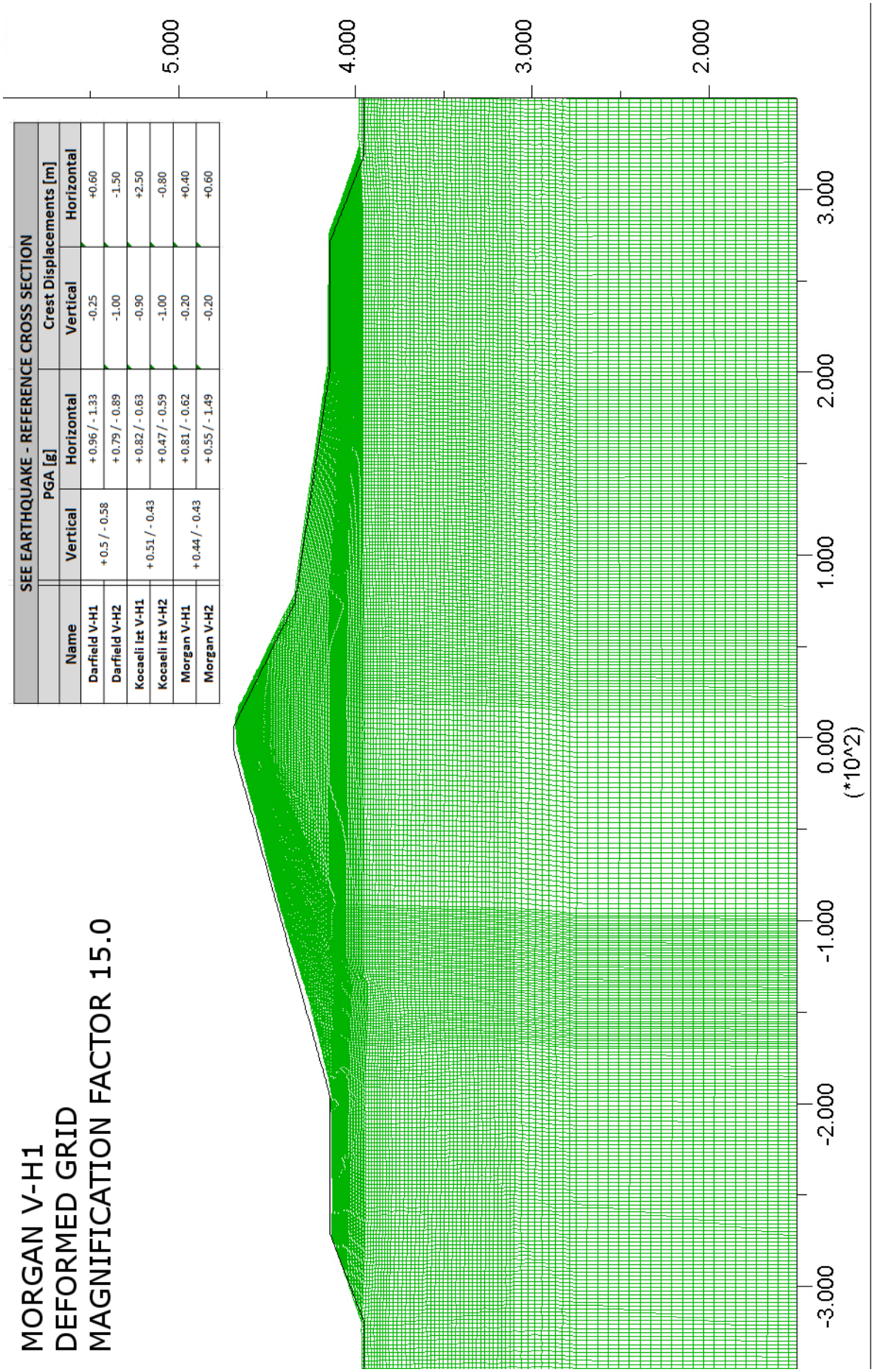

Figure 4-95 SEE earthquake Morgan (V-H1) – Deformed grid (magnification factor 15.0)

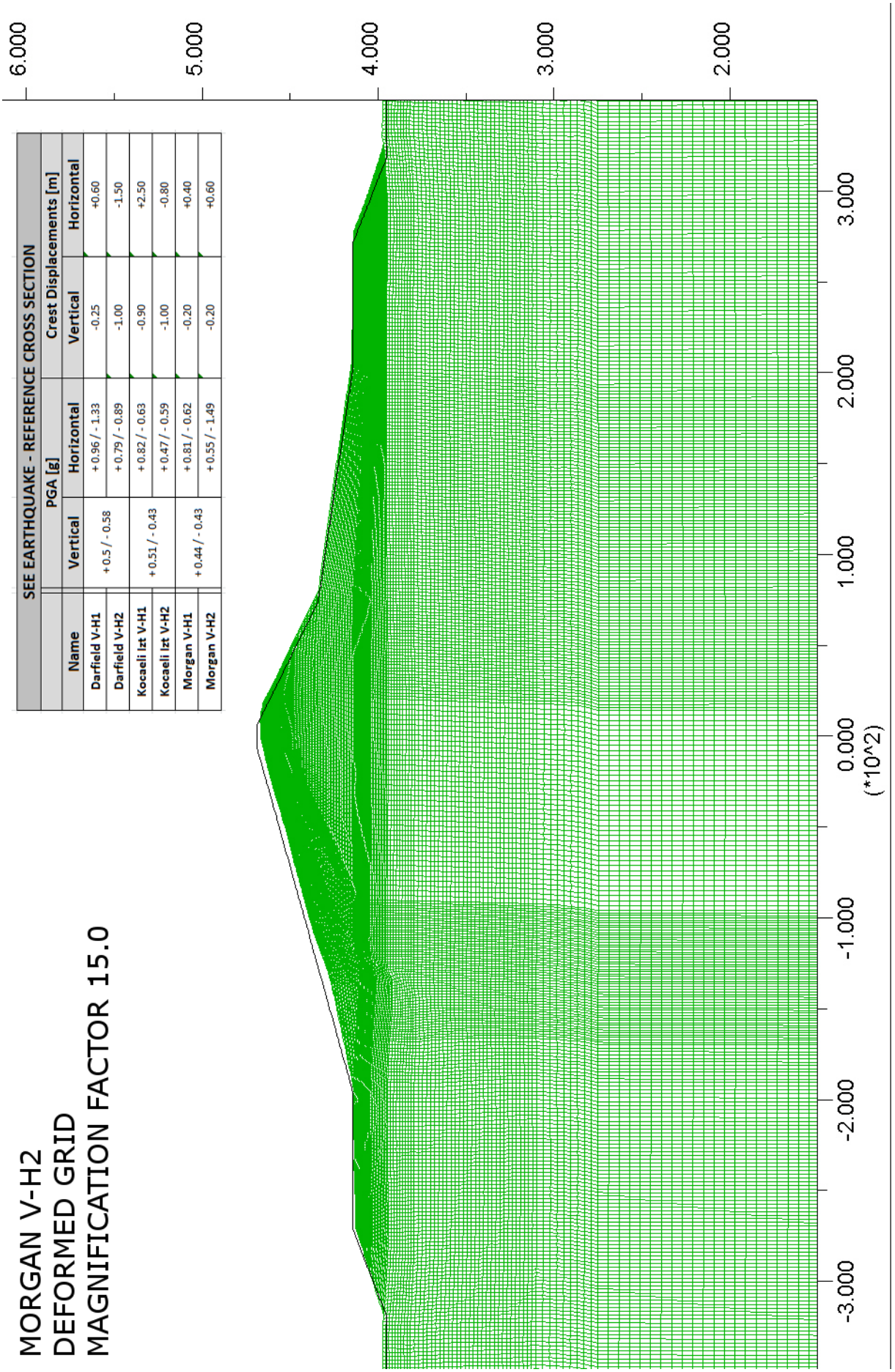

Figure 4-96 SEE earthquake Morgan (V-H2) – Deformed grid (magnification factor 15.0)

4.6.4.1. Dam core stability analysis

Horizontal displacements, as they are recorded at virtual points 1 – 4 of Figure 4-97 during the nonlinear dynamic simulation, are analyzed to verify the stability of the dam core.

Records at points 1 and 2 of Figure 4-97 indicate that this zone deforms almost homogeneously in all the tested cases. This is not the case for the points 3 and 4 (crest of the dam), since the dam at these two points, even if close to each other, behaves differently if either the crest is involved in the upstream slide or not, etc.

Relative horizontal displacements between points 3 and 4 of Figure 4-97 approach 1 meter in all cases but the Morgan earthquakes.

A maximum relative vertical displacement of 1.0 meter is observed between the lowest and the highest part of the dam core for both the Kocaeli V-H1 and V-H2 earthquakes (from Figure 4-102 to Figure 4-105), of about 1.0 meter in both cases.

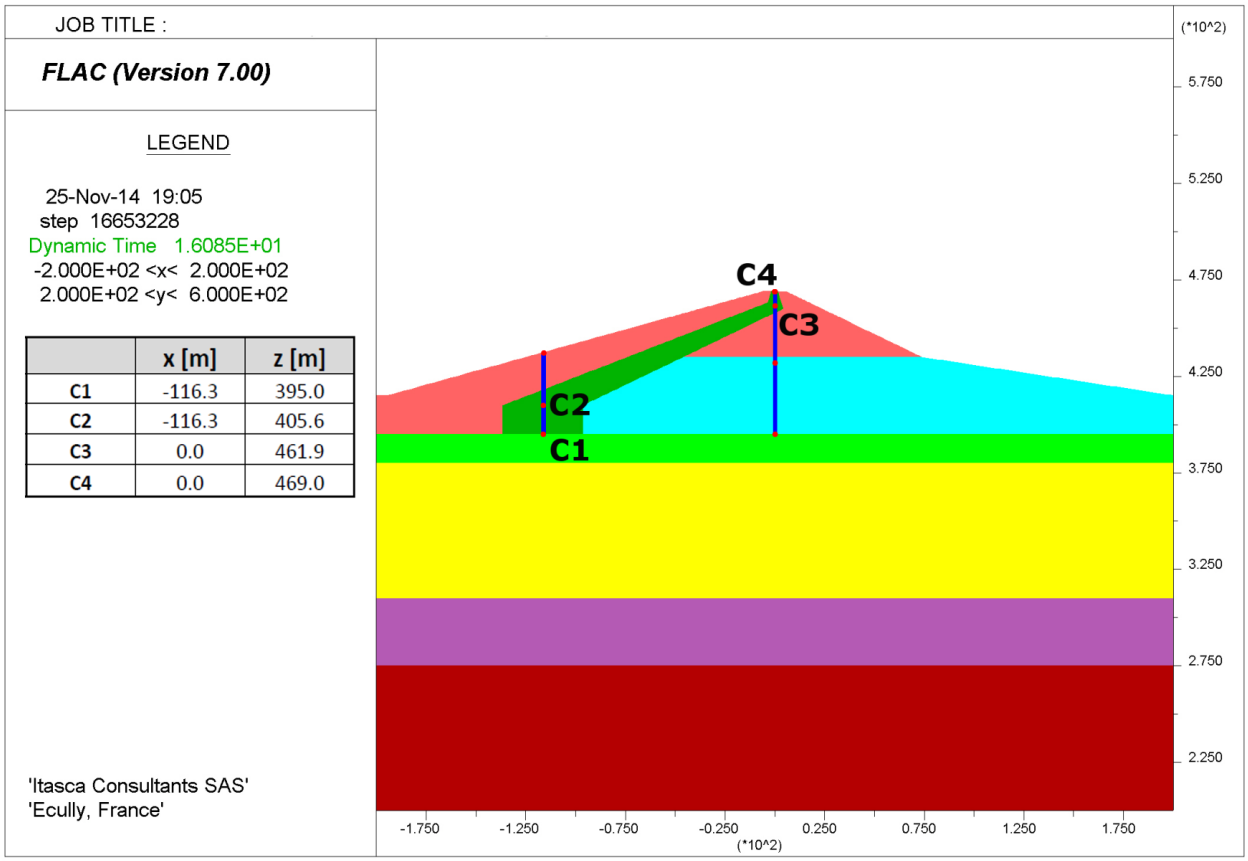

Figure 4-97: virtual points of measurement of displacement for dam core stability analysis

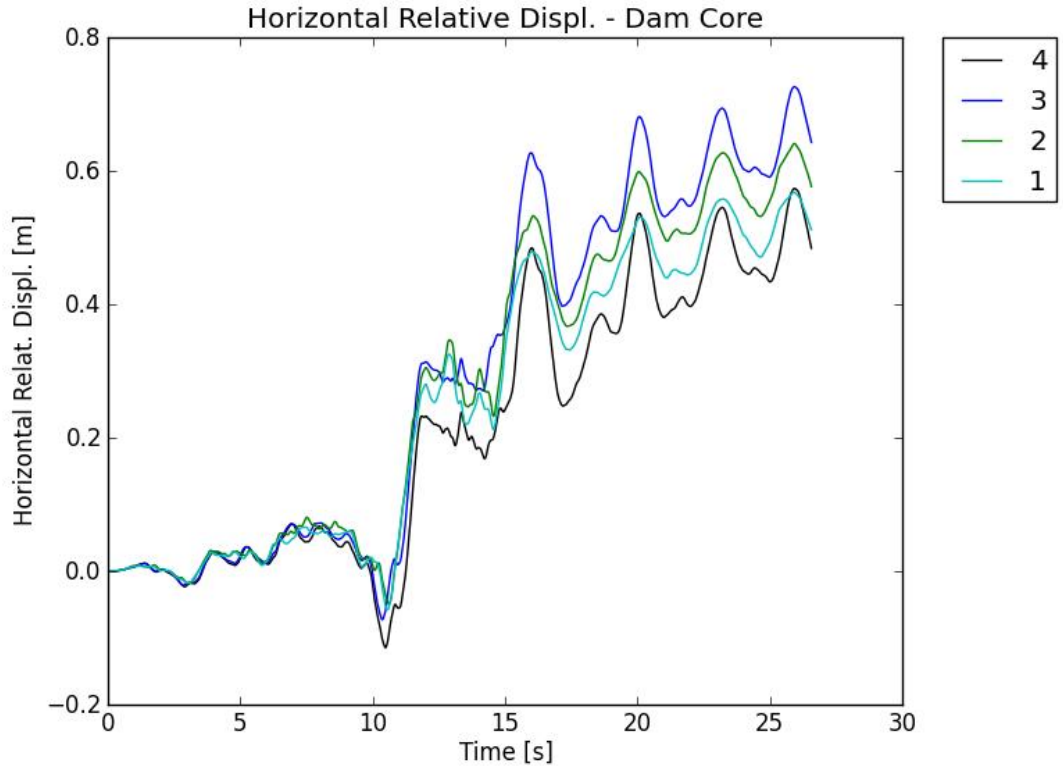

Figure 4-98: Horizontal displacements at points 1 – 4 of Figure 4-97 – SEE Darfield (V-H1)

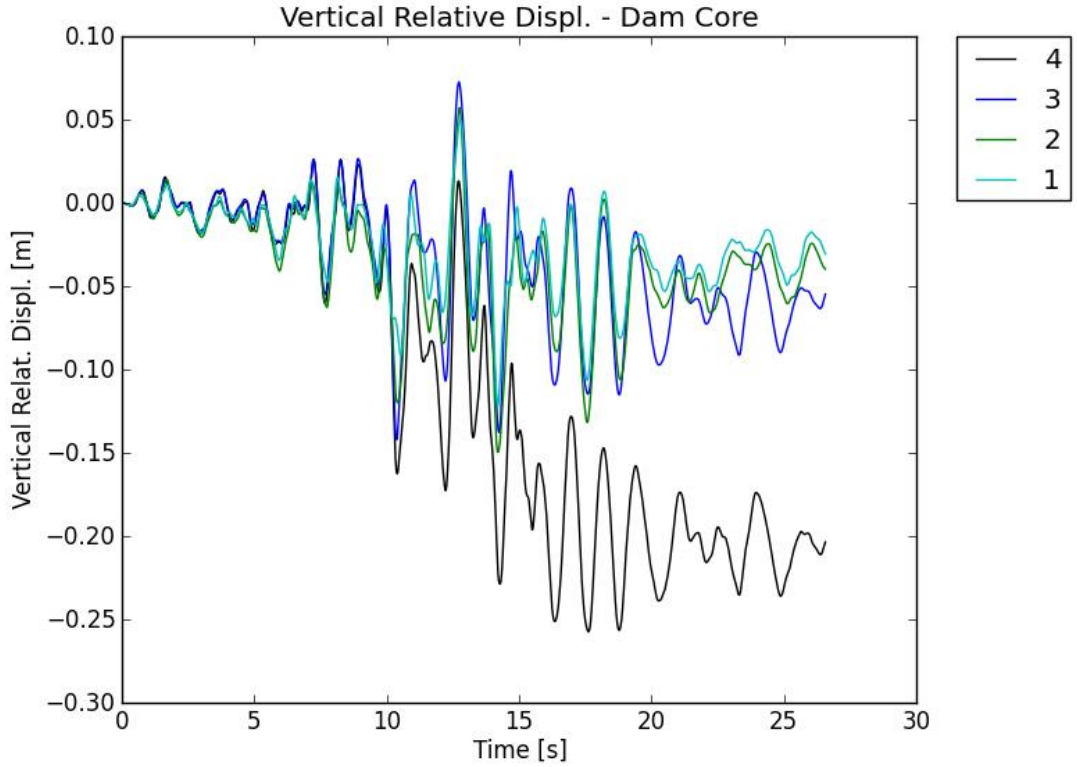

Figure 4-99: Vertical displacements at points 1 – 4 of Figure 4-97 – SEE Darfield (V-H1)

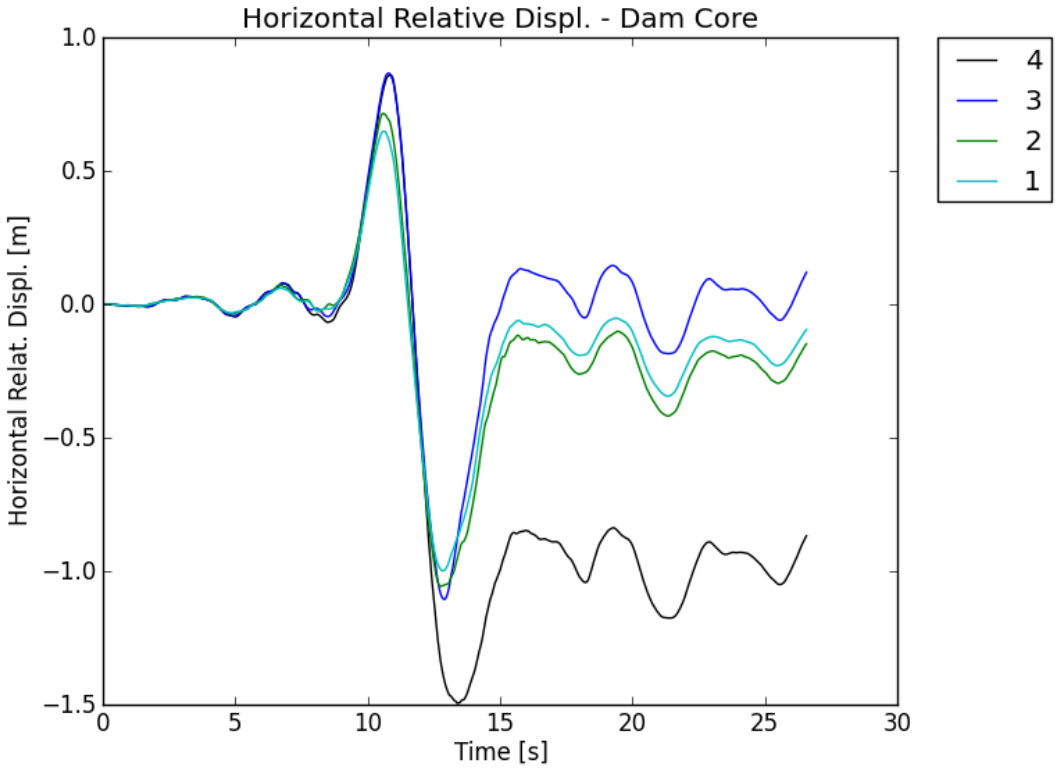

Figure 4-100: Horizontal displacements at points 1 – 4 of Figure 4-97 – SEE Darfield (V-H2)

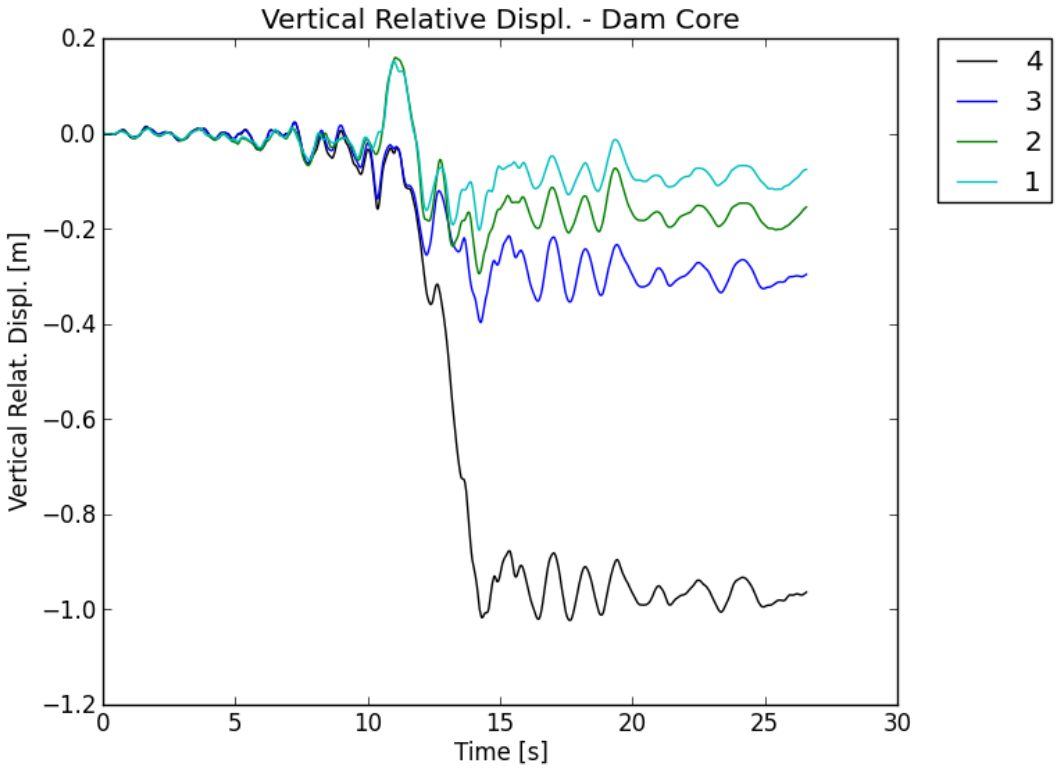

Figure 4-101: Vertical displacements at points 1 – 4 of Figure 4-97 – SEE Darfield (V-H2)

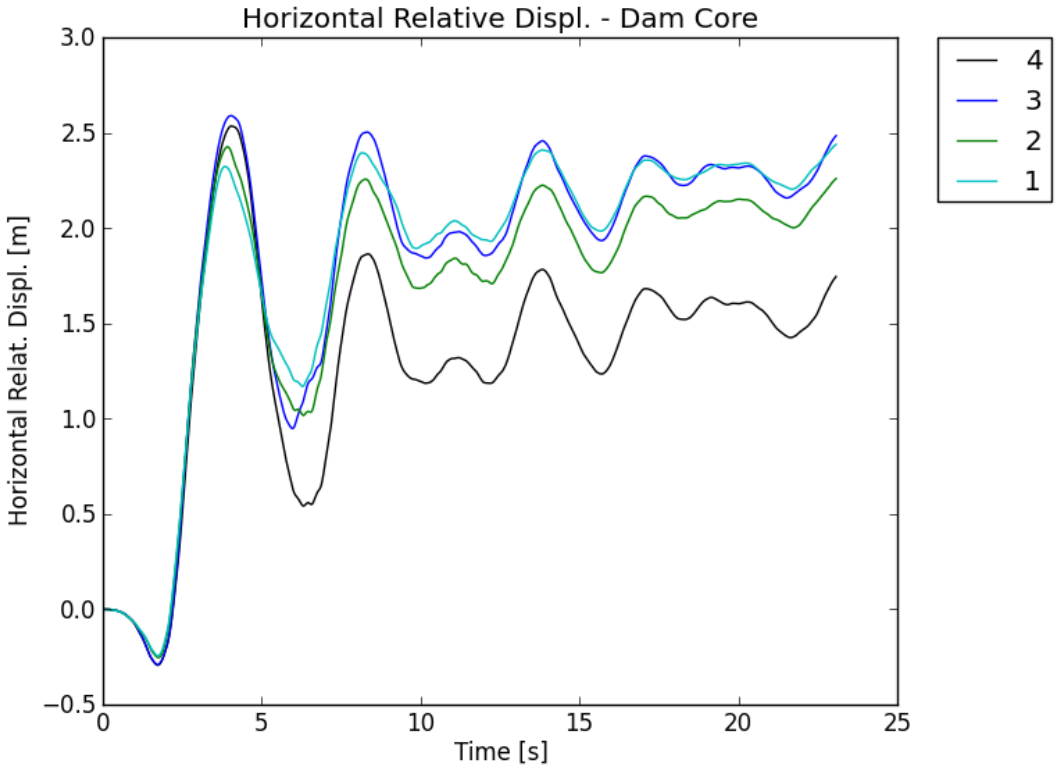

Figure 4-102: Horizontal displacements at points 1 – 4 of Figure 4-97 – SEE Kocaeli (V-H1)

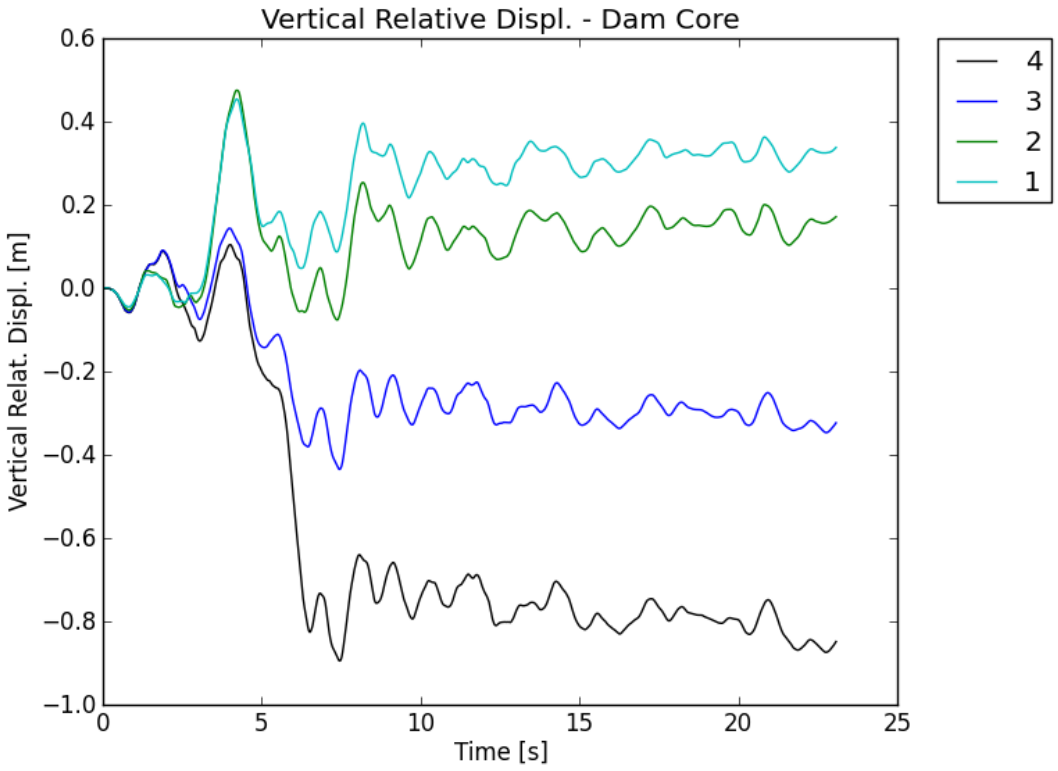

Figure 4-103: Vertical displacements at points 1 – 4 of Figure 4-97 – SEE Kocaeli (V-H1)

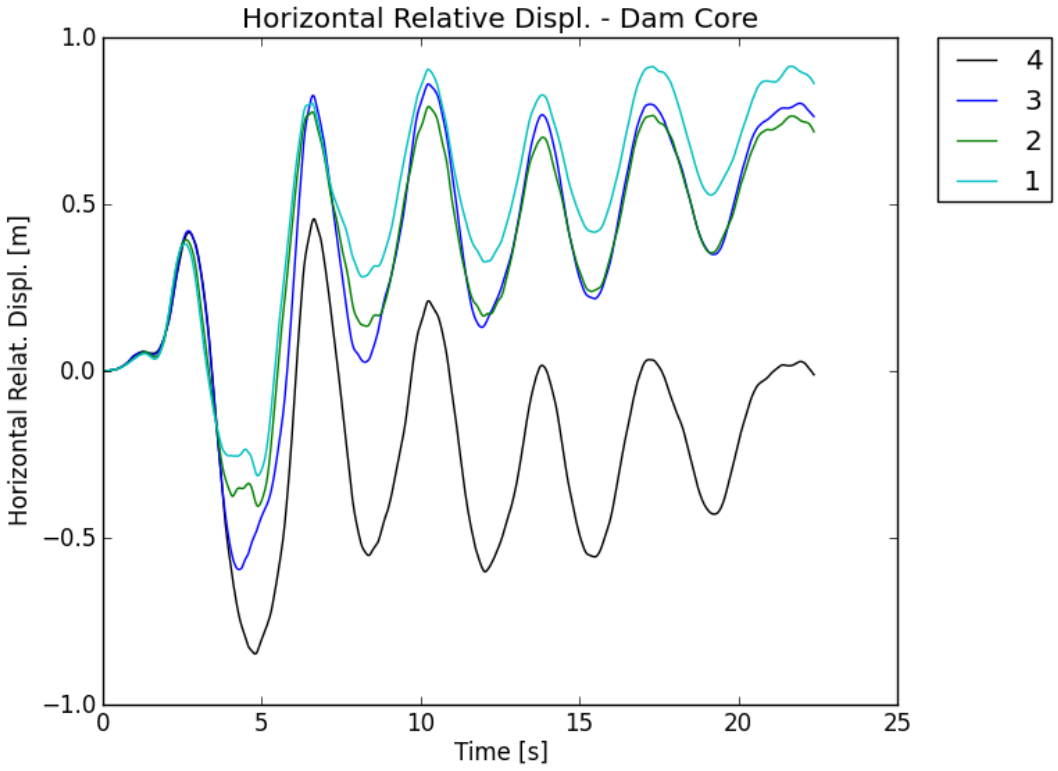

Figure 4-104: Horizontal displacements at points 1 – 4 of Figure 4-97 – SEE Kocaeli (V-H2)

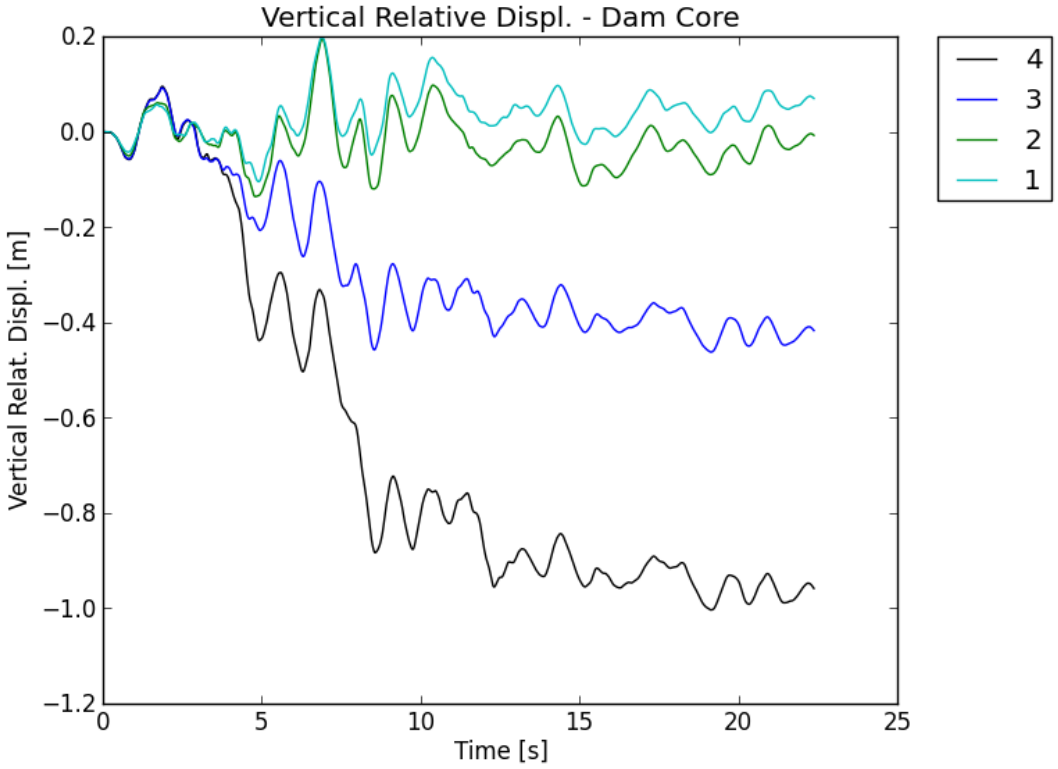

Figure 4-105: Vertical displacements at points 1 – 4 of Figure 4-97 – SEE Kocaeli (V-H2)

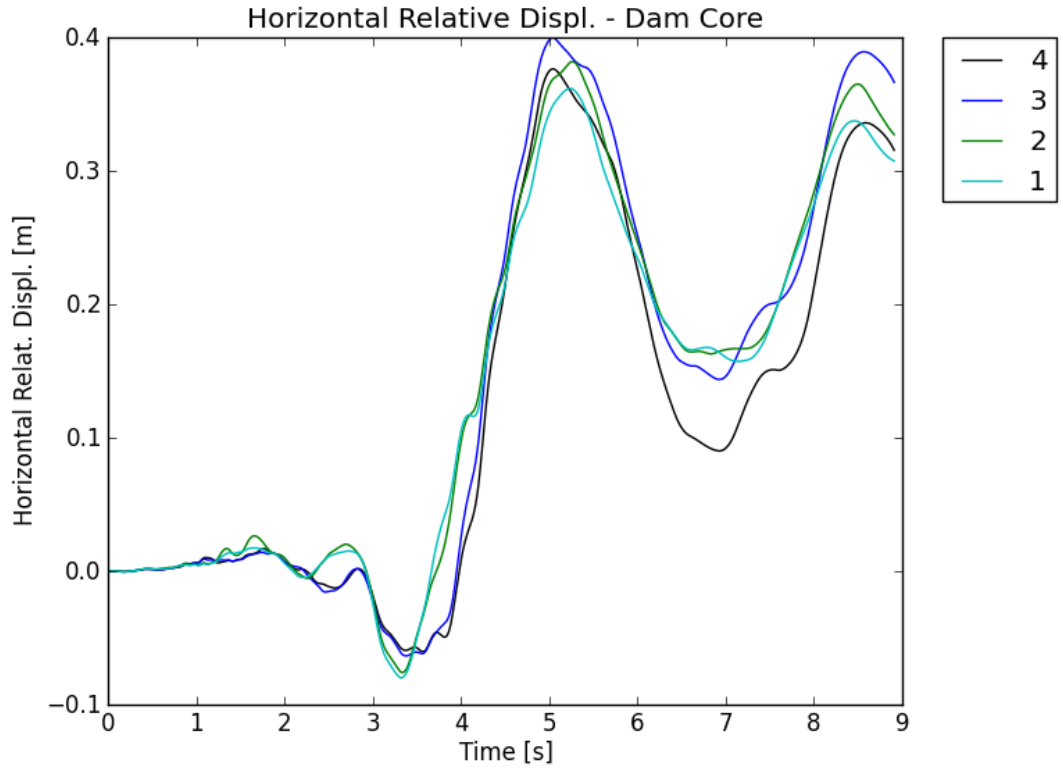

Figure 4-106: Horizontal displacements at points 1 – 4 of Figure 4-97 – SEE Morgan (V-H1)

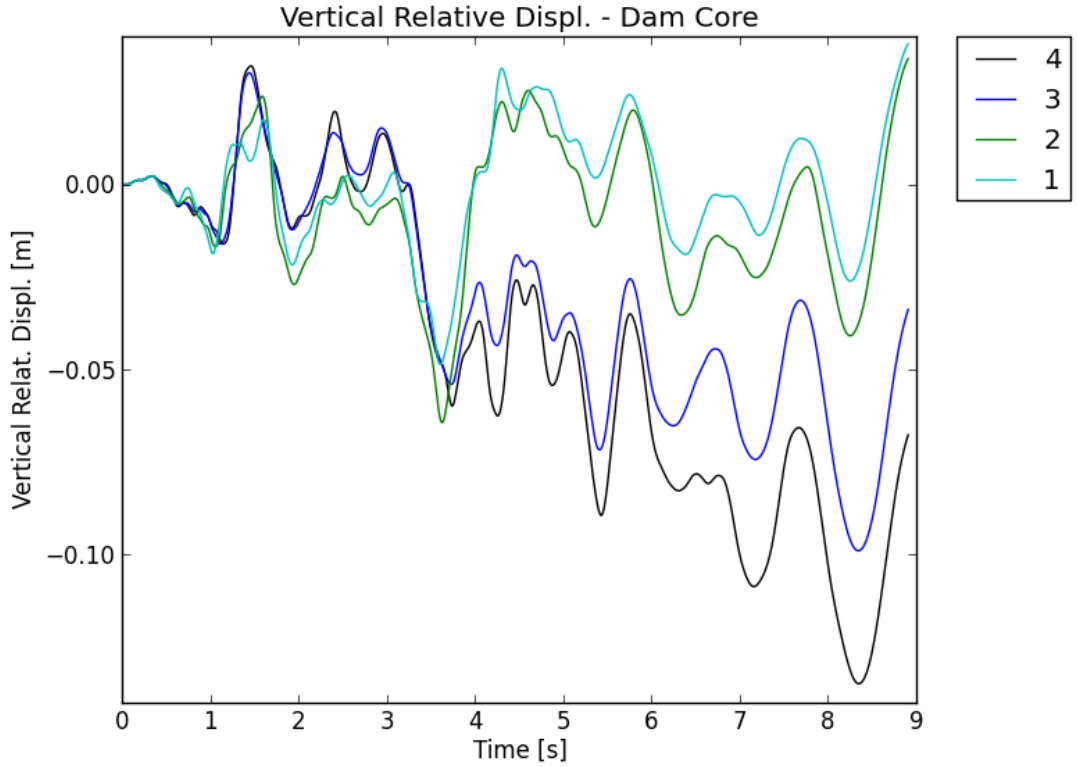

Figure 4-107: Vertical displacements at points 1 – 4 of Figure 4-97 – SEE Morgan (V-H1)

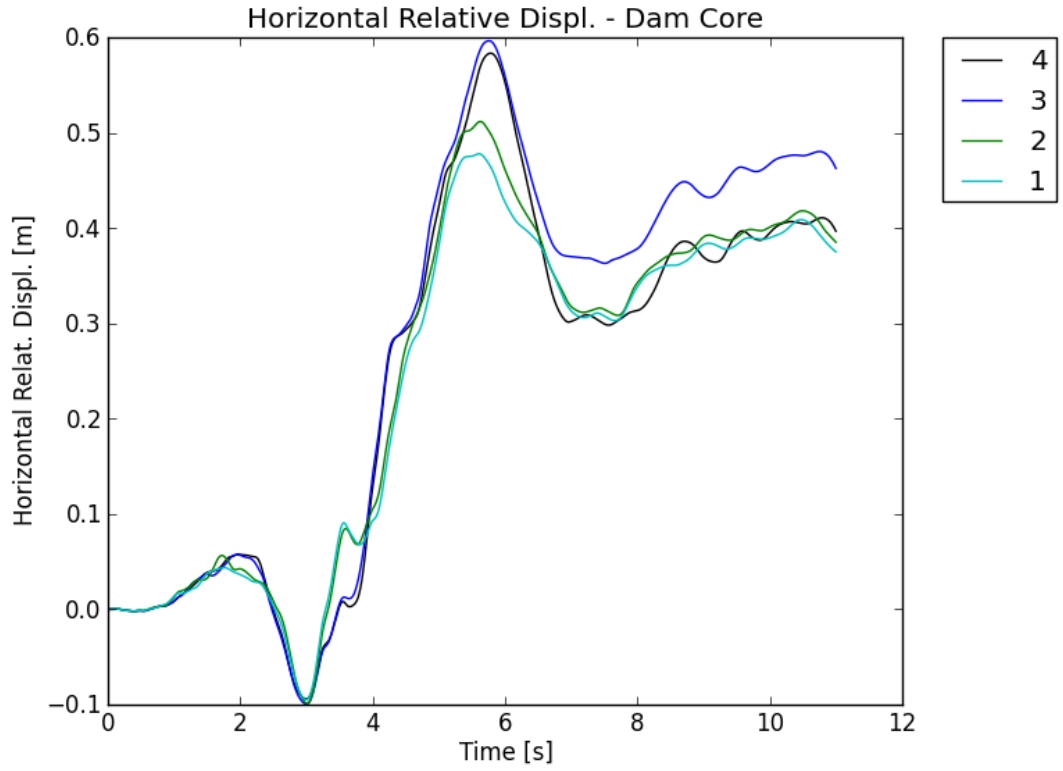

Figure 4-108: Horizontal displacements at points 1 – 4 of Figure 4-97 – SEE Morgan (V-H2)

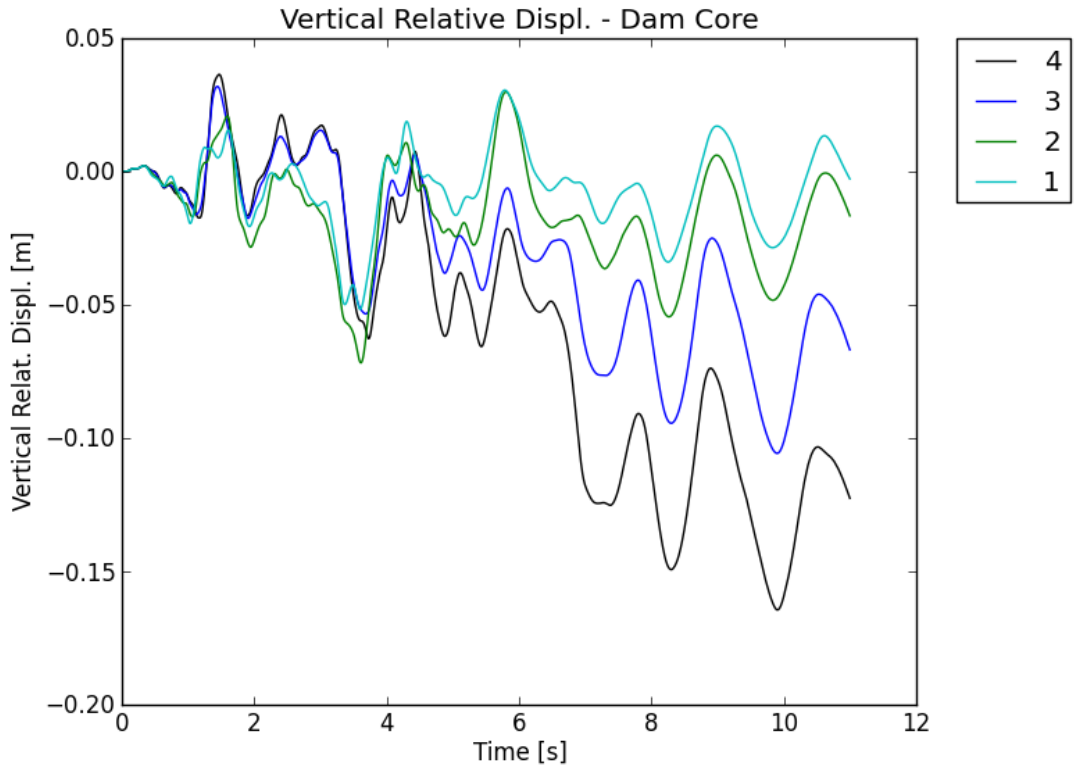

Figure 4-109: Vertical displacements at points 1 – 4 of Figure 4-97 – SEE Morgan (V-H2)

4.6.4.2. Concrete wall stability analysis

The horizontal displacements recorded at virtual points 1 – 8 of Figure 4-110 during the nonlinear dynamic simulation are analyzed to verify their compatibility with the stability of the concrete slurry wall that will be installed in that zones. It is recalled that the concrete wall is not directly included into the model.

Table 4-4 summarizes all the results that were obtained. Figure 4-111 to Figure 4-122 show the horizontal and vertical displacements that were recorded, for all the SEE earthquakes simulated.

The maximum relative horizontal displacement (33 cm) is found for the SEE Kocaeli V-H1 (Figure 4-115), over a length of 38 meters, that corresponds to the distance between points 5-8 on Figure 4-110, i.e. the upper part of the concrete wall.

SEE EARTHQUAKE - CONCRETE SLURRY WALL DISPLACEMENTS				
	PGA [g]		Relative Displacement [m]	Length [m]
Name	Vertical	Horizontal	Horizontal	
Darfield V-H1	+ 0.5 / - 0.58	+ 0.96 / - 1.33	0.09	38m (points 5 - 8)
Darfield V-H2		+ 0.79 / - 0.89	0.09	38m (points 5 - 8)
Kocaeli Izt V-H1	+ 0.51 / - 0.43	+ 0.82 / - 0.63	0.33	38m (points 5 - 8)
Kocaeli Izt V-H2		+ 0.47 / - 0.59	0.18	38m (points 5 - 8)
Morgan V-H1	+ 0.44 / - 0.43	+ 0.81 / - 0.62	0.06	38m (points 5 - 8)
Morgan V-H2		+ 0.55 / - 1.49	0.08	38m (points 5 - 8)

Table 4-4 : SEE earthquakes, nonlinear analysis - Concrete wall relative horizontal displacements

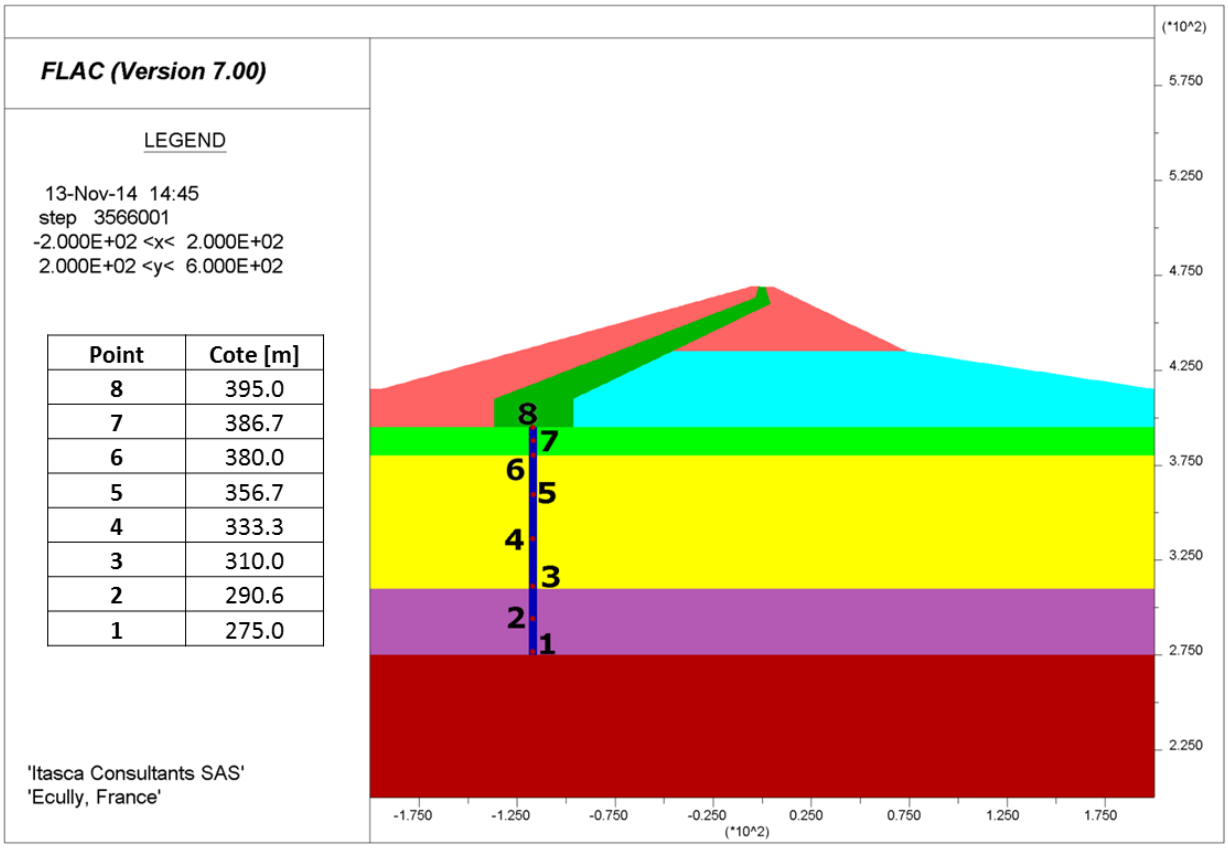

Figure 4-110 : virtual points of measurement of displacement (concrete wall is not modeled)

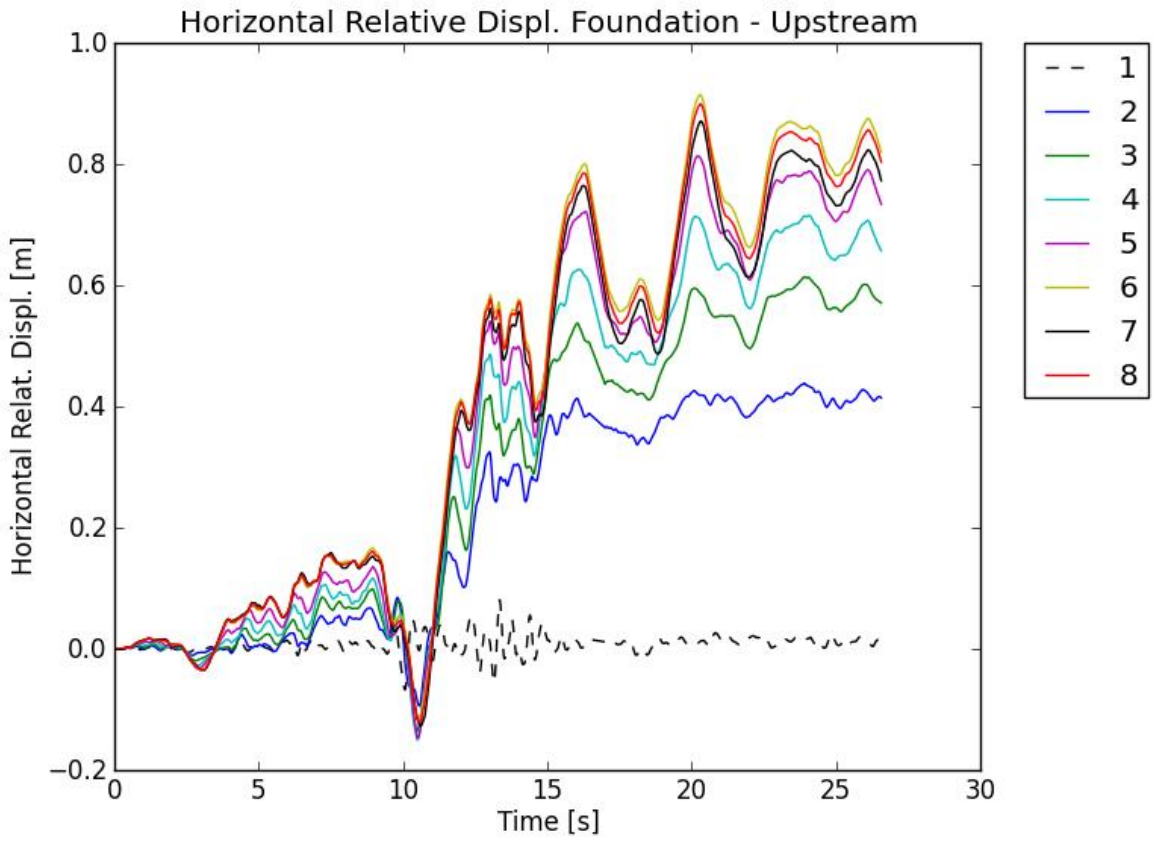

Figure 4-111 Horizontal displacements at points 1 – 8 of Figure 4-110 – SEE Darfield (V-H1)

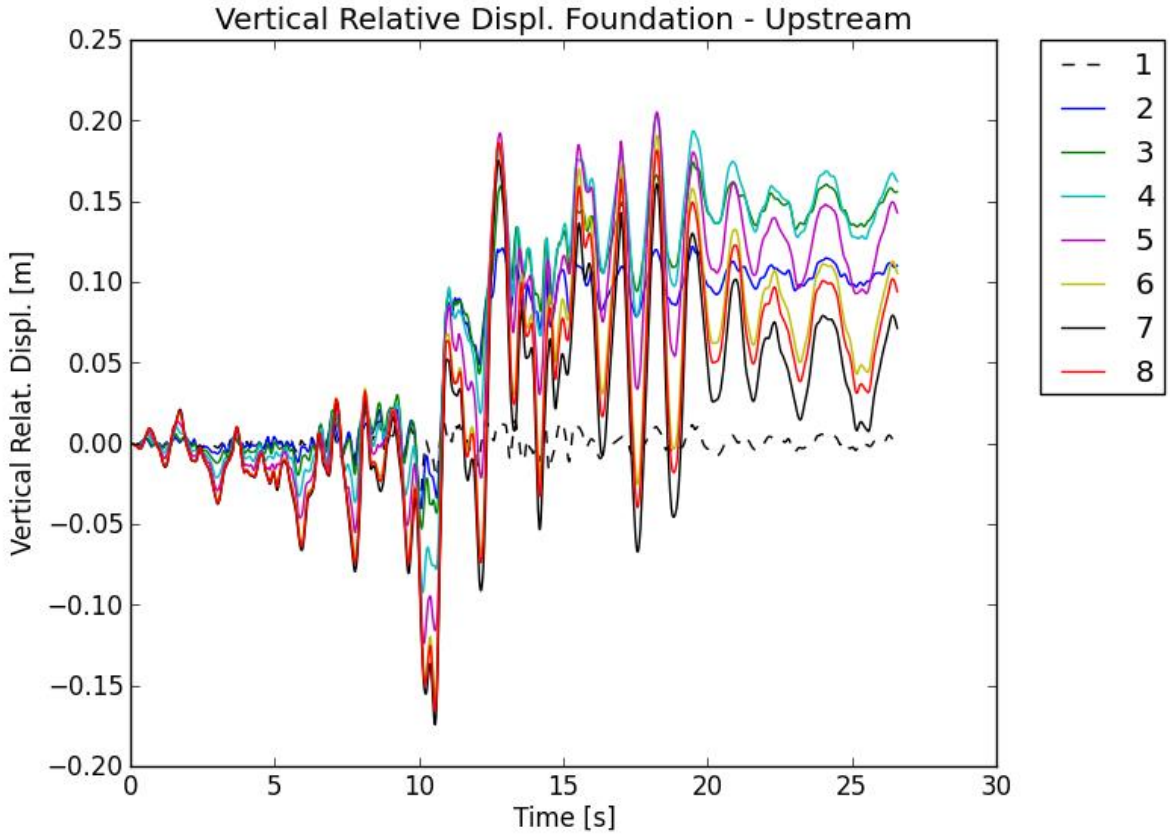

Figure 4-112 Vertical displacements at points 1 – 8 of Figure 4-110 – SEE Darfield (V-H1)

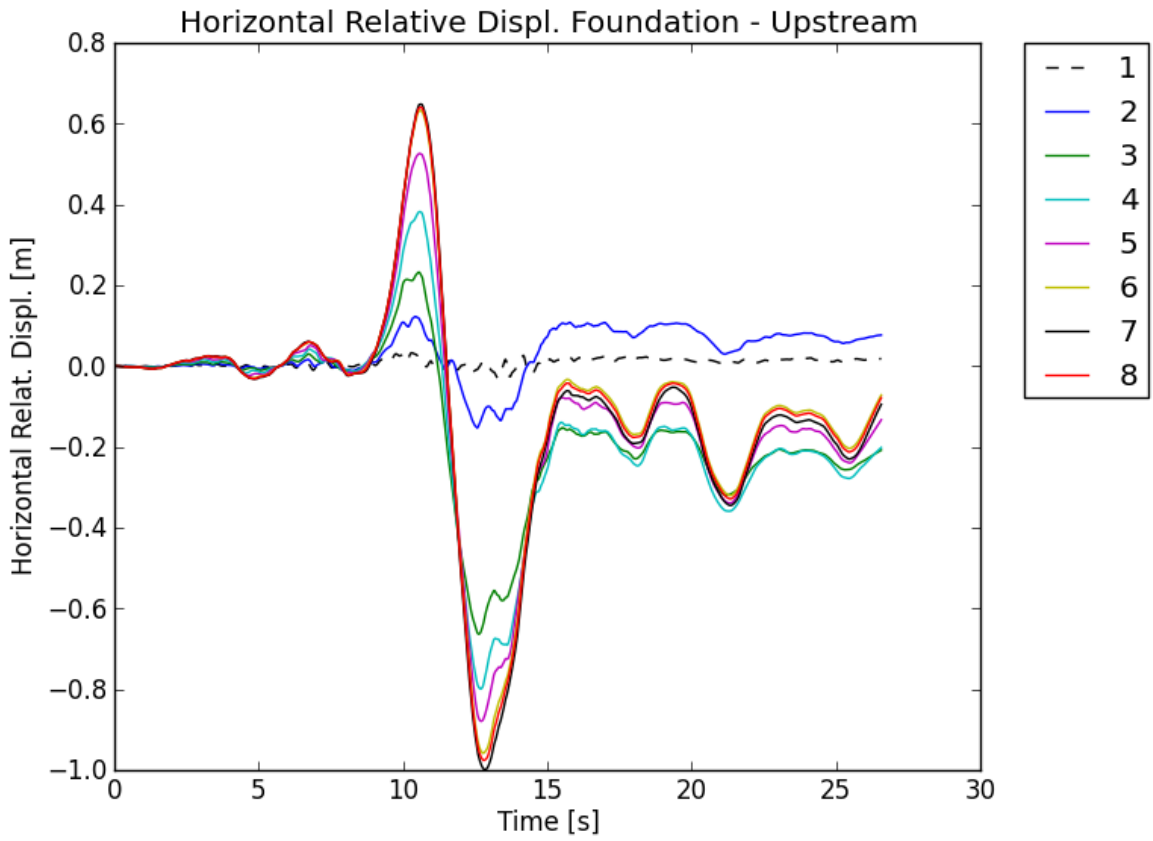

Figure 4-113 Horizontal displacements at points 1 – 8 of Figure 4-110 – SEE Darfield (V-H2)

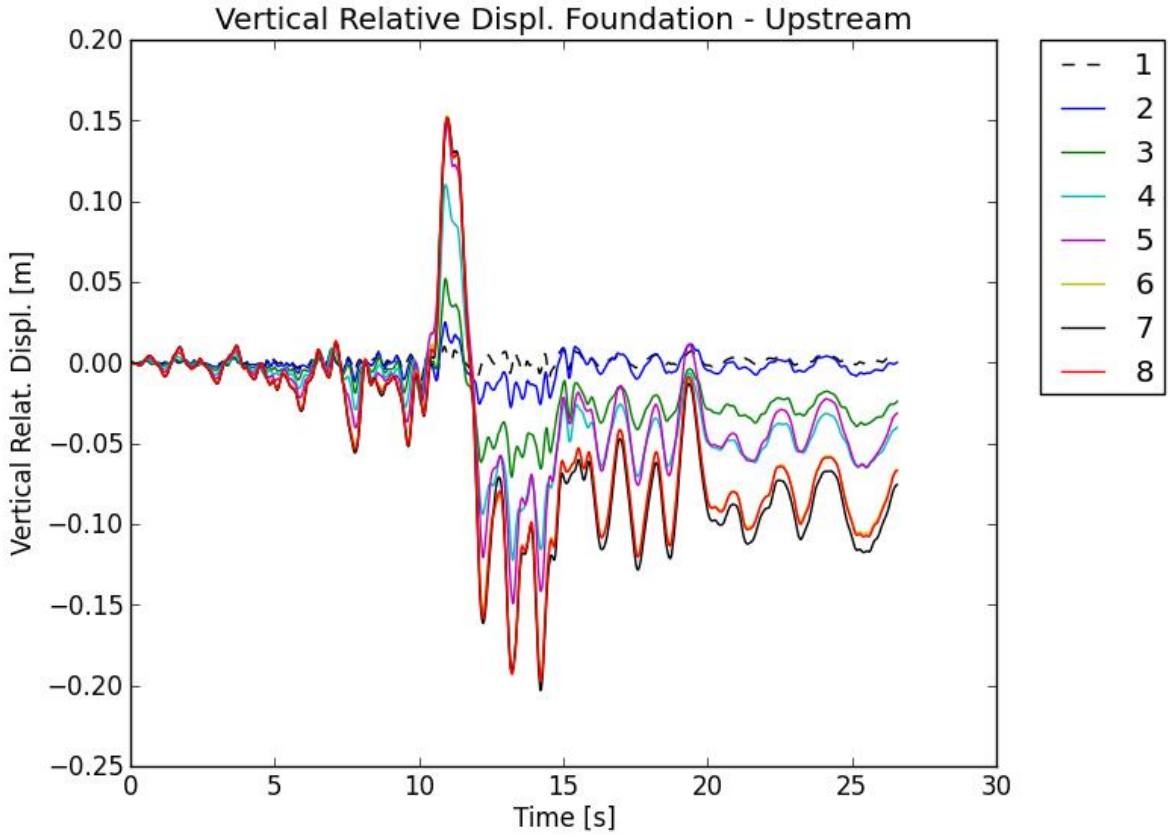

Figure 4-114 Vertical displacements at points 1 – 8 of Figure 4-110 – SEE Darfield (V-H2)

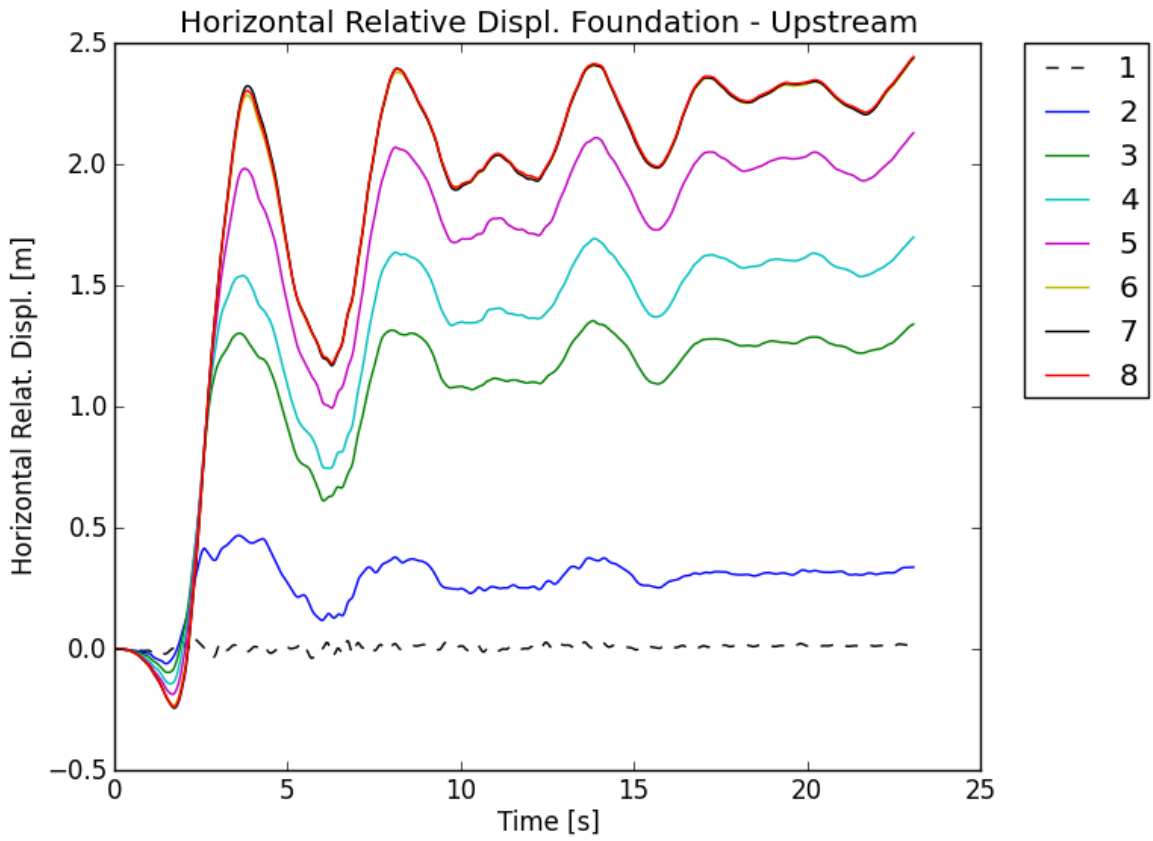

Figure 4-115 Horizontal displacements at points 1 – 8 of Figure 4-110 – SEE Kocaeli (V-H1)

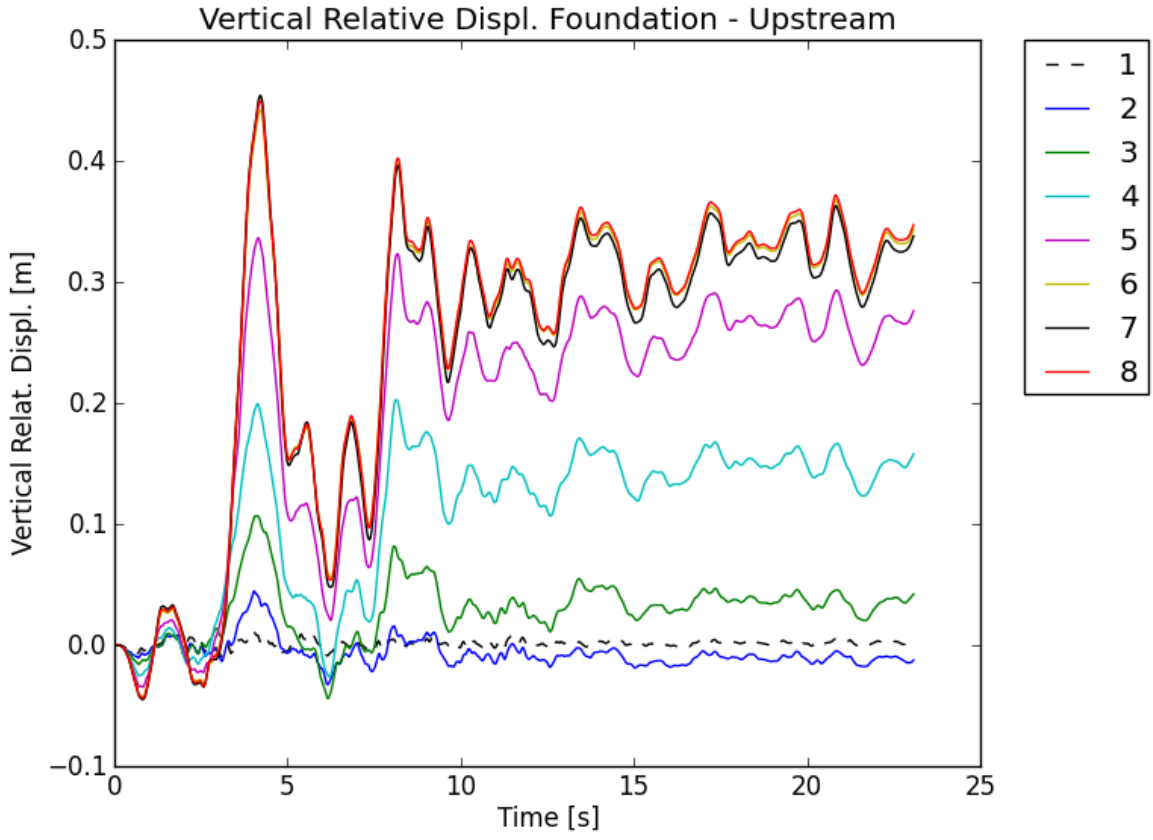

Figure 4-116 Vertical displacements at points 1 – 8 of Figure 4-110 – SEE Kocaeli (V-H1)

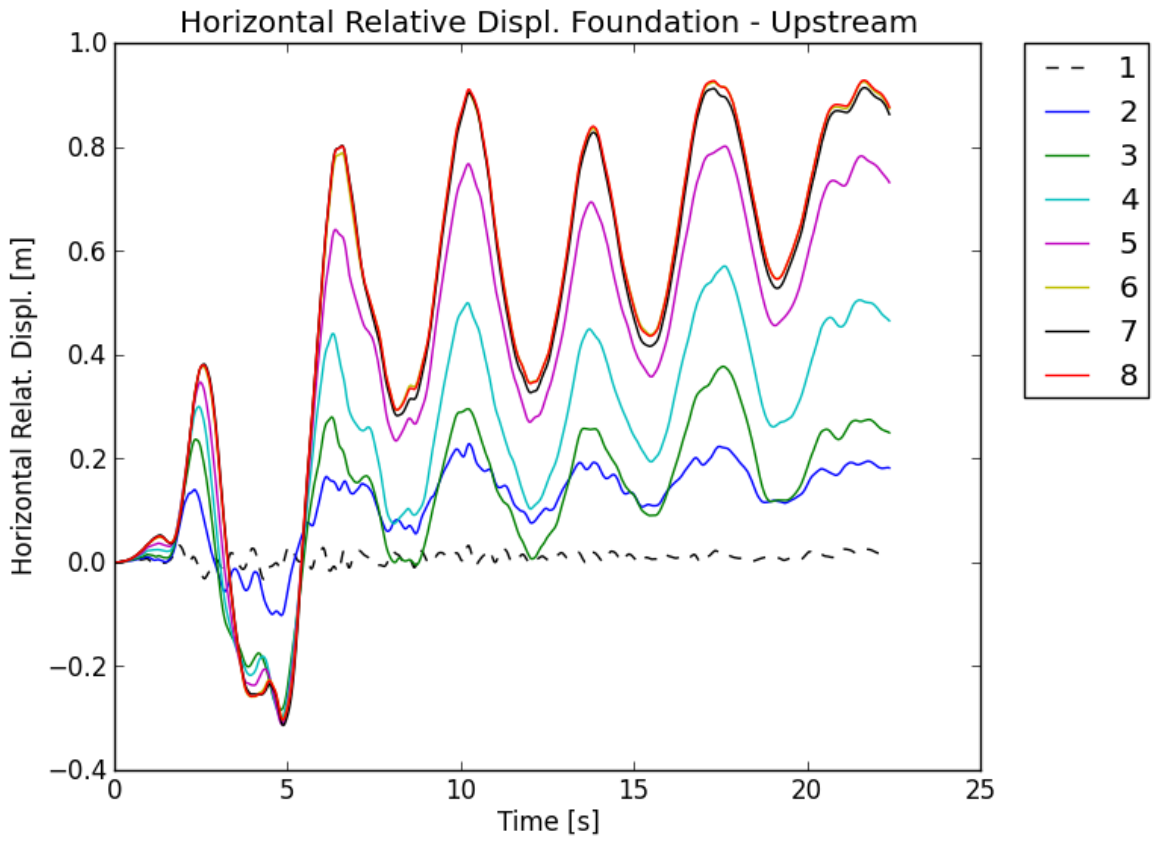

Figure 4-117 Horizontal displacements at points 1 – 8 of Figure 4-110 – SEE Kocaeli (V-H2)

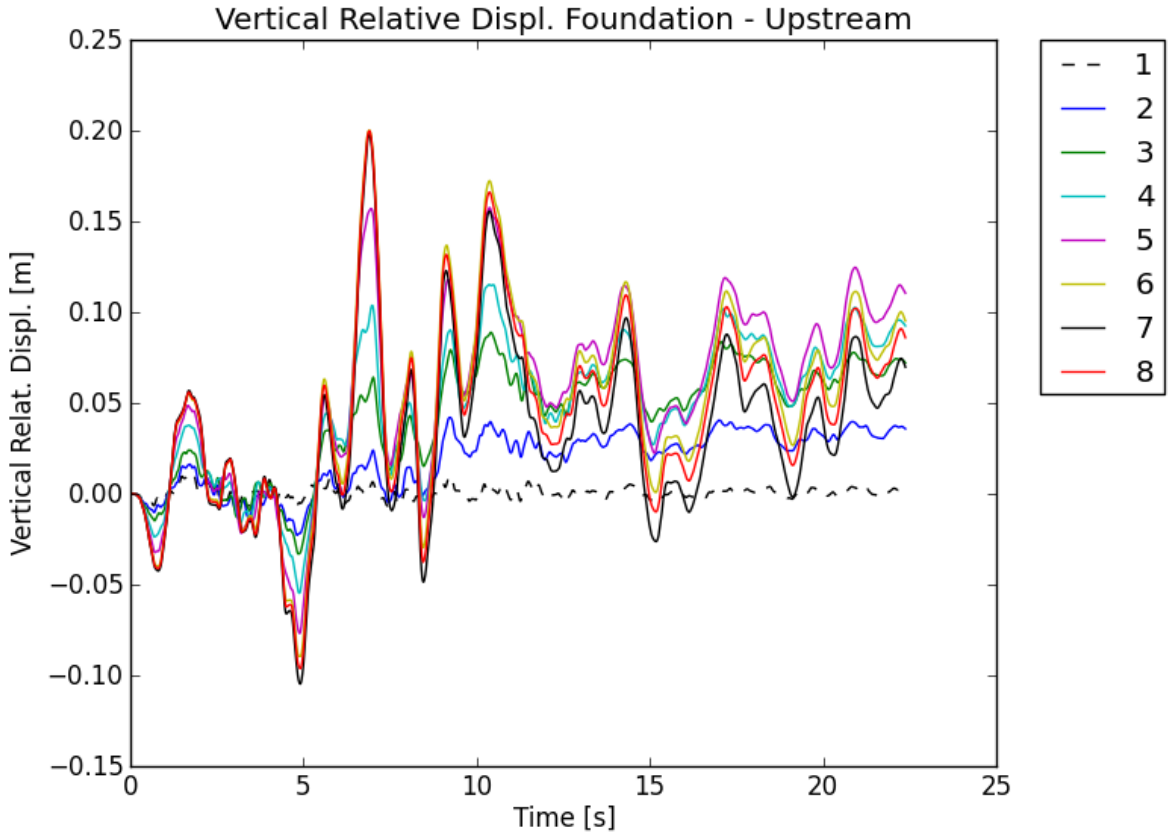

Figure 4-118 Vertical displacements at points 1 – 8 of Figure 4-110 – SEE Kocaeli (V-H2)

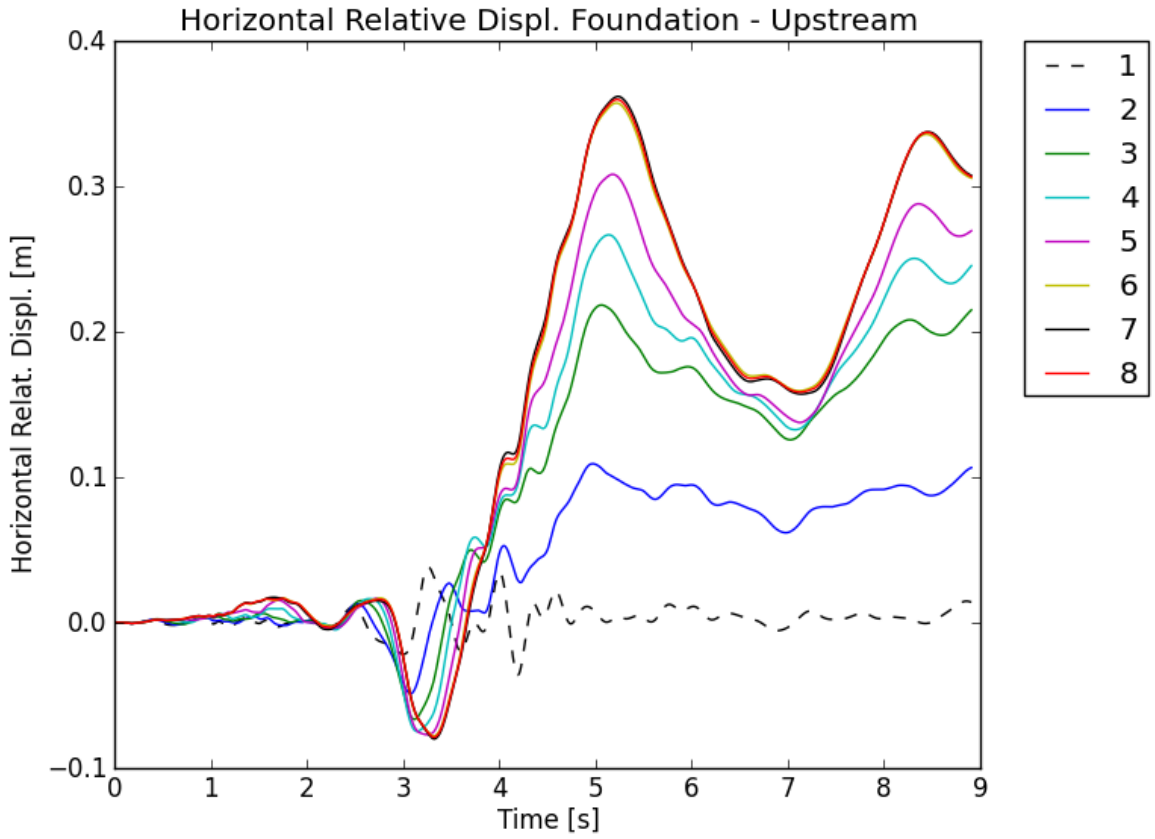

Figure 4-119 Horizontal displacements at points 1 – 8 of Figure 4-110 – SEE Morgan (V-H1)

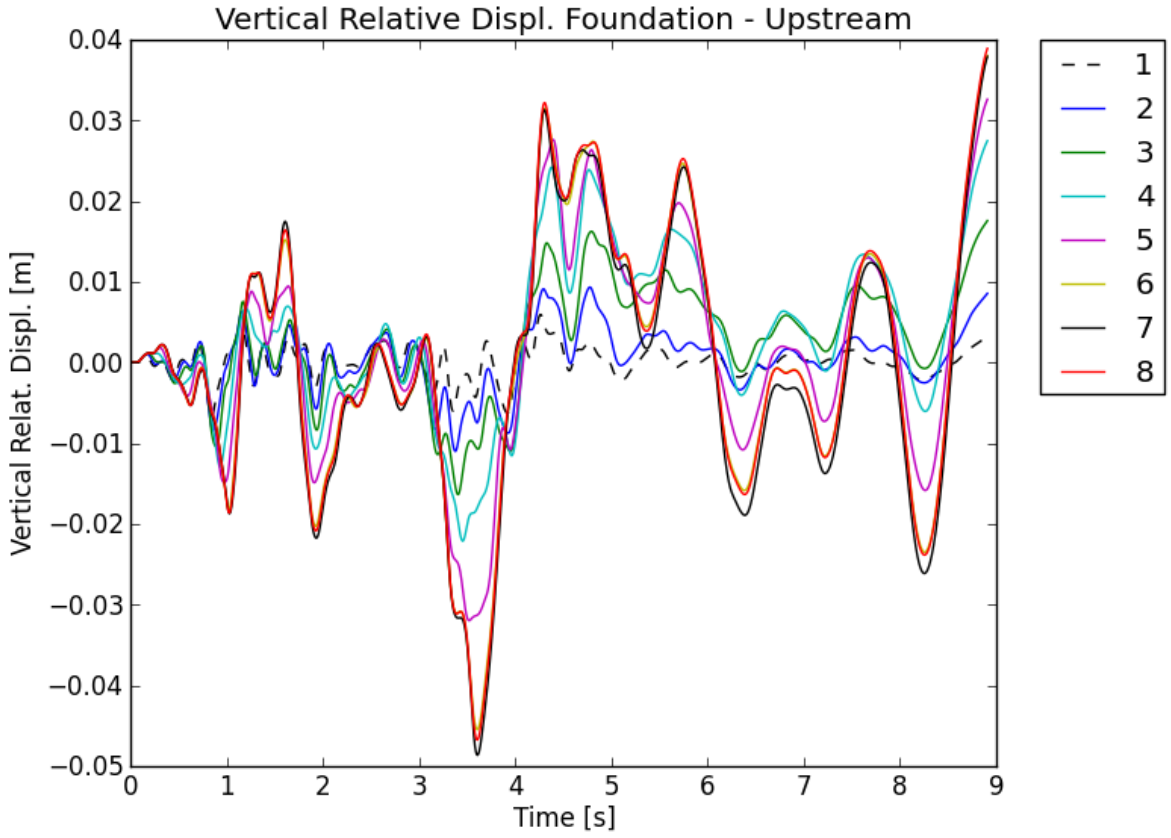

Figure 4-120 Vertical displacements at points 1 – 8 of Figure 4-110 – SEE Morgan (V-H1)

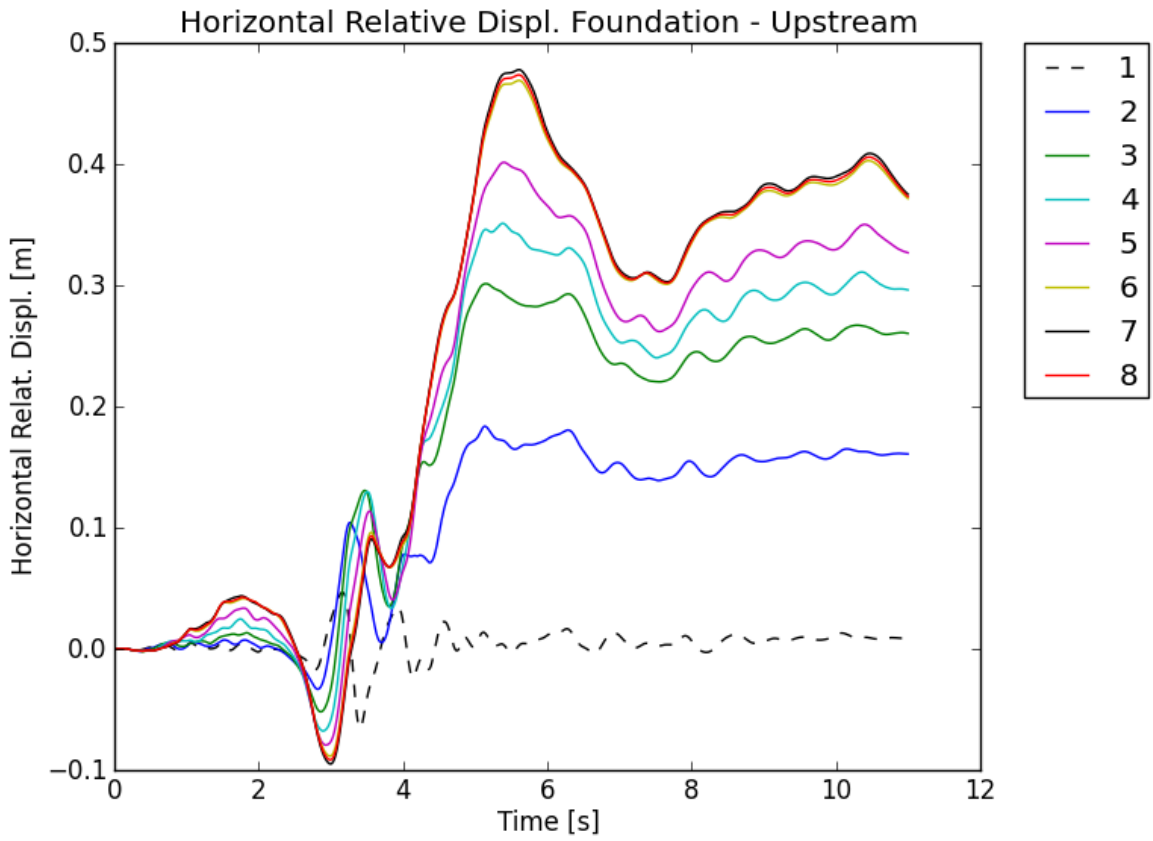

Figure 4-121 Horizontal displacements at points 1 – 8 of Figure 4-110 – SEE Morgan (V-H2)

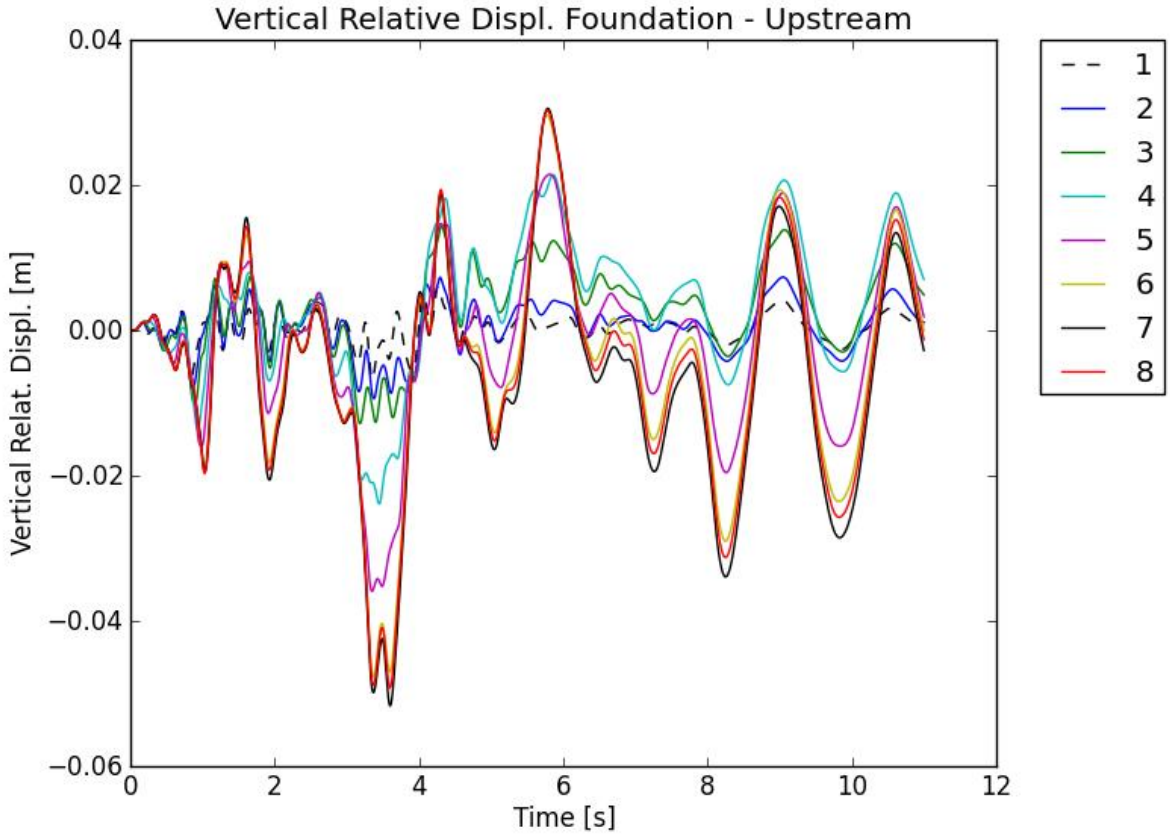

Figure 4-122 Vertical displacements at points 1 – 8 of Figure 4-110 – SEE Morgan (V-H2)

4.6.5. SEE earthquake – Dam founded directly on the bedrock

The simulation of SEE earthquakes considering the dam founded directly on the bedrock have the following properties:

- the influence of the soil foundation on the seismic signal that is applied at the base of the dam is neglected;
- the foundation of the embankment is no more compliant and deformable, but elastic and very stiff.

These two influences contrast somehow with each other: there is no amplification of the signal, then lower velocities are expected at the base of the dam (see Figure 4-45 and Figure 4-46); also, the absence of a deformable foundation provokes the energy of deformation to be all dissipated within the dam.

Table 4-5 summarizes the results that were obtained in terms of maximum displacements at the dam crest. Figure 4-123 to Figure 4-134 show the horizontal and vertical displacements for all the tested cases.

The instability mechanisms that were commented in section 4.6.4 are magnified in this case. The sliding at the upstream occurs for all the tested cases. The embankment feet (upstream and downstream) seem to have gained more stability by substituting the soil foundation by a rigid base.

SEE EARTHQUAKE - DAM FOUNDED ON THE BEDROCK					
		PGA [g]		Max Crest Displacements [m]	
Name		Vertical	Horizontal	Vertical	Horizontal
Darfield V-H1		+ 0.5 / - 0.58	+ 0.96 / - 1.33	-0.60	-0.31
Darfield V-H2			+ 0.79 / - 0.89	-1.20	-1.20
Kocaeli Izt V-H1		+ 0.51 / - 0.43	+ 0.82 / - 0.63	-2.40	-1.00
Kocaeli Izt V-H2			+ 0.47 / - 0.59	-1.90	-1.80
Morgan V-H1		+ 0.44 / - 0.43	+ 0.81 / - 0.62	-0.22	+0.20
Morgan V-H2			+ 0.55 / - 1.49	-0.24	+0.45

Table 4-5 : SEE earthquakes, nonlinear analysis – Dam founded on the bedrock, numerical results

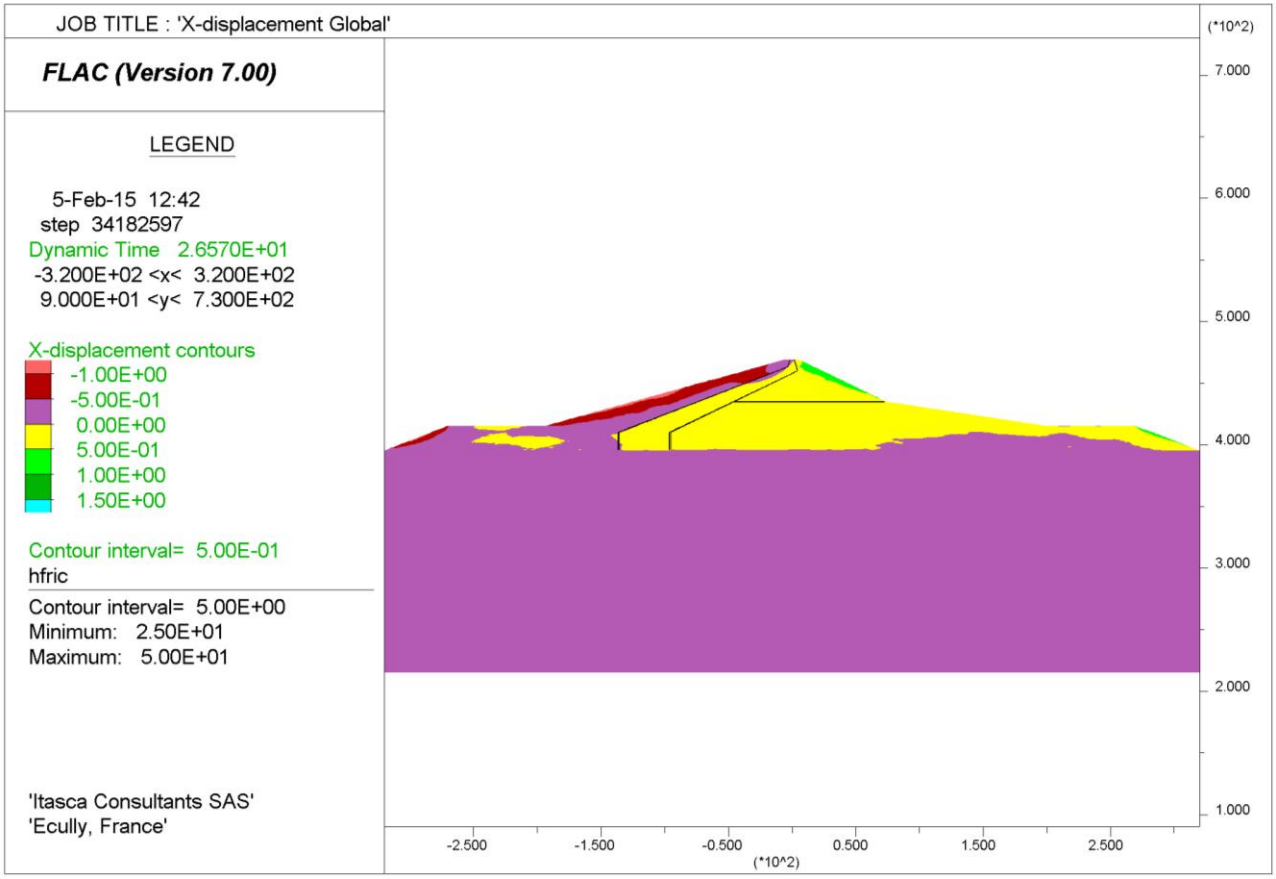

Figure 4-123 : Dam founded on the bedrock - SEE Darfield V-H1- Horizontal displacements

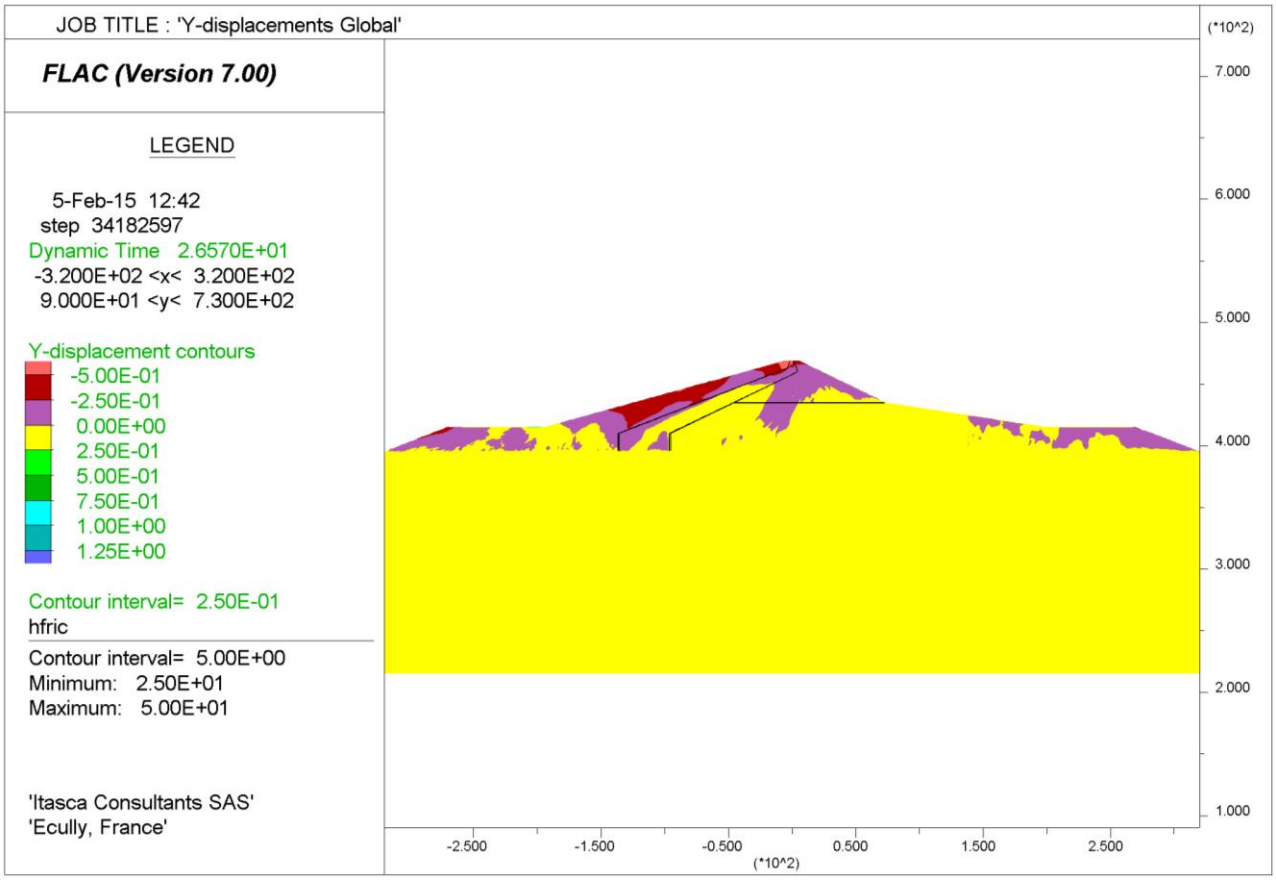

Figure 4-124: Dam founded on the bedrock - SEE Darfield V-H1- Vertical displacements

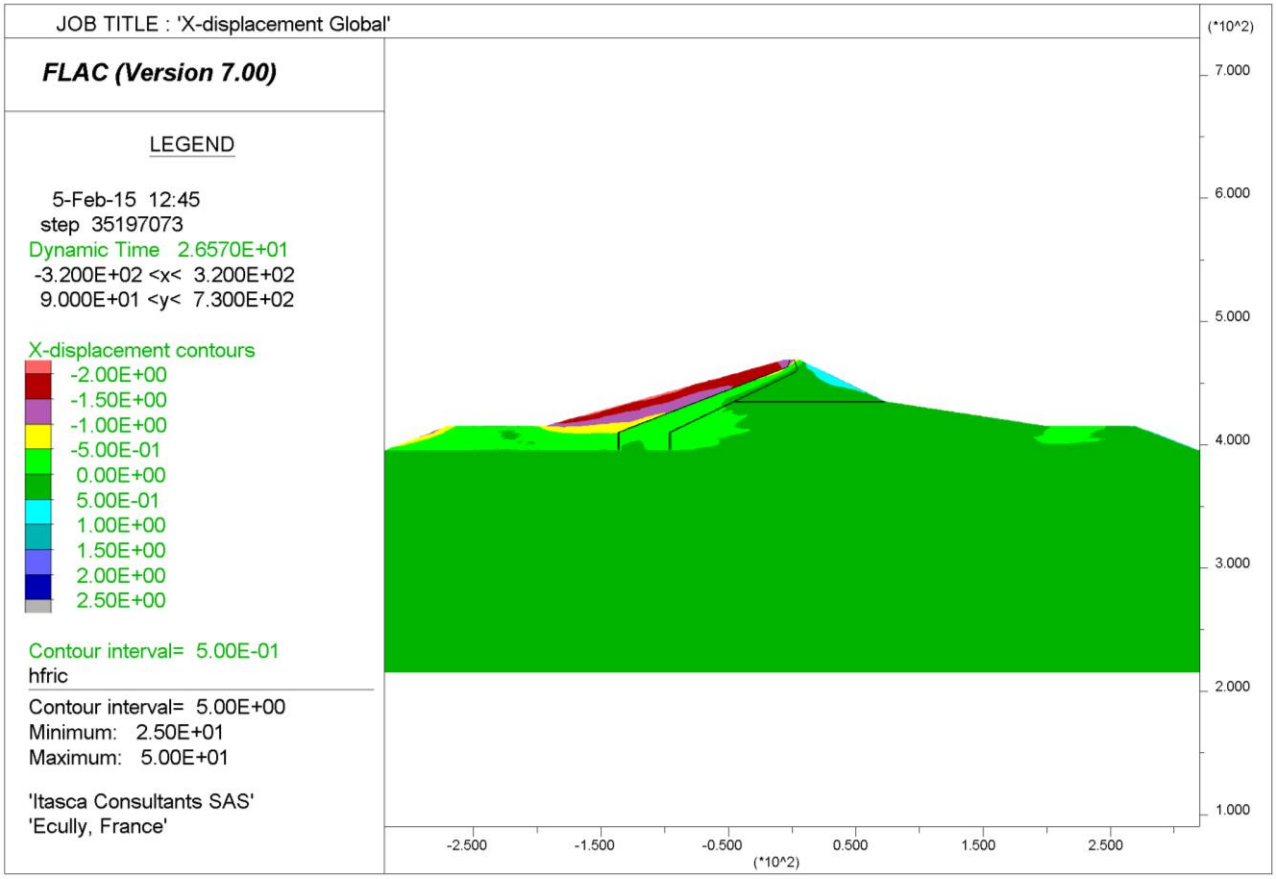

Figure 4-125: Dam founded on the bedrock - SEE Darfield V-H2- Horizontal displacements

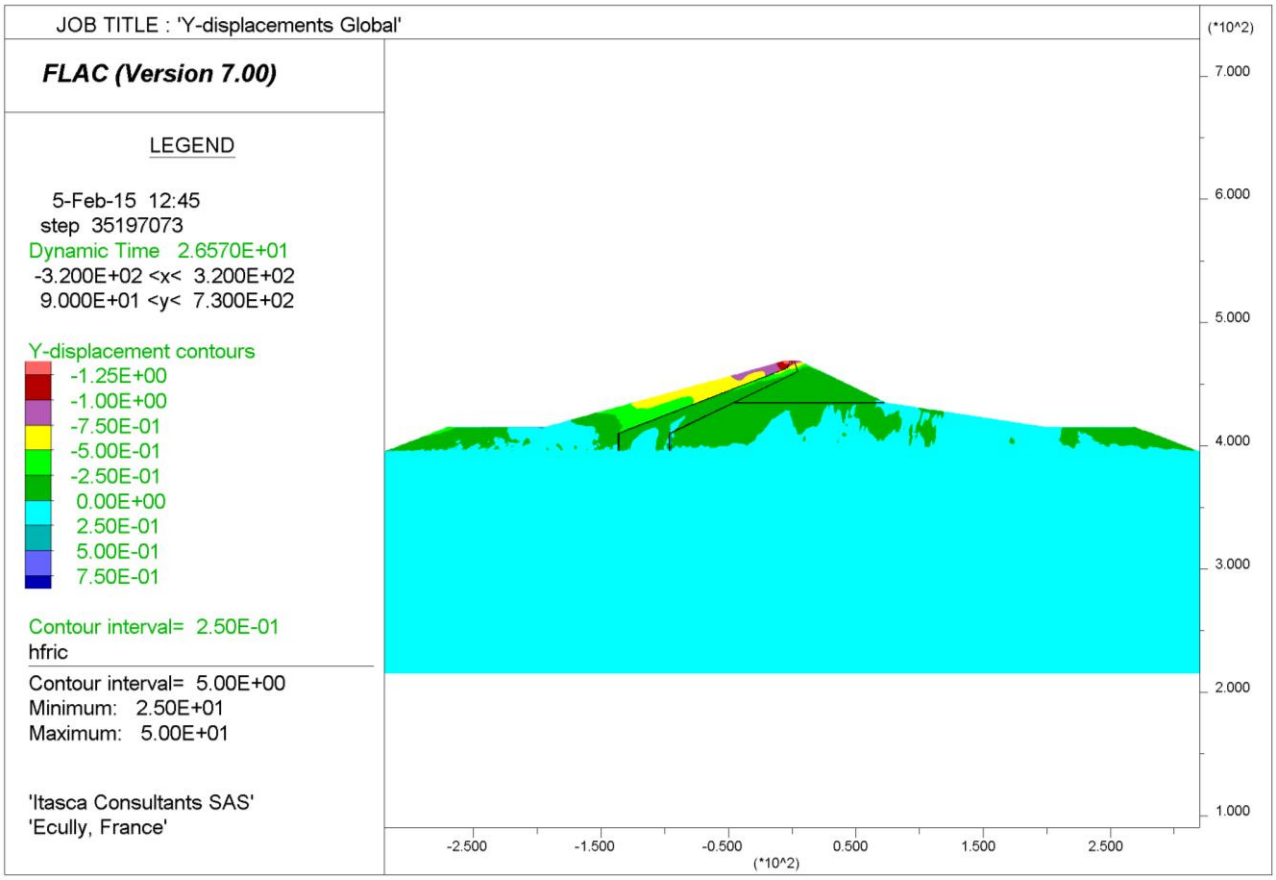

Figure 4-126: Dam founded on the bedrock - SEE Darfield V-H2- Vertical displacements

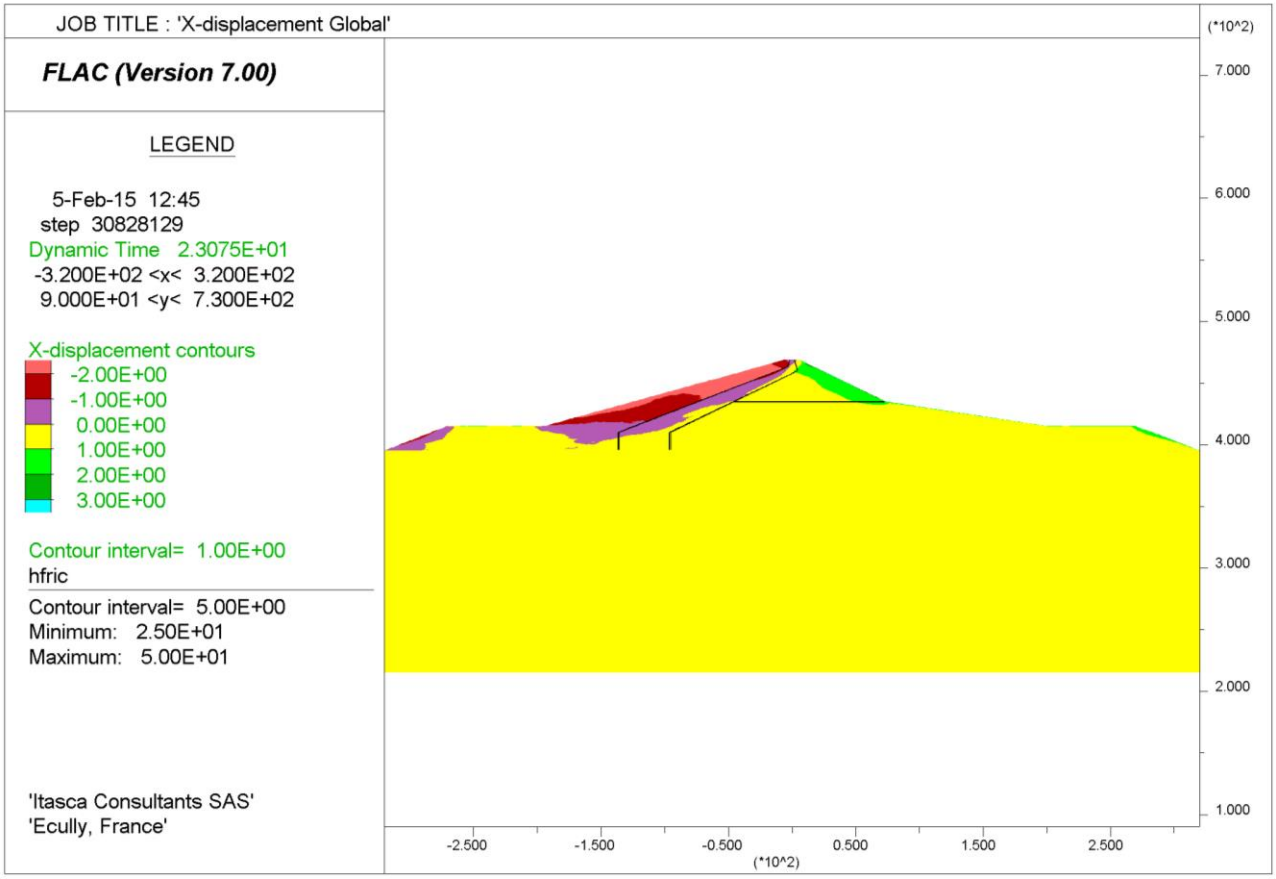

Figure 4-127 : Dam founded on the bedrock - SEE Kocaeli V-H1- Horizontal displacements

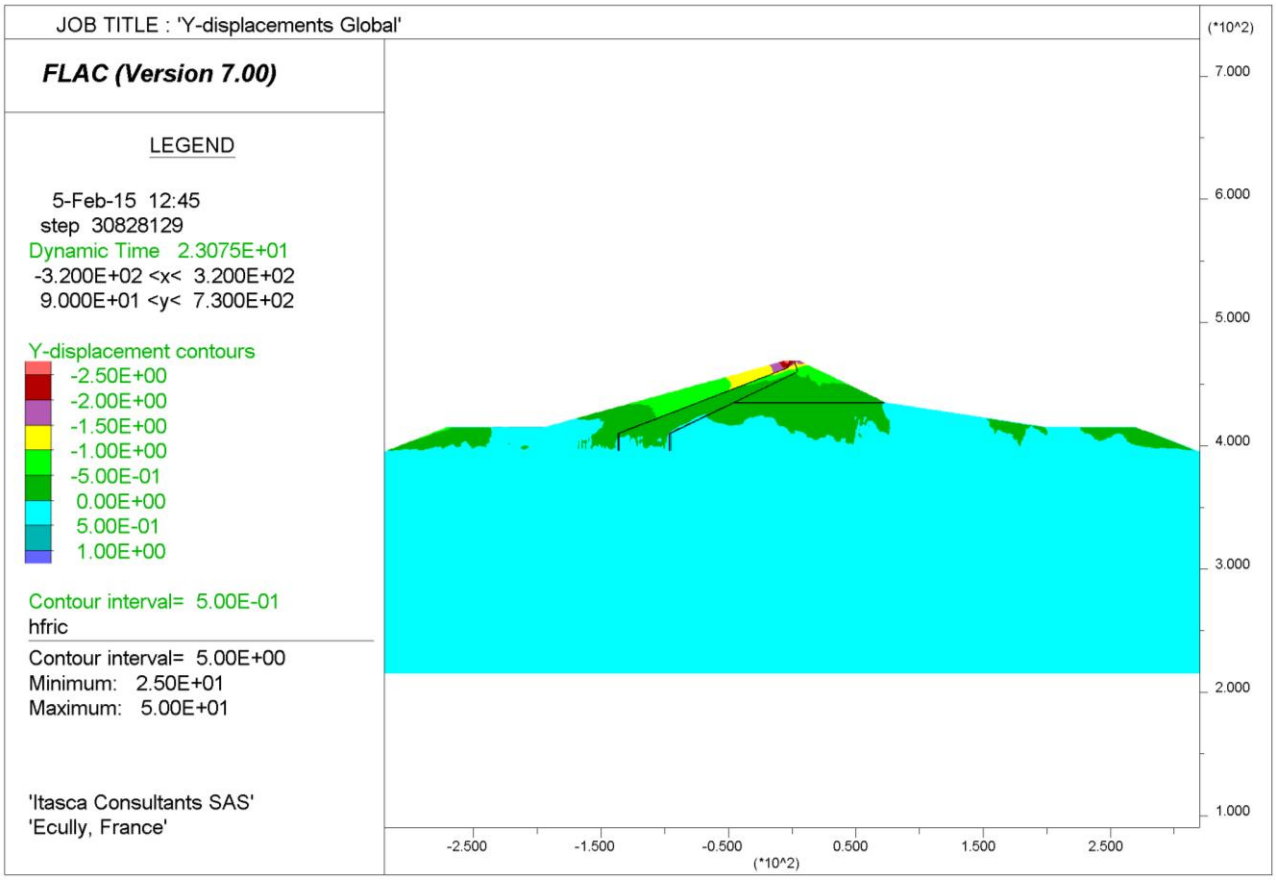

Figure 4-128: Dam founded on the bedrock - SEE Kocaeli V-H1- Vertical displacements

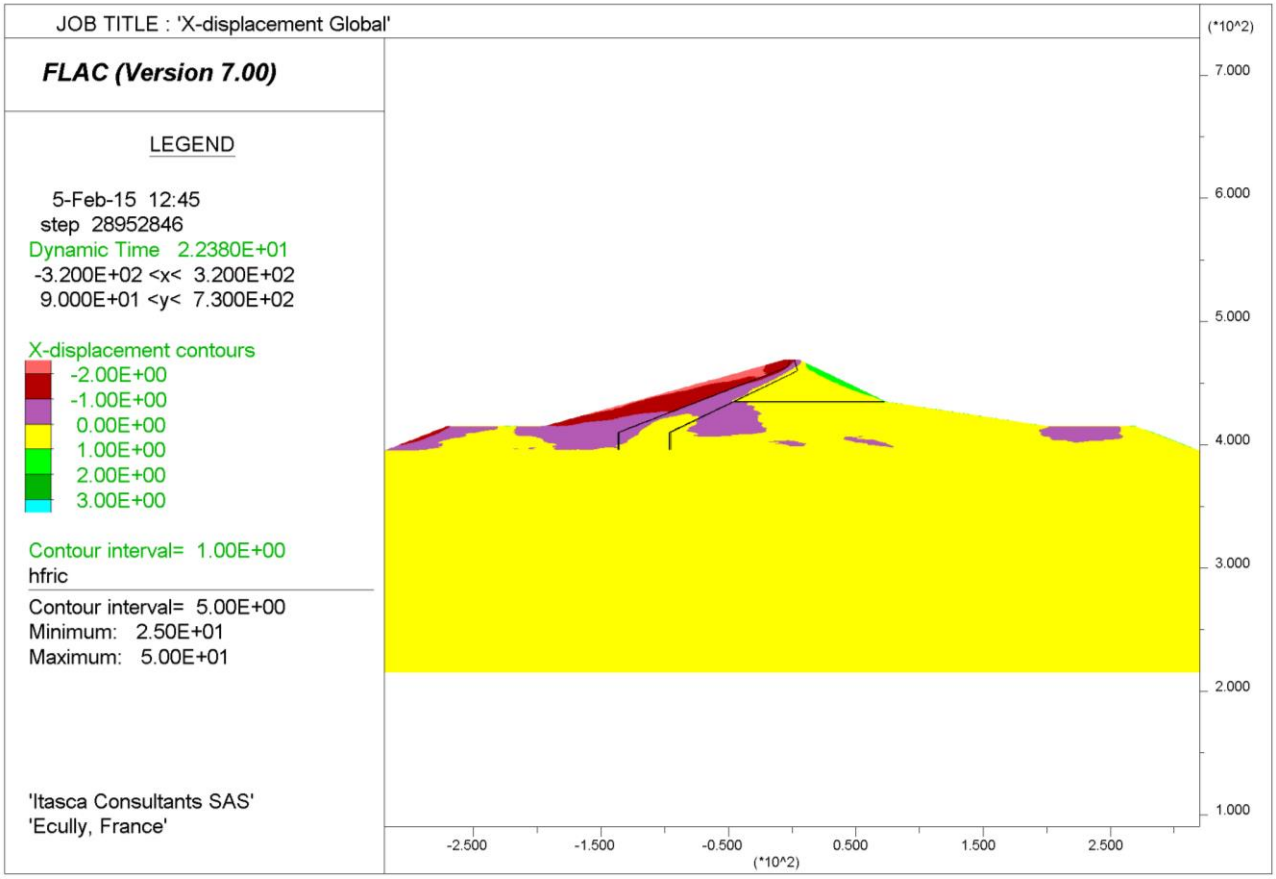

Figure 4-129: Dam founded on the bedrock - SEE Kocaeli V-H2- Horizontal displacements

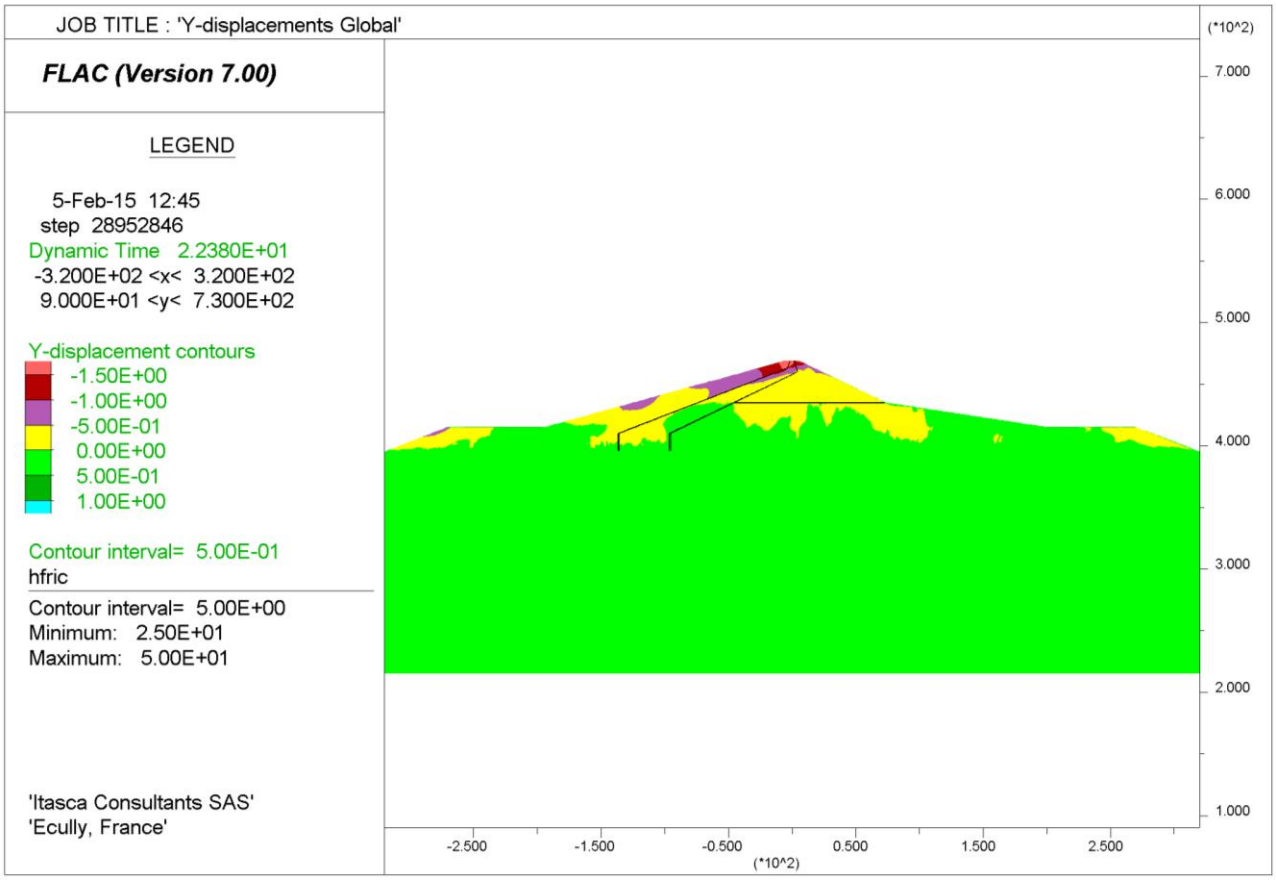

Figure 4-130: Dam founded on the bedrock - SEE Kocaeli V-H2- Vertical displacements

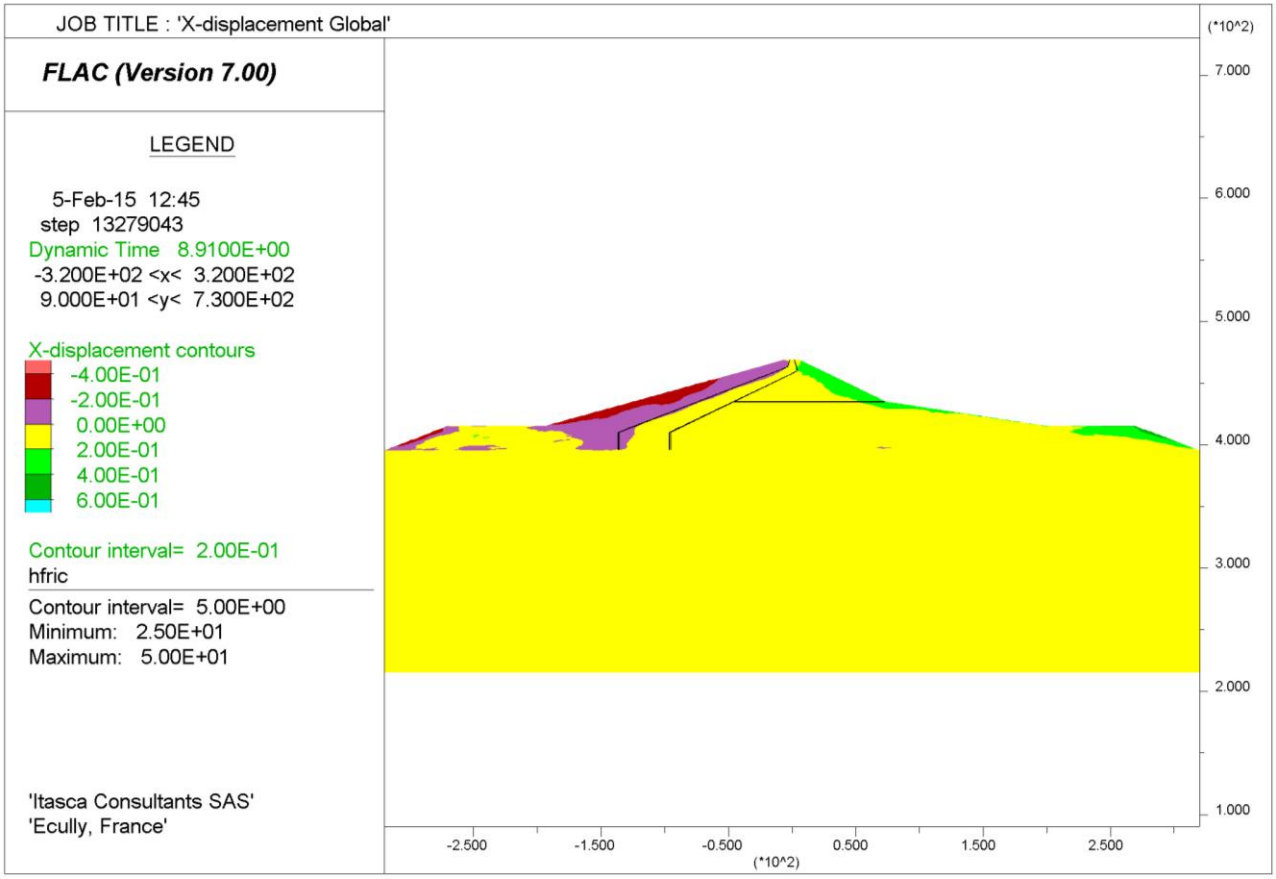

Figure 4-131: Dam founded on the bedrock - SEE Morgan V- H1- Horizontal displacements

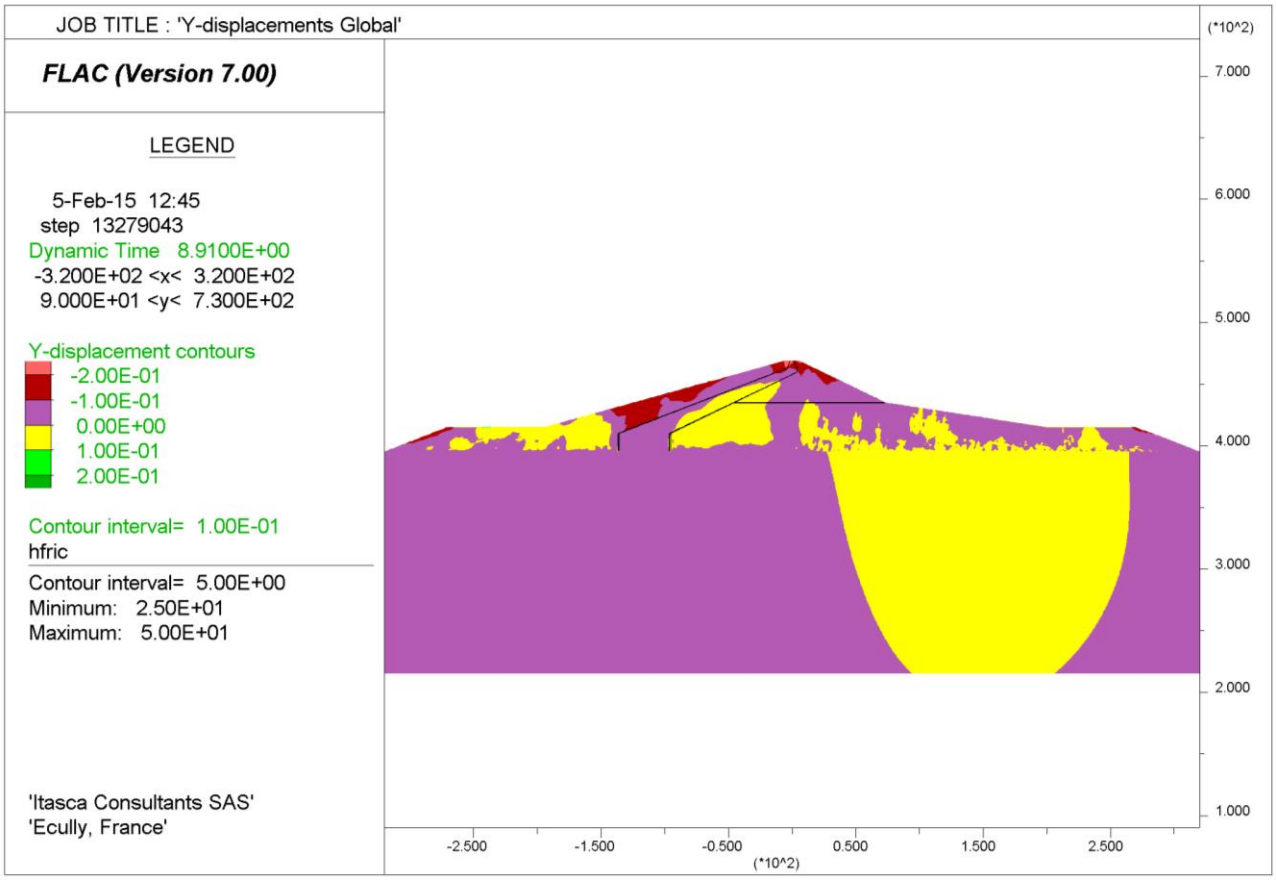

Figure 4-132: Dam founded on the bedrock - SEE Morgan V- H1- Vertical displacements

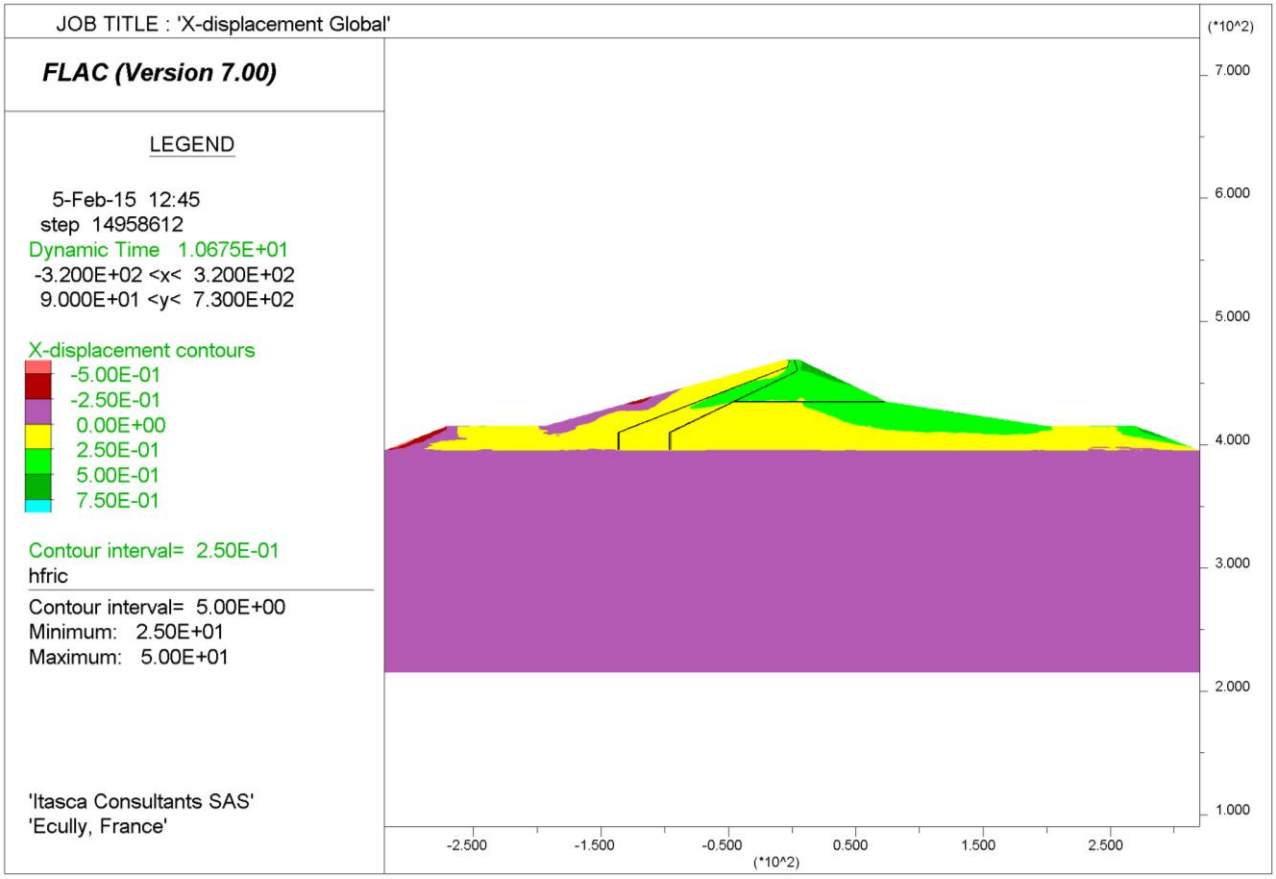

Figure 4-133: Dam founded on the bedrock - SEE Morgan V- H2- Horizontal displacements

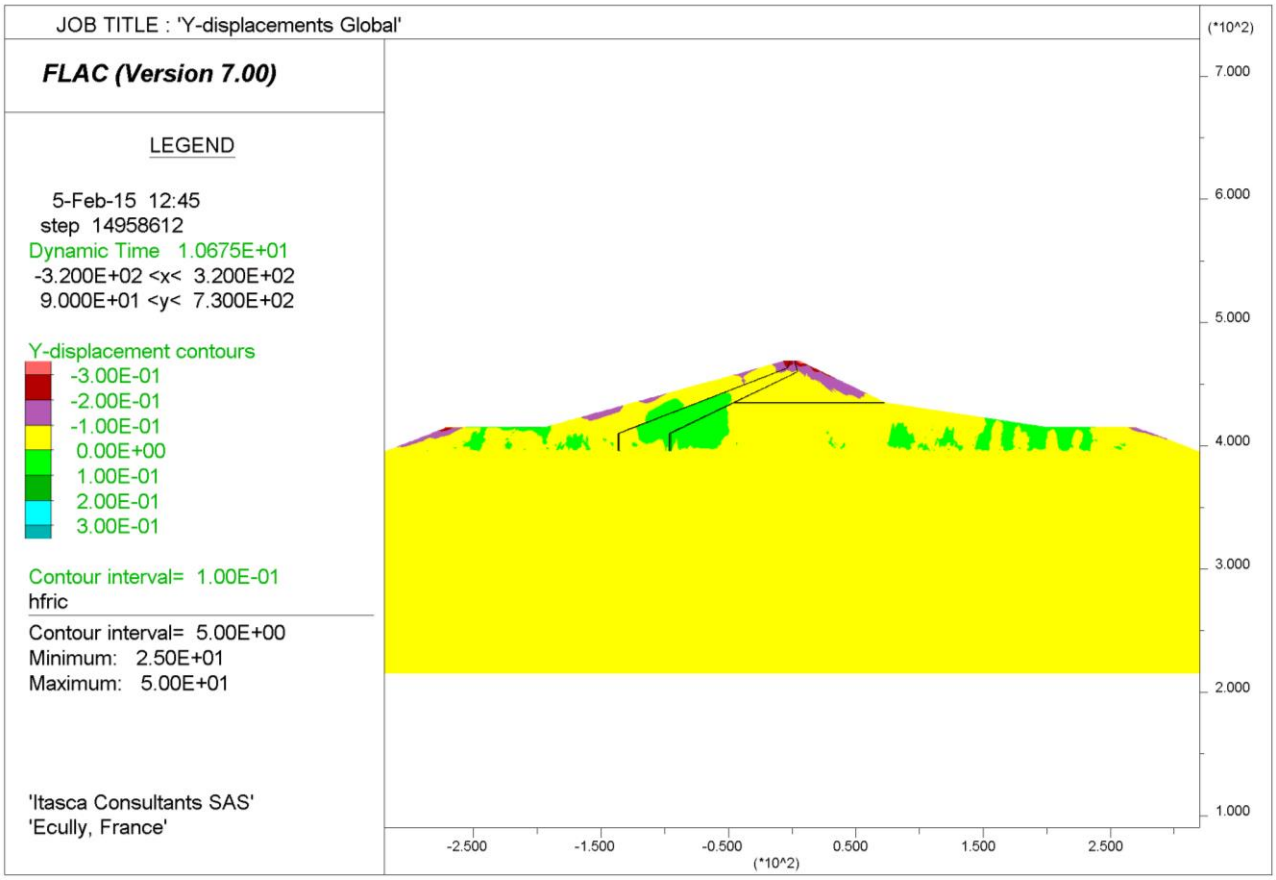

Figure 4-134: Dam founded on the bedrock - SEE Morgan V- H2- Vertical displacements

4.7. Conclusions

Tables that summarize the maximum displacement are presented below.

Table 4-6 summarizes the results of the pseudo-static Newmark's Sliding Block analysis for the SEE earthquakes. Results are commented in section 4.6.3.

Table 4-7 summarizes the results of the nonlinear dynamic analysis considering the SEE earthquakes, commented in section 4.6.4. The analysis of relative horizontal displacements on the concrete slurry wall is presented in section 4.6.4.1 and summarized in Table 4-8.

Table 4-9 summarizes the results obtained by considering the dam founded directly on the bedrock (SEE earthquakes). Results are commented in section 4.6.5.

The dynamic analysis for the *Reference Cross Section* allowed the identification of the zones that undergo to the most important instabilities. The most problematic zone seems to be the upstream slope that fails and undergoes sliding along the interface between the rockfill and the dam core.

For all the tested cases, the maximum vertical displacement at the crest of the dam is far below the maximum admissible displacement, equal to 4 meters, as indicated by NOVEC.

SEE EARTHQUAKE - KOCAELI IZT V-H1			
		Pseudo-static Analysis	
Analysis		Kh [g]	Max Displacement
Downstream		0.17	> 9 m
Upstream		-0.16	> 4 m

Table 4-6 : Pseudo-static analysis – Summary of results

SEE EARTHQUAKE - REFERENCE CROSS SECTION					
		PGA [g]		Max Crest Displacements [m]	
Name		Vertical	Horizontal	Vertical	Horizontal
Darfield V-H1		+ 0.5 / - 0.58	+ 0.96 / - 1.33	-0.25	+0.60
Darfield V-H2			+ 0.79 / - 0.89	-1.00	-1.50
Kocaeli Izt V-H1		+ 0.51 / - 0.43	+ 0.82 / - 0.63	-0.90	+2.50
Kocaeli Izt V-H2			+ 0.47 / - 0.59	-1.00	-0.80
Morgan V-H1		+ 0.44 / - 0.43	+ 0.81 / - 0.62	-0.20	+0.40
Morgan V-H2			+ 0.55 / - 1.49	-0.20	+0.60

Table 4-7 : SEE earthquakes – Nonlinear analysis – Maximum crest displacements

SEE EARTHQUAKE - CONCRETE SLURRY WALL DISPLACEMENTS				
	PGA [g]		Relative Displacement [m]	Length [m]
Name	Vertical	Horizontal	Horizontal	
Darfield V-H1	+ 0.5 / - 0.58	+ 0.96 / - 1.33	0.8	105 (points 1 - 6)
Darfield V-H2		+ 0.79 / - 0.89	0.8	105 (points 1 - 6)
Kocaeli Izt V-H1	+ 0.51 / - 0.43	+ 0.82 / - 0.63	2.4	105 (points 1 - 6)
Kocaeli Izt V-H2		+ 0.47 / - 0.59	0.9	105 (points 1 - 6)
Morgan V-H1	+ 0.44 / - 0.43	+ 0.81 / - 0.62	0.3	105 (points 1 - 6)
Morgan V-H2		+ 0.55 / - 1.49	0.3	105 (points 1 - 6)

Table 4-8 : SEE earthquakes, nonlinear analysis - Concrete wall relative horizontal displacements

SEE EARTHQUAKE - DAM FOUNDED ON THE BEDROCK					
		PGA [g]		Max Crest Displacements [m]	
Name		Vertical	Horizontal	Vertical	Horizontal
Darfield V-H1		+ 0.5 / - 0.58	+ 0.96 / - 1.33	-0.60	-0.31
Darfield V-H2			+ 0.79 / - 0.89	-1.20	-1.20
Kocaeli Izt V-H1		+ 0.51 / - 0.43	+ 0.82 / - 0.63	-2.40	-1.00
Kocaeli Izt V-H2			+ 0.47 / - 0.59	-1.90	-1.80
Morgan V-H1		+ 0.44 / - 0.43	+ 0.81 / - 0.62	-0.22	+0.20
Morgan V-H2			+ 0.55 / - 1.49	-0.24	+0.45

Table 4-9 : SEE earthquakes, nonlinear analysis – Dam founded on the bedrock, crest displacement

5. REAL CROSS SECTION

In this chapter the results obtained considering a new profile for the soil foundation and the embankment are presented. This cross section is labeled "*Real cross section*".

5.1. The geometry

The materials are the same than the ones considered in the *Reference cross section*. The main differences are the following:

- The upstream slope is reduced: it was 1V:3.5H for the *Reference cross section*, it is 1V:4H for the *Real cross section*;
- The profile of the soil foundation represented on Figure 5-1. The layer of alluvial sand is now only below the upstream rockfill and the dam core. The embankment is founded on the clayey silt soil downstream. The profiles of the clayey silt and the alluvial gravel are not more regular, with bedrock that emerges downstream at the free surface.

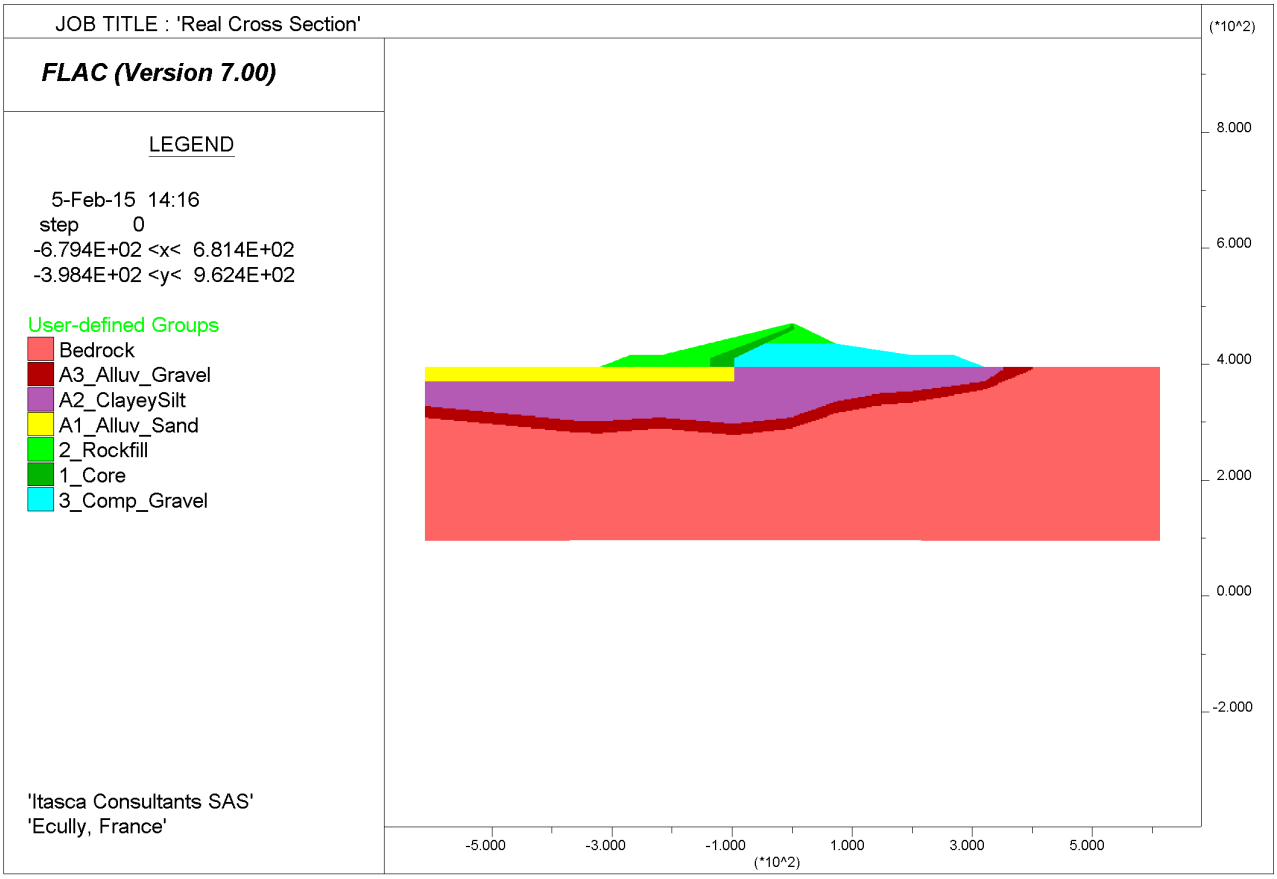

Figure 5-1 : Real cross section – Layout

The position of the concrete wall is unvaried (see Figure 5-2), going from the base of the dam core, down to the top of the bedrock layer. The concrete wall is not introduced in the model.

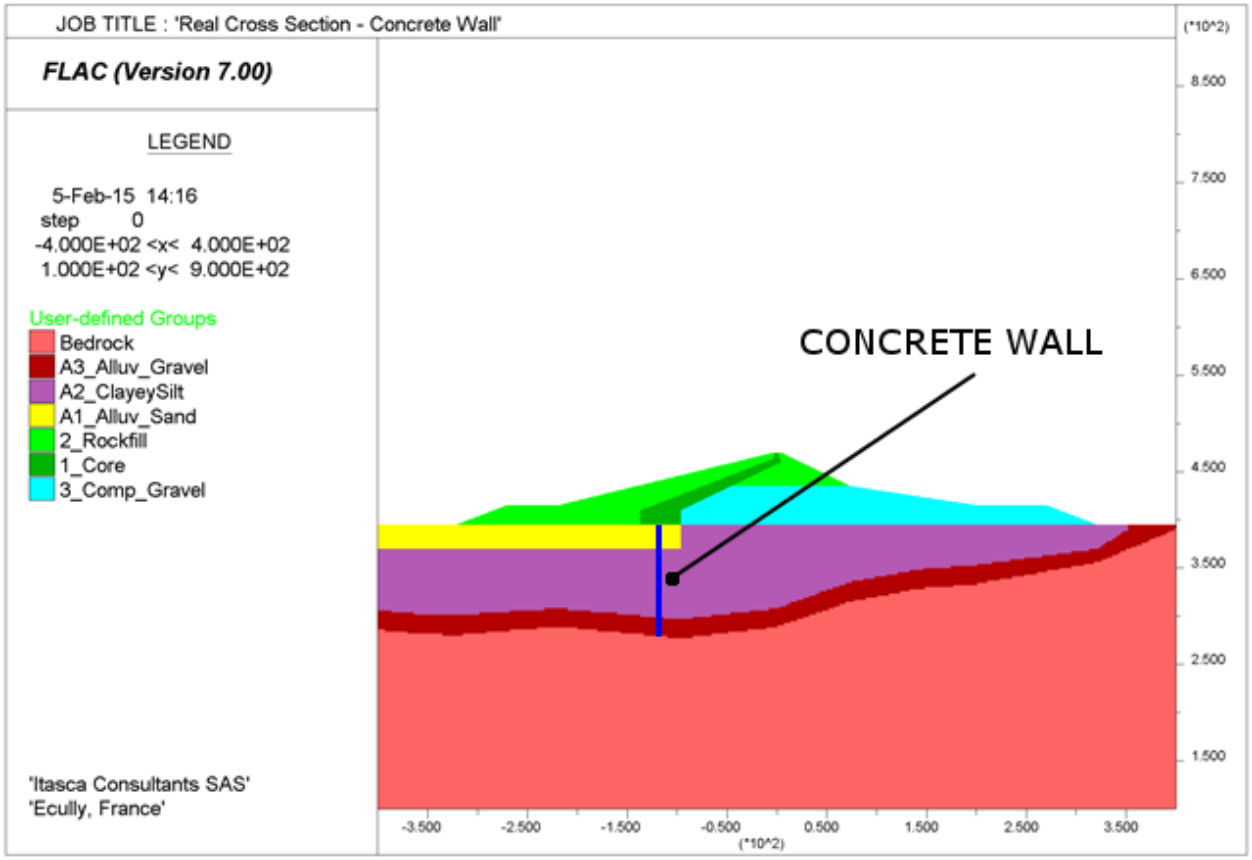

Figure 5-2: Real cross section – Concrete wall

5.2. Mechanical properties

There is no variation in terms of mechanical properties for the *Real cross section* with respect to the *Reference cross section*.

As described in section 3.2.1, a nonlinear-elastic-Mohr-Coulomb model is used to model the whole soil structure for the static part of the analysis. The bedrock layer is assumed to be elastic. For the dam and the foundation materials, variation of the Young's modulus with the confining stress is assumed.

Figure 5-3 and Figure 5-4 show the values of friction angle and dilatancy (see section 3.1.1).

Figure 5-5 and Figure 5-6 show the profiles of bulk modulus and shear modulus, respectively, for the soil foundation layers. These profiles refer to the foundation prior to the construction of the embankment. However, the soil layers are assumed to be consolidated.

The evolution of the confining stress, and its consequences on the value of bulk and shear moduli, is taken into account during the construction of the embankment and the water-filling on the upstream.

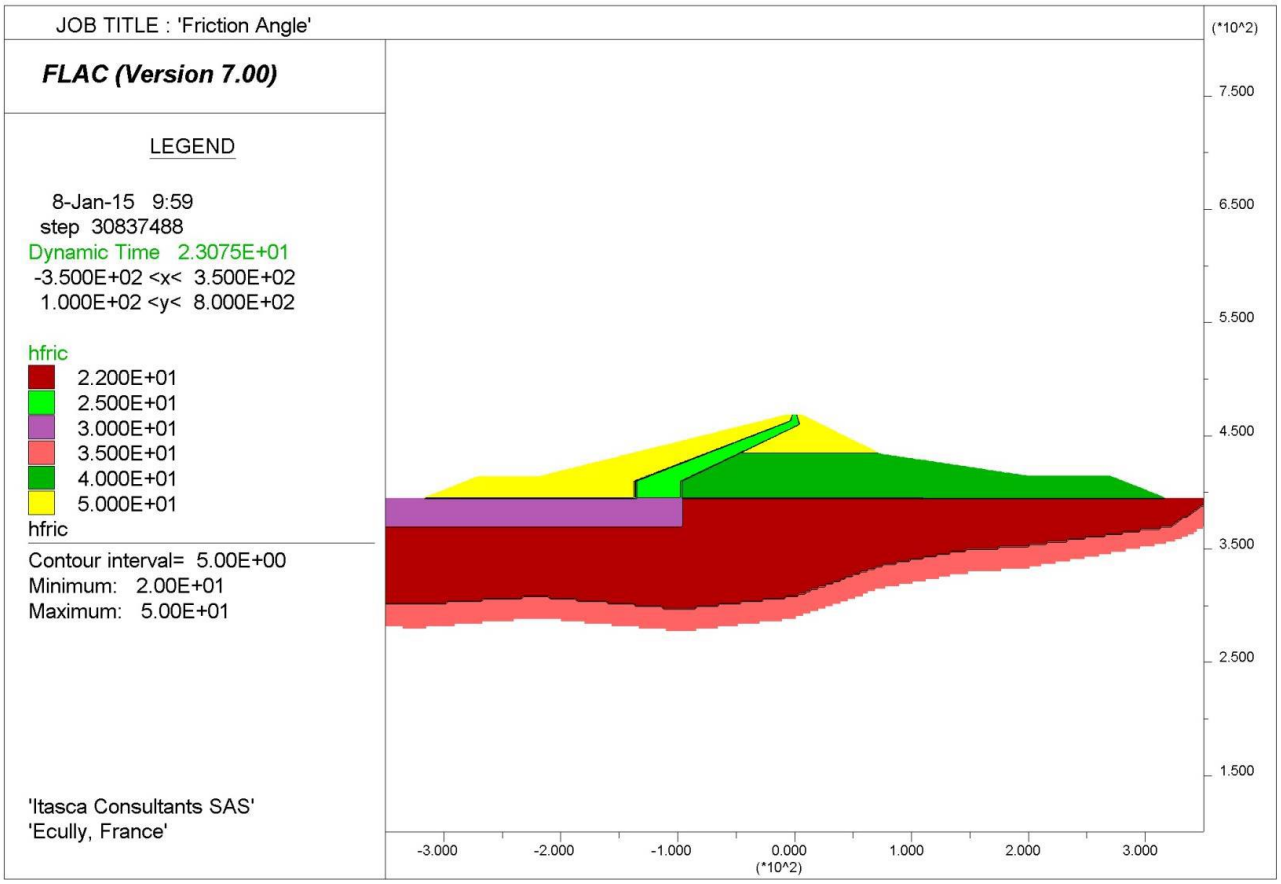

Figure 5-3 : friction angle of the soil foundation and the embankment

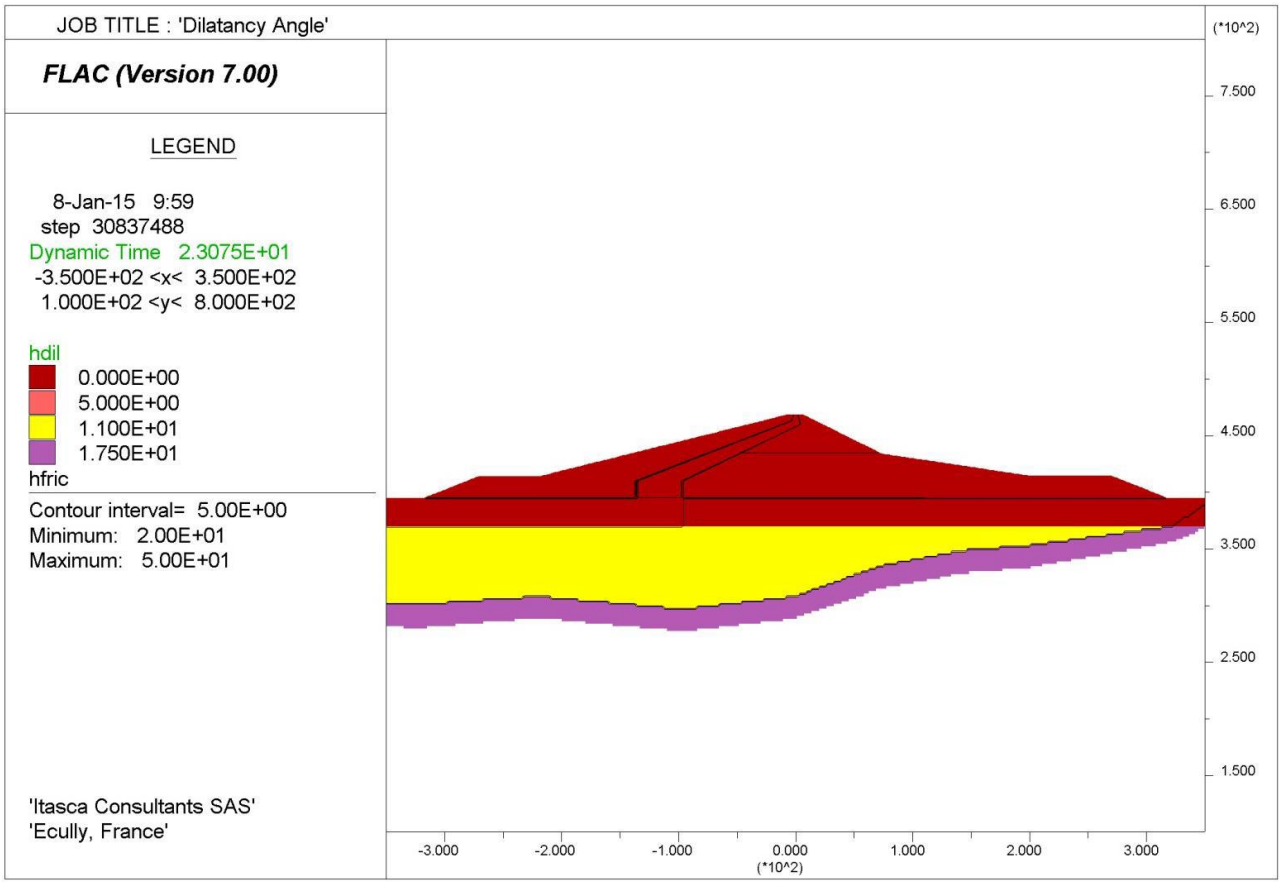

Figure 5-4 : dilatancy of the soil foundation and the embankment

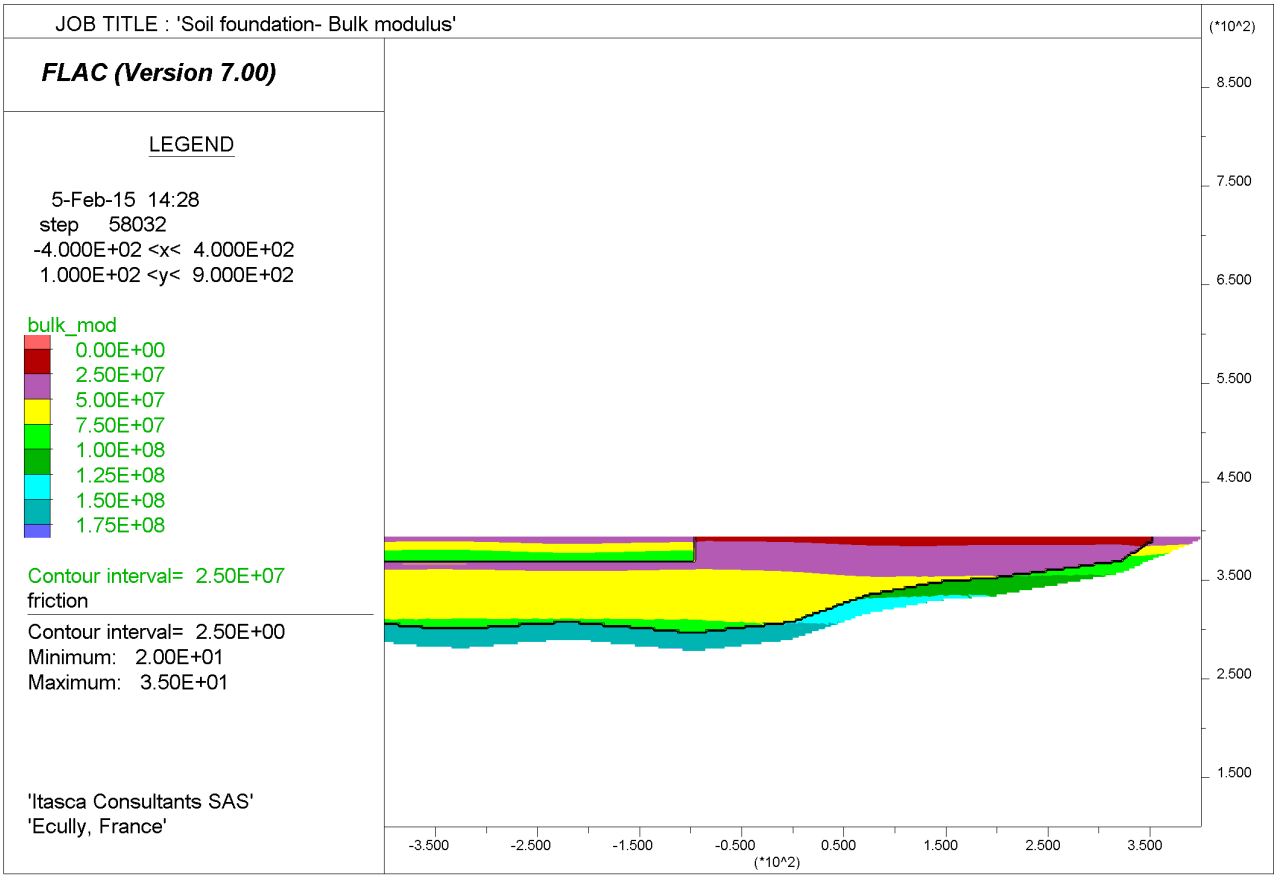

Figure 5-5: bulk modulus of soil foundation layers (consolidated)

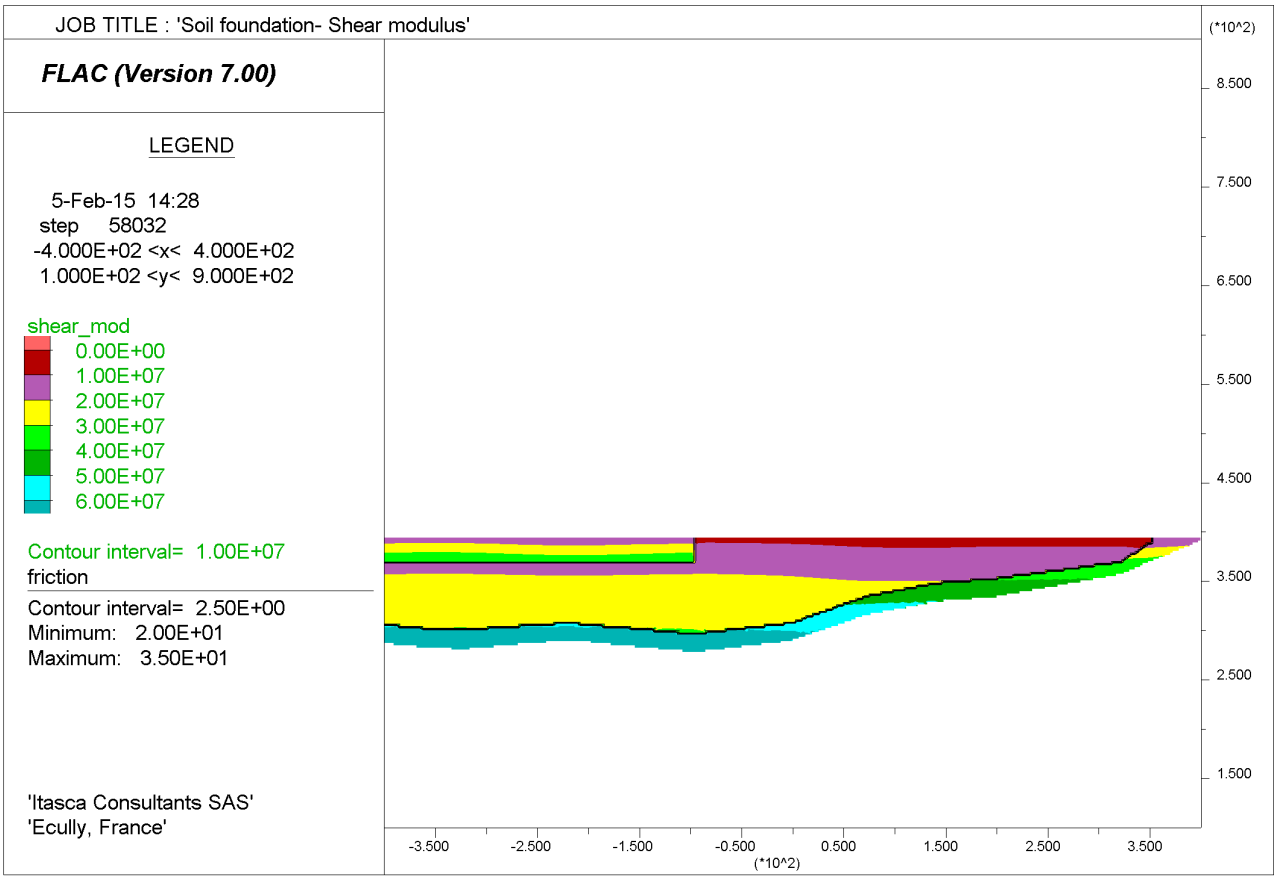

Figure 5-6: shear modulus of soil foundation layers (consolidated)

5.3. Hydraulic properties

The phreatic surface is assumed to coincide with the soil surface, i.e. at elevation 395 meters, at this stage and all along the construction of the embankment. Figure 5-7 shows the pore pressures profile.

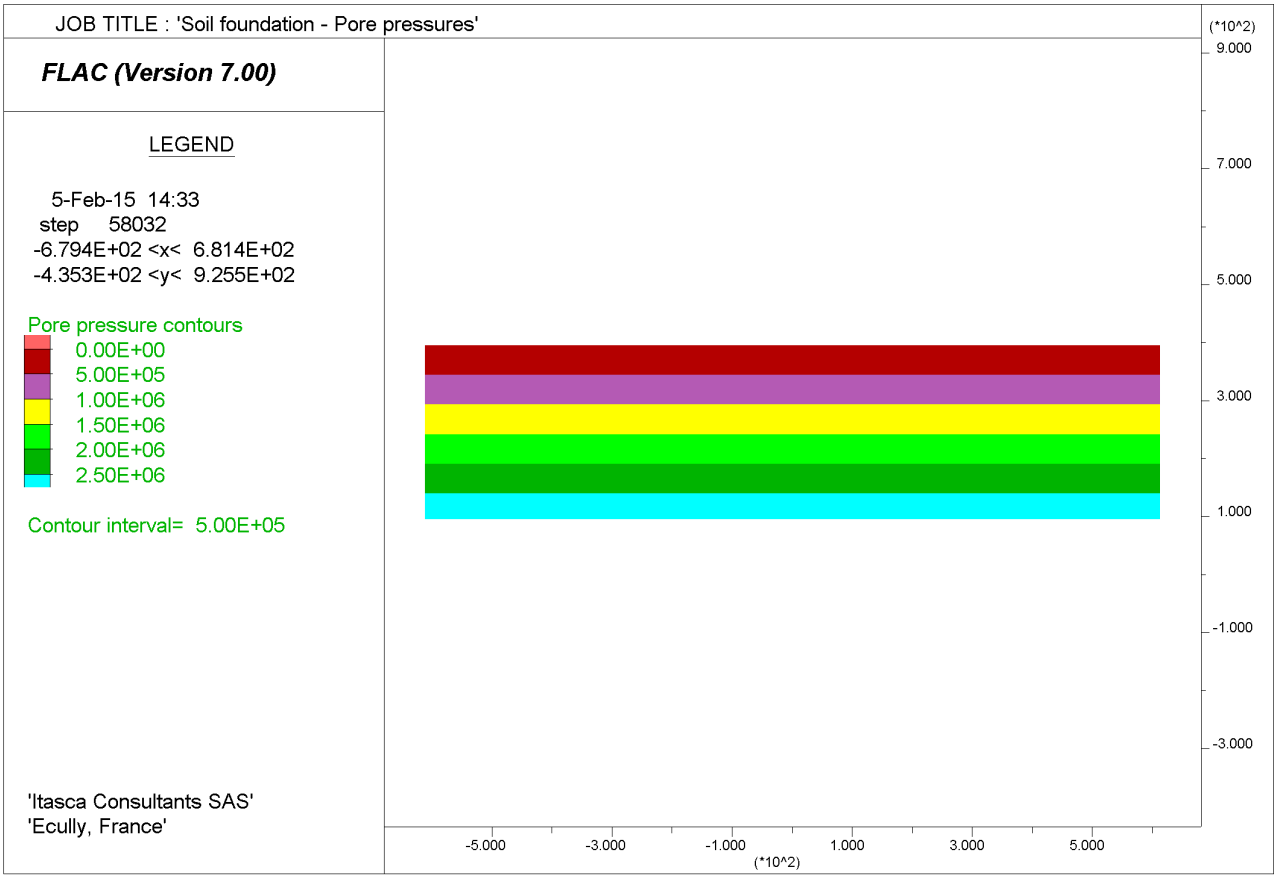

Figure 5-7: embankment foundation – pore pressures profile (water level at the surface)

5.4. Stress initialization

Effective stresses are initialized using the following expressions:

$$\sigma'_{yy}(y) = (\gamma_{sat} - \gamma_w) \cdot y = \gamma' \cdot y \qquad (15)$$

$$\sigma'_{xx}(y) = k_0 \cdot \sigma'_{yy}(y) \qquad (16)$$

$$\sigma'_{zz}(y) = k_0 \cdot \sigma'_{yy}(y) \qquad (17)$$

The coefficient of lateral earth pressure at rest, represented as K0, is assumed to be equal to 0.667 for the first 30 meters of foundation, since in this zone the compaction effects due to the construction of the embankment is assumed to be significant.

K0 = 0.5 below elevation 365 meters.

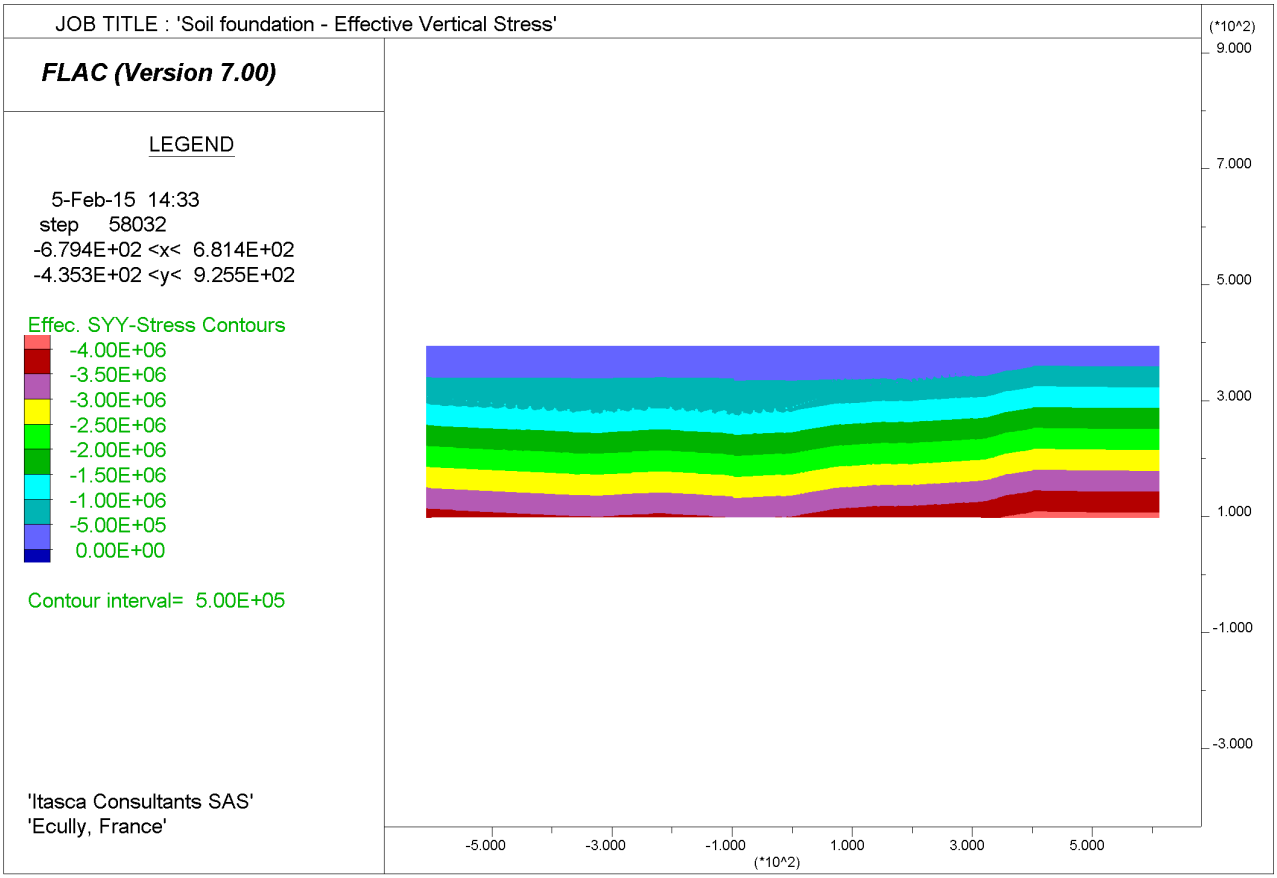

Figure 5-8: effective vertical stress profile prior to the construction of the embankment

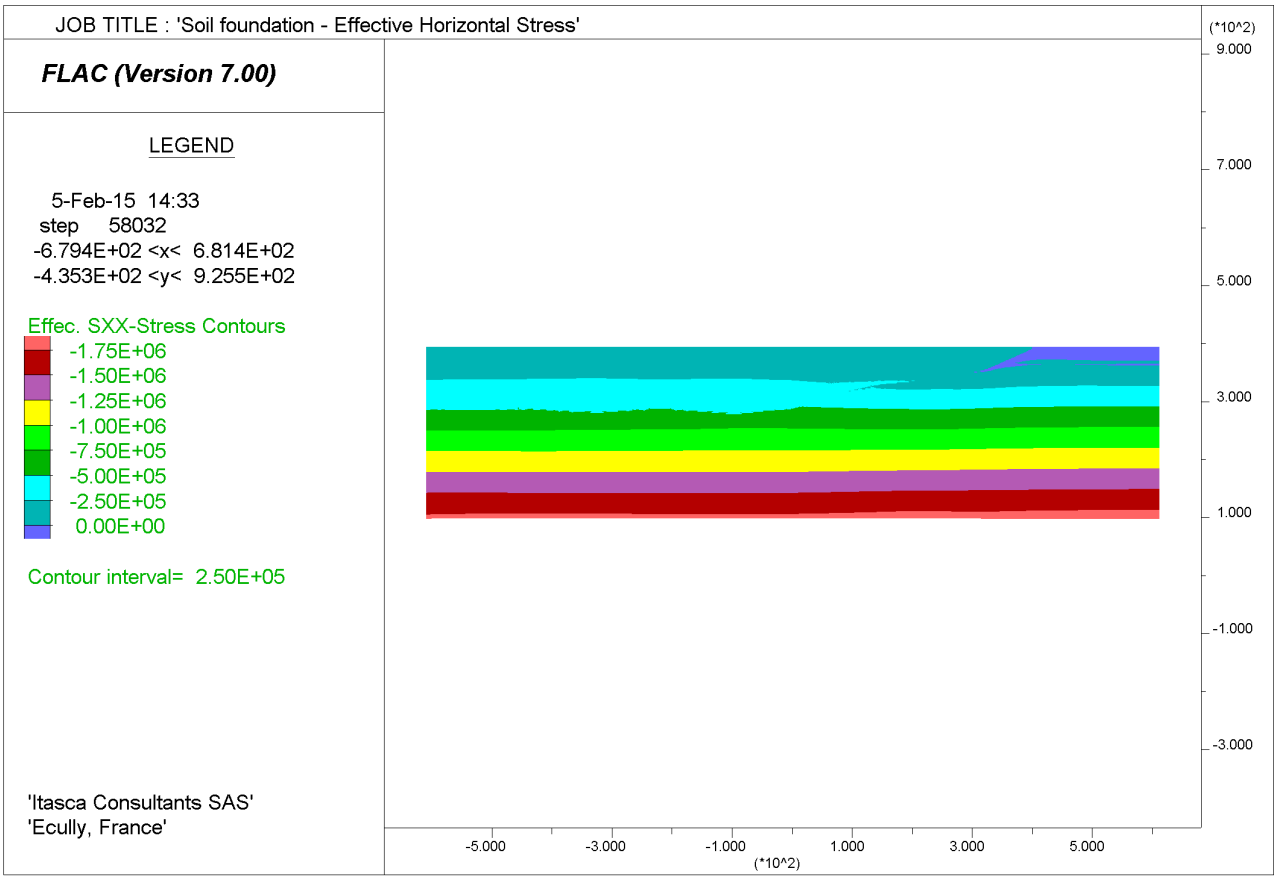

Figure 5-9: effective horizontal stress profile prior to the construction of the embankment

5.5. Simulation of embankment construction

The phases of construction of the embankment are the ones presented in section 4.5, and shown on Figure 4-10 (phase 1, layering of downstream compacted gravel and rockfill, up to elevation 462 meters), Figure 4-11 (phase 2, layering of the dam core and the upstream rockfill, up to elevation 462 meters) and Figure 4-12 (phase 3, layering of the dam crest, up to elevation 469 meters).

5.5.1. Phase 1

The first phase (Phase 1) of embankment construction consists in the layering of downstream compacted gravel (group "3_Comp_Gravel") and rockfill (group "2_Rockfill") up to elevation 462 meters.

Figure 5-10 and Figure 5-11show the horizontal and vertical displacements, respectively, at the end of this phase. The layering of the embankment was subdivided in 12 successive steps. The model is brought to equilibrium after the installation of each layer.

The progressive installation of embankment layers is visible on Figure 5-12, where the horizontal displacements that are represented are measured at points 1 – 8 of Figure 5-13. It is recalled that the concrete wall is not installed yet at this stage.

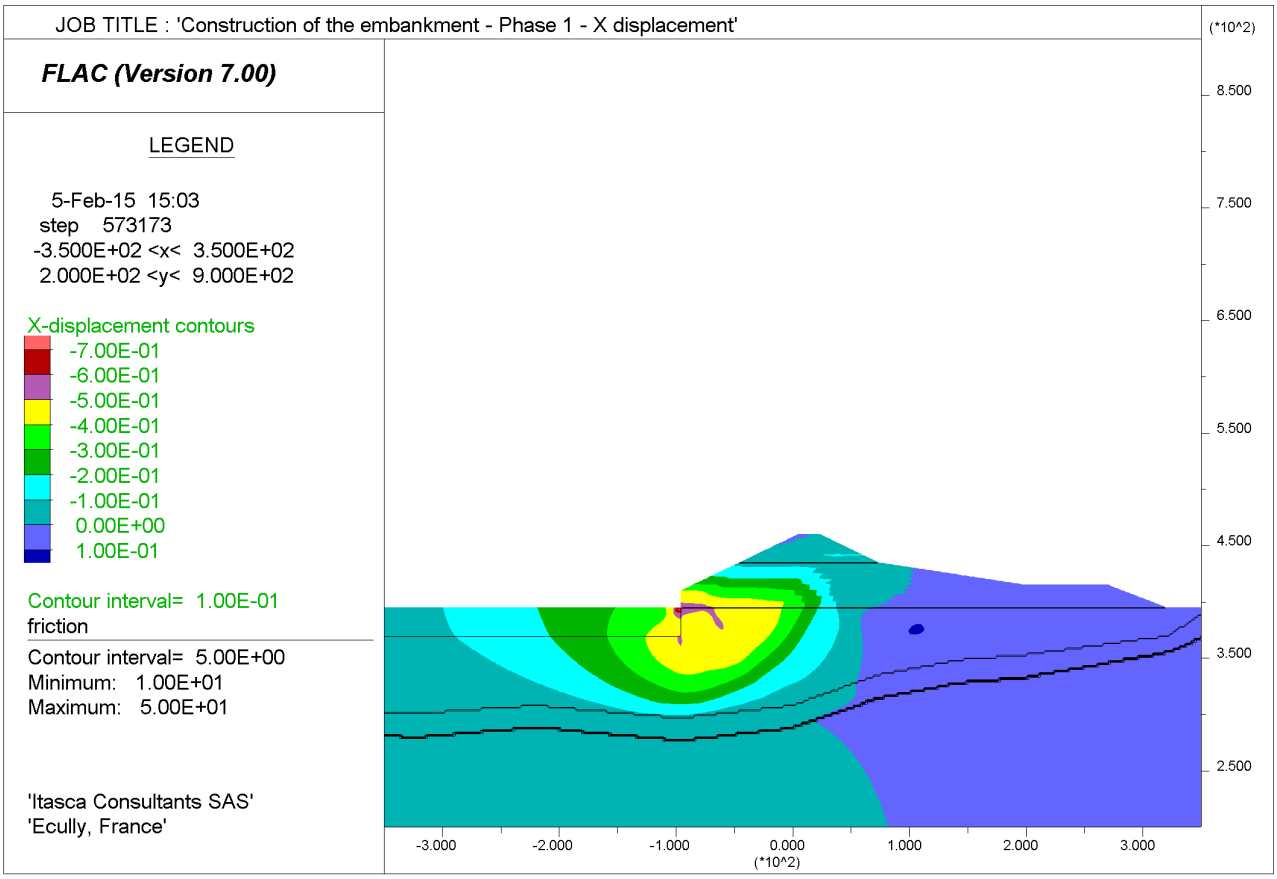

Figure 5-10: Embankment construction – Phase 1 – Horizontal displacements

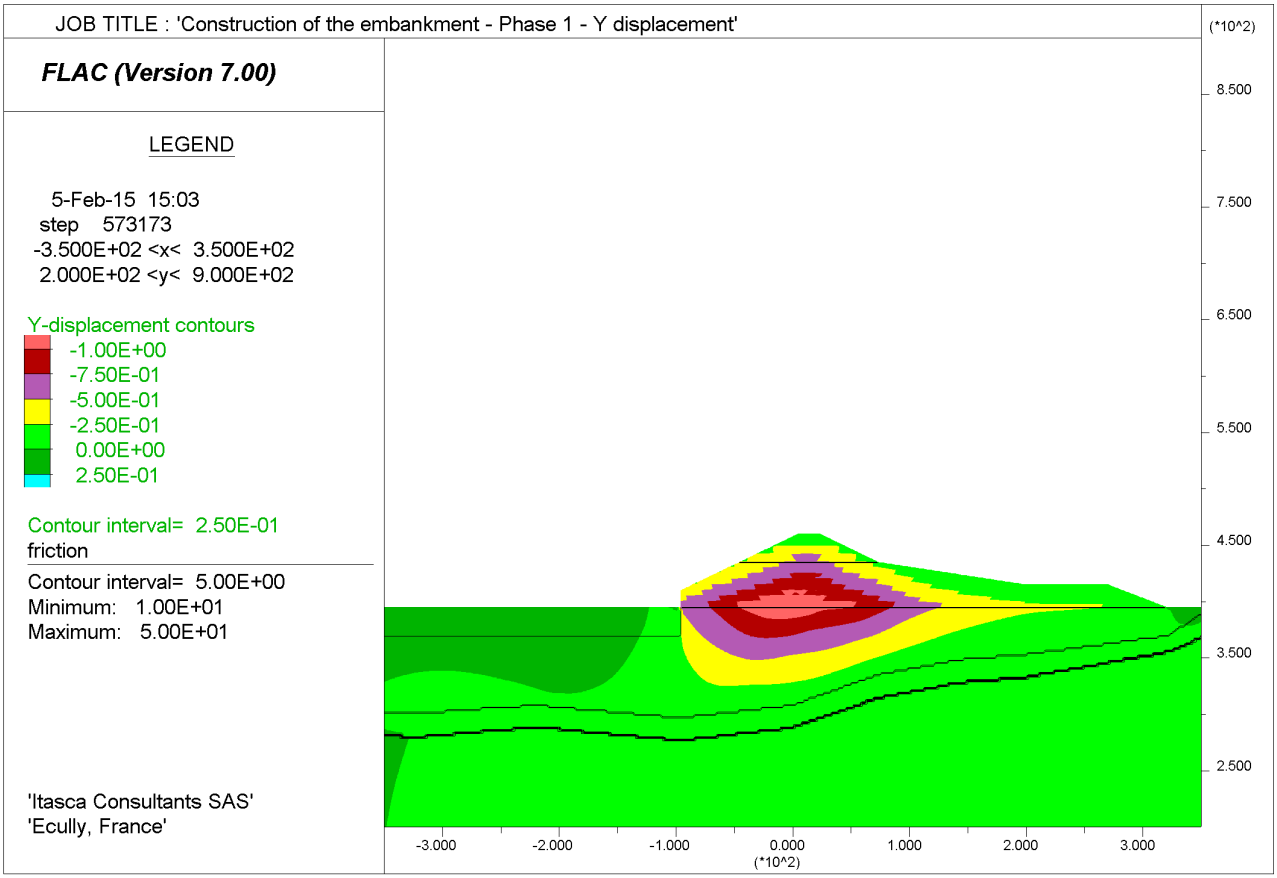

Figure 5-11: Embankment construction – Phase 1 – Vertical displacements

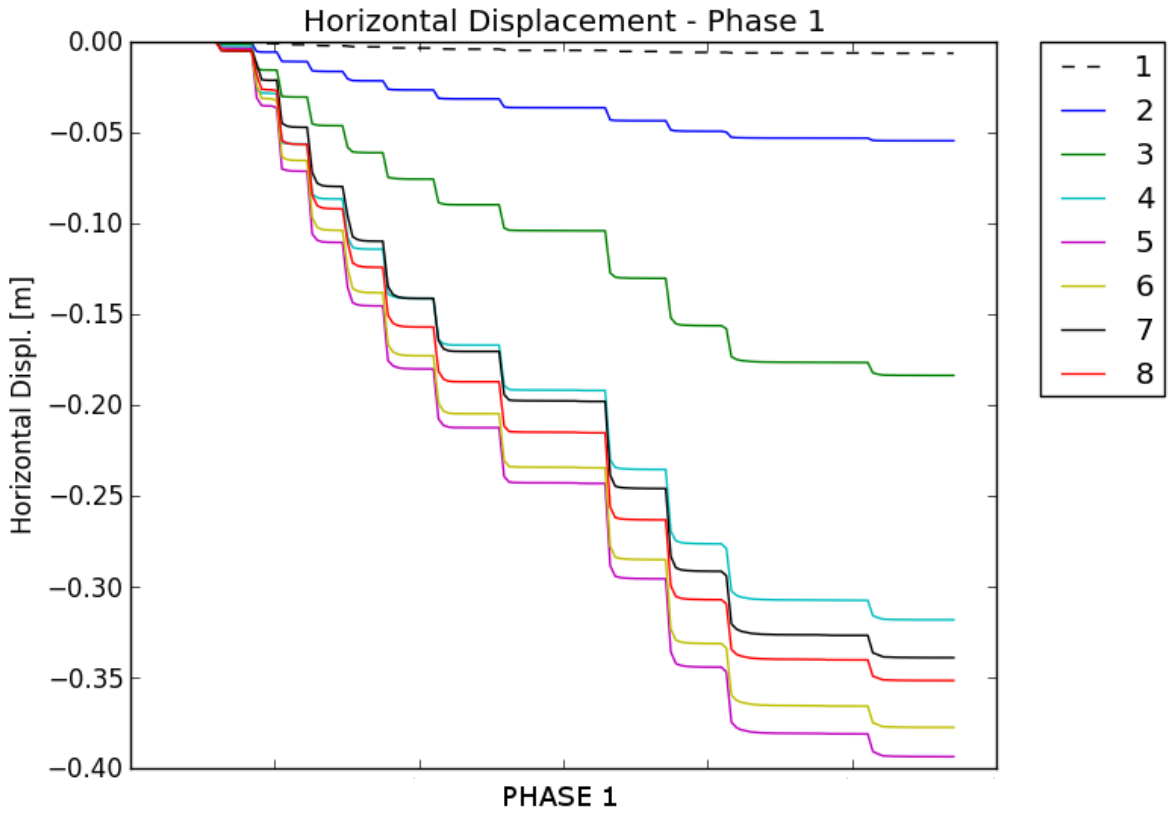

Figure 5-12: Phase 1 - horizontal displacements measured at points 1-8 of Figure 5-13

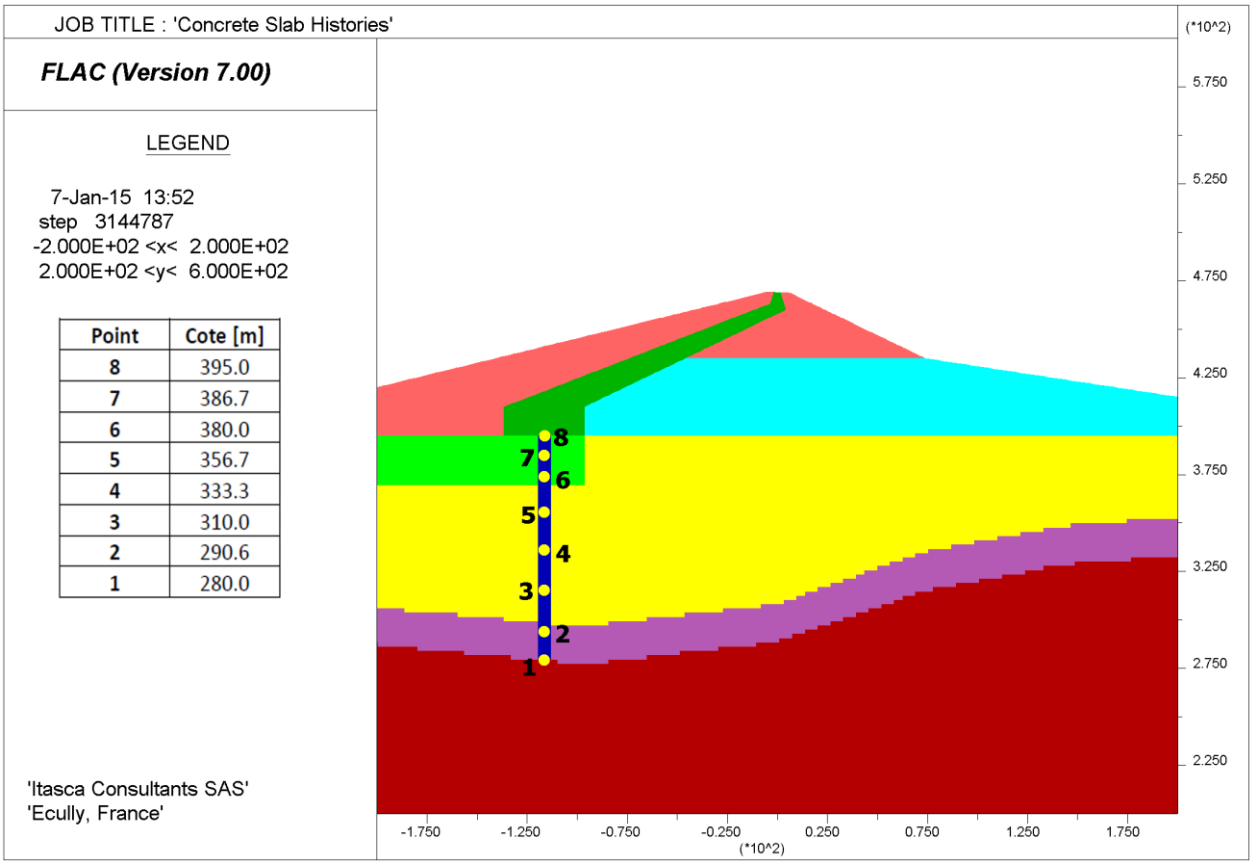

Figure 5-13: virtual points of measurement of displacement (concrete wall is not modeled)

5.5.2. Phase 2

The second phase (Phase 2) of embankment construction consists in the layering (12 steps) of the dam core (group "1_Core") and the upstream rockfill, up to elevation 462 meters. The layering of the embankment was subdivided in 12 successive steps. The model is brought to equilibrium after the installation of each layer.

Figure 5-14 and Figure 5-15 show the horizontal and vertical displacements, respectively, at the end of this phase.

The concrete wall is assumed to be installed before this phase. The induced horizontal displacements are therefore of interest to analyze the eventual occurrence of incompatible differential displacements which could damage it. This is observable in Figure 5-16 : the horizontal displacements, measured at the points of Figure 5-13, denote a differential displacement of 7.5 cm (this was 10cm for the *Reference cross section*) at maximum between the points 1 and 7, i.e. over a length of 107m (62m for the *Reference cross section*).

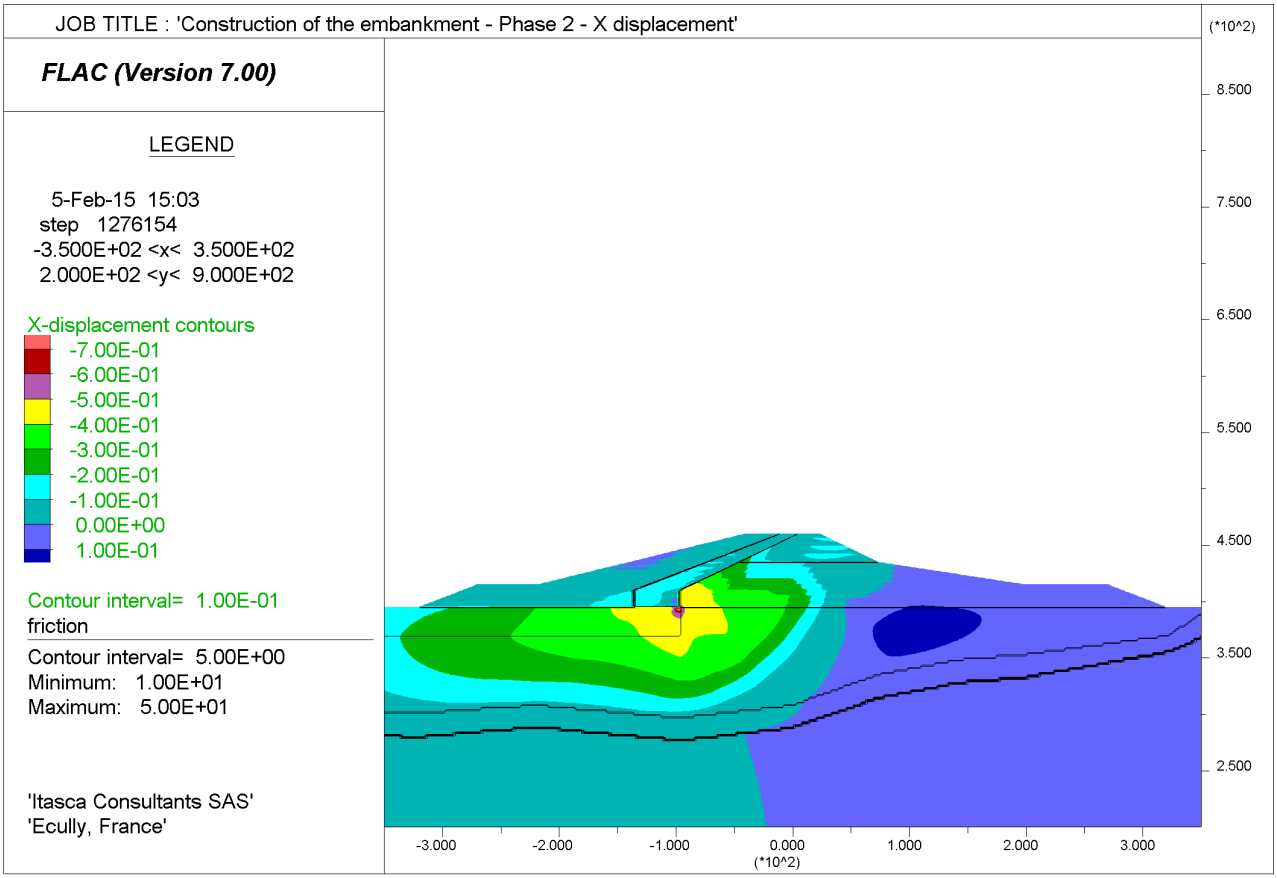

Figure 5-14: Embankment construction – Phase 2 – Horizontal displacements

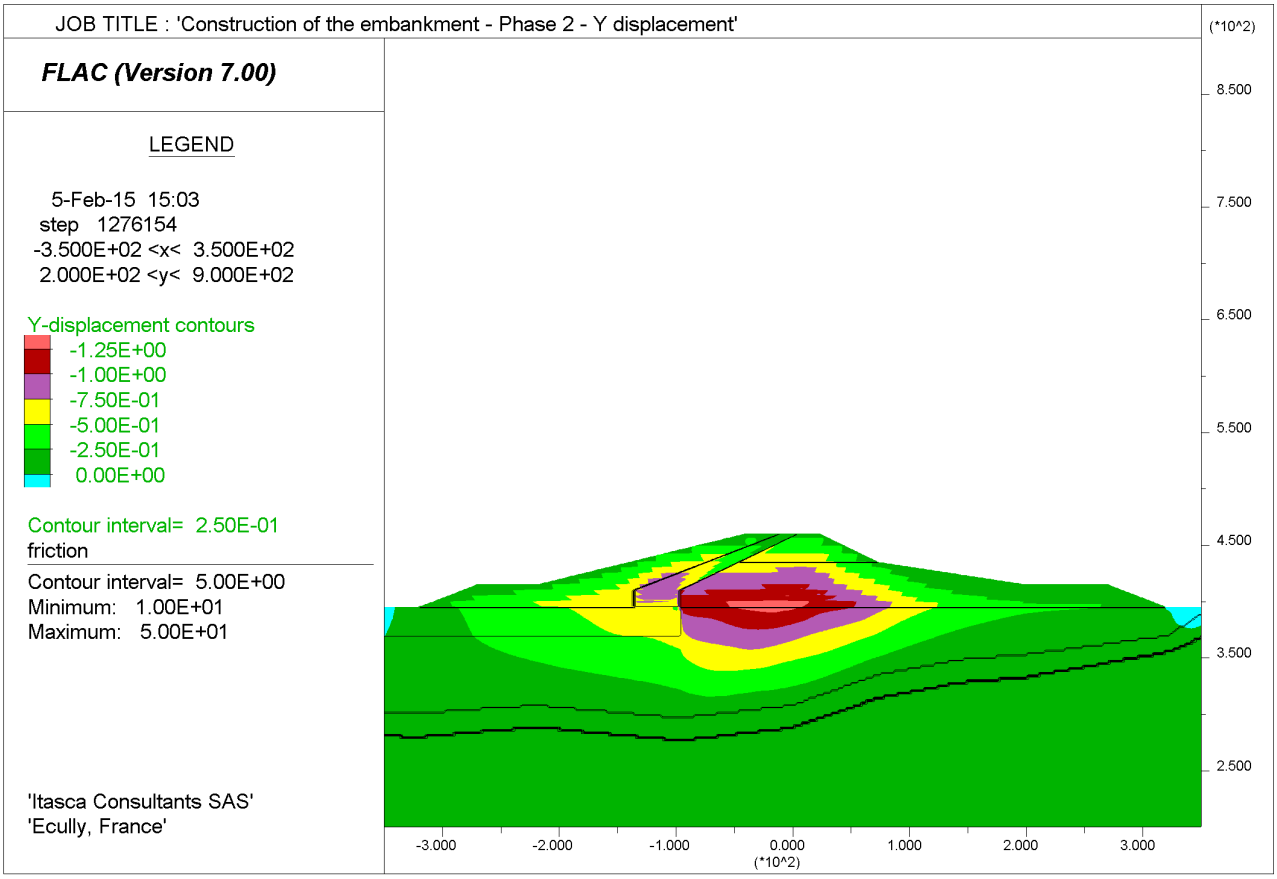

Figure 5-15: Embankment construction – Phase 2 – Vertical displacements

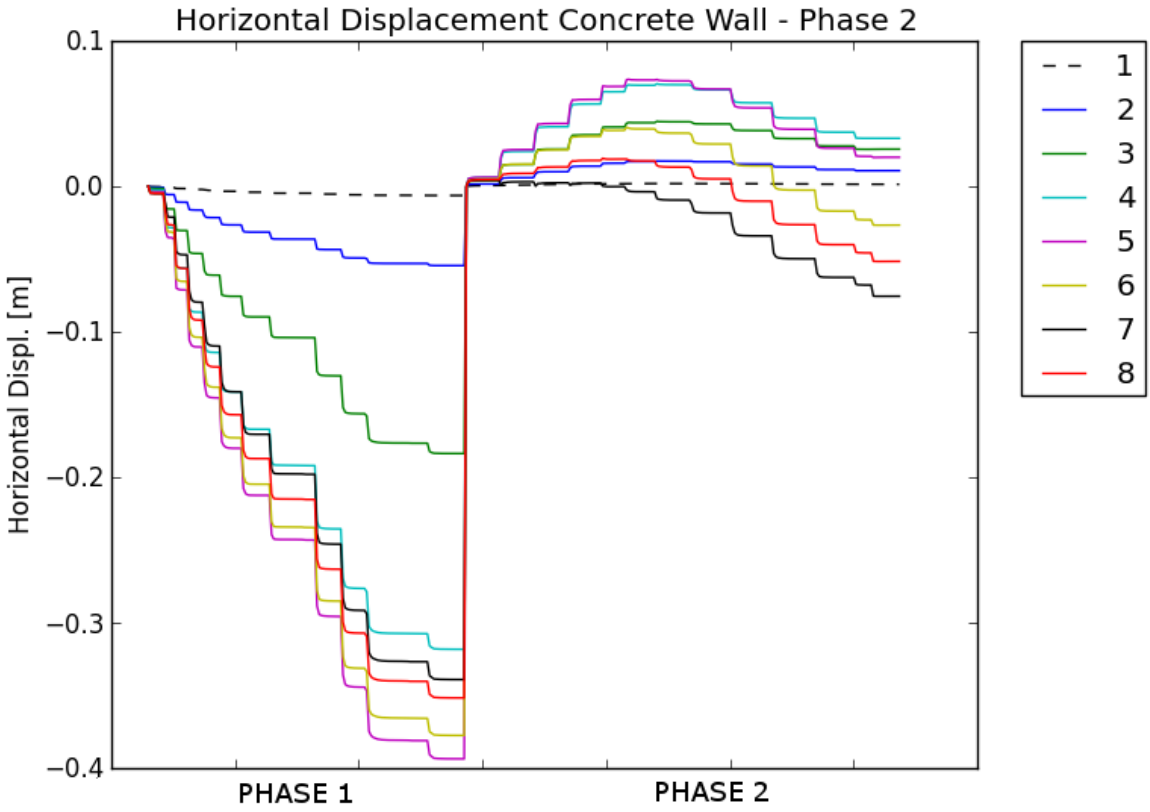

Figure 5-16: Phase 2 - horizontal displacements measured at points 1-8 of Figure 5-13

5.5.3. Phase 3 – End of embankment construction

The third phase (Phase 3) of embankment construction consists in the layering (2 steps) of the dam crest, up to elevation 469 meters.

Figure 5-17 and Figure 5-18 show the horizontal and vertical displacements, respectively, at the end of this phase. The maximum final vertical displacement, at the base of the dam and in correspondence of the central axis, is about 1.25 meters (same as the *Reference cross section* case).

The induced horizontal displacements in correspondence of the concrete wall, after the installation of the dam crest, do not evolve significantly, as shown on Figure 5-19.

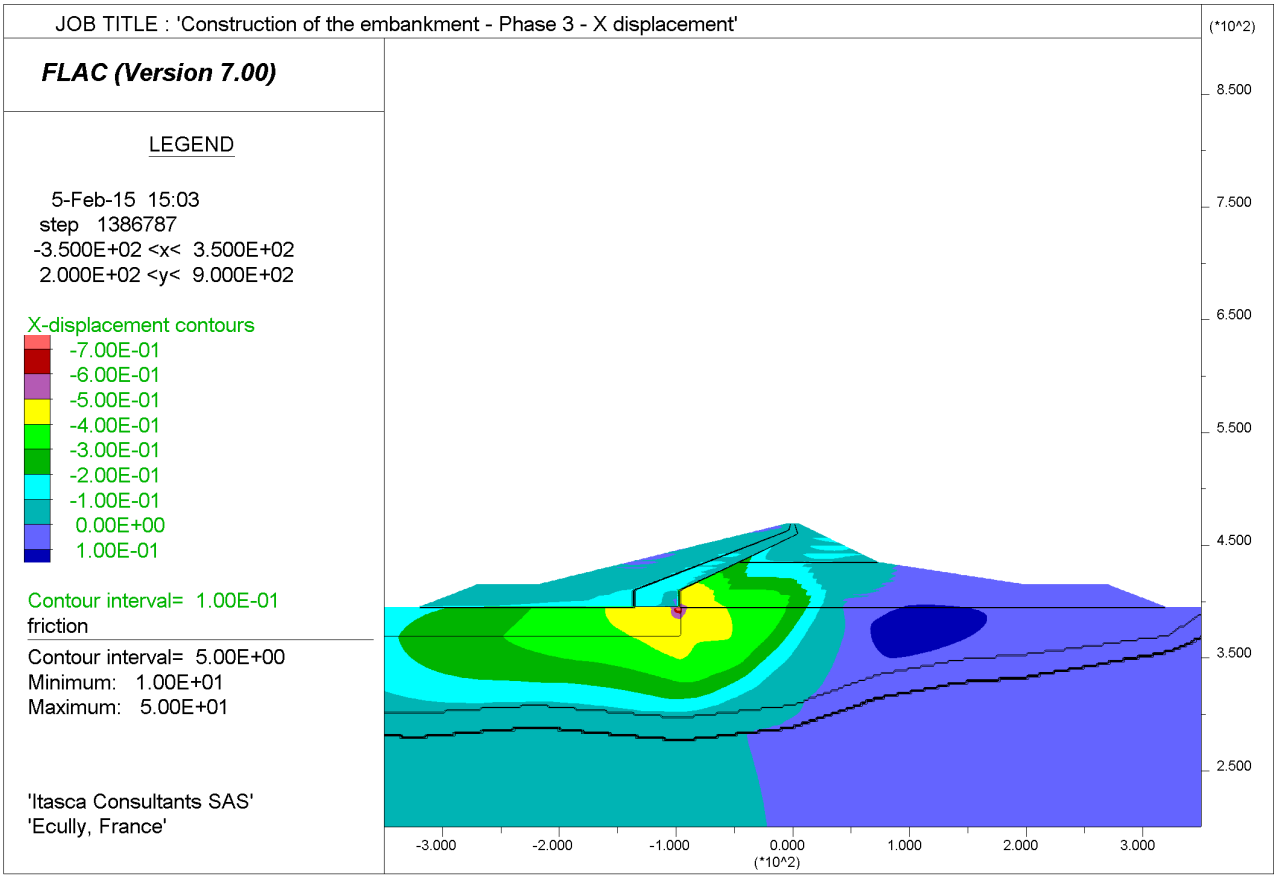

Figure 5-17: Embankment construction – Phase 3 – Horizontal displacements

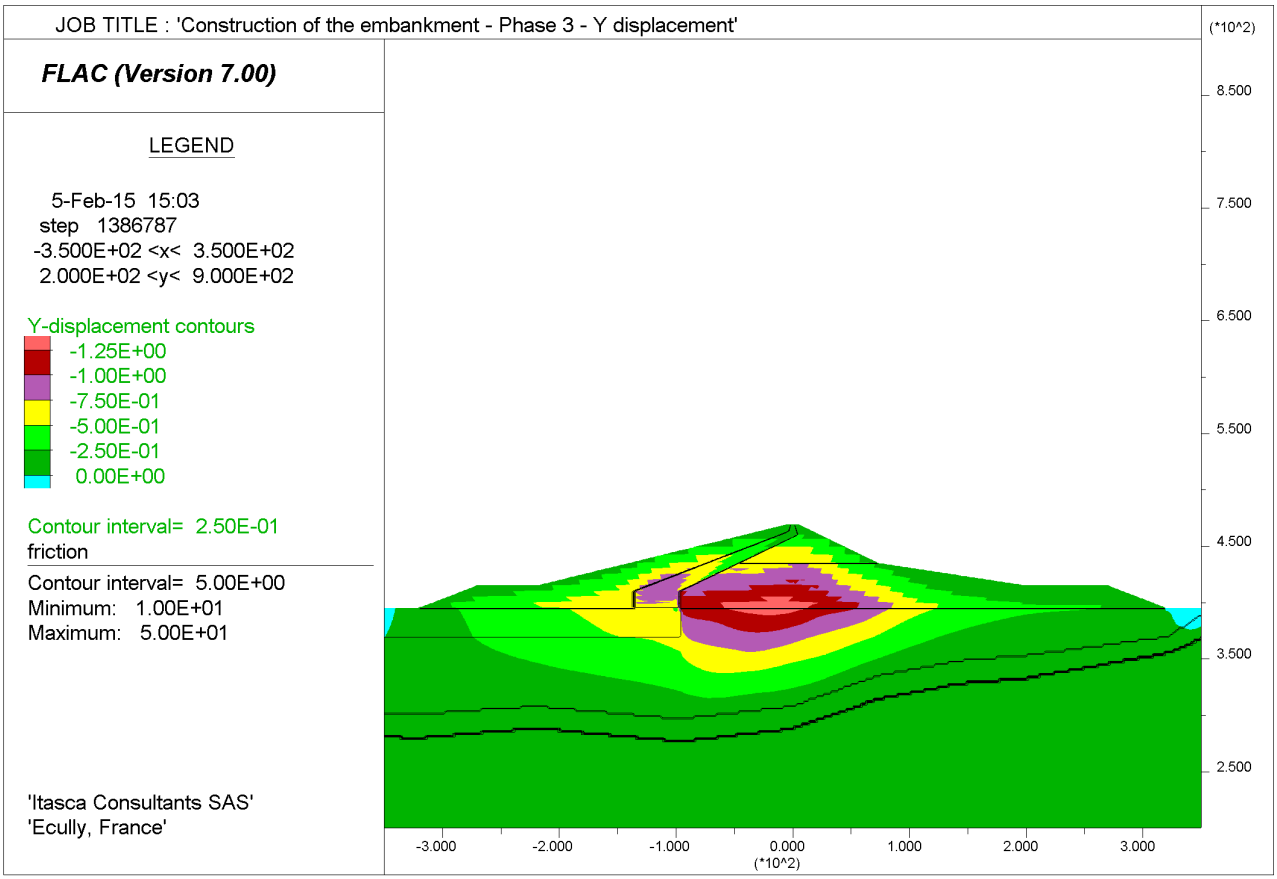

Figure 5-18: Embankment construction – Phase 3 – Vertical displacements

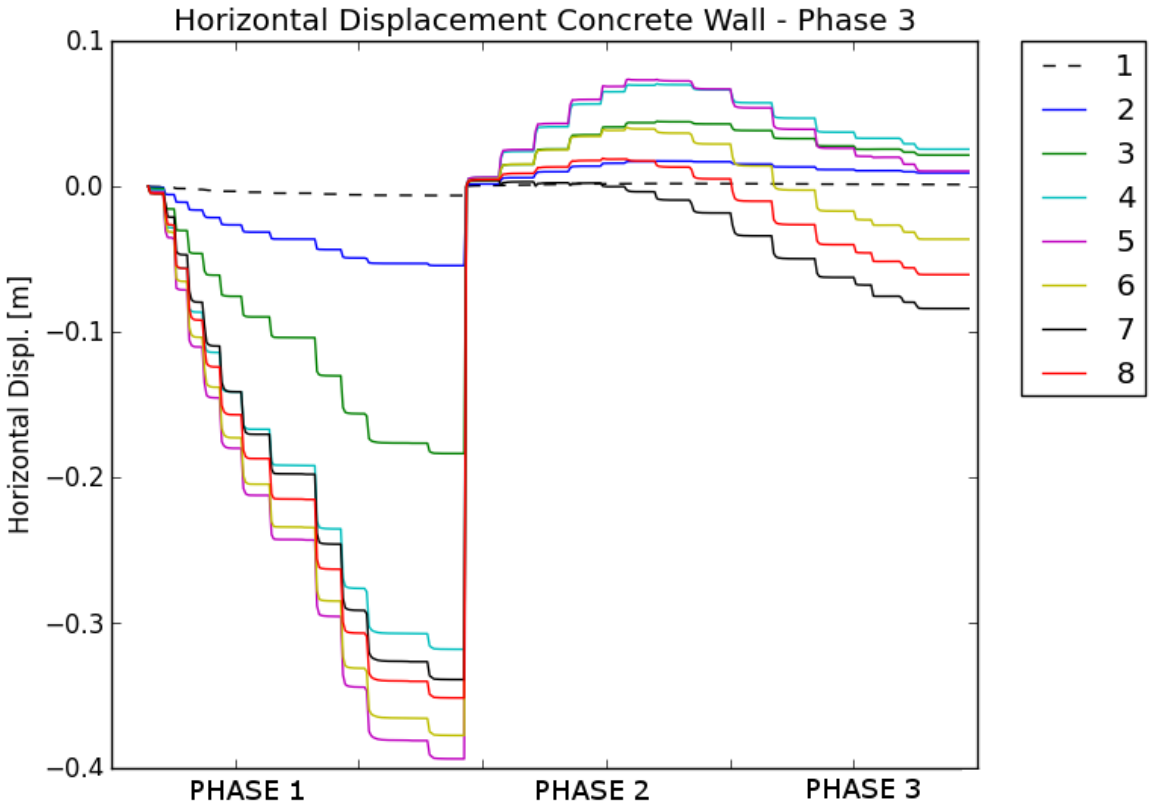

Figure 5-19: Phase 3 - horizontal displacements measured at points 1-8 of Figure 5-13

5.5.4. Reservoir filling

After the construction of the embankment, the water level is raised upstream, up to elevation 462 meters, which is supposed to be the maximum level reached by the reservoir. The rising is gradual and performed in 8 steps.

Figure 5-20 shows the final pore pressure profile at the end of this phase. The pore pressure profile will be maintained at this state all along the dynamic simulation (as mentioned in section 3.2.2, no pore pressure generation is allowed during the dynamic simulation).

Figure 5-21 shows a detail of the pore pressure profile in the embankment: the water is assumed to be perfectly drained by the rockfill and the compacted gravel. Therefore, the phreatic surface follows the interface between the dam core and the rockfill/compacted gravel, and continues along the base of the dam at the downstream.

Figure 5-22 and Figure 5-23 show the final profiles for horizontal and vertical displacements. Figure 5-24 and Figure 5-25 show the final profiles of the effective vertical and horizontal stresses, respectively.

Figure 5-26 shows the evolution of horizontal displacements at points 1 – 8 of Figure 5-13. The 8 steps of the rising water level can easily be recognized. The final relative horizontal displacement is about 0.25 meters (0.35 meters for the *Reference cross section*), between points 1 and 6, i.e. over a length of 105 meters (unvaried from the *Reference cross section* case).

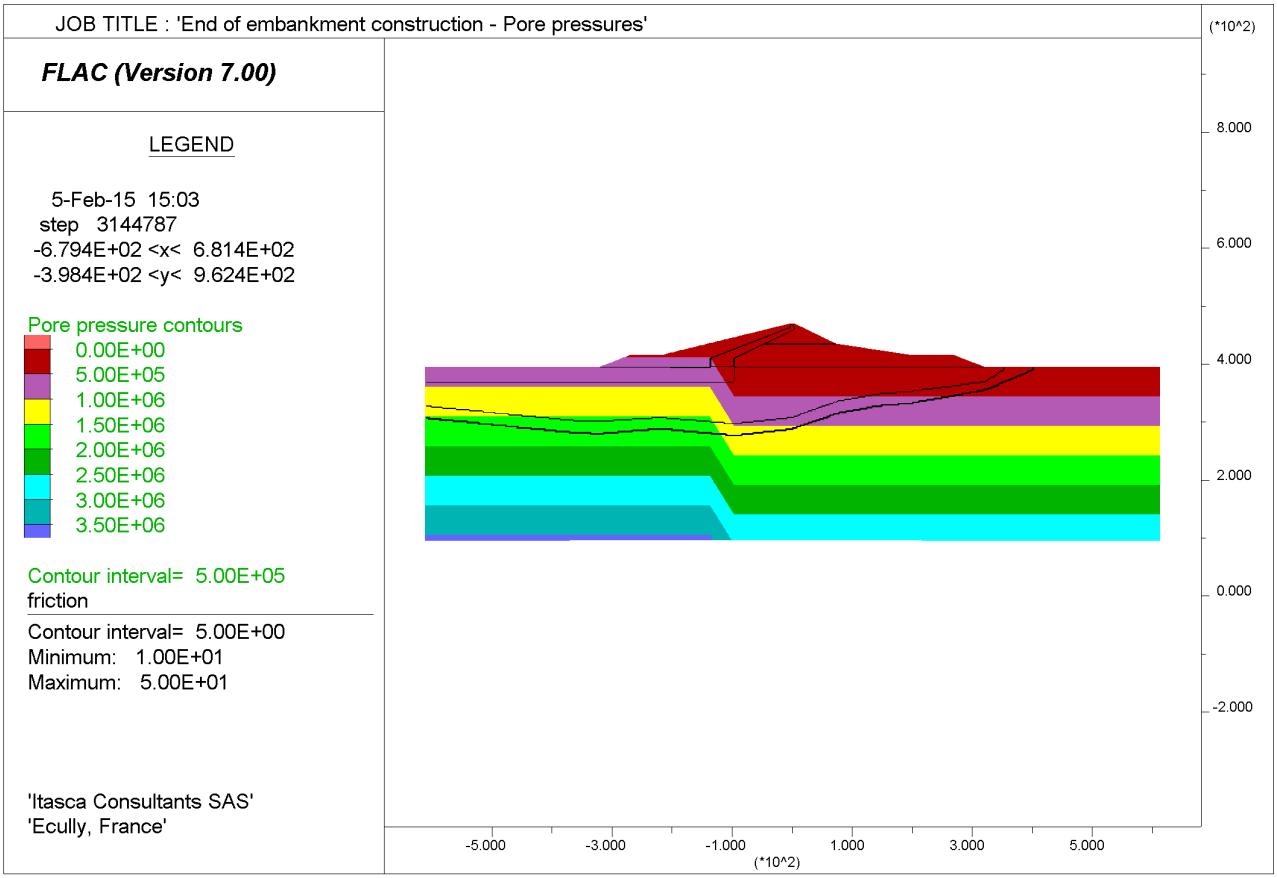

Figure 5-20: upstream water filling – final pore pressure profile

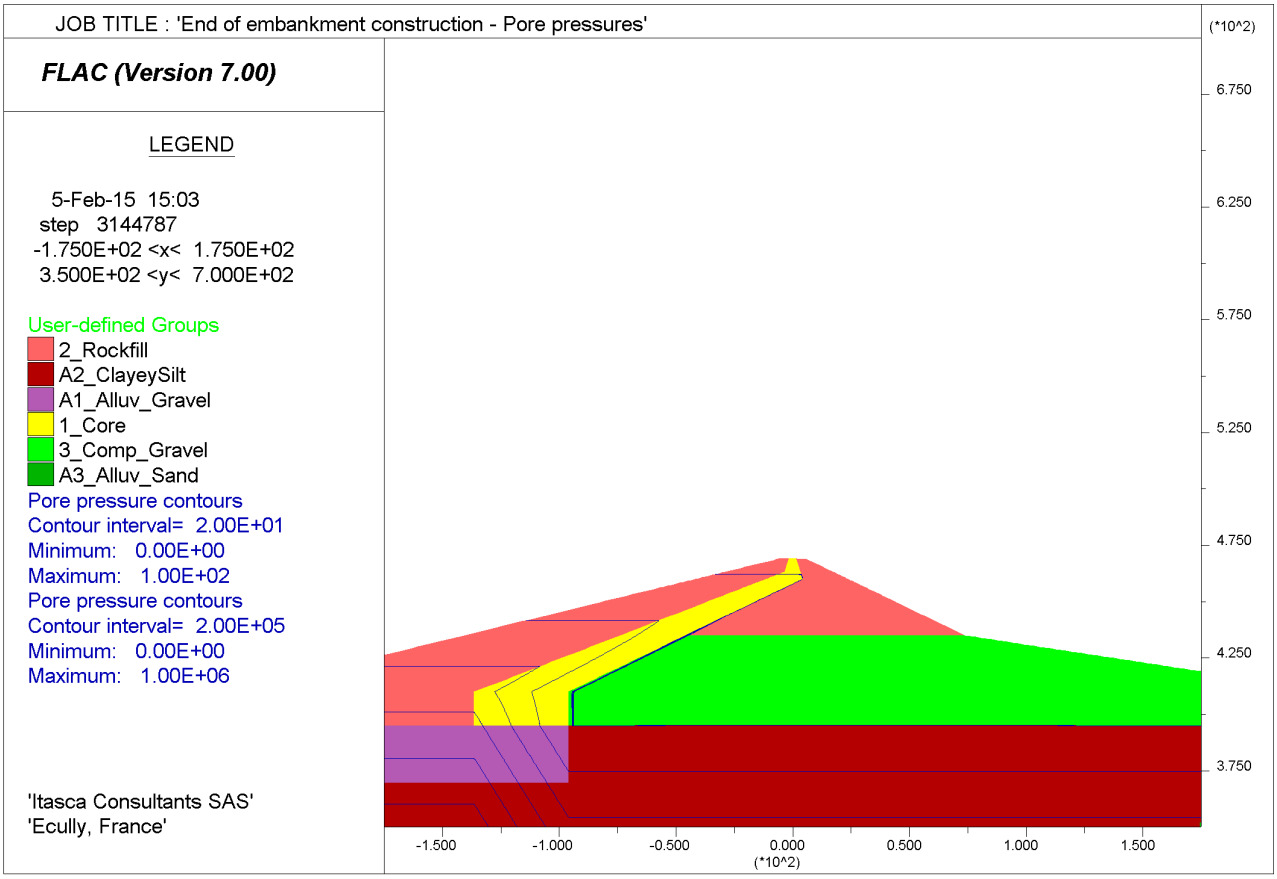

Figure 5-21: upstream water filling – detail of pore pressure profile on dam core

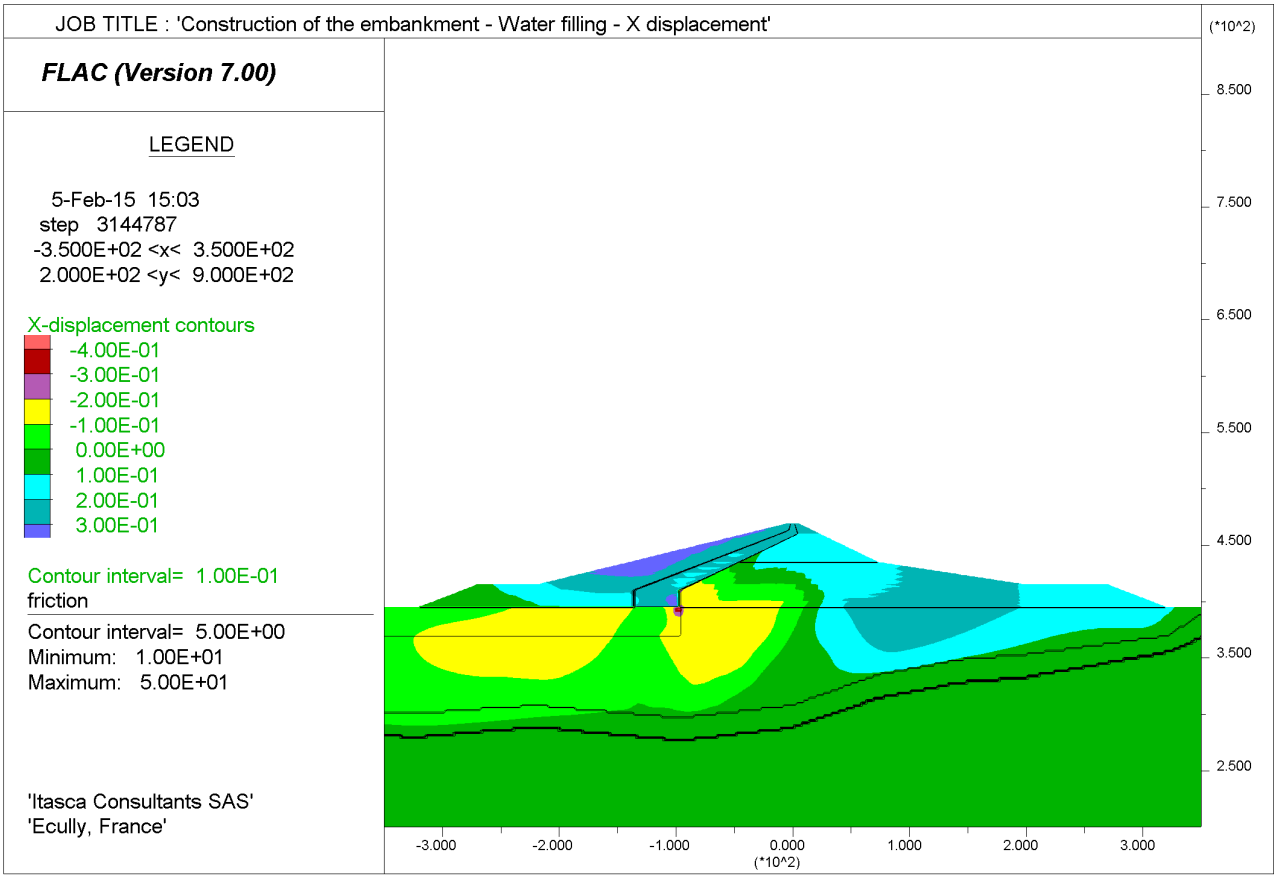

Figure 5-22: embankment construction and upstream water filling – final horizontal displacements

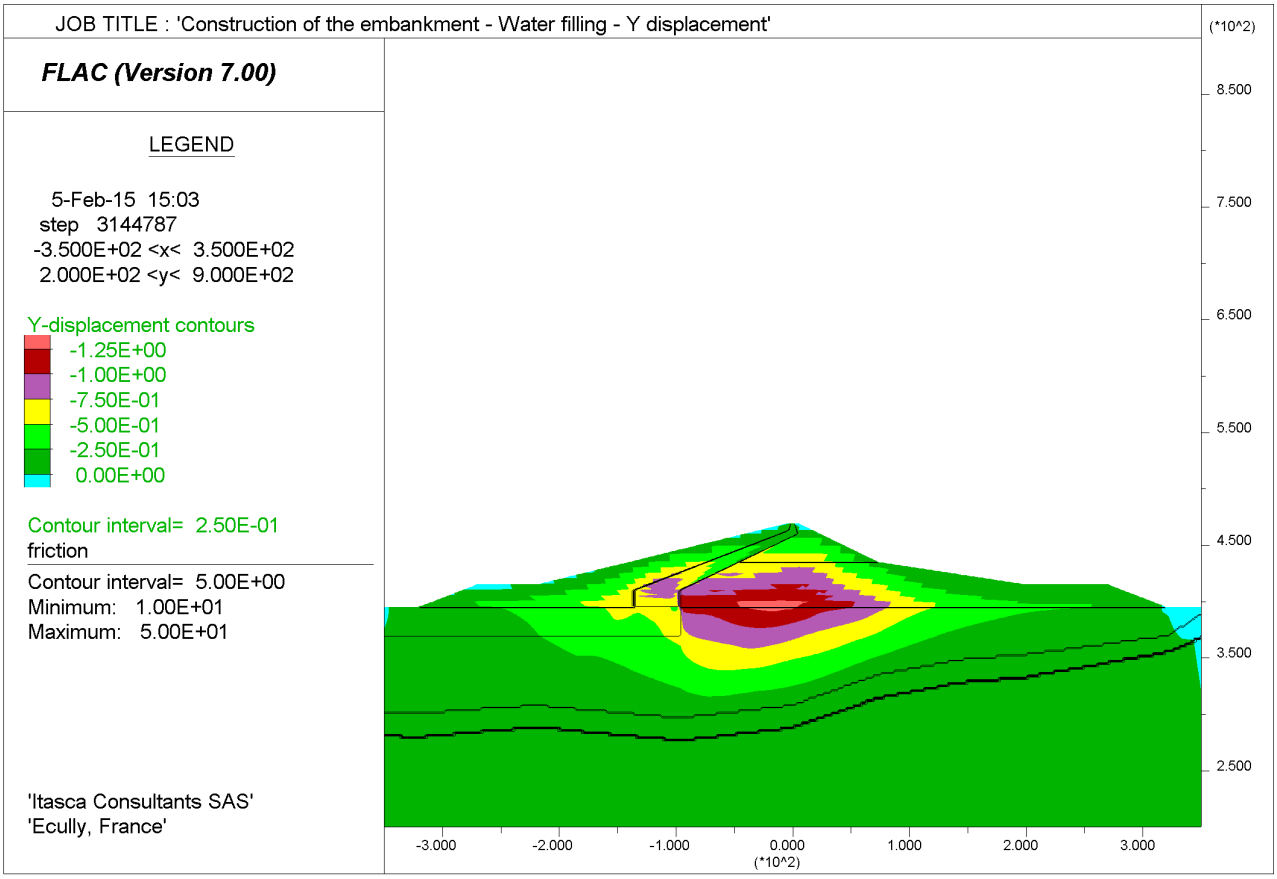

Figure 5-23: embankment construction and upstream water filling – final vertical displacements

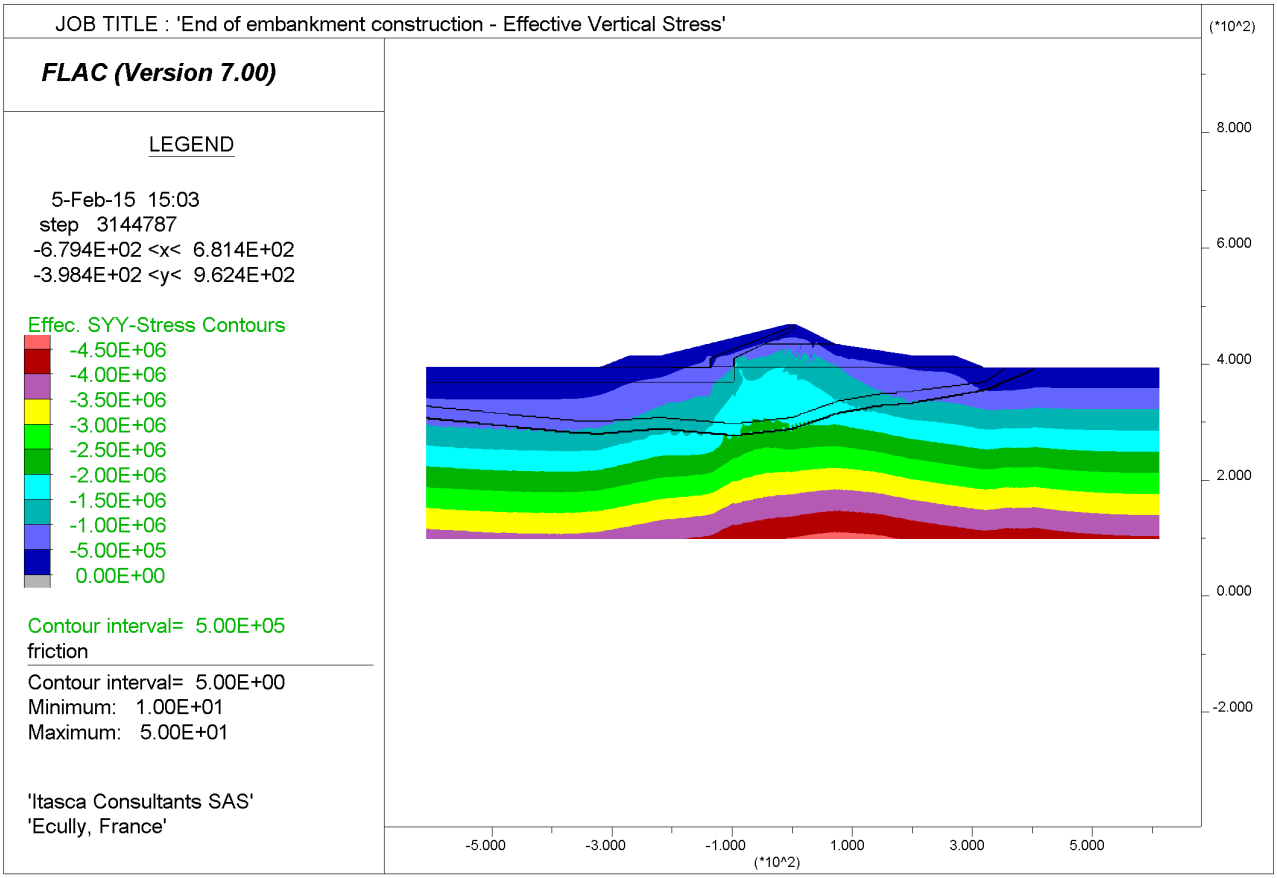

Figure 5-24: embankment construction and upstream water filling – final effective vertical stress

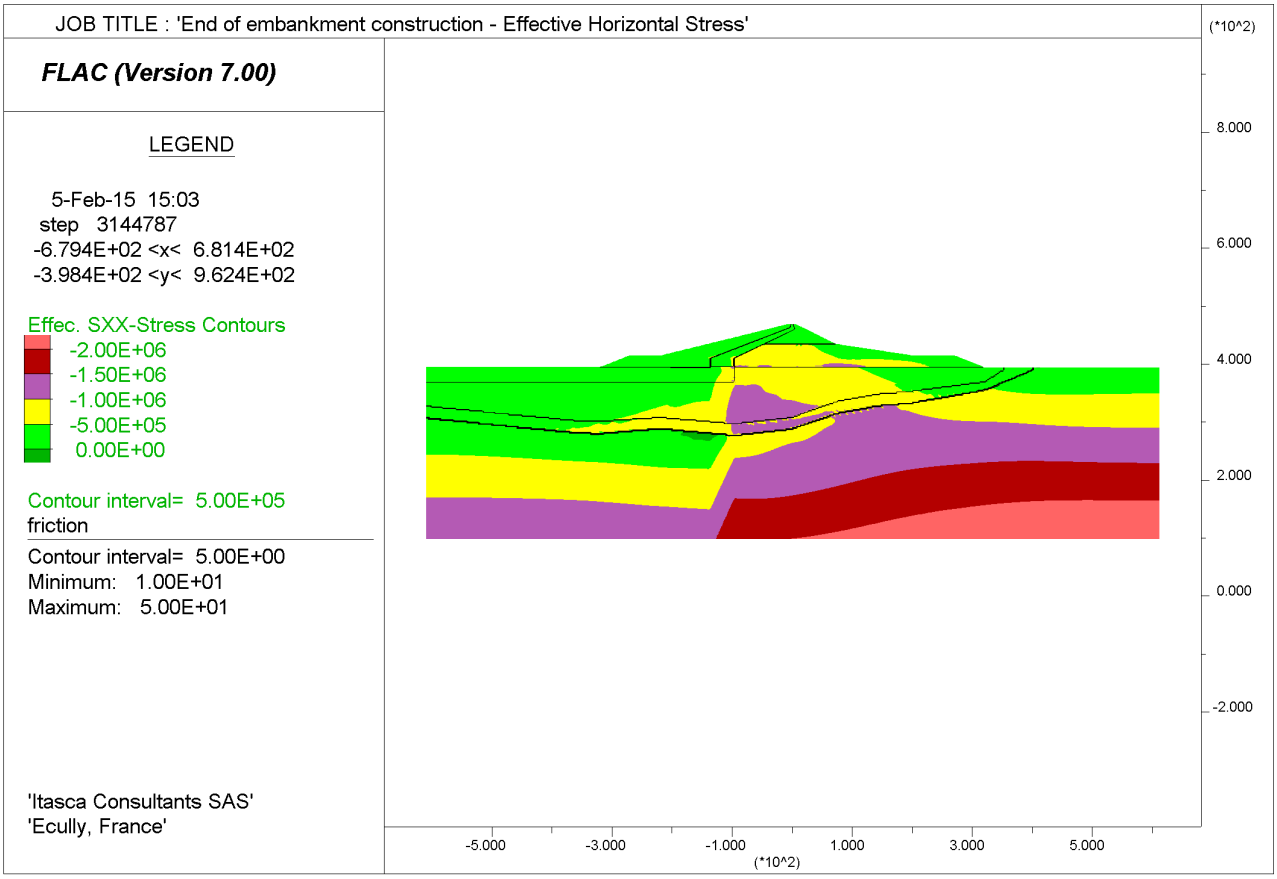

Figure 5-25: embankment construction and upstream water filling – final effective vertical stress

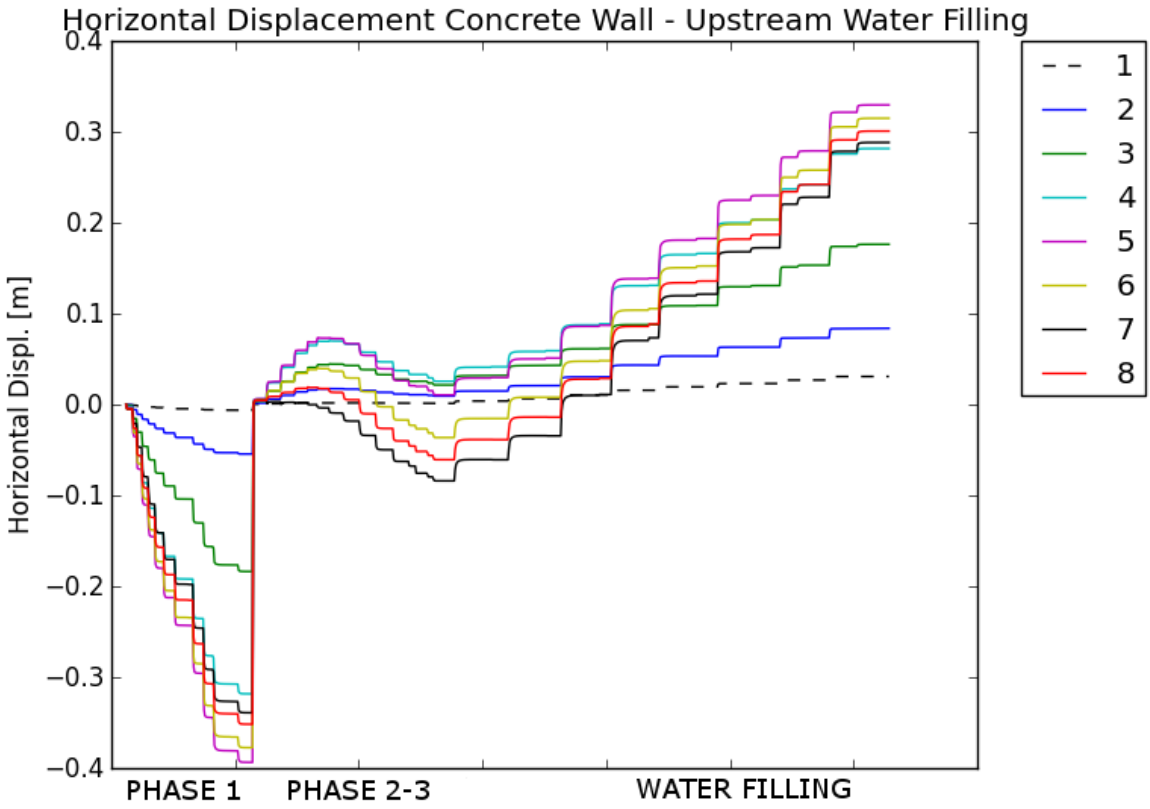

Figure 5-26: embankment construction and upstream water filling – final horizontal displacements measured at points 1 – 8 of Figure 5-13

5.5.5. Conclusions

The construction of the embankment was simulated for a new profile of the dam and the soil foundation, by reproducing the three forecasted phases of construction. The layering of the downstream compacted gravel and rockfill in a first stage (up to elevation 462.0 meters) is of great interest, since it allows the occurrence of a large part of horizontal displacements, prior to the installation of the concrete wall. The successive layering of the dam core, the upstream rockfill and the dam crest, do not constitute a problem for the concrete wall stability.

The final maximum vertical displacement is about 1.25 meters, at center of the embankment base. The same vertical displacement was found for the *Reference cross section* case.

After the completion of the embankment construction, the upstream water level is raised in 8 steps, up to elevation 462 meters. The relative displacement measured at the points (Figure 4-16) where the concrete wall will be installed, reaches a maximum of 25 centimeters over a length of more than 100 meters (points 1 – 6). This is 10 cm less than the *Reference cross section* case.

The stability of the concrete wall is ensured in these conditions.

5.6. Dynamic simulation

The program of dynamic simulations for the *Real cross section* is:

- Pseudo-static Newmark's Sliding Block Analysis, considering the Safety Evaluation Earthquakes, presented in section 5.6.1;
- Nonlinear dynamic analysis, considering the Safety Evaluation Earthquakes, section 5.6.2.

As described in section 3.1.2, the values of the maximum dynamic shear modulus and dynamic bulk modulus are computed by applying a factor to the static values, as obtained at the end of the quasi-static embankment construction and reservoir filling. This factor was estimated to be equal to 3, according to the procedure described in section 3.1.2.

Values of the dynamic maximum shear modulus and dynamic bulk modulus are presented in Appendix 4, section 10.1.

5.6.1. SEE earthquake – Pseudo-static Newmark's Sliding Block analysis

In this section the pseudo-static Newmark's Sliding Block analysis of the Bisri dam is presented, for the *Real Cross Section*, considering the SEE earthquake Kocaeli IZT (V-H1, PGA V + 0.51 / - 0.43 H1 + 0.82 / - 0.63), and following the procedure described in section 4.6.3.

The vertical component of the seismic acceleration, that would lighten the soil, is neglected at this stage. This is a not conservative choice. A complete analysis, including both components of acceleration, will be performed in case a more conservative analysis will be needed.

5.6.1.1. Downstream analysis

Coefficient Kh [*g* units] is varied (increased gradually) to determine the minimum seismic coefficient that causes failure of the dam-foundation structure (see Figure 5-27). A coefficient Kh=0.19 was found. Figure 5-28 and Figure 5-29 show the maximum shear increment and the plastified zones, as they were obtained for Kh=0.19.

The failure involves both the dam and the foundation layers, but it involves the foundation at lower depths, compared to the *Reference Cross Section*, due to the different soil foundation profile and to the presence of the bedrock close to the base of the embankment. Considering a yield acceleration equal to Kh*g, a relative acceleration can be computed (Figure 5-31).

The relative velocity (Figure 5-32) is then calculated by integrating the relative acceleration with respect to time, not taking into account negative values.

The relative displacement is finally obtained by integration of the relative velocity (Figure 5-33). A relative displacement of more than 7 meters is computed (over 9 meters for the *Reference Cross Section* case).

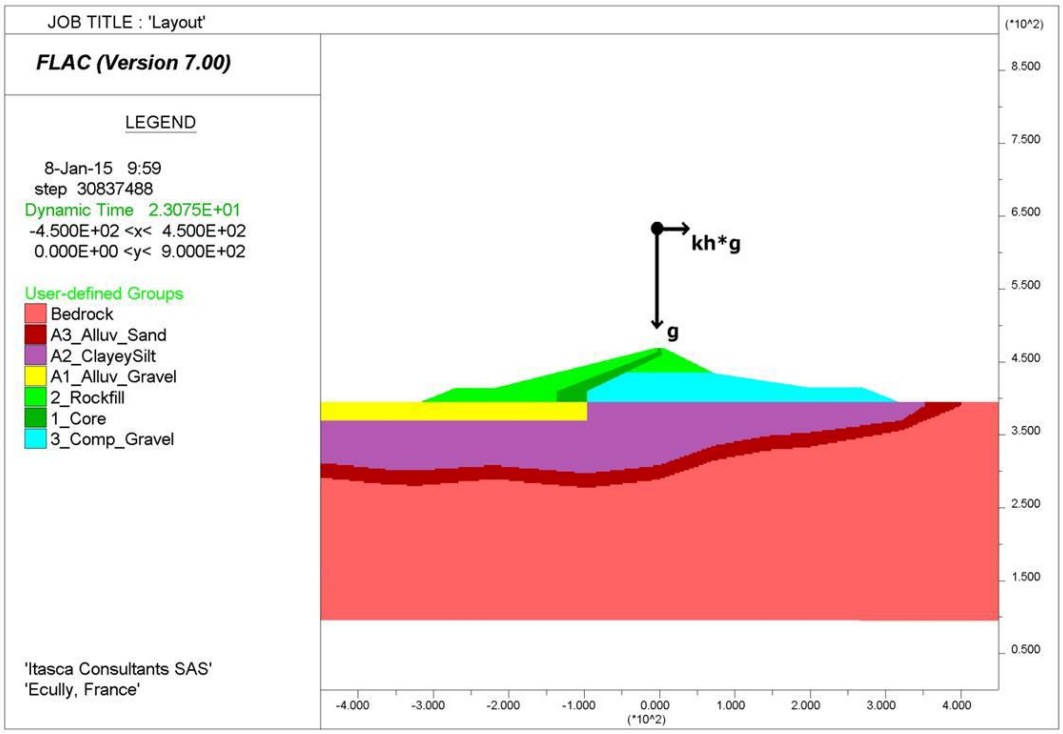

Figure 5-27 : Pseudo-static analysis - Downstream

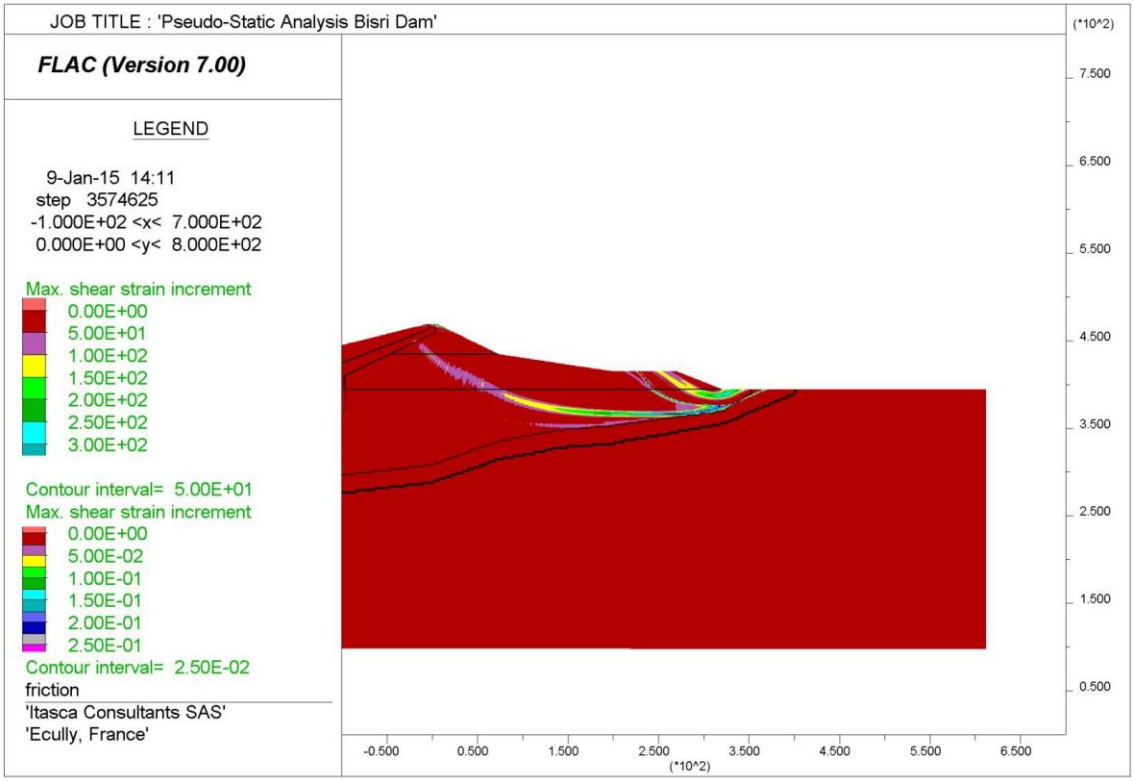

Figure 5-28 : Maximum shear strain increment – Downstream analysis (Kh = 0.17)

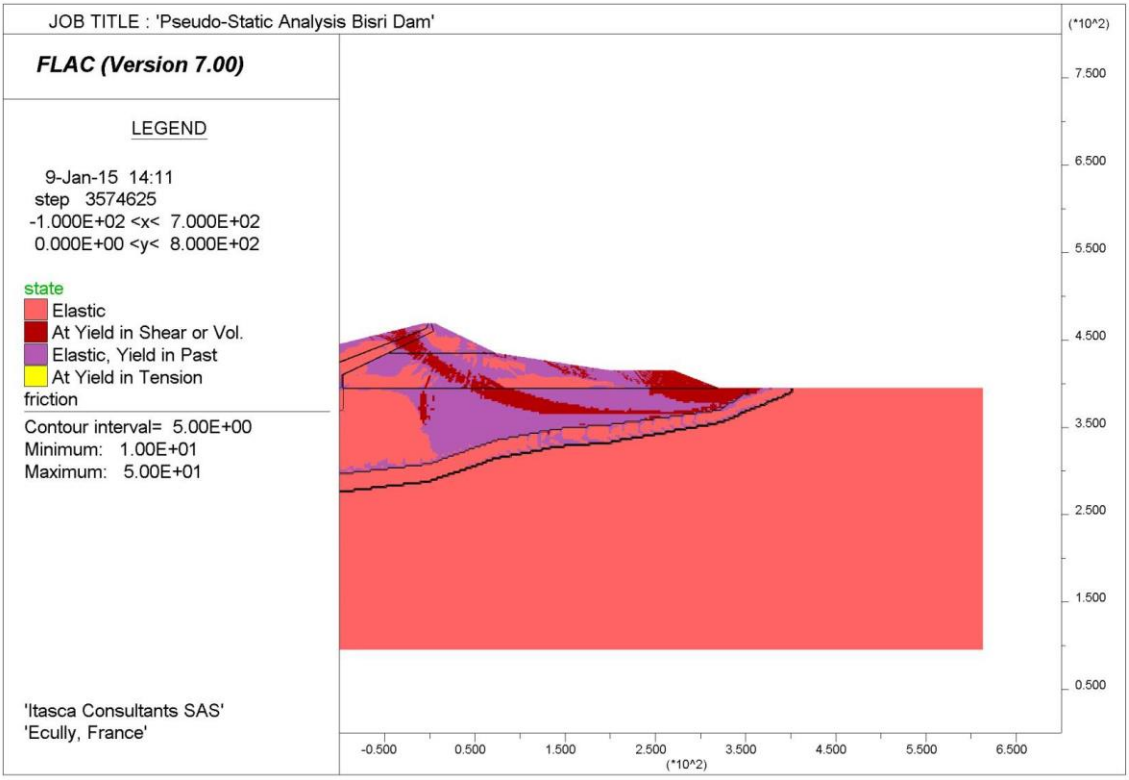

Figure 5-29 : Plasticized zones – Downstream analysis (Kh = 0.17)

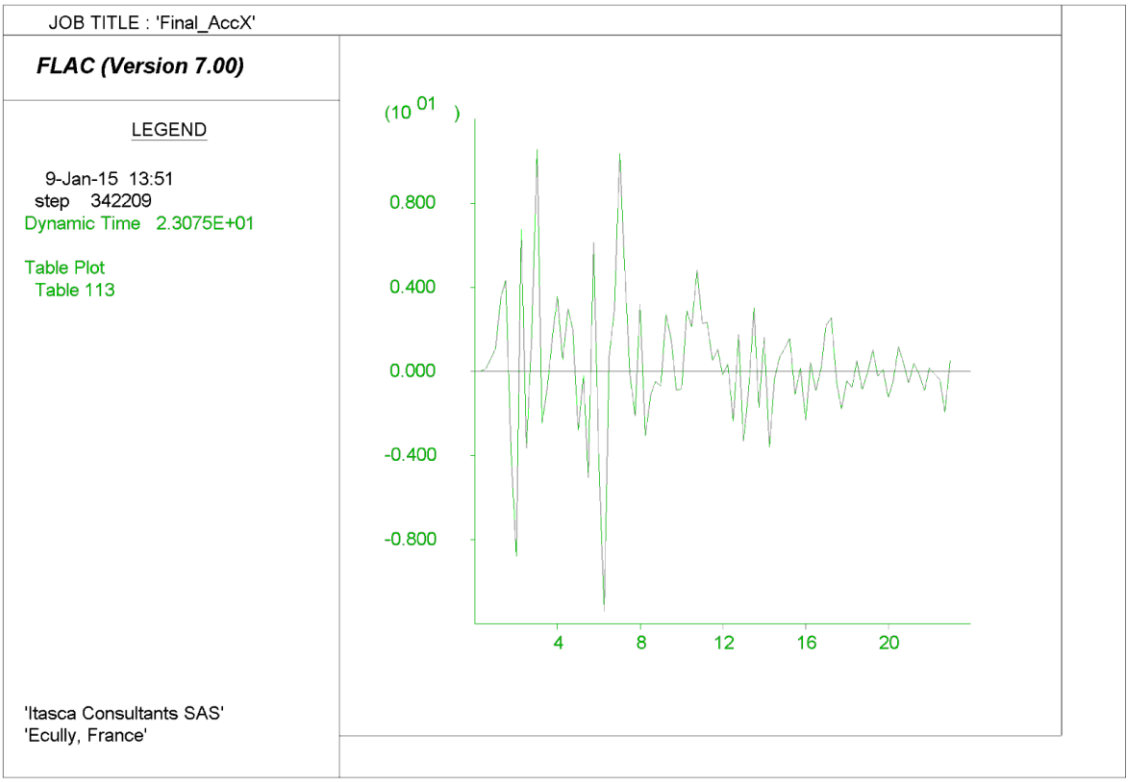

Figure 5-30 : Downstream analysis - Input horizontal acceleration a(t) (KOCAELI IZT V-H1)

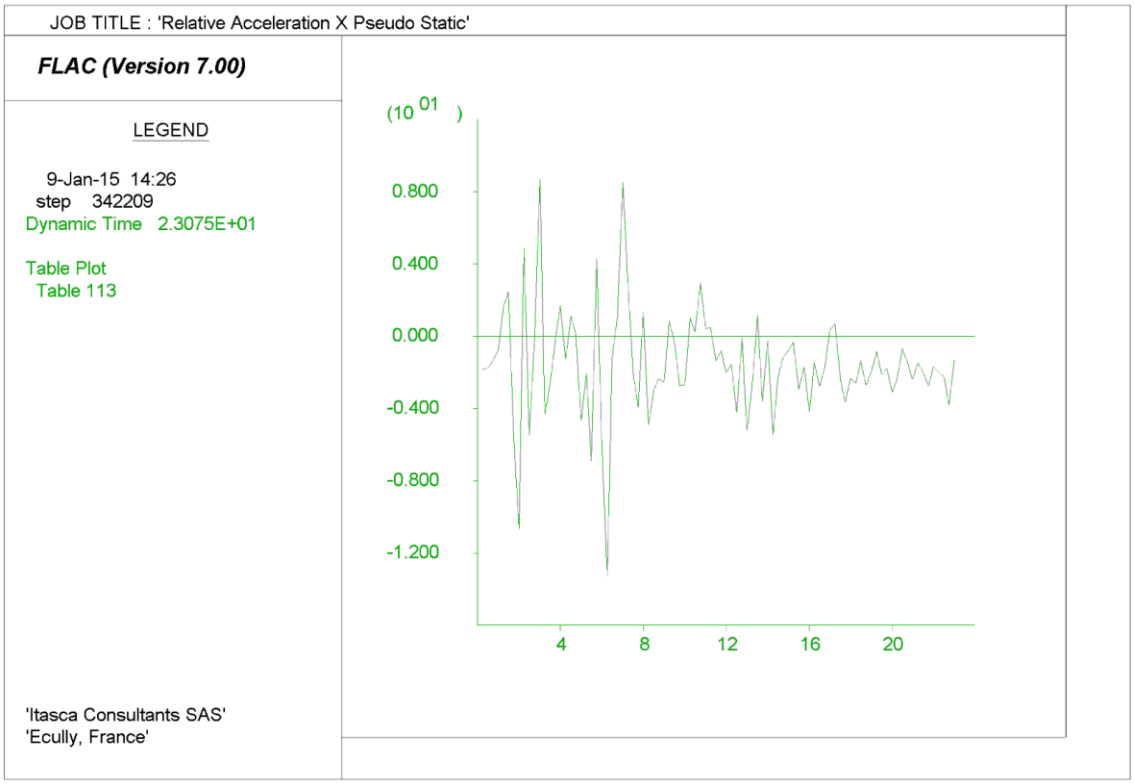

*Figure 5-31 : Downstream analysis - Relative horizontal acceleration ar(t) = a(t) – Kh*g*

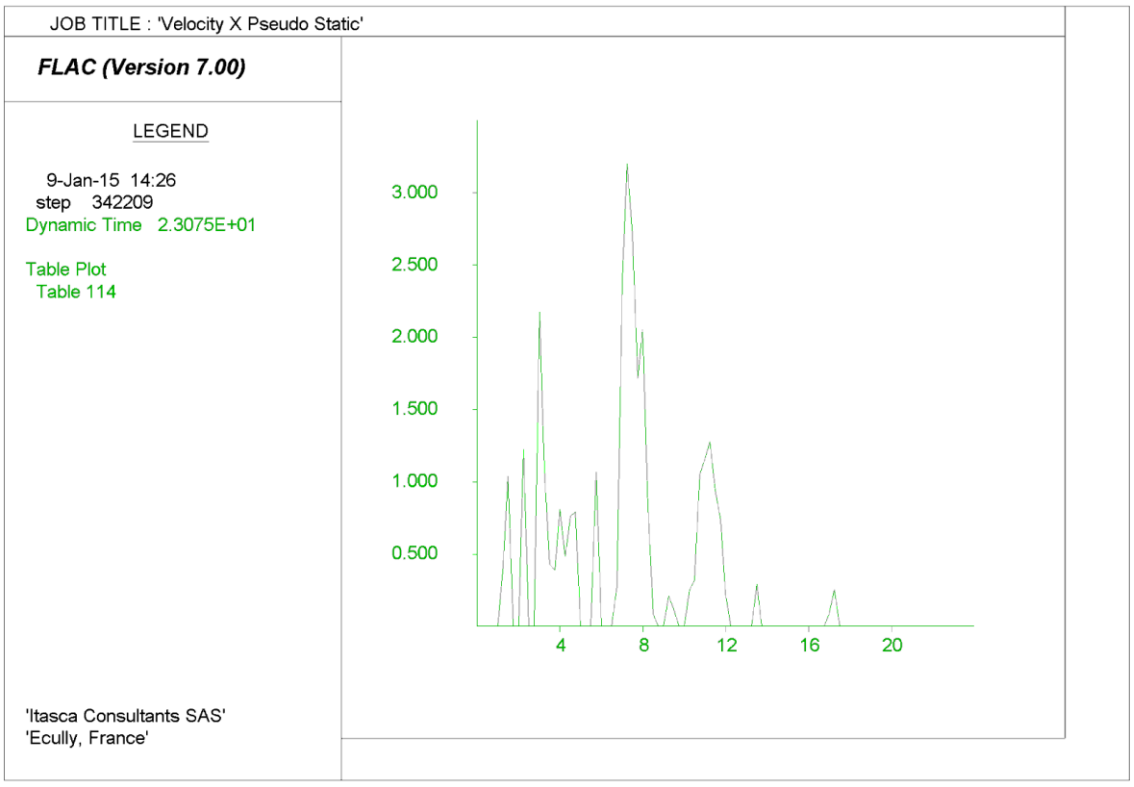

Figure 5-32 : Downstream analysis - Relative velocity (integration of relative acceleration)

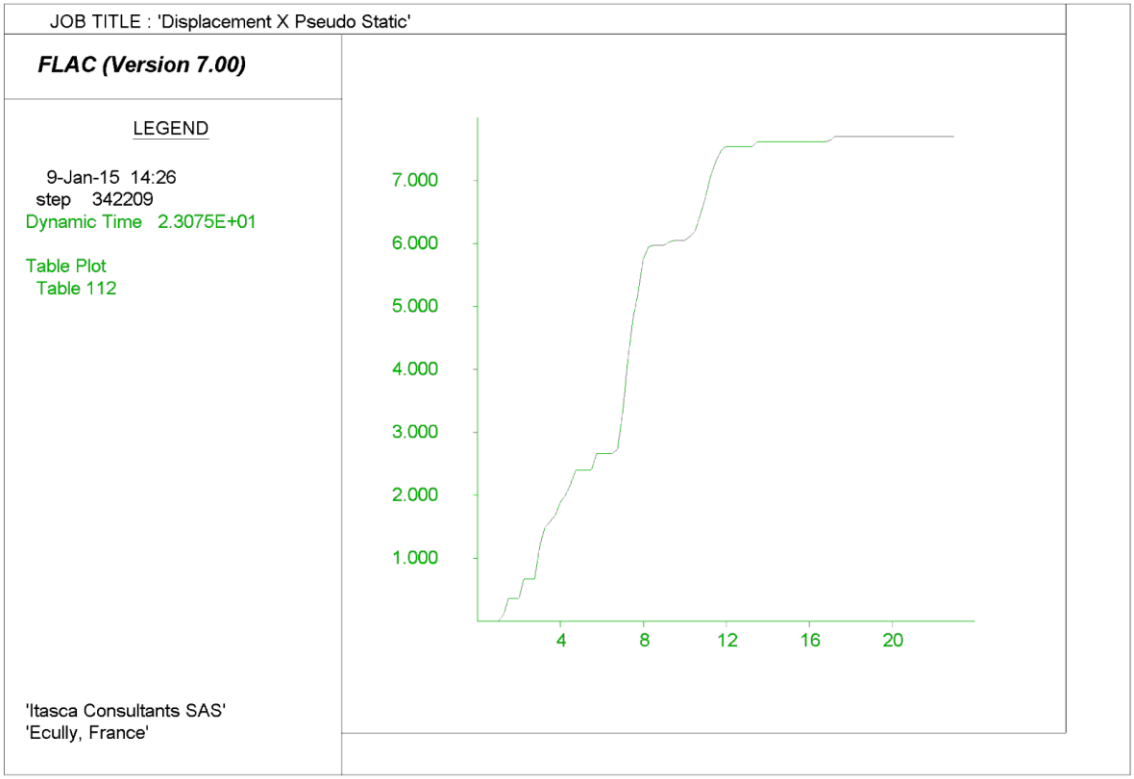

Figure 5-33 : Downstream analysis - Relative displacement (integration of relative velocity)

5.6.1.1. Upstream analysis

Similarly to what it was done for the downstream analysis, an upstream analysis is performed (see Figure 5-34). A coefficient Kh=-0.12 was found. Figure 5-35 and Figure 5-36 show the maximum shear increment and the plasticized zones, as they were obtained for Kh = - 0.12.

Considering a yield acceleration equal to Kh*g, a relative acceleration is computed (Figure 5-38). The relative velocity (Figure 5-39) is then calculated by integrating the relative acceleration with respect to time, not taking into account negative values.

The relative displacement is finally obtained by integration of the relative velocity (Figure 5-40). A negative relative displacement of more than 5 meters is computed (over 4 meters for the *Reference Cross Section* case).

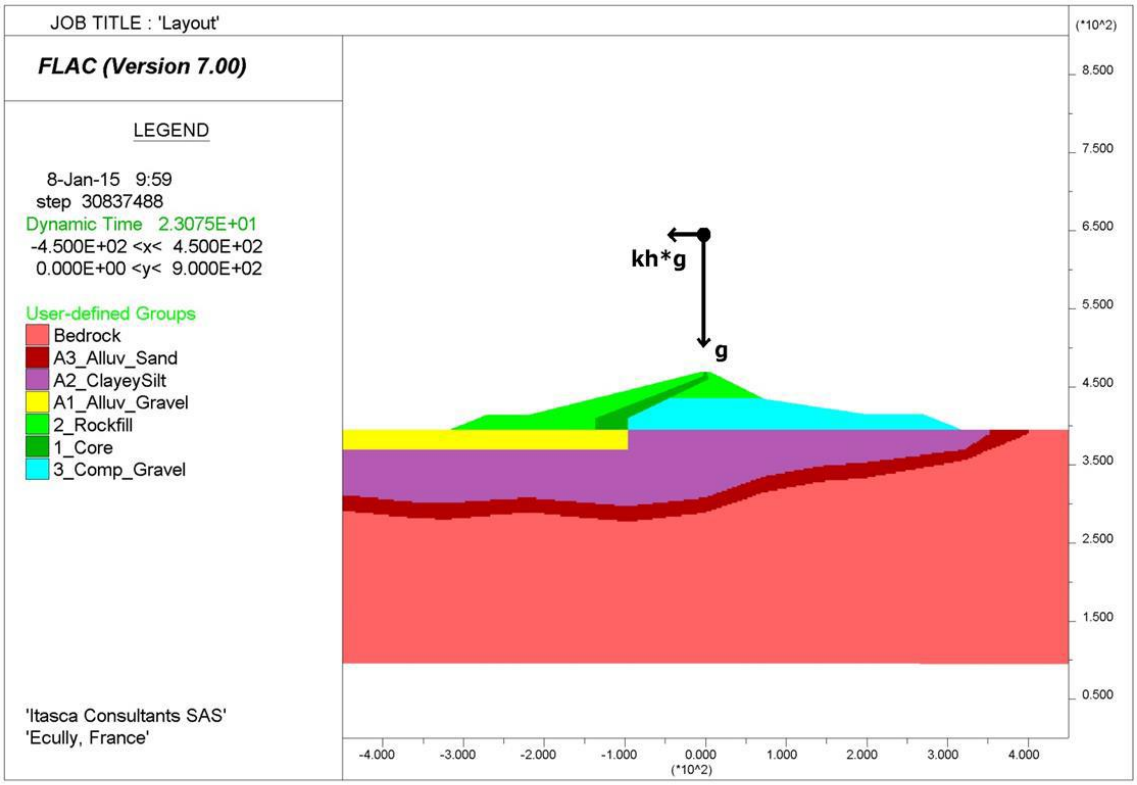

Figure 5-34 : Pseudo-static analysis - Upstream

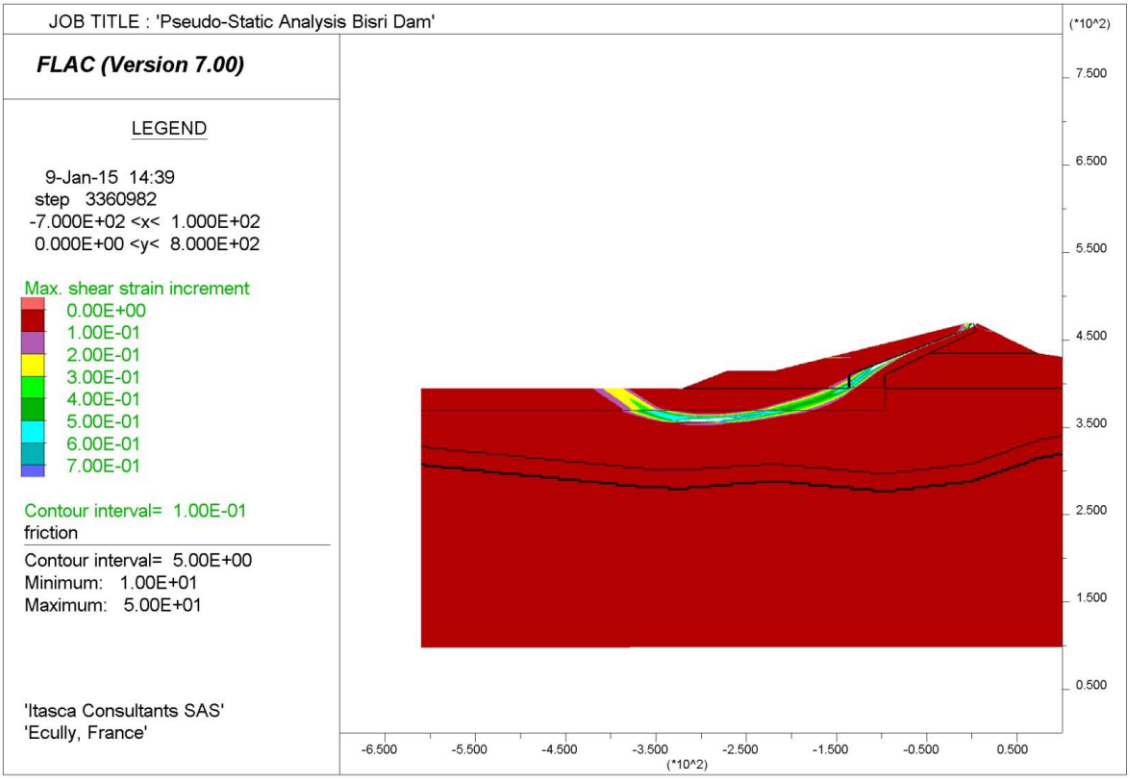

Figure 5-35 : Maximum shear strain increment – Upstream analysis (Kh = 0.17)

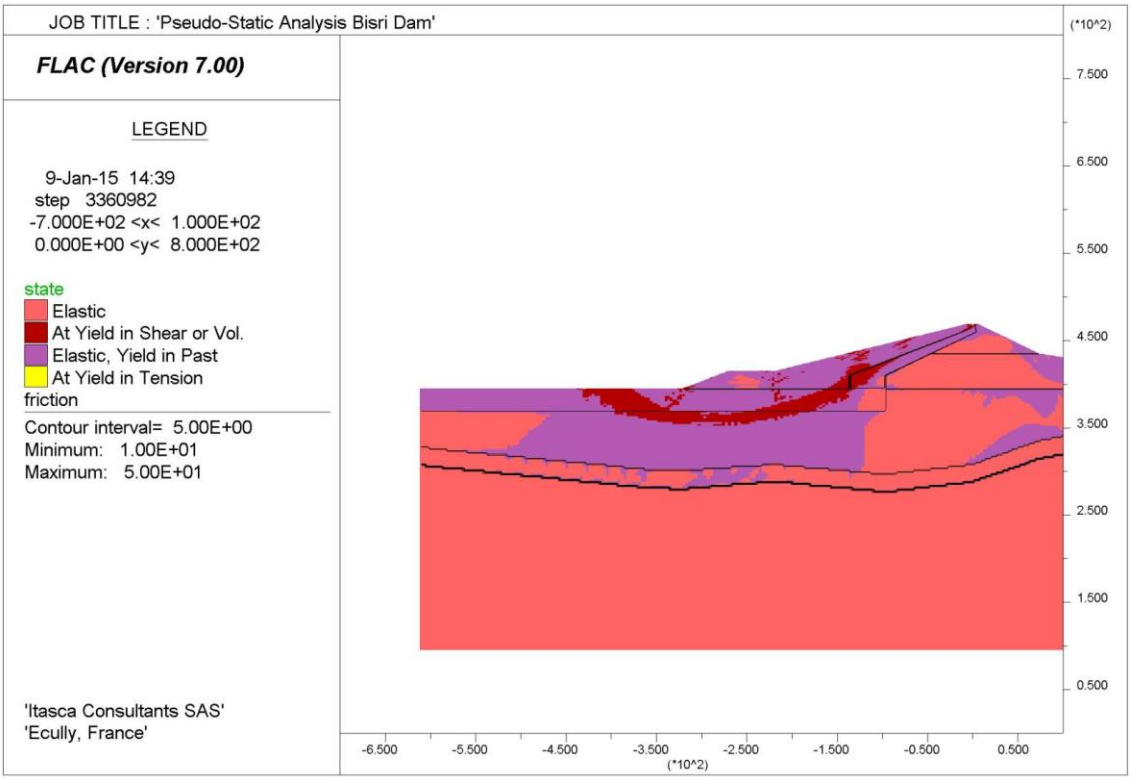

Figure 5-36 : Plasticized zones – Upstream analysis (Kh = 0.17)

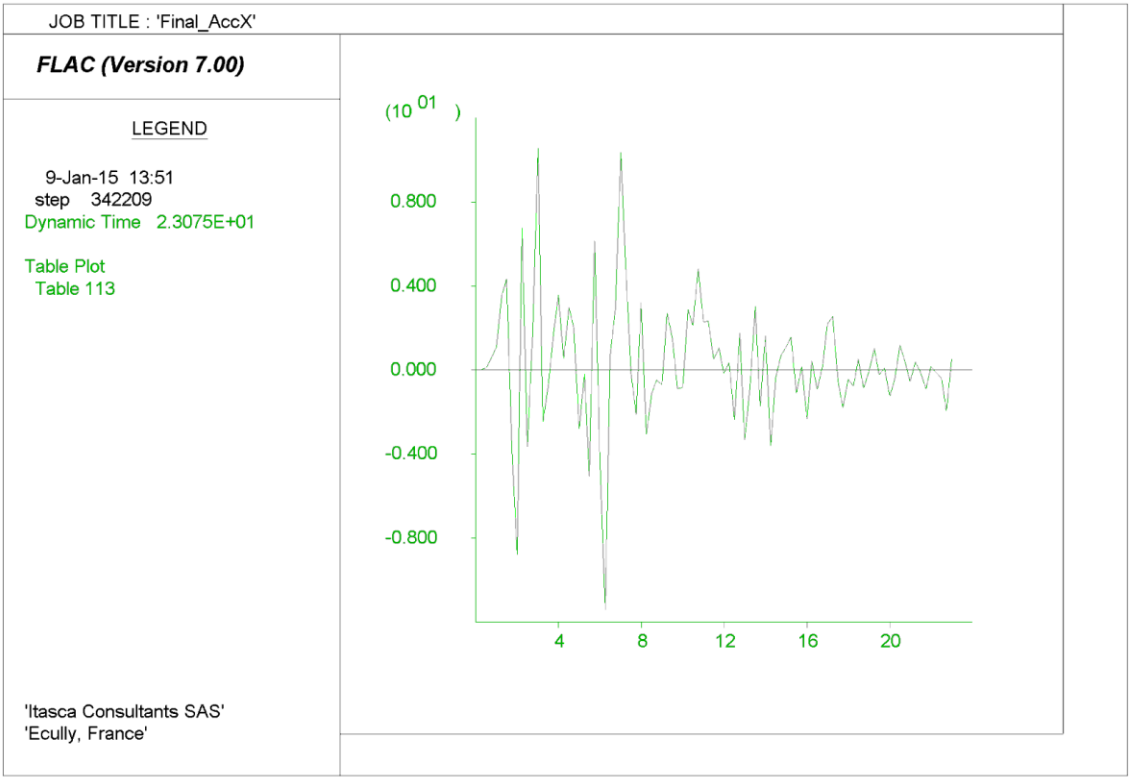

Figure 5-37 : Upstream analysis - Input horizontal acceleration a(t) (KOCAELI IZT V-H1)

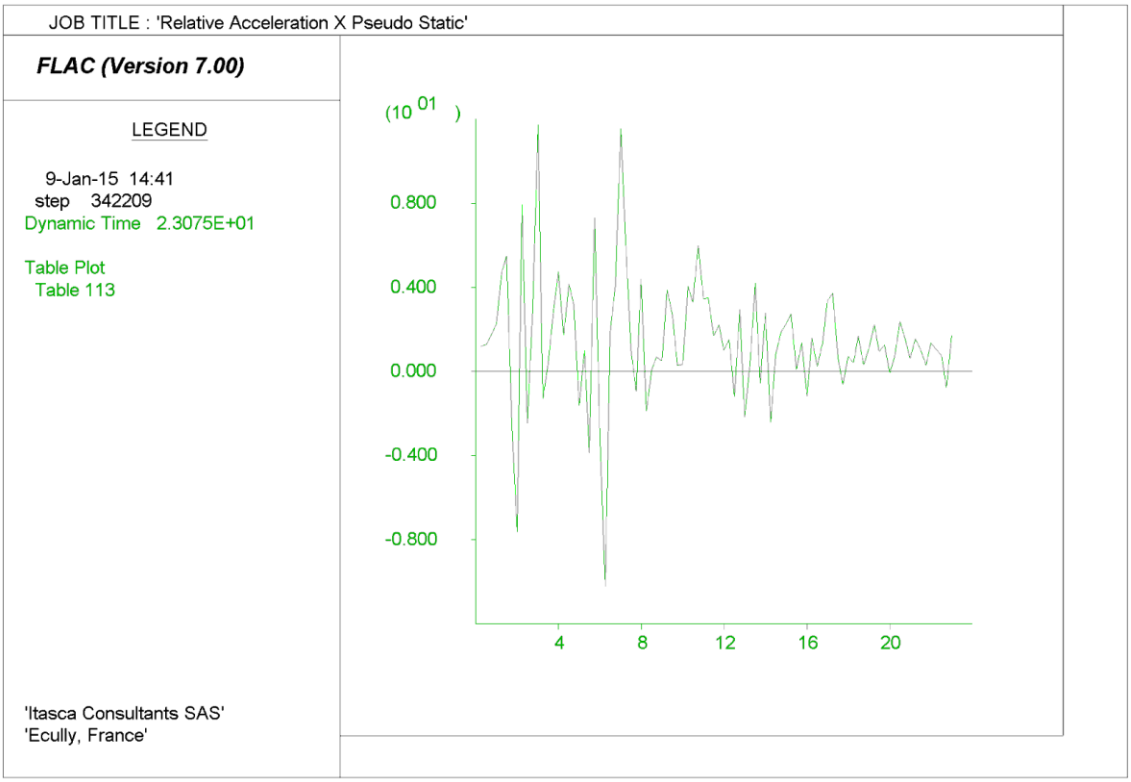

*Figure 5-38 : Upstream analysis - Relative horizontal acceleration ar(t) = a(t) – Kh*g*

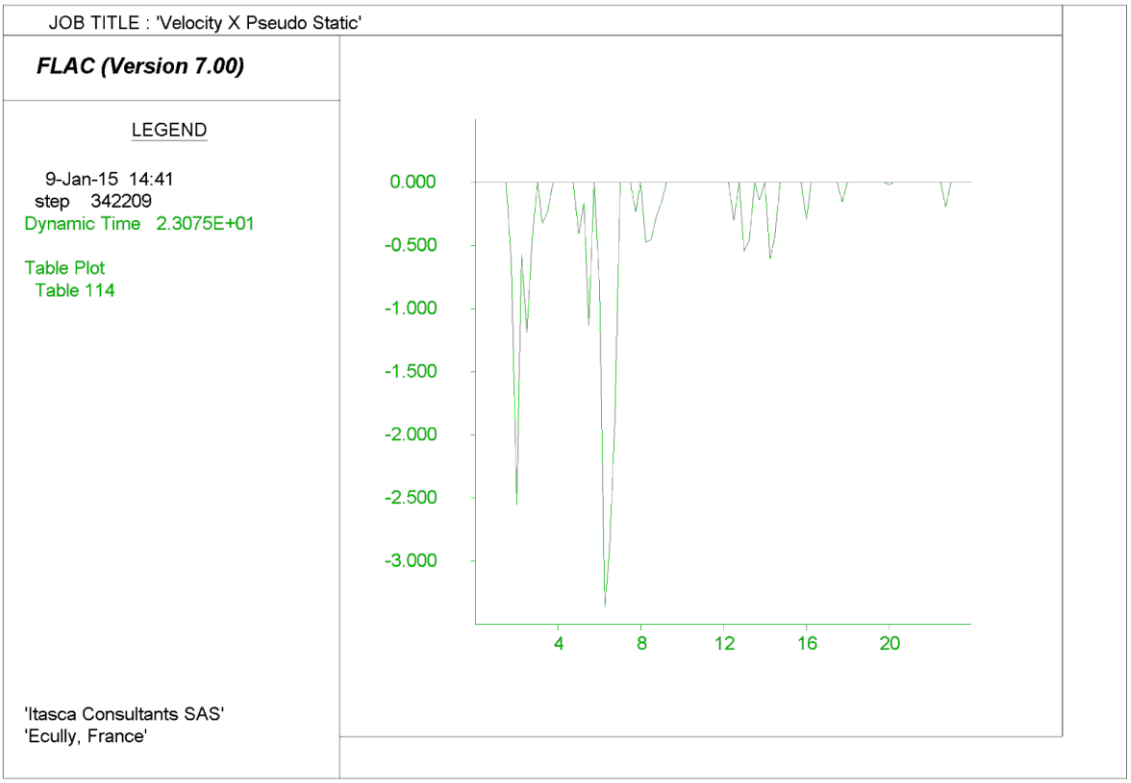

Figure 5-39 : Upstream analysis - Relative velocity (integration of relative acceleration)

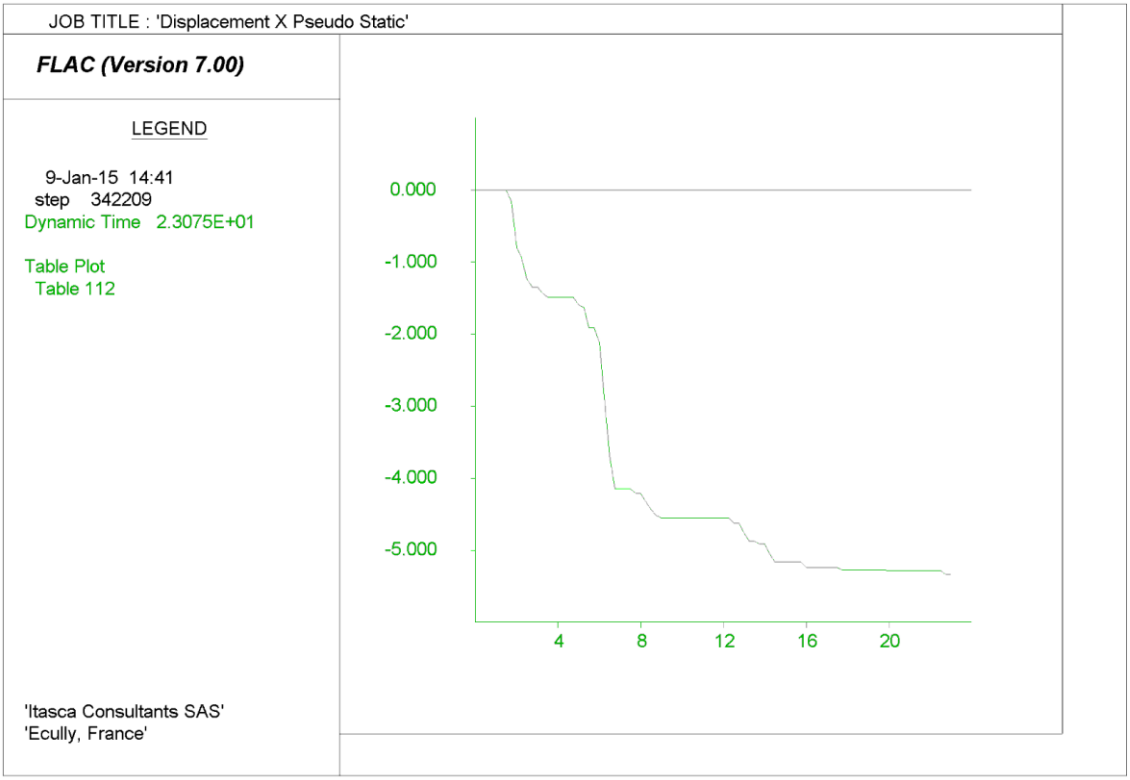

Figure 5-40 : Upstream analysis - Relative displacement (integration of relative velocity)

5.6.1.1. Summary of results and comments

The table below summarizes the results that were obtained and enables a direct comparison with the *Reference Cross Section* case. It is worth noticing that they have to be intended as rigid displacements of the sliding mass along the failure surfaces of Figure 5-28 and Figure 5-35.

SEE EARTHQUAKE - KOCAELI IZT V-H1				
			Pseudo-static Analysis	
Cross Section	**Analysis**		**Kh [g]**	**Max Displacement**
Reference CS	**Downstream**		0.17	> 9 m
	Upstream		-0.16	> 4 m
Real CS	**Downstream**		0.19	> 7 m
	Upstream		-0.12	> 5 m

Table 5-1 : Pseudo-static analysis – Summary of results

The correspondent displacement at the dam crest, noting as *D* the computed displacement along the failure surface (see Figure 5-41) and as α the angle between the vertical and the failure surface, can be computed. For the downstream analysis, an angle α equal to 46° can be measured, therefore a dam crest displacement of about 5m can be estimated. Concerning the upstream analysis, a dam crest vertical displacement of about 3.5m can be estimated, considering an angle α equal to 42° (see Figure 5-42).

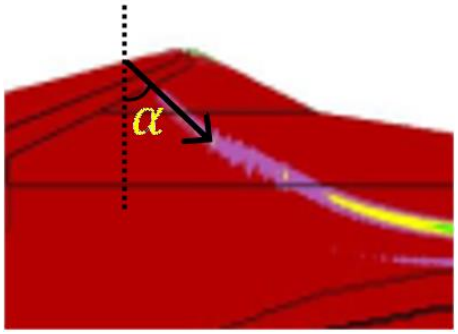

Figure 5-41 : Pseudo-static Newmark's downstream analysis – Displacement at the dam crest

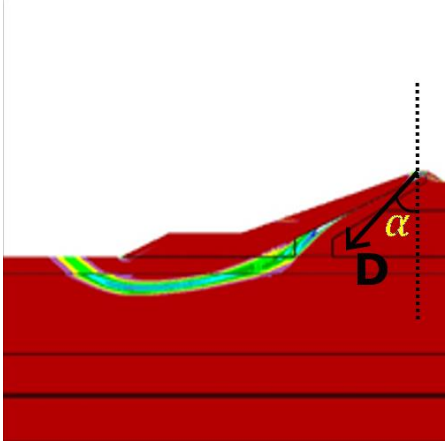

Figure 5-42 : Pseudo-static Newmark's upstream analysis – Displacement at the dam crest

5.6.2. SEE earthquake – Nonlinear analysis

The results of the nonlinear dynamic simulation of the dam-foundation response to the SEE earthquakes are presented in this section. Table 5-2 summarizes the maximum displacements calculated at the dam crest (the maximum displacements that were measured for the *Reference Cross Section* case are reported for comparison in Table 5-3). Displacement fields for all the tested cases are plotted from Figure 5-45 to Figure 5-56. Horizontal displacements that could affect the stability of the slurry concrete wall are analyzed in section 5.6.2.1.

In all cases the vertical displacement at the crest of the dam is again lower than 2 meters, as was the case for the *Reference Cross Section* (the maximum admissible vertical displacement is 4 meters, as indicated by NOVEC).

The main instability process concerns again the foot of the downstream embankment and the upstream slope. The foot of the downstream embankment plastifies for all simulated cases. It is here that the maximum positive horizontal and vertical displacements are encountered. In all cases, the maximum positive horizontal and vertical displacements for this case are higher than the *Reference Cross Section* case ones (see Table 5-2 and Table 5-3). This is due to the different soil foundation profile, with the bedrock daylighting close to the foot of the embankment. Strains tend therefore to concentrate close to the bedrock/foundation interface whereas in the *Reference Cross Section* case the strain localization (failure) was deeper.

The upstream slope remains problematic. Here again, the maximum negative horizontal and vertical displacements are higher than for the *Reference Cross Section* case. Upstream sliding occurs in the

same way as in the *Reference Cross Section* case (Darfield V-H1 in Figure 5-45 and Figure 5-46, Darfield V-H2 in Figure 5-47 and Figure 5-48 and Kocaeli V-H2 in Figure 5-51 and Figure 5-52). The plots of the maximum shear increment (Figure 5-43) and of the magnified grid deformation of Figure 5-44, confirm the relative sliding between the rockfill and the dam core. In fact, it seems that the upstream slope movements are conditioned by the slope of the rockfill/core interface, more than by the rockfill slope itself.

Figure 5-45 and Figure 5-46 show the final horizontal and vertical displacements, respectively, corresponding to the SEE earthquake Darfield LPCC (PGA V + 0.5 / - 0.58 H1 + 0.96 / - 1.33).
Figure 5-47 and Figure 5-48 show the final horizontal and vertical displacements, respectively, corresponding to the SEE earthquake Darfield LPCC (PGA V + 0.5 / - 0.58 H2 + 0.79 / - 0.89).
Figure 5-49 and Figure 5-50 show the final horizontal and vertical displacements, respectively, corresponding to the SEE earthquake Kocaeli IZT (PGA V + 0.51 / - 0.43 H1 + 0.82 / - 0.63).
Figure 5-51 and Figure 5-52 show the final horizontal and vertical displacements, respectively, corresponding to the SEE earthquake Kocaeli IZT (PGA V + 0.51 / - 0.43 H2 + 0.47 / - 0.59).
Figure 5-53 and Figure 5-54 show the final horizontal and vertical displacements, respectively, corresponding to the SEE earthquake Morgan (PGA V + 0.44 / - 0.43 H1 + 0.81 / - 0.62).
Figure 5-55 and Figure 5-56 show the final horizontal and vertical displacements, respectively, corresponding to the SEE earthquake Morgan (PGA V + 0.44 / - 0.43 H2 + 0.55 / - 1.49).

SEE EARTHQUAKE - REAL CROSS SECTION					
		PGA [g]		Max Crest Displacements [m]	
Name		Vertical	Horizontal	Vertical	Horizontal
Darfield V-H1		+ 0.5 / - 0.58	+ 0.96 / - 1.33	-0.40	+0.35
Darfield V-H2			+ 0.79 / - 0.89	-1.40	-1.40
Kocaeli Izt V-H1		+ 0.51 / - 0.43	+ 0.82 / - 0.63	-1.20	+2.20
Kocaeli Izt V-H2			+ 0.47 / - 0.59	-1.50	-1.50
Morgan V-H1		+ 0.44 / - 0.43	+ 0.81 / - 0.62	-0.15	+0.40
Morgan V-H2			+ 0.55 / - 1.49	-0.13	+0.48

Table 5-2 : SEE earthquakes – Maximum crest displacements – Real Cross Section

SEE EARTHQUAKE - REFERENCE CROSS SECTION					
		PGA [g]		Max Crest Displacements [m]	
Name		Vertical	Horizontal	Vertical	Horizontal
Darfield V-H1		+ 0.5 / - 0.58	+ 0.96 / - 1.33	-0.25	+0.60
Darfield V-H2			+ 0.79 / - 0.89	-1.00	-1.50
Kocaeli Izt V-H1		+ 0.51 / - 0.43	+ 0.82 / - 0.63	-0.90	+2.50
Kocaeli Izt V-H2			+ 0.47 / - 0.59	-1.00	-0.80
Morgan V-H1		+ 0.44 / - 0.43	+ 0.81 / - 0.62	-0.20	+0.40
Morgan V-H2			+ 0.55 / - 1.49	-0.20	+0.60

Table 5-3 : SEE earthquakes – Maximum crest displacements – Reference Cross Section

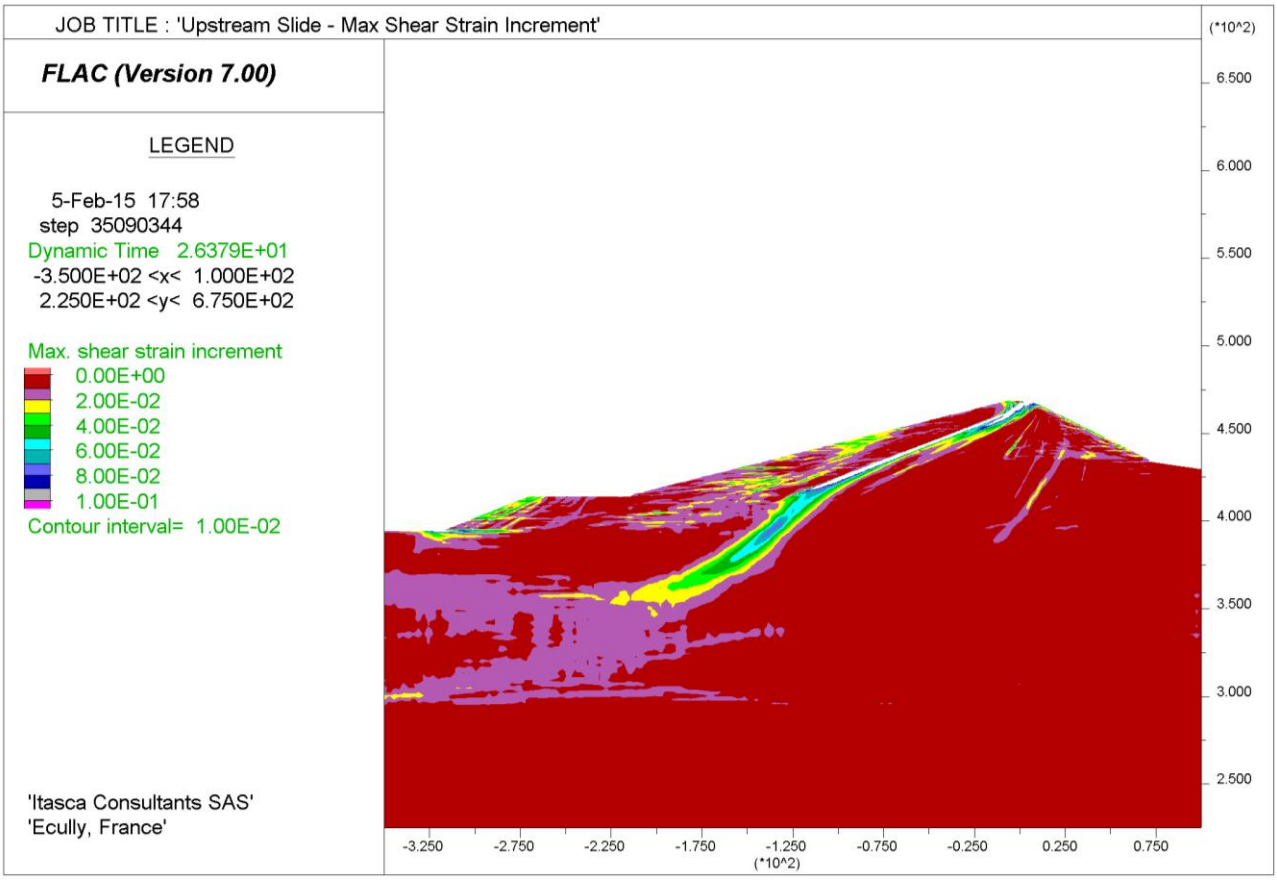

Figure 5-43: Upstream rockfill sliding – Maximum shear strain increment (SEE Darfield V-H2)

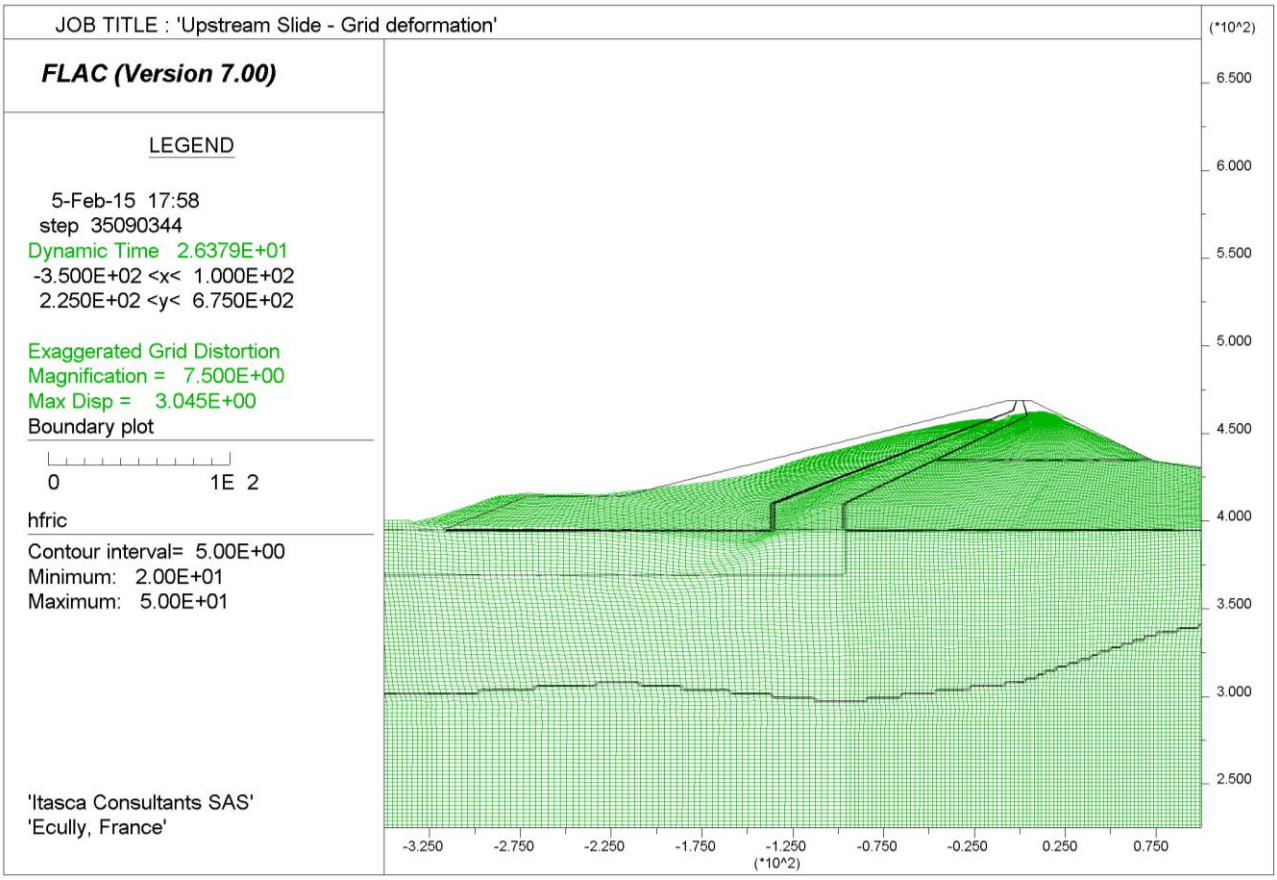

Figure 5-44: Upstream rockfill sliding – Grid magnified deformation (SEE Darfield V-H2)

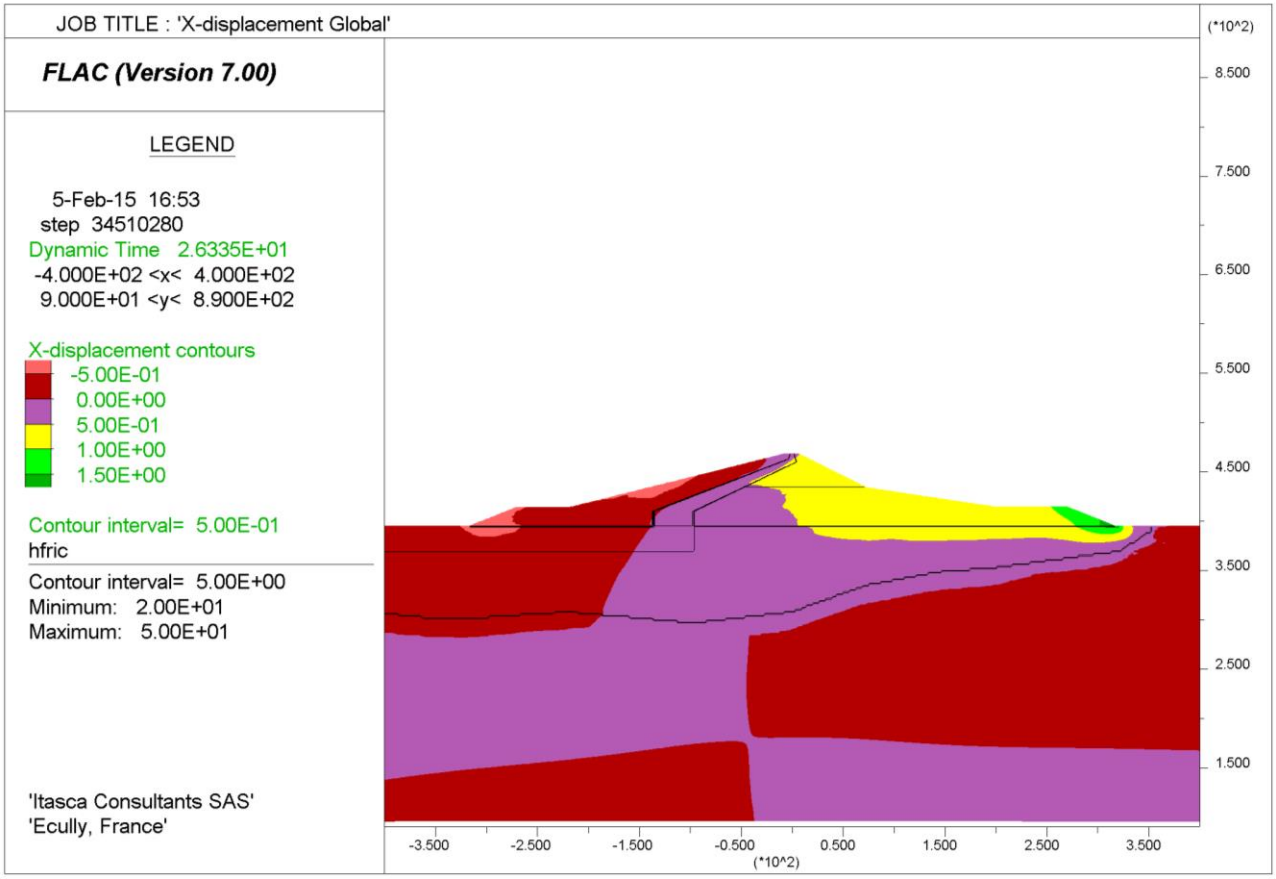

Figure 5-45 Nonlinear analysis – SEE earthquake Darfield LPCC (V-H1)
Final horizontal displacements

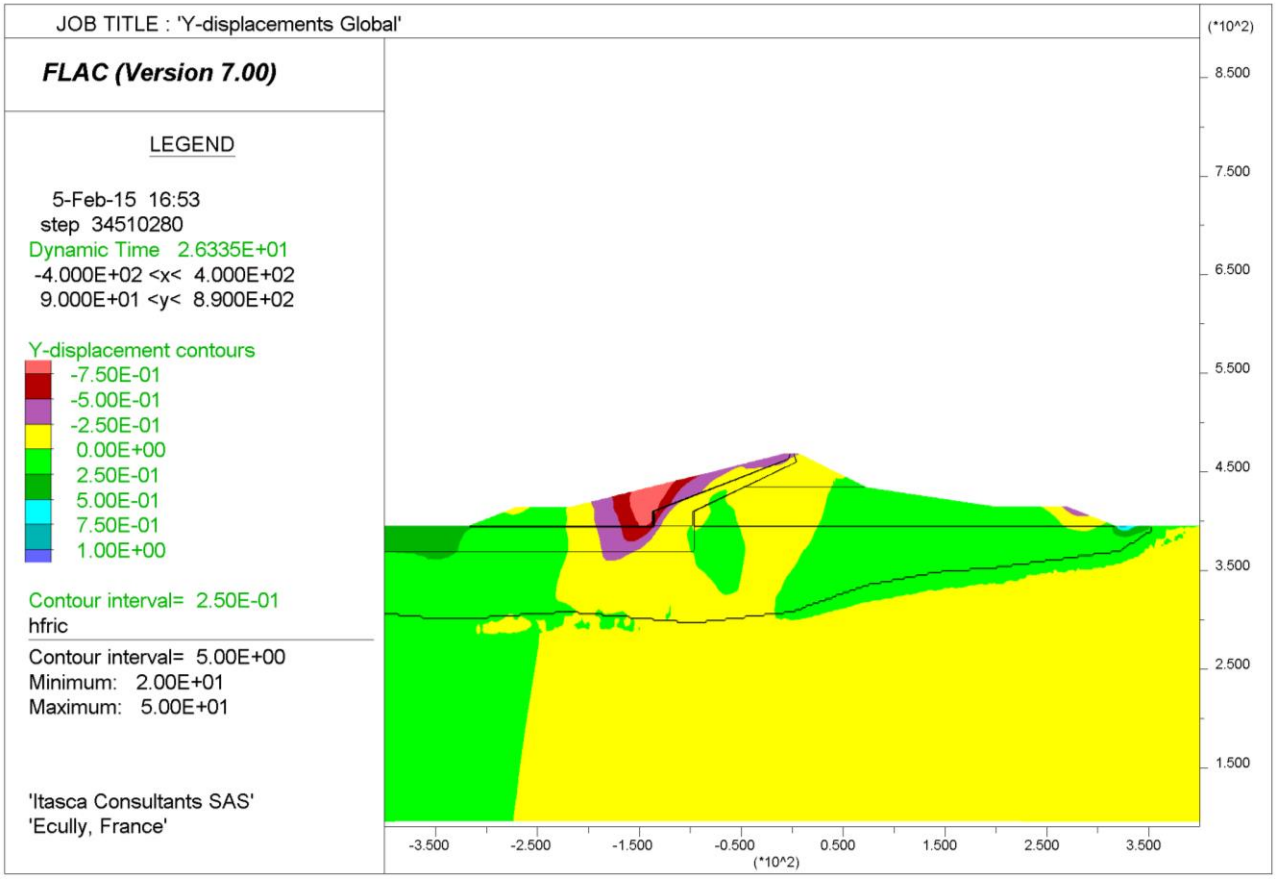

Figure 5-46 Nonlinear analysis – SEE earthquake Darfield LPCC (V-H1)
Final vertical displacements

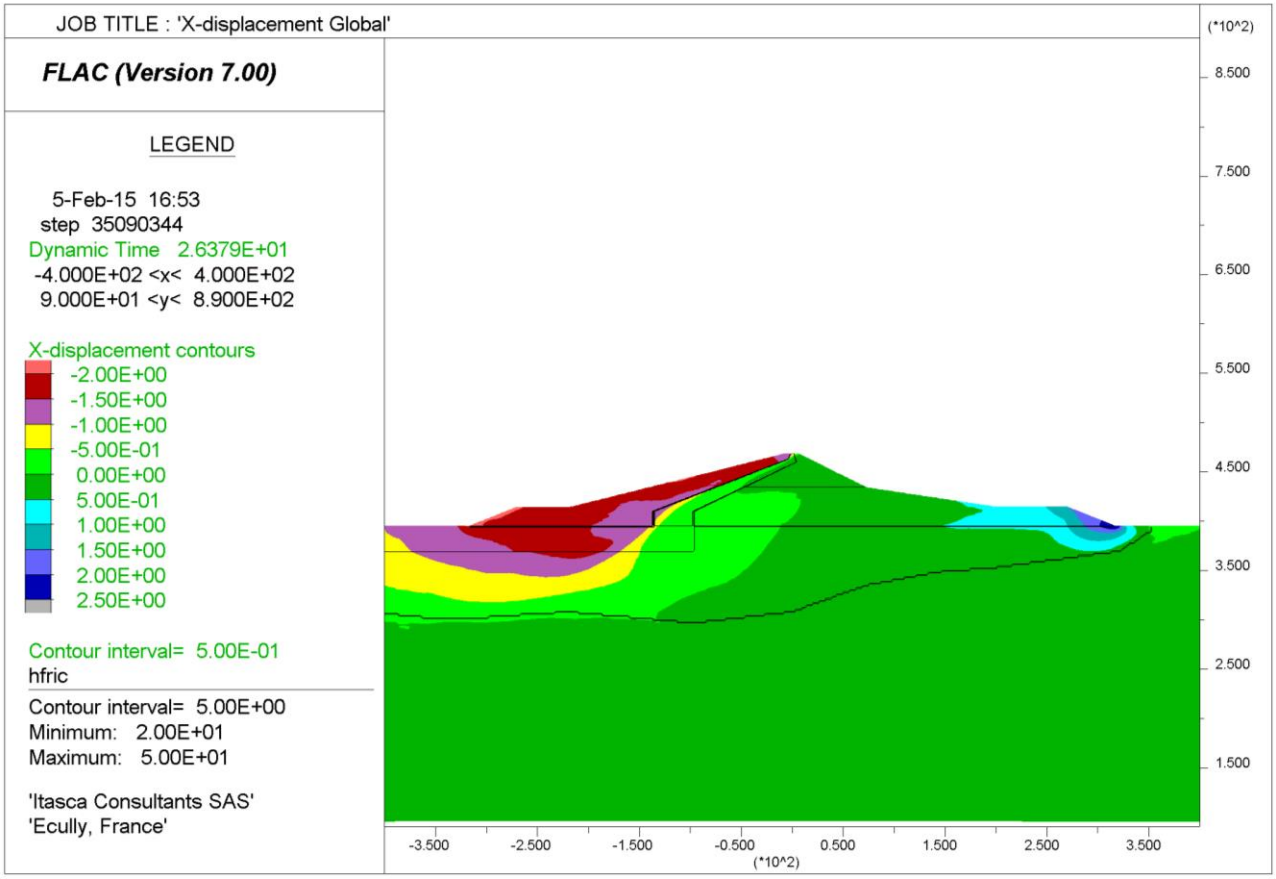

Figure 5-47 Nonlinear analysis – SEE earthquake Darfield LPCC (V-H2)
Final horizontal displacements

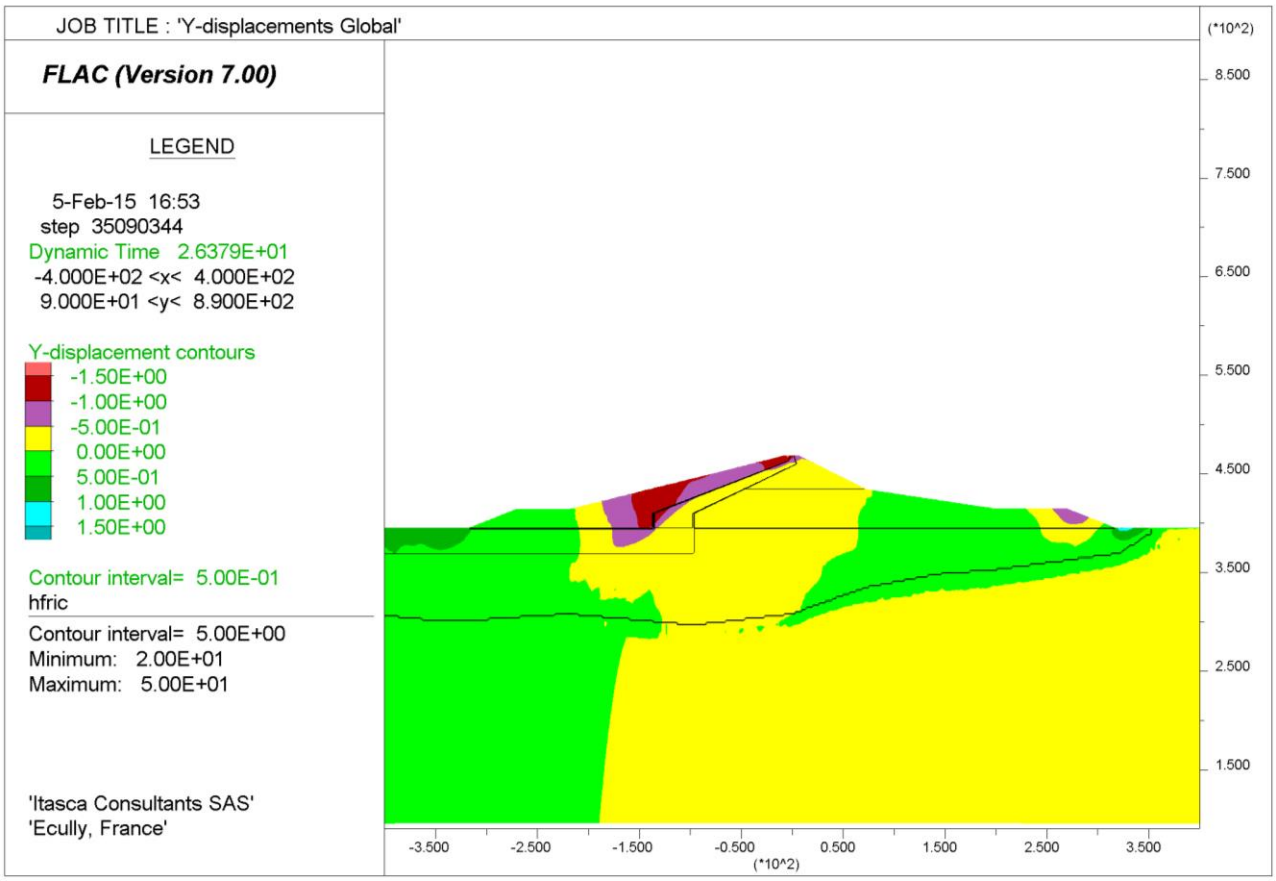

Figure 5-48 Nonlinear analysis – SEE earthquake Darfield LPCC (V-H2)
Final vertical displacements

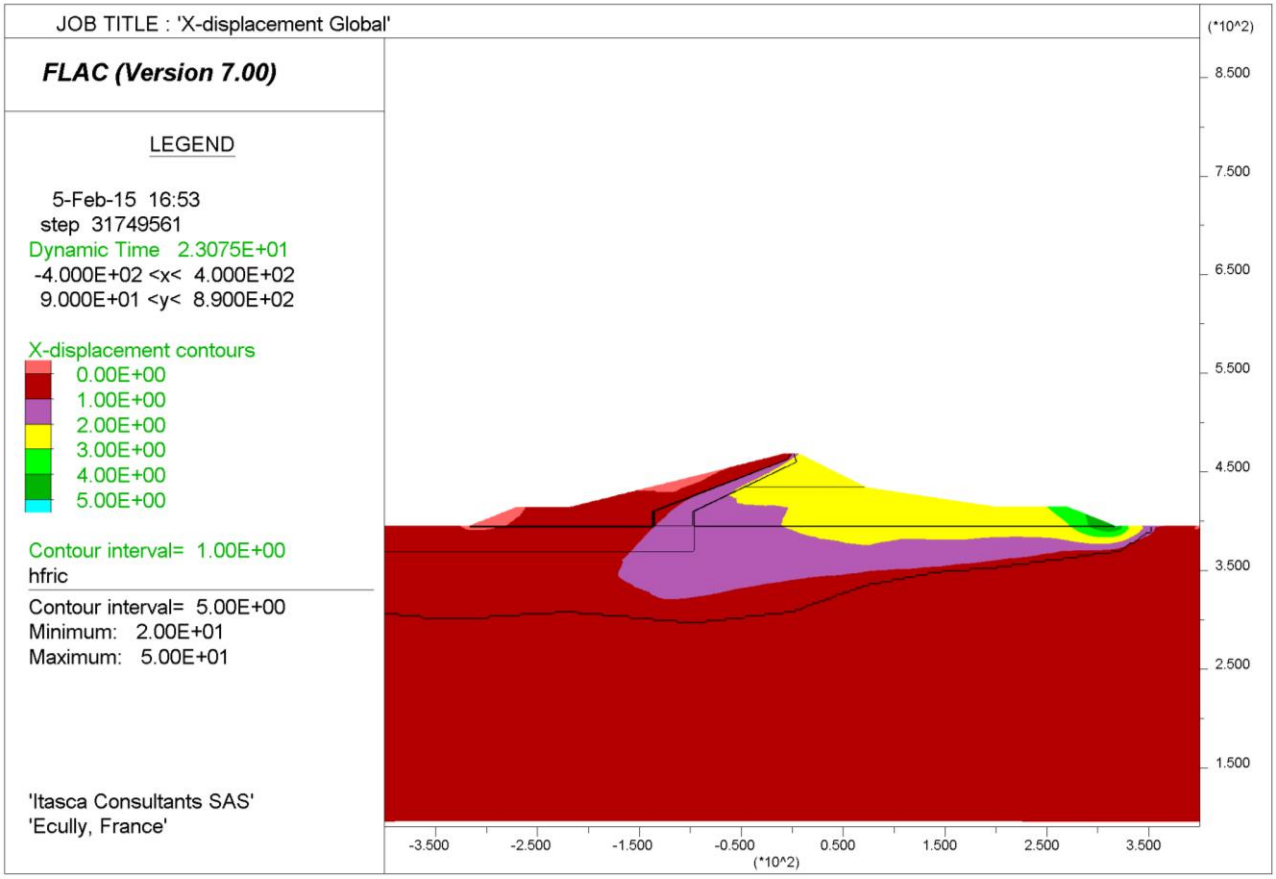

Figure 5-49 Nonlinear analysis – SEE earthquake Kocaeli IZT (V-H1)
Final horizontal displacements

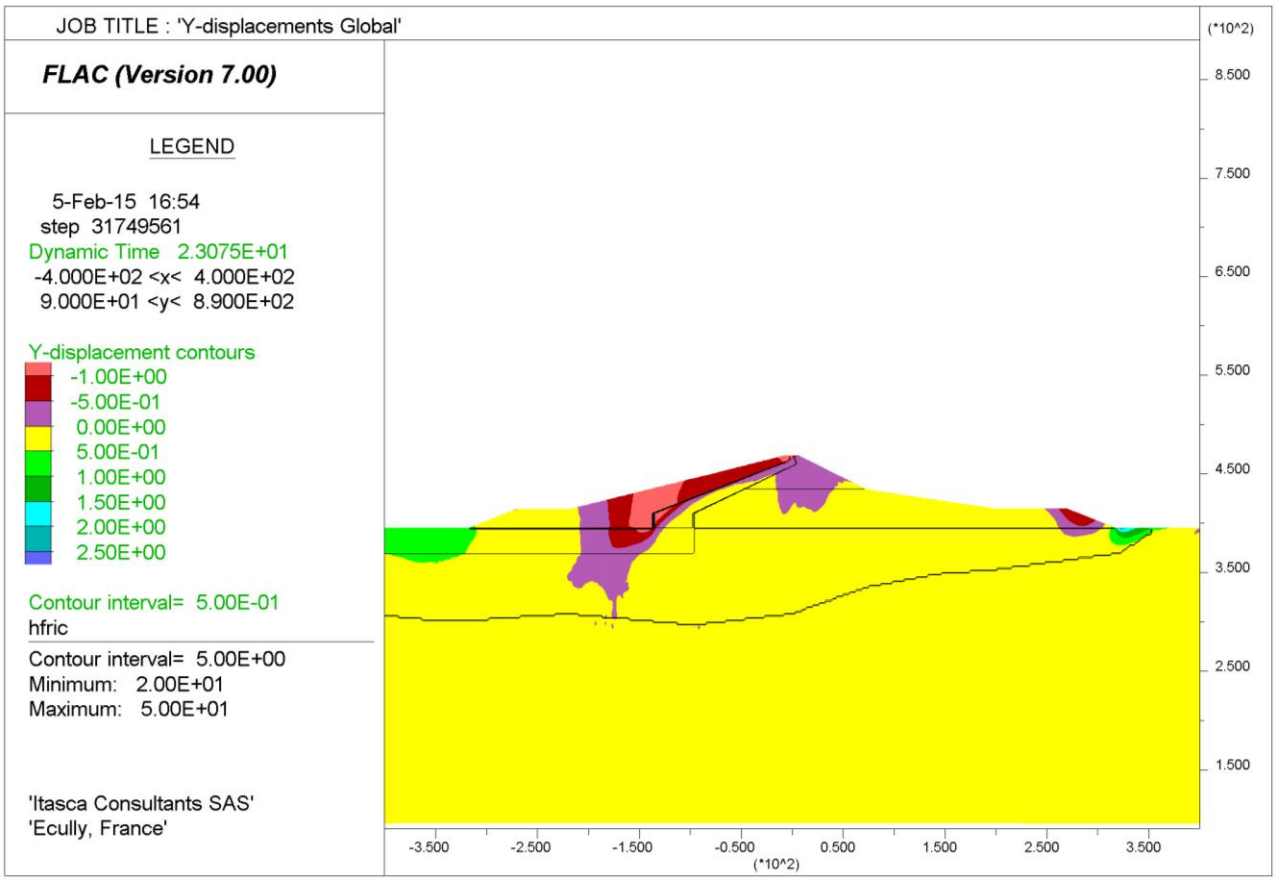

Figure 5-50 Nonlinear analysis – SEE earthquake Kocaeli IZT (V-H1)
Final vertical displacements

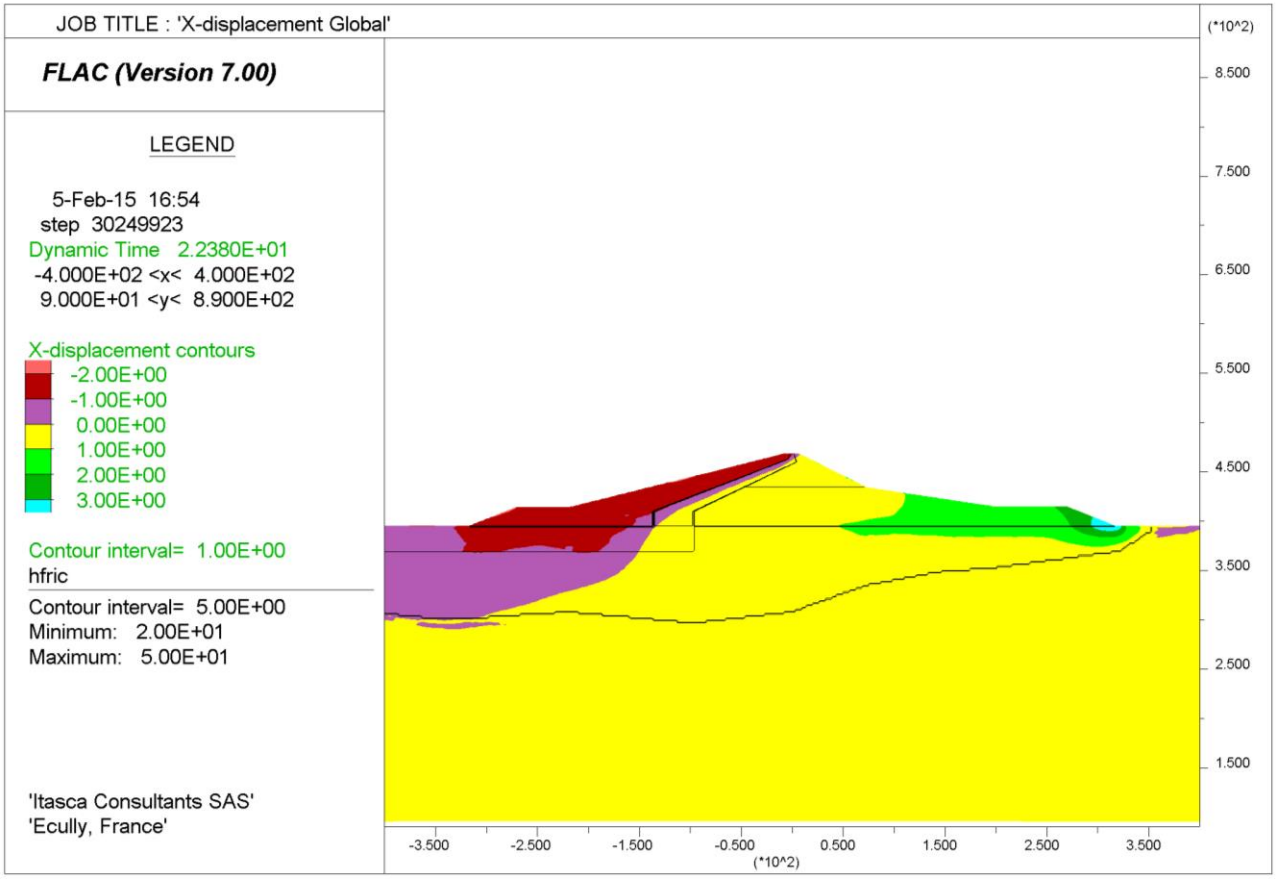

Figure 5-51 Nonlinear analysis – SEE earthquake Kocaeli IZT (V-H2)
Final horizontal displacements

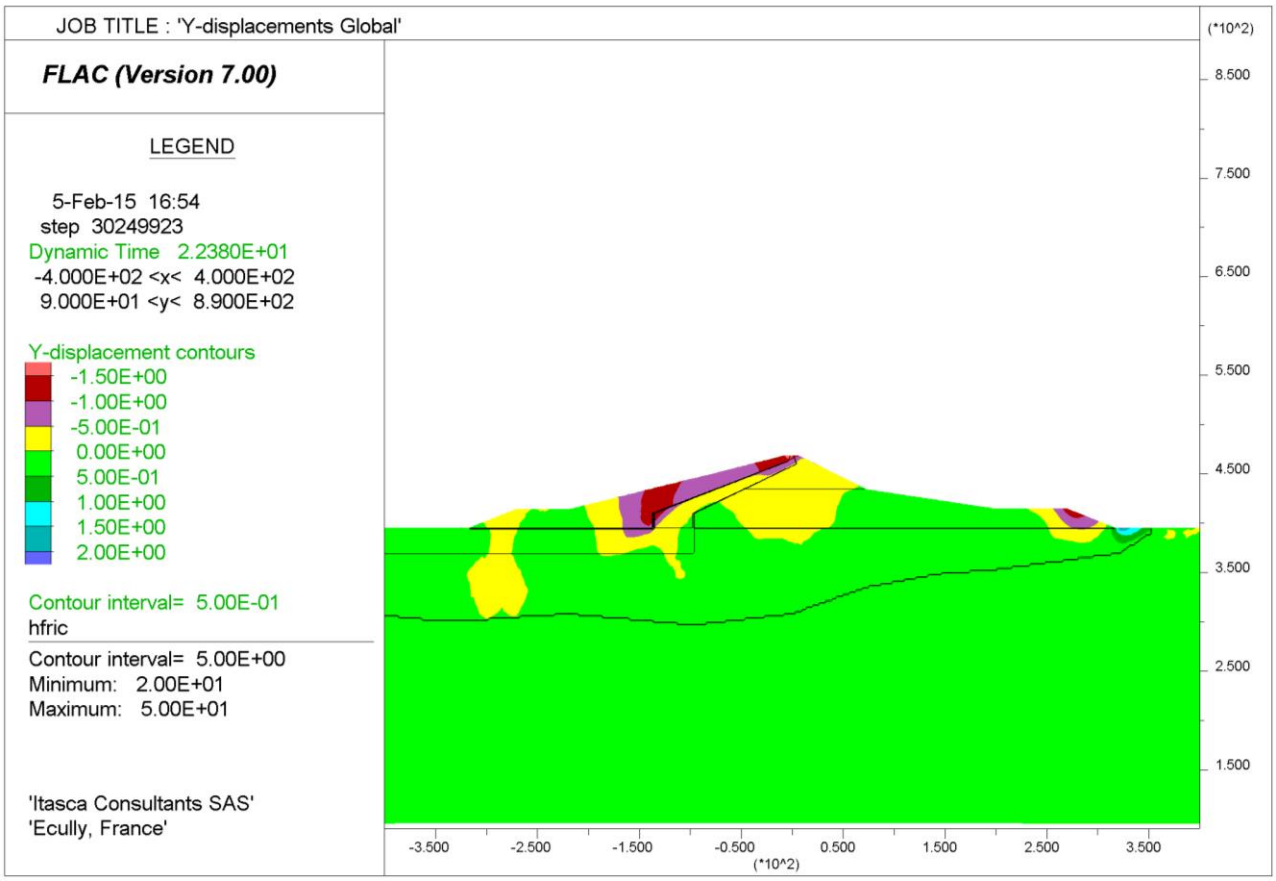

Figure 5-52 Nonlinear analysis – SEE earthquake Kocaeli IZT (V-H2)
Final vertical displacements

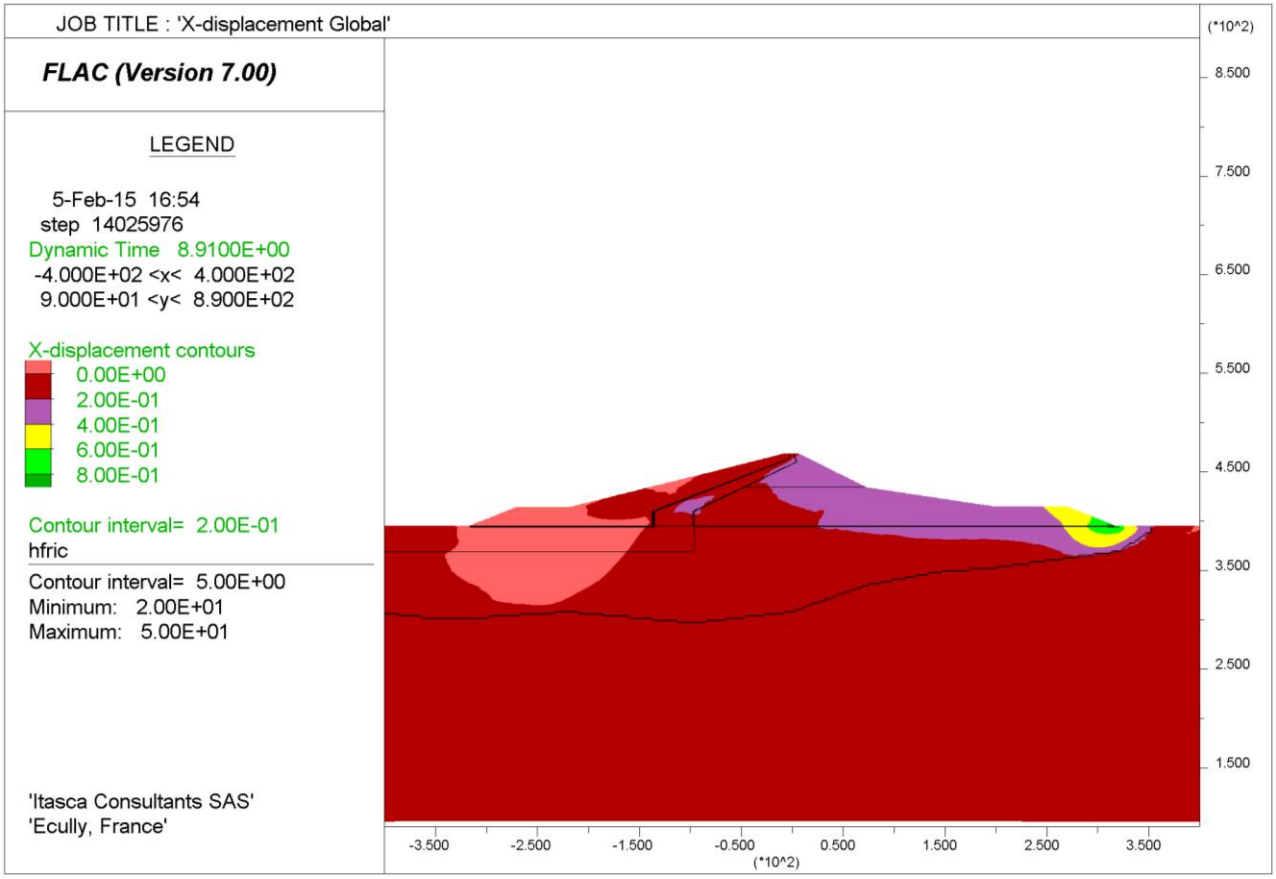

Figure 5-53 Nonlinear analysis – SEE earthquake Morgan (V-H1)
Final horizontal displacements

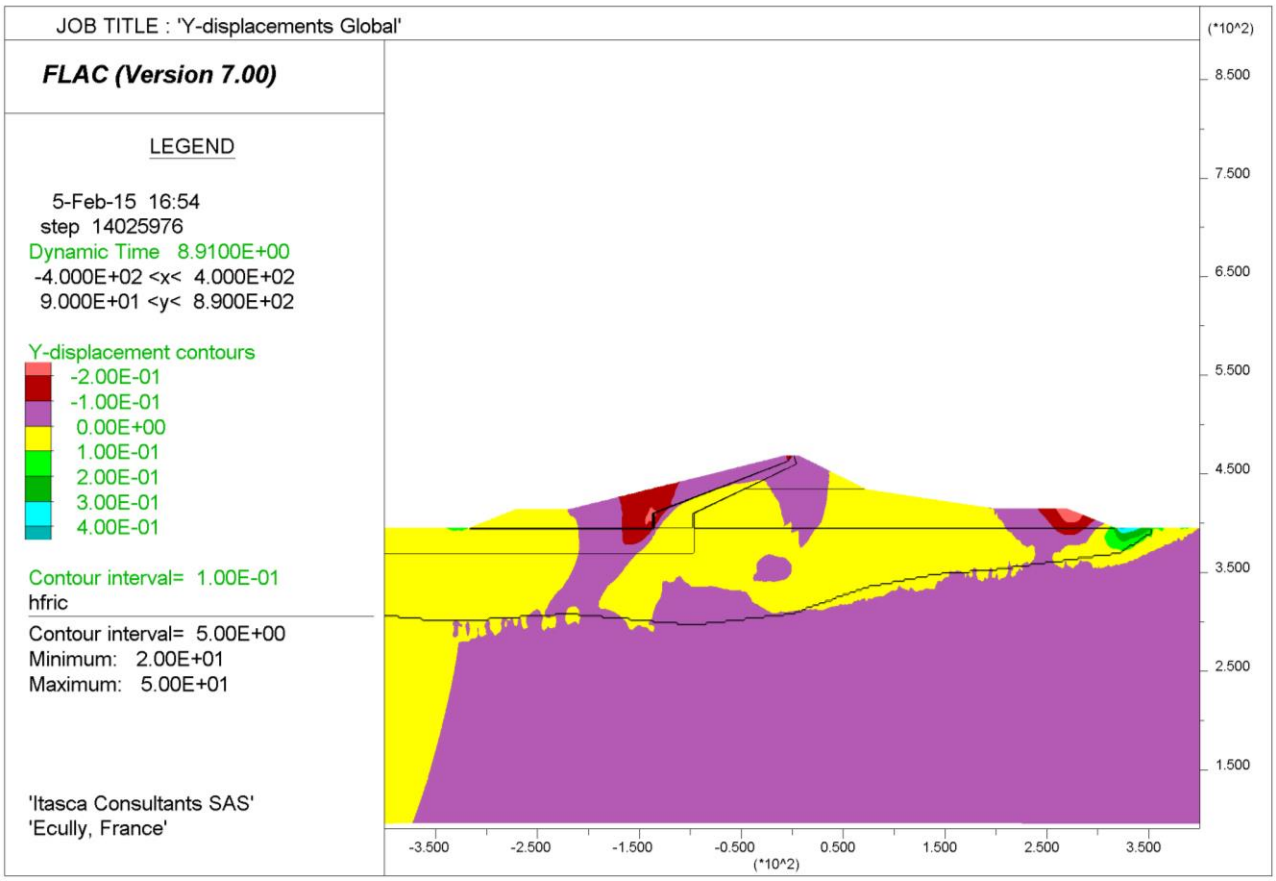

Figure 5-54 Nonlinear analysis – SEE earthquake Morgan (V-H1)
Final vertical displacements

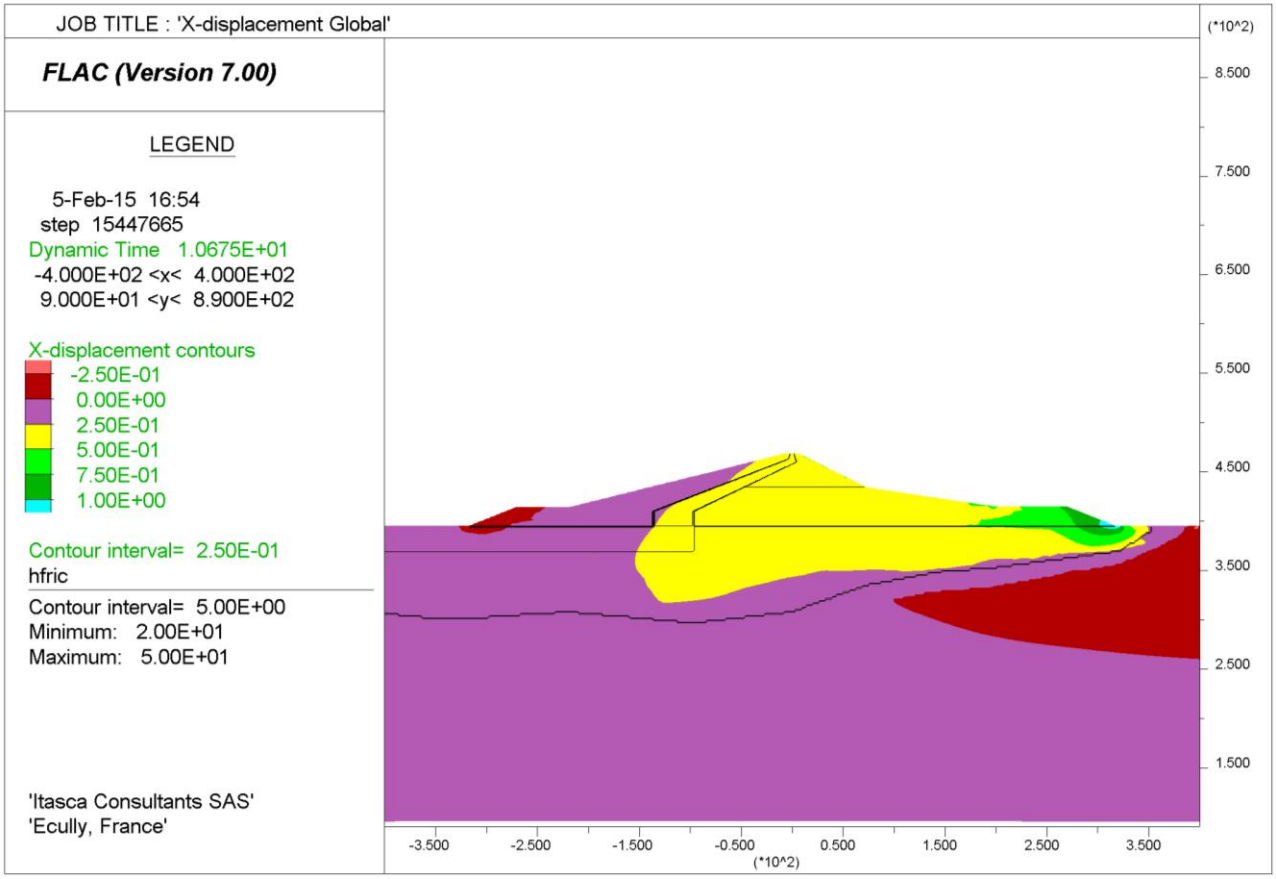

Figure 5-55 Nonlinear analysis – SEE earthquake Morgan (V-H2)
Final horizontal displacements

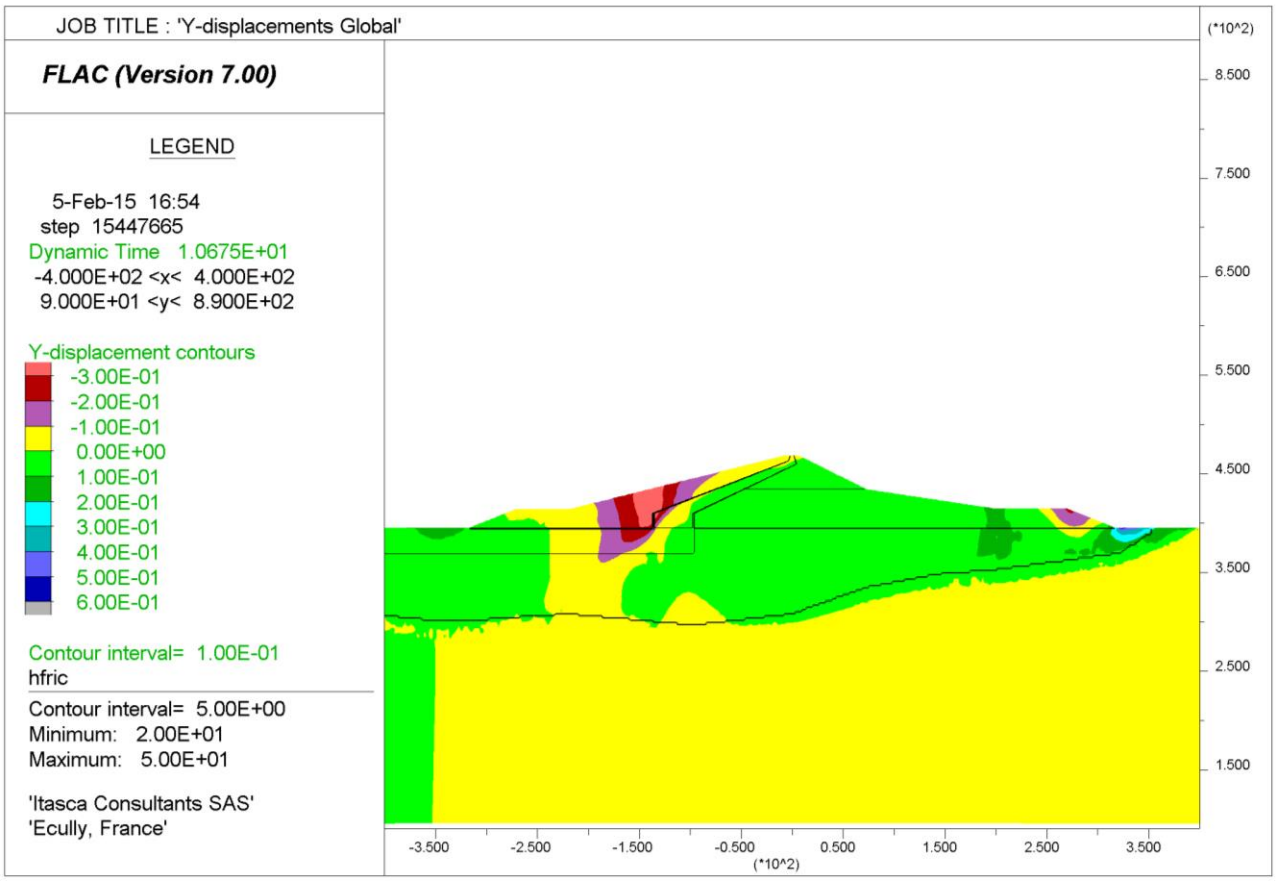

Figure 5-56 Nonlinear analysis – SEE earthquake Morgan (V-H2)
Final vertical displacements

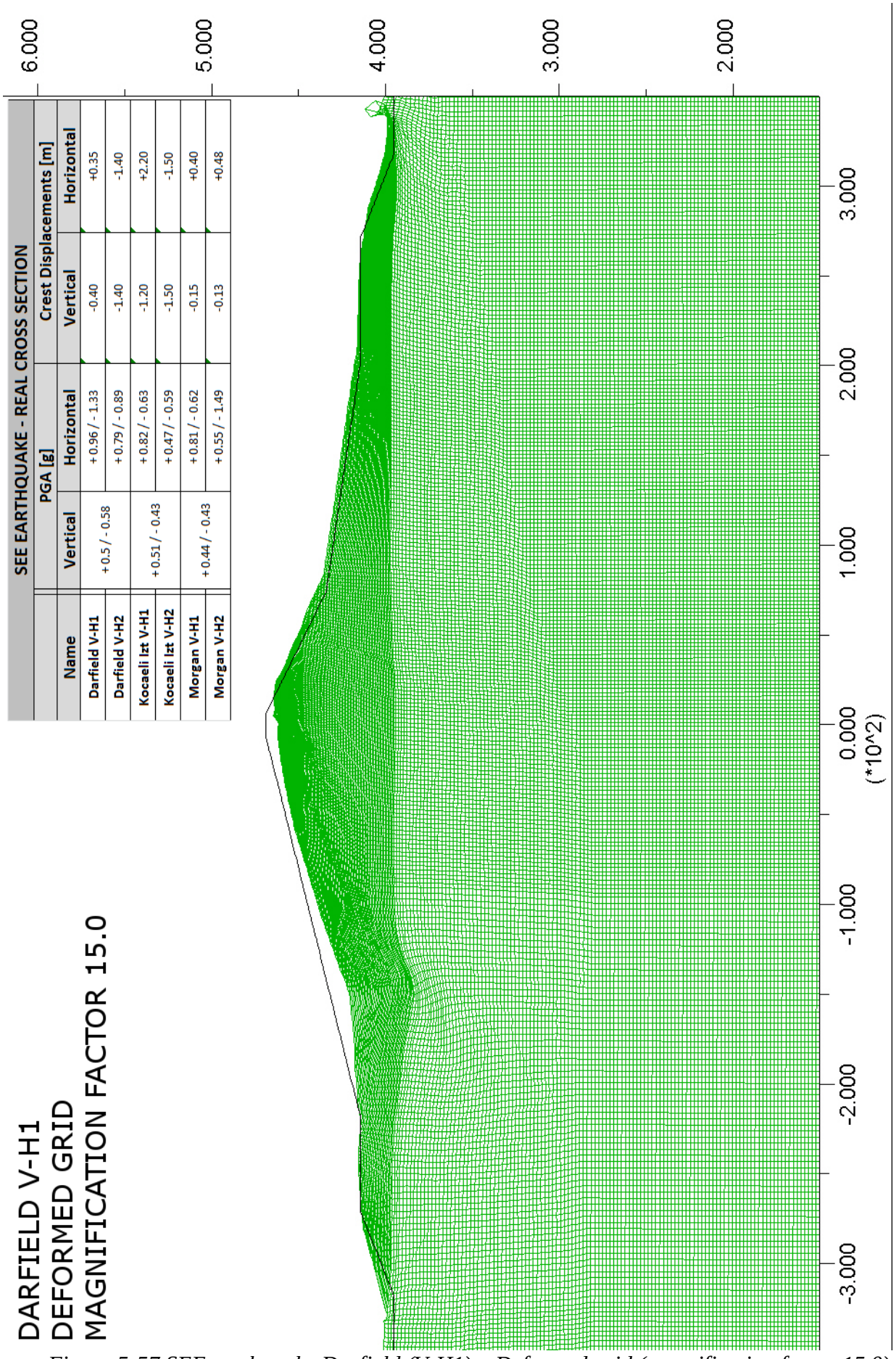

Figure 5-57 SEE earthquake Darfield (V-H1) – Deformed grid (magnification factor 15.0)

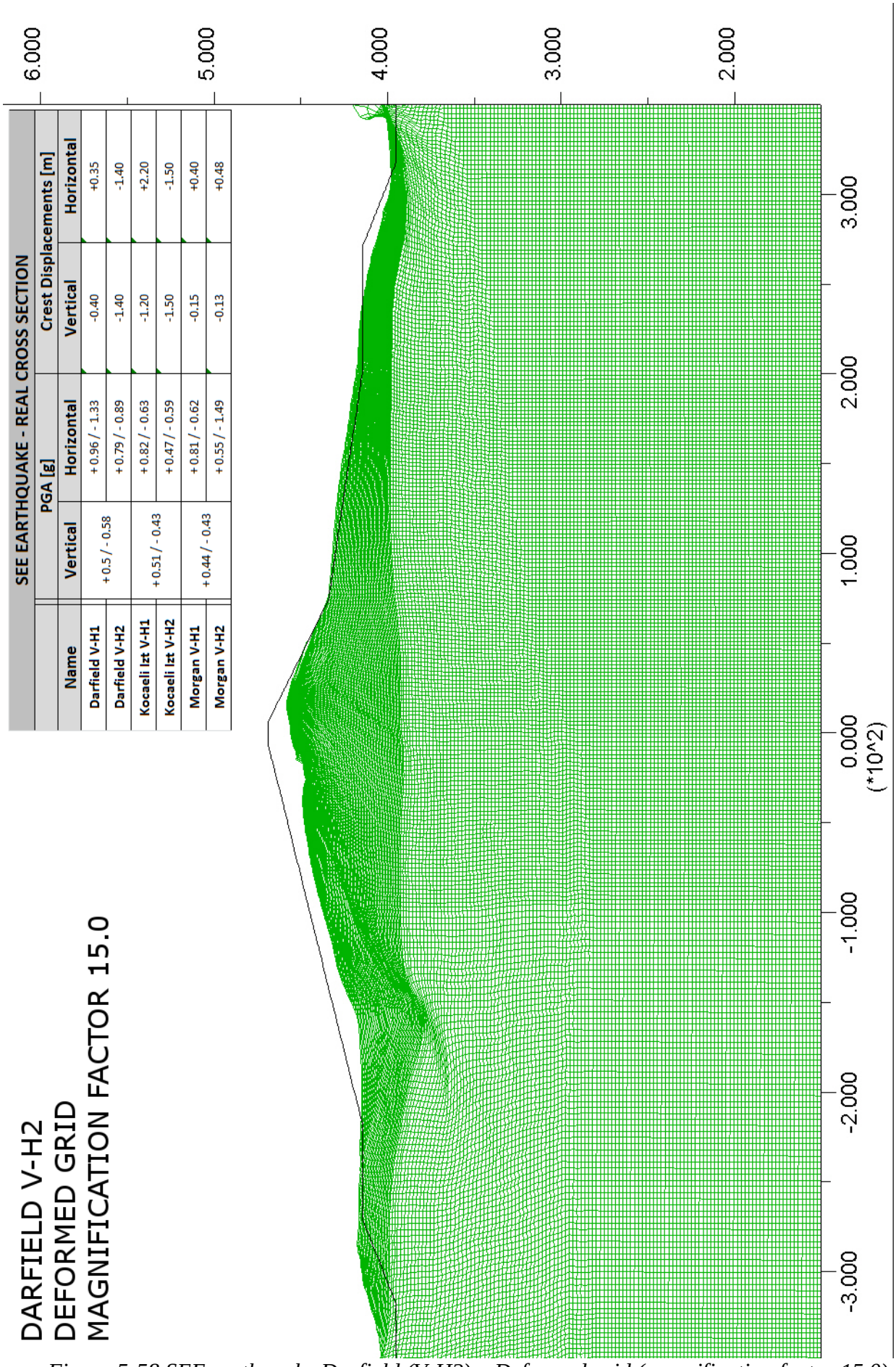

Figure 5-58 SEE earthquake Darfield (V-H2) – Deformed grid (magnification factor 15.0)

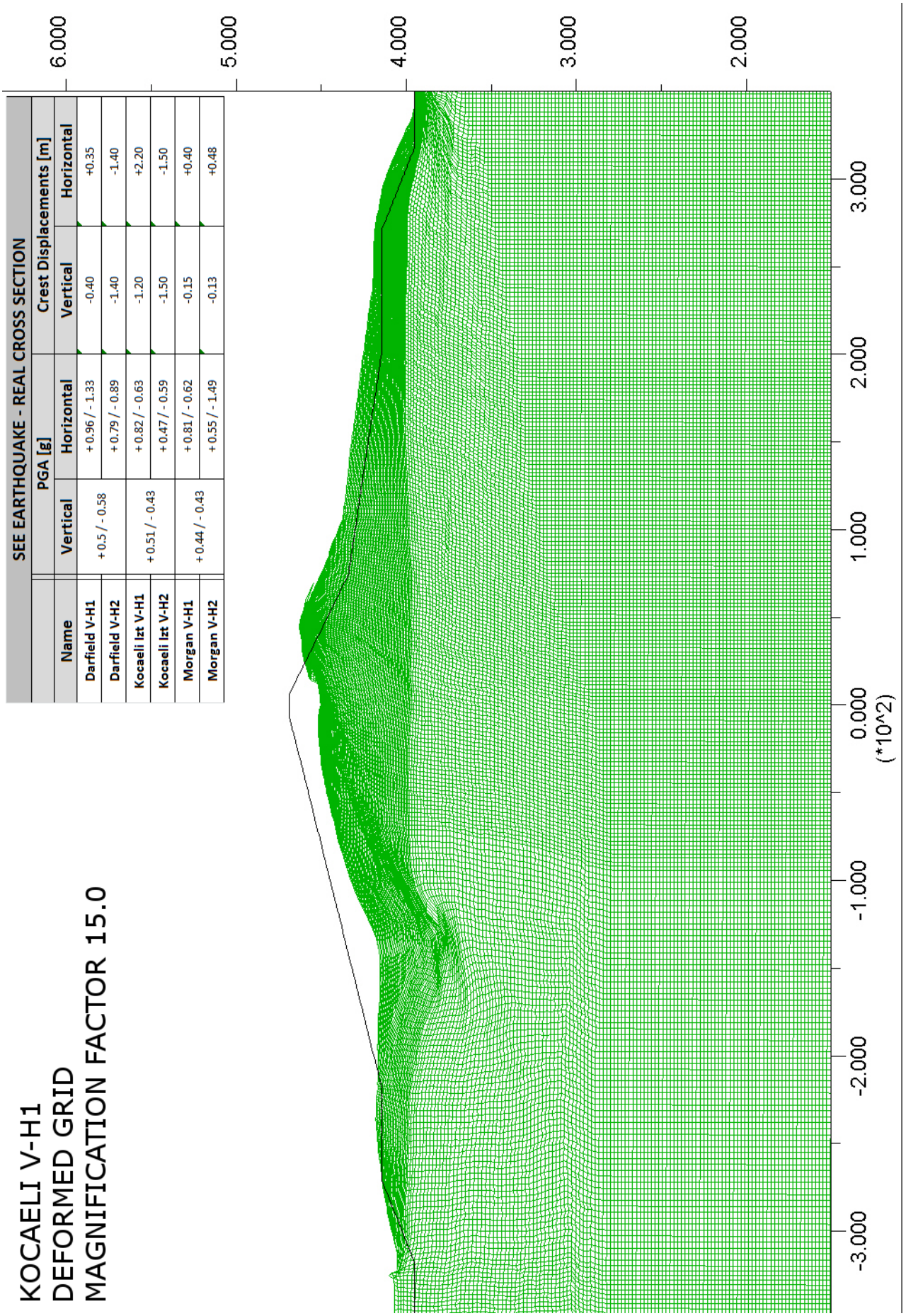

Figure 5-59 SEE earthquake Kocaeli (V-H1) – Deformed grid (magnification factor 15.0)

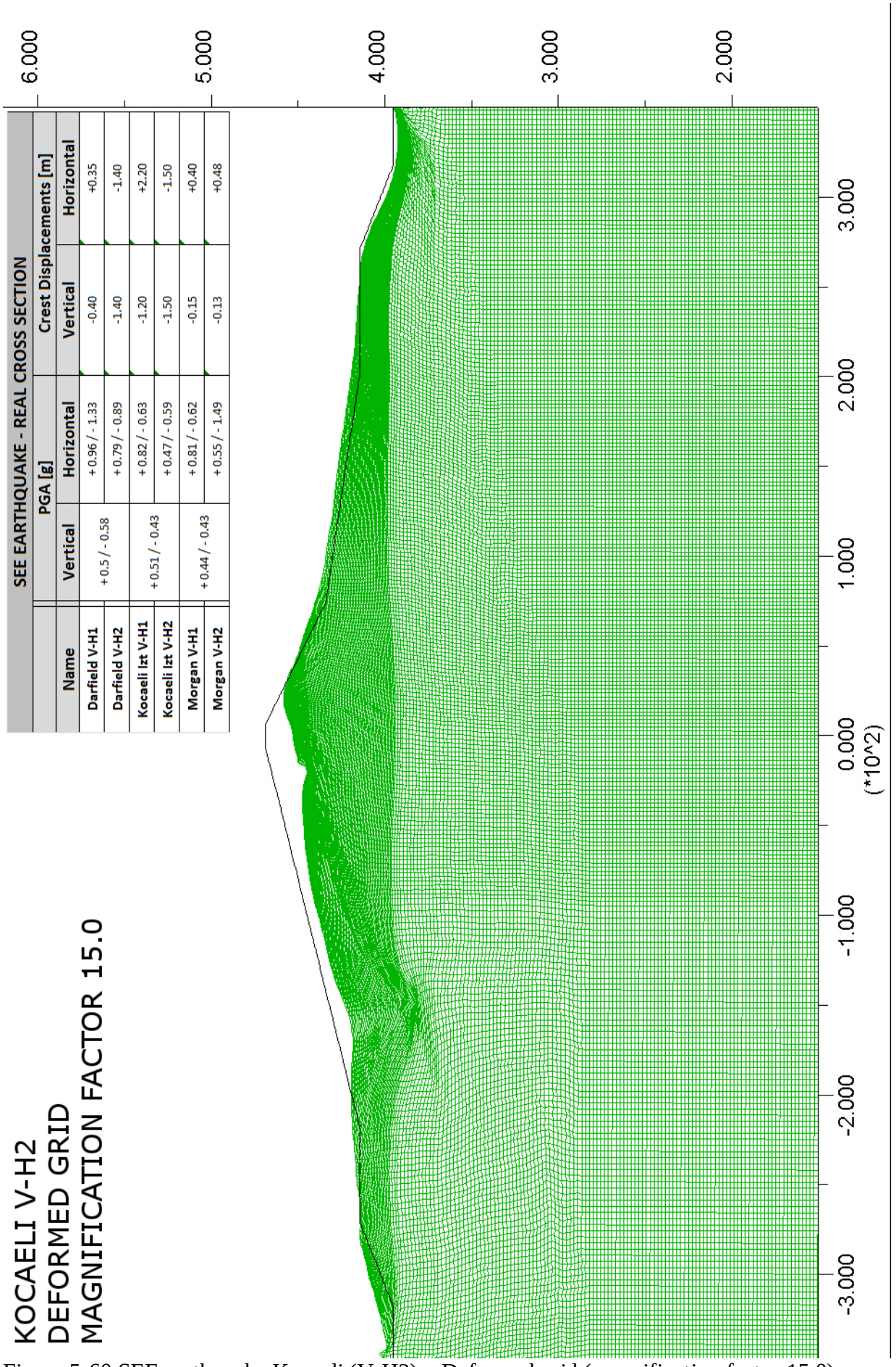

Figure 5-60 SEE earthquake Kocaeli (V-H2) – Deformed grid (magnification factor 15.0)

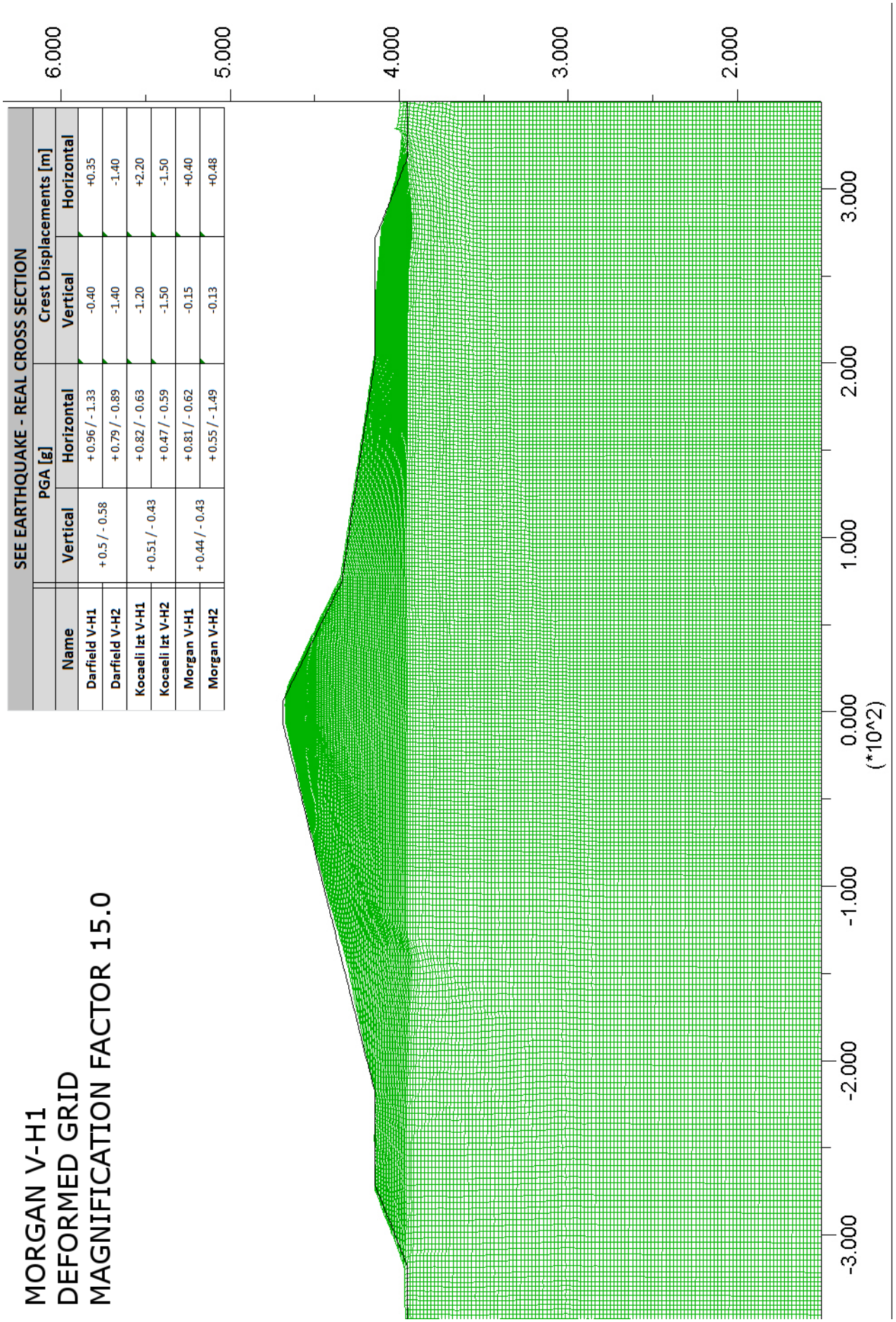

Figure 5-61 SEE earthquake Morgan (V-H1) – Deformed grid (magnification factor 15.0)

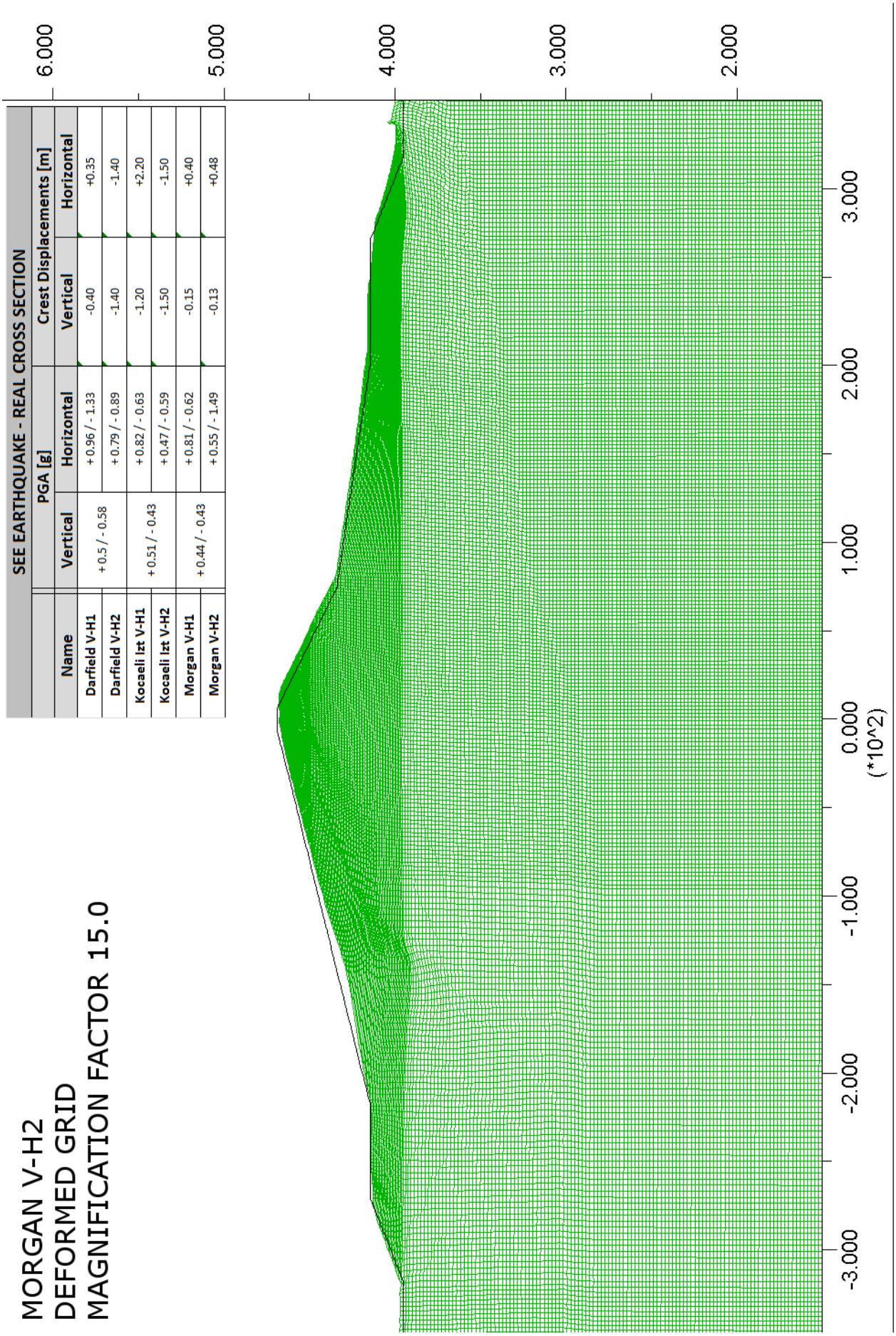

Figure 5-62 SEE earthquake Morgan (V-H2) – Deformed grid (magnification factor 15.0)

5.6.2.1. Dam core stability analysis

Horizontal displacements recorded at points 1 – 4 of Figure 5-63 during the nonlinear dynamic simulation, are analyzed to verify the stability of the dam core.

The same considerations noted for the *Reference Cross Section* case (section 4.6.4.1) are valid in this case.

Relative horizontal displacements at the crest (between points 3 and 4 of Figure 5-63) are in some case around 1.25 meters (e.g. Darfield V-H2, Figure 5-66, Kocaeli V-H1 and V-H2, Figure 5-68 and Figure 5-70).

Relative vertical displacements of about 1.2-1.5 meters, between the lowest and the highest part of the dam core, are observed for the Kocaeli V-H1 and V-H2 earthquakes (Figure 5-69 and Figure 5-71), and for Darfield V-H2 (Figure 5-67).

Relative displacements are generally higher than for the *Reference Cross Section* case.

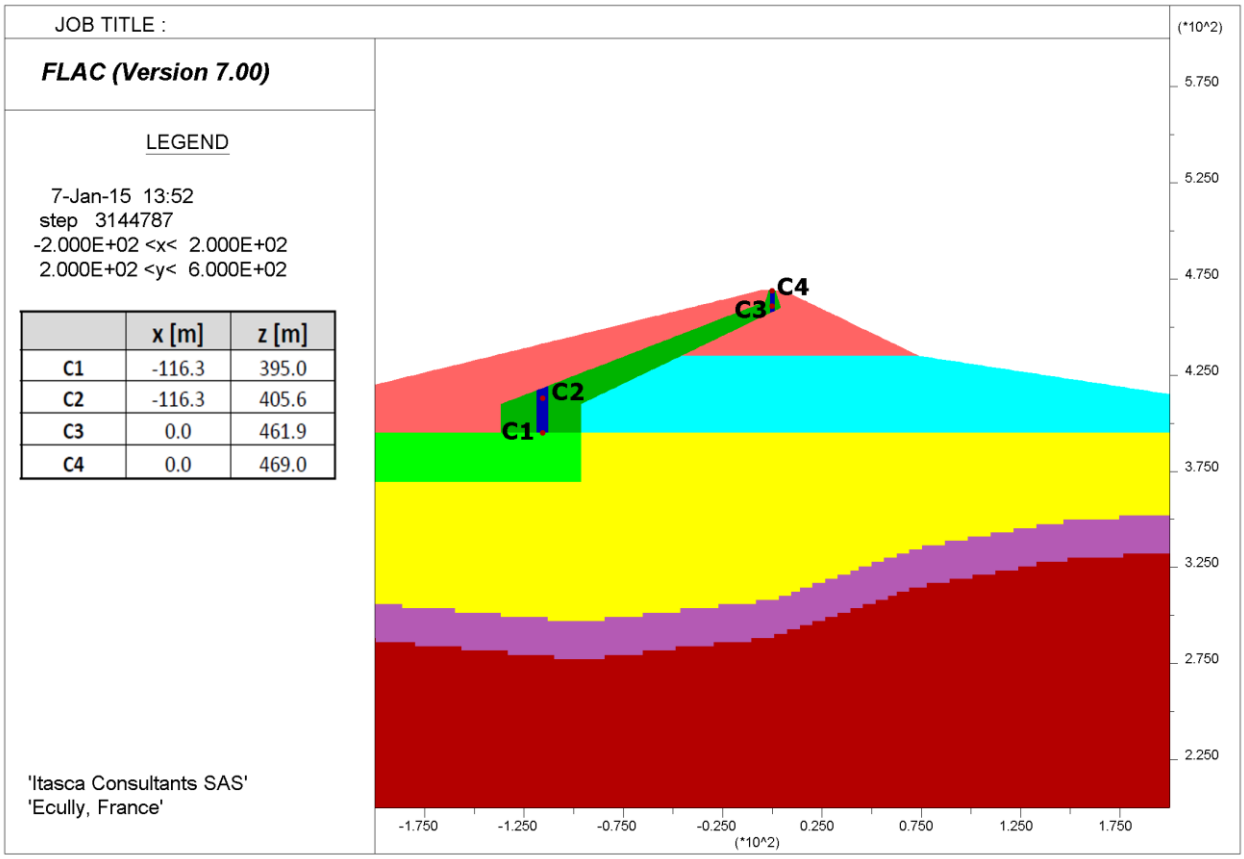

Figure 5-63: virtual points of measurement of displacement for dam core stability analysis

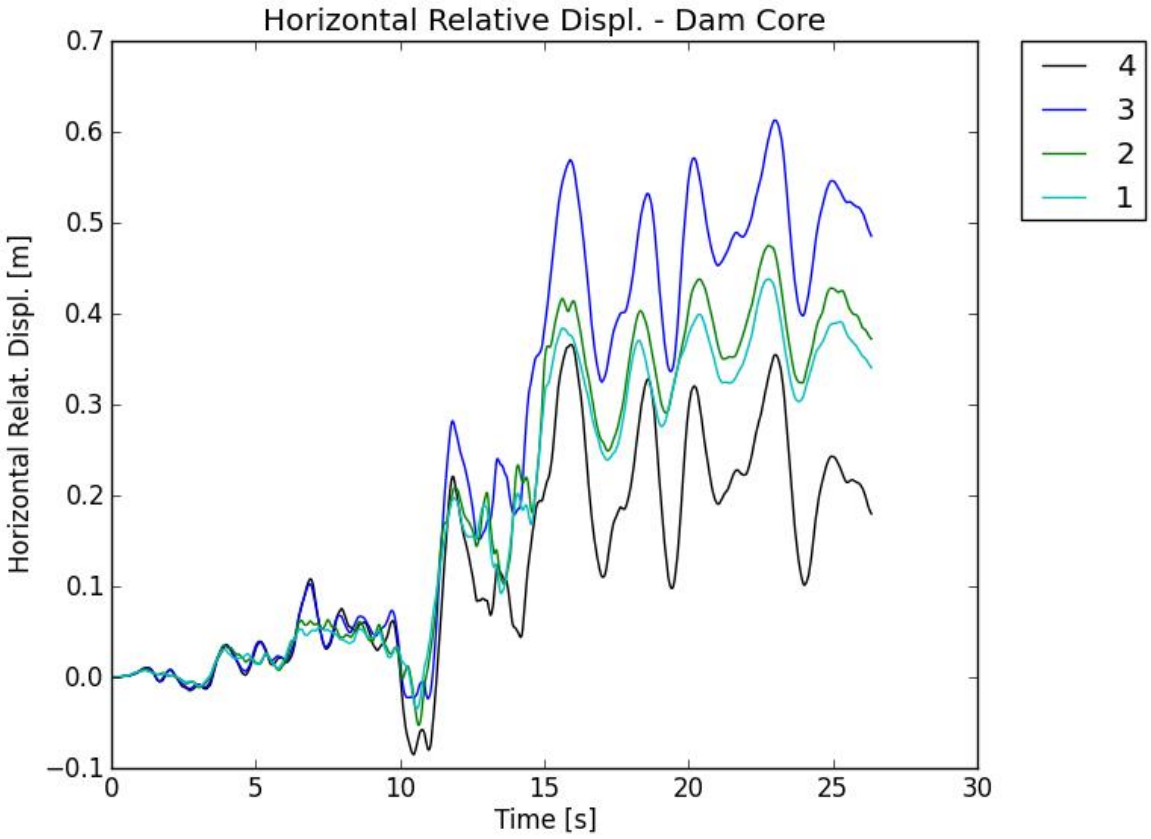

Figure 5-64: Horizontal displacements at points 1 – 4 of Figure 5-63 – SEE Darfield (V-H1)

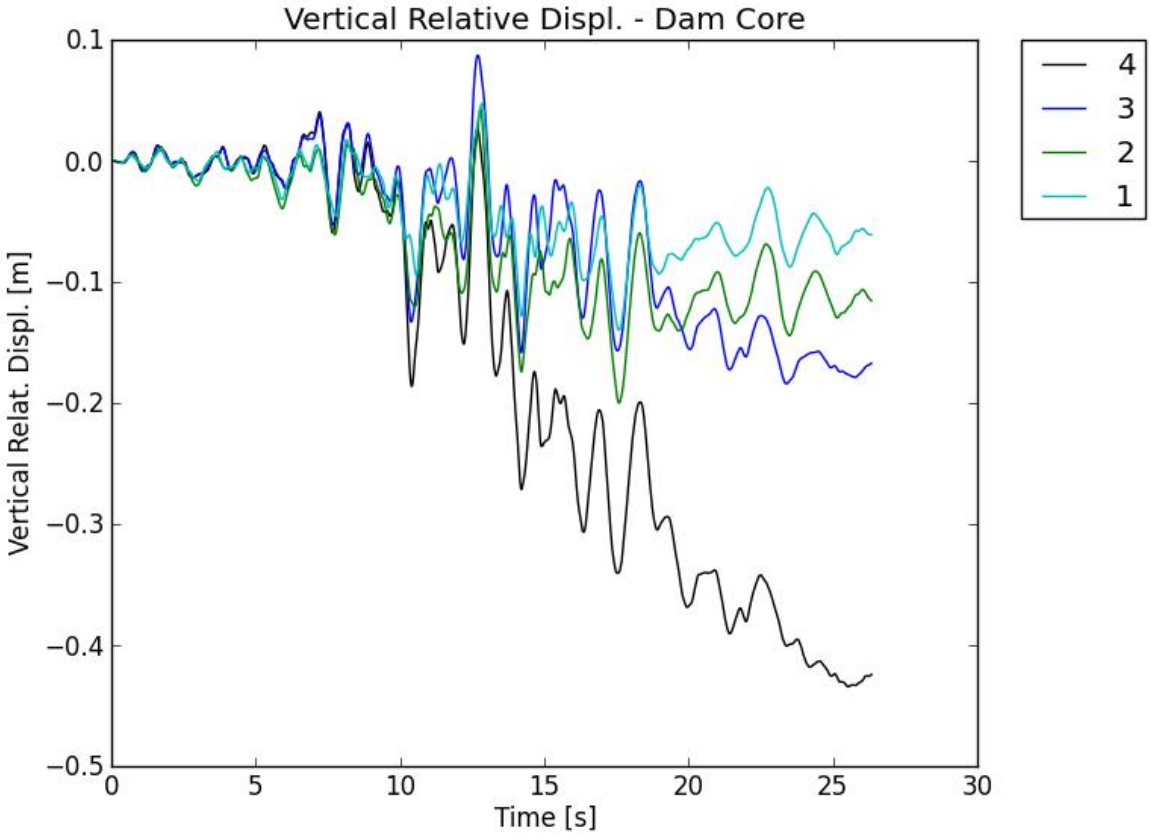

Figure 5-65: Vertical displacements at points 1 – 4 of Figure 5-63 – SEE Darfield (V-H1)

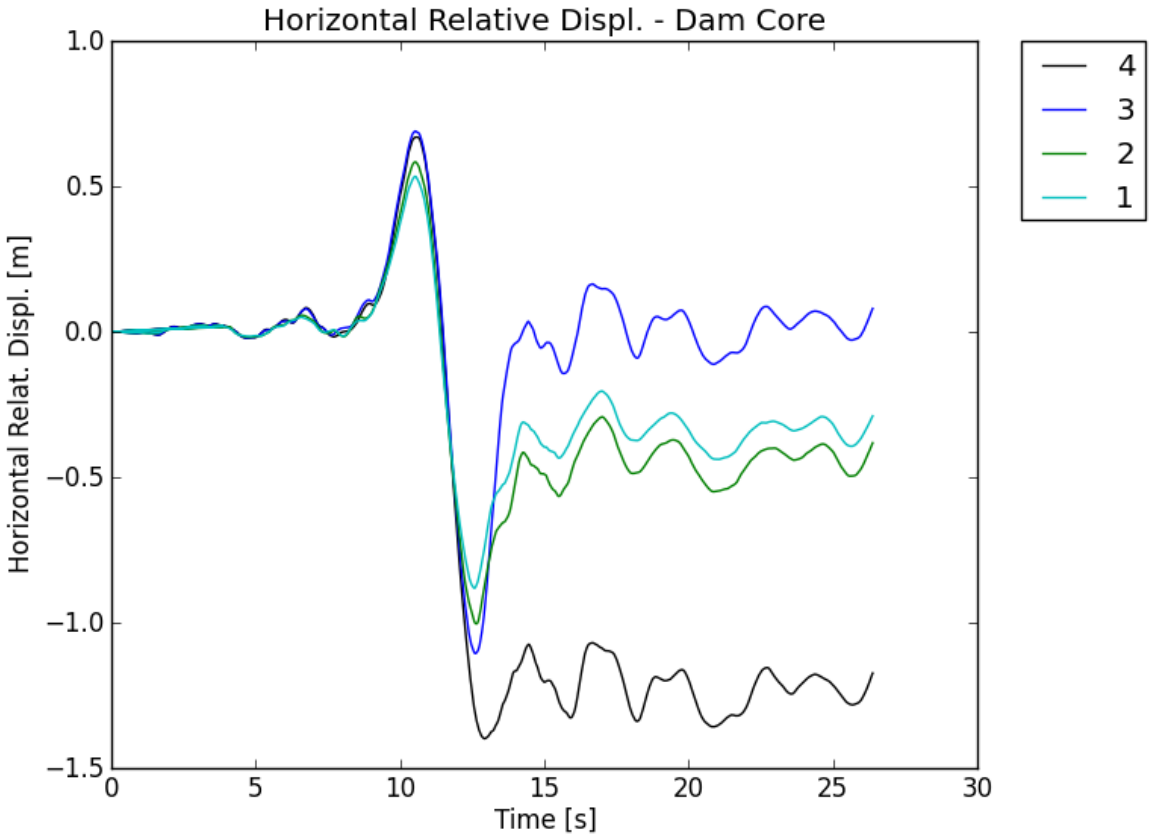

Figure 5-66: Horizontal displacements at points 1 – 4 of Figure 5-63 – SEE Darfield (V-H2)

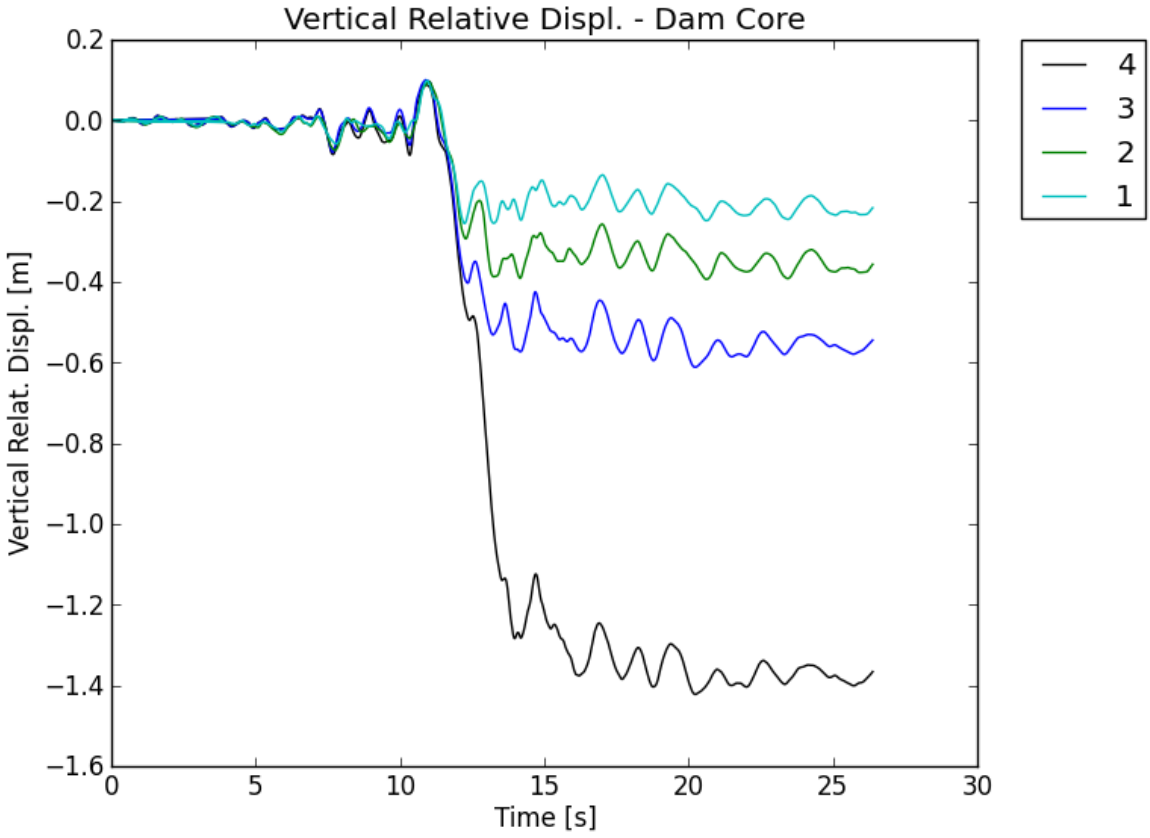

Figure 5-67: Vertical displacements at points 1 – 4 of Figure 5-63 – SEE Darfield (V-H2)

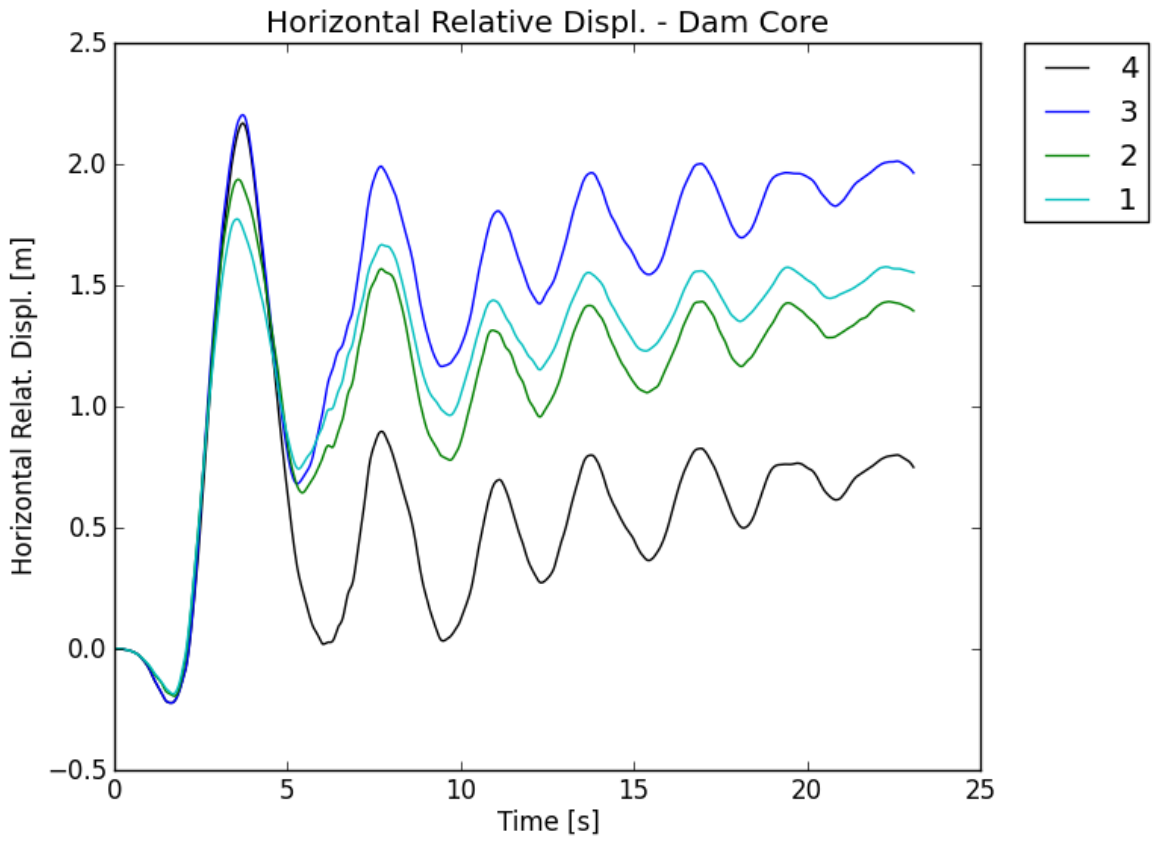

Figure 5-68: Horizontal displacements at points 1 – 4 of Figure 5-63 – SEE Kocaeli (V-H1)

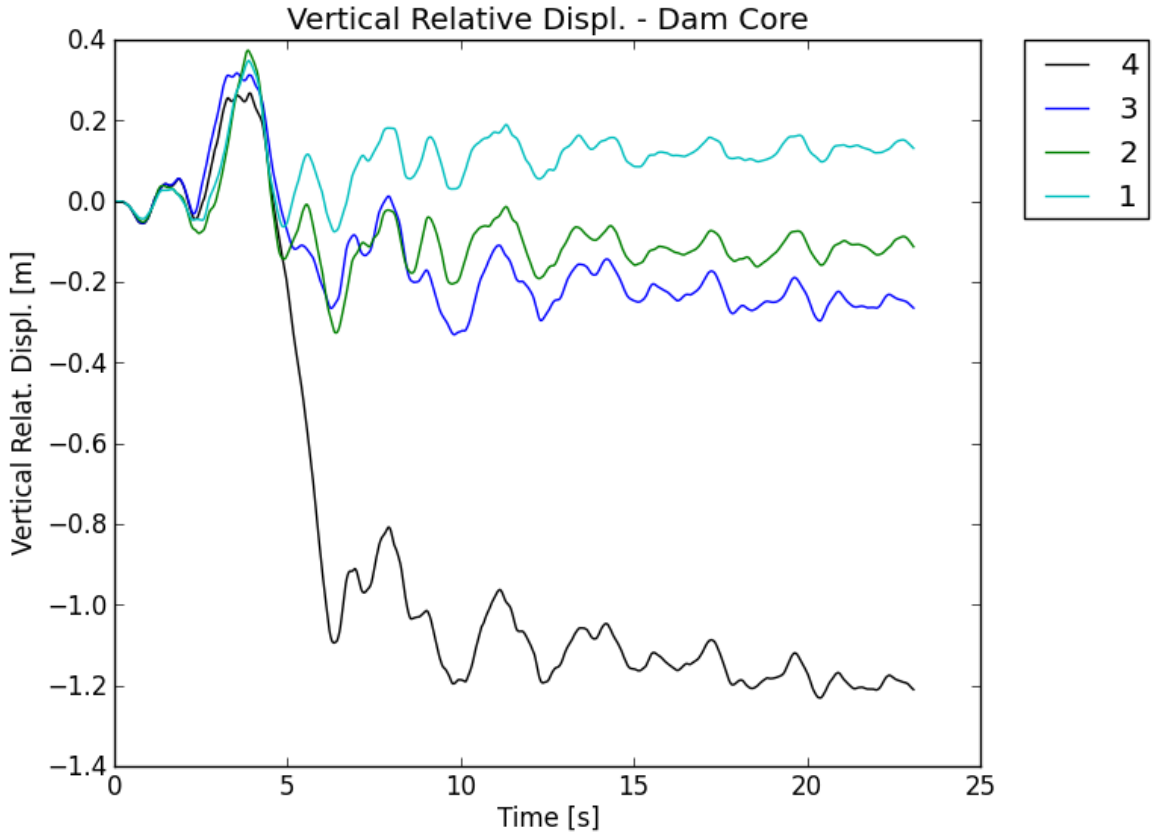

Figure 5-69: Vertical displacements at points 1 – 4 of Figure 5-63 – SEE Kocaeli (V-H1)

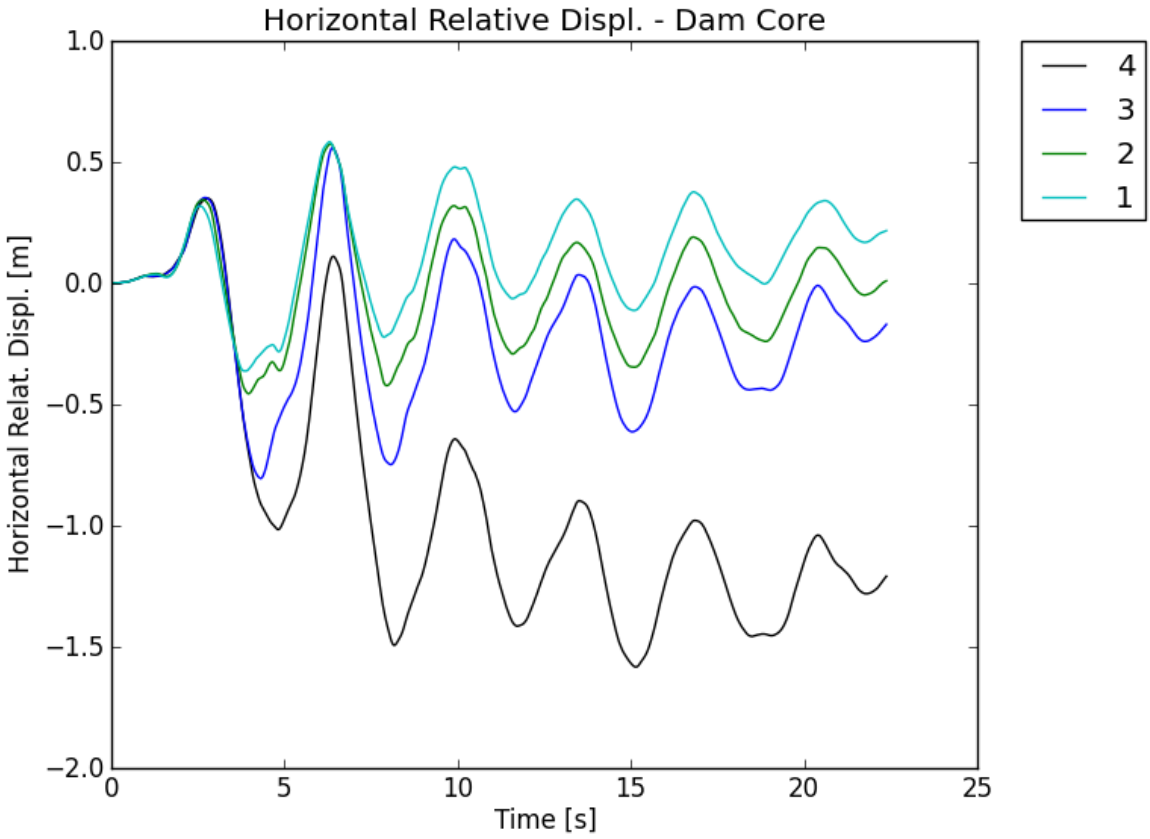

Figure 5-70: Horizontal displacements at points 1 – 4 of Figure 5-63 – SEE Kocaeli (V-H2)

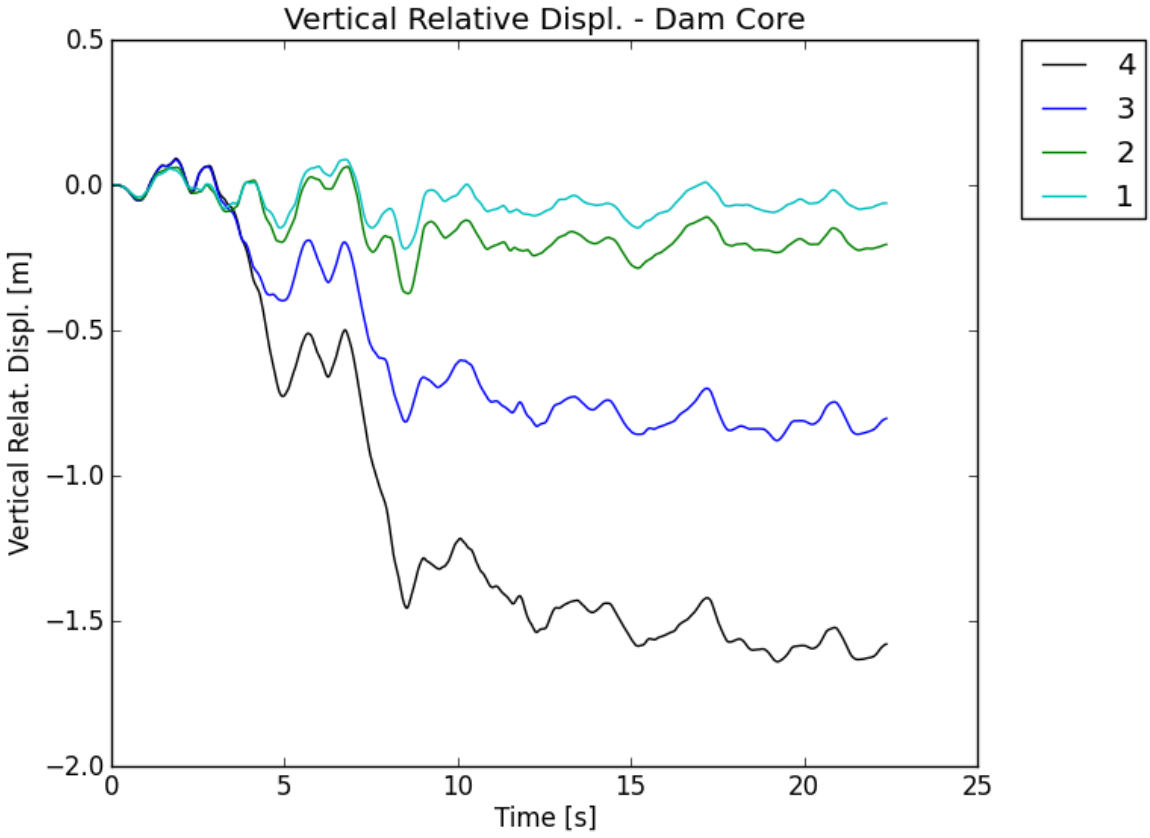

Figure 5-71: Vertical displacements at points 1 – 4 of Figure 5-63 – SEE Kocaeli (V-H2)

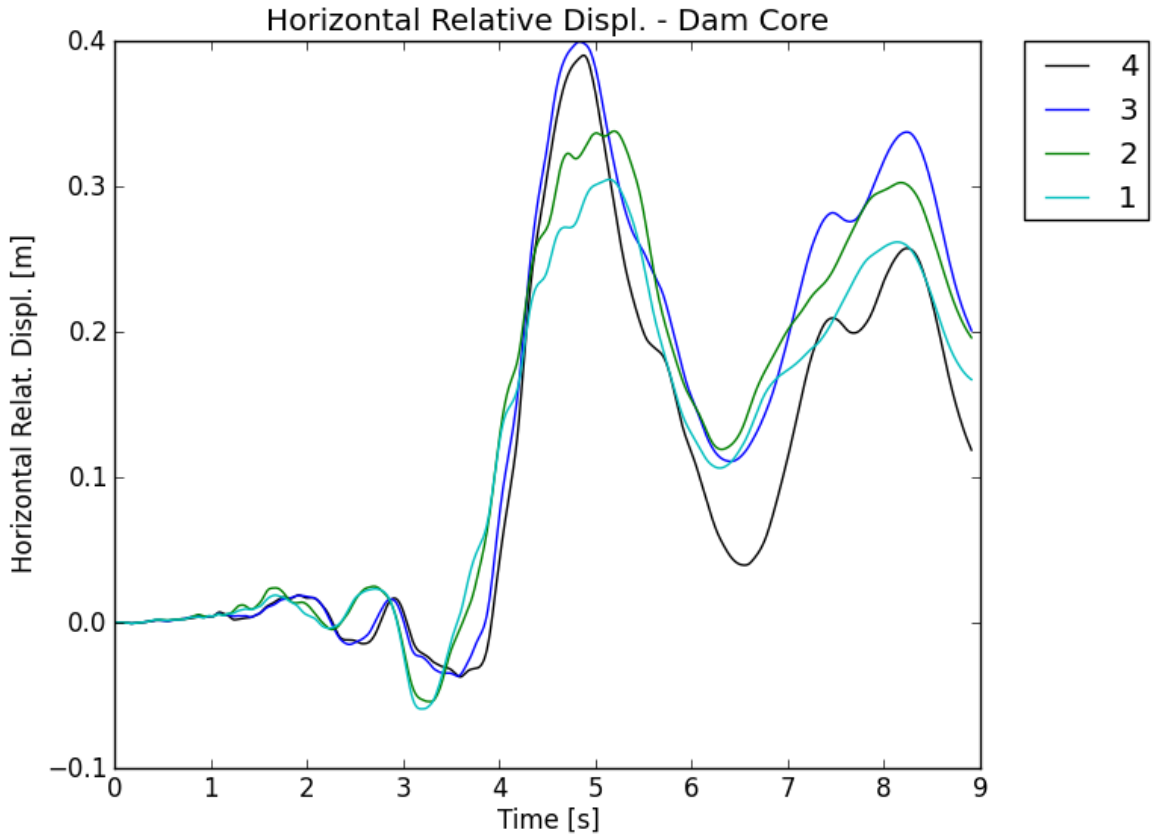

Figure 5-72: Horizontal displacements at points 1 – 4 of Figure 5-63 – SEE Morgan (V-H1)

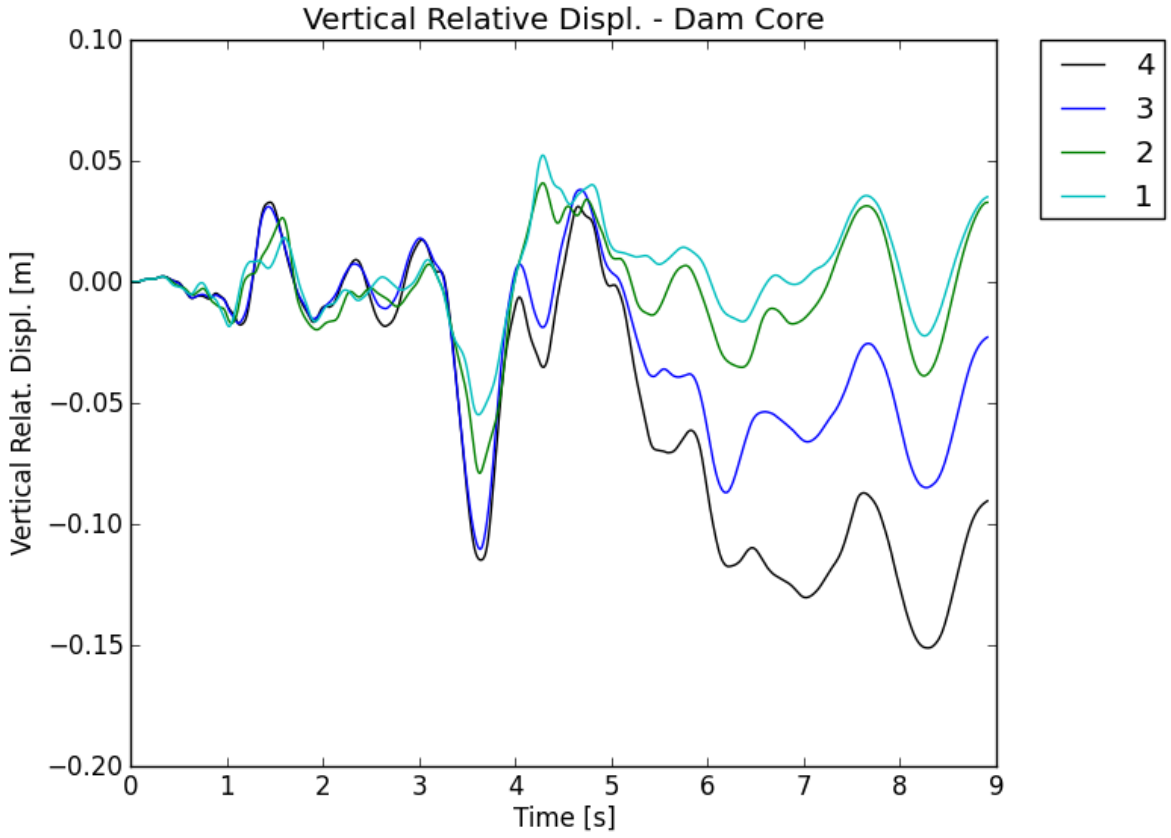

Figure 5-73: Vertical displacements at points 1 – 4 of Figure 5-63 – SEE Morgan (V-H2)

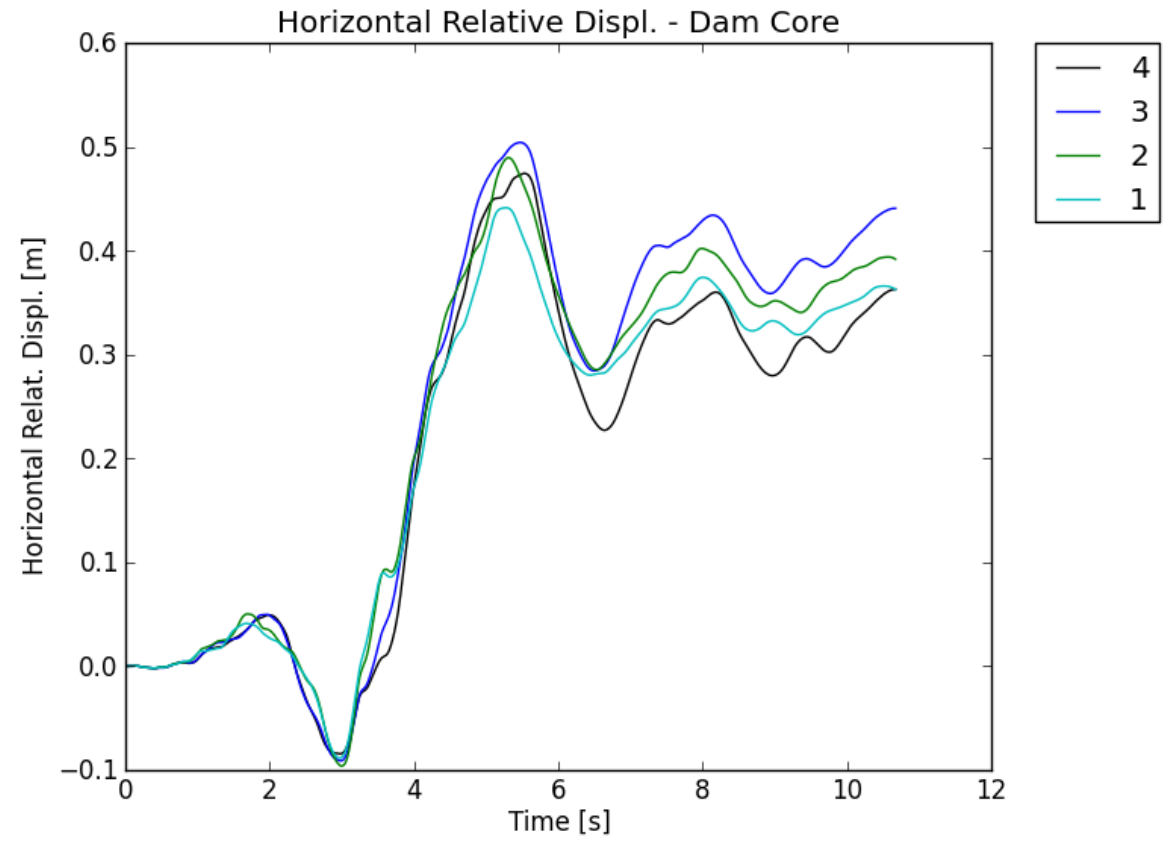

Figure 5-74: Horizontal displacements at points 1 – 4 of Figure 5-63 – SEE Morgan (V-H2)

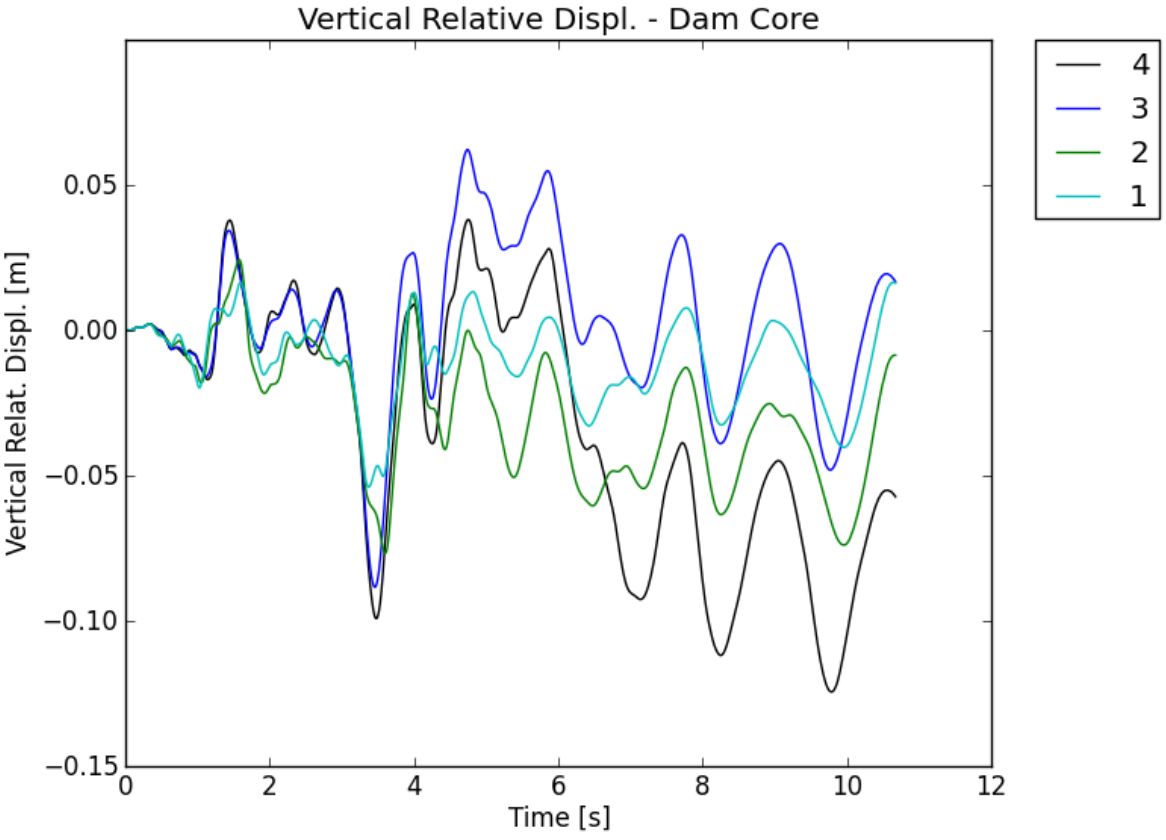

Figure 5-75: Vertical displacements at points 1 – 4 of Figure 5-63 – SEE Morgan (V-H2)

5.6.2.2. Concrete wall stability analysis

The horizontal displacements, as they are recorded at points 1 – 8 of Figure 5-76 during the nonlinear dynamic simulation, are analyzed to verify their compatibility with the stability of the concrete slurry wall that will be installed in that zones. It is recalled that the concrete wall is not directly included into the model.
Table 5-4 summarizes the results obtained. Figure 5-77 to Figure 5-88 show the horizontal and vertical displacements recorded, for all the SEE earthquakes simulated.

The maximum relative horizontal displacement (29cm) is found for the SEE Kocaeli V-H1 (Figure 5-81), over a length of 38 meters , that corresponds to the distance between points 5-8 on Figure 5-76, i.e. the upper part of the concrete wall. The maximum relative displacement was equal to 33cm for the *Reference Cross Section* case.

SEE EARTHQUAKE - CONCRETE SLURRY WALL DISPLACEMENTS				
	PGA [g]		Relative Displacement [m]	Length [m]
Name	Vertical	Horizontal	Horizontal	
Darfield V-H1	+ 0.5 / - 0.58	+ 0.96 / - 1.33	0.08	38m (points 5 - 8)
Darfield V-H2		+ 0.79 / - 0.89	0.13	38m (points 5 - 8)
Kocaeli Izt V-H1	+ 0.51 / - 0.43	+ 0.82 / - 0.63	0.29	38m (points 5 - 8)
Kocaeli Izt V-H2		+ 0.47 / - 0.59	0.12	38m (points 5 - 8)
Morgan V-H1	+ 0.44 / - 0.43	+ 0.81 / - 0.62	0.08	38m (points 5 - 8)
Morgan V-H2		+ 0.55 / - 1.49	0.06	38m (points 5 - 8)

Table 5-4 : SEE earthquakes, nonlinear analysis - Concrete wall relative horizontal displacements

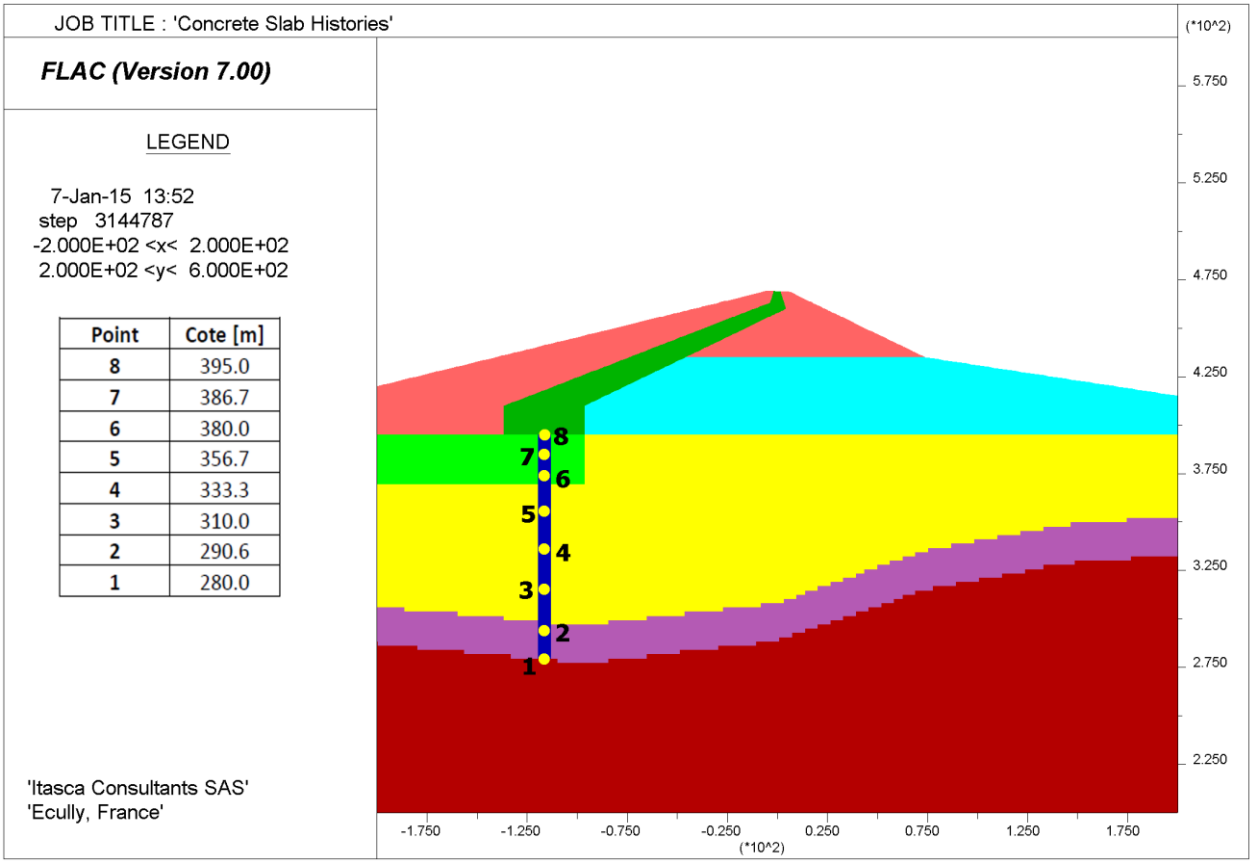

Figure 5-76: virtual points of measurement of displacement (concrete wall is not modeled)

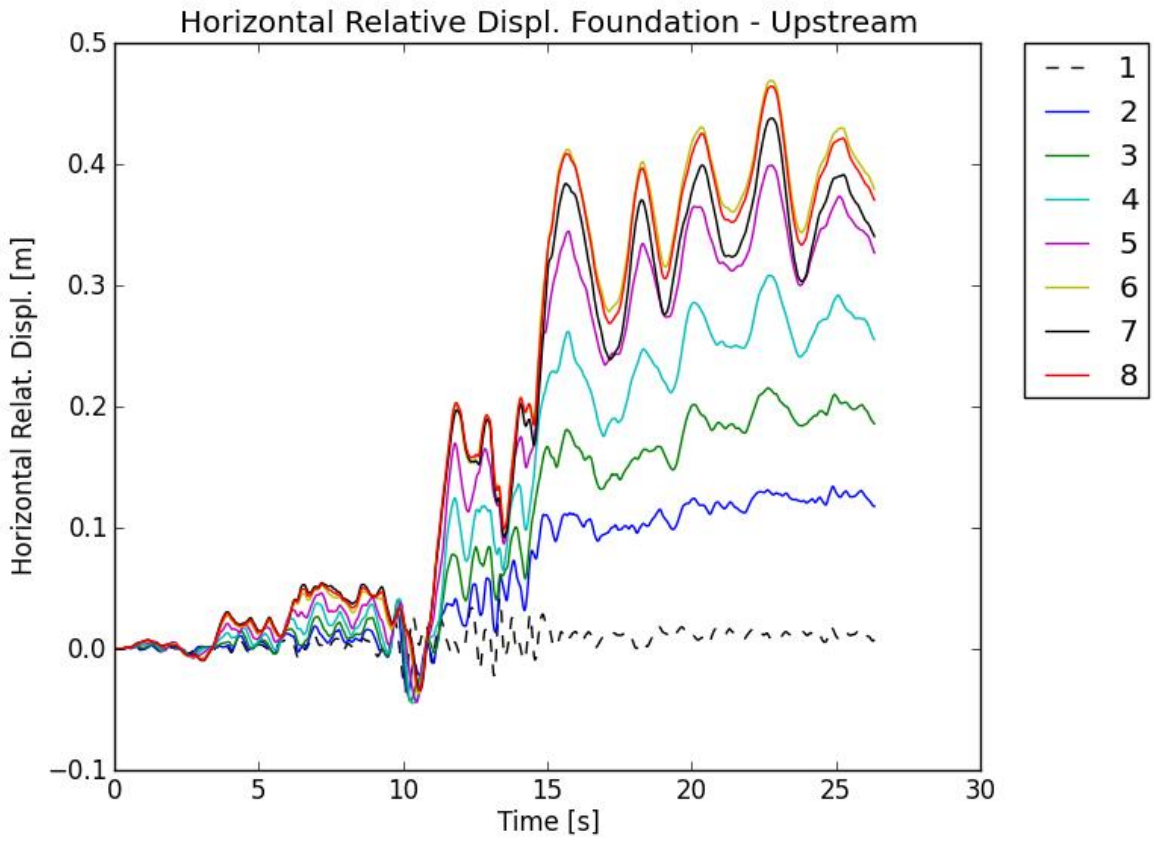

Figure 5-77: Horizontal displacements at points 1 – 8 of Figure 5-76 – SEE Darfield (V-H1)

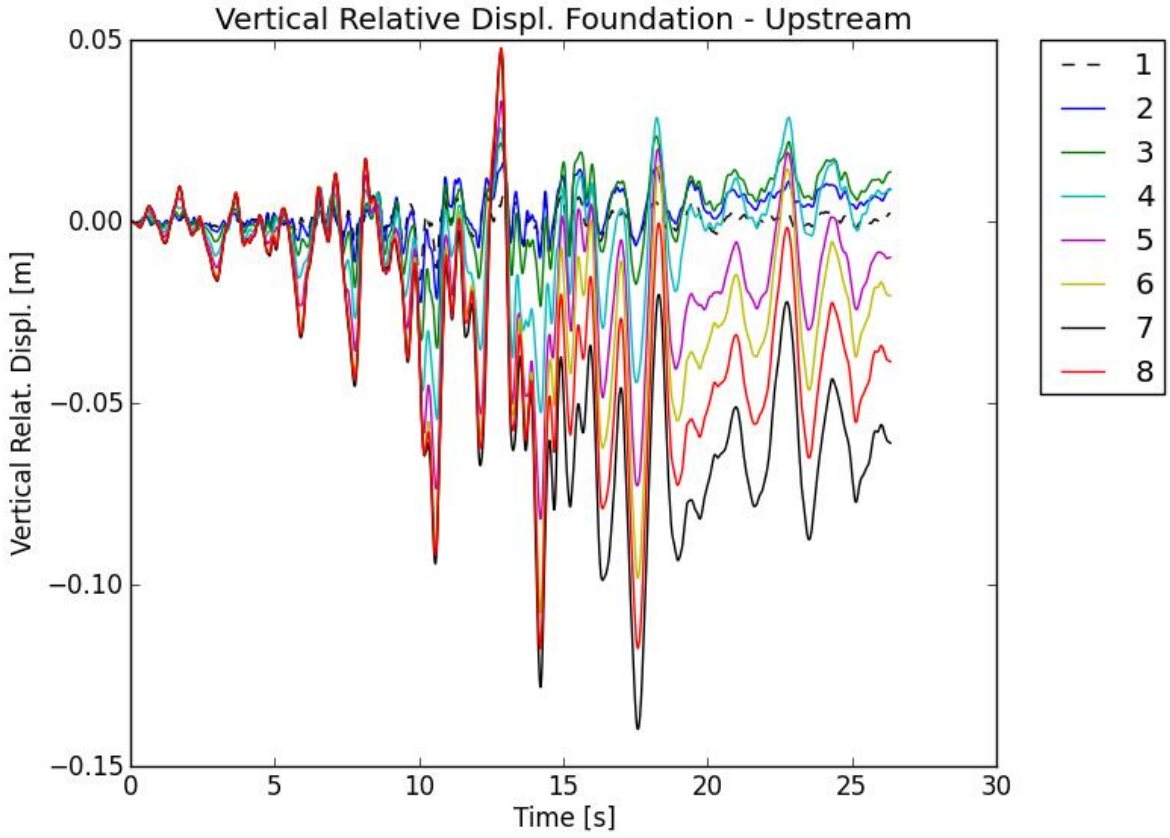

Figure 5-78: Vertical displacements at points 1 – 8 of Figure 5-76 – SEE Darfield (V-H1)

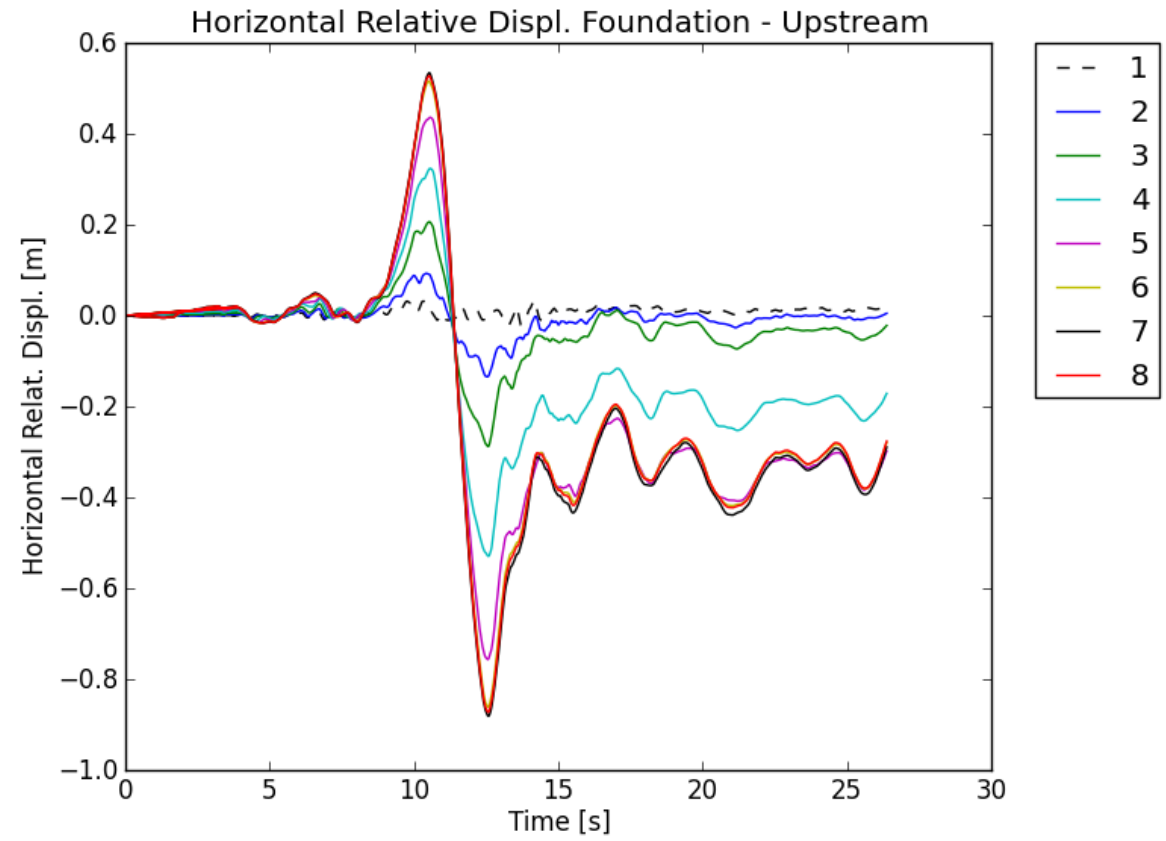

Figure 5-79: Horizontal displacements at points 1 – 8 of Figure 5-76 – SEE Darfield (V-H2)

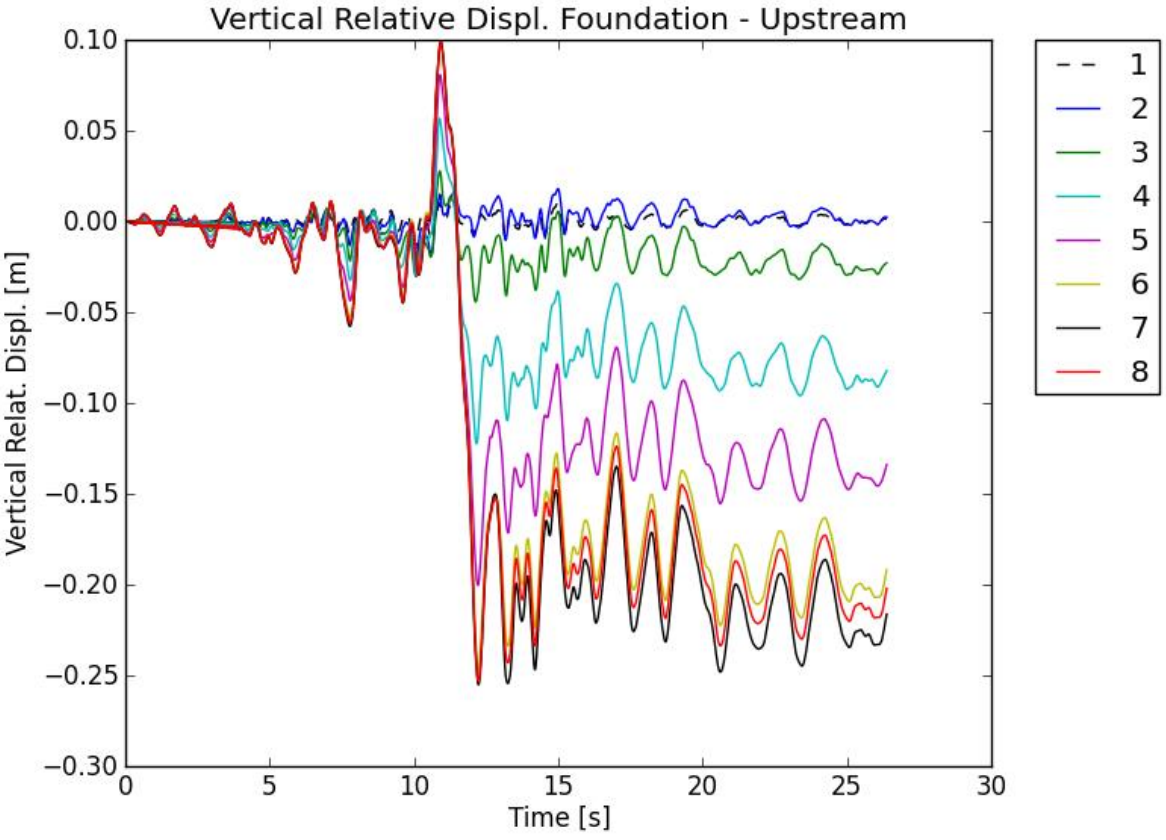

Figure 5-80: Vertical displacements at points 1 – 8 of Figure 5-76 – SEE Darfield (V-H2)

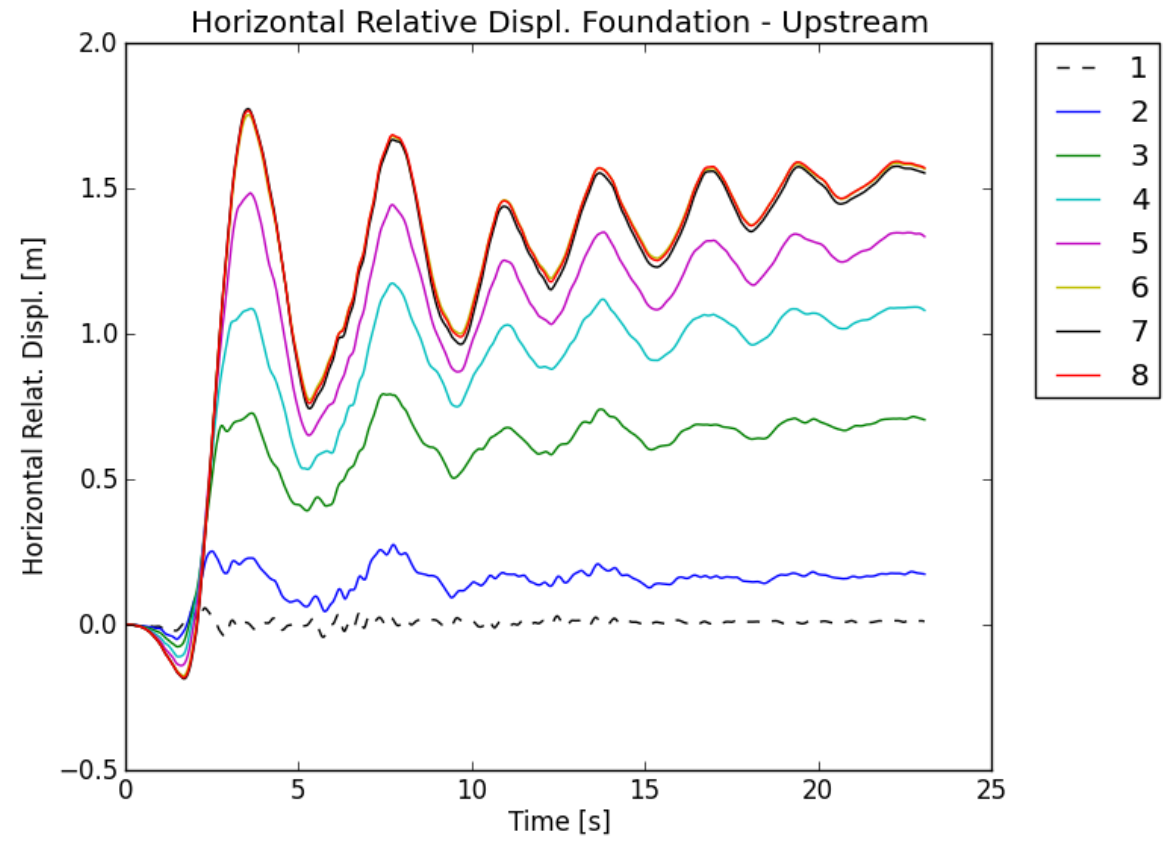

Figure 5-81: Horizontal displacements at points 1 – 8 of Figure 5-76 – SEE Kocaeli (V-H1)

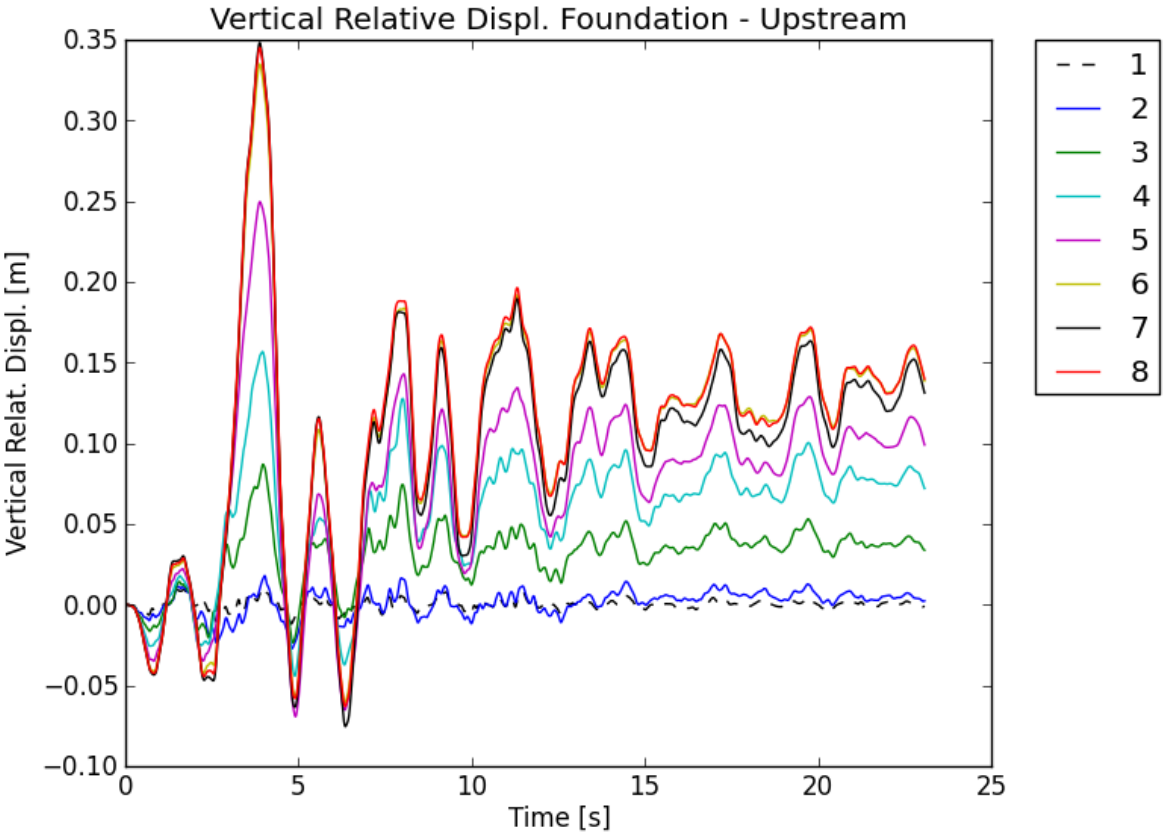

Figure 5-82: Vertical displacements at points 1 – 8 of Figure 5-76 – SEE Kocaeli (V-H1)

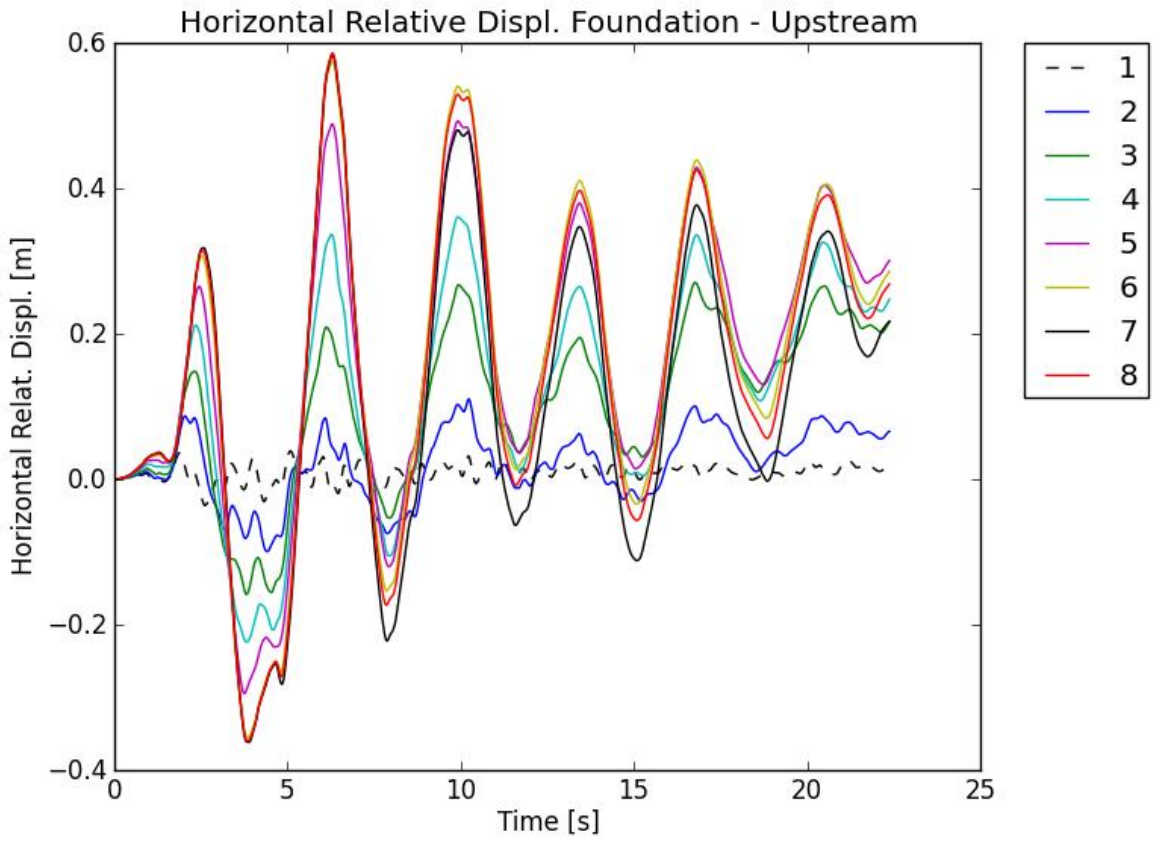

Figure 5-83: Horizontal displacements at points 1 – 8 of Figure 5-76 – SEE Kocaeli (V-H2)

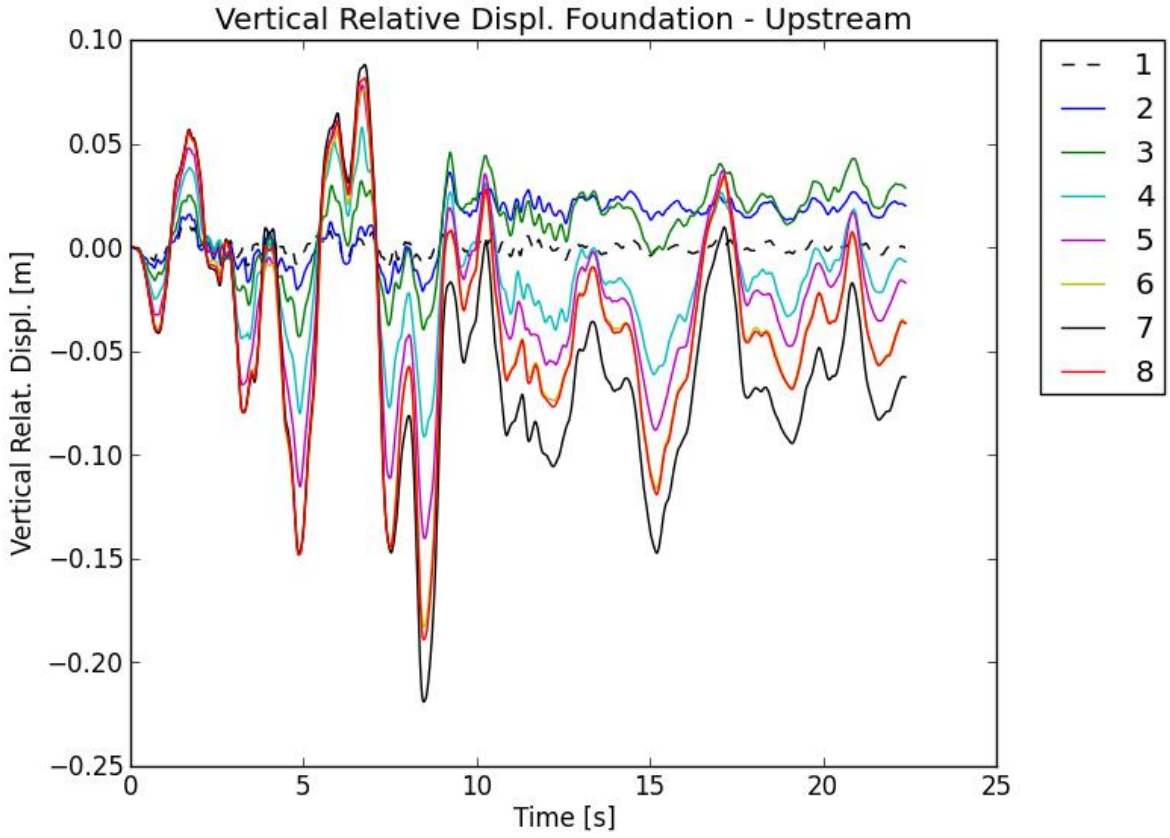

Figure 5-84: Vertical displacements at points 1 – 8 of Figure 5-76 – SEE Kocaeli (V-H2)

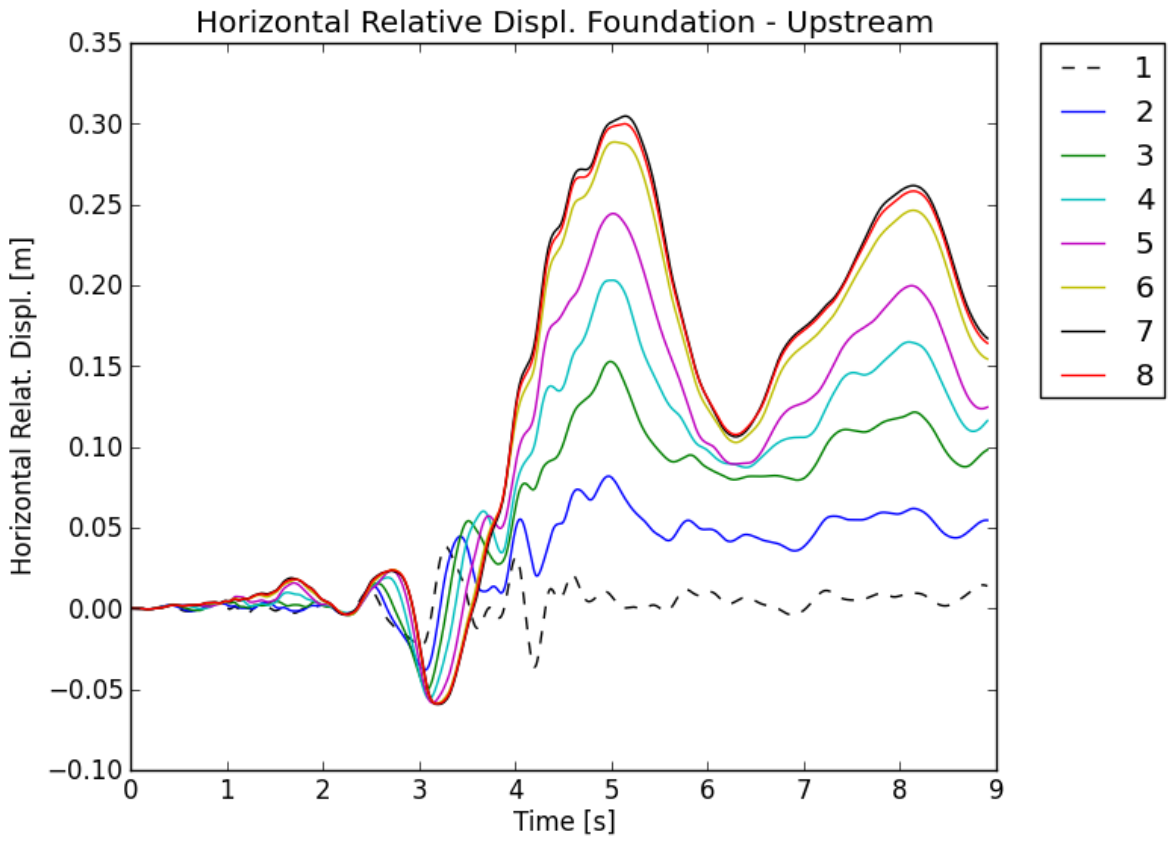

Figure 5-85: Horizontal displacements at points 1 – 8 of Figure 5-76 – SEE Morgan (V-H1)

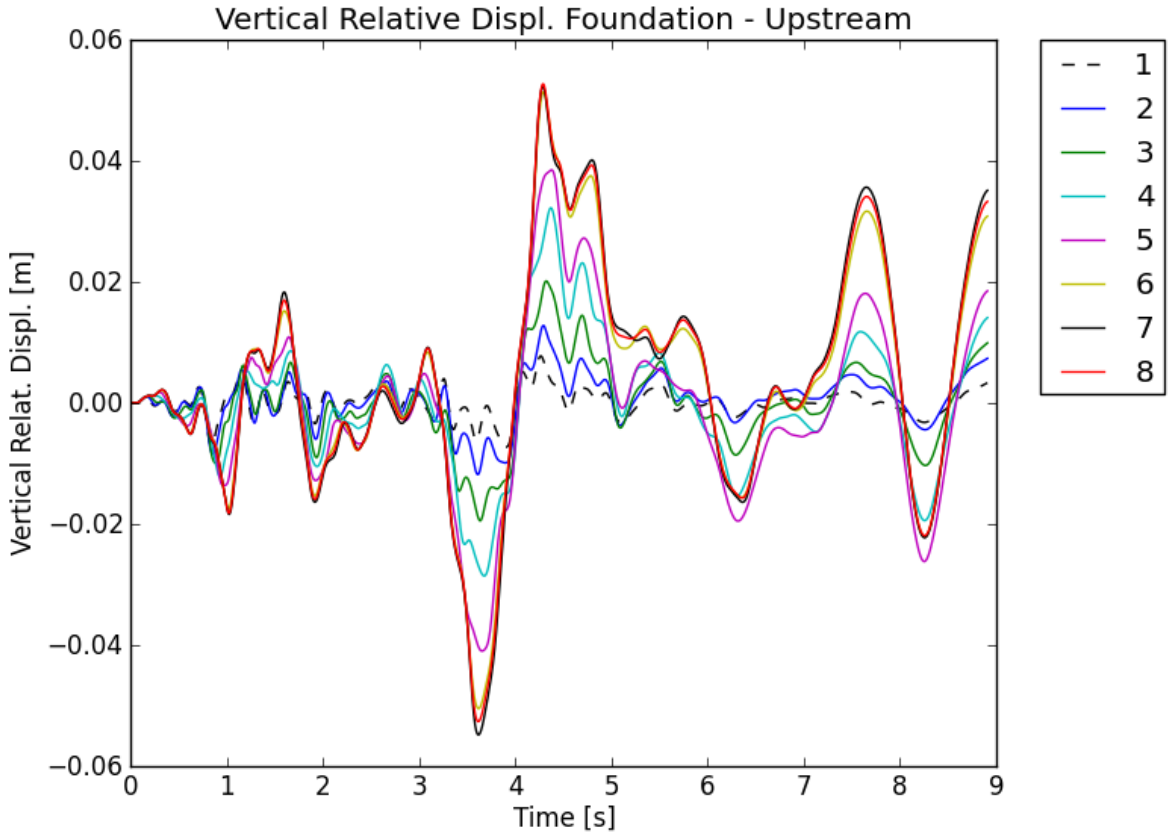

Figure 5-86: Vertical displacements at points 1 – 8 of Figure 5-76 – SEE Morgan (V-H1)

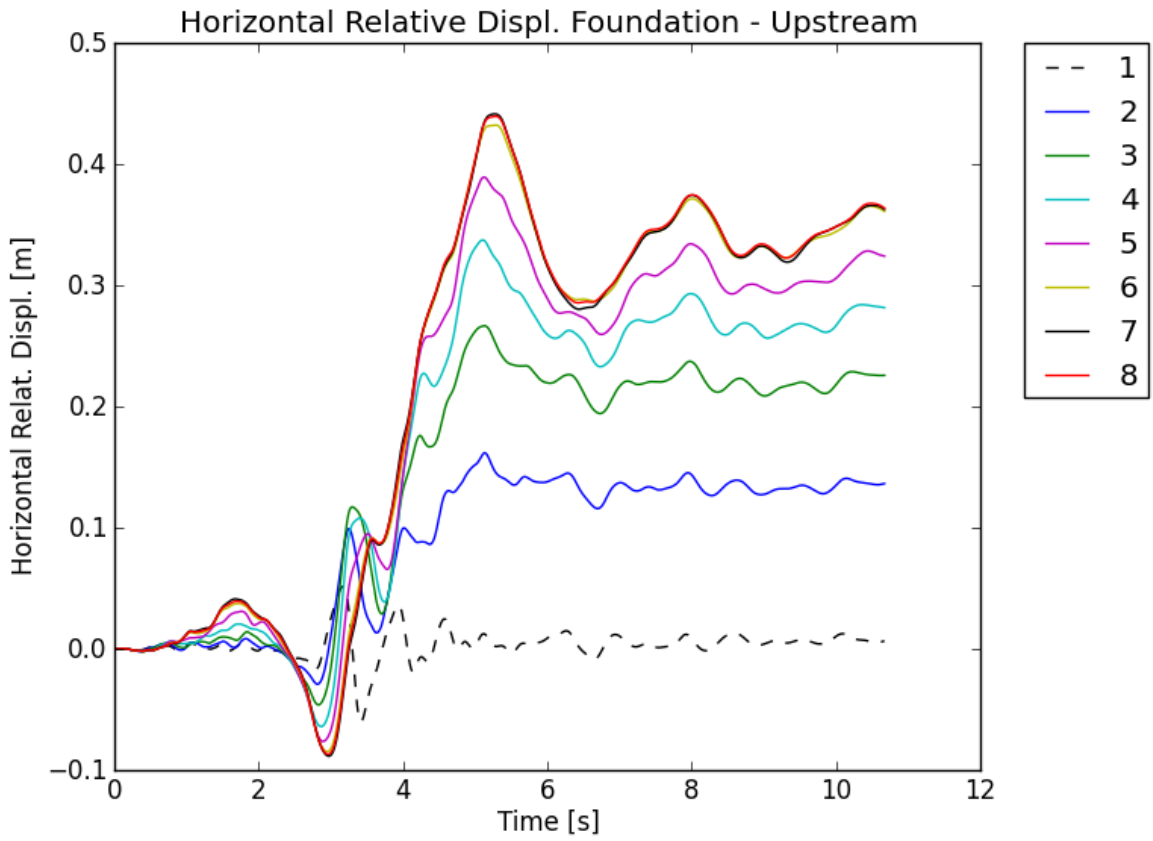

Figure 5-87: Horizontal displacements at points 1 – 8 of Figure 5-76 – SEE Morgan (V-H2)

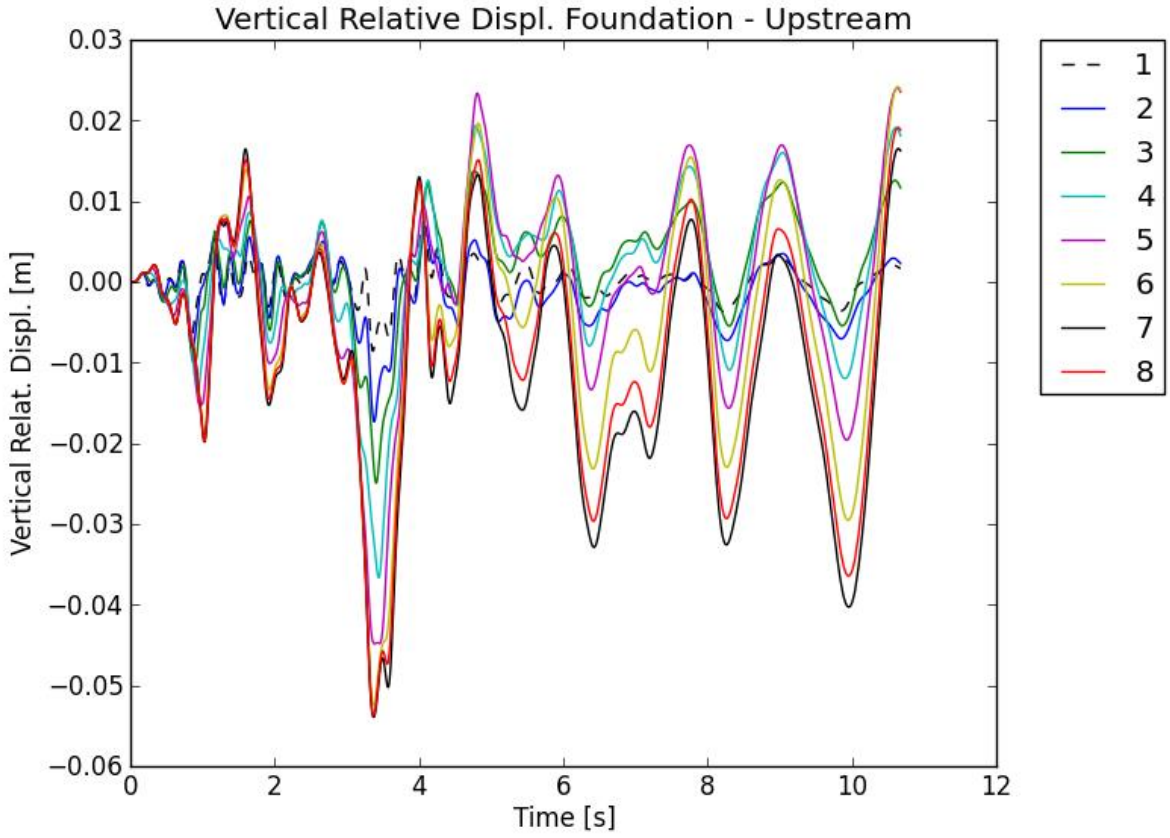

Figure 5-88: Vertical displacements at points 1 – 8 of Figure 5-76 – SEE Morgan (V-H2)

5.7. Conclusions

Tables that summarize the maximum displacement are represented below.

Table 5-5 summarizes the results of the pseudo-static Newmark's Sliding Block analysis for the SEE earthquakes. Results are commented in section 5.6.1.

Table 5-6 summarizes the results of the nonlinear dynamic analysis considering the SEE earthquakes, commented in section 5.6.2. The analysis of relative horizontal displacements on the concrete slurry wall is presented in section 5.6.2.2 and summarized in Table 5-7.

The dynamic analysis for the *Real Cross Section* confirms the results obtained for the *Reference Cross Section* case. The most problematic zone is confirmed to be the upstream slope, which slides along the interface between the rockfill and the dam core.

For all the tested cases, the maximum vertical displacement at the crest of the dam is far below the maximum admissible displacement, equal to 4 meters, as indicated by NOVEC.

SEE EARTHQUAKE - KOCAELI IZT V-H1				
			Pseudo-static Analysis	
Cross Section	Analysis		Kh [g]	Max Displacement
Reference CS	Downstream		0.17	> 9 m
	Upstream		-0.16	> 4 m
Real CS	Downstream		0.19	> 7 m
	Upstream		-0.12	> 5 m

Table 5-5 : Pseudo-static analysis – Summary of results

SEE EARTHQUAKE - REAL CROSS SECTION					
		PGA [g]		Max Crest Displacements [m]	
Name		Vertical	Horizontal	Vertical	Horizontal
Darfield V-H1		+ 0.5 / - 0.58	+ 0.96 / - 1.33	-0.40	+0.35
Darfield V-H2			+ 0.79 / - 0.89	-1.40	-1.40
Kocaeli Izt V-H1		+ 0.51 / - 0.43	+ 0.82 / - 0.63	-1.20	+2.20
Kocaeli Izt V-H2			+ 0.47 / - 0.59	-1.50	-1.50
Morgan V-H1		+ 0.44 / - 0.43	+ 0.81 / - 0.62	-0.15	+0.40
Morgan V-H2			+ 0.55 / - 1.49	-0.13	+0.48

Table 5-6 : SEE earthquakes – Maximum crest displacements – Real Cross Section

SEE EARTHQUAKE - CONCRETE SLURRY WALL DISPLACEMENTS				
	PGA [g]		Relative Displacement [m]	Length [m]
Name	Vertical	Horizontal	Horizontal	
Darfield V-H1	+ 0.5 / - 0.58	+ 0.96 / - 1.33	0.45	105 (points 1 - 6)
Darfield V-H2		+ 0.79 / - 0.89	0.9	105 (points 1 - 6)
Kocaeli Izt V-H1	+ 0.51 / - 0.43	+ 0.82 / - 0.63	1.75	105 (points 1 - 6)
Kocaeli Izt V-H2		+ 0.47 / - 0.59	0.58	105 (points 1 - 6)
Morgan V-H1	+ 0.44 / - 0.43	+ 0.81 / - 0.62	0.3	105 (points 1 - 6)
Morgan V-H2		+ 0.55 / - 1.49	0.05	105 (points 1 - 6)

Table 5-7 : SEE earthquakes, nonlinear analysis - Concrete wall relative horizontal displacements

6. CONCLUSIONS

6.1. Construction of the embankment

Concerning the simulation of the construction of the embankment, the following conclusions can be formulated:

- **The maximum vertical displacement** at the base of the embankment is of **1.25 meters**, for both cross sections. It is worth noting that the soil is assumed to be **consolidated** prior to the construction of the embankment. The weight of the construction increases the confinement stress, resulting in an improvement of the deformability properties of the soil foundation materials (bulk and shear moduli are function of confinement stress). The vertical displacement are therefore under estimated;
- The sequence of construction of the embankment allows the **limitation of horizontal displacements** at the level of the **concrete slurry wall**. In fact, most displacements occur in the phase before the concrete wall installation. Later relative horizontal displacements reach **35 cm** over a length of more than 100 meters for the *Reference Cross Section* case, and **25 cm** centimeters over a length of more than 100 meters for the *Real Cross Section* case. **The stability of the concrete wall is ensured** at this stage;

6.2. Dynamic analysis

Concerning the nonlinear dynamic analysis, the following conclusions can be formulated:

- The **linear analysis** (Operating Basis Earthquake) for the *Reference Cross Section* case allowed the identification of **potentially instable zones** under seismic loading: these are the embankment feet, upstream and downstream, the crest, and the upstream slope.
- The **nonlinear analysis** (Operating Basis Earthquake) for the *Reference Cross Section* case confirmed the indications of the linear analysis. Displacements in all the tested cases are below any warning level;
- A **pseudo-static Newmark's Sliding Block analysis** (Safety Evaluation Earthquake) was performed for both the *Reference Cross Section* case and the *Real Cross Section* case. The results are more **pessimistic** than the nonlinear numerical analysis; considering a failure surface that extends over both the dam and the foundation layers, the computed **displacements** are **very large**. Some **qualitative comparison** can be done between the two cases that were tested, characterized by two considerably different soil foundation profiles. The downstream analysis yields a failure surface that involves all the foundation layers for the *Reference Cross Section* case (down to a depth of 100 meters), but is found to be superficial for the *Real Cross Section* case, consistently with of the low thickness of the downstream foundation, with the bedrock approaching the ground surface. The highest displacements can be expected downstream for the latter case, because the energy of deformation that was dissipated within the foundation and the embankment for the *Reference Cross Section* case, is dissipated almost only within the embankment for the *Real Cross Section* case;
- The **nonlinear analysis** (Safety Evaluation Earthquake) allowed the evaluation of maximum displacements on the two cases that were tested, the *Reference Cross Section* case and the *Real Cross Section* case. In all cases the vertical displacement at the crest of the dam is lower than 2 meters, compared to a maximum admissible displacement, equal to 4 meters, as indicated by NOVEC.

The **main instability** concerns **the foot of the downstream embankment** and the **upstream** slope. The foot of the downstream embankment plastifies for all the simulated cases, and shows the maximum positive horizontal and vertical displacements. In all cases, the maximum positive horizontal and vertical displacements are higher in the *Real Cross Section* case (see Table 6-1 and Table 6-2). This is due to the different soil foundation profile, with the bedrock daylighting close to the foot of the embankment for that case. Strains tend to concentrate close to the bedrock/foundation interface whereas in the *Reference Cross Section* case the strain localization (failure) occurs deeper.

The **upstream slope** seems to be a **problematic zone**. The maximum negative horizontal and vertical displacements are generally higher in the *Real Cross Section* case (see Table 6-1 and Table 6-2). The plots of the maximum shear increment confirmed that **sliding occurs** at the interface between the rockfill and the dam core.

SEE EARTHQUAKE - REAL CROSS SECTION					
		PGA [g]		Max Crest Displacements [m]	
Name		Vertical	Horizontal	Vertical	Horizontal
Darfield V-H1		+ 0.5 / - 0.58	+ 0.96 / - 1.33	-0.40	+0.35
Darfield V-H2			+ 0.79 / - 0.89	-1.40	-1.40
Kocaeli Izt V-H1		+ 0.51 / - 0.43	+ 0.82 / - 0.63	-1.20	+2.20
Kocaeli Izt V-H2			+ 0.47 / - 0.59	-1.50	-1.50
Morgan V-H1		+ 0.44 / - 0.43	+ 0.81 / - 0.62	-0.15	+0.40
Morgan V-H2			+ 0.55 / - 1.49	-0.13	+0.48

Table 6-1 : SEE earthquakes – Maximum crest displacements – Real Cross Section

SEE EARTHQUAKE - REFERENCE CROSS SECTION					
		PGA [g]		Max Crest Displacements [m]	
Name		Vertical	Horizontal	Vertical	Horizontal
Darfield V-H1		+ 0.5 / - 0.58	+ 0.96 / - 1.33	-0.25	+0.60
Darfield V-H2			+ 0.79 / - 0.89	-1.00	-1.50
Kocaeli Izt V-H1		+ 0.51 / - 0.43	+ 0.82 / - 0.63	-0.90	+2.50
Kocaeli Izt V-H2			+ 0.47 / - 0.59	-1.00	-0.80
Morgan V-H1		+ 0.44 / - 0.43	+ 0.81 / - 0.62	-0.20	+0.40
Morgan V-H2			+ 0.55 / - 1.49	-0.20	+0.60

Table 6-2 : SEE earthquakes – Maximum crest displacements – Reference Cross Section

7. APPENDIX 1

7.1. Mohr-coulomb model - Incremental Elastic Law

In the *FLAC* implementation of this model, principal stresses $\sigma_1, \sigma_2, \sigma_3$ are used, the out-of-plane stress, σ_{zz} being recognized as one of these. The principal stresses and principal directions are evaluated from the stress tensor components, and ordered so that (recall that compressive stresses are negative):

$$\sigma_1 \leq \sigma_2 \leq \sigma_3 \qquad \textit{(Eq. 1)}$$

The corresponding principal strain increments $\Delta e_1, \Delta e_2, \Delta e_3$ are decomposed as follows:

$$\Delta e_i = \Delta e_i^e + \Delta e_i^p \qquad \textit{(Eq. 2)}$$

where the superscripts *e* and *p* refer to elastic and plastic parts, respectively, and the plastic components are nonzero only during plastic flow. The incremental expression of Hooke's law in terms of principal stress and strain has the form:

$$\Delta\sigma_1 = \alpha_1 \Delta e_1^e + \alpha_2 (\Delta e_2^e + \Delta e_3^e) \qquad \textit{(Eq. 3)}$$
$$\Delta\sigma_2 = \alpha_1 \Delta e_2^e + \alpha_2 (\Delta e_1^e + \Delta e_3^e) \qquad \textit{(Eq. 4)}$$
$$\Delta\sigma_3 = \alpha_1 \Delta e_3^e + \alpha_2 (\Delta e_1^e + \Delta e_2^e) \qquad \textit{(Eq. 5)}$$

where $\alpha_1 = K + 4G/3$ and $\alpha_2 = K - 2G/3$.

7.1.1.1. Mohr-coulomb model - Yield and Potential Functions

The failure envelope is defined from point A to point B by the Mohr-Coulomb yield function f^s of the form:

$$f^s = \sigma_1 - \sigma_3 N_\phi + 2c\sqrt{N_\phi} \qquad \textit{(Eq. 6)}$$

and from B to C by a tension yield function f^t of the form:

$$f^t = \sigma^t - \sigma_3 \qquad \textit{(Eq. 7)}$$

where ϕ is the friction angle, c is the cohesion, σ^t is the tensile strength and:

$$N_\phi = \frac{1+\sin\phi}{1-\sin\phi} \qquad \textit{(Eq. 8)}$$

With the ordering convention of eq. 10, the failure criterion may be represented in the plane (σ_1, σ_3) is illustrated in Figure 7-1:

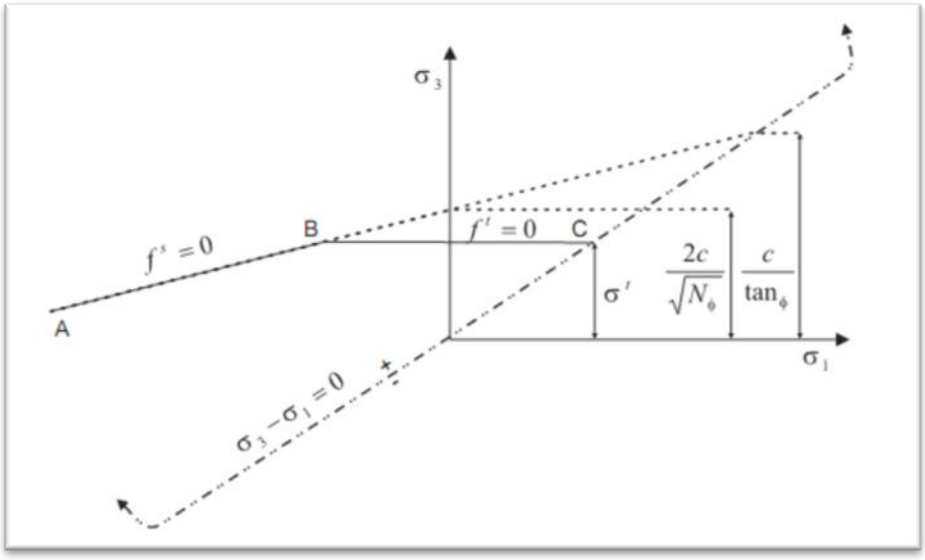

Figure 7-1 : Mohr-Coulomb failure criterion in FLAC

8. APPENDIX 2

8.1. Calibration of the UBCHyst model

Here below, the parameters that were obtained by the calibration of the model UBCHyst, for the dam and the foundation materials, are summarized.

CALIBRATION – Group 1 (Core)			
sxx	**hn**	**hn1**	**hrf**
200	4.00	0.80	0.90
400	4.20	0.77	0.92
600	4.30	0.75	0.95
800	4.50	0.73	0.98
1000	4.70	0.71	0.98

CALIBRATION – Group 2 (Rockfill)			
sxx	**hn**	**hn1**	**hrf**
200	4.0	0.6	0.90
400	5.0	0.6	0.95
600	6.0	0.6	0.98

CALIBRATION – Group 3 (comp. gravel)			
sxx	**hn**	**hn1**	**hrf**
200	8.00	0.70	0.80
400	9.00	0.70	0.85
600	10.00	0.70	0.90
800	11.00	0.70	0.95
1000	12.00	0.70	0.98

CALIBRATION – Group A1 (Alluv. Sand)			
sxx	**hn**	**hn1**	**hrf**
200	2.00	0.70	0.80
400	2.25	0.70	0.85
600	2.75	0.75	0.90
800	2.75	0.75	0.95
1000	3.00	0.80	0.98

CALIBRATION – Group A2 (Alluv. Clay)			
sxx	**hn**	**hn1**	**hrf**
200	1.50	0.75	0.90
400	1.75	0.75	0.95
600	1.75	0.70	0.95
800	2.00	0.70	0.95
1000	2.25	0.70	0.95
1200	2.50	0.70	0.98
1400	2.50	0.70	0.98

CALIBRATION – Group A3 (Alluv. Gravel)			
sxx	**hn**	**hn1**	**hrf**
200	6.00	0.65	0.90
400	7.00	0.65	0.90
600	9.00	0.65	0.90
800	10.00	0.70	0.90
1000	11.00	0.75	0.90

9. APPENDIX 3

9.1. Values of dynamic maximum shear modulus and dynamic bulk modulus – Reference Cross Section

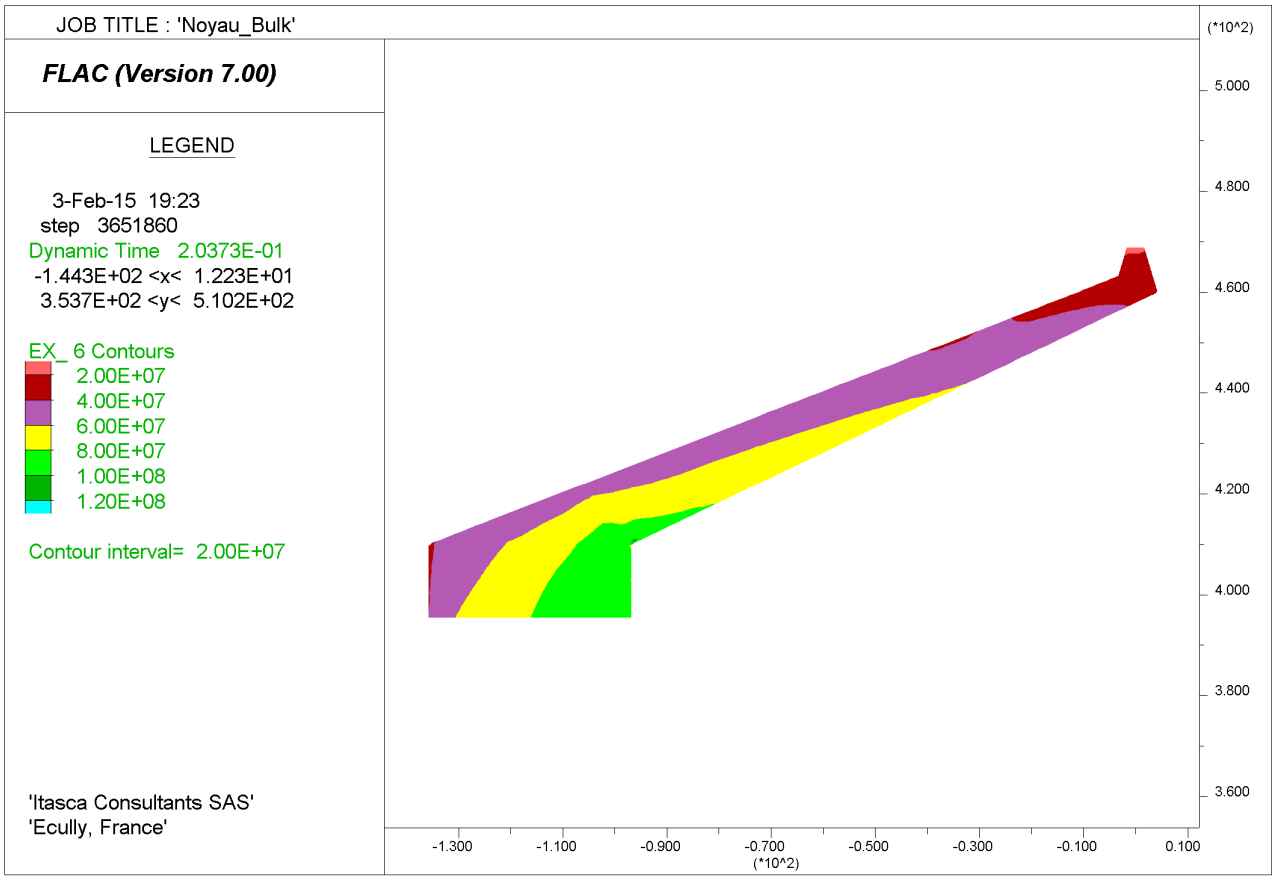

Figure 9-1 : dynamic maximum shear modulus of dam core(reference cross section)

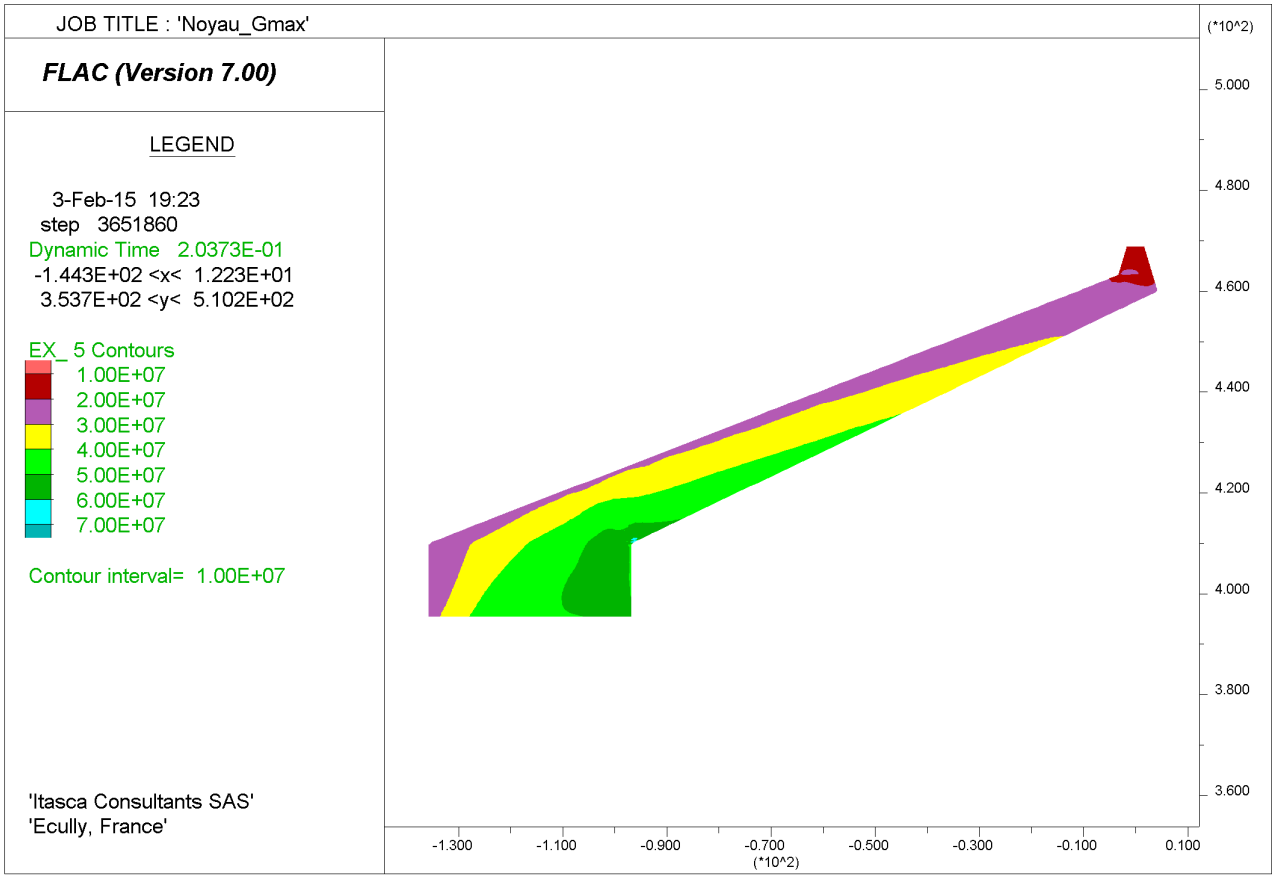

Figure 9-2: dynamic bulk modulus of dam core (reference cross section)

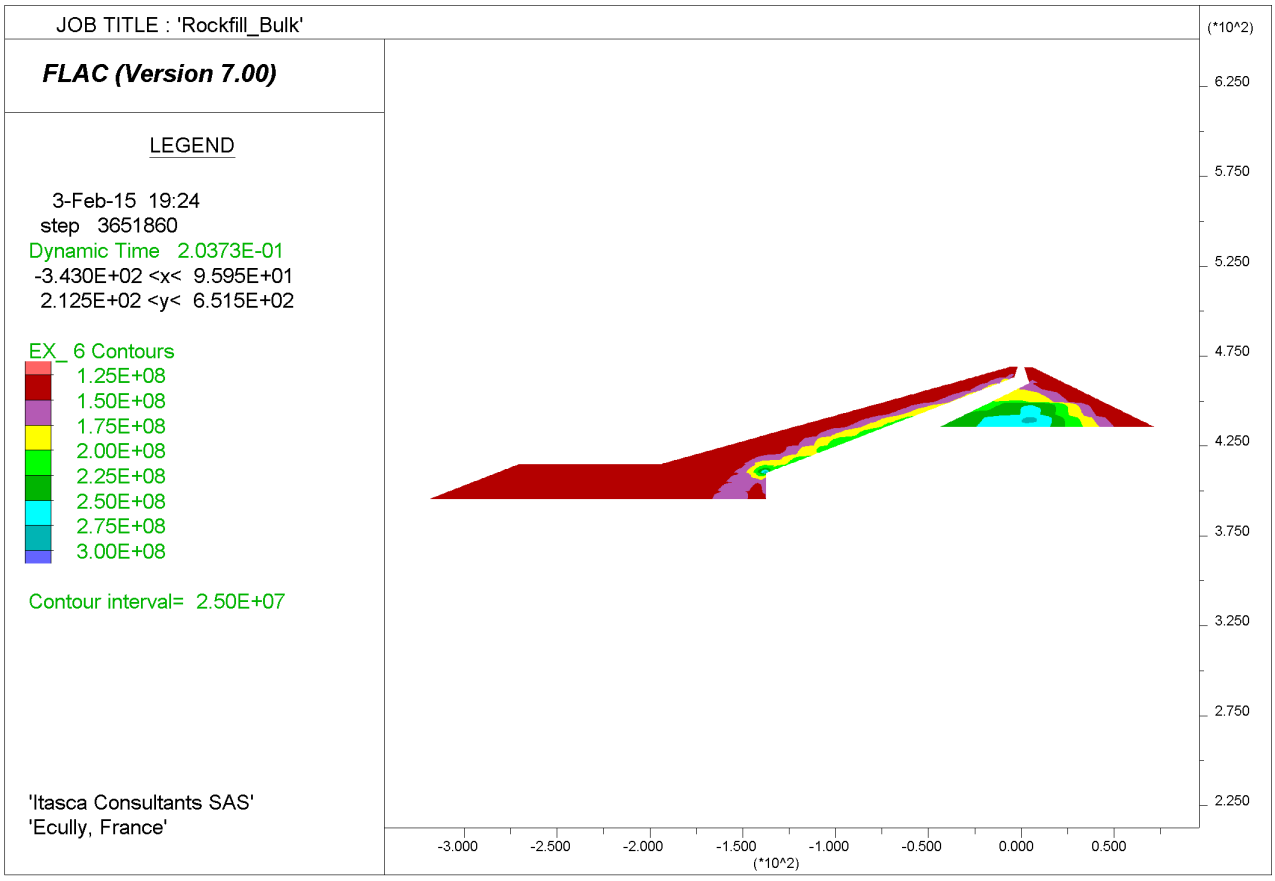

Figure 9-3: dynamic maximum shear modulus of rockfill (reference cross section)

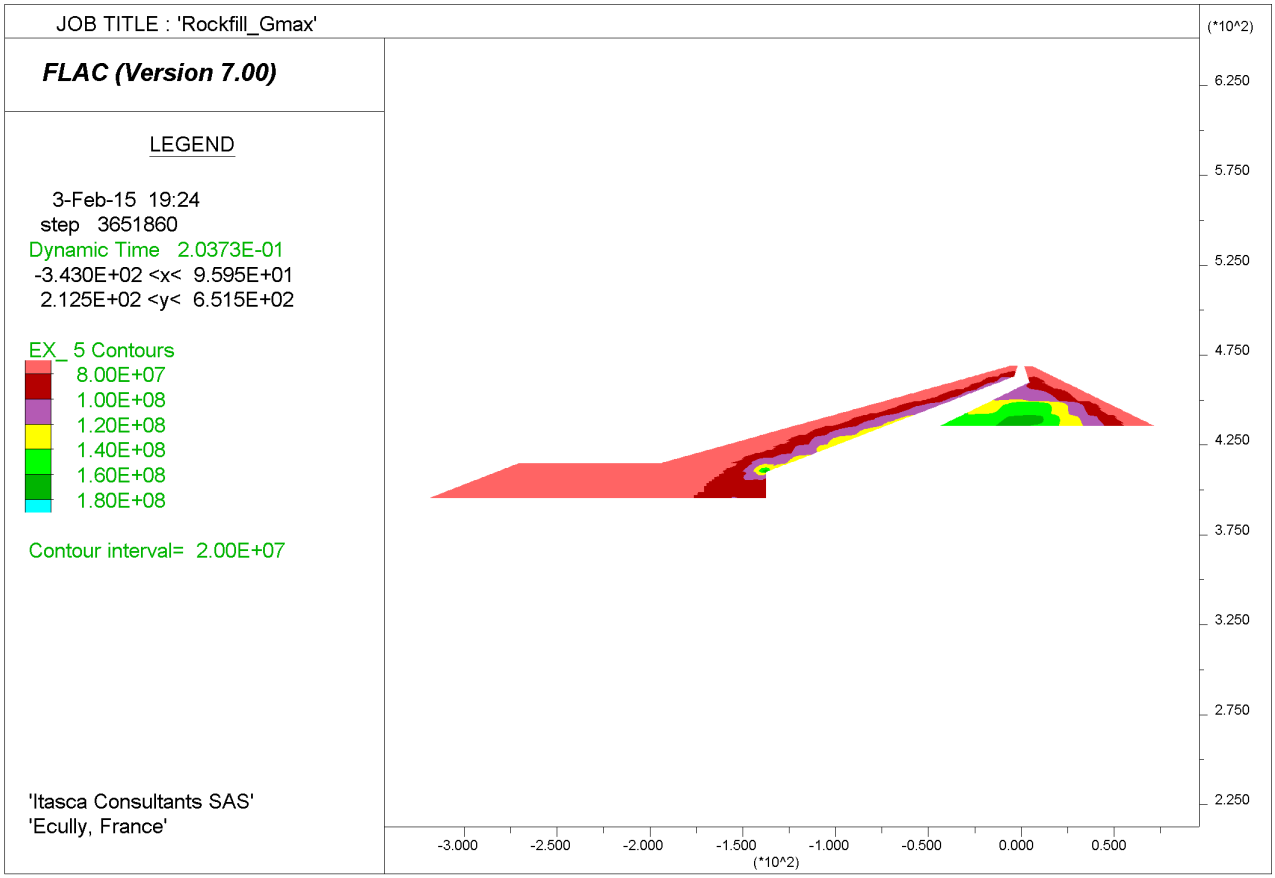

Figure 9-4: dynamic bulk modulus of rockfill (reference cross section)

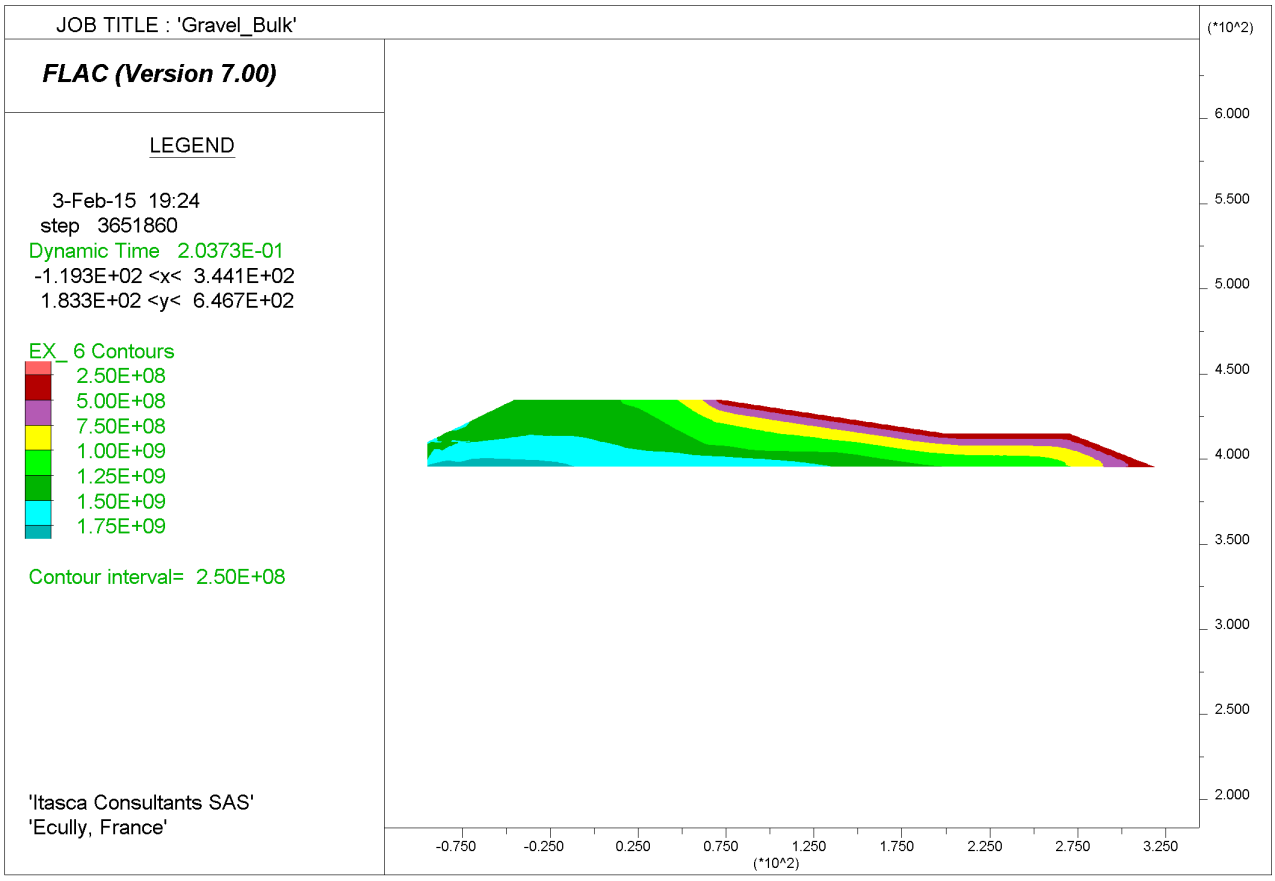

Figure 9-5: dynamic maximum shear modulus of compacted gravel (reference cross section)

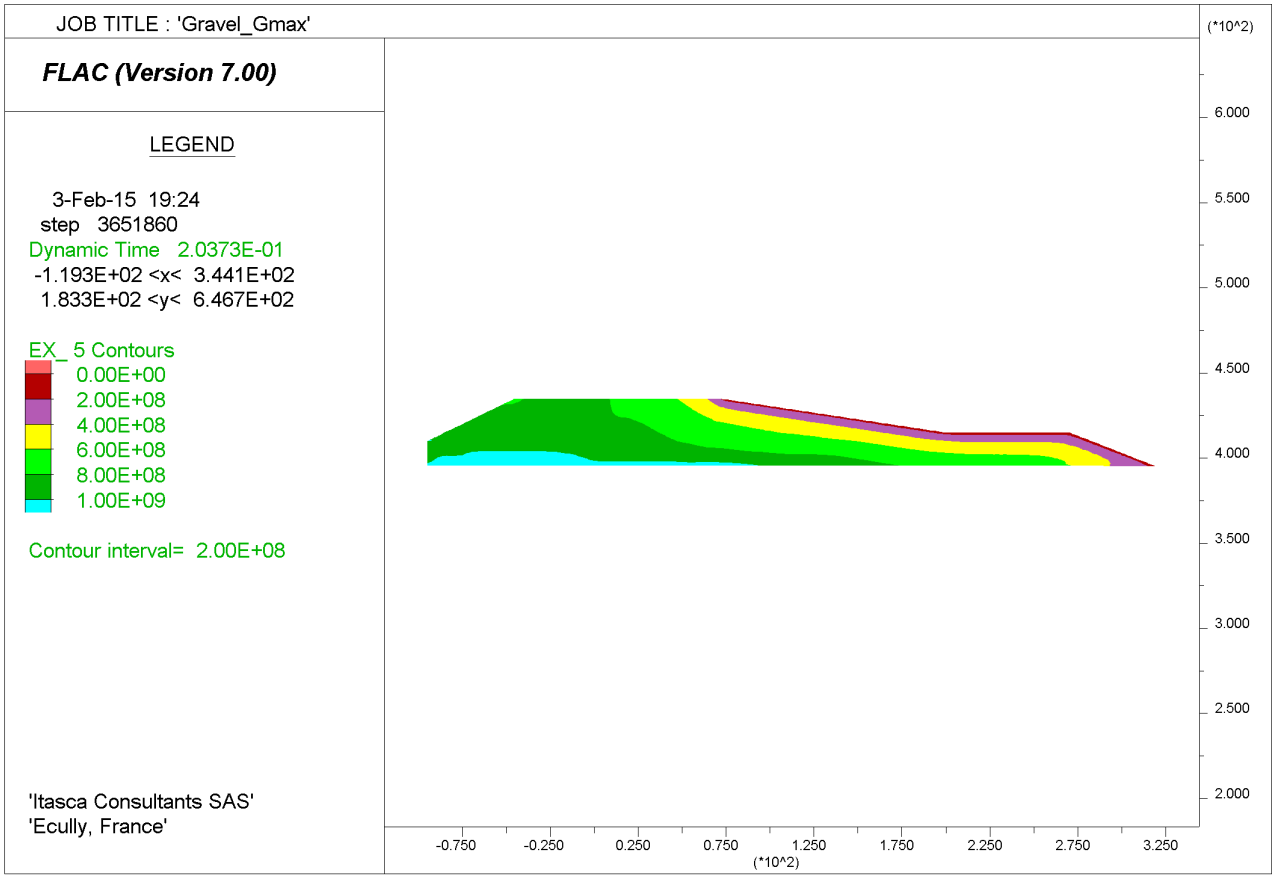

Figure 9-6: dynamic bulk modulus of compacted gravel (reference cross section)

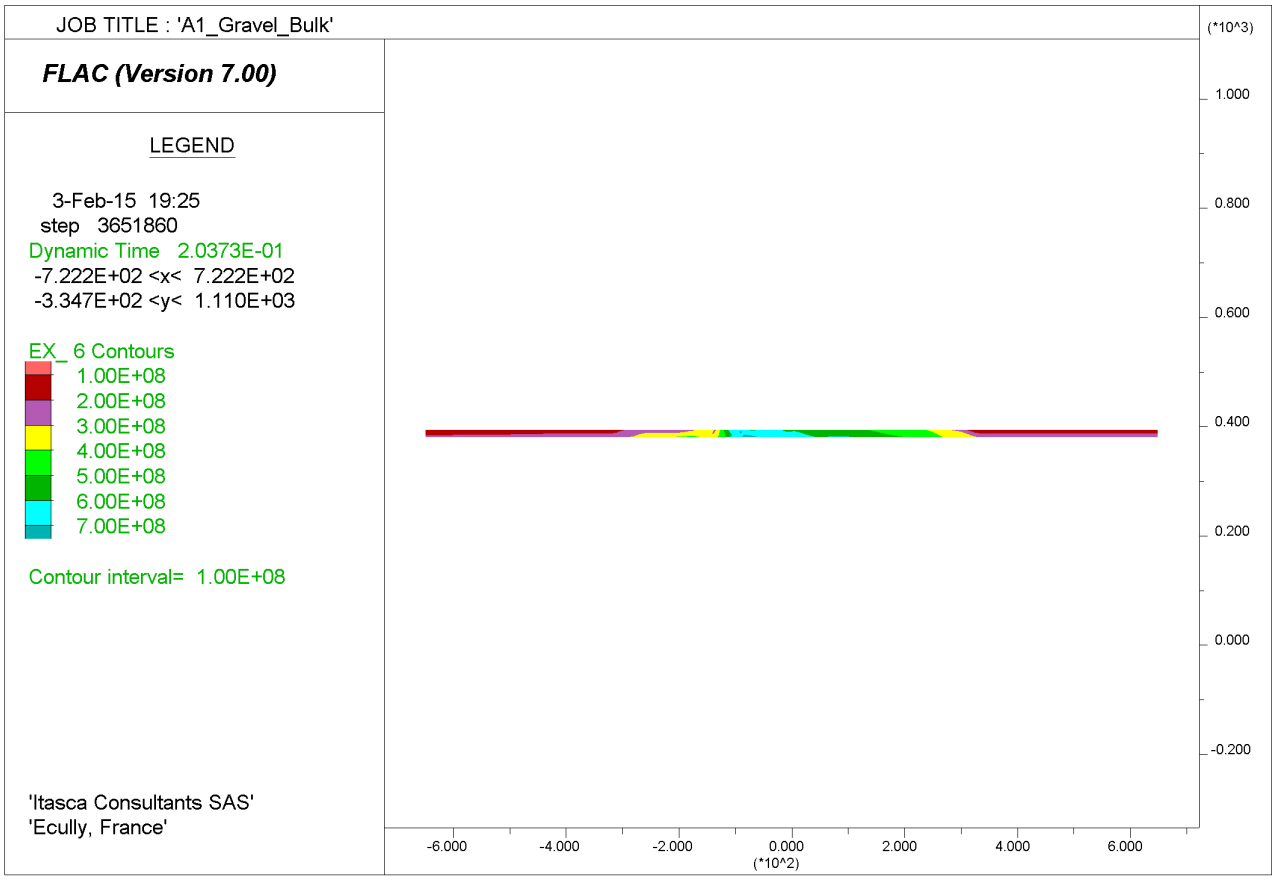

Figure 9-7: dynamic maximum shear modulus of alluvial sand (reference cross section)

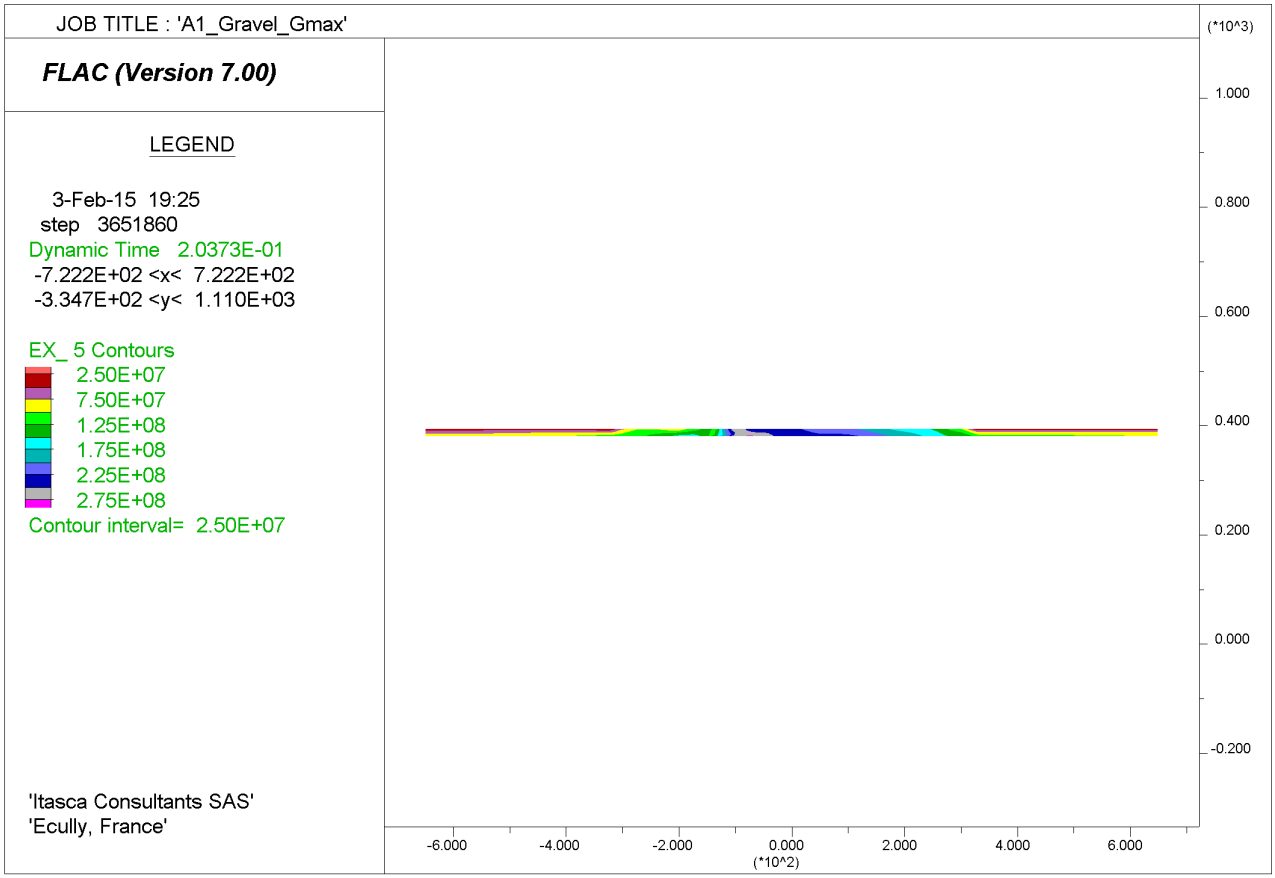

Figure 9-8: dynamic bulk modulus of alluvial sand (reference cross section)

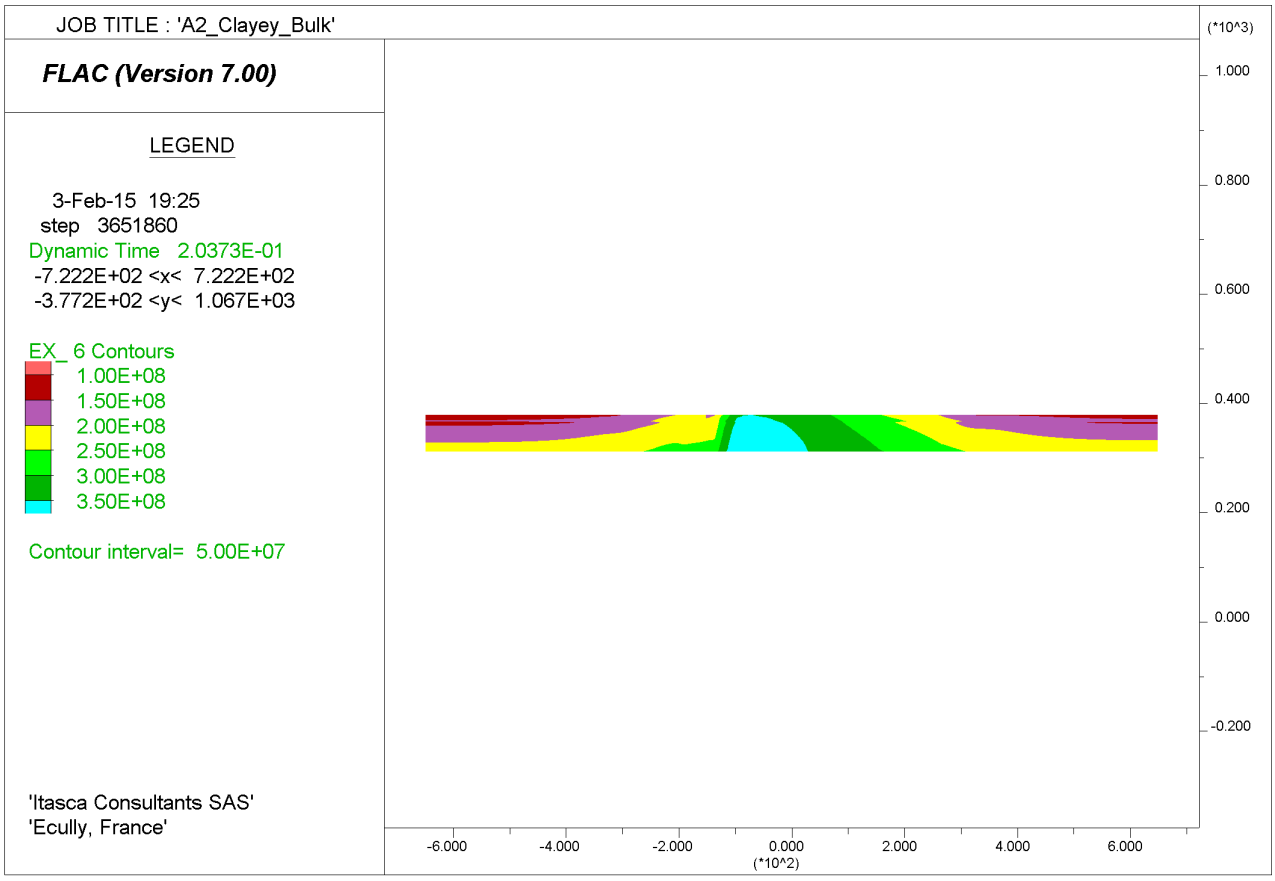

Figure 9-9: dynamic maximum shear modulus of clayey silt (reference cross section)

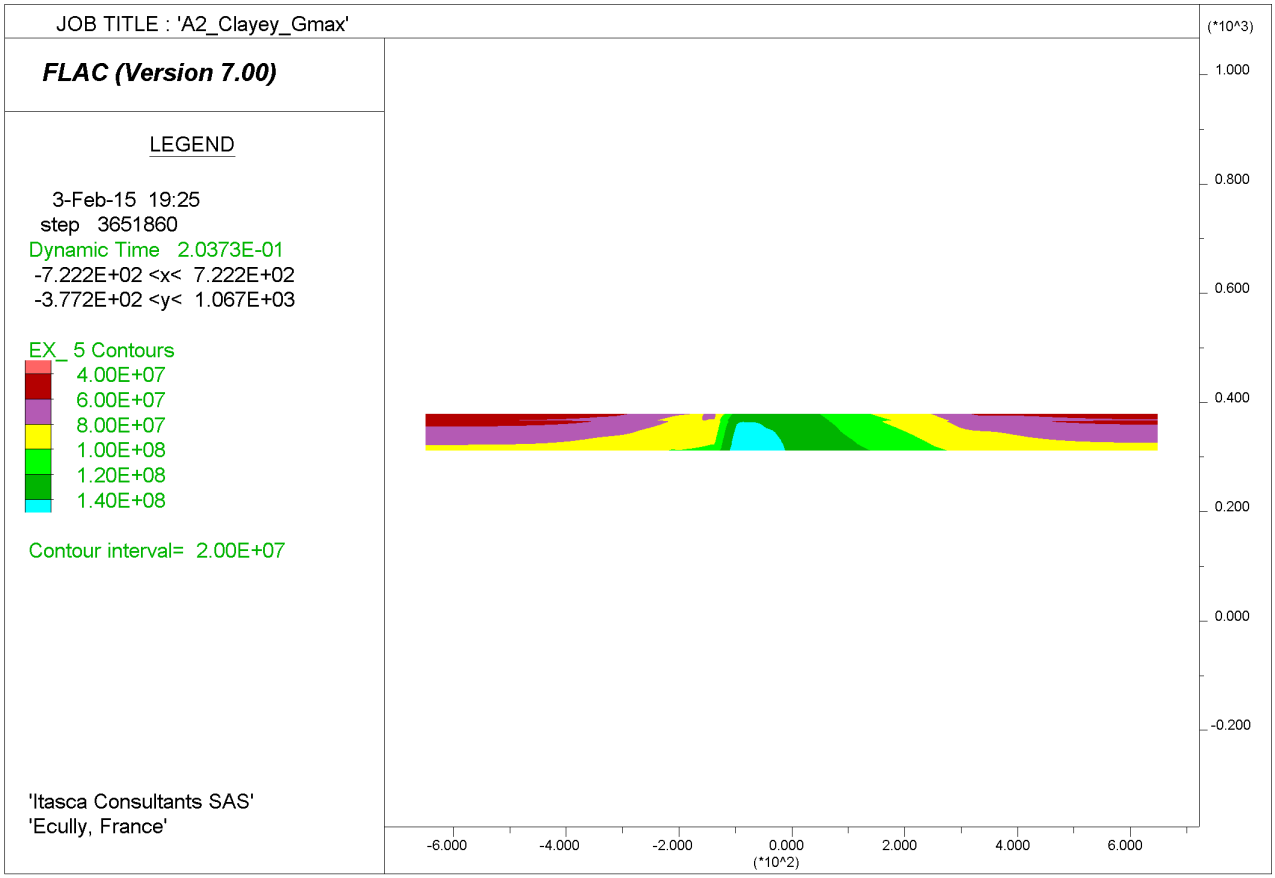

Figure 9-10: dynamic bulk modulus of clayey silt (reference cross section)

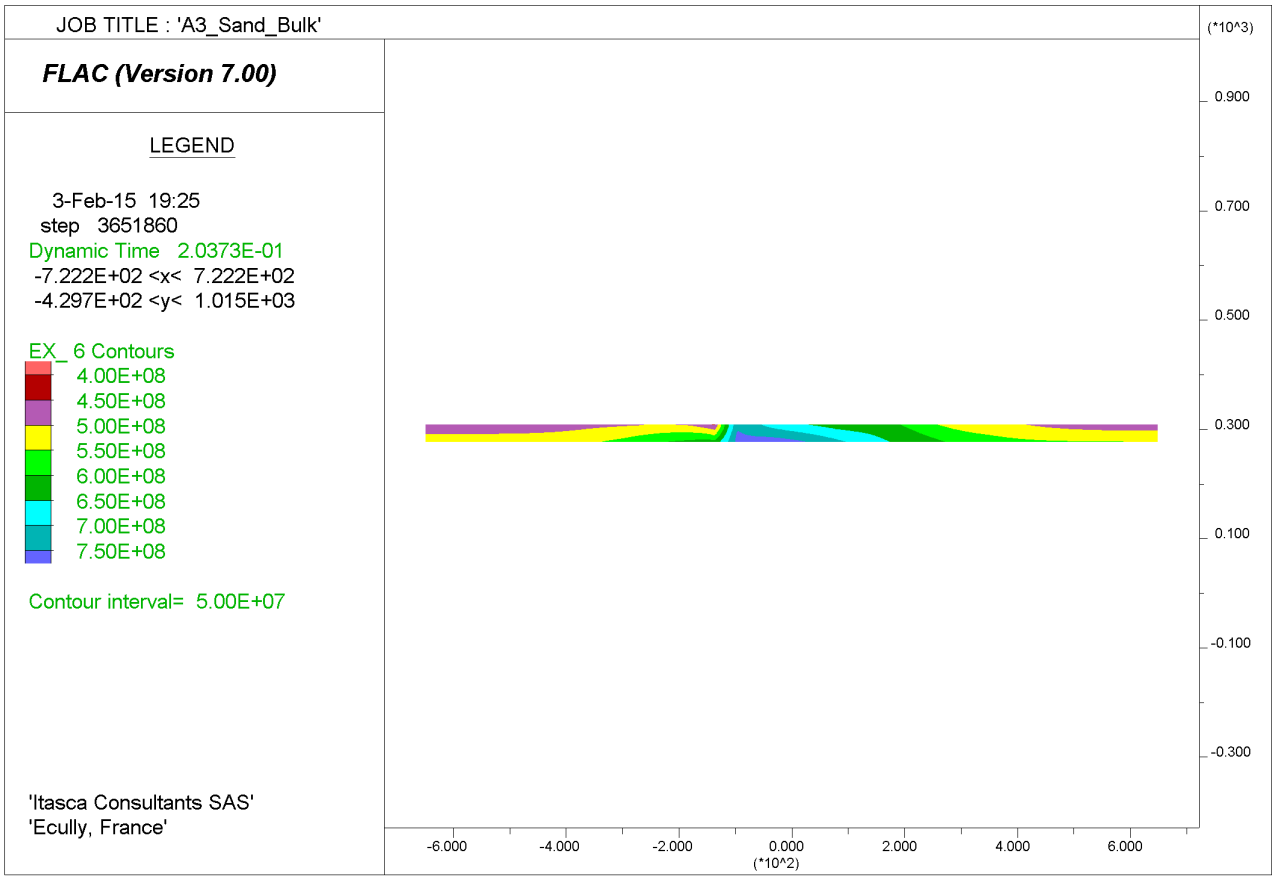

Figure 9-11: dynamic maximum shear modulus of alluvial gravel (reference cross section)

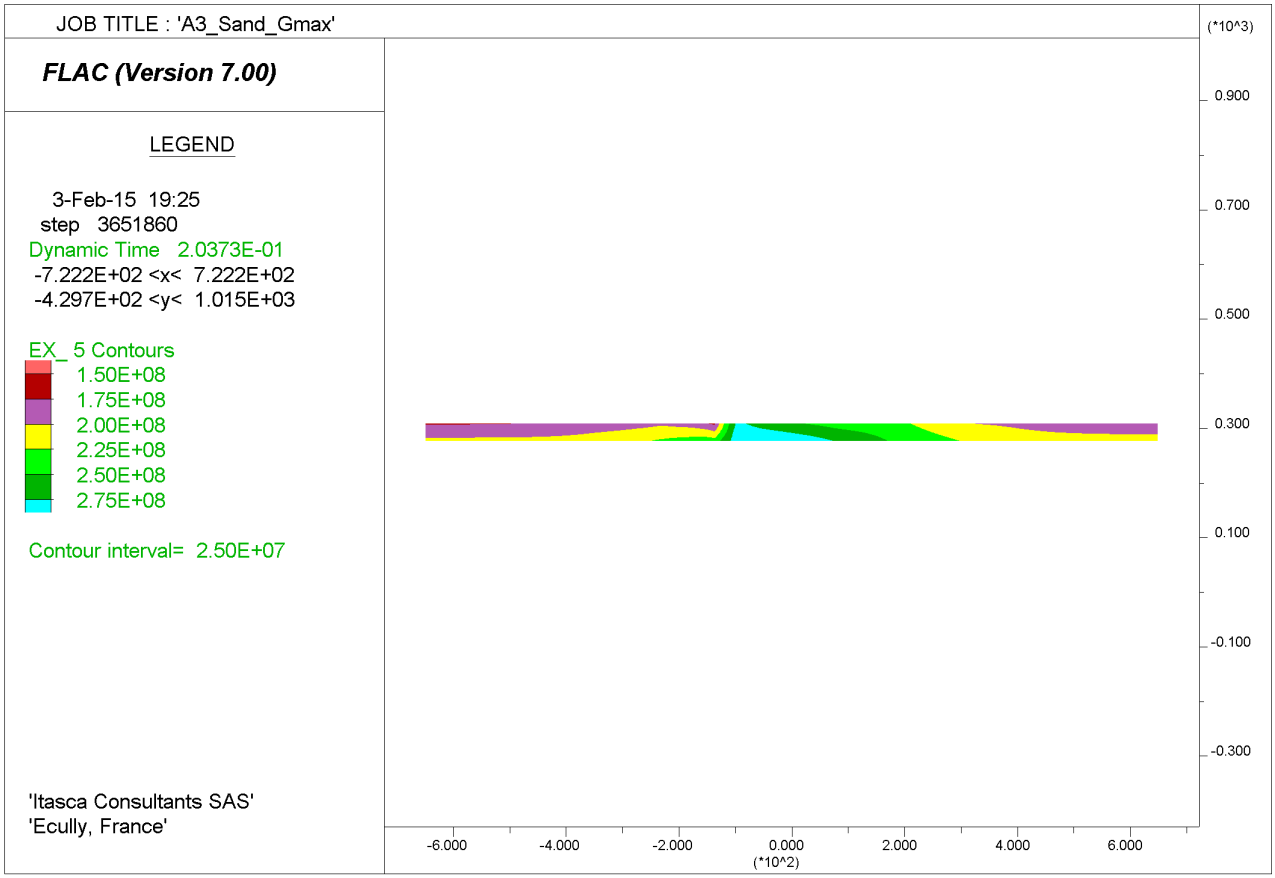

Figure 9-12: dynamic bulk modulus of alluvial gravel (reference cross section)

10. APPENDIX 4

10.1. Values of dynamic maximum shear modulus and dynamic bulk modulus – Real Cross Section

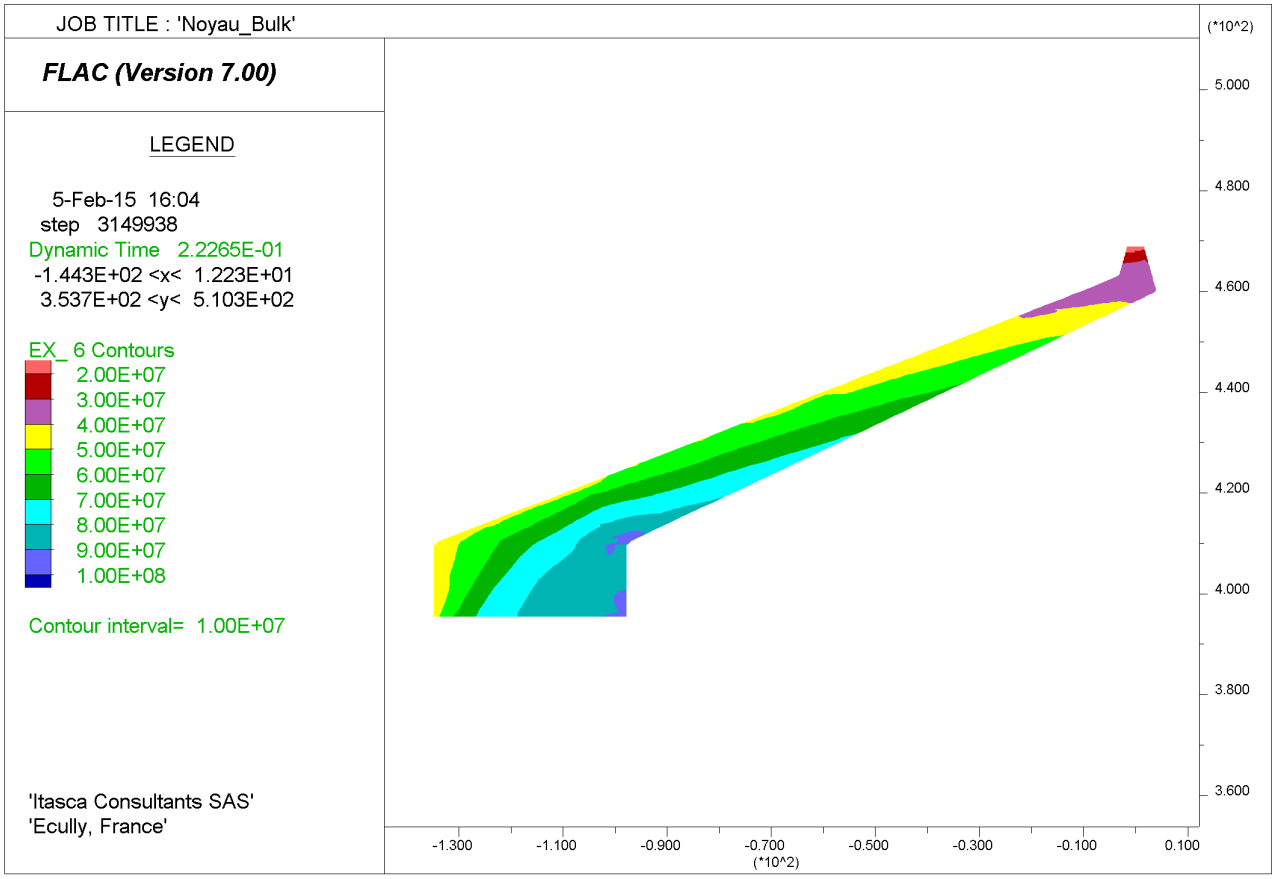

Figure 10-1 dynamic bulk modulus of dam core (real cross section)

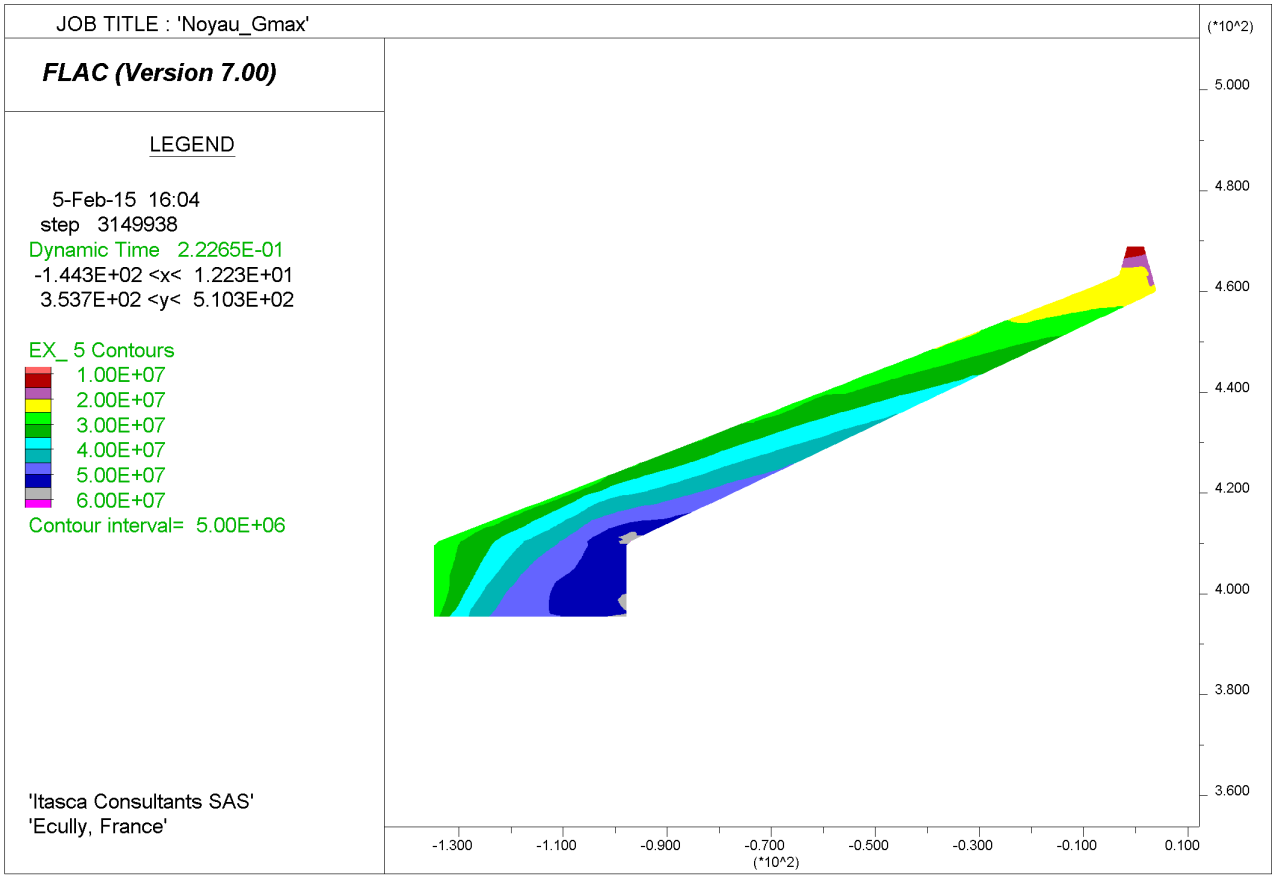

Figure 10-2 dynamic maximum shear modulus of dam core (real cross section)

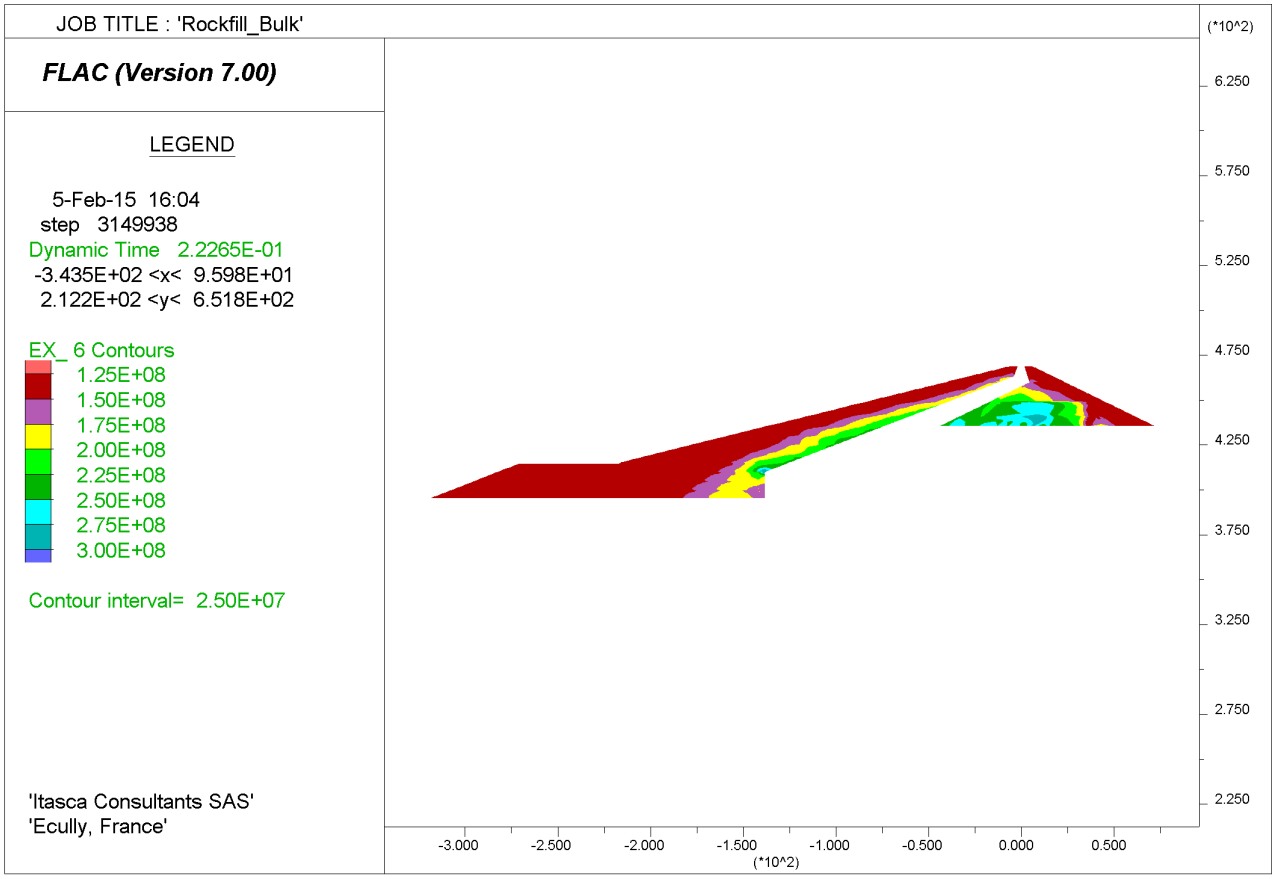

Figure 10-3 dynamic bulk modulus of rockfill (real cross section)

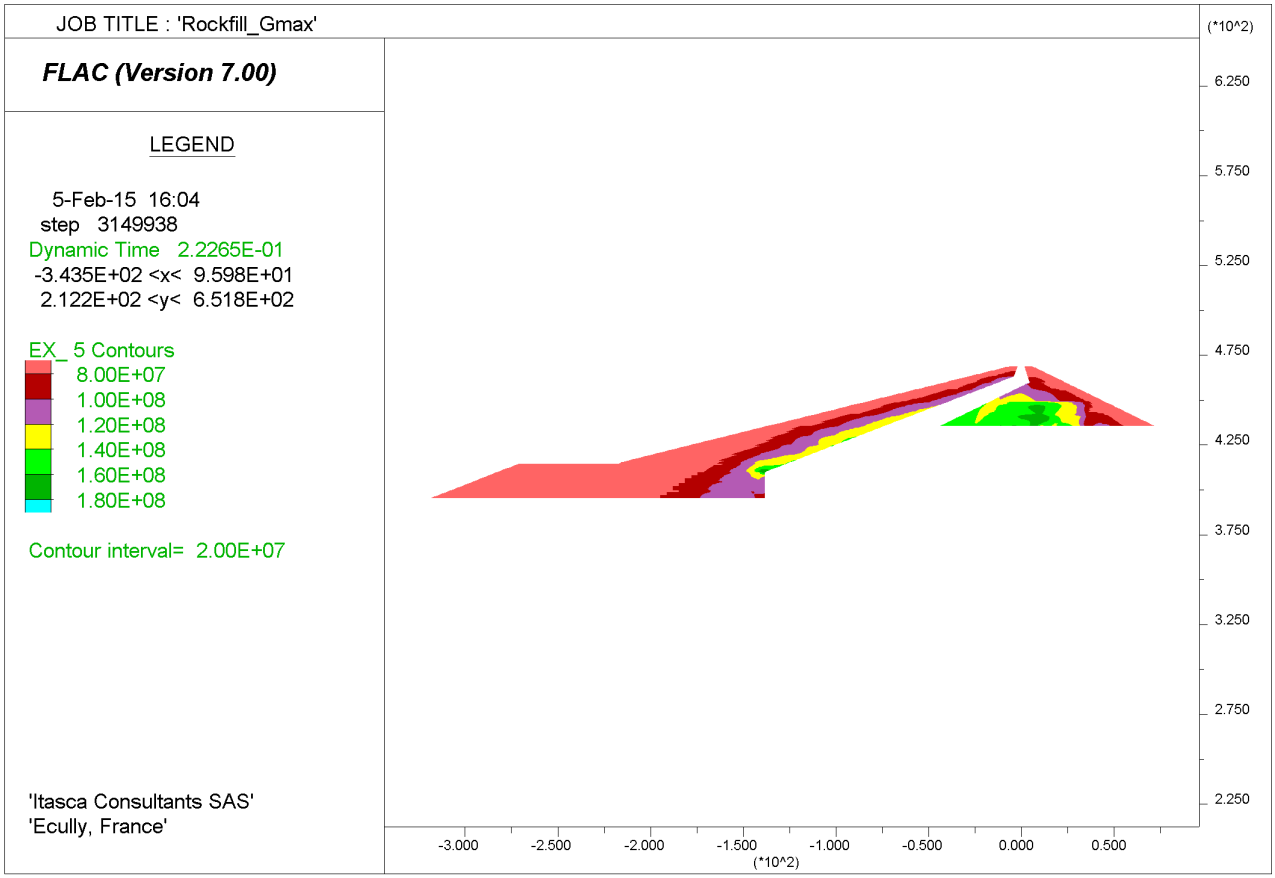

Figure 10-4 dynamic maximum shear modulus of rockfill (real cross section)

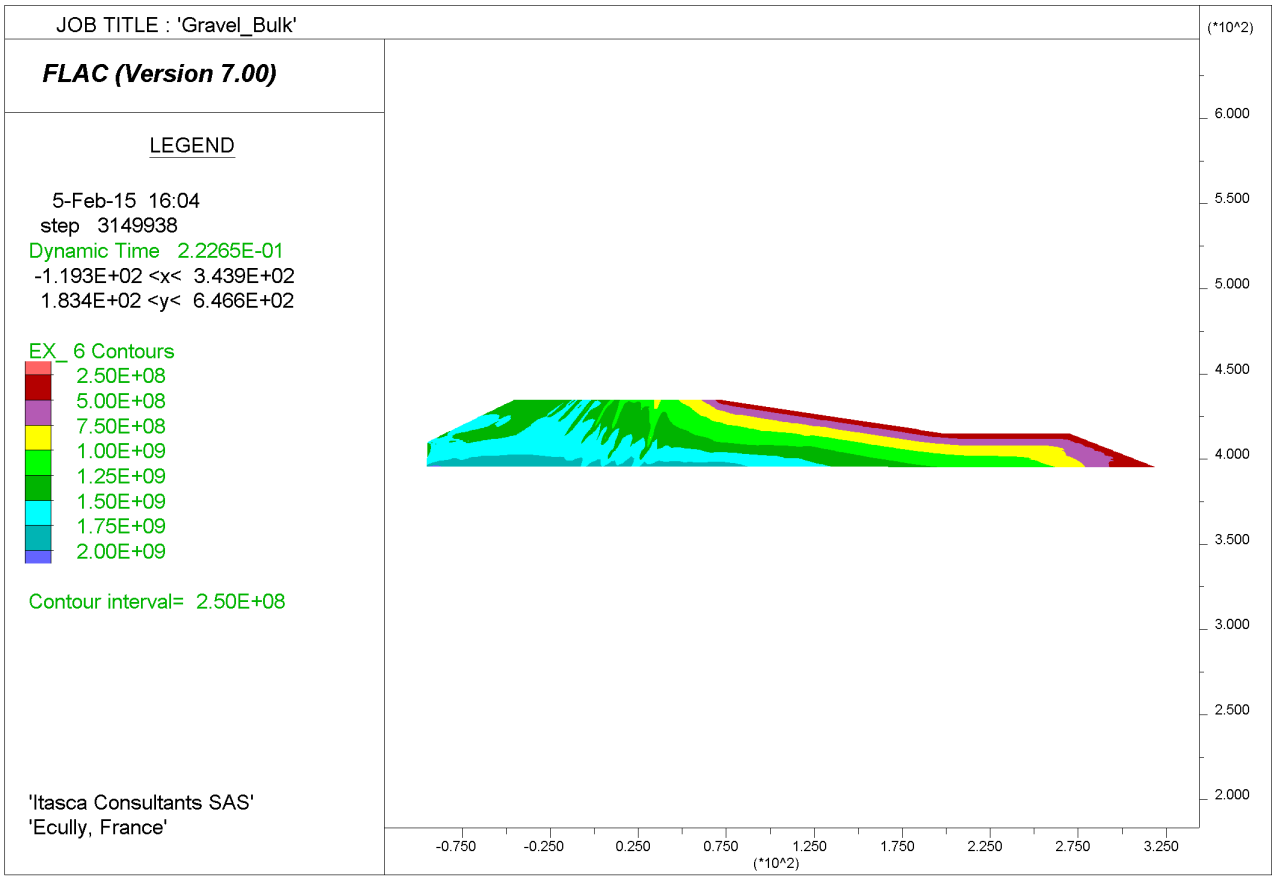

Figure 10-5 dynamic bulk modulus of compacted gravel (real cross section)

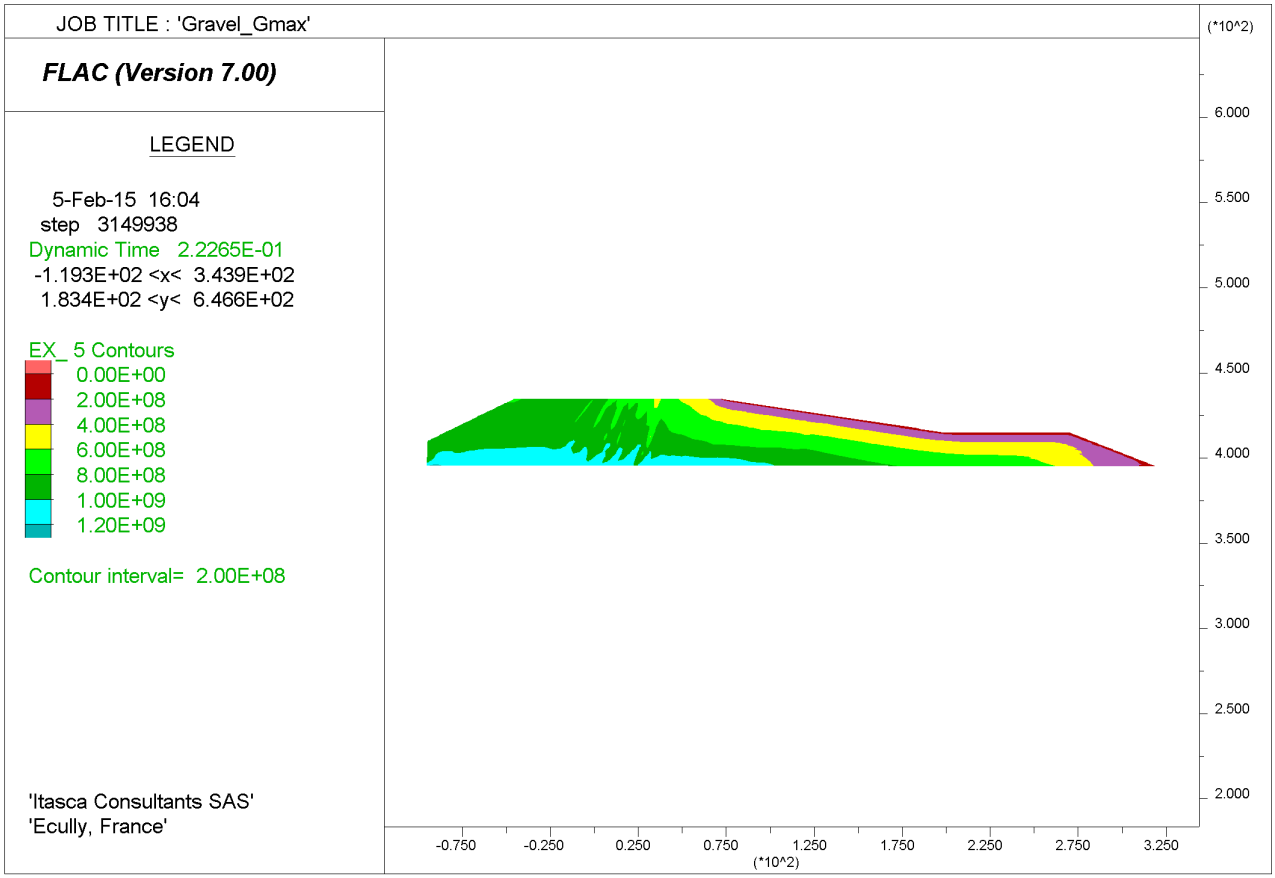

Figure 10-6 dynamic maximum shear modulus of compacted gravel (real cross section)

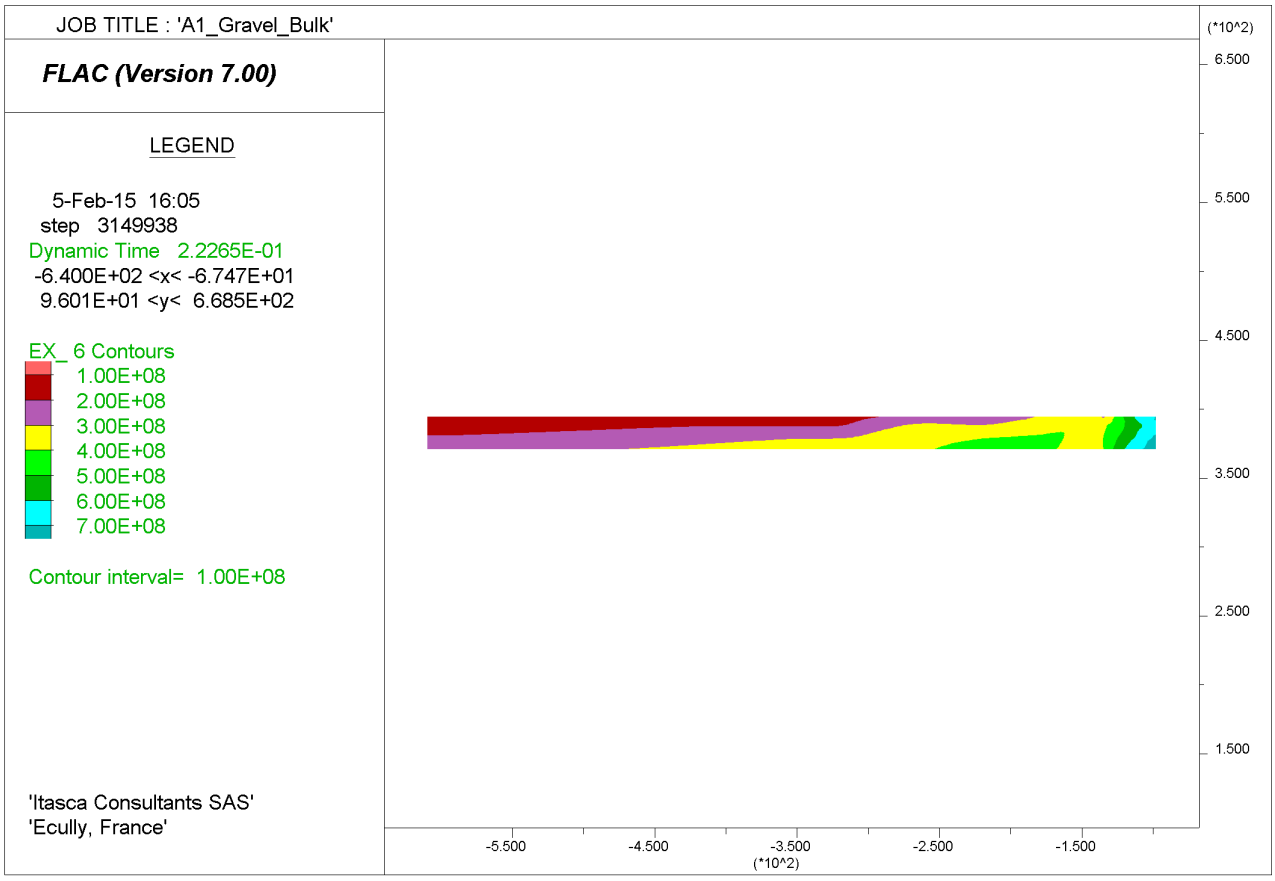

Figure 10-7 dynamic bulk modulus of alluvial sand (real cross section)

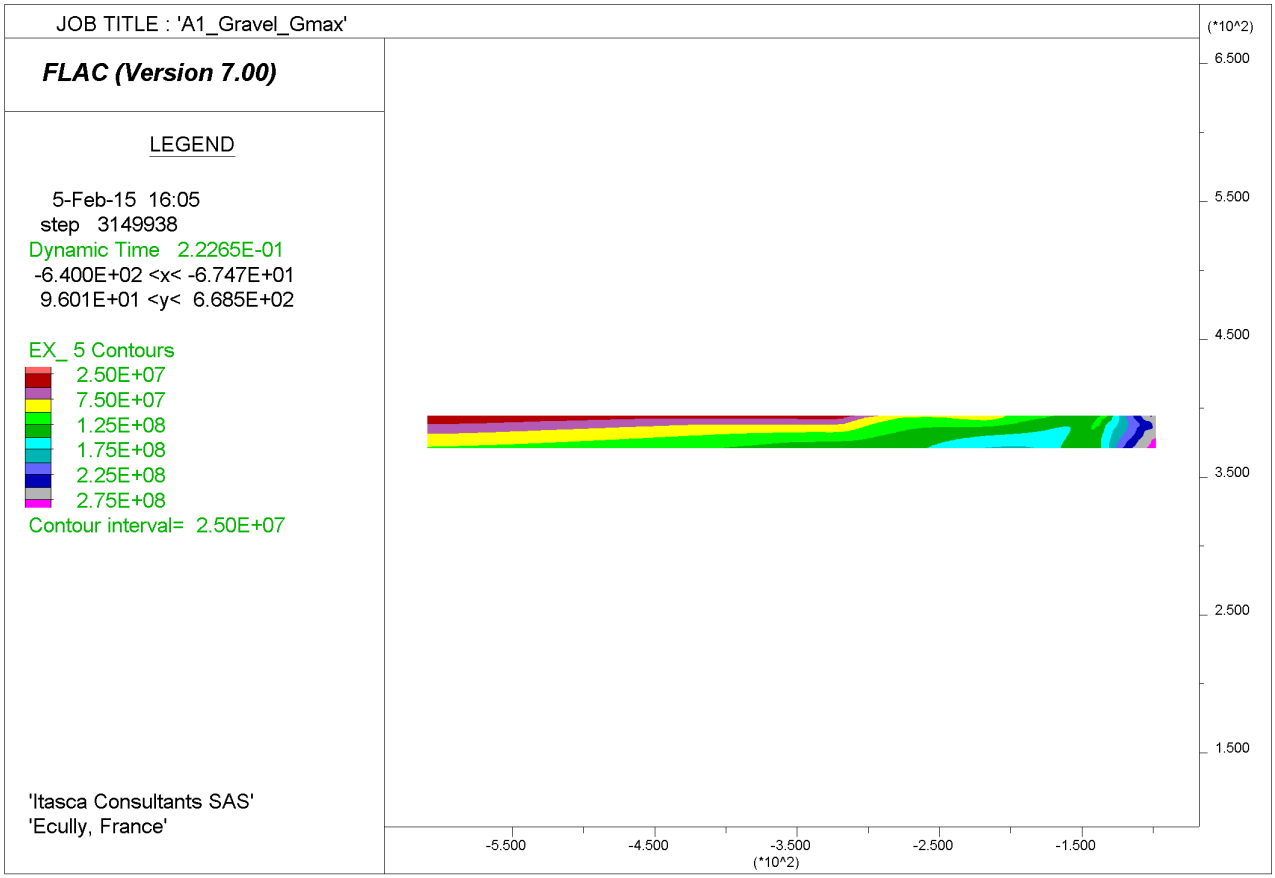

Figure 10-8 dynamic maximum shear modulus of alluvial sand (real cross section)

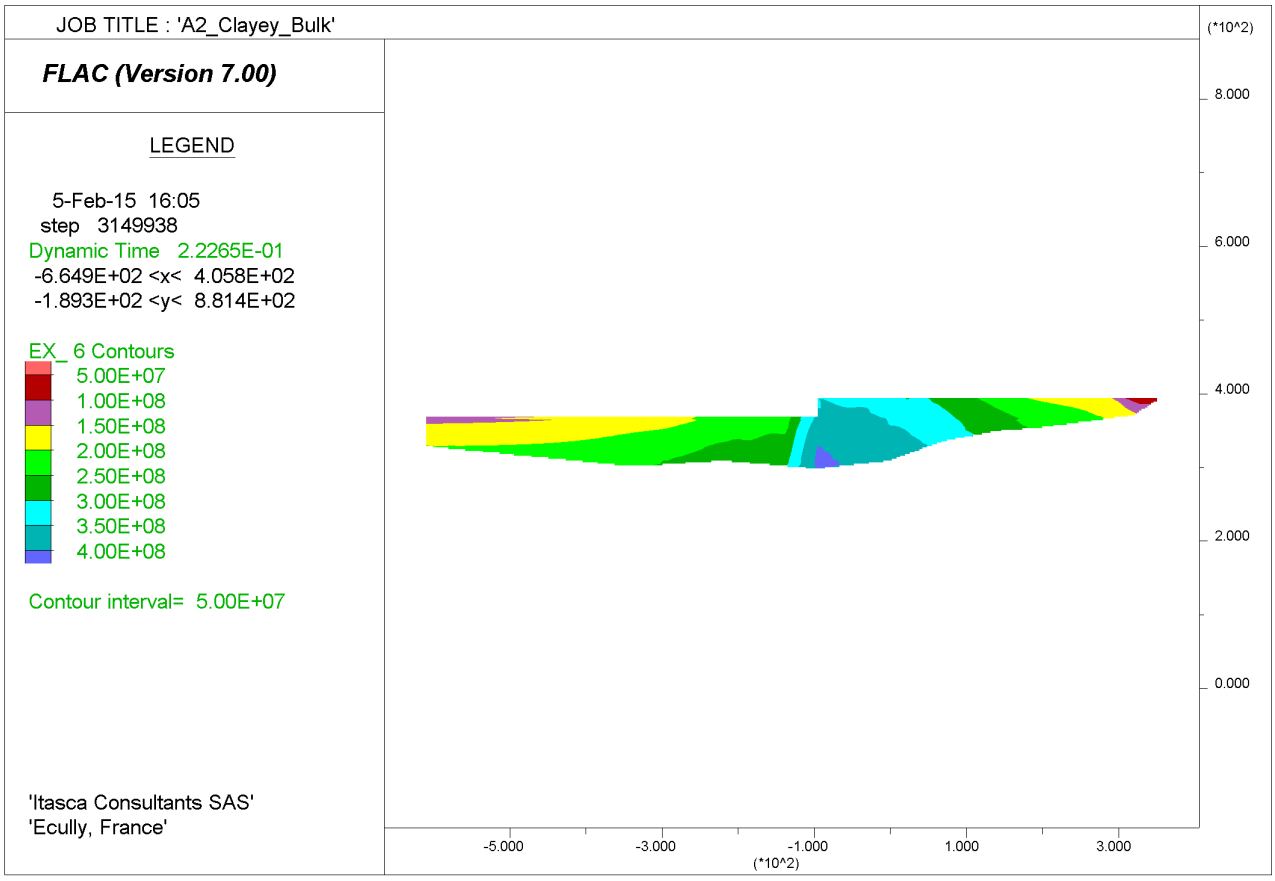

Figure 10-9 dynamic bulk modulus of clayey silt (real cross section)

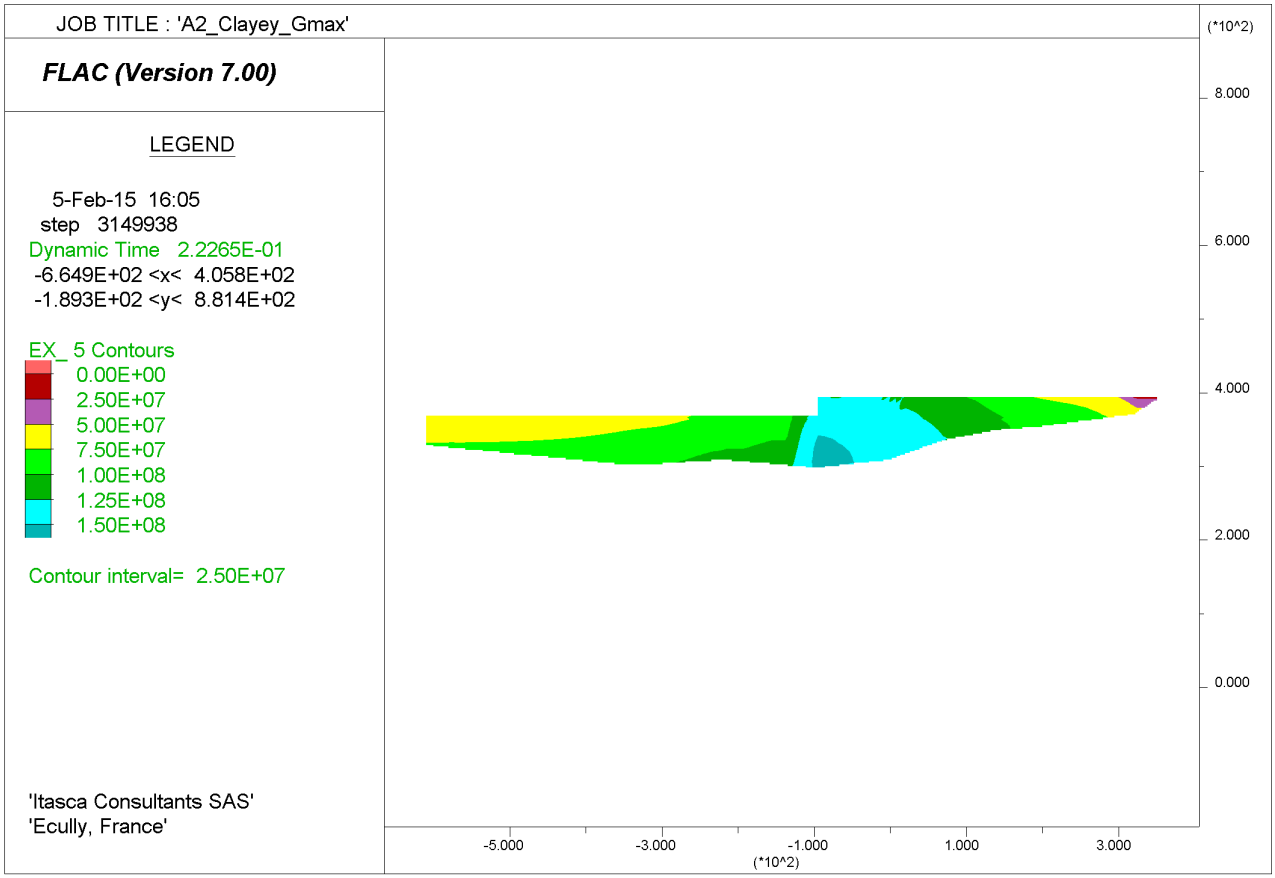

Figure 10-10 dynamic maximum shear modulus of clayey silt (real cross section)

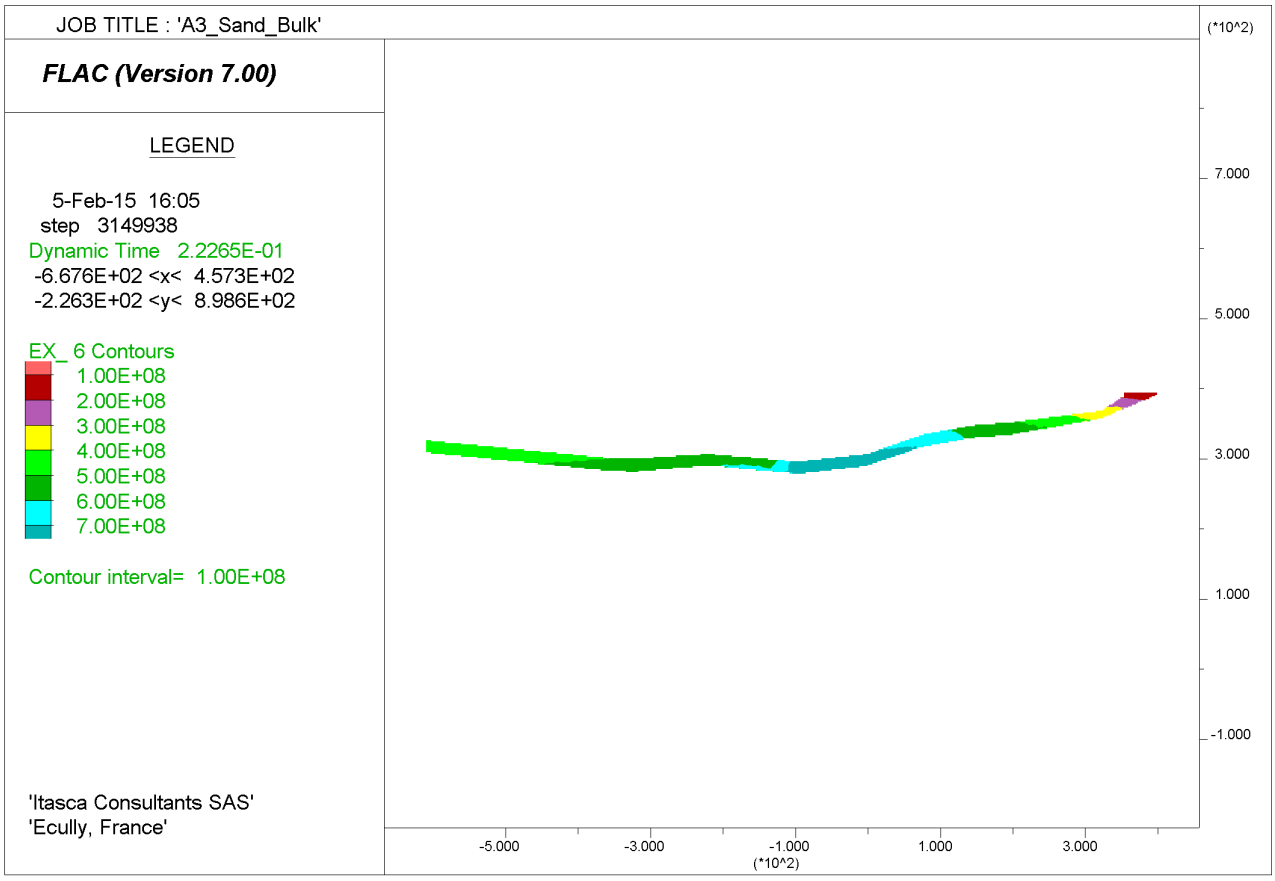

Figure 10-11 dynamic bulk modulus of alluvial gravel (real cross section)

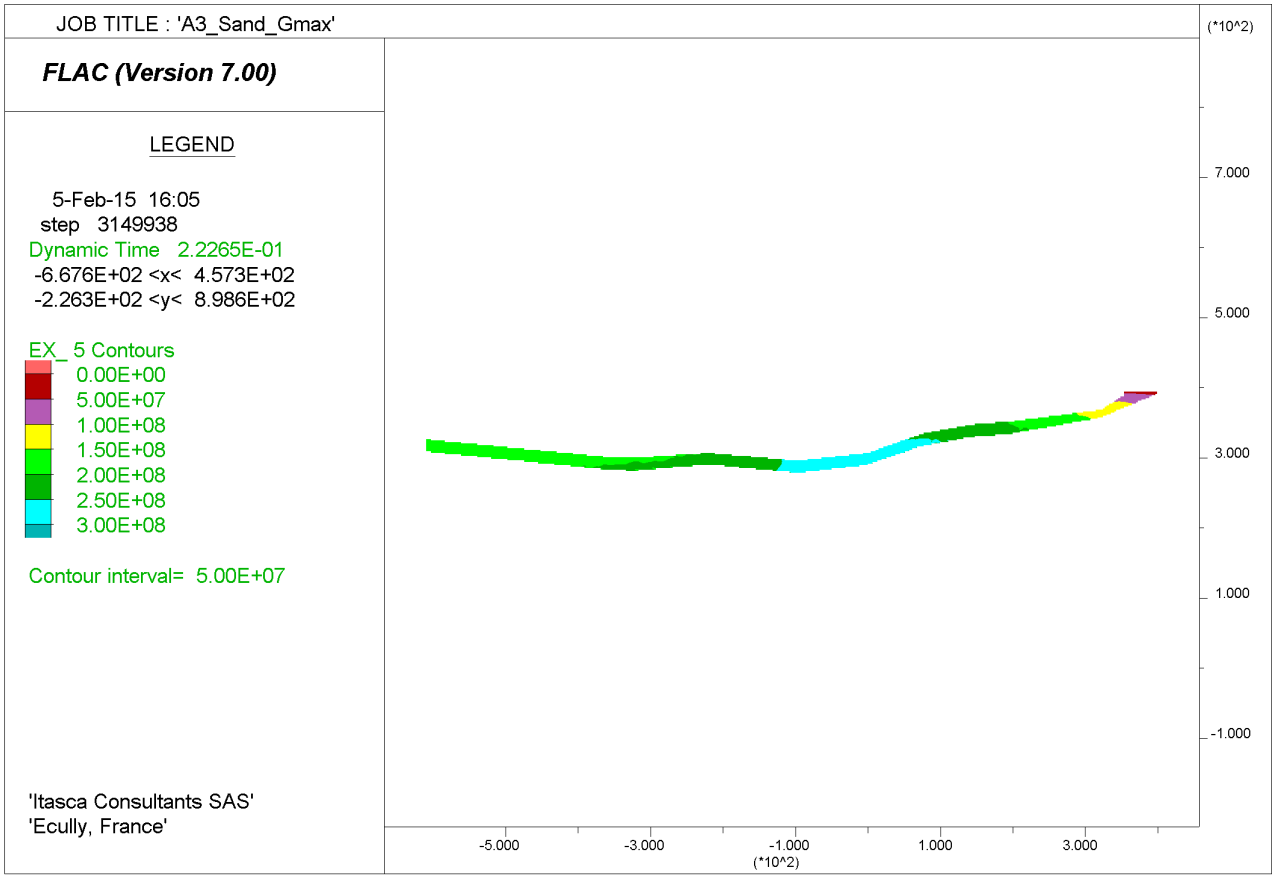

Figure 10-12 dynamic maximum shear modulus of alluvial gravel (real cross section)

11. APPENDIX 5

This section presents the results that were obtained using an undrained behavior for the clayey silt foundation layer. Such analysis was suggested by the amplification of the vertical component of acceleration after the passage through the above mentioned layer (see section 3.5.1). The amplification is in fact quite important. It was thougth that this might be due to the "drained" hypothesis. The objective of this simulation was to check if the results were significantly different.

The results, for the *reference cross section*, considering the KOCAELI V-H2 earthquake, are presented and compared to the results that were obtained adopting a *drained* bulk modulus for the soil foundation layers (section 4.6.4).

The « undrained » modulus for the clayey foundation layer is computed using the following expression:

$$K_{undrained} = K_{drained} + K_w \cdot n$$

Considering a porosity n=0.51, the undrained modulus is almost ten times higher than the *drained* one.

Figure 11-1 shows the comparison of the Fourier transform (FFT) of the horizontal component of the signal, as it is measured at the bedrock outcrop (input signal, Figure 11-1 *left*), and the FFT of the signal measured after passage through the soil foundation. This allows highlighting the effect of soil foundation layers on the amplification of the signal. It can be observed how low frequencies are amplified, whereas high frequencies are dissipated.

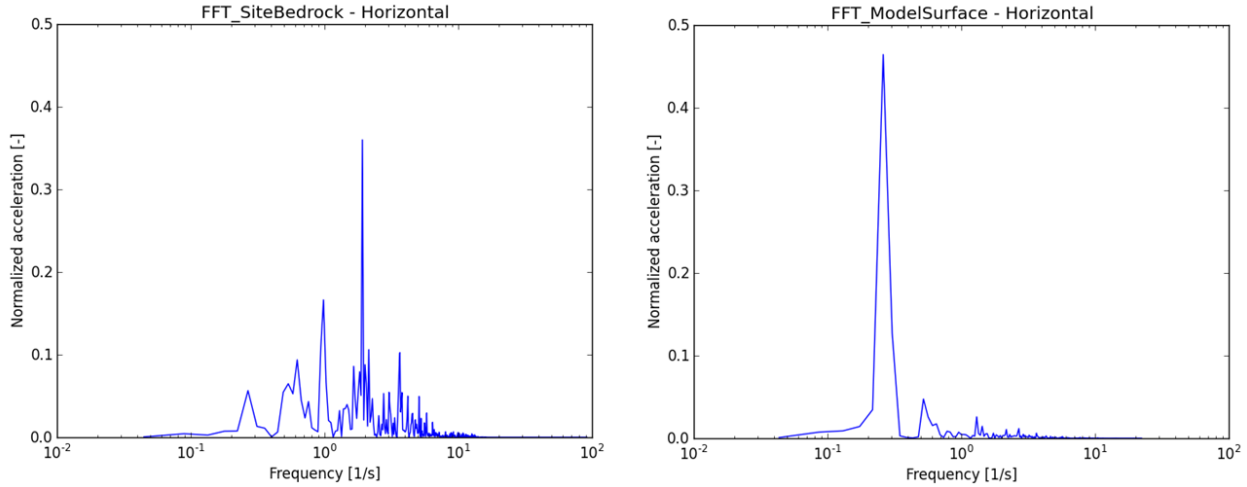

Figure 11-1 : FFT of horizontal acceleration measured at the bedrock outcrop (left) and at the top of the soil foundation (right). Undrained modulus.

Figure 11-2 shows the same comparison for the vertical component of acceleration. The same effects are observed.

Figure 11-3 compares the FFT of the horizontal acceleration measured at the model surface with the FFT of the signal as it was measured considering a *drained* modulus for the clayey silt layer. The amplification of the signal is slightly higher for the *undrained* case, but the difference can be considered as negligible.

Figure 11-4 shows the same comparison for the vertical component of acceleration. As expected, the amplification is more important for the *drained* case than the *undrained* case.

The final results issued from the dynamic simulation are compared to evaluate the incidence of such difference in terms of amplification of the signal.

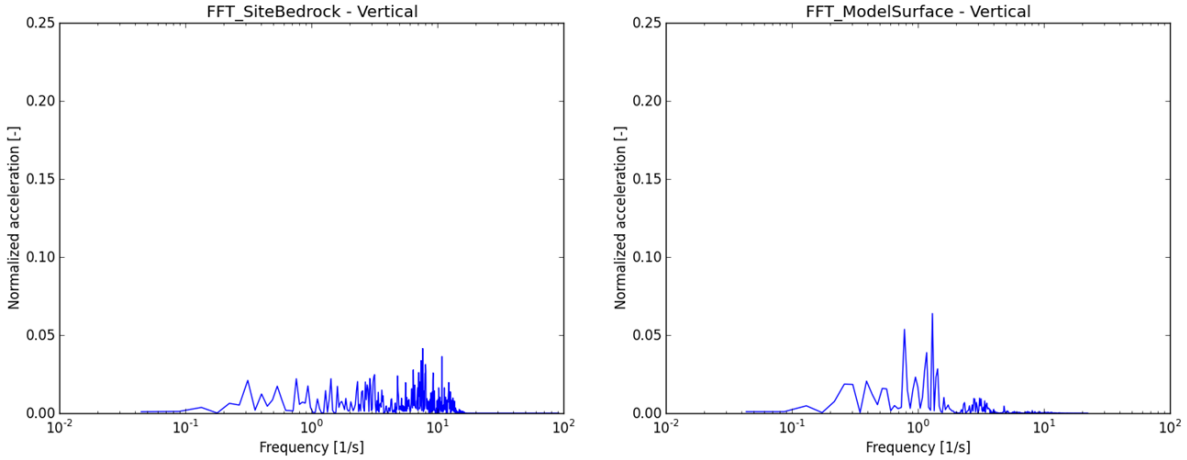

Figure 11-2 : FFT of vertical acceleration measured at the bedrock outcrop (left) and at the top of the soil foundation (right). Undrained modulus.

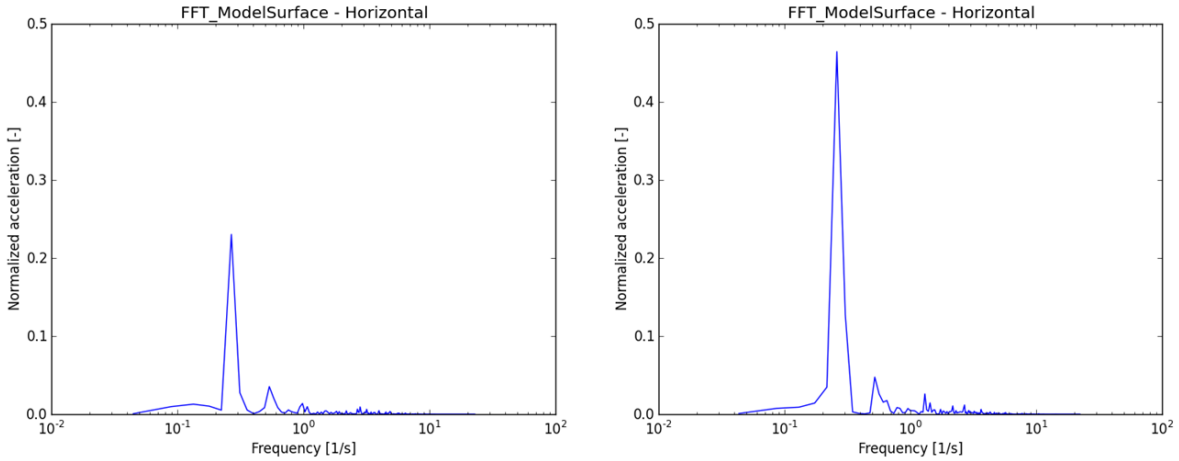

Figure 11-3 : FFT of horizontal acceleration measured at the model surface. Result obtained considering a drained *modulus (left) and an* undrained *modulus (right) for the clayey silt layer.*

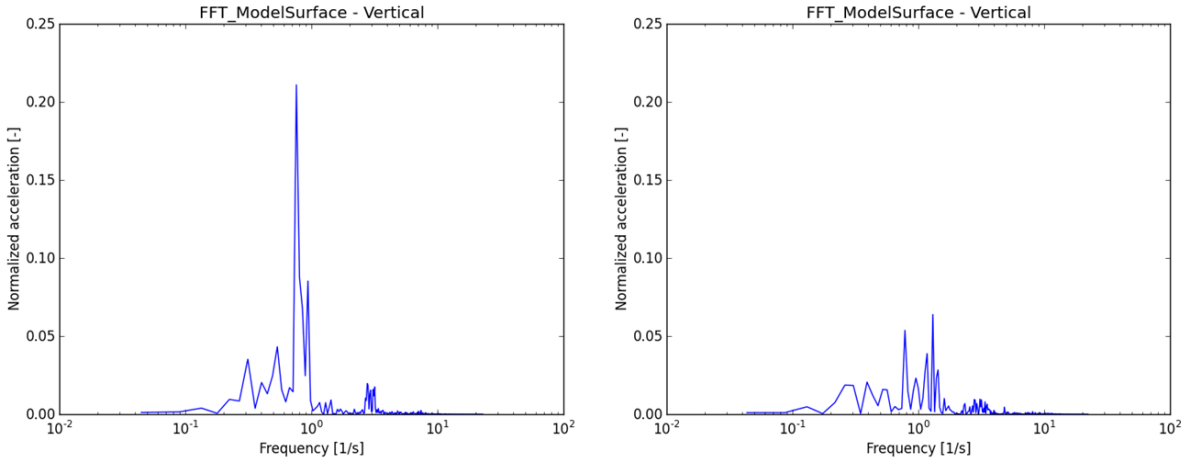

Figure 11-4 : FFT of vertical acceleration measured at the model surface. Result obtained considering a drained *modulus (left) and an* undrained *modulus (right) for the clayey silt layer.*

11.1. Comparison of final displacements

Figure 11-5 and Figure 11-6 show the comparison of the horizontal and the vertical displacement fields, respectively. It can be noticed how the mechanisms of deformation are very similar. Some difference is observed in terms of displacement magnitude.

Figure 11-7 summarizes the displacements that were measured. The differences are small enough to be considered as negligible.

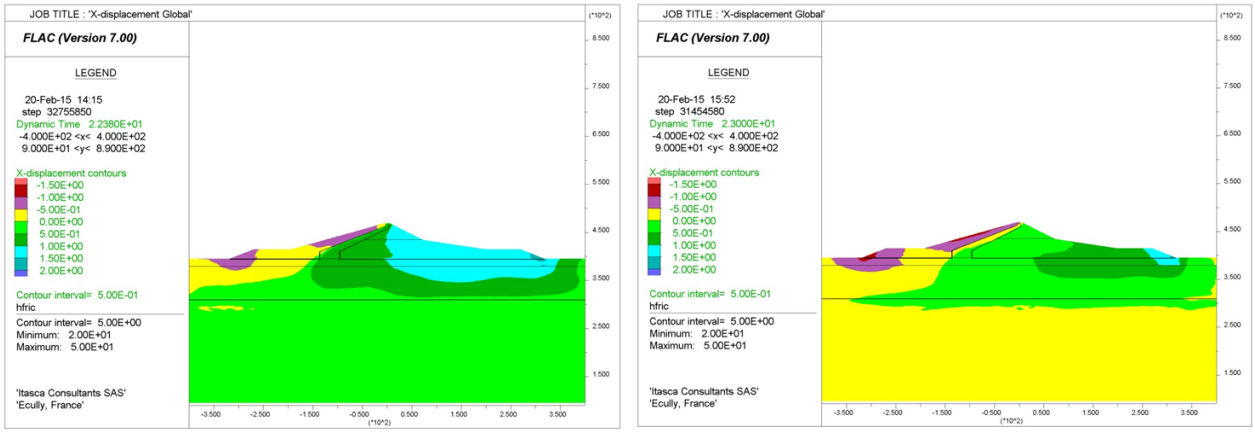

Figure 11-5 : Horizontal displacements field. Result obtained considering a drained *modulus (left) and an* undrained *modulus (right) for the clayey silt layer.*

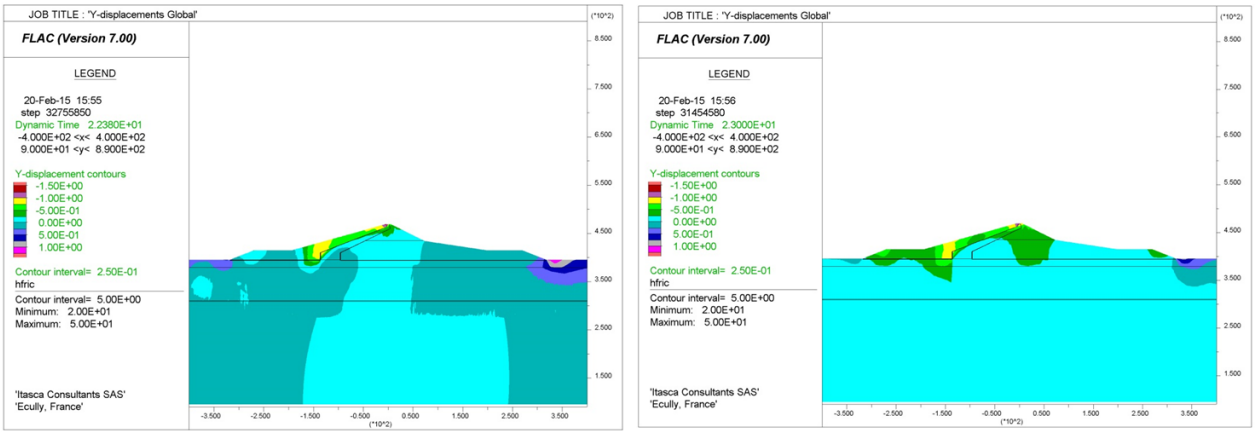

Figure 11-6 : Vertical displacements field. Result obtained considering a drained *modulus (left) and an* undrained *modulus (right) for the clayey silt layer.*

SEE KOCAELI V-H2 -- COMPARISON DRAINED/UNDRAINED					
		PGA [g]		Max Crest Displacements [m]	
Name		Vertical	Horizontal	Vertical	Horizontal
"Drained" case		+ 0.51 / - 0.43	+ 0.47 / - 0.59	-1.0	-0.8
"Undrained" case		+ 0.51 / - 0.43	+ 0.47 / - 0.59	-1.0	-1.0

Figure 11-7 : Comparison of max crest displacements between the drained *and the* undrained *case.*